University of Nottingham
UK | CHINA | MALAYSIA

Investigations into β_2-adrenoceptor pharmacology: kinetic analysis, mechanotransduction and allosteric modulation

Sean A. Cullum, BSc (Hons) MScR

Thesis submitted to the University of Nottingham
for the degree of Doctor of Philosophy

September 2023

This thesis is entirely the candidate's own work. The experiments described in this thesis were performed by the author between October 2019 and March 2023 in the Cell Signalling Research Group, University of Nottingham. No part of this work has been submitted previously for a degree or any other qualification at any University.

Abstract

The β_2-adrenoceptor (β_2AR) is a prototypical class A member of the G protein-coupled receptor (GPCR) superfamily of membrane-bound receptors. Activation of the β_2AR is associated primarily with the relaxation of airway and vascular smooth muscle and has been targeted extensively by β-agonists to treat pulmonary diseases. This thesis has investigated several underexplored aspects of β_2AR pharmacology to improve our understanding of the mechanisms underpinning GPCR action. Quantifying endogenous β_2AR-mediated cAMP signalling kinetics in HEK293 cells revealed that partial (but not full) agonists exhibited reduced maximal initial rates of signal generation (IR_{max}) compared with their maximal responses (E_{max}), likely reflecting slower rates of receptor desensitisation. Moreover, preincubation of slowly dissociating antagonists greatly reduced agonist E_{max} and IR_{max} values due to hemi-equilibrium conditions. These findings were not observed upon β_2AR overexpression because of increased receptor reserve. Kinetic analysis of β_2AR responses has provided valuable new insights into ligand-receptor interactions. Receptor overexpression also exposed a mechanosensory function of the β_2AR whereby a transient cAMP signal was measured after application of a sustained linear motion to cells, which may be physiologically relevant in the vascular system. This response was potentiated or inhibited by agonists and inverse agonists, respectively. Mutagenic removal of three N-glycosylation sites (Asn6, Asn15 and Asn187) resulted in a substantial reduction of the mechanical response, suggesting receptor extracellular N-glycan chains are responsible for conferring β_2AR mechanosensitivity. Finally, functional characterisation of five β_2AR-derived pepducins (ICL3-2, ICL3-7, ICL3-8, ICL3-9 and ICL1-15) uncovered possible allosteric agonist activity, although this was inconclusive due to the variability and small magnitude of responses. No evidence was found of pepducin binding to detergent-solubilised β_2AR, however several pepducins modestly increased receptor dissociation rates of either F-propranolol (ICL3-7) or formoterol (ICL3-9, ICL1-15) in native membranes, indicative of allosteric modulation. This thesis contributes to a greater understanding of the kinetics of β_2AR signalling, receptor mechanotransduction and allosteric modulation by pepducins.

Publications arising from this thesis

Papers

Cullum, S. A., Veprintsev, D. B. & Hill, S. J. 2023. Kinetic analysis of endogenous β_2-adrenoceptor-mediated cAMP GloSensor^{TM} responses in HEK293 cells. *British Journal of Pharmacology*, 180, 1304-1315.

Abstracts

Cullum, S. A., Veprintsev, D. B. & Hill, S. J. 2021. The molecular basis for allosteric modulation of the β_2-adrenoceptor by pepducins.

- Oral communication at IMPACT: MRC DTP Annual Symposium, January 2021. Online event.
- Poster presentation at University of Nottingham School of Life Sciences PGR Symposium, July 2021. Online event.

Cullum, S. A., Veprintsev, D. B. & Hill, S. J. 2022. Kinetic analysis of endogenous β_2-adrenoceptor-mediated cAMP GloSensor^{TM} responses in HEK293 cells.

- Oral communication at University of Nottingham School of Life Sciences PGR Symposium, July 2022. University of Nottingham, UK.
- Poster presentation at 4GPCRnet International Symposium, September 2022. Universität Leipzig, Germany.
- Poster presentation at IRN iGPCRnet Meeting, September-October 2022. Universität Würzburg, Germany.

Acknowledgements

I would firstly like to thank my supervisors, Professor Steve Hill and Professor Dmitry Veprintsev, for giving me the opportunity to undertake this PhD project and for all their support and guidance over the last four years. Both have been absolutely excellent supervisors throughout my time in their labs, providing constant encouragement, confidence and advice and helping me through the many difficult moments. Steve and Dmitry have taught me so much, not just about GPCRs and pharmacology, but also to think independently as a scientist and to present my work in a concise and engaging manner. It is largely thanks to their influence that I have decided to continue to pursue a career in science. I am also grateful to the Medical Research Council (MRC) for funding my PhD.

Special mentions must also go to Dr. Mark Soave, Dr. David Sykes and Dr. Simon Platt, each of whom have played important roles at different stages of my PhD, for teaching me many new experimental techniques and taking the time for regular discussions about my project and general day-to-day advice in the lab. The Institute of Cell Signalling (ICS) has been such a fantastic place to work for these years and I have made many great friends who have provided so much support, joy and countless laughs. I will remember the time I spent in ICS very fondly and Nottingham will always feel like home to me.

I also want to give a massive thanks to my parents, Janet and Laurence, for simply being the most supportive and loving parents I could ever ask for. I'm so grateful for everything you've done and sacrificed to help me get this far and for the endless moral (and often financial...) support. I really can never repay you! The same goes to my sister, Lauren, and to the rest of my family and friends who have always been there for me whenever I've needed them.

Finally, and most importantly, to Octavia. I'm so lucky to have had you by my side throughout my PhD. You've been a constant supply of optimism, support, love and especially fun (and goofiness!). You've always believed in me and pushed me to keep going, even when I didn't believe in myself. I can never thank you enough, especially for your understanding over the past year. I truly couldn't have achieved this without you and I can't wait for our next adventure together.

Abbreviations

ATP	Adenosine triphosphate
AUC	Area under curve
$A_{2A}AR$	Adenosine receptor 2A
$A_{2B}AR$	Adenosine receptor 2B
BCA	Bicinchoninic acid
B_{max}	Maximal specific binding
BRET	Bioluminescence resonance energy transfer
BSA	Bovine serum albumin
cAMP	Cyclic adenosine monophosphate
CHAPSO	3-[(3-Cholamidopropyl)dimethylammonio]-2-hydroxy-1-propanesulfonate
CHO cells	Chinese Hamster Ovary cells
CHS	Cholesteryl hemisuccinate tris salt
CMC	Critical micelle concentration
CMV	Human cytomegalovirus immediate early promoter
CNG	Cyclic nucleotide-gated ion channels
COPD	Chronic obstructive pulmonary disease
CRE	cAMP response element
CREB	cAMP response element-binding protein
CRE-SPAP	cAMP response element-mediated secreted placental alkaline phosphatase
Cryo-EM	Cryogenic electron microscopy
DAG	Diacylglycerol
ddH_2O	Double distilled water
DDM	N-Dodecyl-β-D-maltopyranoside

DEA	Diethanolamine
DMEM	Dulbecco's Modified Eagle Medium
DMSO	Dimethyl sulfoxide
DNA	Deoxyribonucleic acid
E. coli	*Escherichia coli*
ECL	Extracellular loop
ECM	Extracellular matrix
EC_{50}	Half-maximal response concentration
EDTA	Ethylenediamine tetraacetic acid
E_{max}	Maximal response
EPAC	Exchange proteins activated by cAMP
ER	Endoplasmic reticulum
ERK	Extracellular-signal-regulated kinase
FCS	Foetal calf serum
F-propranolol	Fluorescent β_2AR antagonist (S)-propranolol-green
FRET	Fluorescence/Förster resonance energy transfer
GDP	Guanosine diphosphate
GEF	Guanine nucleotide exchange factor
GPCR	G protein-coupled receptor
GppNHp	Guanosine-5'-[(β,γ)-imido]triphosphate tetralithium salt
GRK	G protein-coupled receptor kinase
GTP	Guanosine triphosphate
HaBSS	Hanks' balanced salt solution
HBSS	HEPES buffered saline solution
HEK293 cells	Human Embryonic Kidney 293 cells

HEPES	4-(2-Hydroxyethyl)-1-piperazineethanesulfonic acid
HTRF	Homogenous time-resolved fluorescence
IBMX	3-Isobutyl-1-methylxanthine
ICI-118551	(±)-1-[2,3-(Dihydro-7-methyl-1*H*-inden-4-yl)oxy]-3-[(1-methylethyl)amino]-2-butanol hydrochloride
ICL	Intracellular loop
IC_{50}	Half-maximal inhibition concentration
IL_{50}	Half-maximal kinetic inhibition concentration
I_{max}	Maximal inhibition
IR_{max}	Maximal initial rate of signal generation
IP_3	Inositol 1,4,5-trisphosphate
JNK	c-Jun N-terminal kinase
K_D	Equilibrium dissociation constant
K_I	Inhibition constant
k_{off}	Dissociation rate constant
k_{on}	Association rate constant
LABA	Long-acting β-agonist
LB broth	Luria-Bertani broth
LMNG	Lauryl maltose neopentyl glycol
L_{50}	Half-maximal initial rate concentration
MAPK	Mitogen-activated protein kinase
NaCl	Sodium chloride
NAL	Neutral allosteric ligand
NAM	Negative allosteric modulator
NanoBRET	Nanoluciferase-based bioluminescence resonance energy transfer

NECA	5’-(N-Ethylcarboxamido)adenosine
NLuc	Nanoluciferase
NMR	Nuclear magnetic resonance
NSB	Non-specific binding
OD	Optical density
PAM	Positive allosteric modulator
PBS	Phosphate buffered saline
PCR	Polymerase chain reaction
PDE	Phosphodiesterase enzyme
PEI	Polyethylenimine
Pen/Strep	Penicillin-streptomycin
PIP_2	Phosphatidylinositol 4,5-bisphosphate
PI_3K	Phosphatidylinositol-3 kinase
PKA	Protein kinase A
PKC	Protein kinase C
PLC	Phospholipase C
PLD	Phospholipase D
pNPP	4-Nitrophenyl phosphate disodium salt hexahydrate
RGS	Regulators of G protein signalling
RhoGEF	Rho guanine nucleotide exchange factor
RIIβB	cAMP-binding domain from PKA regulatory subunit
RIU	Relative intensity units of luminescence
SABA	Short-acting β-agonist
SCM	Sulfo-cyanine3 maleimide
SFM	Serum-free media
SPAP	Secreted placental alkaline phosphatase

SR	Sarcoplasmic reticulum
$TetO_2$	Tetracycline operator sequences
TetR	Tetracycline repressor protein
ThermoBRET	Thermostability bioluminescence resonance energy transfer
ThermoFRET	Thermostability fluorescence/Förster resonance energy transfer
TM	Transmembrane domain
T_m	Melting temperature
TR-FRET	Time-resolved fluorescence/Förster resonance energy transfer
tsNLuc	Thermostable nanoluciferase
VEGF	Vascular endothelial growth factor
αAR	α-adrenoceptor
βAR	β-adrenoceptor
β_1AR	β_1-adrenoceptor
β_2AR	β_2-adrenoceptor
β_3AR	β_3-adrenoceptor
8-CPT-cAMP	8-(4-Chlorophenylthio)adenosine 3',5'-cyclic monophosphate sodium salt

Table of contents

Chapter 1

General introduction

1.1 – G protein-coupled receptors

1.1.1 – Introduction to G protein-coupled receptors

G protein-coupled receptors (GPCRs), also termed seven-transmembrane (7TM) receptors, are a large superfamily of membrane proteins which comprise seven membrane-spanning α-helices (transmembrane domains; TM1-7) which are connected by three intracellular (ICL1-3) and three extracellular (ECL1-3) loops and contain an intracellular carboxyl (C-) terminus and an extracellular amino (N-) terminus (Schertler et al., 1993; Van Neuren et al., 1999; Palczewski et al., 2000; Hanson and Stevens, 2009; Alexander et al., 2017). Figure 1.1 illustrates the simplified general GPCR structure. The human genome is known to encode at least 800 GPCRs (Lander et al., 2001; Venter et al., 2001; Fredriksson et al., 2003; Foord et al., 2005; Alexander et al., 2017) and they are expressed almost ubiquitously throughout mammalian tissues, where they regulate a plethora of physiological processes by transducing a wide range of extracellular stimuli into intracellular downstream signalling pathways (Ji et al., 1998; Foord et al., 2005; Luttrell, 2008; Regard et al., 2008). Therefore, GPCR dysregulation is unsurprisingly implicated in a vast number of diseases and these receptors have become critical targets for therapeutic treatment (Hauser et al., 2017; Shimada et al., 2019; Congreve et al., 2020). It is estimated that approximately one third of all current FDA-approved drugs target GPCRs directly (Rask-Andersen et al., 2011; Hauser et al., 2017; Santos et al., 2017) and they continue to show promise for further development of improved therapeutics in the future. Naturally, gaining a better understanding of GPCR pharmacology is vital to aid in this endeavour.

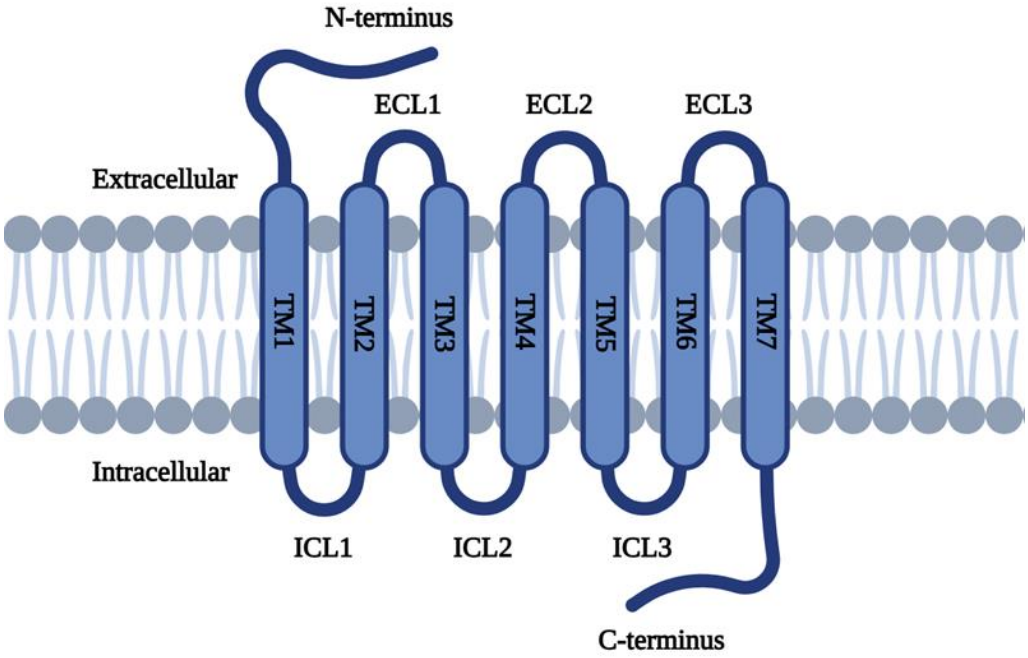

Figure 1.1: The general GPCR structure including seven transmembrane domains (TM1-7) connected by three extracellular (ECL1-3) and three intracellular (ICL1-3) loops with an extracellular N-terminus and intracellular C-terminus. This diagram was created using BioRender.com.

1.1.2 – GPCR classification

Due to the large size of the GPCR superfamily, it is necessary to split this into several distinct subfamilies. All GPCRs share a general structure and mechanism of signal transduction, however there is still considerable diversity between GPCRs in terms of the types of ligands they recognise, as well as their specific structures and functions (Ji et al., 1998; Luttrell, 2008). GPCRs have been divided into subfamilies (or classes) by numerous different methods, including by amino acid sequence homology, ligand type and function (Ji et al., 1998; Schiöth and Fredriksson, 2005; Gao and Wang, 2006; Lagerström and Schiöth, 2008; Gacasan et al., 2017). One such method, known as the 'GRAFS' system, which has become the most established system to classify GPCRs into subfamilies and is based on the phylogenetic origin of the receptors, comprises five classes: glutamate, rhodopsin, adhesion, frizzled/taste 2 and secretin (Schiöth and Fredriksson, 2005; Lagerström and Schiöth, 2008; Katritch et al., 2013; Hu et al., 2017). Of these, the rhodopsin subfamily (often instead referred to as class A, based on the previous classical system) is by far the largest group, comprising roughly 80% of the GPCR superfamily. Therefore, based on sequence homology, class A GPCRs can be further differentiated into four subclasses (α, β, γ and δ) (Schiöth and Fredriksson, 2005; Lagerström and Schiöth, 2008; Katritch et al., 2013; Hu et al., 2017).

1.1.3 – General GPCR structure and mechanism of signal transduction

The first GPCR to have its three-dimensional structure solved using x-ray crystallography was rhodopsin by Palczewski et al. (2000). Since then, hundreds of GPCR crystal structures have been resolved bound to different ligands and intracellular proteins and in distinct conformational states (Zhang et al., 2015a; Congreve et al., 2020; Gusach et al., 2020). This work has advanced our understanding of GPCR structural biology and has enabled a structure-based approach to rational drug design, ultimately leading to improved therapeutics. Although GPCRs share a common general structure, there is still much diversity

between different GPCR families. The extracellular loops and N-terminus represent the most variable regions of GPCRs, enabling the recognition of extremely diverse ligands such as photons, ions, neurotransmitters, hormones, lipids and more (Ji et al., 1998; Kobilka, 2007; Strotmann et al., 2011; Wheatley et al., 2012; Katritch et al., 2013; Stevens et al., 2013; Zhang et al., 2015a). The N-terminus varies not only in sequence but also in length, with some GPCRs comprising N-termini as short as 10 amino acids whilst others, particularly adhesion GPCRs, can span up to approximately 600 residues (Ji et al., 1998; Kobilka, 2007; Gacasan et al., 2017). The seven transmembrane domains, which provide the core receptor structure and are primarily responsible for transducing extracellular stimuli into intracellular signals, are extremely well conserved and have served as identifiers of GPCRs in genetic sequences (Strotmann et al., 2011; Katritch et al., 2013; Stevens et al., 2013; Lu and Wu, 2016). The generally moderate sequence homology of intracellular regions allows them to interact with a number of intracellular proteins to initiate downstream signalling cascades (Kobilka, 2007; Stevens et al., 2013; Lu and Wu, 2016; Gacasan et al., 2017). Additionally, most GPCRs comprise a C-terminal α-helix (helix 8) which is also involved in interactions with intracellular proteins (Santos et al., 2006; Zhang et al., 2015a).

Upon binding of extracellular agonists, GPCRs undergo a common mechanism of activation and signal transduction, whereby a conformational change results in increased coupling to intracellular effector proteins (Kobilka, 2007; Rosenbaum et al., 2009; Venkatakrishnan et al., 2013). In general, this involves structural changes to several conserved GPCR motifs, primarily located within the transmembrane domain, which form networks of inter-helical contacts that stabilise the receptor and act as microswitches during receptor activation (Katritch et al., 2013; Venkatakrishnan et al., 2013; Zhang et al., 2015a; Gacasan et al., 2017). Firstly, the D/ERY motif resides at the cytoplasmic end of TM3 and acts as an ionic lock which stabilises the inactive receptor conformation, thus hindering intracellular protein binding (Rovati et al., 2007; Vogel et al., 2008; Katritch et al., 2013; Zhang et al., 2015a). It does this by formation of an interhelical salt bridge between the positively charged arginine residue ($R^{3.50}$; using Ballesteros-Weinstein numbering, where the first number refers to the TM

helix and the second denotes the residue position relative to the most conserved residue in the helix which is defined as 50 (Ballesteros and Weinstein, 1995)) of the D/ERY sequence on TM3 and a neighbouring negatively charged aspartate or glutamate residue (D/E$^{6.30}$) from TM6, which is generally broken and replaced by new interactions upon transition of the receptor to an active conformation (Rovati et al., 2007; Vogel et al., 2008; Katritch et al., 2013; Zhang et al., 2015a). The CWxP motif on TM6, which is referred to as the rotamer toggle switch, acts as a trigger for the change in receptor conformation to an active state (Shi et al., 2002; Katritch et al., 2013; Zhang et al., 2015a; Filipek, 2019). Upon orthosteric agonist binding, the side chain of the conserved tryptophan residue (W$^{6.48}$) of the CWxP motif is rotated which facilitates the outward movement of TM6 away from TM3 at the intracellular surface, critical for GPCR activation (Shi et al., 2002; Katritch et al., 2013; Zhang et al., 2015a; Filipek, 2019). Simultaneously, the NPxxY motif residing on TM7 also plays a role in receptor activation, where inward rotation of the tyrosine residue (Y$^{7.53}$) sterically blocks the return of TM6 back toward TM3, thus stabilising the active conformation of the receptor (Rosenbaum et al., 2009; Katritch et al., 2013; Zhang et al., 2015a; Venkatakrishnan et al., 2016).

1.2 – Intracellular proteins

1.2.1 – Heterotrimeric G proteins

Activated GPCRs couple to several intracellular proteins including primarily the heterotrimeric effector proteins known as heterotrimeric GTP-binding proteins (G proteins; hence the name G protein-coupled receptors) which are comprised of α, β and γ subunits (Downes and Gautam, 1999; Hillenbrand et al., 2015). There are several distinct subtypes of each of these G protein subunits; 21 G_{α}, six G_{β} and 12 G_{γ} subtypes, some of which are expressed only in specific tissues while others are more widely distributed (Downes and Gautam, 1999; Neves et al., 2002; Wettschureck and Offermanns, 2005; Anantharaman et al., 2011; Flock et al., 2015). The G_{α} subtypes are further divided into four classes, $G_{\alpha s}$, $G_{\alpha i}$, $G_{\alpha q}$ and $G_{\alpha 12/13}$, based on sequence similarities and their abilities to initiate distinct downstream pathways (Neves et al., 2002; Cabrera-Vera et al., 2003; Syrovatkina et al., 2016). Assembly of the G protein subunits into the heterotrimeric protein is relatively unrestricted between subtypes, meaning that up to 700 distinct $G_{\alpha\beta\gamma}$ complexes may exist which could provide substantial diversity in their specific functional roles (Pierce et al., 2002; Hillenbrand et al., 2015). GPCRs also have distinct preferences for different G protein complexes, further increasing the variety of downstream signalling responses (Flock et al., 2015; Hillenbrand et al., 2015).

Coupling to the intracellular surface of GPCRs initiates conformational changes in G proteins whereby they transition to an active state by undergoing nucleotide exchange, substituting a GDP molecule bound to the G_{α} subunit for GTP (Pierce et al., 2002; Cabrera-Vera et al., 2003; Flock et al., 2015). The active GTP-bound G_{α} subunit then dissociates from the $G_{\beta\gamma}$ complex which generally remains tightly bound together, and both components of the G protein can subsequently initiate downstream signalling cascades (Pierce et al., 2002; Cabrera-Vera et al., 2003; Luttrell, 2008). G_{α} possesses intrinsic GTPase activity thereby naturally hydrolysing the bound GTP molecule back into GDP, which leads to reassociation of the heterotrimeric G protein subunits and termination of GPCR-induced signalling (Cabrera-Vera et al., 2003; Luttrell, 2008). Additionally, this

process can be accelerated by regulators of G protein signalling (RGS), which are intracellular proteins that target G_{α} and catalyse GTP hydrolysis (Berman et al., 1996; De Vries et al., 2000; Ross and Wilkie, 2000).

The signalling pathways initiated by the activated G protein are dependent on the class of the G_{α} subunit. The $G_{\alpha s}$ class (containing G_s and G_{olf}) stimulates the enzymatic effector adenylate cyclase which catalyses the synthesis of cyclic adenosine monophosphate (cAMP) from adenosine triphosphate (ATP) by the removal of two phosphate groups, increasing the concentration of cAMP inside cells (Sunahara et al., 1996; Cabrera-Vera et al., 2003; Wettschureck and Offermanns, 2005; Syrovatkina et al., 2016). cAMP is a universal second messenger molecule which has several functions including activation of protein kinase A (PKA), exchange proteins activated by cAMP (EPAC) and cyclic nucleotide-gated ion channels (CNG) (Neves et al., 2002; Wettschureck and Offermanns, 2005; Serezani et al., 2008; Kamenetsky et al., 2006). When cAMP binds to the regulatory subunits of PKA, which is a serine/threonine kinase enzyme, the activated catalytic subunits dissociate and subsequently phosphorylate numerous targets, including GPCRs, other kinases and transcription factors, such as cAMP response element-binding protein (CREB) (Chin et al., 2002; Kopperud et al., 2003; Serezani et al., 2008). Contrastingly, the $G_{\alpha i}$ class (comprising G_{i1}, G_{i2}, G_{i3}, G_{oA}, G_{oB}, G_{t1}, G_{t2}, G_g and G_z) inhibits adenylate cyclase to reduce cytosolic cAMP concentration, thus opposing the action of $G_{\alpha s}$ (Sunahara et al., 1996; Cabrera-Vera et al., 2003; Wettschureck and Offermanns, 2005; Syrovatkina et al., 2016).

$G_{\alpha q}$ (which comprises G_q, G_{11}, G_{14}, G_{15} and G_{16}) instead targets the β subtype of phospholipase C (PLC), which in turn catalyses the hydrolysis of the membrane-bound phosphatidylinositol 4,5-bisphosphate (PIP_2) into inositol 1,4,5-trisphosphate (IP_3) and diacylglycerol (DAG) (Neves et al., 2002; Cabrera-Vera et al., 2003; Wettschureck and Offermanns, 2005; Syrovatkina et al., 2016). IP_3 diffuses through the cytosol and acts as a second messenger to bind IP_3 ion channel receptors (IP_3Rs) bound to the sarcoplasmic (SR) and endoplasmic (ER) reticulum membranes, causing the release of calcium ions from intracellular stores (Exton, 1996; Rhee and Bae, 1997; Neves et al., 2002; Bootman, 2012).

Moreover, DAG signals through protein kinase C (PKC)-mediated pathways (Neves et al., 2002; Bootman, 2012; Syrovatkina et al., 2016). Finally, $G_{\alpha 12/13}$ (including G_{12} and G_{13}) regulates cell growth and actin cytoskeleton organisation through the GTPase Rho guanine nucleotide exchange factor (RhoGEF) and is also involved in further downstream signalling events like phospholipase D (PLD) and mitogen-activated protein kinase (MAPK) activation (Kozasa, 1998; Cabrera-Vera et al., 2003; Kurose, 2003; Syrovatkina et al., 2016). The exact signalling functions of each of these G_{α} subunits is dependent not only on the specific subtype within each G_{α} class, but also on the cell type in which they are expressed (Wettschureck and Offermanns, 2005).

In addition to G_{α}-dependent signalling, the dissociated $G_{\beta\gamma}$ complex can also mediate downstream pathways through interactions with numerous effectors including MAPK, PLC, adenylate cyclase, various potassium and calcium ion channels and also G protein-coupled receptor kinases (GRKs) (Logothetis et al., 1987; Tang and Gilman, 1991; Boyer et al., 1992; Inglese et al., 1995; Herlitze et al., 1996; Clapham and Neer, 1997; Stoffel et al., 1997; Cabrera-Vera et al., 2003). The $G_{\beta\gamma}$ dimer is thought to play a particularly significant role after $G_{\alpha i}$ protein activation (Neves et al., 2002; Wettschureck and Offermanns, 2005).

1.2.2 – GRKs and arrestins

GPCRs can also couple to other intracellular proteins, most notably GRKs and arrestins which are primarily associated with regulating GPCR-G protein signalling (Ferguson et al., 1996; Krupnick and Benovic, 1998; Premont and Gainetdinov, 2007). GRKs are serine/threonine kinases which bind to the C-terminal tail of activated GPCRs, becoming activated themselves and subsequently phosphorylating specific patterns of serine and threonine residues at the receptor C-terminus (Kühn, 1978; Benovic et al., 1986; Palczewski et al., 1991; Chen et al., 1993; Fredericks et al., 1996; Komolov and Benovic, 2018). This plays a major role in attenuating G protein-mediated signalling because phosphorylation of GPCRs increases their affinity for arrestin recruitment (Ferguson et al., 1996; Moore et al., 2007a; Black et al., 2016). There are seven

members of the GRK family (GRKs1-7), divided into 3 subfamilies; GRK1 (GRK1 and GRK7; primarily located in the retina), GRK2 (GRK2 and GRK3; ubiquitously expressed) and GRK4 (GRK4, GRK5 and GRK6; widely distributed except GRK4 which is primarily expressed in the testes) (Moore et al., 2007a; Premont and Gainetdinov, 2007; Black et al., 2016). Except for GRK5, which is membrane-bound (Ferguson et al., 1996), GRKs are generally soluble in the cytosol but localise at the cell membrane by distinct methods (Ferguson et al., 1996; Krupnick and Benovic, 1998; Gurevich and Gurevich, 2019). GRK2 and GRK3, for example, comprise a unique binding site for the $G_{\beta\gamma}$ complex which facilitates anchorage to the membrane and subsequent recognition of GPCR phosphorylation sites (Pitcher et al., 1992; Koch et al., 1993; Touhara et al., 1994; Lodowski, 2003).

The specific patterns of GRK-mediated phosphorylation of serine and threonine residues on the GPCR C-terminus directly influences arrestin binding affinity for the receptor (Oakley et al., 2001; Reiter et al., 2012; Black et al., 2016). Arrestins are cytosolic scaffolding proteins which interact at the intracellular loops and C-terminus of activated GPCRs to sterically uncouple G protein binding, thereby regulating GPCR function by terminating G protein-dependent signalling pathways; a process called receptor desensitisation (Lohse et al., 1990; Ferguson et al., 1996; Krupnick and Benovic, 1998; Oakley et al., 2001; Gurevich and Gurevich, 2006; Moore et al., 2007a). Four subtypes of arrestin are known to exist, arrestin-1 (visual arrestin), arrestin-2 (β-arrestin-1), arrestin-3 (β-arrestin-2) and arrestin-4 (X-/C-arrestin or cone arrestin), of which visual arrestin and cone arrestin are found exclusively in the retina and are involved in photoreceptor function, while the two β-arrestins are almost universally expressed and interact with most GPCRs (Pfister et al., 1985; Lohse et al., 1990; Attramadal et al., 1992; Murakami et al., 1993; Krupnick and Benovic, 1998; Premont and Gainetdinov, 2007). Just as GPCRs have distinct preferences for G protein subtypes, they also comprise differing abilities to couple to arrestin subtypes (Pierce et al., 2002; Reiter et al., 2012; Gurevich and Gurevich, 2013).

Beyond receptor desensitisation, another important regulatory function of β-arrestins is the trafficking of GPCRs, where receptors can be internalised from

the cell membrane by endocytosis (Ferguson et al., 1996; Moore et al., 2007a; Black et al., 2016). In this process, β-arrestins act as adapters and recruit other proteins including β_2-adaptin and clathrin to facilitate sequestration of GPCRs via clathrin-coated pits into early endosomes (Ferguson et al., 1996; Goodman et al., 1996; Krueger et al., 1997; Laporte et al., 1999; Drake et al., 2006). Internalised receptors are subsequently either recycled back to the cell surface membrane in a dephosphorylated, re-sensitised state or alternatively transported through a series of late endosomes and ultimately to lysosomes for protein degradation (Ferguson et al., 1996; Krueger et al., 1997; Drake et al., 2006; Moore et al., 2007a). Moreover, β-arrestins are also implicated in modulating G protein-independent signalling of GPCRs through interactions with numerous signalling molecules including several MAPKs such as extracellular-signal-regulated kinases (ERKs), c-Jun N-terminal kinases (JNKs) and p38 kinases (Luttrell et al., 1999; Dewire et al., 2007; Black et al., 2016; Gurevich and Gurevich, 2019). The exact signalling pathways initiated are dependent on β-arrestin conformation, which is in turn influenced by the different patterns (or 'barcode') of GRK-mediated phosphorylation of serine and threonine residues on the receptor C-terminus (Liggett, 2011; Nobles et al., 2011; Xiao and Liu, 2016). Nevertheless, it remains unresolved as to whether β-arrestins actually play a direct role in the mediation of signal transduction or instead simply act as scaffolding proteins to facilitate localisation of other effector proteins, forming a signalosome (Morrison and Davis, 2003; Luttrell, 2005; Shenoy and Lefkowitz, 2005; Dewire et al., 2007; Gutkind and Kostenis, 2018; Gurevich and Gurevich, 2019).

1.3 – Concepts in GPCR pharmacology

1.3.1 – Classification of ligand activity

It is useful to classify ligands based upon their differing activities at GPCRs. An agonist can be defined as a ligand which is capable of inducing a signalling response at the receptor by stabilising the receptor's active state (Stephenson, 1956; Neubig et al., 2003; Weis and Kobilka, 2018). Agonists can also be split into full agonists and partial agonists, whereby a full agonist elicits a maximal receptor response while a partial agonist only produces a submaximal response at the receptor (Stephenson, 1956; Neubig et al., 2003; Weis and Kobilka, 2018). The magnitude of the maximal response produced (often measured in terms of E_{max}) is dependent on the agonist's intrinsic efficacy for the receptor, which describes the efficiency with which the bound ligand can confer an active receptor conformation and thus transduce downstream signalling pathways (Stephenson, 1956; Neubig et al., 2003; Kenakin, 2013; Weis and Kobilka, 2018). In some cases, ligands may appear as full agonists in certain assay systems but act as partial agonists in different conditions, depending on coupling efficiencies of the system, degrees of signal amplification and receptor expression levels (Hoyer and Boddeke, 1993; Whaley et al., 1994; McDonnell et al., 1998; McDonald et al., 2003).

Contrastingly, an inverse agonist is a ligand which stabilises the receptor's inactive conformation (thus comprising negative intrinsic efficacy) and therefore reduces the receptor's constitutive activity, which is the ability of the receptor to spontaneously switch to an active conformation and initiate signalling in the absence of a bound ligand (Costa and Herz, 1989; Neubig et al., 2003; Greasley and Clapham, 2006; Berg and Clarke, 2018; Weis and Kobilka, 2018). At low or endogenous receptor expression levels, it is often not possible to interpret inverse agonist behaviour as the GPCR constitutive activity is too small to detect, occasionally leading to mischaracterisation of inverse agonists as neutral antagonists (Milligan, 2003; Chanrion et al., 2008; Berg and Clarke, 2018). An antagonist is any ligand which binds to the receptor without altering its conformational equilibrium, thus it has no efficacy and does not modulate

receptor constitutive activity (Stephenson, 1956; Neubig et al., 2003; Greasley and Clapham, 2006; Weis and Kobilka, 2018). They can however inhibit the response mediated by an agonist (or inverse agonist) at the receptor, which they do by directly competing for the receptor binding site, assuming both ligands are orthosteric (Neubig et al., 2003; Greasley and Clapham, 2006; Weis and Kobilka, 2018). Orthosteric and allosteric ligands are discussed later (see 1.3.3 – GPCR allostery and allosteric modulation).

Alongside efficacy, binding affinity (usually measured in terms of K_D, the concentration at which 50% of the ligand is bound to receptor) is another important property in ligand characterisation, which defines the strength of the ligand binding interactions with the receptor (Stephenson, 1956; Neubig et al., 2003; Kenakin, 2013). Another useful pharmacological parameter is ligand potency, which is a measure of its functional activity at the receptor and is influenced by both the affinity and efficacy of the ligand (generally expressed as EC_{50}, the concentration at which 50% of the maximal response is achieved) (Stephenson, 1956; Neubig et al., 2003; Kenakin, 2013). Defining and comparing ligand pharmacological parameters by performing binding and signalling assays has provided extremely useful insights into ligand-receptor interactions and their underlying mechanisms (Kenakin, 2019; Zhao and Furness, 2019). Figure 1.2 demonstrates the general effects on receptor signalling that are observed in response to different types of ligands.

In addition to these standard pharmacological parameters of ligand activity, it is becoming increasingly clear that understanding the kinetics of both ligand-receptor binding and also signalling responses may be equally important (Sykes et al., 2019; Hoare et al., 2020b). In ligand binding experiments, two kinetic binding parameters can be determined, the association and dissociation rate constants (k_{on} and k_{off}, respectively), which define the equilibrium-based K_D parameter ($K_D = k_{off}/k_{on}$) (Sykes et al., 2014; Bosma et al., 2017; Sykes et al., 2019). Since drug-receptor equilibrium conditions are rarely achieved *in vivo*, using these kinetic binding parameters to reveal previously unknown drug properties such as receptor residence time could contribute toward more accurate therapeutic optimisation (Bosma et al., 2017; Sykes et al., 2019). Moreover,

elucidating the kinetics of receptor signalling responses using functional assays, which has become possible due to the development of novel biosensors that continuously measure GPCR signalling in real-time, has already proven pivotal in advancing our understanding of receptor signalling mechanisms (Calebiro et al., 2009; Klein Herenbrink et al., 2016; Lane et al., 2017; Paek et al., 2017). The recent derivation of kinetic equations which can be fit to time-course data to quantify new kinetic ligand parameters, initial rate of signal generation (which can be applied to determine kinetic measures of efficacy and potency, IR_{max} and L_{50}) as well as k_1 and k_2 (which define the regulatory mechanisms counteracting the signal) will further aid in improved characterisation of ligand activity (Hoare et al., 2018; Hoare et al., 2020b). More extensive detail on the importance of understanding GPCR signalling kinetics is provided in Chapter 3 (see 3.1), particularly in the specific context of β_2-adrenoceptor (β_2AR)-mediated cAMP signals.

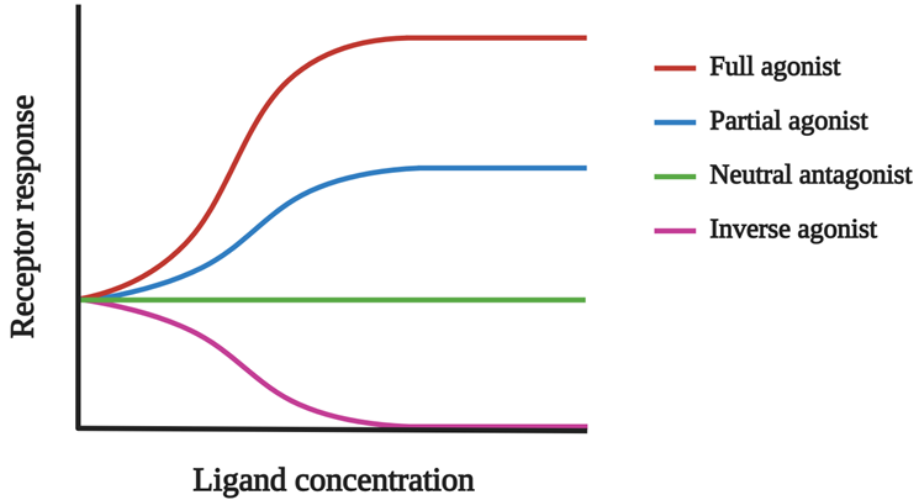

Figure 1.2: Example concentration-response curves observed in response to application of a full agonist (maximal response), partial agonist (submaximal response), neutral antagonist (no effect on basal activity) and inverse agonist (reduction of basal activity) to a receptor. This diagram was created using BioRender.com.

1.3.2 – Ternary complex models of GPCR activation

There have been several models developed in order to explain ligand binding and activation of GPCRs. The ternary complex model, first described by De Lean et al. (1980), stated that activation of the GPCR was dependent on the formation of a ternary complex of agonist, receptor and G protein, which resulted in the initiation of a signalling response (De Lean et al., 1980; Park et al., 2008; Kenakin, 2017). Additionally, agonist affinity for mediating formation of the complex was altered by the presence of guanine nucleotides, for example GTP (De Lean et al., 1980; Park et al., 2008; Kenakin, 2017). It eventually became clear however that GPCRs comprised constitutive activity and could signal spontaneously in the absence of a bound agonist (Costa and Herz, 1989). Therefore, the ternary complex model was extended to include the existence of receptors in the activated state in the absence of ligand; this was therefore termed the extended ternary complex model (Samama et al., 1993; Park et al., 2008; Kenakin, 2017), which is depicted in Figure 1.3. The model has since been updated further to the cubic ternary complex model which accommodates the ability of the inactive state of the receptor to bind G protein (Weiss et al., 1996; Kenakin, 2017).

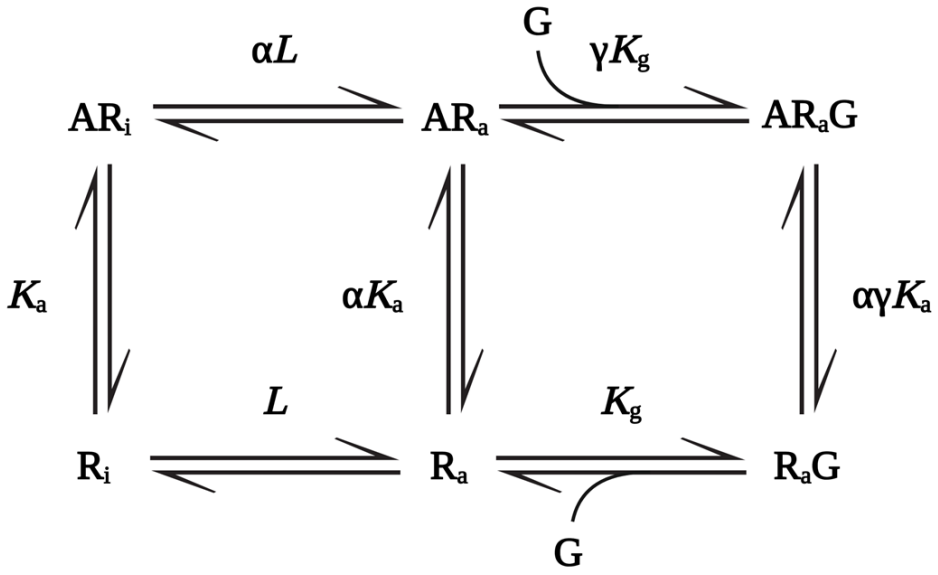

Figure 1.3: The extended ternary complex model of GPCR activation, where '*A*' is the agonist, 'R_i' is the receptor in its inactive state, 'R_a' is the receptor in its active state, '*G*' is the G protein, 'K_a' and 'K_g' relate to the binding affinities of the agonist and G protein, respectively, 'α' and 'γ' describe efficacy and '*L*' refers to the spontaneous activation of the receptor in absence of agonist (constitutive activity) (Samama et al., 1993). This diagram was created using BioRender.com.

1.3.3 – GPCR allostery and allosteric modulation

An orthosteric ligand is any ligand which binds at the same receptor binding pocket as the endogenous ligand, known as the orthosteric site (Christopoulos et al., 2014). The transduction of the signal from the extracellular orthosteric site upon agonist binding to the intracellular effector protein binding site is an allosteric mechanism because the sites are not directly connected, instead they interact via networks of amino acids throughout the protein (Christopoulos and Kenakin, 2002; Süel et al., 2003; Clarkson et al., 2006; Reynolds et al., 2011; Chen et al., 2020). Allostery is defined as the long-range communication between spatially distinct molecular sites (Reynolds et al., 2011; Chen et al., 2020). The presence of several conserved GPCR motifs which act as microswitches of receptor activation (see 1.1.3 – General GPCR structure and mechanism of signal transduction) is critical for initiating substantial structural changes which propagate throughout the transmembrane core (Süel et al., 2003; Chen et al., 2020). These microswitches are not in direct contact and only connect indirectly through much less conserved residues, which likely contributes to the diversity of GPCR functional responses (Süel et al., 2003; Chen et al., 2020). It may be possible to exploit GPCR allostery to target accessible 'hotspots' at the surfaces of receptors to regulate a specific beneficial effect at a distant site, however these intramolecular networks are poorly understood at present (Reynolds et al., 2011; Chen et al., 2020).

Other than the orthosteric site, many GPCRs also comprise other topologically distinct regions which may also interact with ligands; these are termed allosteric sites and the ligands which bind to them are called allosteric ligands (May et al., 2007; Christopoulos et al., 2014). Just like orthosteric ligands, allosteric ligands may act as agonists, inverse agonists or neutral antagonists to either increase, reduce or have no effect on basal receptor signalling (May et al., 2007; Christopoulos et al., 2014). Additionally, some allosteric ligands do not alter receptor activity on their own but instead act as modulators of orthosteric ligand activity, fine-tuning receptor responses either by potentiation (positive allosteric modulators; PAMs) or inhibition (negative allosteric modulators; NAMs) of orthosteric ligand affinity or efficacy (May et al., 2007; Christopoulos et al.,

2014). Some ligands interact with allosteric sites but have no effect on orthosteric ligand activity (neutral allosteric ligands; NALs) (May et al., 2007; Christopoulos et al., 2014). Similar to the coupling allostery between orthosteric binding sites and effector binding sites, allosteric sites may be connected to both orthosteric and effector binding sites through their own distinct intramolecular networks of amino acid residues (May et al., 2007; Chen et al., 2020).

Ligands acting at allosteric sites can potentially exhibit several therapeutic advantages over orthosteric ligands (Christopoulos and Kenakin, 2002; May et al., 2007; Conn et al., 2009; Keov et al., 2011). Firstly, they may have increased receptor subtype selectivity as they act at sites comprising much greater structural diversity (May et al., 2007; Conn et al., 2009; Keov et al., 2011). GPCR orthosteric sites are often highly conserved between subtypes in order to bind endogenous ligands, whereas allosteric regions primarily serve structural roles and hence are under lower evolutionary pressure (May et al., 2007; Christopoulos et al., 2014). Another advantage of allosteric ligands is that they provide a saturable 'ceiling level' of effect whereby further increases in ligand dose do not further amplify target responses (Christopoulos and Kenakin, 2002; May et al., 2007; Keov et al., 2011). This is related to the cooperativity factor of the allosteric ligand-receptor interaction, which describes the ability of a given modulator to alter a specific receptor's functional activity (Leach et al., 2007; May et al., 2007; Keov et al., 2011). Therefore, larger doses of allosteric ligands may be administered without risking increased toxicity (May et al., 2007; Keov et al., 2011). An allosteric ternary complex model has been developed to describe the cooperativity factor between an allosteric ligand and its orthosteric ligand-bound target receptor (Leach et al., 2007). An additional unique feature of allosteric ligands is 'probe-dependence', which describes the differing (and sometimes opposing) abilities of an allosteric ligand to modulate receptor responses induced by distinct orthosteric ligands (May et al., 2007; Keov et al., 2011; Valant et al., 2012). Despite their therapeutic potential, relatively few allosteric GPCR drugs have been clinically approved so far (Dorr et al., 2005; Nemeth, 2013), but this number promises to accelerate in the future (Conn et al., 2009; Wild et al., 2014; Wold et al., 2019). In Chapter 5 (see 5.1), allosteric modulation of the β_2AR is discussed specifically.

1.3.4 – Biased signalling

A very important recent discovery in GPCR pharmacology has been the phenomenon of biased signalling (or functional selectivity). Most GPCRs are able to recruit several intracellular proteins including distinct G protein subtypes and β-arrestins, leading to transduction of several diverse signalling pathways (Kobilka and Deupi, 2007; Smith et al., 2018). Biased signalling occurs when the activated receptor preferentially recruits a specific intracellular protein and therefore selectively initiates (or inhibits) certain downstream pathways over others, for example a G protein pathway over β-arrestin or alternatively a G_s protein pathway over other G proteins, rather than activation (or inhibition) of all pathways equally (Shukla et al., 2014a; Wootten et al., 2018; Smith et al., 2018). Ligands which promote receptor biased signalling are termed biased ligands (Shukla et al., 2014a; Wootten et al., 2018; Smith et al., 2018). It is likely that biased ligands stabilise distinct active conformations of the receptor which have differing binding affinities for effector proteins, thus enhancing recruitment of some downstream binding partners and reducing others (Shukla et al., 2014a; Wootten et al., 2018; Kobilka and Deupi, 2007; Smith et al., 2018). This is because structurally diverse ligands form specific interactions at the receptor binding site, thereby disrupting distinct intramolecular allosteric networks of residues throughout the receptor transmembrane core which modify the specific conformational changes occurring at the intracellular effector binding site (Shukla et al., 2014a; Wootten et al., 2018; Kobilka and Deupi, 2007; Smith et al., 2018). Moreover, these distinct receptor conformations may affect not only the binding but also the subsequent action of effector proteins, for example G protein binding to GTP (and hence efficacy of signalling responses) can be affected by different conformational changes in the G_α subunit (Shukla et al., 2014a; Furness et al., 2016; Wootten et al., 2018). Additionally, β-arrestin interactions with downstream signalling molecules can also be altered, which may be in part due to receptor recruitment of different GRK isoforms and the resulting distinct GRK phosphorylation barcodes (Kohout et al., 2004; Shukla et al., 2008; Zidar et al., 2009).

Biased ligands have now been reported for a wide range of GPCRs. In addition to ligands acting at the orthosteric binding site, allosteric ligands also offer promise as biased signalling molecules (Pupo et al., 2016; Slosky et al., 2021; Berg and Clarke, 2018). There is however an ongoing debate regarding the biased signalling phenomenon, specifically whether different measurements of ligand activity show true ligand bias between downstream pathways or can instead simply be attributed to partial agonism, cell-specific effects like varying degrees of effector expression or signal amplification (system bias) and differences in the detection sensitivities of the experimental assays (observational bias) (Gundry et al., 2017; Azevedo Neto et al., 2020; Gillis et al., 2020; Thompson et al., 2016; Kenakin and Christopoulos, 2013). This has been particularly exemplified in the case of the mu opioid receptor (μOR), whereby several purportedly G protein-biased μOR agonists (oliceridine, PZM21 and SR-17018) were actually shown to exhibit partial agonism at the receptor which was originally interpreted as bias, likely due to differences in coupling and amplification of the G protein and β-arrestin pathways (Gillis et al., 2020). Furthermore, it is important to consider differences in the kinetics of signalling responses, as this has been found to influence the interpretation of biased signalling previously (Klein Herenbrink et al., 2016; Lane et al., 2017).

Biased signalling offers a potentially revolutionary breakthrough for the development of more effective drugs which can exhibit higher efficacy for the desired physiological response while reducing side effects due to diminished signalling through non-specific pathways (Whalen et al., 2011; Rankovic et al., 2016; Slosky et al., 2021). However, an improved understanding of the structure-activity relationships underpinning biased signalling mechanisms is still required in order to facilitate the rational design of new biased drugs.

1.3.5 – Mechanostimulation of GPCRs

In addition to the activation of receptors in response to binding by an agonist ligand, some receptors can also be activated by exposure to mechanical stimuli (Chachisvilis et al., 2006; Erdogmus et al., 2019; Hu et al., 2022; Wilde et al.,

2022). Sensitivity to mechanical stimuli has been recorded in numerous receptor types previously including integrins (Katsumi et al., 2004; Friedland et al., 2009; Ross et al., 2013; Sun et al., 2016), ions channels (Sukharev et al., 1994; Liu and Montell, 2015; Ranade et al., 2015; Gaub and Müller, 2017) and GPCRs (Chachisvilis et al., 2006; Erdogmus et al., 2019; Hu et al., 2022; Wilde et al., 2022; Hardman et al., 2023). Within the GPCR superfamily, it is a particularly common feature of adhesion GPCRs, which likely respond to mechanical stimuli by autoproteolysis of their N-terminal fragment, exposing the tethered *Stachel* peptide to activate the receptor (Scholz et al., 2015; Lin et al., 2022; Scholz et al., 2023). Other examples of GPCRs which have been shown to possess mechanosensory functions include the angiotensin type 1 receptor (AT_1R) (Zou et al., 2004; Yatabe et al., 2009; Rakesh et al., 2010; Poudel et al., 2023), proton sensing receptor GPR68 (Wei et al., 2018; Xu et al., 2018), apelin receptor (APJ) (Scimia et al., 2012; Busch et al., 2015), histamine 1 receptor (H_1R) (Erdogmus et al., 2019), bradykinin B_2 receptor (B_2R) (Groves et al., 1995; Chachisvilis et al., 2006), the parathyroid hormone type 1 receptor (PTH_1R) (Zhang et al., 2009) and the β_2AR (Virion et al., 2019; Marullo et al., 2020).

Mechanical stimulation of receptors has been implicated in numerous physiological roles, such as senses of touch, hearing and pain, cell growth and apoptosis, immune responses, bone growth and remodelling, embryonic development and a wide range of cardiovascular processes (Aceto and Baker, 1990; Katsumi et al., 2004; Chalfie, 2009; Zhang et al., 2009; Schwartz, 2010; Storch et al., 2012; Liu and Montell, 2015; Scholz et al., 2015; De Belly et al., 2022; Wilde et al., 2022). Specifically, receptor mechanotransduction in vascular endothelial cells stimulated by the flow of blood in vessels plays important roles in vascular remodelling and angiogenesis, vasodilation, myogenic vasoconstriction, inflammatory responses and atheroprotection, and dysregulation of these processes is linked to diseases like hypertension and atherosclerosis (Davies, 1995; Groves et al., 1995; Chachisvilis et al., 2006; Busch et al., 2015; Chistiakov et al., 2017; Xu et al., 2018; Erdogmus et al., 2019; Hong et al., 2020; Tanaka et al., 2021; Hu et al., 2022).

The specific mechanisms by which mechanosensitive GPCRs detect and transduce mechanical stimuli into intracellular signalling pathways remain largely unknown, although flow- or stress-induced changes in cell membrane structure, tension and fluidity are implicated in promoting the adoption of active receptor conformations by shifting GPCR conformational equilibrium (Cantor, 1997; Chachisvilis et al., 2006; Zhang et al., 2009; Erdogmus et al., 2019; Hu et al., 2022; Poudel et al., 2023). Ligand application has been extensively shown to modulate GPCR mechanotransduction, either by potentiation (agonists) or inhibition (inverse agonists) of the signalling response (Groves et al., 1995; Zou et al., 2004; Chachisvilis et al., 2006; Zhang et al., 2009; Scimia et al., 2012; Busch et al., 2015; Erdogmus et al., 2019). Furthermore, it has been suggested that mechanical stimulation of GPCRs confers an active receptor conformation distinct to that induced by agonist-binding (Zhang et al., 2009; Storch et al., 2012; Wang et al., 2018; Erdogmus et al., 2019; Poudel et al., 2023). This may involve a distinct rotation of TM7 as well as a more pronounced elongation of the intracellular helix 8 domain during activation, which has been reported as an essential domain for mediating mechanical activation in the H_1R (Yasuda et al., 2008; Erdogmus et al., 2019; Hardman et al., 2023). Finally, N-glycan chains attached to GPCRs by receptor N-glycosylation may also play a critical role in conferring mechanosensitivity, having recently been shown to directly mediate β_2AR transduction of traction forces from meningococcus pili into β-arrestin-biased signalling pathways, resulting in bacterial crossing of the blood-brain barrier (Coureuil et al., 2010; Virion et al., 2019; Marullo et al., 2020). This is comprehensively discussed in Chapter 4 (see 4.1).

1.4 – Adrenoceptors

1.4.1 – Classification of α- and β-adrenoceptors

The adrenoceptors (or adrenergic receptors) are a family of class A GPCRs (within the α subclass of class A GPCRs) which respond endogenously to catecholamines such as adrenaline and noradrenaline (Ahlquist, 1948; Langer, 1974; Katritch et al., 2013). Adrenaline is a hormone which is critical in maintaining metabolic homeostasis, while noradrenaline is the major neurotransmitter of the sympathetic nervous system (Laverty, 1978; Goldstein, 2001). The physiological effects of these catecholamines are mediated by adrenoceptors expressed in many different cell types (Minneman et al., 1979; Minneman et al., 1981; Small et al., 2003). These receptors were originally divided into two subfamilies, α-adrenoceptors, (αARs) and β-adrenoceptors (βARs), due to the differential effects of catecholamines in smooth muscle cells (Ahlquist, 1948; Minneman et al., 1981). However, the αARs have since been further split based on relative potencies of agonists, distinct G protein coupling, physiological functions and sequence homology, resulting in three groups of adrenoceptors; α_1ARs (comprising α_{1A}AR, α_{1B}AR and α_{1D}AR), α_2ARs (α_{2A}AR, α_{2B}AR and α_{2C}AR) and βARs (β_1AR, β_2AR and β_3AR) (Lands et al., 1967a; Lands et al., 1967b; Langer, 1974; Berthelsen and Pettinger, 1977; Minneman et al., 1981; Stiles et al., 1984; Wilson et al., 1984; Small et al., 2003; Bylund, 2007), as outlined in Figure 1.4.

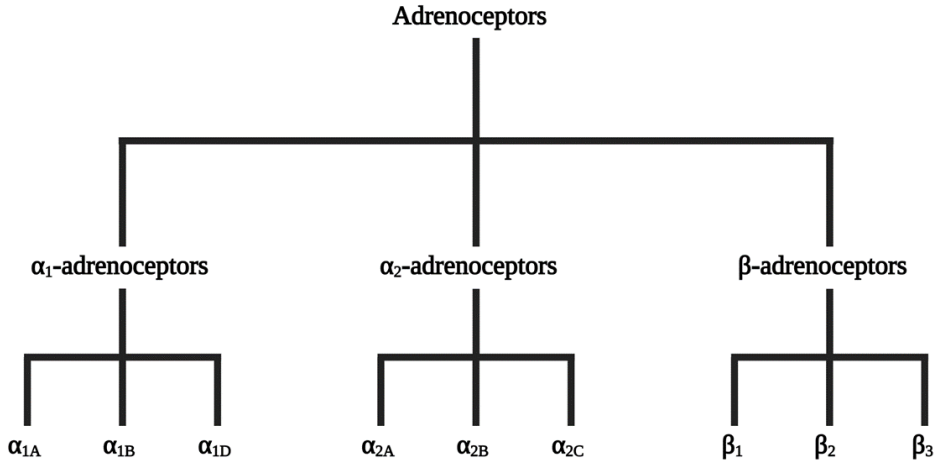

Figure 1.4: The classification of the adrenoceptor family of GPCRs which is subdivided into three subfamilies, α_1ARs (α_{1A}AR, α_{1B}AR and α_{1D}AR), α_2ARs (α_{2A}AR, α_{2B}AR and α_{2C}AR) and βARs (β_1AR, β_2AR and β_3AR) This diagram was created using BioRender.com.

1.4.2 – Physiological roles of adrenoceptors

Members of the α_1AR and α_2AR subfamilies couple to G_q proteins and G_i proteins, respectively, as well as β-arrestins (Docherty, 1998; Hein, 2006; Akinaga et al., 2019). βARs instead couple primarily to G_s proteins and β-arrestins, although both β_2AR and β_3AR have also been reported to bind G_i proteins (Daaka et al., 1997; Zamah et al., 2002; Kobilka, 2011). All adrenoceptors are expressed prevalently in neurons throughout both the central and peripheral nervous systems, where they are responsible for a number of processes including regulation of blood pressure, memory storage and retrieval, sedation, analgesia and inhibition of neurotransmitter release (Ruffolo and Hieble, 1994; Nicholas et al., 1996; Murchison et al., 2004; Hein, 2006; Akinaga et al., 2019). They also play important roles in mediating vascular tone in vascular smooth muscle and endothelial cells, as well as modulating cardiac rate and contractility in the heart (Minneman et al., 1981; Stiles et al., 1984; Ruffolo, 1985; Reid, 1986; Brodde, 1993; Guimarães and Moura, 2001; Vanhoutte, 2001; Dessy and Balligand, 2010; Akinaga et al., 2019). While αARs are generally linked with mediating muscle contraction (vasoconstriction, uterine contraction), βARs are associated with muscle relaxation (vasodilation, bronchodilation, uterine relaxation) (Stiles et al., 1984; Muramatsu et al., 1990; Barnes, 1993; Hrometz et al., 1999; Chotani et al., 2004; Tanaka et al., 2005; Otsuka et al., 2008). Most adrenoceptor subtypes are expressed in white and brown adipocytes, where they have been linked with mediating glucose uptake, lipolysis and adipocyte differentiation (Langin et al., 1995; Stich et al., 1999; Merlin et al., 2018; Evans et al., 2019). The adrenoceptors are also implicated in the regulation of various additional functions including in the kidneys, gastrointestinal tract, genitourinary system, pancreas and other organs (Ruffolo and Hieble, 1994; Andersson et al., 1997; Hein, 2006; Otsuka et al., 2008; Fagerholm et al., 2011; Akinaga et al., 2019; Archer et al., 2021). The specific functions of the β_2AR are explored in more depth shortly (see 1.5.2 – Physiological functions and therapeutic relevance of the β_2-adrenoceptor).

1.5 – The β_2-adrenoceptor

1.5.1 – Determination of β_2-adrenoceptor structure

The β_2-adrenoceptor (β_2AR) is often described as a 'prototypical' or model class A GPCR due to the extensive studies of the β_2AR which have been used to understand the structure and function of GPCRs more generally (Dohlman et al., 1991; Lefkowitz, 2004; Kobilka, 2013). Purification of the β_2AR (Cerione et al., 1984b) and subsequent cloning of the receptor's cDNA (the first receptor with which this was accomplished) (Dixon et al., 1986) revealed a high degree of sequence homology with rhodopsin, which ultimately led to the foundation of the GPCR superfamily of membrane receptors and paved the way for classification of GPCRs by sequence homology and structure (Lefkowitz, 2004; Kobilka, 2013; Barwich and Bschir, 2017). The primary sequence of the β_2AR is displayed in Figure 1.5. Further insights into β_2AR structure were provided by the development of chimeric or mutant receptors which enabled identification of ligand-binding sites at the extracellular and transmembrane domains and effector-binding sites at the intracellular regions (Kobilka et al., 1988; Ostrowski et al., 1992; Strader et al., 1994; Lefkowitz, 2004).

After rhodopsin (Palczewski, 2000), the β_2AR became the second GPCR to have its three-dimensional structure solved by x-ray crystallography, and the first in the presence of a diffusible bound ligand (Cherezov et al., 2007; Rasmussen et al., 2007), shown in Figure 1.6. Later, the active β_2AR-G_s protein complex became the first resolved crystal structure of a GPCR coupled to a G protein (Rasmussen et al., 2011b). These crystal structures allowed direct visualisation of receptor-effector binding and structural comparison of the β_2AR in its inactive and active states, including the large outward extension of TM6 during activation and relatively minor changes in the ligand binding pocket such as the small inward movement of TM5 (Rasmussen et al., 2011b; Kobilka, 2013; Bang and Choi, 2015). Numerous further β_2AR crystal structures, as well as structures derived from cryogenic electron microscopy (cryo-EM), have now been resolved in complex with distinct binding partners and in different conformations (Hanson et al., 2008; Wacker et al., 2010; Rasmussen et al., 2011a; Rosenbaum

et al., 2011; Westfield et al., 2011; Ring et al., 2013; Shukla et al., 2014b; Masureel et al., 2018; Zhang et al., 2020). The determination of three-dimensional GPCR structures has represented an extremely significant advancement in the field of GPCR structural biology and has ultimately enabled the structure-based, rational design of improved therapeutics for these receptors (Congreve et al., 2020).

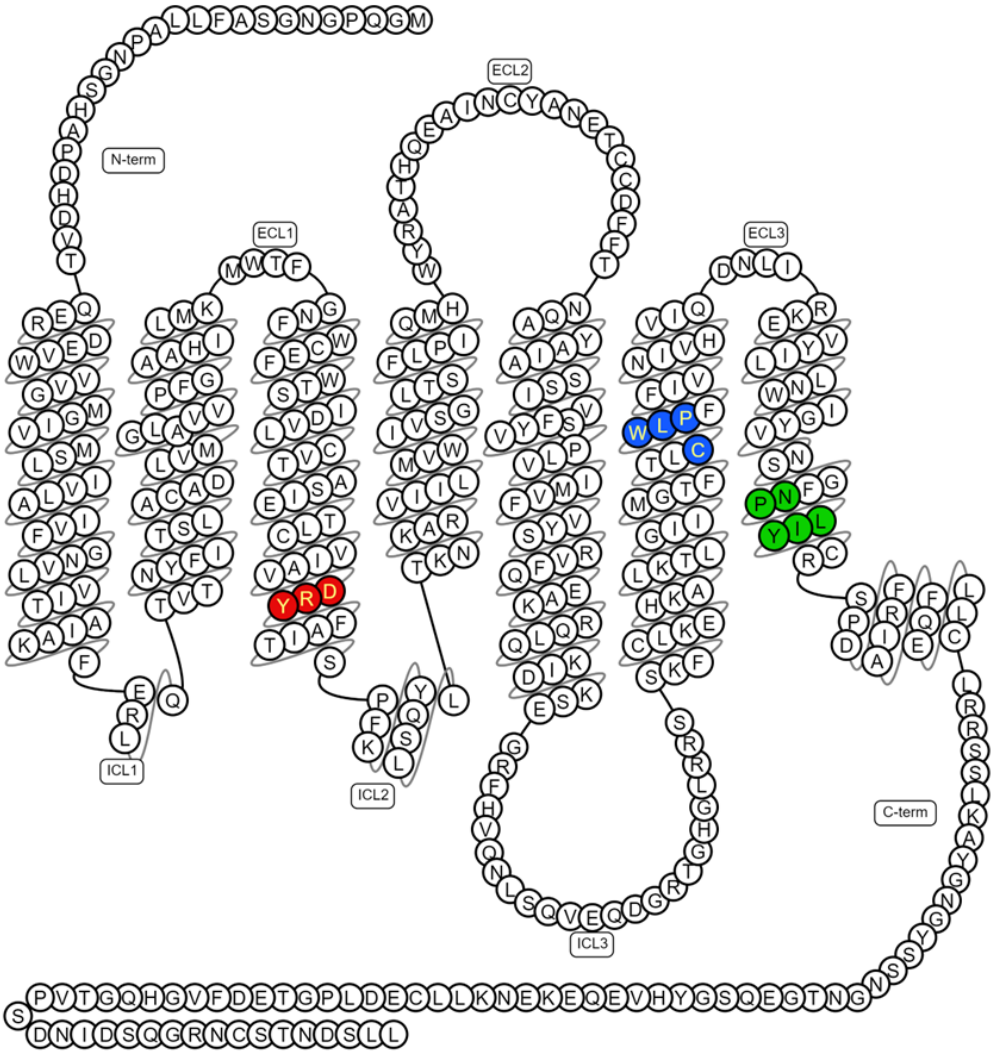

Figure 1.5: A snake plot of the human β_2AR showing the primary sequence of amino acid residues with three conserved GPCR motifs highlighted: D/ERY (red), CWxP (blue) and NPxxY (green). This diagram was adapted using www.gpcrdb.org (Pándy-Szekeres et al., 2018).

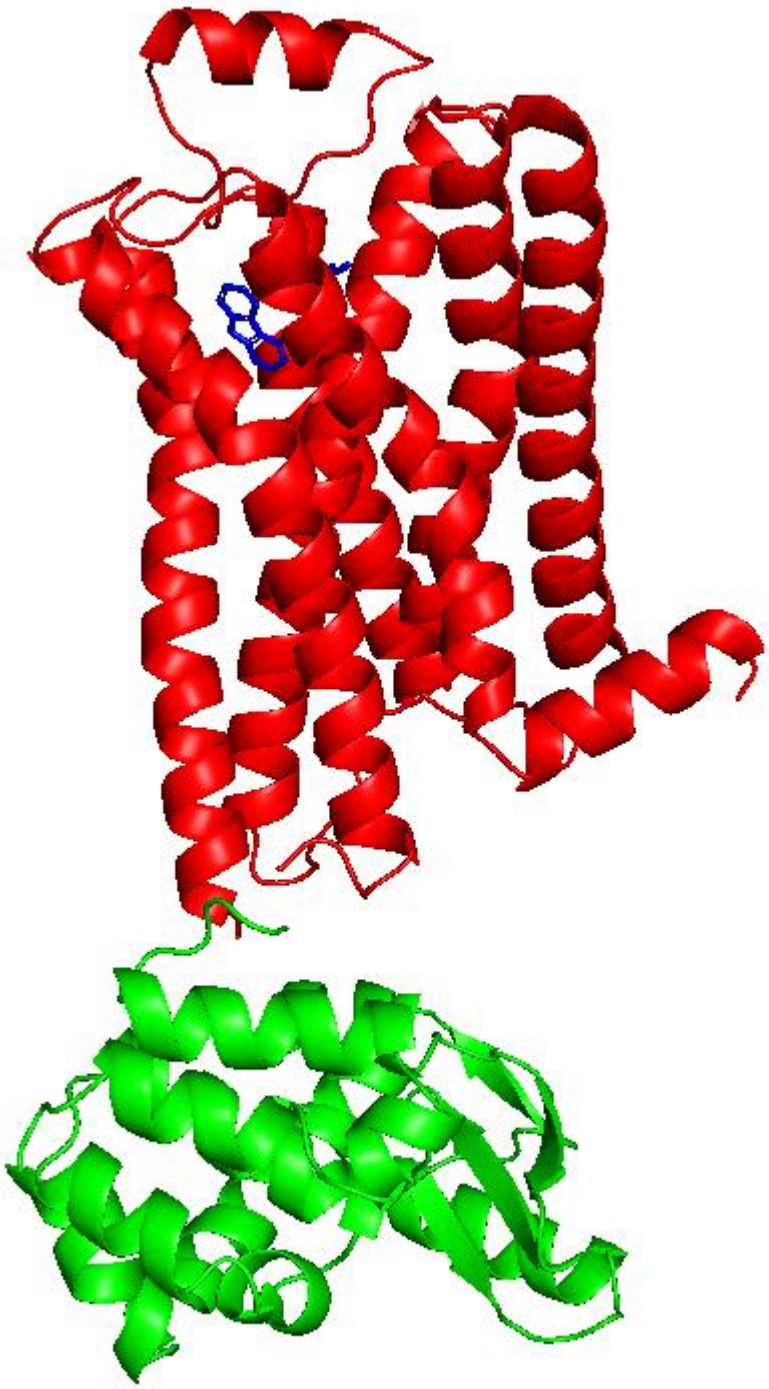

Figure 1.6: The crystal structure of the human β_2AR (red) fused to the T4-lysozyme protein (green) and bound to the partial inverse agonist carazolol (blue), determined by Cherezov et al. (2007). This image was adapted using PyMol (PDB: 2RH1).

1.5.2 – Physiological functions and therapeutic relevance of the β_2-adrenoceptor

As with many members of the adrenoceptor family, the β_2AR is distributed widely throughout many tissues in mammals (Minneman et al., 1981; Daly and McGrath, 2011). Most prevalently, the β_2AR is found in smooth muscle, in particular in airway and vascular smooth muscle but also in the gastrointestinal tract, bladder, uterus and other organs where it is responsible for mediating muscle relaxation (Horinouchi et al., 2003; Li et al., 2004; Takemoto et al., 2008; Penn and Benovic, 2011). The physiological roles of the β_2AR expressed in smooth muscle and several other tissues and cell types are explored throughout this section, including the cell signalling pathways which are involved and the therapeutic significance of targeting the receptor for treatment of relevant diseases.

Airway smooth muscle, which resides in the trachea and bronchioles in the lung, plays a critical role in regulating bronchomotor tone (Amrani and Panettieri, 2003; Panettieri et al., 2008). The β_2AR is prevalently expressed in airway smooth muscle, as well as inflammatory cells such as mast cells and neutrophils in the lung, and mediates bronchodilation which causes a widening of the airways via cAMP-mediated inhibition of airway smooth muscle contraction, in addition to reversing cell proliferation and inflammation (Barnes, 1998; Billington and Penn, 2003; Moldoveanu et al., 2009; Billington et al., 2013). Hence, the β_2AR has been targeted extensively in the treatment of pulmonary diseases including asthma and chronic obstructive pulmonary disease (COPD) (Bai, 1992; Donohue, 2004; Tashkin and Fabbri, 2010). Asthma is defined as the reversible narrowing of the airway due to inflammation and contraction caused by airway hyperresponsiveness and is extremely common, affecting approximately 300 million individuals worldwide (Masoli et al., 2004; Welte and Groneberg, 2006; Cukic et al., 2012). Meanwhile COPD refers to the irreversible and progressive limitation of airflow due to persistent inflammation and bronchoconstriction and is a leading cause of global mortality (Lopez et al., 2006; Welte and Groneberg, 2006; Cukic et al., 2012). Constriction of airway smooth muscle is mediated largely by G_q-coupled receptors including the M_3

muscarinic acetylcholine receptor (M_3 mAChR), histamine H_1R and bradykinin B_2R (Barnes, 1998; Billington and Penn, 2003; Billington et al., 2013). G_q protein-mediated activation of PLCβ and subsequent IP_3 production increases release of calcium ions from intracellular stores, which promotes calcium-calmodulin complex formation and consequent activation of myosin light chain kinase (Barnes, 1998; Billington and Penn, 2003; An et al., 2007; Mahn et al., 2010). This is followed by phosphorylation of myosin light chains which then interact with the actin cytoskeleton to directly mediate contraction of airway smooth muscle (Barnes, 1998; Billington and Penn, 2003; An et al., 2007; Mahn et al., 2010). Additionally, cell proliferation and inflammation induced by mitogenic growth factors and pro-inflammatory cytokines further contribute toward the obstruction of airways in individuals with asthma and COPD (Johnson et al., 2001; Howarth et al., 2004; Mahn et al., 2010).

The β_2AR, alongside several other G_s-coupled GPCRs such as the prostaglandin E_2 receptor (PGE_2R) and prostacyclin receptor (PGI_2R), stimulates an increase cytosolic cAMP production by adenylate cyclase, which in turn activates both PKA and EPAC (Barnes, 1998; Billington and Penn, 2003; Billington et al., 2013). PKA-mediated phosphorylation of intracellular proteins subsequently elicits several bronchodilatory effects, for example phosphorylation of some G_q-coupled receptors and PLCβ inhibits IP_3 generation while phosphorylation of IP_3Rs reduces the binding affinity of IP_3 for the receptor, all of which results in reduced release of calcium ions from intracellular stores (Barnes, 1998; Billington and Penn, 2003; Billington et al., 2013). PKA additionally phosphorylates myosin light chain kinase, thereby reducing myosin light chain phosphorylation and subsequent bronchoconstrictive activity (Barnes, 1998; Billington and Penn, 2003; Billington et al., 2013). Other actions of PKA which promote bronchodilation also include potassium channel activation promoting potassium ion efflux from cells and hyperpolarisation of airway smooth muscle, as well as downregulation of gene transcription of several pro-inflammatory cytokines via CREB (Barnes, 1998; Ammit et al., 2000; Hall, 2000; Hallsworth et al., 2001; Billington and Penn, 2003). Potassium channels are also activated directly by the $G_{\alpha s}$ subunit (Kume et al., 1994; Hall, 2000; Billington and Penn, 2003). EPAC is also implicated in PKA-independent airway smooth muscle

relaxation and anti-inflammatory effects via GTPase Rap1 and MAPK pathways (Roscioni et al., 2009; Grandoch et al., 2010; Roscioni et al., 2011; Billington et al., 2013). Finally, both PKA and EPAC may induce anti-mitogenic effects to prevent aberrant cell proliferation in airway smooth muscle (Kassel et al., 2008; Yan et al., 2011).

Drugs which selectively activate the β_2AR (β-agonists) have long been used to combat pulmonary diseases, including short-acting β-agonists (SABAs; salbutamol, terbutaline) and long-acting β-agonists (LABAs; salmeterol, formoterol, indacaterol), which are classed based on their duration of action (Moore et al., 1998; Lötvall, 2001; Donohue, 2004; Naline et al., 2007; Tashkin and Fabbri, 2010; Ejiofor and Turner, 2013). In addition to duration of action, these β-agonists can be differentiated by their intrinsic efficacies and rates of onset of action, as summarised in Table 1.1. These different pharmacological properties influence the clinical utility of the drugs, for example β-agonists with a fast onset of action are more suitable for urgent use in rescue therapy upon sudden acute asthma symptoms, while β-agonists with a long duration of action are preferential for chronic maintenance therapy to prevent the onset of symptoms (D'Alonzo et al., 1994; Moore et al., 1998; Naline et al., 2007; Tashkin and Fabbri, 2010). Although they have generally proven very effective bronchodilators, prolonged use of β-agonists, particularly LABAs, has been associated with attenuated responsiveness, causing β_2AR tachyphylaxis, tolerance and impairment of asthma control which can result in an increased risk of fatal asthmatic attack (Sears et al., 1990; Johnson, 1998; Beasley et al., 1999; Sears and Lötvall, 2005; Walker et al., 2011). This effect likely relates to the GRK-mediated recruitment of β-arrestins to the β_2AR which causes desensitisation of the response by uncoupling the β_2AR-G_s protein signalling pathway and also downregulates β_2AR cell surface expression via receptor internalisation (Johnson, 1998; Hanania et al., 2002; Deshpande et al., 2008; Walker et al., 2011; Billington et al., 2013). Therefore, the identification of biased β-agonists which can selectively activate G_s protein-mediated pathways without promoting β-arrestin recruitment could lead to the development of improved therapeutics targeting the β_2AR for the treatment of pulmonary diseases like asthma and COPD (Walker et al., 2011; Billington and Hall, 2012).

Clinically used β-agonist	Intrinsic efficacy (full or partial agonist)	Rate of onset of action	Duration of action
Salbutamol	Partial agonist	Fast (3-5 min)	Short-acting (4-6 h)
Terbutaline	Partial agonist	Medium (10-30 min)	Short-acting (4-6 h)
Salmeterol	Partial agonist	Slow (20-60 min)	Long-acting (~12 h)
Formoterol	Full agonist	Fast (3-5 min)	Long-acting (~12 h)
Indacaterol	Full agonist	Fast (3-5 min)	Ultra long-acting (~24 h)

Table 1.1: Pharmacological and clinical properties of five commonly used β-agonists for the treatment of pulmonary diseases such as asthma and COPD (Moore et al., 1998; Ullman and Svedmyr, 1988; Palmqvist et al., 1999; Lötvall, 2001; Hanania et al., 2002; Sears and Lötvall, 2005; Beeh et al., 2007; Brookman et al., 2007; Naline et al., 2007; Sturton et al., 2007; Rennard et al., 2008; Rosethorne et al., 2010; Tashkin and Fabbri, 2010).

The β_2AR also mediates relaxation of vascular smooth muscle (Feldman and Gros, 1998; Ferguson and Feldman, 2014). In a similar process to the relaxation of airway smooth muscle, activation of the β_2AR stimulates G_s protein coupling which leads to elevated cytosolic cAMP concentrations in vascular smooth muscle cells, promoting relaxation (Haynes et al., 1992; Aiello et al., 1998; Feldman and Gros, 1998; Ferro et al., 1999; Ferguson and Feldman, 2014). In addition, vascular endothelial cells express the β_2AR and are also implicated in vasodilation, likely in part through nitric oxide synthesis (Gray and Marshall, 1992; Ferro et al., 1999; Leblais et al., 2007). Due to its importance in regulating vascular tone and thus blood pressure, dysregulation of vascular β_2AR is associated with hypertension, whereby blood pressure is persistently too high (Feldman and Gros, 1998; Ferguson and Feldman, 2014). Although β_2AR expression is generally not downregulated in individuals with hypertension, β_2AR coupling to G_s protein is often impaired which hinders the stimulation of downstream vasodilatory pathways (Feldman and Gros, 1998; Feldman and Gros, 2006; Ferguson and Feldman, 2014). The expression of the β_2AR in the vascular system varies throughout different blood vessels, thus stimulation of the β_2AR is likely to be more relevant for regulating vascular tone and blood flow in some vessels than in others (Vatner et al., 1986; Gaspardone et al., 1991; Barbato, 2009). The β_1AR and β_3AR are also expressed to differing degrees throughout the vasculature and play similar physiological roles to the β_2AR (Vatner et al., 1986; Gaspardone et al., 1991; Leblais et al., 2007; Barbato, 2009). Some βAR antagonists (β-blockers) which actually exhibit β-arrestin bias (carvedilol, nebivolol) have been shown to promote vasodilation and thus protect against hypertension (Rosendorff, 1993; Rath et al., 2012; Wachter and Gilbert, 2012).

Although the β_1AR is the predominant subtype of adrenoceptor in cardiac tissue, the β_2AR is also implicated in heart function (Freedman and Lefkowitz, 2004; Madamanchi, 2007; Pérez-Schindler et al., 2013). In cardiac myocytes, both subtypes elicit positive inotropic responses (increased contraction of cardiac muscle) via the G_s-coupled signalling pathway in which PKA-mediated phosphorylation of intracellular proteins including troponin I and L-type calcium channels promotes contractility (Freedman and Lefkowitz, 2004; Madamanchi,

2007; Pérez-Schindler et al., 2013; Woo and Xiao, 2012). The cardiac β_2AR has also been shown to couple G_i protein which both inhibits the G_s-mediated pathway and also plays an important cardioprotective role by regulating hypertrophy and cardiac myocyte apoptosis via $G_{\beta\gamma}$ activation of the phosphatidylinositol-3 kinase (PI_3K) signalling cascade (Pavoine and Defer, 2005; Madamanchi, 2007; Woo and Xiao, 2012; Pérez-Schindler et al., 2013). Due to the relevance of βAR signalling in the heart, β-blockers (propranolol, carvedilol, bisoprolol) have been used extensively to treat cardiovascular diseases such as heart failure, cardiac arrythmias and atrial fibrillation (Wachter and Gilbert, 2012; Woo and Xiao, 2012; Dézsi and Szentes, 2017).

Furthermore, the β_2AR (and β_1AR) has been demonstrated to be overexpressed in malignant tumours and is implicated in mediating cancer progression by promoting angiogenesis through upregulation of vascular endothelial growth factor (VEGF) and other proangiogenic factors, as well as preventing apoptosis of tumour cells and inducing tumour invasion and metastasis (Chakroborty et al., 2009; Sardi et al., 2013; Kim-Fuchs et al., 2014; Creed et al., 2015; Pon et al., 2016; Velmurugan et al., 2019). In particular, the role of the β_2AR in breast cancer has been well studied (Madden et al., 2011; Wilson et al., 2015; Chang et al., 2016; Pon et al., 2016; Kurozumi et al., 2019; Gillis et al., 2021). Some evidence has suggested the potential therapeutic value of β-blockers in cancer treatment, which may be capable of inhibiting proliferation and inducing apoptosis in cancer cells (Stanojkovic et al., 2005; Shan et al., 2011; Kozanoglu et al., 2013; Zhou et al., 2016; Montoya et al., 2019; Gillis et al., 2021). Other notable physiological and pathophysiological functions of the β_2AR include regulation of glycogenesis and glucogenesis in the liver to maintain glucose homeostasis (Lessard et al., 2009; Cipolletta et al., 2017), microglia-mediated neuroinflammation associated with Parkinson's disease and other neurodegenerative disorders (Peterson et al., 2014; Mittal et al., 2017; Velmurugan et al., 2019; Magistrelli and Comi, 2020) and wake-promoting activity in sleep disorders (Berridge et al., 2005; Berridge et al., 2012).

1.6 – Pepducins

1.6.1 – Structure and derivation of pepducins

Pepducins are a relatively novel class of allosteric ligands of GPCRs which act at the intracellular surface of their target receptors (Covic et al., 2002a; Carlson et al., 2012; Zhang et al., 2015b). They comprise short peptide sequences (generally 10-20 amino acid residues) which derive from the sequences of one of the three intracellular loops or the C-terminal tail of the target GPCR and are N-terminally linked by a peptide bond to a lipid group, usually a palmitate or steroid (Covic et al., 2002a; Carlson et al., 2012; Zhang et al., 2015b). Since first being described by Covic et al. (2002a), pepducins have now been developed for a range of GPCRs including most prominently protease-activated receptors (PAR_1, PAR_2 and PAR_3) (Covic et al., 2002a; Covic et al., 2002b; Hollenberg et al., 2004; Wielders et al., 2007; Agarwal et al., 2008; Cisowski et al., 2011; Sevigny et al., 2011) and chemokine receptors ($CXCR_1$, $CXCR_2$ and $CXCR_4$) (Kaneider et al., 2005; Tchernychev et al., 2010; Janz et al., 2011; O'Callaghan et al., 2012b; Quoyer et al., 2013), but also for other GPCRs including the formyl peptide receptor 2 (FPR_2) (Lee et al., 2010), melancortin-4 receptor (MC_4R) (Covic et al., 2002a), sphingosine 1-phosphate receptor 3 (S_1P_3R) (Licht et al., 2003) and the β_2AR (Carr et al., 2014). β_2AR-derived pepducins are discussed further in Chapter 5 (see 5.1). The secondary structures of the peptide sequences of pepducins are largely unknown and are likely quite flexible, but interestingly the nuclear magnetic resonance (NMR) structure of the PAR_1 pepducin, P1pal-7, showed it maintained an α-helical structure similar to that of the receptor ICL3, from which it is derived (Zhang et al., 2012).

1.6.2 – Mechanisms of action and functions of pepducins

The lipid group provides a hydrophobicity which enables pepducins to traverse cell membranes in a reversible manner by penetrating into the outer layer of the phospholipid bilayer and passively flipping (in a reversible manner) across the transmembrane core to the intracellular side, where they remain anchored to the

inner layer of the bilayer by the lipid group (Covic et al., 2002a; Covic et al., 2002b; Wielders et al., 2007; Carlson et al., 2012; Tsuji et al., 2013; Zhang et al., 2015b). From here the peptide moiety can interact at the intracellular surface of their cognate receptor to either promote or inhibit downstream signalling (Covic et al., 2002a; Carlson et al., 2012; Zhang et al., 2015b). This process is illustrated in Figure 1.7. Pepducins have been shown to act as allosteric agonists, inverse agonists, PAMs and NAMs (Tressel et al., 2011; Carlson et al., 2012; O'Callaghan et al., 2012a). Several previous studies have also reported biased signalling by pepducins (Quoyer et al., 2013; Carr et al., 2014; Hollenberg et al., 2014; Carr et al., 2016b). Pepducins generally exhibit a considerable degree of selectivity for the GPCR from which they are derived, however some pepducins show polypharmacology at several receptor subtypes, especially when there is extremely high homology between the intracellular loops, for example in the case of $CXCR_1$ and $CXCR_2$ (Kaneider et al., 2005). The general mechanisms by which pepducins modulate receptor activity are not well understood, although they are thought to stabilise distinct receptor conformational states (Carlson et al., 2012; O'Callaghan et al., 2012a). While most pepducins are thought to modulate downstream signalling by interactions with the receptor near the effector binding site, some β_2AR-derived agonist pepducins were shown to act receptor-independently, thereby likely interacting with G_s protein directly to initiate downstream signalling (Carr et al., 2014). This is discussed further in Chapter 5 (see 5.1).

Pepducins represent a potential novel route for the design of improved drugs and, as such, recent work has focused on investigating the therapeutic utility of pepducin action. The $CXCR_4$ pepducin, ATI-2341, is derived from ICL1 of the receptor and acts as an allosteric agonist to stimulate G_i-mediated signalling pathways (Tchernychev et al., 2010). ATI-2341 was able to induce chemotaxis in cells expressing the $CXCR_4$ and mediated the release of polymorphonuclear neutrophils and haematopoietic stem and progenitor cells from the bone marrow, suggesting a potential use for recruitment of stem cells for bone marrow transplantation (Tchernychev et al., 2010). Additionally, the PAR_1 ICL3-derived pepducin, P1pal-7, has been shown to act as an antagonist to inhibit PAR_1-mediated platelet aggregation without altering bleeding or coagulation (Zhang

et al., 2012). P1pal-7 also inhibited ERK-mediated tumour growth in primary lung cancer cell lines, whereas the ICL1-derived PAR_1 pepducin antagonist, P1pal-i1, was less effective (Cisowski et al., 2011). Furthermore, a β-arrestin biased β_2AR pepducin, ICL1-9, has been reported to reduce G_i-coupled signalling in cardiomyocytes to facilitate improved cardiac contractility and to promote β-arrestin recruitment to initiate anti-apoptotic pathways (Carr et al., 2016b; Grisanti et al., 2018). The treatment of pulmonary diseases with biased pepducins has also been explored. β_2AR-derived G_s-biased agonists ICL3-8 and ICL3-9 were tested for their ability to block airway smooth muscle contraction induced by carbachol, however they proved ineffective (Carr et al., 2016a). Instead, several G_q-biased antagonist pepducins deriving from PAR_1, H_1R and M_3 mAChR were more successful at reversing bronchoconstriction (Carr et al., 2016a; Panettieri et al., 2018). Finally, the $S1P_3$R-derived pepducin, KRX-725, was able to induce pro-angiogenic ERK signalling and mediate neovascularisation *in vivo*, implying a potential use for pepducin therapeutics in the cardiovascular system (Licht et al., 2003). Further studies into the pharmacokinetics and pharmacodynamics of pepducins are required to confirm their suitability for use as therapeutics. Regardless, pepducins have become useful pharmacological tools in the studies of GPCR mechanisms of action and signal transduction.

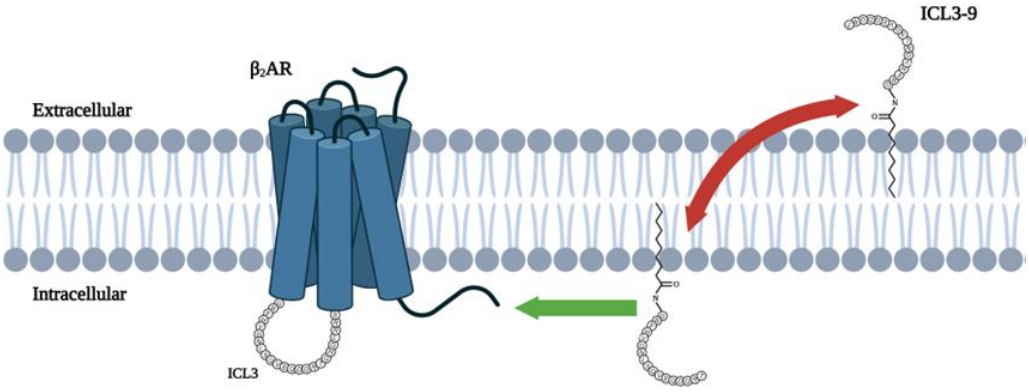

Figure 1.7: The general mechanism of pepducin action at GPCRs using as an example the β_2AR pepducin, ICL3-9, which is derived from ICL3 of the receptor. After incorporation of the palmitate tag into the outer layer of the cell membrane, the pepducin reversibly flips to the inner layer of the membrane, where the peptide sequence can subsequently interact with the intracellular surface of the target GPCR (Covic et al., 2002a; Carlson et al., 2012; Zhang et al., 2015b). This diagram was created using BioRender.com.

1.7 – Thesis aims

The β_2AR is one of the most well-studied GPCRs and has been used as a model system for understanding GPCR structure and function. However, much knowledge is still to be gained surrounding the pharmacology of GPCRs, which should facilitate the underlying ambition of developing improved therapeutics and treatments for diseases. Thus, the general aim of this thesis was to investigate several underexplored aspects of β_2AR pharmacology in the hope that this will contribute towards that goal. This thesis therefore focused on three main objectives:

1. To quantify the kinetic parameters of β_2AR-mediated cAMP signalling responses to reveal new information regarding the kinetics of complex ligand-receptor interactions, under both low (endogenous) and high (stable overexpression) receptor expression conditions.

2. To investigate the mechanosensory function of the β_2AR and determine the underlying mechanism responsible for conferring β_2AR sensitivity to mechanostimulation.

3. To characterise the functional activity of several β_2AR-derived pepducins to allosterically modulate receptor-mediated signal transduction and to assess their ability to bind (or modulate the binding of orthosteric ligands) at the β_2AR.

Chapter 2

Materials and methods

2.1 – Materials

2.1.1 – Cell lines and DNA constructs

Human Embryonic Kidney 293 (HEK293) cells stably expressing the cAMP GloSensor^{TM} 20F construct (termed HEK293Gwt cells) were obtained from Promega (Madison, WI, USA). Chinese Hamster Ovary (CHO) cells stably overexpressing human β_2AR and the cAMP response element-mediated secreted placental alkaline phosphatase (CRE-SPAP) reporter (CHO-CRE-SPAP-β_2AR cells), or just the CRE-SPAP reporter alone (CHO-CRE-SPAPwt cells), were gifted by Prof. Jillian G. Baker (COMPARE, University of Nottingham, UK). The T-Rex^{TM} cell line (HEK293 cells stably expressing the tetracycline repressor protein (TetR), termed HEK293TR cells) was obtained from ThermoFisher Scientific (Loughborough, UK). DH5α competent *E. coli* cells were purchased from New England Biolabs (Hitchin, UK).

The pcDNA3.1(+) plasmid containing the human wildtype β_2AR with N-terminal HiBiT (HiBiT-β_2ARwt) was developed by Dr. Mark Soave in the lab of Prof. Stephen J. Hill (COMPARE, University of Nottingham, UK). The pcDNA4/TO plasmids containing the human β_2AR with N-terminal Twin-Strep affinity purification tag and SNAP tag (TS-SNAP-β_2AR) construct and with N-terminal Twin-Strep affinity purification tag and thermostable nanoluciferase (TS-tsNLuc-β_2AR) were both developed by Dr. Bradley L. Hoare in the lab of Prof. Dmitry B. Veprintsev (COMPARE, University of Nottingham, UK). The pcDNA3.1(+) and pcDNA4/TO mammalian expression vector plasmids were originally purchased from ThermoFisher Scientific (Loughborough, UK). The DNA insert fragments (HiBiT-β_2AR_N6A_N15A and HiBiT-β_2AR_N6A_N15A_N187A) were purchased from Twist Bioscience (South San Francisco, CA, USA). Finally, the primers for these DNA inserts were obtained from Sigma-Aldrich (Gillingham, UK).

2.1.2 – Chemicals and reagents

The GloSensor™ cAMP reagent, Nano-Glo® Luciferase Assay System, Nano-Glo® HiBiT Lytic Detection System, PureYield™ Plasmid Mini-prep System, PureYield™ Plasmid Maxi-prep System, Wizard® SV Gel and PCR Clean-up System, the restriction endonucleases KnpI and XbaI, thermostable alkaline phosphatase (TSAP), MULTI-CORE™ buffer, FuGENE™ HD and 1 kb DNA ladder were purchased from Promega (Madison, WI, USA). The Zymoclean™ Gel DNA Recovery Kit was purchased from Zymo Research (Irvine, CA, USA). The components of the Q5 Mastermix: Q5 hotstart high-fidelity DNA polymerase, deoxynucleoside triphosphates (dNTPs) and Q5 reaction buffer; T4 DNA ligase, ligase buffer 100 bp DNA ladder and loading dye were all obtained from New England Biolabs (Hitchin, UK). 4-Nitrophenyl phosphate disodium salt hexahydrate (pNPP), isoprenaline hydrochloride (isoprenaline), salmeterol, propranolol, (±)-1-[2,3-(dihydro-7-methyl-1*H*-inden-4-yl)oxy]-3-[(1-methylethyl)amino]-2-butanol hydrochloride (ICI-118551), bisoprolol, carazolol, 5'-(N-ethylcarboxamido)adenosine (NECA), 8-(4-chlorophenylthio)adenosine 3',5'-cyclic monophosphate sodium salt (8-CPT-cAMP), 3-isobutyl-1-methylxanthine (IBMX), rolipram, dimethyl sulfoxide (DMSO), bovine serum albumin (BSA), saponin, diethanolamine (DEA), glycerol, ethidium bromide, acetylated BSA, 4-(2-hydroxyethyl)-1-piperazineethanesulfonic acid (HEPES), sodium pyruvate, sodium chloride (NaCl), magnesium sulphate ($MgSO_4$), ethylenediamine tetraacetic acid (EDTA), Tris acetate, IDTE buffer, Hanks' Balanced Salt Solution (HaBSS), tetracycline hydrochloride (tetracycline), Dulbecco's Modified Eagle Medium (DMEM), DMEM/nutrient mixture F12 Ham, L-glutamine, phosphate buffered saline (PBS), trypsin-EDTA, foetal calf serum (FCS), penicillin-streptomycin (Pen/Strep), poly-D-lysine, cholesteryl hemisuccinate tris salt (CHS), ampicillin sodium salt (ampicillin), Luria-Bertani (LB) broth, agarose and bicinchoninic acid (BCA) protein determination assay kit were all purchased from Sigma-Aldrich (Gillingham, UK). Forskolin, formoterol hemifumarate (formoterol), salbutamol hemisulfate (salbutamol) and alprenolol hydrochloride (alprenolol) were purchased from Tocris Bioscience (Bristol, UK). Carvedilol was obtained from ACROS Organics (Geel, Belgium). Potassium chloride (KCl), calcium

chloride dihydrate ($CaCl_2.2H_2O$), sodium hydrogen carbonate ($NaHCO_3$) and L-ascorbic acid were purchased from BDH (Mumbai, India). D-Glucose anhydrous was purchased from ThermoFisher Scientific (Loughborough, UK). Zeocin, hygromycin B and Opti-mem were from Invitrogen (Waltham, MA, USA). CellAura fluorescent β_2AR antagonist (S)-propranolol-green (F-propranolol) was purchased from Hello Bio (Bristol, UK). Polyethylenimine (PEI) transfection reagent was purchased from Polysciences (Warrington, PA, USA). Cellstripper® non-enzymatic cell dissociation solution was purchased from Corning (Corning, NY, USA). N-Dodecyl-β-D-maltopyranoside (DDM), lauryl maltose neopentyl glycol (LMNG) and 3-[(3-cholamidopropyl)dimethylammonio]-2-hydroxy-1-propanesulfonate (CHAPSO) were from Anatrace (Maumee, OH, USA). Sulfo-cyanine3 maleimide (SCM) was purchased from Lumiprobe (Hunt Valley, MD, USA). Guanosine-5'-[(β,γ)-imido]triphosphate tetralithium salt (GppNHp) was from Jena Bioscience (Jena, Germany). The SNAP-Lumi4-Tb labelling reagent and Tag-lite buffer (5x) were obtained from Cisbio (Codolet, France). The β_2AR-derived pepducins intracellular loop (ICL) 3-2, ICL3-7, ICL3-8, ICL3-9 and ICL1-15 were obtained from Almac (Craigavon, UK). Any other chemicals, reagents and plasticware used were from Sigma-Aldrich (Gillingham, UK).

2.2 – Solubilisation of pepducins

Five pepducins derived from the β_2AR, four from the third intracellular loop (ICL3-2, ICL3-7, ICL3-8, ICL3-9) and one from the first intracellular loop (ICL1-15), were purchased in lyophilised form from Almac (Craigavon, UK). Each of the pepducins contained an N-terminal palmitate tag for cell membrane translocation and anchoring (Covic et al., 2002a; Wielders et al., 2007; Johannessen et al., 2011). The amino acid sequence and molecular mass of each pepducin is displayed in Table 2.1. Stocks of the lyophilised pepducins were stored at -20 °C. To solubilise pepducins, samples were dissolved to 1 mM in sterile-filtered double-distilled water (ddH_2O) containing 10% (ICL3-2, ICL3-7, ICL3-8) or 50% (ICL3-9, ICL1-15) sterile DMSO by a series of brief sonication cycles (approximately 5x 10 s) in a sonication water bath with intermittent heating in an incubator at 37 °C until samples were fully dissolved (15-30 min total). An initial attempt to solubilise ICL3-9 in ddH_2O containing 10% DMSO (as had been performed with ICL3-2, ICL3-7 and ICL3-8 previously) was unsuccessful, and the undissolved solution was re-lyophilised by a process of freeze drying, kindly performed by Dr. Eleonora Comeo (COMPARE, University of Nottingham, UK). Due to this, and the limited amount of sample of ICL3-9 and ICL1-15 specifically, these remaining pepducins were instead solubilised in ddH_2O containing 50% DMSO, to increase the solubility of these peptides. After solubilisation, samples were then split into 10 µL aliquots and stored frozen at -20 °C until defrosted for use in assays.

Pepducin	Amino acid sequence	Molecular mass (g/mol)
ICL3-2	Pal-VYSRVFQEAKRQLQKIDKSEGRF	3050.9
ICL3-7	Pal-AKRQLQKIDKSEGRFHV	2278.5
ICL3-8	Pal-LQKIDKSEGRFHV	1795.2
ICL3-9	Pal-GRFHVQNLSQVEQDGRT	2209.3
ICL1-15	Pal-IAKFERLQTVTN	1657.0

Table 2.1: Amino acid sequences and molecular mass of the five β_2AR-derived pepducins with N-terminal palmitate tags, purchased from Almac (Craigavon, UK).

2.3 – Molecular biology

2.3.1 – DNA insert fragment and primer design

Two DNA insert fragments were purchased from Twist Bioscience (South San Francisco, CA, USA), which both comprised nucleotide sequences encoding the human β_2AR with an N-terminal HiBiT tag (connected by a linker consisting of the following amino acid sequence: GSSGGSSGGS) and several mutations within the β_2AR sequence, namely either a double mutation of the asparagine residues Asn6 and Asn15 to alanine residues (Ala) (HiBiT-β_2AR_N6A_N15A fragment) or a triple mutation including the same two N-terminal asparagine residues in addition to another asparagine residue Asn187, residing on ECL2, also to alanine (HiBiT-β_2AR_N6A_N15A_N187A fragment). These DNA fragments were flanked by KpnI (5' end) and XbaI (3' end) restriction sites for digestion, as well as Twist Universal Adapters (identical short nucleotide sequences) distal to the restriction sites on each end to enable use of the same primers for each fragment during PCR amplification of the DNA. Each insert was approximately 1.5 kb in length. The translated amino acid sequences of these DNA inserts are stated in Supplementary Table 8.1. No DNA insert containing HiBiT-tagged wildtype β_2AR (HiBiT-β_2ARwt) was required at this stage because this construct had already been made and ligated into a pcDNA3.1(+) plasmid previously by Dr. Mark Soave in the lab of Prof. Stephen J. Hill (COMPARE, University of Nottingham, UK). It should also be noted that, in both of the DNA inserts, as in the HiBiT-β_2ARwt plasmid, the methionine residue Met1 has been switched to leucine (Leu) because the start codon was not required here, due to the receptor N-terminal HiBiT tag.

Additionally, Table 2.2 shows the forward and reverse primer (purchased from Sigma-Aldrich, Gillingham, UK) sequences and molecular mass, as well as GC content and predicted melting temperatures (T_m). Since the bonding of G and C bases is stronger than that of A and T bases (due to the formation of three hydrogen bonds instead of two), the GC content of designed primers is important for determining their melting temperatures, and thus the required PCR reaction annealing temperatures. High GC content is generally avoided to prevent PCR

annealing temperatures becoming too high. Moreover, particularly high GC content can contribute toward the formation of primer secondary structures or dimerisation which can hinder DNA amplification (Kumar and Kaur, 2014).

Primer	Sequence (5'-3')	Molecular mass (g/mol)	GC content (%)	T_m (°C)
Twist Adapter Forward	CAATCCGCCCTCACTACAACCG	6569	59.0	71.4
Twist Adapter Reverse	TCCCTCATCGACGCCAGAGTAG	6680	59.0	69.7

Table 2.2: Designed primer nucleotide sequences, molecular mass, GC content and T_m values for the PCR amplification reaction.

2.3.2 – Amplification of DNA inserts by polymerase chain reaction

Polymerase chain reaction (PCR) is a technique used to specifically and efficiently amplify DNA in an exponential manner using a thermostable DNA polymerase enzyme to catalyse the assembly of new nucleotides to single DNA strands (Eckert and Kunkel, 1991; Bartlett and Stirling, 2003). This method was used here to substantially increase the number of copies of the DNA insert fragments (HiBiT-β_2AR_N6A_N15A and HiBiT-β_2AR_N6A_N15A_N187A) prior to the digestion and ligation reactions. The DNA inserts were initially resuspended and diluted to 50 ng/µL in TE buffer (10 mM Trip, 0.1 mM EDTA. Meanwhile, forward and reverse primers designed for complementation with the DNA inserts were diluted to 100 µM in IDTE buffer. For the PCR reaction, a Q5 Mastermix was made, comprising 0.5 ng template DNA (DNA insert) 0.5 µM forward primer, 0.5 µM reverse primer, 0.5 U Q5 hot start high-fidelity DNA polymerase, 200 µM (dNTPs) and 1X Q5 reaction buffer, made up to 25 µL final volume with nuclease-free H_2O. The same conditions were used for the independent PCR reactions of both DNA inserts, displayed in Table 2.3.

To verify that the PCR reactions were successful, 5 µL samples of the products were added to 1 µL loading dye and run on a 2% agarose gel (made up in TAE buffer; 40 mM Tris-acetate, 1 mM EDTA; with 0.002% ethidium bromide which binds to DNA to dye it for ultraviolet visualisation) for 30 min at 100 V. The gels were then visualised under UV light and band sizes were determined by comparison with a DNA ladder. Both samples showed bands at approximately 1.5 kb, indicating that the DNA had been amplified successfully in both cases.

The remaining DNA products from the PCR reactions were then purified according to the 'Wizard® SV Gel and PCR Clean-up System' from Promega (Madison, WI, USA). Briefly, 20 µL PCR product was added to 20 µL Membrane Binding Solution, transferred to a Minicolumn and incubated at room temperature for 3 min. After centrifugation for 1 min at 16,000 x *g*, 700 µL Membrane Wash Solution containing ethanol was added, followed by a further centrifugation for 1 min at 16,000 x *g* and discard of the flowthrough. This step

was then repeated with 500 µL Membrane Wash Solution and centrifugation for 5 min at 16,000 x *g*. The Minicolumn was incubated at room temperature for 1 min to allow remaining ethanol to evaporate, then transferred to a fresh 1.5 mL microcentrifuge tube followed by the addition of 30 µL nuclease-free H_2O, subsequent incubation for a further 5 min at room temperature and a final centrifugation for 1 min at 16,000 x *g* to ensure all DNA had eluted2. Finally, the concentration of DNA was quantified by measuring absorbance at 260 nm of the DNA samples using a DeNovix FS-11 spectrophotometer (DeNovix, Wilmington, DE, USA). The purity of samples was also estimated by additionally measuring absorbance at 280 nm and 230 nm and calculating the 260/280 nm and 260/230 nm absorbance ratios. Ratios of approximately >1.8 and >2.0, respectively, were considered pure. The is because ratios lower than these values may indicate the contamination of compounds which absorb at either 280 nm or 230 nm wavelength (Boesenberg-Smith et al., 2012).

PCR step (20 cycles each)	Temperature (°C)	Time (s)
Denaturation	95	10
Annealing	70	10
Extension	72	45

Table 2.3: PCR conditions used in the amplification of the DNA insert fragments. The steps were repeated for 20 cycles in total.

2.3.3 – DNA restriction digestion

Restriction digestion reactions were then performed with both of the purified DNA inserts, as well as a pcDNA3.1(+) vector plasmid. Restriction endonucleases are a large family of enzymes which bind with high affinity to specific DNA sequences and cleave double-stranded DNA at specific nucleotides (either within or adjacent to the binding sequence) (Pingoud and Jeltsch, 2001). The DNA insert fragments each comprised a KpnI and XbaI restriction site (at the 5' and 3' ends, respectively, of the desired receptor construct sequence but within the Twist Universal Adaptors which were therefore cleaved out), so the restriction endonucleases KpnI (15 U) and XbaI (15 U) were added to a digestion reaction mix comprising 2 µg DNA insert, 3 µg acetylated BSA, 1X MULTI-CORE^{TM} restriction enzyme buffer and made up to 30 µL with nuclease-free H_2O. A similar digestion reaction mix was also made using 2 µg pcDNA3.1(+) plasmid (which also contains the relevant KpnI and XbaI restriction sites) instead of the DNA inserts, plus the addition of 2 U thermostable alkaline phosphatase (TSAP) to remove the phosphate groups from the cleaved pcDNA3.1(+) plasmid (important to prevent re-ligation of vector later). The digestion reactions for the two inserts and the pcDNA3.1(+) vector were all performed separately by incubation at room temperature for 1.5 h, followed by heat inactivation of the enzymes at 65 °C for 15 min. The restriction endonucleases cut both the DNA inserts and the pcDNA plasmid with sticky ends, which will be complementary with each other.

After completion of the digestion reaction, 30 µL digested DNA (insert or vector) and 6 µL loading dye were added together and run on a 0.8% agarose gel (made up in TAE buffer with 0.002% ethidium bromide) for 30 min at 100 V as performed earlier. This time, however, the resulting DNA bands were cut from the gel with a scalpel and the mass of each gel slice was weighed in a 1.5 mL microcentrifuge tube. These slices were subsequently dissolved and the DNA extracted and purified using the 'Zymoclean^{TM} Gel DNA Recovery Kit' from Zymo Research (Irvine, CA, USA). Briefly, 300 µL Agarose Dissolving Buffer was added to the gel slice per 100 mg gel weighed and incubated at 55 °C for 10 min, followed by mixing by inversion. Once the gel was completely dissolved,

the solution was transferred to a Zymo-Spin™ Column and centrifuged for 1 min at 16,000 x *g*. 200 µL DNA wash buffer containing ethanol was added to the column and centrifuged for 30 s at 16,000 x *g*. This step was then repeated. Finally, the column was transferred to a fresh 1.5 mL microcentrifuge tube and 6 µL DNA elution buffer was added and again centrifuged for 1 min at 16,000 x *g*. DNA concentration and purity was then assessed with a DeNovix FS-11 spectrophotometer (DeNovix, Wilmington, DE, USA).

2.3.4 – Ligation of DNA inserts with plasmid vector

Next, the pcDNA3.1(+) plasmid vector was ligated individually with the each of the DNA inserts. This was done by creating a ligation reaction mix consisting of 1 µL T4 DNA ligase, 2 µL DNA insert, 1 µL plasmid vector, 1X ligase buffer and made up to a final volume of 20 µL with nuclease-free H_2O. The ligation mixture was incubated at room temperature for 1 h for ligation to occur between the insert and the vector DNA, whereby the ligase enzyme catalyses the synthesis of phosphodiester bonds between the DNA backbone fragments (Lehman, 1974), and the complementary sticky ends of the two fragments join together. This ligation reaction requires at least one of the two DNA components to be phosphorylated. Therefore, by dephosphorylating the vector by application of TSAP during the digestion step as described previously, the vector is only able to be ligated to the phosphorylated DNA inserts rather than, for example, any remaining fragment of the vector DNA which was digested out previously. Once complete, the enzyme was heat-inactivated by incubation at 65 °C for 10 min. Two new complete DNA plasmids have therefore now been constructed: pcDNA3.1(+) HiBiT-β_2AR_N6A_N15A and pcDNA3.1(+) HiBiT-β_2AR_N6A_N15A_N197A. Both constructs should be identical to the pcDNA3.1(+) HiBiT-β_2ARwt plasmid with the exception of the two or three single point mutations within the β_2AR receptor. This would later be confirmed by preparing and sending DNA samples for whole plasmid sequencing by Plasmidsaurus (Eugene, OR, USA). Supplementary Figure 8.1 depicts the pcDNA3.1(+) HiBiT-β_2ARwt whole plasmid sequence map.

2.3.5 – DNA transformation into competent cells

Transformations of the two newly constructed plasmids, pcDNA3.1(+) HiBiT-β_2AR_N6A_N15A and pcDNA3.1(+) HiBiT-β_2AR_N6A_N15A_N187A, as well as the previously generated plasmids pcDNA3.1(+) HiBiT-β_2ARwt and pcDNA4/TO TS-SNAP-β_2AR, generously gifted by Dr. Mark Soave and Dr. Bradley L. Hoare, respectively (both from COMPARE, University of Nottingham, UK), were performed by 1 µL addition of the DNA to 25 µL DH5α competent *E. coli* cells and incubated on ice for 30 min. The cells were then heat shocked at 42 °C for 30 s to allow uptake of the DNA plasmid into the bacterial cells, followed by a further 2 min incubation on ice. 250 µL LB broth was added to the cells and they were incubated on a shaker at 37 °C for 1 h at 225 rpm. 50 µL of the transformed cell preparation and 50 µL LB broth was then spread onto LB agar plates containing 50 µg/mL ampicillin and incubated at 37 °C for approximately 18 h. Each of the plasmids contain an ampicillin resistance gene in addition to the gene encoding the desired receptor construct, so any bacterial cells which survived and formed colonies on the agar plate should successfully express the desired plasmid. Once colonies had formed, the agar plates were stored at 4 °C until required for the next step.

2.3.6 – Preparation of DNA constructs by Mini-prep/Maxi-prep

Single colonies of transformed bacterial cells were picked from the agar plates using a pipette tip and inoculated into 5 mL LB broth containing 50 µg/mL ampicillin and incubated on a shaker at 37 °C for 8 h at 225 rpm to propagate the transformed bacteria and eliminate any remaining untransformed bacteria. This preparation was then transferred to 200 mL LB broth containing 50 µg/mL ampicillin and incubated on a shaker at 37 °C for a further 18 h at 225 rpm to allow exponential bacterial cell growth. Plasmid DNA was then extracted from the bacterial cells and purified using, depending on the quantities of DNA required, either the 'PureYield^{TM} Plasmid Mini-prep System' or the 'PureYield^{TM} Plasmid Maxi-prep System' (both purchased from Promega, Madison, WI, USA), according to the manufacturer's protocol. Briefly, maxi-

prep was performed by the following steps: bacterial cells were pelleted by centrifugation of the 200 mL preparation for 10 min at 5,000 x *g*, followed by resuspension in 12 mL Cell Resuspension Solution. The cells were then lysed by addition of 12 mL Cell Lysis Solution and cellular debris (including genomic DNA) was precipitated by adding 12 mL Neutralisation Solution. Cell debris was pelleted by centrifugation for 20 min at 14,000 x *g* and discarded. During these steps the plasmid DNA is separated from genomic DNA because its relatively small size allows fast reannealing after initial denaturation, thus it remains soluble while genomic DNA is pelleted during centrifugation (Birnboim and Doly, 1979). Plasmid DNA was then purified using a PureYield™ Clearing Column and PureYield™ Maxi Binding Column stacked onto a vacuum manifold. After several wash steps, including addition of 5 mL Endotoxin Removal Wash and 20 mL Column Wash solutions, DNA was eluted via an Eluator™ Vacuum Elution Device into a 1.5 mL microcentrifuge tube by addition of 1 mL nuclease-free water. The concentration and purity of the DNA was then tested using a DeNovix FS-11 spectrophotometer (DeNovix, Wilmington, DE, USA). The plasmid DNA was then stored at -20 °C until required for use. A similar process was carried out for DNA mini-preps, but on a smaller scale.

2.4 – Cell culture

2.4.1 – Passaging cells

HEK293 and CHO cells were cultured and used in experiments in this project. HEK293 cells were cultured in DMEM supplemented with 2 mM L-glutamine and 10% FCS, while CHO cells were cultured in DMEM/nutrient mixture F-12 Ham supplemented with 2 mM L-glutamine and 10% FCS. Supplemented DMEM and DMEM/nutrient mixture F-12 Ham are both referred to as media throughout. Cells were grown in sterile conditions in uncoated T75 tissue culture flasks and stored in cell culture incubators at 37 °C and 5% CO_2. Once grown to confluency (70-90%), cells were washed with PBS and dislodged from the T75 flask surface by 5 min incubation with 1 mL 1X trypsin-EDTA in PBS at room temperature (HEK293 cells) or 37 °C and 5% CO_2 (CHO cells), then added to 9 mL media and pelleted by centrifugation for 4 min at 1,000 x *g*. This was followed by discarding of the supernatant and resuspension in 10 mL media. Cells were then split to a lower cell density (typically a 1:10, 1:20 split) and returned to a new T75 flask for continuation of the cell line.

2.4.2 – Seeding cells in assay plates

HEK293G (wildtype and β_2AR-overexpressing) cells and CHO-CRE-SPAP (wildtype and β_2AR-overexpressing) cells were seeded in 96-well plates for the cAMP GloSensor™ assay and the CRE-SPAP assay, respectively, as follows. Cells were grown to confluency and dislodged from the T75 flask as described above (see 2.4.1 – Passaging cells). After centrifugation for 4 min at 1,000 x *g* and resuspension in 10 mL media, HEK293G cells were seeded at 30,000 cells/well (measured by haemocytometer) into white walled, clear bottomed 96-well plates (pre-treated with 10 µg/mL poly-D-lysine for improved cell adhesion to the well surface) with 100 µL media/well. The seeded plates were then incubated at 37 °C and 5% CO_2 for 24 h prior to cAMP GloSensor™ assay.

For assays involving transient overexpression of β_2AR constructs contained within the pcDNA3.1(+) plasmids (HiBiT-β_2ARwt, HiBiT-β_2AR_N6A_N15A, HiBiT-β_2AR_N6A_N15A_N187A or pcDNA3.1(+) empty vector control), HEK293G cells were instead first seeded at 500,000 cells/well into clear 6-well plates with 2 mL media/well and incubated at 37 °C and 5% CO_2 for 6 h. Transfection mixture consisting of 700 µL Opti-mem containing 3% (21 µL) FuGENE^{TM} HD and 10 ng/µL (7 µg) DNA (3:1 FuGENE^{TM} HD:DNA ratio) was preincubated at room temperature for 10 min, followed by 100 µL dropwise addition to each well of the 6-well plates and incubation at 37 °C and 5% CO_2 for 18 h. FuGENE^{TM} HD is a non-liposomal transfection reagent which forms a complex with DNA, facilitating translocation of DNA across cell membranes. Cells were then dislodged from the 6-well plates with 500 µL 1X trypsin-EDTA in PBS and seeded at 40,000 cells/well into white walled, clear bottomed 96-wells plates (pre-treated with 10 µg/mL poly-D-lysine) with 100 µL media/well. The seeded plates were then incubated at 37 °C and 5% CO_2 for 24 h prior to cAMP GloSensor^{TM} assay.

CHO cells were instead resuspended in 60 mL media, 10 mL of which was used to seed each of a maximum of six clear 96-well plates with 100 µL media/well. The seeded plates were then incubated at 37 °C and 5% CO_2 for 48 h prior to CRE-SPAP assay. After 24 h, media was aspirated from each well and replaced with 100 µL serum-free media (SFM; DMEM/nutrient mixture F-12 Ham supplemented with 2 mM L-glutamine but not FCS) to reduce basal production of SPAP during the final 24 h prior to assay.

2.4.3 – Cryopreservation of cells

Stocks of cells were also frozen in liquid nitrogen for long-term storage for use in future studies. Cells grown to confluency were dislodged from the T75 flask as described above (see 2.4.1 – Passaging cells), followed by resuspension in 2 mL cell freezing media (filter sterilised FCS containing 10% DMSO). Two 1 mL aliquots of cells in cell freezing media were transferred into 2 mL cryovials which were stored at -80 °C for 24 h in a Mr. Frosty storage container containing

isopropanol to reduce rate of freezing in order to maintain cell viability. The cryovials were then transferred to a liquid nitrogen dewar for long-term storage at -196 °C.

2.5 – Generation of new stable cell lines

2.5.1 – DNA transfection and antibiotic selection of cells

Untransfected HEK293G cells which endogenously express the β_2AR at extremely low levels (Friedman et al., 2002; Goulding et al., 2021a; Goulding et al., 2021b), were termed HEK293G wild-type (HEK293Gwt) in this study. In order to study a high receptor expression system, a new HEK293G cell line stably overexpressing the β_2AR was generated by transfection of HEK293Gwt cells with the pcDNA4/TO TS-SNAP-β_2AR plasmid. These cells were termed HEK293G-β_2AR. A confluent T75 flask of HEK293Gwt cells was split as described above (see 2.4.1 – Passaging cells) and transferred to a new T75 flask at high density (1:3 split) in 20 mL media containing 1% penicillin-streptomycin (Pen/Strep). After preincubation together for 20 min at room temperature, 500 µL Opti-mem containing 3% (15 µL) PEI transfection reagent and 10 ng/µL (5 µg) pcDNA4/TO TS-SNAP-β_2AR DNA (3:1 PEI:DNA ratio) were added to the T75 flask containing the cells and incubated at 37 °C and 5% CO_2 for 48 h to allow transfection of the cells with the DNA. PEI is a cationic (positively charged) polymer which binds to the negatively charged DNA molecules and enables translocation across negatively charged cell membranes via endocytosis (Boussif et al., 1995; Sonawane et al., 2003). The pcDNA4/TO plasmid contains a zeocin antibiotic resistance gene, so 50 µg/mL zeocin was applied for selection of the cells which had been successfully transfected and expressed the desired β_2AR construct. Since the HEK293G cells already stably expressed the cAMP GloSensor^{TM} plasmid, which comprises a hygromycin B antibiotic resistance gene, 100 µg/mL hygromycin B was applied simultaneously with zeocin to maintain cAMP GloSensor^{TM} plasmid expression. Application of both antibiotics was repeated every 3-4 days for 2-3 weeks until colonies formed and eventually the cells grew to confluency, indicating that the cells were stably expressing both the β_2AR and cAMP GloSensor^{TM} plasmids.

2.5.2 – Dilution cloning to generate clonal cells

As the stable, mixed population HEK293G-β_2AR cells likely varied in their expression levels of the β_2AR due to differential transfection efficiency between cells within the population, dilution cloning was then performed to produce a clonal cell line derived from a single cell, ensuring all cells deriving from this clone would share the same level of β_2AR expression. Once grown to confluency in a T75 flask, HEK293G-β_2AR cells were trypsinised and dislodged from the T75 flask, pelleted and subsequently resuspended in 20 mL media. Then 20 µL was taken and added to another 20 mL media (1 in 1,000 dilution) in a 50 mL Falcon tube. The cells were further diluted by adding the following volumes to 10 different 50 mL Falcon tubes, each containing a further 20 mL media: 200 µL, 180 µL, 160 µL, 140 µL, 120 µL, 100 µL, 80 µL, 60 µL, 40 µL and 20 µL. Each of these cell dilutions were seeded into all wells of separate 96-well plates at 200 µL/well (10 plates total). The 96-well plates were incubated at 37 °C and 5% CO_2 for 3-4 days. All wells from each plate were then checked for the presence of a single colony of cells and marked. Any wells containing no cells were discarded, as were wells containing multiple colonies of cells (as these populations had derived from multiple original cells). 48 single colony wells were found throughout the 10 plates and taken forward. Once confluent, cells were trypsinised and transferred into 24-well plates, then eventually 6-well plates. Cells were screened for their ability to produce a cAMP GloSensor™ signal in response to the direct adenylate cyclase activator forskolin, the β_2AR agonist isoprenaline in presence and absence of inverse agonist ICI-118551, and for their basal response after application of vehicle (see 4.3.1). Four clonal candidates were taken forward and screened further until one clonal cell line was eventually selected.

2.6 – Membrane preparation

In order to prepare membranes for membrane-based assays, HEK293TR cells were first induced for high expression of the receptor of interest, followed in some cases (TR-FRET assays) by Terbium-labelling of the receptor, and finally the cells were homogenised to produce membranes with high receptor expression. For thermoBRET assays, HEK293TR cells overexpressing the TS-tsNLuc-β_2AR construct (stable cell line generated by Dr. Bradley L. Hoare, COMPARE, University of Nottingham, UK) were used. For TR-FRET assays, HEK293TR cells overexpressing the TS-SNAP-β_2AR construct (stable cell line generated by Dr. David A. Sykes, COMPARE, University of Nottingham, UK) were used.

2.6.1 – Tetracycline induction of protein expression

HEK293TR cells stably expressing the desired receptor construct (described above), were grown to confluence in a T175 flask and were then treated with fresh media containing 1 µg/mL tetracycline and incubated at 37 °C and 5% CO_2 for 48 h to induce maximal receptor expression. The HEK293TR cell line (T-REx^{TM} cell line, ThermoFisher Scientific, Loughborough, UK) stably expresses the tetracycline repressor protein (TetR) which represses transcription of the protein of interest by binding to the tetracycline operator sequences ($TetO_2$) of the human cytomegalovirus immediate early (CMV) promotor in the pcDNA4/TO plasmid (Yao et al., 1998). The application of tetracycline reverses this repression of gene transcription as tetracycline binds to TetR to inhibit its binding to the $TetO_2$ and the result is extremely high expression of the desired protein (Yao et al., 1998).

2.6.2 – Terbium-labelling of receptors

For TR-FRET assays, after tetracycline induction of high TS-SNAP-β_2AR expression in HEK293TR cells, the receptor construct was then Terbium-

labelled. After 48 h incubation with tetracycline at 37 °C and 5% CO_2, T175 flasks containing induced cells were washed twice with 10 mL PBS and once with 10 mL Tag-lite buffer (diluted to 1x in ddH_2O), followed by treatment with 10 mL Tag-lite buffer containing 100 nM SNAP-Lumi4-Tb labelling reagent and incubation at 37 °C and 5% CO_2 for 1 h. The SNAP-tag® is a peptide tag which derives from the O^6-guanine nucleotide alkyltransferase enzyme which binds specifically and covalently to the benzyl guanine group attached to the Terbium in the SNAP-Lumi4-Tb labelling reagent (Maurel et al., 2008). Cells were then washed twice with 10 mL PBS to remove the remaining unreacted SNAP-Lumi4-Tb labelling reagent. This step was not necessary for thermoBRET assays and thus was not performed in HEK293TR cells expressing the TS-tsNLuc-β_2AR construct.

2.6.3 – Homogenisation of cell membranes

Tetracycline-induced HEK293TR cells expressing either TS-tsNLuc-β_2AR or Terbium-labelled TS-SNAP-β_2AR were then dislodged from the T175 flask by 3 mL Cellstripper® non-enzymatic cell dissociation solution (used instead of trypsin-EDTA here to reduce risk of membrane protein cleavage), added to 7 mL DMEM and pelleted by centrifugation for 10 min at 1,000 x *g*. The supernatant was discarded and cells were either frozen and stored at -80 °C for later use or taken forward for membrane homogenisation. Cells taken forward were resuspended in 20 mL ice-cold buffer B (10 mM HEPES, 10 mM EDTA in ddH_2O, pH 7.45) and then homogenised for 10x 1 s bursts (on the high setting 6) using an Ultra-Turrax tissue homogeniser kit (IKA-Werke GmbH & Co., Staufen, Germany). This was followed by centrifugation at 4 °C for 5 min at 600 x *g* to pellet any remaining whole cells, nuclei, and other large debris. The resulting pellet was discarded and the supernatant was then centrifuged at 4 °C for 30 min at 48,000 x *g*. The pellet was then resuspended again in 20 mL buffer B and this homogenisation process was repeated one more time (but instead performing 6x 1 s bursts, again on setting 6) and, following another centrifugation at 4 °C for 30 min at 48,000 x *g*, pellets were this time resuspended

in 1 mL buffer C (10 mM HEPES, 0.1 mM EDTA in ddH_2O, pH 7.45). The resulting membranes were split into 20 µL aliquots and frozen at -80 °C.

2.6.4 – Protein concentration determination of membranes

To determine the concentration of the desired receptor construct in the homogenised membranes, the BCA protein determination assay kit was used with BSA as the standard for comparison of protein concentration. Bicinchoninic acid (BCA) forms a complex with reduced copper ions which has a strong absorbance at 562 nm. Reduction of copper ions is protein concentration-dependent, hence measuring absorbance at 562 nm provides an accurate estimate of protein concentration in the solution (Walker, 2009). Therefore, absorbance was measured in terms of optical density at 562 nm ($OD_{562\ nm}$) for a range of BSA concentrations (0.1 mg/mL – 1 mg/mL) and for three dilutions of the TS-tsNLuc-β_2AR or Terbium-labelled TS-SNAP-β_2AR membranes (1/10, 1/20, 1/50) to generate a standard curve for BSA and use this to estimate the protein concentration of the membranes by plotting a line of best-fit through the BSA absorbance values. Figure 2.1 displays an example standard curve generated for BSA, used to determine the protein concentration of the diluted TS-tsNLuc-β_2AR membrane samples, and thus estimate the protein concentration of the original undiluted membranes.

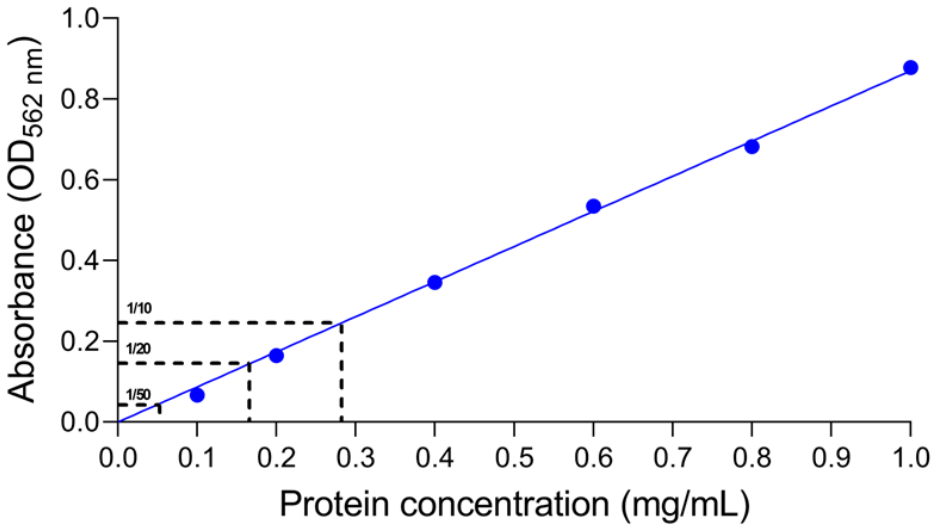

Figure 2.1: Example standard curve using the BCA protein determination assay kit. Absorbance ($OD_{562\ nm}$) was measured for a range of BSA concentrations (0.1 mg/mL – 1 mg/mL) and for three dilutions of TS-SNAP-β_2AR membranes (1/10, 1/20, 1/50) to generate a BSA standard curve from which to estimate the protein concentration in the membranes. A line of best-fit (blue) is plotted through the BSA absorbance values and the membrane dilution absorbance values are used to estimate membrane protein concentration.

2.7 – cAMP GloSensor™ assay

The cAMP GloSensor™ luminescence assay was performed according to the manufacturer's instructions (Promega, Madison, WI, USA). Briefly, after 24 h incubation at 37 °C and 5% CO_2 after cell plating (see 2.4.2 – Seeding cells in assay plates), wells were checked under a microscope for cell viability and confluence (80-90%). Media was then aspirated from each well of the 96-well plate and HEK293G cells were incubated in 50 µL HEPES buffered saline solution (HBSS; 2 mM sodium pyruvate, 145 mM NaCl, 10 mM D-glucose, 5 mM KCl, 1 mM $MgSO_4.7H_2O$, 10 mM HEPES, 1.3 mM $CaCl_2.2H_2O$, 1.5 mM $NaHCO_3$ in ddH_2O, pH 7.45) containing 3% GloSensor™ reagent at 37 °C and 5% CO_2 for 2 h. This was to allow the GloSensor™ reagent to translocate across the cell membranes and equilibrate inside cells. The GloSensor™ biosensor consists of a firefly luciferase enzyme genetically fused to the cAMP-binding domain of a protein kinase A (PKA) regulatory subunit (RIIβB) (Fan et al., 2008; Binkowski et al., 2011). The GloSensor™ reagent derives from the substrate luciferin which is oxidised by the firefly luciferase enzyme to oxyluciferin to produce luminescence upon cAMP binding to RIIβB and the subsequent luciferase conformational change (Fan et al., 2008; Binkowski et al., 2011). For work involving pepducins, 0.1% BSA and 0.1% or 0.5% DMSO were also added to the HBSS. BSA was used to reduce peptide binding to plasticware, while DMSO was applied to ensure an equal concentration throughout each condition to negate any minor effects of DMSO from pepducin stocks on the basal cAMP response. A white seal was placed on the clear back of the plate before reading to prevent loss of luminescence.

For agonist studies, luminescence was measured immediately after addition of a further 50 µL HBSS containing agonist (2x final concentration) or vehicle control (HBSS or DMSO). Luminescence was measured continuously over 60 min using an open luminescence channel (on 3,600 gain), reading each well once every minute, by a PHERAstar FSX microplate reader (BMG Labtech, Offenburg, Germany) while maintained at 37 °C. Increases in luminescence are indicative of intracellular cAMP accumulation, thus, the temporal changes in relative cytosolic cAMP concentration were measured upon agonist or vehicle

addition. Baseline luminescence was also measured in each well prior to any addition. For agonist vs antagonist/inverse agonist/allosteric modulator studies, the same process was performed with the additional preincubation of 5 µL HBSS containing antagonist/inverse agonist/allosteric modulator (20x final concentration) or vehicle, 30 min prior to application of agonist (2x final concentration) or vehicle. Studies involving phosphodiesterase inhibitors also included 30 min preincubation of 5 µL HBSS containing phosphodiesterase inhibitor (20x final concentration) or vehicle. All conditions were performed in at least triplicate within each plate. Where conditions were repeated in more than three replicates within a plate, this is stated throughout.

In some cases, cells were initially incubated with 90 µL HBSS containing 3% GloSensor™ reagent and subsequently treated with 10 µL HBSS containing ligand (10x final concentration) or vehicle in order to study the large mechanostimulatory response in HEK293G-β_2AR cells. Where this is the case, it is stated throughout. Additionally, in other cases, luminescence reads were briefly paused once (at 30 min) or several times (at 15, 30 and 45 min), in order to either open and subsequently close the PheraStar FSX door (including outward-inward movement of microplate in the tray) or to shake the microplate within the PheraStar FSX (using either linear or orbital shake protocols) to study receptor mechanical responses further. These conditions are clearly stated where relevant. A graphical representation of the activation and subsequent luminescence emission of the GloSensor™ biosensor is displayed in Figure 2.2, which also includes the β_2AR-mediated cAMP signalling pathway and regulatory mechanisms counteracting the signal.

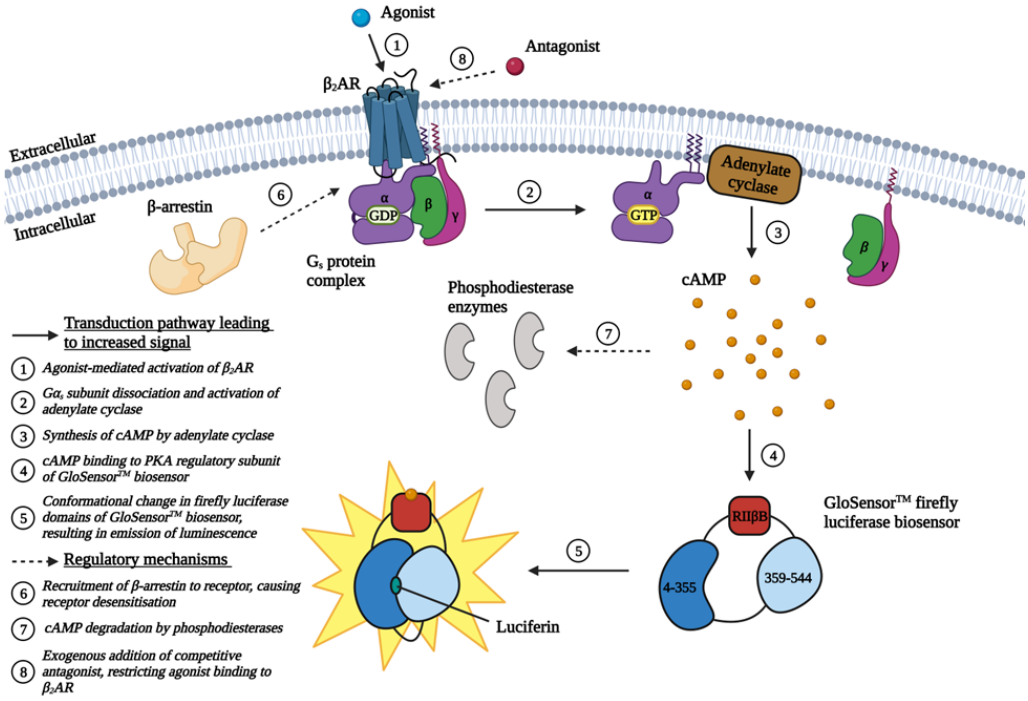

Figure 2.2: cAMP GloSensor™ assay. The mechanism of the β_2AR-mediated cAMP signalling pathway leading to activation and subsequent luminescence emission of the GloSensor™ biosensor. After agonist-mediated β_2AR activation (1), recruited G_s protein undergoes nucleotide exchange (GDP for GTP) resulting in the α subunit dissociating from the βγ subunits and activating adenylate cyclase (2). Synthesis of cAMP by adenylate cyclase is subsequently increased (3) and cytosolic cAMP binds to the PKA regulatory subunit (RIIβB) of the GloSensor™ biosensor (4), initiating a conformational change in the firefly luciferase domains of the biosensor which, in the presence of the enzyme substrate luciferin (cAMP reagent), results in the emission of luminescence (5). The intensity of luminescence is measured in real-time to indicate changes in relative cAMP concentration inside cells. Several regulatory mechanisms counteract the cAMP signalling response, including receptor desensitisation by recruitment of β-arrestin (6), degradation of cytosolic cAMP by phosphodiesterase enzymes (7) and the exogenous addition of a β_2AR antagonist which competes with the agonist for the receptor orthosteric binding site, thus inhibiting β_2AR activation (8). This diagram was created using BioRender.com.

2.8 – HiBiT-LgBiT complementation assay

This assay was used to determine relative surface expression of transiently transfected β_2AR constructs with N-terminal HiBiT tags (HiBiT-β_2ARwt, HiBiT-β_2AR_N6A_N15A, HiBiT-β_2AR_N6A_N15A_N187A and pcDNA3.1(+) control) in HEK293G cells. High BiT (HiBiT) is a high affinity (K_D: 700 pM) derivative of the small nanoluciferase subunit (11 amino acid peptide) which complements with the large subunit Large BiT (LgBiT; 18 kDa) to form the complete nanoluciferase enzyme as part of the NanoLuc® Binary Technology (NanoBiT; Promega, Madison, WI, USA) (Dixon et al., 2016; Schwinn et al., 2018). Upon complementation, the complete enzyme becomes active and, in the presence of the furimazine substrate, produces luminescence which can be measured to determine relative HiBiT-tagged protein expression (Dixon et al., 2016; Schwinn et al., 2018). After 24 h incubation at 37 °C and 5% CO_2 after cell plating (see 2.4.2 – Seeding cells in assay plates), each well was checked for cell confluency and viability. From each relevant well of the 96-well plate, media was aspirated and HEK293G cells were then incubated with 50 µL HBSS at 37 °C and 5% CO_2 for 2 h. This was followed by simultaneous addition of 0.2% purified LgBiT protein and 0.25% Nano-Glo® luciferase assay substrate (a furimazine derivative) in 50 µL HBSS to the cells and incubation at 37 °C for 5 min (to allow for equilibration of LgBiT and the furimazine-based substrate with the HiBiT tagged at the extracellular surface of the receptor) before a single luminescence measurement of each well was taken by a PHERAstar FSX microplate reader (BMG Labtech, Offenburg, Germany) using an open luminescence channel (on 2,000 gain). Since LgBiT is too large to pass through the cell membrane, this method provides an estimate of the cell surface expression of the HiBiT-tagged protein (Soave et al., 2020). The HiBiT-LgBiT complementation assay is shown in Figure 2.3.

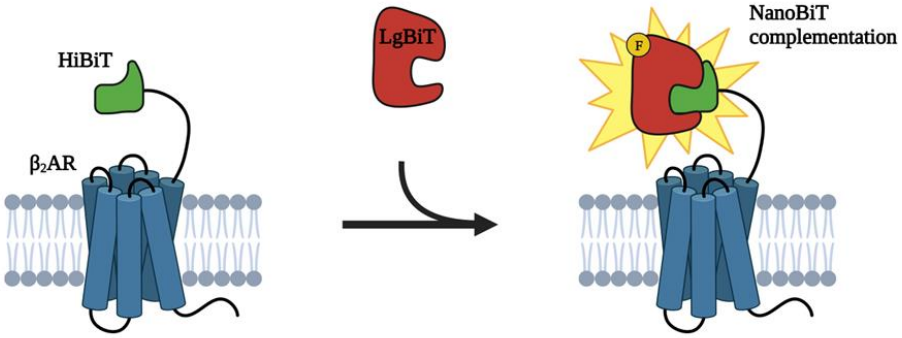

Figure 2.3: HiBiT-LgBiT complementation assay. Exogenously applied LgBiT binds with high affinity to the HiBiT attached to the N-terminus of the β_2AR to form the complete nanoluciferase enzyme (NanoBiT). In the presence of the enzyme substrate furimazine (Nano-Glo® luciferase assay substrate; denoted by 'F'), the complete nanoluciferase emits luminescence which is subsequently measured to report on receptor expression at the cell surface. This diagram was created using BioRender.com.

2.9 – CRE-SPAP assay

For the CRE-SPAP gene transcription assay, 48 h after cell plating and 24 h after treatment with SFM (see 2.4.2 – Seeding cells in assay plates), SFM was aspirated from each well of the 96-well plate. For agonist studies, cells were then incubated in 100 µL SFM containing agonist or vehicle control (HBSS or DMSO) at 37 °C and 5% CO_2 for 5 h to initiate CRE-mediated gene transcription of SPAP. Phosphorylation of CRE-binding protein (CREB) in the nucleus by the catalytic subunits of PKA (downstream of cAMP) activates CREB and other transcriptional proteins to bind to one of the six repeating CRE palindromic sequences (TGACGTCA) in the promotor region of the SPAP gene to initiate gene transcription (Montminy et al., 1990; Lalli and Sassone-Corsi, 1994; Hill et al., 2001). For work involving pepducins, 0.1% BSA and 0.1% or 0.5% DMSO were also added to the SFM for the same reasons as outlined above (see 2.7 – cAMP GloSensor^{TM} assay). For agonist vs antagonist/inverse agonist/allosteric modulator studies, the same process was performed with the additional preincubation of 5 µL SFM containing antagonist/inverse agonist/allosteric modulator (20x final concentration) or vehicle, 30 min prior to application of agonist or vehicle.

After 5 h, SFM containing ligands was aspirated from wells and replaced with 40 µL fresh SFM and cells were incubated at 37 °C and 5% CO_2 for a further 1 h, thus allowing SPAP production and secretion over hour 5 to 6, which was later measured. Cells were then heat-inactivated at 65 °C for 30 min to degrade endogenous alkaline phosphatases, but not the reporter protein SPAP which has high thermal stability and does not degrade at 65 °C (Cullen and Malim, 1992; Cassinotti and Weitz, 1994; Hill et al., 2001). The plate was then allowed to cool to room temperature, after which 100 µL DEA buffer (100 mM DEA, 280 mM NaCl, 0.5 mM $MgCl_2.H_2O$ in ddH_2O, pH 9.85) containing 5 mM pNPP dye was applied to each well and plates were incubated at 37 °C for 1 h before absorbance at 405 nm was read by a Dynex MRX microplate reader (Dynex Technologies, Chantilly, VA, USA) at room temperature. The phosphate group of pNPP is hydrolysed by the phosphatase activity of SPAP, leaving p-nitrophenol (pNP) and resulting in a colour change from clear to yellow in the alkaline conditions

of the DEA buffer (Cullen and Malim, 1992; Hill et al., 2001). Thus, the CRE-mediated SPAP production and secretion from cells was quantified by measuring absorbance at 405 nm. All conditions were performed in triplicate within each plate. An illustration of the CRE-SPAP assay including the full signalling pathway from β_2AR activation to CRE-mediated transcription of SPAP and subsequent secretion from cells is provided in Figure 2.4.

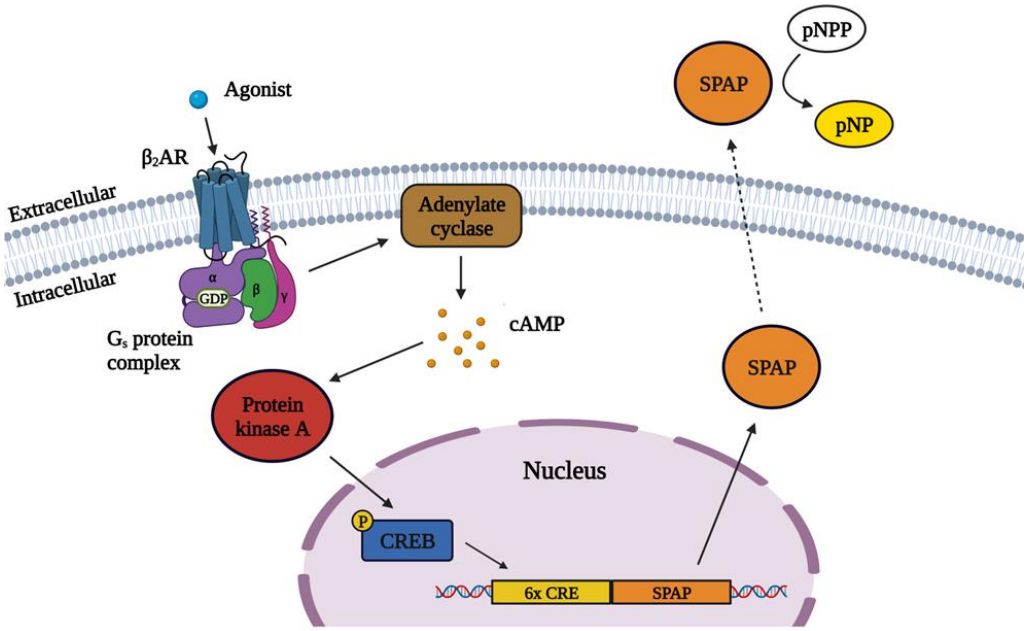

Figure 2.4: CRE-SPAP assay. The signalling pathway leading to CRE-mediated SPAP production and subsequent cellular secretion. Agonist stimulation of the β_2AR and subsequent adenylate cyclase activation by G_s protein results in cAMP binding to protein kinase A (PKA) regulatory subunits. PKA catalytic subunits then phosphorylate (denoted by 'P') cAMP response element-binding proteins (CREB) in the nucleus, which bind to one of six repeating CRE palindromic sequences (TGACGTCA) in the SPAP reporter gene promoter region, initiating transcription of SPAP. After translation of the protein and secretion from cell, SPAP hydrolyses the phosphate group of the dye pNPP, which is added to the buffer, producing pNP and resulting in a colour change from clear to yellow. Quantification of the colour change by absorbance measurements at 405 nm indicates the relative CRE-mediated SPAP production. This diagram was created using BioRender.com.

2.10 – ThermoBRET assay

All ligands, reagents and membranes were kept on ice throughout the assay preparation stages of all thermoBRET assays. Most of the thermoBRET work presented was performed using the standard CORE buffer with high salt concentration (20 mM HEPES, 150 mM NaCl, 10% glycerol, 0.5% BSA in ddH_2O, pH 7.45), although some experiments were performed in CORE buffer lacking salt (NaCl removed). Similarly, the solubilisation buffer (CORE buffer containing detergent for receptor solubilisation) composition lacked salt in these conditions, and this is stated where relevant. After induction of receptor expression and subsequent membrane homogenisation (see 2.6 – Membrane preparation), TS-tsNLuc-β_2AR membranes were first diluted to 80 µg/mL in 500 µL CORE buffer. Membranes were pelleted by centrifugation at 4 °C for 30 min at 16,900 x *g* and supernatant was carefully discarded to remove EDTA without dislodging the membrane pellet. The pellet was then resuspended in 200 µL solubilisation buffer and placed on shaker at 4 °C for 20 min at 1,000 rpm to solubilise the receptor. Generally, 1% N-dodecyl-β-D-maltopyranoside (DDM) was used as the solubilisation detergent throughout (unless otherwise stated), but 1% DDM + 0.2% cholesteryl hemisuccinate tris salt (CHS) + 1% 3-[(3-cholamidopropyl)dimethylammonio]-2-hydroxy-1-propanesulfonate (CHAPSO) or 0.5% lauryl maltose neopentyl glycol (LMNG) or 0.5% LMNG + 0.2% CHS + 1% CHAPSO conditions were also tested. The solution was then centrifuged again at 4 °C for 30 min at 16,900 x *g* to pellet any remaining unsolubilised membranes and the 200 µL supernatant (solubilised receptor) was added to 1.8 mL CORE buffer containing 1 µM sulfo-cyanine3 maleimide (SCM) dye. SCM dye is a thiol-reactive fluorophore which binds to cysteine residues residing predominantly in the transmembrane regions of GPCRs (Hoare et al., 2023).

9 µL of this solution was applied to each well of a 384-well plate with 1 µL ligand (10x final concentration) or vehicle (CORE buffer or DMSO). For pepducin experiments, 1 µL pepducin was also added (10x final concentration) prior to melting (including 30 min preincubation of either pepducin or orthosteric ligand in some cases). A final DMSO concentration of 1.5% was used

in each well, or 2.5% when pepducins were included. 1% DMSO controls (referring to the extra 1% DMSO applied to make a final 2.5% concentration) were used in these experiments to ensure no observed effects were due to the increased DMSO concentration in the wells. A foil seal was tightly covered over the top of the 384-well plate to prevent liquid evaporation from the wells and the plate was then heated in a GeneTouch^{TM} Thermocycler (Bioer, Hangzhou, China) either over a 30 °C temperature gradient across the plate (to determine receptor melting temperature; T_m) or at a constant temperature (using different ligand concentrations to determine ligand IC_{50} values) for 30 min before rapid cooling back to 4 °C. 5 µL CORE buffer containing 30 µM Nano-Glo® luciferase assay substrate (10 µM final concentration in wells) was added to each well and the 550LP/450BP80 nanoBRET emission ratio was measured for six cycles by a PHERAstar FSX microplate reader (BMG Labtech, Offenburg, Germany) at room temperature. Due to overlapping donor-acceptor excitation-emission spectra, when the donor and acceptor come into close proximity (~10 nm), the luminescence emitted by the donor is absorbed by the acceptor and subsequently emitted as fluorescence (Hoare et al., 2023). Therefore, the nanoBRET ratio measures the ratio of emission of the tsNLuc donor (~450 nm wavelength emission) and the SCM dye acceptor (~550 nm wavelength emission) (England et al., 2016; Hoare et al., 2023). All conditions were performed in singlet within each plate and the mean of the six repeated cycles was calculated. In Figure 2.5A, the principles of the thermoBRET assay are illustrated, while the overlapping donor-acceptor excitation-emission spectra are depicted in Figure 2.5B.

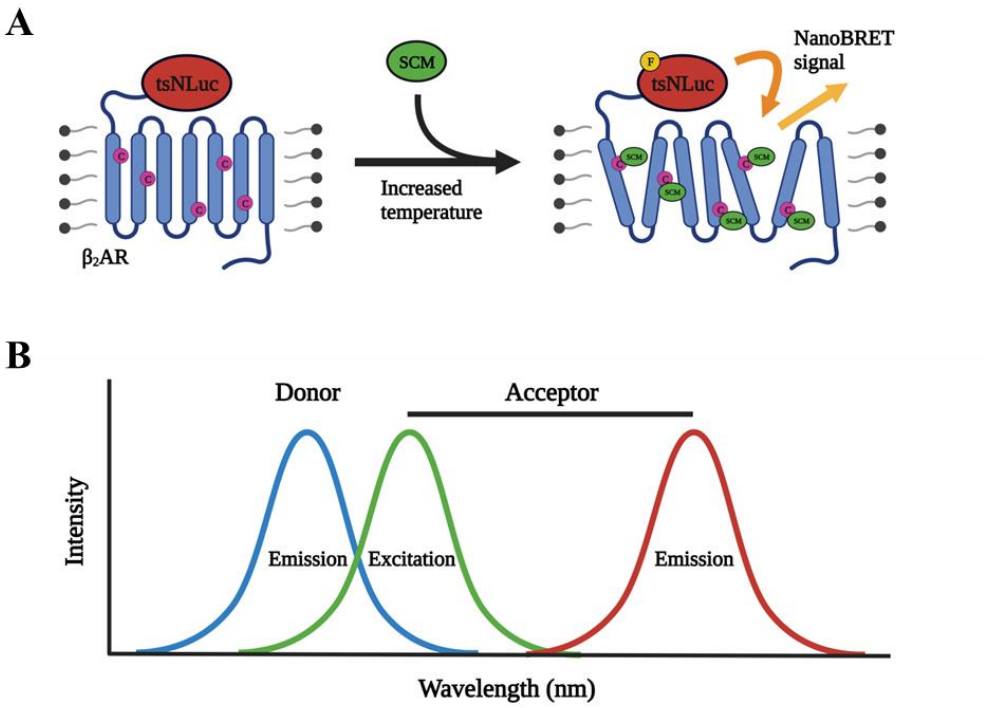

Figure 2.5: ThermoBRET assay. (A) The detergent-solubilised β_2AR with an N-terminally tagged thermostable nanoluciferase (tsNLuc) donor is incubated over an increasing temperature gradient to denature the protein, causing protein unfolding and exposing the cysteine residues (denoted by 'C') residing in the receptor transmembrane domains to the SCM acceptor dye which binds covalently. After subsequent addition of furimazine (Nano-Glo® luciferase assay substrate; denoted by 'F'), the nanoBRET ratio can be measured which is used to determine receptor thermostability (in terms of melting temperature; T_m). (B) The thermoBRET donor-acceptor excitation-emission spectra whereby the wavelength of donor emission overlaps with the acceptor excitation wavelength, allowing BRET to occur. The nanoBRET ratio is the ratio of donor luminescence and acceptor fluorescence. This diagram was created using BioRender.com.

2.11 – TR-FRET assay

All ligands, reagents and membranes were kept on ice throughout the assay preparation stages of all TR-FRET assays. To first determine the binding kinetics of the fluorescently labelled tracer ligand F-propranolol, 29 µL TR-FRET assay buffer (5 mM HEPES, 0.1% BSA, 0.02% pluronic F-127, 0.1% saponin in HaBSS, pH 7.45) was added to each well of a 384-well plate with either 0.5 µL F-propranolol (100x final concentration, ranging between 0.98 nM – 125 nM) or vehicle (1% DMSO) and either 0.5 µL alprenolol (100x final concentration of 3 µM) as the non-specific binding (NSB) control or vehicle (1% DMSO) for the total binding condition. For work involving pepducins, 0.5 µL pepducin (100x final concentration of 10 µM) or vehicle was also added. Homogenised Terbium-labelled TS-SNAP-β_2AR membranes (see 2.6 – Membrane preparation) were diluted to 50 ng/µL in 1 mL TR-FRET assay buffer containing 100 µM GppNHp. GppNHp is a non-hydrolysable analogue of GTP which binds to a G protein to prevent coupling to GPCRs (Ibarrondo et al., 1989). Using the PHERAstar FSX liquid injectors, 20 µL membrane solution was applied to each well for a final membrane concentration of 20 ng/µL (1 µg total membrane per well), and the 520/620 nm x10,000 homogenous time-resolved fluorescence (HTRF) emission ratio was measured continuously for 20 min, reading each well once every 10 s using a PHERAstar FSX microplate reader (BMG Labtech, Offenburg, Germany) at room temperature. This measures the ratio of emission of the Terbium donor (~620 nm wavelength emission) (Degorce et al., 2009) and the F-propranolol acceptor (~520 nm wavelength emission) (Farmer et al., 2022). All conditions were performed in singlet.

For competition binding experiments, a similar process was performed, but with the additional application of a competing unlabelled β_2AR ligand, namely 0.5 µL formoterol (100x final concentration, ranging between 0.21 nM – 450 nM) or vehicle (1% DMSO). F-propranolol was consistently applied at its approximate calculated K_D concentration of 4 nM (applied to plate at 100x the final concentration). The membrane solution was again applied via the PHERAstar FSX liquid injectors and the 520/620 nm x10,000 HTRF emission ratio was measured continuously for 20 min, this time reading each well once

every 7 s on the plate reader at room temperature. Again, all conditions were performed in singlet. The principles of the TR-FRET assay are displayed in Figure 2.6A, while Figure 2.6B illustrates the differences between the short-lived background fluorescence and the long-lived Terbium fluorescence which is taken advantage of during the measurement of the TR-FRET signal.

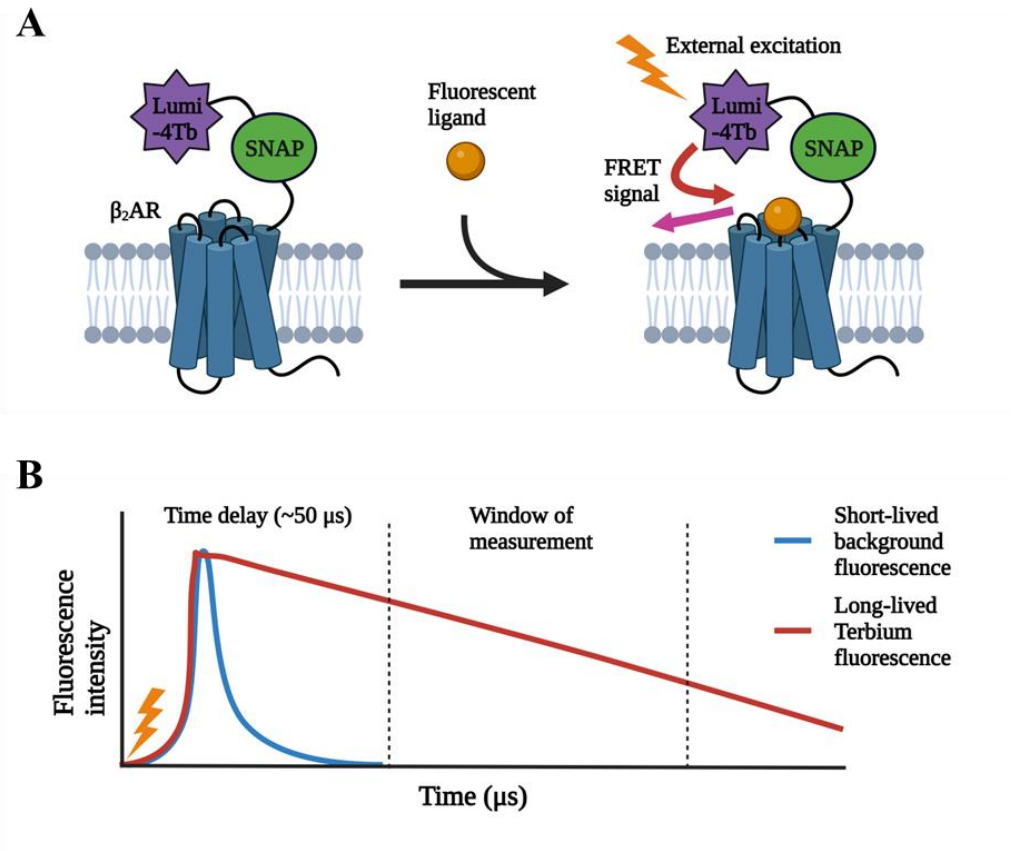

Figure 2.6: TR-FRET assay. (A) Application of a fluorescent tracer ligand to the Terbium-labelled, SNAP-tagged β_2AR in homogenised native cell membranes results in a TR-FRET signal upon external excitation due to the close proximity (~10 nm) of the Terbium (donor) and tracer ligand (acceptor). The TR-FRET ratio is measured to determine labelled tracer ligand (or unlabelled competitor ligand) kinetic binding parameters to the β_2AR. (B) The relatively long-lived Terbium fluorescence emission enables the TR-FRET signal-to-noise ratio to be improved by introducing a short time delay (~50 μs) after external excitation to allow the generally short-lived fluorescence from background compounds to decay before measurement of the signal. This diagram was created using BioRender.com.

2.12 – Data analysis and statistics

Data were analysed and presented using GraphPad Prism 8 software (San Diego, CA, USA). Results are generally expressed as mean ± standard error of mean (SEM) from three, five or six separate experiments, unless otherwise stated. The exact number of independent experiments '*n*' is stated throughout.

2.12.1 – Functional assays

In the cAMP GloSensor™ assay, peak responses were determined as the maximal signal in each trace. Area under curve (AUC) responses were determined as the total accumulated luminescence signal over the measured 60 min period. The kinetic parameters, initial rate, k_1 and k_2, were determined by curve fitting of the kinetic equation (Equation 3) to cAMP GloSensor™ luminescence time-course data, according to Hoare et al. (2020b). A graphical representation of this kinetic curve fitting to ligand-stimulated cAMP time-course data and the resulting kinetic parameters is presented in Figure 2.7. In contrast, the CRE-SPAP assay is simply an endpoint point assay with no kinetic dimension to the measurement. Therefore, since just one absolute value was received for each condition (per replicate), no peak, AUC or initial rate parameters could be determined in this assay.

Throughout the cAMP GloSensor™ assay, parallel measurements were made at each time-point following addition of vehicle (HBSS or DMSO) in place of agonist under the same experimental conditions. For tests involving HEK293Gwt cells with low, endogenous β_2AR expression, these values were subtracted from the equivalent agonist-induced data at each time-point to provide a baseline-corrected time-course. This was performed to improve the fitting of the kinetic equation to the time-course data. However, for tests involving HEK293G-β_2AR cells with high β_2AR expression, baseline correction of agonist signals was not required to fit the kinetic equation adequately and in fact hindered the analysis of agonists vs preincubated inverse agonists due to the inhibiting effect of inverse agonists to the baseline cAMP response. In addition,

unlike the equivalent in HEK293Gwt cells, the large response to vehicle observed in HEK293G-β_2AR cells was primarily mediated by the β_2AR. Thus, baseline-correction was not deemed appropriate in those cases.

Upon data normalisation to construct concentration-response curves, cAMP GloSensor^{TM} data obtained from HEK293Gwt cells were normalised between 0 (representing the basal response which had been corrected to zero) and a maximal concentration of high efficacy agonist as 100% (usually 1 μM isoprenaline or 100 μM forskolin). Agonist data obtained from HEK293G-β_2AR cells were instead normalised between the uncorrected HBSS (mechanical) cAMP response as 0% and a maximal concentration of high efficacy agonist as 100% (usually 1 nM isoprenaline). However, HEK293G-β_2AR inverse agonist data were instead normalised between absolute zero luminescence as 0% and the uncorrected HBSS (mechanical) response as 100%. For GloSensor^{TM} assays, agonist and inverse agonist peak concentration-response curves were fitted to sigmoidal curves using the relevant Hill equations (Equations 1 and 2, respectively) to determine pharmacological ligand parameters, whilst agonist initial rate concentration-response curves were fitted to sigmoidal curves using the modified Hill equation (Equation 4) to determine kinetic ligand parameters. CRE-SPAP data were also normalised between the basal gene transcription response as 0% and a maximal concentration of high efficacy agonist as 100%. All agonist concentration-response curves derived from CRE-SPAP data were fitted to sigmoidal curves using the Hill equation (Equation 1) to determine ligand parameters.

During Schild regression analyses, under equilibrium conditions (observed in high receptor expression conditions, and in low receptor expression conditions when a fast-dissociating antagonist is used) dose ratios were calculated using the half-maximal (EC_{50}) agonist responses (Arunlakshana and Schild, 1959; Tallarida and Murray, 1987). Whereas, under non-equilibrium conditions (observed when a slow-dissociating antagonist is used in low receptor expression conditions), whereby a reduction in maximal agonist response is observed by antagonist application, equieffective agonist response concentrations (where all conditions show a constant level of response, occurring within the linear phase

of the sigmoidal curve) were instead selected to determine dose ratios (Christopoulos et al., 1999). Figures 2.8A and 2.8B illustrate the methods used to determine the agonist concentrations for dose ratio calculation under both equilibrium and non-equilibrium conditions. Schild plots were then constructed using the Schild equation (Equation 5) and fitted with a linear regression line equation (Equation 6) to determine antagonist K_D values, represented by the x-intercept of the line. For determining partial agonist K_D values, the modified Gaddum equation (Equation 7) was instead applied.

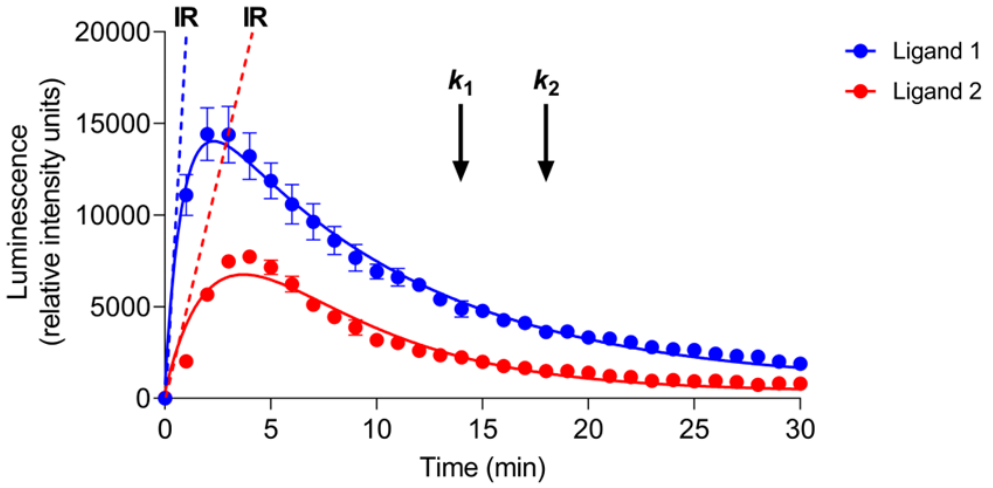

Figure 2.7: Graphical representation of the kinetic curve fitting of cAMP GloSensor™ time-course data, according to Hoare et al. (2020b), and subsequent derivation of kinetic parameters including 'IR' (the initial linear phase of signal generation), 'k_1' and 'k_2' (rate constants relating to the regulatory mechanisms counteracting the signal) after application of a full agonist (ligand 1; blue) and a partial agonist (ligand 2; red) to HEK293Gwt cells. Data points represent mean ± standard error of mean (SEM) of triplicate measurements, expressed as relative luminescence intensity units (RIU) of luminescence.

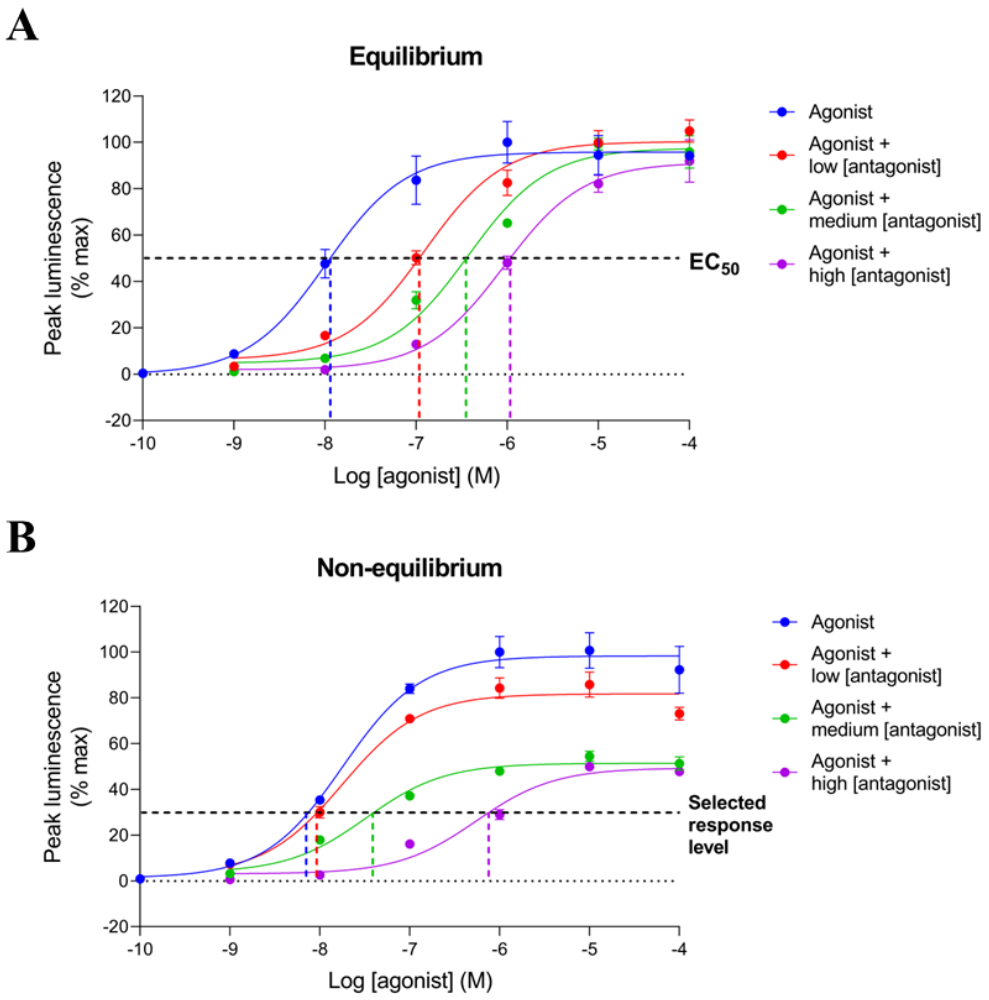

Figure 2.8: Example cAMP GloSensor™ agonist vs antagonist concentration response curves to illustrate the calculation of dose ratios under equilibrium (A) and non-equilibrium (B) conditions. The black dotted line depicts the selected response level taken in these examples to determine equieffective concentrations of agonist in each antagonist condition (illustrated by the x-intercepts of the blue, red, green and purple lines). From these, the dose ratios are determined, and Schild plots can be constructed.

2.12.2 – Ligand binding assays

For the thermoBRET assay, the mean 550LP/450BP80 nanoBRET emission ratio was calculated from the six repeated cycles measured for each condition within the same experiment. Upon construction of receptor melting curves using temperature gradients, data were normalised against their own minimal (0%) and maximal (100%) nanoBRET ratio values in each individual experiment and fitted to a Boltzmann sigmoidal equation (Equation 8) to determine T_m values. Where the nanoBRET ratio reduced at higher temperatures, likely due to protein aggregation and loss of signal (Hoare et al., 2023), these datapoints were excluded from the curve fitting but are still displayed in the relevant Figures. For orthosteric ligand IC_{50} curves, data were instead normalised against the signal measured in absence of ligands (vehicle; 100%) and the highest tested concentration of the ligand (100 μM; 0%). Log IC_{50} values were then determined by fitting the data to the Hill equation (Equation 2). For pepducin-based isothermal thermoBRET studies, the zero was instead determined by a formoterol control (10 μM or 100 μM).

In TR-FRET tracer saturation binding experiments, the mean F-propranolol total and non-specific binding (NSB) 520/620 nm x1000 HTRF emission ratios taken from six repeated measurements at equilibrium (between 19-20 min after assay start) were determined. Mean NSB was subtracted from mean total emission ratio to calculate specific binding and all values were normalised against the maximal specific binding at the highest concentration of the fluorescent ligand (125 nM; 100%). Saturation plots were then constructed and both total and NSB (Equation 9), as well as specific binding (Equation 10) were fit globally to one-site binding models to determine the equilibrium dissociation constant, K_D. To obtain association and dissociation rate constants *(*k_{on} and k_{off}, respectively), the specific binding data (calculated from total and NSB 520/620 nm x1000 HTRF emission ratios measured every 10 s for 20 min) were fit globally to an association kinetics equation (Equation 11). The kinetic K_D values of the fluorescent ligand were then calculated by k_{off} / k_{on}.

For TR-FRET competition binding experiments, specific binding values taken from six repeated measurements at equilibrium (between 19-20 min after assay

start) were normalised between the maximal specific binding of the fluorescent ligand in the absence of competing unlabelled ligand (100%) and the specific binding in the presence of the highest concentration of competing unlabelled ligand (450 nM; 0%). The specific binding data were fit to an IC_{50} curve (Equation 12) using the previously calculated tracer equilibrium K_D value, and the determined IC_{50} value for the unlabelled ligand was subsequently converted into the equilibrium inhibition constant, K_I, according the method previously described by Cheng and Prusoff (1973) (Equation 13). The unlabelled ligand k_{on} and k_{off} values were determined by globally fitting the specific binding data (calculated from total and NSB 520/620 nm x1000 HTRF emission ratios measured every 7 s for 20 min) to the kinetic binding model developed by Motulsky and Mahan (1984) (Equation 14), and the kinetic K_I values of the competing ligand were then calculated by k_{off} / k_{on}. To aid in the fitting of the competition association kinetics data to the Motulsky-Mahan model, data were constrained to the first 10 min of measured values after addition of both the fluorescent tracer and unlabelled competitor ligand. Attempts to fit the entire 20 min data to the model often resulted in poor fits whereby the k_3 value (referring to the k_{on} of the competing ligand) could not be determined.

2.12.3 – Relevant equations

The Hill equation, shown in Equation 1, was used to fit agonist concentration-response data to a standard sigmoidal curve, where '*E*' represents the magnitude of response, 'E_{max}' represents the maximal response magnitude, '[*A*]' is the ligand concentration, 'EC_{50}' is the half-maximal response concentration and '*n*' is the Hill coefficient (Hill, 1910; Neubig et al., 2003).

$$\frac{\mathrm{E}}{\mathrm{E_{max}}} = \frac{[\mathrm{A}]^{\mathrm{n}}}{\mathrm{EC_{50}^{n}} + [\mathrm{A}]^{\mathrm{n}}}$$

Equation 1

Inverse agonist concentration-response data were also fit to a sigmoidal curve by using the Hill Equation, displayed in Equation 2, where '*I*' represents the

magnitude of inhibition, 'I_{max}' represents the maximal inhibition, '[A]' is the ligand concentration, 'IC_{50}' is the half-maximal inhibition concentration and 'n' is the Hill coefficient (Hill, 1910; Neubig et al., 2003).

$$\frac{\mathrm{I}}{\mathrm{I_{max}}} = \frac{[\mathrm{A}]^{\mathrm{n}}}{\mathrm{IC_{50}^{n}} + [\mathrm{A}]^{\mathrm{n}}}$$

Equation 2

The "rise-and-fall-to-baseline time-course" equation, shown in Equation 3, was used to fit cAMP GloSensor™ luminescence time-course data to a kinetic curve, according to Hoare et al. (2020b), where '*IR*' is a fitting constant (in units of y-units.t^{-1}), which is equal to the initial rate of signalling, the initial linear phase of signal generation upon ligand addition, 'k_1' and 'k_2' are two regulatory rate constants (in units of t^{-1}) which are responsible for attenuating the initial rate of response (e.g., due to desensitisation) and the decay of the cAMP response (e.g., due to phosphodiesterase activity), which cause the signal to peak and then decline back towards baseline (Hoare et al., 2020b), 't' refers to the time-point and '*Baseline*' is the level of baseline response. Equation 3 was provided as a plug-in which was downloaded into GraphPad Prism 8 software (San Diego, CA, USA) (Hoare et al., 2020b). k_1 was assumed to be the larger of the two rate constant values and this was handled by constraining k_1 to be greater than k_2. In all cases, rate constant values were constrained to be greater than zero.

$$\mathrm{y} = \frac{\mathrm{IR}}{\mathrm{k_1} - \mathrm{k_2}}\left(\mathrm{e}^{-\mathrm{k_2 t}} - \mathrm{e}^{-\mathrm{k_1 t}}\right) + \mathrm{Baseline}$$

Equation 3

Concentration-response data for the initial rates were fit to a variable slope Hill equation, displayed in Equation 4, where '*IR*' represents the initial rate of signalling, 'IR_{max}' is the maximal initial rate response, '[A]' is the ligand concentration, 'L_{50}' is the half maximal initial rate concentration and 'n' is the Hill coefficient.

$$\frac{\mathrm{IR}}{\mathrm{IR_{max}}} = \frac{[\mathrm{A}]^{\mathrm{n}}}{\mathrm{L}_{50}^{\mathrm{n}} + [\mathrm{A}]^{\mathrm{n}}}$$

Equation 4

Schild plots were fitted using the Schild equation, displayed in Equation 5, where '*r*' refers to the dose ratio (the ratio of agonist concentrations required to produce a specific response in the presence and absence of antagonist), '[*B*]' is the antagonist concentration and 'K_D' is the equilibrium dissociation constant (Arunlakshana and Schild, 1959; Tallarida and Murray, 1987).

$$\mathrm{Log(r-1) = Log[B] - Log(K_D)}$$

Equation 5

Subsequent log K_D values were determined by employing the linear regression line, as stated in Equation 6, where '*y*' and '*x*' refer to the respective values of the y-axis and x-axis, '*m*' is the slope of the line and '*c*' is the y-axis intercept. The x-axis intercept provides the antagonist log K_D value.

$$\mathrm{y = mx + c}$$

Equation 6

When determining the affinity of a partial agonist, the Gaddum equation was modified using the method described by Stephenson (1956), shown in Equation 7, where 'K_D' is the equilibrium dissociation constant, '[*B*]' is the partial agonist concentration, '[A_1]' is the concentration of the agonist when the response magnitude is equal in the presence or absence of the partial agonist, '[A_2]' is the concentration of the agonist causing a selected response level in absence of the partial agonist and '[A_3]' is the concentration of the agonist causing the same selected level of response in presence of the partial agonist (Stephenson, 1956).

$$K_D = \frac{Y \times [B]}{1 - Y}$$

$$Y = \frac{[A_1] - [A_2]}{[A_3]}$$

Equation 7

To determine receptor melting temperature (T_m) values, the Boltzmann sigmoidal equation, displayed in Equation 8, was applied to receptor melting curves whereby '*Y*' is the relative concentration of the receptor in the unfolded state, '*X*' is the temperature, 'T_m' is the temperature at which half of the receptors are unfolded (melting temperature) and '*Bottom*', '*Top*' and '*Slope*' refer to the bottom, top and slope of the sigmoidal curve, respectively (Dubois et al., 2009).

$$Y = Bottom + \frac{(Top - Bottom)}{1 + \exp \times \left(\frac{T_m - X}{Slope}\right)}$$

Equation 8

For F-propranolol saturation binding, the total and non-specific (NSB) data were fit globally to a one-site binding model equation, shown in Equation 9, where 'B_{max}' is the maximal specific binding, '*[L]*' is the concentration of the fluorescent ligand, 'K_D' is the equilibrium dissociation constant, '*slope*' refers to the slope of the linear non-specific binding and '*Background*' is the Y-axis intercept (Sykes and Charlton, 2018).

$$\text{Total binding} = \left(\frac{B_{max} \times [L]}{(K_D + [L])}\right) + (Slope \times [L] + Background)$$

Equation 9

Specific binding for F-propranolol at equilibrium was obtained by subtracting NSB from total binding and was fitted to a one-site binding model equation, shown in Equation 10, where 'B_{max}' is the maximal specific binding, '*[L]*' is the concentration of the fluorescent ligand and 'K_D' is the equilibrium dissociation constant (Sykes and Charlton, 2018).

$$\text{Specific binding} = \frac{\mathrm{B_{max}} \times [\mathrm{L}]}{(\mathrm{K_D} + [\mathrm{L}])}$$

Equation 10

The specific binding kinetics of the F-propranolol tracer were fitted globally to simultaneously calculate k_{on} and k_{off} values using an association kinetics equation, shown in Equation 11, where 'k_{obs}' refers to the observed rate of association, '*[L]*' is the concentration of the fluorescent ligand, 'k_{on}' is the association rate constant, 'k_{off}' is the dissociation rate constant, '*Y*' refers to the level of receptor-bound fluorescent ligand, 'Y_{max}' is the maximal level of receptor-bound fluorescent ligand (at equilibrium) and '*X*' is units of time (Bosma et al., 2017).

$$\mathrm{k_{obs}} = [\mathrm{L}] \times \mathrm{k_{on}} + \mathrm{k_{off}}$$

$$\mathrm{Y} = \mathrm{Y_{max}} \times \left(1 - \exp\left(-1 \times \mathrm{k_{obs}} \times \mathrm{X}\right)\right)$$

Equation 11

The equilibrium binding data for competing unlabelled ligands were fitted to a one-site binding model equation, stated in Equation 12, where '*Y*' refers to the level of receptor-bound fluorescent ligand, '*Log* IC_{50}' is the logarithmic concentration of the unlabelled ligand which displaces 50% of the fluorescent ligand binding and '*Bottom*' and '*Top*' refer to the bottom and top of the specific binding curve, respectively (Sykes and Charlton, 2018).

$$\mathrm{Y} = \frac{(\mathrm{Top} - \mathrm{Bottom})}{(1 + 10^{(\mathrm{X} - \mathrm{Log\,IC_{50}})}) + \mathrm{Bottom}}$$

Equation 12

The IC_{50} values calculated from the competitive ligand inhibition curves were then used to determine K_I values using the method developed by Cheng and Prusoff (1973), displayed in Equation 13, where 'K_I' is the inhibition constant of the unlabelled ligand, 'IC_{50}' is the concentration of the unlabelled ligand which displaces 50% of the fluorescent ligand binding, '*[L]*' is the concentration of the

fluorescent ligand and 'K_D' is the equilibrium dissociation constant of the fluorescent ligand.

$$K_I = \frac{IC_{50}}{1 + \left(\frac{[L]}{K_D}\right)}$$

Equation 13

The specific binding kinetics of the competitive unlabelled ligands were fitted to the model developed by Motulsky and Mahan (1984) to determine k_{on} and k_{off} values using Equation 14, where 'K_1' refers to the k_{on} of the fluorescent ligand, 'K_2' refers to the k_{off} of the fluorescent ligand, 'K_3' refers to the k_{on} of the unlabelled ligand, 'K_4' refers to the k_{off} of the unlabelled ligand, '*[L]*' is the concentration of the fluorescent ligand, '*[I]*' is the concentration of the unlabelled ligand, 'B_{max}' is the maximal specific binding, '*Y*' refers to the specific binding and '*X*' is units of time.

$$K_A = K_1[L] + K_2$$

$$K_B = K_3[I] + K_4$$

$$S = \sqrt{((K_A - K_B)^2 + 4 \times K_1 \times K_3 \times L \times I \times 10^{-18})}$$

$$K_F = 0.5 \times (K_A + K_B + S)$$

$$K_S = 0.5 \times (K_A + K_B - S)$$

$$Q = \frac{B_{max} \times K_1 \times L \times 10^{-9}}{K_F - K_S}$$

$$Y = Q \times \left(\frac{K_4 \times (K_F - K_S}{K_F \times K_S} + \frac{K_4 - K_F}{K_F}\exp^{(-K_F \times X)} - \frac{K_4 \times K_S}{K_S}\exp^{(-K_S \times X)}\right)$$

Equation 14

2.12.4 – Statistical analysis

Statistical analyses were also performed using GraphPad Prism 8 software (San Diego, CA, USA). Statistical significance of data was tested using unpaired, two-tailed *t*-test or either one-way or two-way ANOVA and Tukey's multiple comparisons test. Post-hoc tests were run only if F achieved $P < 0.05$ and there was no significant variance inhomogeneity. The relevant statistical test used is stated in each case. Throughout the study, $P < 0.05$ was used as the level for significance ($P \geq 0.05$ = ns, $P < 0.05$ = *, $P < 0.01$ = **, $P < 0.001$ = ***, $P < 0.0001$ = ****).

Chapter 3

Pharmacological and kinetic analysis of endogenous β_2-adrenoceptor-mediated cAMP GloSensor^{TM} responses in HEK293 cells

3.1 – Introduction

Conventionally in pharmacological studies of receptors, various ligand concentrations are employed and functional responses are measured at a set time-point, or at a peak response level, in order to construct concentration-response curves from which classic pharmacological ligand parameters can be determined such as efficacy (maximal response; E_{max}) and potency (EC_{50}) (Stephenson, 1956; Black and Leff, 1983; Kenakin, 2009; Zhu et al., 2019; Finlay et al., 2020; Hoare et al., 2020b). Subsequent comparisons of relative ligand activities has helped to provide new insights into the mechanisms underlying ligand-receptor interactions, which is crucial for the development of improved therapeutics (Kenakin, 2019; Zhao and Furness, 2019). However, this standard pharmacological analysis assumes that the system is in a state of equilibrium, which often is not actually the case. Furthermore, it cannot distinguish between the mechanism responsible for generating the signal (transduction by the agonist-occupied receptor) and those which counteract the signal, causing it to decline (regulatory mechanisms including receptor desensitisation and breakdown of second messengers like cAMP) (Moore et al., 2007a; Zhu et al., 2019; Hoare et al., 2020b; Hoare et al., 2022). This can distort the observed parameters for efficacy and potency taken from measurements at distinct time-points, or at the peak response in non-equilibrium conditions (Klein Herenbrink et al., 2016; Bdioui et al., 2018; Zhu et al., 2019; Hoare et al., 2022), which may account for the discrepancies between these ligand parameters in the literature.

Recently, there has been an increased focus on GPCR signalling kinetics. Newly developed biosensors have allowed the continuous measurement of GPCR signals over a period, which has made it possible to visualise and quantify the entire time-course of a receptor response (Lohse et al., 2008; Lohse et al., 2012; Goulding et al., 2018; Greenwald et al., 2018; Dijon et al., 2021; Wright and Bouvier, 2021). Hoare et al. (2020b) have now derived equations with can fit these time-course data to a curve, enabling kinetic parameters of the signal to be calculated, including the maximal initial rate of signal generation (IR_{max}), which is related to ligand efficacy, and kinetic potency (L_{50}) (Hoare et al., 2020b; Hoare et al., 2022). According to Hoare et al. (2020b), most time-course data fit within

one of four classic curve shapes based upon the nature of the regulatory mechanisms involved, each of which can be defined by a distinct equation. The initial rate parameter quantifies the initial linear generation of the signal immediately after ligand addition, prior to the onset of the counteractive effect of the regulation (Hoare et al., 2020b; Hoare et al., 2022). The regulatory mechanisms can also be defined by the two rate constants, k_1 and k_2 (Hoare et al., 2020b; Hoare et al., 2022). Previous analyses of time-course data have already expanded our understanding of receptor regulation (Shear et al., 1976; Paek et al., 2017), biased signalling (Klein Herenbrink et al., 2016; Lane et al., 2017; Hoare et al., 2020a) and new spatiotemporal mechanisms including internalised GPCR signalling (Calebiro et al., 2009; Ferrandon et al., 2009; Irannejad et al., 2013). Applying this new kinetic analysis to functional time-course data could uncover new insights into both the pharmacological and kinetic properties of ligands and improve the characterisation of ligand-receptor interactions.

This study has utilised real-time measurements of luminescence using the cAMP GloSensor™ biosensor (Promega, Maddison, WI, USA) to detect changes in β_2AR-mediated cAMP production under low, endogenous receptor expression in HEK293 cells (Friedman et al., 2002; Thomas and Smart, 2005; Goulding et al., 2021a; Goulding et al., 2021b). The cAMP GloSensor™ biosensor comprises a firefly luciferase enzyme which is genetically fused to the cAMP-binding domain of a regulatory subunit (RIIβB) of protein kinase A (PKA) (Fan et al., 2008; Binkowski et al., 2011). The binding of cAMP to the PKA subunit causes a conformational shift in the luciferase enzyme to an active state, catalysing the oxidation of the enzyme substrate 'GloSensor™ reagent' (a derivative of the endogenous substrate luciferin), which results in an increase in the emission of luminescence (Fan et al., 2008; Binkowski et al., 2011). The measured luminescence intensity is proportional to relative cytosolic cAMP concentration, hence this technique indirectly measures β_2AR functional activity. Here, the kinetics of agonist-mediated β_2AR responses were monitored by curve fitting cAMP GloSensor™ luminescence time-course data according to the method outlined by Hoare et al. (2020b). Classic pharmacological ligand parameters (E_{max}, log EC_{50}) are compared with equivalent newly established kinetic

parameters (IR_{max}, log L_{50}) for several β_2AR agonists in live cells endogenously expressing the receptor at very low levels (Friedman et al., 2002; Thomas and Smart, 2005; Goulding et al., 2021a; Goulding et al., 2021b). Additionally, the impact of β_2AR competitive antagonists of differing dissociation rates on agonist pharmacological and kinetic parameters under hemi-equilibrium conditions is assessed. Finally, estimates for ligand binding affinities at the β_2AR are made and compared using both standard peak response data and also kinetic initial rates. Much of the data presented in this Chapter has recently been published in *British Journal of Pharmacology* (Cullum et al., 2023).

3.2 – Materials and methods

Cell culture

HEK293 cells stably expressing the cAMP GloSensor™ biosensor (HEK293Gwt) were used throughout this Chapter and were passaged and seeded into 96-well assay plates as described previously in Chapter 2 (See 2.4 – Cell culture).

cAMP GloSensor™ assay

All of the data presented in this Chapter were obtained by performing the cAMP GloSensor™ assay. This technique was performed as described in Chapter 2 (see 2.7 – cAMP GloSensor™ assay).

Data analysis and statistics

Analysis of the data was carried out as stated in Chapter 2 (see 2.12 – Data analysis and statistics).

3.3 – Results

3.3.1 – Initial characterisation of the cAMP GloSensor™ luminescence assay

Initial attempts to characterise cAMP production in HEK293 cells stably expressing the cAMP GloSensor™ biosensor were performed by measurement of luminescence immediately after application of a variety of ligands acting at distinct targets within the cells. These cells are referred to throughout as HEK293G wildtype (HEK293Gwt) cells as they do not overexpress any target receptors and instead the native, endogenously expressed receptor responses were being studied. Forskolin directly activates the cAMP-synthesising adenylate cyclase enzyme by binding in the catalytic cleft of the enzyme (Seamon and Daly, 1981; Zhang et al., 1997). Isoprenaline and salmeterol are both agonists of the β_2-adrenoceptor (β_2AR) which is expressed in HEK293 cells at low levels (Friedman et al., 2002; Thomas and Smart, 2005; Goulding et al., 2021a; Goulding et al., 2021b), but comprise differing intrinsic efficacies for the receptor, with isoprenaline generally being considered a full agonist while salmeterol is classed as a partial agonist. NECA instead acts as a non-selective adenosine receptor agonist, therefore targeting both A_{2A} and A_{2B} receptors (A_{2A}AR and A_{2B}AR) which are also expressed in HEK293 cells (Cooper et al., 1997; Thomas and Smart, 2005; Goulding et al., 2018). Activation of the β_2AR, A_{2A}AR and A_{2B}AR indirectly promote the production of cAMP via their coupling to the adenylate cyclase stimulatory G_s protein (Stiles et al., 1984; Fredholm et al., 1994). 8-chlorophenylthio-cAMP (8-CPT-cAMP) is a highly cell membrane-permeable analogue of cAMP which has been used as an agonist of cAMP-dependent pathways due to its ability to mimic the action of cAMP (Connolly et al., 1992; Parvathenani et al., 1998; Won and Oh, 2000; Li et al., 2016). It should therefore bind to the PKA regulatory subunit of the GloSensor™ biosensor directly to induce the conformational rearrangement of the firefly luciferase enzyme, resulting in the measured luminescence emission.

The transient changes in cAMP GloSensor™ luminescence measured over 60 min after application of maximal concentrations of forskolin (100 μM)

isoprenaline (1 μM), salmeterol (1 μM), NECA (10 μM) and 8-CPT-cAMP (100 μM), as well as a vehicle control (HBSS) to HEK293Gwt cells are shown in Figure 3.1A. Each ligand initially stimulated a rapid increase in luminescence to a peak level, indicating increased concentration of cAMP inside the cells, followed by a decline of the signal back towards the baseline as the cytosolic cAMP concentration subsequently decreases. The profile of these time-course data varied greatly between the tested ligands. For example, the cAMP response produced by salmeterol achieved a vastly diminished peak amplitude when compared with that of isoprenaline (isoprenaline E_{max}: 70.62% ± 5.09% of 100 μM forskolin E_{max}, salmeterol E_{max}: 24.04% ± 2.04%; $P < 0.0001$), owing to its reduced efficacy for activating the β_2AR. Meanwhile, although the peak response produced by NECA is similar to that of isoprenaline ($P > 0.05$), after reaching its peak the NECA response declines at a visibly slower rate. Although the forskolin-mediated cAMP response also decays at a relatively slow rate, the direct action of 8-CPT-cAMP at the GloSensor^{TM} biosensor elicits much slower rates of both the stimulation and degradation phases of the response compared with any of the other tested ligands. Interestingly, the application of HEPES buffered saline solution (HBSS) as the vehicle control also caused a small but notable cAMP response. By testing each of the ligands at a range of concentrations, concentration-response curves were generated, displayed in Figure 3.1B, by normalising the peak response produced at each concentration of the ligands between the maximal 100 μM forskolin response (100%) and the vehicle control response (0%) and fitting to a standard sigmoidal curve using the Hill equation (Equation 1). Each ligand stimulated cAMP production in a concentration-dependent manner, and the potencies (log EC_{50}) and relative maximal responses (E_{max}) of each ligand were calculated and are shown in Table 3.1. No log EC_{50} value was determined for 8-CPT-cAMP because the response did not reach the top of the curve within the tested concentration range.

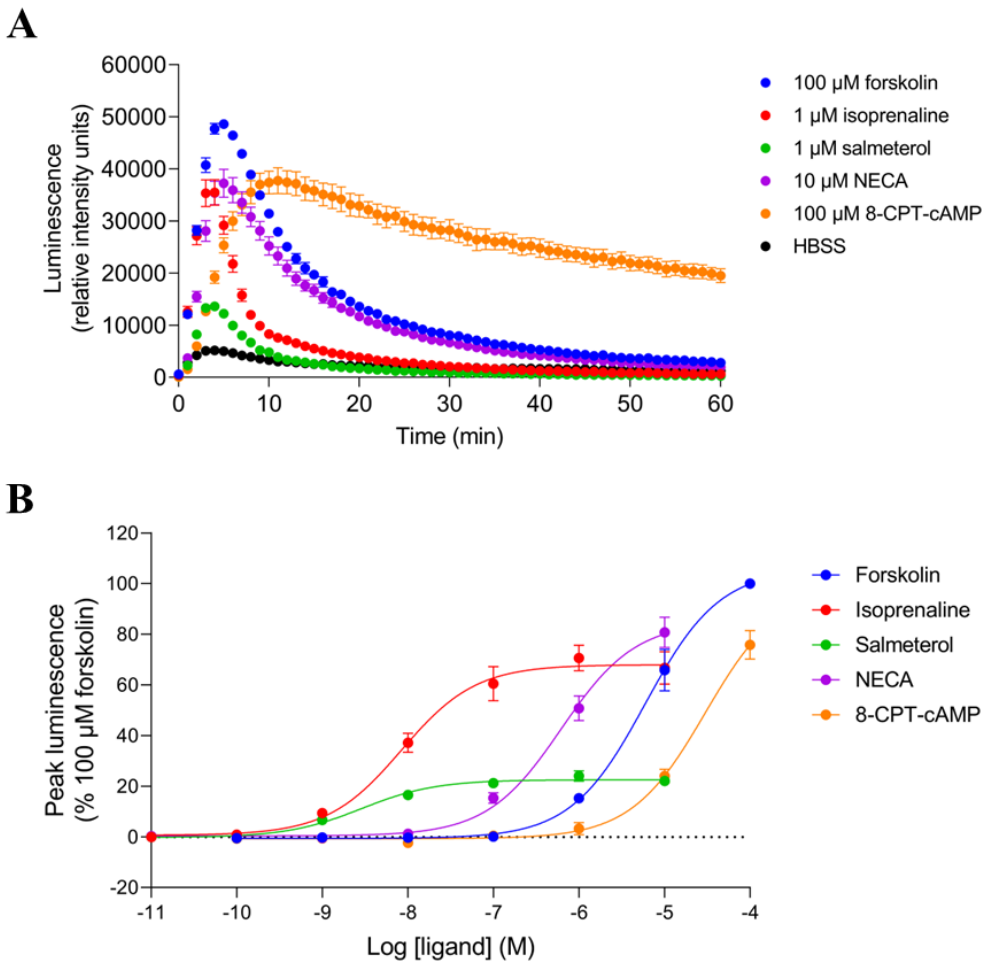

Figure 3.1: GloSensor™ luminescence stimulated by ligand-mediated cAMP production. (A) Representative GloSensor™ luminescence time-course data in one experiment over 60 min following application of maximal concentrations of forskolin (100 µM), isoprenaline (1 µM), salmeterol (1 µM), NECA (10 µM) and 8-CPT-cAMP (100 µM), as well as HBSS (vehicle) to HEK293Gwt cells. Data points represent mean ± standard error of mean (SEM) of triplicate measurements, expressed as relative intensity units (RIU) of luminescence. Similar data were obtained in five independent experiments. (B) Mean peak concentration-response curves for forskolin, isoprenaline, salmeterol, NECA and 8-CPT-cAMP in HEK293Gwt cells expressed as a percentage of 100 µM forskolin. Data points represent mean ± SEM from five independent experiments (n = 5). Significant differences were determined by a one-way ANOVA with Tukey's multiple comparisons test.

Ligand	E_{max} (% 100 µM forskolin) ± SEM	Log EC_{50} (M) ± SEM
Forskolin	100	-5.18 ± 0.13
Isoprenaline	70.62 ± 5.09	-8.08 ± 0.11
Salmeterol	24.04 ± 2.04	-8.53 ± 0.05
NECA	80.77 ± 6.00	-6.21 ± 0.01
8-CPT-cAMP	75.85 ± 5.65	N/A

Table 3.1: Ligand mean E_{max} and log EC_{50} values ± SEM determined for forskolin, isoprenaline, salmeterol, NECA and 8-CPT-cAMP from concentration-response curves obtained by cAMP GloSensor^{TM} in HEK293Gwt cells from five independent experiments (n = 5). No log EC_{50} value was determined for 8-CPT-cAMP.

Because catecholamines (including isoprenaline) are known to degrade rapidly due to oxidation, isoprenaline responses were compared in the presence and absence of the antioxidant ascorbic acid (0.01% added in the HBSS buffer; Figures 3.2A and 3.2B), which prevents catecholamine oxidation (Bendich et al., 1986; Hughes and Smith, 2011). However, the addition of ascorbic acid had no effect on the maximal response achieved by isoprenaline (E_{max}: 59.33% ± 6.81% of 100 μM forskolin compared with 64.00% ± 9.69%; $P > 0.05$) or its measured potency (log EC_{50}: -8.14 ± 0.13 compared with -8.16 ± 0.15; $P > 0.05$) in these experiments. In addition, no change was seen on the profile of the time-course of isoprenaline response.

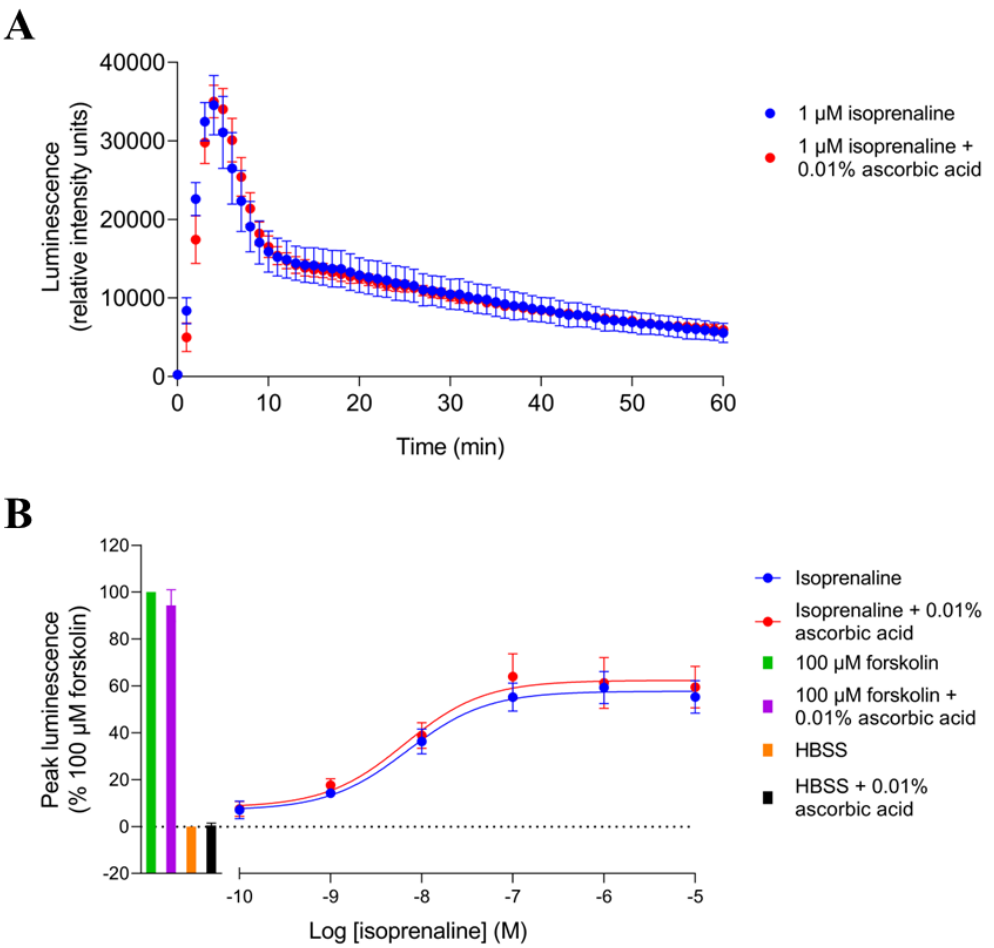

Figure 3.2: GloSensor™ luminescence stimulated by isoprenaline in the presence and absence of ascorbic acid. (A) Combined GloSensor™ luminescence time-course data over 60 min following application of 1 µM isoprenaline in the presence and absence of 0.01% ascorbic acid to HEK293Gwt cells. Data points represent mean ± SEM, expressed as relative intensity units (RIU) of luminescence, from three independent experiments (n = 3). (B) Mean peak concentration-response curves for isoprenaline in the presence and absence of 0.01% ascorbic acid, plus 100 µM forskolin and HBSS (vehicle) controls in HEK293Gwt cells, expressed as a percentage of 100 µM forskolin. Data points represent mean ± SEM from three independent experiments (n = 3). Significant differences were determined by an unpaired t-test.

It has previously been shown that the cAMP-synthesising adenylate cyclase enzyme displays a synergistic activation by forskolin and $G_{\alpha s}$ protein, whereby the presence of forskolin increases the binding affinity of $G_{\alpha s}$ to the enzyme, and vice-versa, (Dessauer et al., 1997; Insel and Ostrom, 2003), and the simultaneous binding of both potentiates adenylate cyclase activation and subsequent production of cAMP (Darfler et al., 1982; McHugh Sutkowski et al., 1994; Insel and Ostrom, 2003). Therefore, to determine whether forskolin had any potentiating effects on β_2AR-mediated GloSensor^{TM} cAMP production, HEK293Gwt cells were treated with a concentration range of isoprenaline or HBSS (vehicle) in the presence or absence of 30 min preincubated 10 nM forskolin. On its own this low concentration of forskolin would elicit minimal or no stimulation of cAMP production. As shown in Figure 3.3, preincubated forskolin did amplify the peak isoprenaline response, albeit only to a small degree (23.03% ± 9.86% increase in peak isoprenaline response, as a percentage of 1 μM isoprenaline response; $P < 0.05$). Forskolin had no effect on the potency of isoprenaline, however (isoprenaline log EC_{50}: -8.17 ± 0.04, compared with isoprenaline + 10 nM forskolin log EC_{50}: -8.20 ± 0.04; $P > 0.05$). Moreover, application of 10 nM forskolin alone did elicit a modest but significant response over basal in this assay (4.37% ± 0.87%; $P < 0.01$).

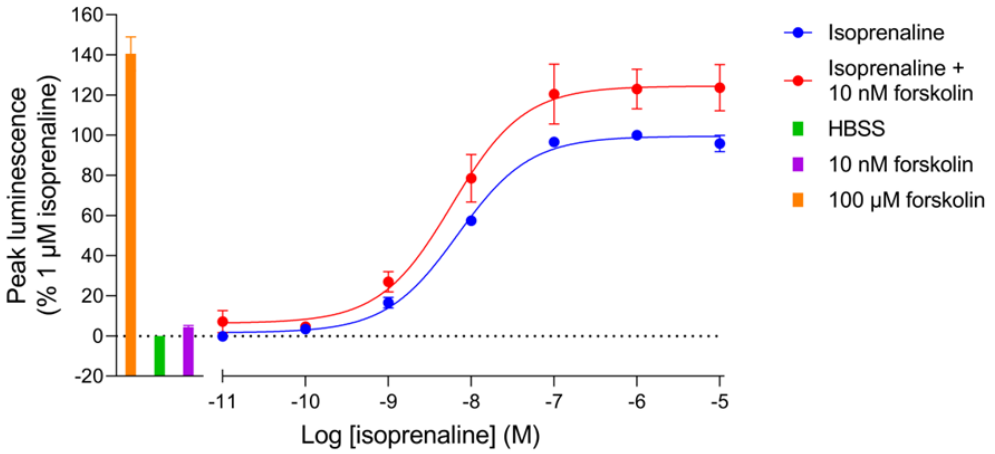

Figure 3.3: GloSensor^{TM} luminescence stimulated by isoprenaline in the presence and absence of 30 min preincubated forskolin. Mean peak concentration-response curves for isoprenaline in the presence and absence of 10 nM forskolin, plus 100 µM forskolin, 10 nM forskolin and HBSS (vehicle) controls in HEK293Gwt cells, expressed as a percentage of 1 µM isoprenaline. Data points represent mean ± SEM from five independent experiments (n = 5). Significant differences were determined by an unpaired t-test.

Cyclic nucleotide phosphodiesterases (PDEs) are cytosolic enzymes which hydrolyse the phosphodiester bonds of cyclic nucleotides to convert them to their non-cyclical counterpart, for example cAMP to AMP, thus regulating second messenger concentration inside cells (Francis et al., 2000; Ghosh et al., 2009). The use of inhibitors of PDEs has thus been exploited extensively to amplify and prolong cAMP responses by preventing breakdown of the cyclic nucleotide (Morgan et al., 1993; Hopkinson et al., 2000; Ghosh et al., 2009). In order to better understand the role that PDEs play in shaping receptor responses by degradation of cAMP, PDE inhibitors were tested in the cAMP GloSensor^{TM} luminescence assay. Figure 3.4A shows the effect of 30 min preincubation of two PDE inhibitors, the non-selective IBMX (100 μM) and the PDE4-selective rolipram (10 μM) on the time-course of the maximal isoprenaline response (1 μM), while Figures 3.4C (peak) and 3.4D (AUC) display the effect of varying concentrations of the PDE inhibitors on the maximal isoprenaline cAMP response. Both IBMX (85.19% ± 9.26% increase at 100 μM; $P < 0.0001$) and rolipram (58.24% ± 4.22% increase at 10 μM; $P < 0.05$) concentration-dependently amplified the peak magnitude of the isoprenaline-mediated cAMP response. The effect on the AUC was even more pronounced, with both PDE inhibitors prolonging the duration of the response by reducing the rate of signal decay (410% ± 29.06% increase by 100 μM IBMX; $P < 0.0001$; 246.57% ± 9.32% increase by 10 μM rolipram; $P < 0.001$). IBMX and rolipram enhanced both peak ($P > 0.05$) and AUC ($P > 0.05$) isoprenaline responses similarly. Addition of both IBMX and rolipram simultaneously did not significantly potentiate the peak response further than IBMX alone (97.99% ± 14.79% increase by 100 μM IBMX + 1 μM rolipram, compared with 85.19% ± 9.26% increase by 100 μM IBMX alone; $P > 0.05$), whereas it considerably further enhanced the total AUC response (645.66% ± 55.08% increase by 100 μM IBMX + 1 μM rolipram, compared with 410% ± 29.06% increase by 100 μM IBMX alone; $P < 0.01$). Finally, addition of IBMX (288.76% ± 57.63% increase in peak at 100 μM; $P < 0.0001$; 283.94% ± 39.97% increase in AUC; $P < 0.0001$) but not rolipram (40.54% ± 25.21% increase by 10 μM; $P > 0.05$; 51.79% ± 19.26% increase in AUC; $P > 0.05$) also potentiated the small basal response after application of vehicle control (HBSS), displayed in Figures 3.4B, 3.4E and

3.4F. Tables 3.2 and 3.3 summarise the effects of PDE inhibitors on the isoprenaline and HBSS response, respectively.

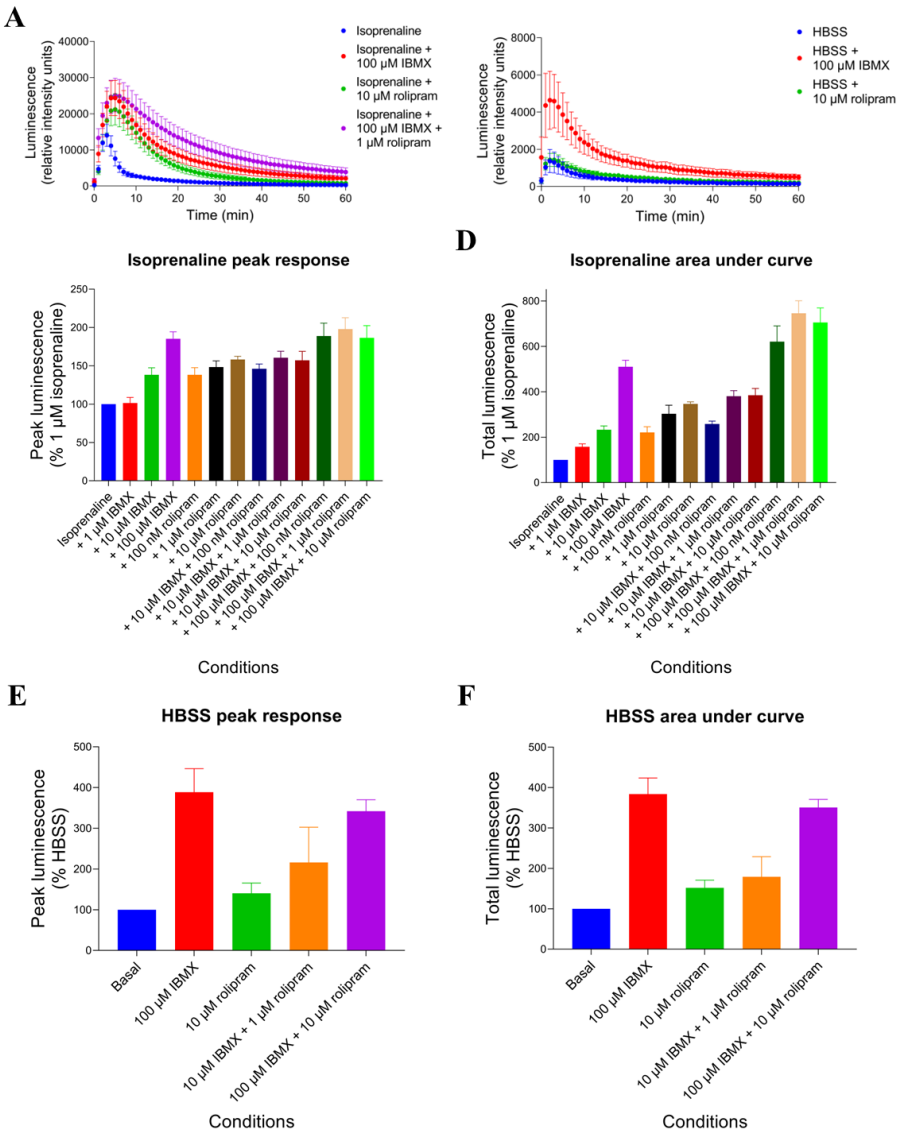

Figure 3.4: GloSensor™ luminescence stimulated by isoprenaline or HBSS (vehicle) in the presence and absence of 30 min preincubated phosphodiesterase (PDE) inhibitors. (A, B) Combined GloSensor™ luminescence time-course data over 60 min following application of 1 µM isoprenaline (A) or HBSS (vehicle; B) in the presence and absence of 100 µM IBMX, 10 µM rolipram or 100 µM IBMX plus 1 µM rolipram (A only) to HEK293Gwt cells. Data points represent mean ± SEM, expressed as relative intensity units (RIU) of luminescence, from five independent experiments (n = 5). (C-F) Bar charts displaying mean peak response (C, E) and AUC (D, F) for 1 µM isoprenaline (C, D) or HBSS (vehicle; E, F) in the presence and absence of IBMX (1 µM – 100 µM), rolipram (100 nM – 10 µM), or both in HEK293Gwt cells, expressed as a percentage of 1 µM isoprenaline (C, D) or HBSS (vehicle; E, F). Data points represent mean ± SEM from five independent experiments (n = 5).

Condition	Peak response (% 1 µM isoprenaline) ± SEM	AUC (% 1 µM isoprenaline) ± SEM
Isoprenaline	100	100
Isoprenaline + 1 µM IBMX	101.48 ± 7.25	157.73 ± 13.21
Isoprenaline + 10 µM IBMX	138.25 ± 9.21	232.62 ± 16.83
Isoprenaline + 100 µM IBMX	185.19 ± 9.26 ****	510.01 ± 29.06 ****
Isoprenaline + 100 nM rolipram	138.23 ± 9.44	221.31 ± 24.89
Isoprenaline + 1 µM rolipram	148.37 ± 8.18	303.09 ± 37.84 *
Isoprenaline + 10 µM rolipram	158.24 ± 4.22 *	346.57 ± 9.32 ***
Isoprenaline + 10 µM IBMX + 100 nM rolipram	146.21 ± 6.19	257.94 ± 13.39
Isoprenaline + 10 µM IBMX + 1 µM rolipram	160.58 ± 8.53 **	380.47 ± 24.74 ****
Isoprenaline + 10 µM IBMX + 10 µM rolipram	157.25 ± 11.75 *	385.02 ± 29.93 ****
Isoprenaline + 100 µM IBMX + 100 nM rolipram	188.88 ± 16.90 ****	620.86 ± 69.10 ****

Isoprenaline + 100 μM IBMX + 1 μM rolipram	197.99 ± 14.79 ****	745.66 ± 55.08 ****
Isoprenaline + 100 μM IBMX + 10 μM rolipram	186.47 ± 16.14 ****	705.00 ± 64.57 ****

Table 3.2: Isoprenaline mean peak response and AUC ± SEM determined in the presence and absence of increasing concentrations of the PDE inhibitors IBMX, rolipram or both, expressed as a percentage of 1 μM isoprenaline obtained by cAMP GloSensor^{TM} in HEK293Gwt cells from five independent experiments (n = 5). Significant differences in isoprenaline peak response and AUC to those seen in absence of PDE inhibitors are indicated, determined by a one-way ANOVA with Tukey's multiple comparisons test. $P < 0.05$ was used as the level for significance ($P < 0.05$ = *, $P < 0.01$ = **, $P < 0.001$ = ***, $P < 0.0001$ = ****).

Condition	Peak response (% HBSS) ± SEM	AUC (% HBSS) ± SEM
HBSS	100	100
HBSS + 100 μM IBMX	388.76 ± 57.63 **	383.94 ± 39.97 ****
HBSS + 10 μM rolipram	140.54 ± 25.21	151.79 ± 19.26
HBSS + 10 μM IBMX + 1 μM rolipram	216.14 ± 86.42	179.10 ± 49.85
HBSS + 100 μM IBMX + 10 μM rolipram	342.02 ± 28.17 *	350.80 ± 19.81 ***

Table 3.3: HBSS (vehicle) mean peak response and AUC ± SEM determined in the presence and absence of the PDE inhibitors IBMX, rolipram or both, expressed as a percentage of HBSS (vehicle) obtained by cAMP GloSensor^{TM} in HEK293Gwt cells from five independent experiments (n = 5). Significant differences in isoprenaline peak response and AUC to those seen in absence of PDE inhibitors are indicated, determined by a one-way ANOVA with Tukey's multiple comparisons test. $P < 0.05$ was used as the level for significance ($P < 0.05$ = *, $P < 0.01$ = **, $P < 0.001$ = ***, $P < 0.0001$ = ****).

3.3.2 – Pharmacological and kinetic characterisation of β_2-adrenoceptor agonist activity under endogenous receptor expression

Four distinct β_2AR agonists were used in order to perform pharmacological and kinetic analyses of β_2AR-mediated cAMP responses using the cAMP GloSensor^{TM} assay. Two of these ligands, isoprenaline and formoterol, are considered full agonists with relatively high efficacy for β_2AR activation, while the other two, salbutamol and salmeterol, are partial agonists with lower efficacy (Baker et al., 2003b; Baker et al., 2003a; Hoffmann et al., 2004; Baker, 2010). Combined time-course data for each agonist and forskolin are presented in Figure 3.5A, whilst individual representative traces fitted with kinetic curve fitting according to Hoare et al. (2020b) are shown in Figures 3.5B-3.5F. Throughout the rest of Chapter 3, all GloSensor^{TM} time-course data has been 'baseline-corrected' (by subtraction of the HBSS response at equivalent time-points) in order to adjust for the small vehicle control response observed throughout these assays, which likely results from activation of other endogenous receptors in HEK293 cells (discussed in Chapter 4). This also aided in the proper fitting of the kinetic equation to the time-course data. Peak luminescence values produced by each concentration of ligand were normalised against 1 μM isoprenaline and taken to construct peak concentration-response curves, fitted to a standard sigmoidal curve using the Hill equation (Equation 1), displayed in Figure 3.6. Each ligand stimulated a concentration-dependent cAMP response. The largest peak response was produced by 100 μM forskolin. Comparing the β_2AR ligands, maximal responses of the full agonists isoprenaline and formoterol were similar ($P > 0.05$), although formoterol elicited a 10-fold more potent response than isoprenaline ($P < 0.0001$). Both partial agonists salbutamol and salmeterol produced considerably reduced maximal responses compared with both isoprenaline and formoterol ($P < 0.0001$ in each case). Additionally, salbutamol and salmeterol maximal responses were similar ($P > 0.05$), albeit salmeterol acted with almost 100-fold more potency for the β_2AR. A full summary of the calculated maximal responses (E_{max}) and potencies (log EC_{50}) for each β_2AR ligand is shown in Table 3.4.

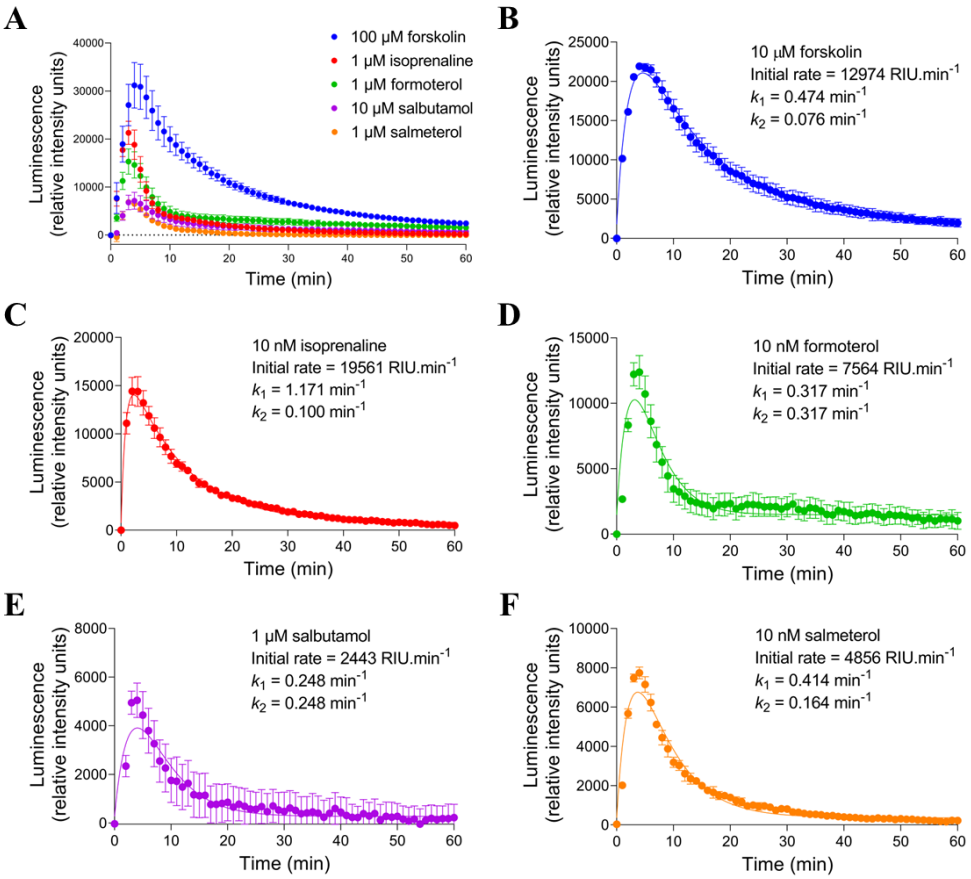

Figure 3.5: GloSensor™ luminescence stimulated by ligand-mediated cAMP production. (A) Combined GloSensor™ luminescence time-course data over 60 min following application of maximal concentrations of forskolin (100 µM), isoprenaline (1 µM), formoterol (1 µM), salbutamol (10 µM) and salmeterol (1 µM) to HEK293Gwt cells. Data points represent mean ± SEM, expressed as relative intensity units (RIU) of luminescence, from five independent experiments (n = 5). (B-F) Representative GloSensor™ luminescence time-course data in one experiment over 60 min following application of 10 µM forskolin (B), 10 nM isoprenaline (C), 10 nM formoterol (D), 1 µM salbutamol (E) and 10 nM salmeterol (F) to HEK293Gwt cells, fitted with time-course curve fitting according to Hoare et al. (2020b). Derived kinetic parameters (initial rate, k_1 and k_2 values) are displayed for each ligand. Data points represent mean ± SEM of triplicate measurements, expressed as relative intensity units (RIU) of luminescence. Similar data were obtained in five independent experiments.

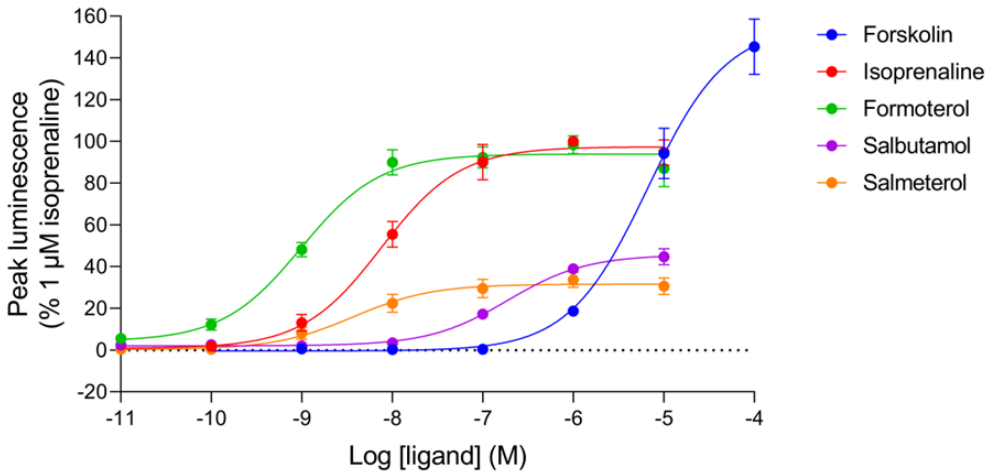

Figure 3.6: GloSensor™ luminescence stimulated by ligand-mediated cAMP production. Mean peak concentration-response curves for forskolin, isoprenaline, formoterol, salbutamol and salmeterol in HEK293Gwt cells expressed as a percentage of 1 µM isoprenaline. Data points represent mean ± SEM from five independent experiments (n = 5). Significant differences were determined by a one-way ANOVA with Tukey's multiple comparisons test.

Curve fitting of time-course data to a kinetic equation (Equation 3) according to Hoare et al. (2020b) allowed for quantification of kinetic parameters of the signal, including the initial rate of signal generation, as well as two rate constants, k_1 and k_2, relating to the regulatory mechanisms responsible for attenuating the receptor response (receptor desensitisation) and the degradation of cAMP (phosphodiesterase activity). This was presented graphically in Chapter 2 (Figure 2.7). Determined initial rate parameters for increasing concentrations of isoprenaline are depicted by the dashed lines in Figure 3.7A, whereby the steepening gradient of the lines indicates the acceleration in the initial rate of signal generation with increasing ligand concentration, up to a maximal level. For clarity, just the first five minutes of response after isoprenaline addition are shown in this graph. As with peak response, the initial rate parameter for each ligand increased concentration-dependently and these initial rate values were normalised against 1 μM isoprenaline. 'Initial rate' concentration-response curves were then generated and fitted to a sigmoidal curve using the modified Hill equation (Equation 4), shown in Figure 3.7B. Following a similar trend to the peak response data, isoprenaline and formoterol maximal initial rates were similar ($P > 0.05$), but formoterol kinetic potency was almost 10-fold higher ($P < 0.01$). Consistent with their partial agonism, salbutamol and salmeterol both showed markedly reduced maximal initial rates to those of isoprenaline and formoterol ($P < 0.0001$ in each case). Salbutamol and salmeterol maximal initial rates were also similar ($P > 0.05$), but salmeterol kinetic potency was much higher ($P < 0.0001$). The full set of calculated maximal initial rates (IR_{max}) and kinetic potencies (log L_{50}) are stated in Table 3.4 for comparison with E_{max} and log EC_{50} values. Direct comparison of the E_{max} and IR_{max} for each ligand has been performed in Figure 3.8, normalised against the reference ligand isoprenaline. The partial agonists salbutamol and salmeterol showed significantly reduced IR_{max} values compared with their E_{max} ($P < 0.05$ for both), relative to isoprenaline. Formoterol on the other hand showed no significant difference ($P > 0.05$). Moreover, the forskolin IR_{max} was also markedly reduced compared with its E_{max} ($P < 0.01$).

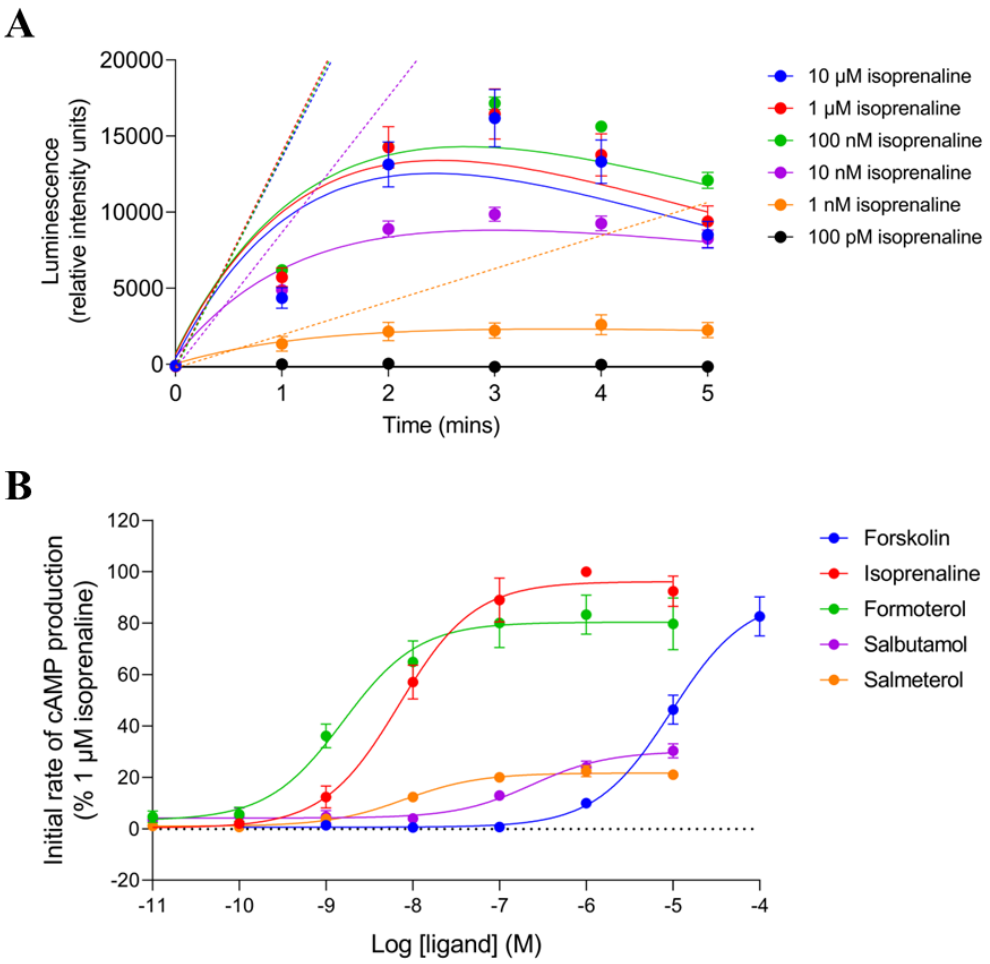

Figure 3.7: GloSensor™ luminescence stimulated by ligand-mediated cAMP production. (A) Representative GloSensor™ luminescence time-course data in one experiment over 5 min following application of isoprenaline (100 pM – 10 µM) to HEK293Gwt cells, fitted with time-course curve fitting, according to Hoare et al. (2020b), with derived initial rates represented by dashed lines. Data points represent mean ± SEM of triplicate measurements, expressed as relative intensity units (RIU) of luminescence. Similar data were obtained in five independent experiments. (B) Mean initial rate concentration-response curves for forskolin, isoprenaline, formoterol, salbutamol and salmeterol in HEK293Gwt cells expressed as a percentage of 1 µM isoprenaline. Data points represent mean ± SEM from five independent experiments (n = 5). Significant differences were determined by a one-way ANOVA with Tukey's multiple comparisons test.

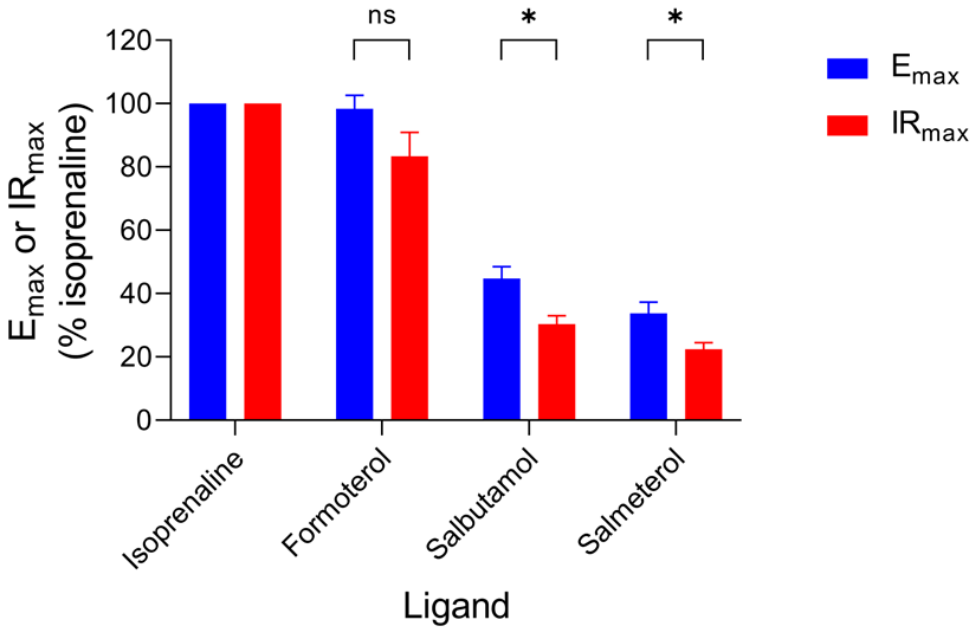

Figure 3.8: GloSensor^{TM} luminescence stimulated by agonist-mediated cAMP production. Bar chart comparisons of mean E_{max} and IR_{max} values for isoprenaline, formoterol, salbutamol and salmeterol, relative to isoprenaline in HEK293Gwt cells. Data points represent mean ± SEM expressed as a percentage of isoprenaline from five independent experiments (n = 5). Significant differences are indicated, determined by an unpaired t-test. $P < 0.05$ was used as the level for significance ($P \geq 0.05$ = ns, $P < 0.05$ = *).

Agonist	E_{max} (% 1 µM isoprenaline) ± SEM	IR_{max} (% 1 µM isoprenaline) ± SEM	Log EC_{50} (M) ± SEM	Log L_{50} (M) ± SEM
Isoprenaline	100	100	-8.10 ± 0.12	-8.13 ± 0.12
Formoterol	98.38 ± 4.31	83.36 ± 7.62	-9.00 ± 0.04	-8.80 ± 0.07
Salbutamol	44.74 ± 3.80	30.34 ± 2.75	-6.73 ± 0.01	-6.68 ± 0.14
Salmeterol	33.72 ± 3.60	22.41 ± 2.16	-8.39 ± 0.12	-8.08 ± 0.11

Table 3.4: Agonist mean E_{max}, IR_{max}, log EC_{50} and log L_{50} values ± SEM determined for isoprenaline, formoterol, salbutamol and salmeterol from concentration-response curves obtained by cAMP GloSensor™ in HEK293Gwt cells from five independent experiments (n = 5).

The time-course data throughout this study all show an initial increase in signal due to β_2AR-mediated stimulation of cAMP synthesis, followed by a decline back to baseline due to the action of regulatory mechanisms such as receptor desensitisation and breakdown of cAMP by PDEs (Hoare et al., 2020b). To assess the effect of PDEs on the kinetics of the β_2AR-mediated cAMP response, the nonselective PDE inhibitor IBMX and the PDE4-selective rolipram were used. As previously reported (see 3.3.1), both 100 μM IBMX ($P < 0.0001$) and 10 μM rolipram ($P < 0.01$) significantly increased peak 1 μM isoprenaline response (Figure 3.9B) and reduced the rate of decay of the signal. By applying the kinetic curve fitting to the isoprenaline time-course in the presence of the PDE inhibitors, as demonstrated in Figure 3.9A, kinetic parameters of the signal could also be calculated (Hoare et al., 2020b). Despite the marked effects on peak response, no change was observed in the initial rate of signal generation by isoprenaline by either PDE inhibitor ($P > 0.05$ for both; Figure 3.9C). Since the rate constants k_1 and k_2 relate to regulatory mechanisms including PDE-mediated breakdown of cAMP, the effect of PDE inhibitors on these rate constants was also of considerable interest. This kinetic analysis revealed that IBMX significantly reduced the k_2 rate constant ($P < 0.01$) but not k_1 ($P > 0.05$), whilst rolipram instead altered the k_1 rate constant ($P < 0.05$) despite having no effect on k_2 ($P > 0.05$). These data are shown in Table 3.5. Throughout the rest of the study, k_1 and k_2 have simply been used as operational rate constants to aid in kinetic curve fitting in order to define the initial rate of signal generation, which is the main focus in this study.

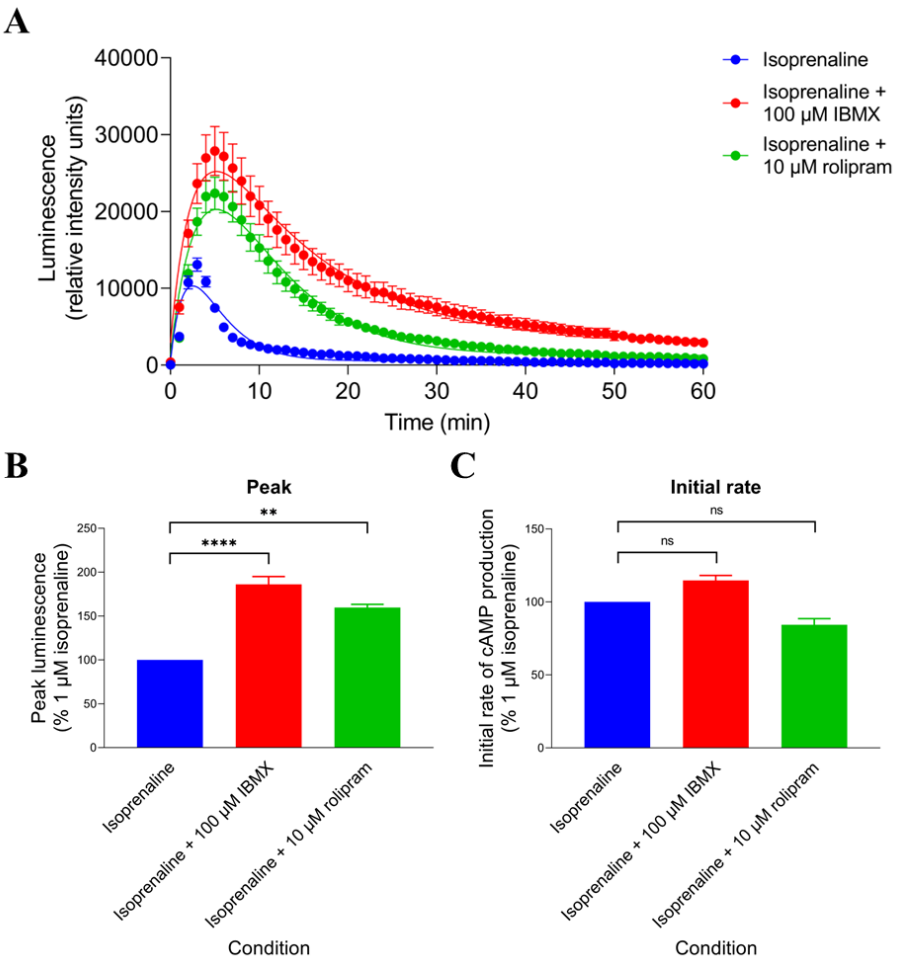

Figure 3.9: GloSensor™ luminescence stimulated by isoprenaline in the presence and absence of 30 min preincubated PDE inhibitors. (A) Representative GloSensor™ luminescence time-course data in one experiment over 60 min following application of 1 µM isoprenaline in the presence and absence of 100 µM IBMX or 10 µM rolipram to HEK293Gwt cells, fitted with time-course curve fitting according to Hoare et al. (2020b). Data points represent mean ± SEM of triplicate measurements, expressed as relative intensity units (RIU) of luminescence. Similar data were obtained in five independent experiments. (B, C) Bar charts displaying mean peak response (B) and initial rate (C) for 1 µM isoprenaline in the presence and absence of 100 µM IBMX or 10 µM rolipram in HEK293Gwt cells, expressed as a percentage of 1 µM isoprenaline. Data points represent mean ± SEM from five independent experiments (n = 5). Significant differences in responses to those seen in absence of PDE inhibitors are indicated, determined by a one-way ANOVA with Tukey's multiple comparisons test. $P < 0.05$ was used as the level for significance ($P \geq 0.05$ = ns, $P < 0.01$ = **, $P < 0.0001$ = ****).

Condition	Peak response (% 1 µM isoprenaline)	Initial rate (% 1 µM isoprenaline)	k_1 (min^{-1})	k_2 (min^{-1})
Isoprenaline	100	100	0.50 ± 0.20	0.38 ± 0.04
Isoprenaline + 100 µM IBMX	186.04 ± 9.05 ****	114.77 ± 3.42	0.44 ± 0.10	0.09 ± 0.01 **
Isoprenaline + 10 µM rolipram	159.71 ± 3.67 **	84.38 ± 4.20	0.23 ± 0.05 *	0.17 ± 0.02

Table 3.5: Isoprenaline mean peak response, initial rate, k_1 and k_2 values ± SEM determined in the presence and absence of the PDE inhibitors IBMX or rolipram obtained by cAMP GloSensor™ in HEK293Gwt cells from five independent experiments (n = 5). Significant differences in responses to those seen in absence of PDE inhibitors are indicated, determined by a one-way ANOVA with Tukey's multiple comparisons test. $P < 0.05$ was used as the level for significance ($P < 0.05$ = *, $P < 0.01$ = **, $P < 0.0001$ = ****).

3.3.3 – Pharmacological and kinetic characterisation of β_2-adrenoceptor antagonist activity under endogenous receptor expression

To further study endogenous β_2AR pharmacology using the cAMP GloSensor^{TM} assay, four antagonists (or inverse agonists), propranolol, ICI-118551, carvedilol and bisoprolol, were tested on HEK293Gwt cells. Although there was a minor decrease in the HBSS response at concentrations below 1 μM (for example, 100 nM ICI-118551 caused a 3.37% ± 0.90% reduction in HBSS response; $P < 0.05$), at higher concentrations (1 μM or higher), none of the β_2AR antagonists had any effect on intracellular cAMP levels ($P > 0.05$ for each condition). These results are displayed in Figures 3.10A and 3.10B, normalised against the maximal isoprenaline response for reference. This lack of clear inhibitory action was expected due to the low endogenous expression of β_2AR in HEK293 cells (Friedman et al., 2002; Goulding et al., 2021a; Goulding et al., 2021b). Thus, there was no (or very little) detectable constitutive β_2AR activity to be reduced, so inverse agonists instead appeared as classical antagonists here.

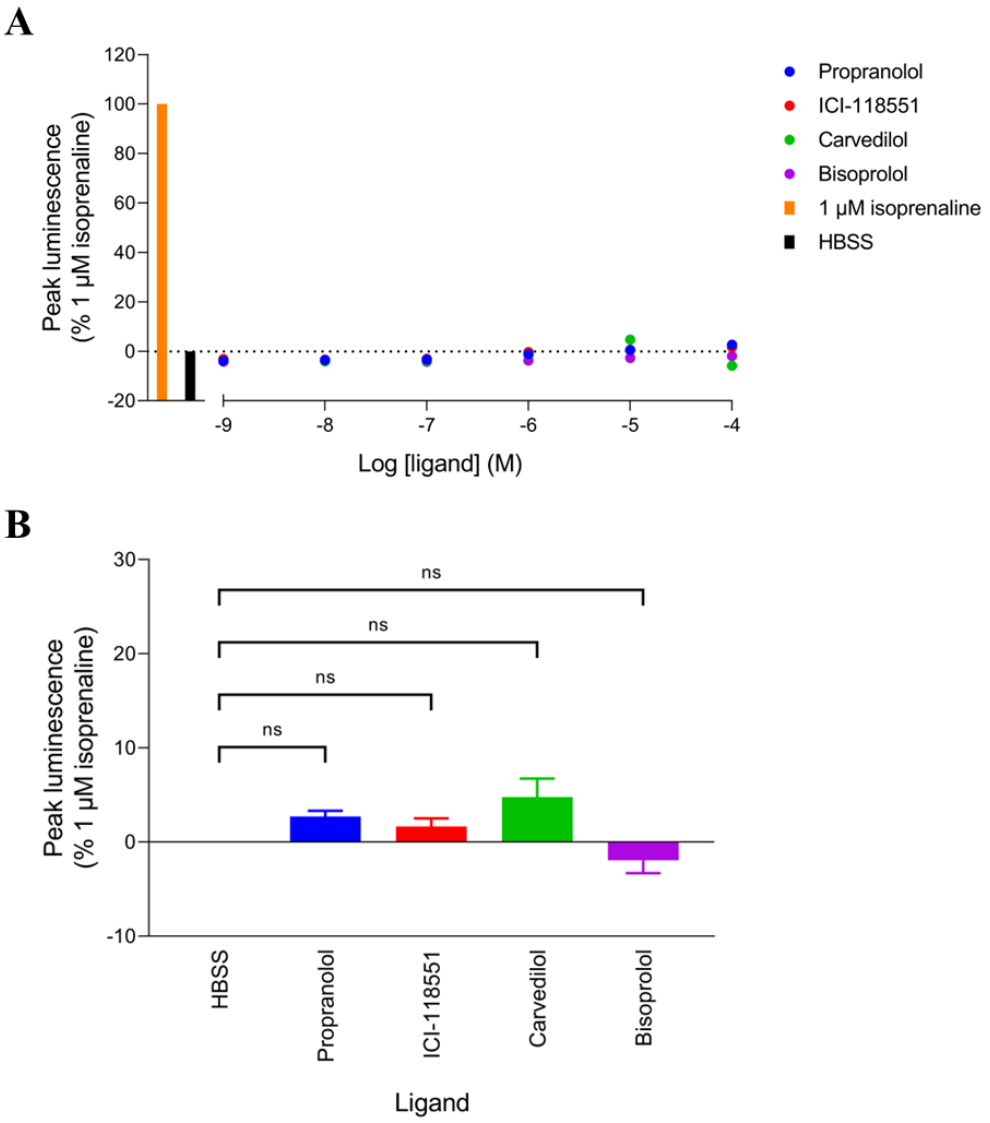

Figure 3.10: GloSensor™ luminescence measured after application of antagonists/inverse agonists. (A, B) Mean peak concentration-response curves (A) and bar chart displaying mean peak response (B) for propranolol, ICI-118551, carvedilol and bisoprolol (each 10 µM shown in B), plus 1 µM isoprenaline (A only) and HBSS (vehicle) controls in HEK293Gwt cells, expressed as a percentage of 1 µM isoprenaline. Data points represent mean ± SEM from five independent experiments (n = 5). Significant differences from HBSS (vehicle) are indicated, determined by a one-way ANOVA with Tukey's multiple comparisons test. $P < 0.05$ was used as the level for significance ($P \geq 0.05$ = ns).

Next, to study the effect of competing antagonists on agonist-stimulated endogenous β_2AR responses, each of the four antagonists/inverse agonists were preincubated with HEK293Gwt cells for 30 min (to allow binding equilibrium with endogenous β_2AR to be reached), followed by application of agonist (isoprenaline or formoterol). The observed changes in the 1 μM isoprenaline time-courses by increasing concentrations of each antagonist are represented in Figures 3.11A-3.11D. With the exception of bisoprolol, each of the antagonists caused a concentration-dependent reduction in the maximal responses of both isoprenaline (each $P < 0.0001$; Figures 3.12A-3.12C) and formoterol (each $P < 0.0001$; Figures 3.13A-3.13C), indicative of an insurmountable antagonism. In each case, the reduction in response maxima reached a plateau, whereby subsequent increases in antagonist concentration did not further decrease E_{max}, instead reducing agonist potency ($P < 0.0001$). Contrastingly, bisoprolol did not affect agonist maximal responses ($P > 0.05$ throughout), except for a slight reduction in isoprenaline (but not formoterol) E_{max} at the highest tested bisoprolol concentration (10 μM; $P < 0.01$), instead simply eliciting a parallel rightward shift in the potency of both agonists ($P < 0.0001$; Figures 3.12D and 3.13D). A clear correlation was found between the degree of reduction of agonist maximal responses by the antagonists and their respective dissociation rates at the β_2AR according to Sykes et al. (2014), whereby the slower the dissociation rate of the antagonist, the more pronounced the effect on agonist E_{max}, in the following order: carvedilol (dissociation rate: 0.033 ± 0.01 min^{-1}) < ICI-118551 (0.21 ± 0.03 min^{-1}) < propranolol (0.46 ± 0.05 min^{-1}) < bisoprolol (6.86 ± 2.09 min^{-1}) (Sykes et al., 2014), with carvedilol almost abolishing both isoprenaline and formoterol peak responses entirely (88.54% ± 0.26% reduction in isoprenaline E_{max}, 89.82% ± 1.26% reduction in formoterol E_{max}).

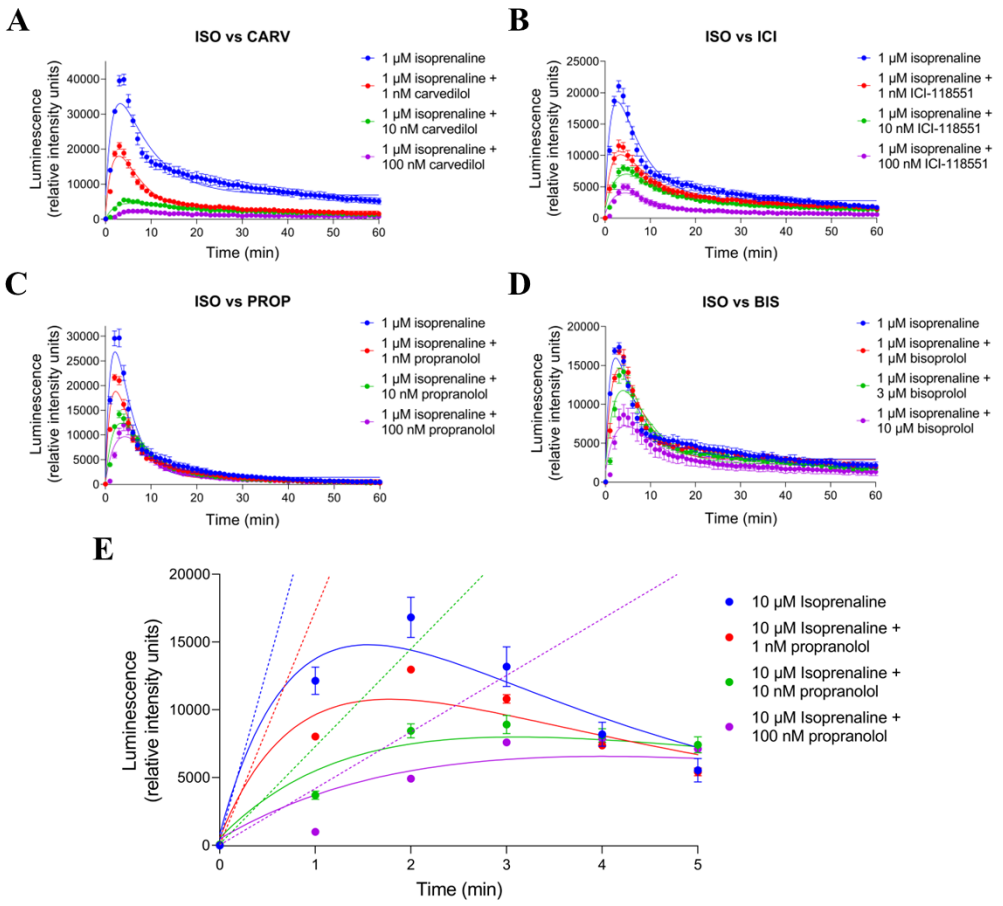

Figure 3.11: GloSensor™ luminescence stimulated by isoprenaline in the presence and absence of 30 min preincubated antagonists/inverse agonists. (A-E) Representative GloSensor™ luminescence time-course data in one experiment over 60 min (A-D) or 5 min (E) following application of 1 µM isoprenaline (ISO) in the presence and absence of carvedilol (CARV; 1 nM – 100 nM; A), ICI-118551 (ICI; 1 nM – 100 nM; B), propranolol (PROP; 1 nM – 100 nM; C, E) and bisoprolol (BIS; 1 µM – 10 µM; D) to HEK293Gwt cells, fitted with time-course curve fitting according to Hoare et al. (2020b), with derived initial rates indicated by dashed lines (E only). Data points represent mean ± SEM of triplicate measurements, expressed as relative intensity units (RIU) of luminescence. Similar data were obtained in five independent experiments.

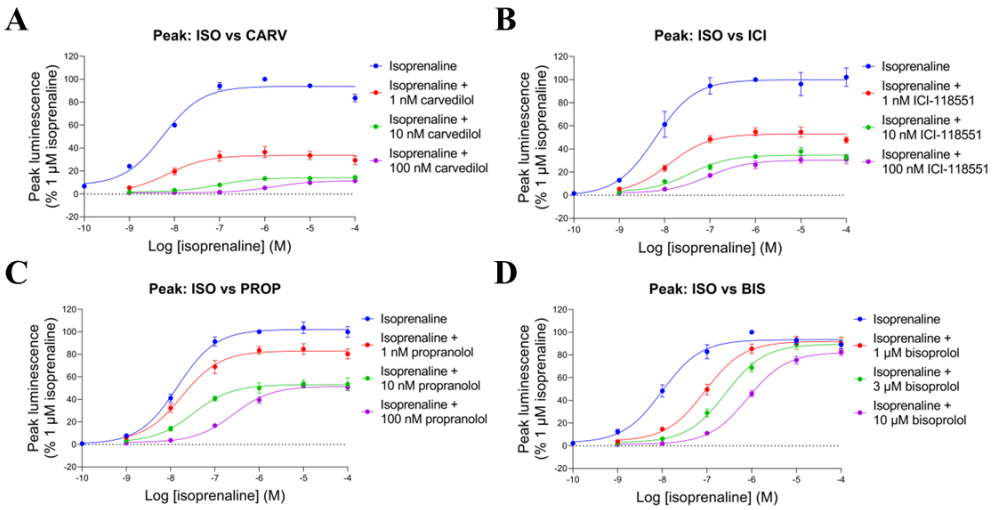

Figure 3.12: GloSensor^{TM} luminescence stimulated by isoprenaline in the presence and absence of 30 min preincubated antagonists/inverse agonists. (A-D) Mean peak concentration-response curves for isoprenaline (ISO) in the presence and absence of carvedilol (CARV; 1 nM – 100 nM; A), ICI-118551 (ICI; 1 nM – 100 nM; B), propranolol (PROP; 1 nM – 100 nM; C) and bisoprolol (BIS; 1 µM – 10 µM; D) in HEK293Gwt cells, expressed as a percentage of 1 µM isoprenaline. Data points represent mean ± SEM from five independent experiments (n = 5).

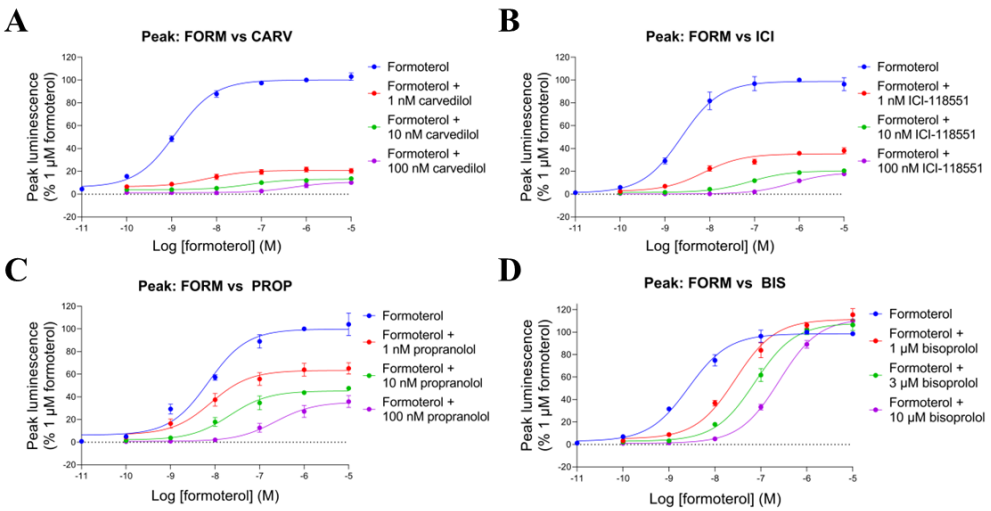

Figure 3.13: GloSensor^{TM} luminescence stimulated by formoterol in the presence and absence of 30 min preincubated antagonists/inverse agonists. (A-D) Mean peak concentration-response curves for formoterol (FORM) in the presence and absence of carvedilol (CARV; 1 nM – 100 nM; A), ICI-118551 (ICI; 1 nM – 100 nM; B), propranolol (PROP; 1 nM – 100 nM; C) and bisoprolol (BIS; 1 µM – 10 µM; D) in HEK293Gwt cells, expressed as a percentage of 1 µM formoterol. Data points represent mean ± SEM from five independent experiments (n = 5).

Kinetic analysis of these agonist responses in the presence and absence of the preincubated antagonists allowed for the calculation of the initial rate parameter in each condition. Figure 3.11E shows the first five minutes of a representative isoprenaline-mediated cAMP response after preincubation of increasing propranolol concentrations, or vehicle. The decreasing gradients of the dashed lines (which represent the calculated initial rate parameter) reveal that antagonist addition reduces the initial rate of signal generation mediated by the agonist. Indeed, each antagonist suppressed the maximal initial rates of both isoprenaline (each $P < 0.0001$; Figures 3.14A-3.14D) and formoterol (each $P < 0.0001$; Figures 3.15A-3.15D) in a concentration-dependent manner. In each case, the reduction in agonist IR_{max} was more drastic than that of the E_{max} ($P < 0.05$ or less) and even bisoprolol caused a substantial reduction in maximal initial rate of both agonists, depicted in Figures 3.16A and 3.16B. The degree of reduction in agonist IR_{max} remained in the same order as with E_{max}, correlating with antagonist dissociation rates (Sykes et al., 2014). The log shift in agonist EC_{50} and L_{50} values did not differ at the maximal concentrations of any of the antagonists ($P > 0.05$). The full sets of agonist E_{max}, log EC_{50}, IR_{max} and log L_{50} values in the presence and absence of increasing concentrations of propranolol, ICI-118551, carvedilol and bisoprolol are presented in Tables 3.6 (isoprenaline) and 3.7 (formoterol).

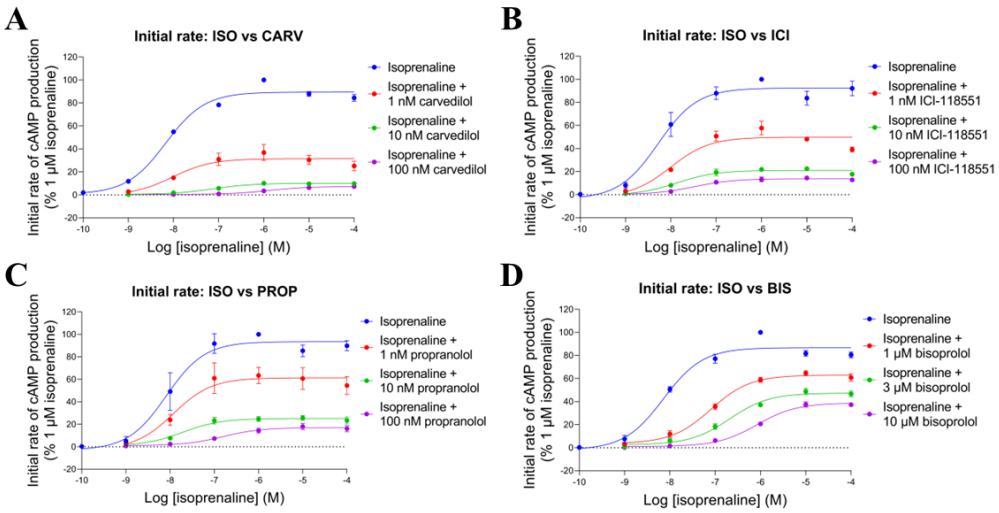

Figure 3.14: GloSensor^{TM} luminescence stimulated by isoprenaline in the presence and absence of 30 min preincubated antagonists/inverse agonists. (A-D) Mean initial rate concentration-response curves for isoprenaline (ISO) in the presence and absence of carvedilol (CARV; 1 nM – 100 nM; A), ICI-118551 (ICI; 1 nM – 100 nM; B), propranolol (PROP; 1 nM – 100 nM; C) and bisoprolol (BIS; 1 µM – 10 µM; D) in HEK293Gwt cells, expressed as a percentage of 1 µM isoprenaline. Data points represent mean ± SEM from five independent experiments (n = 5).

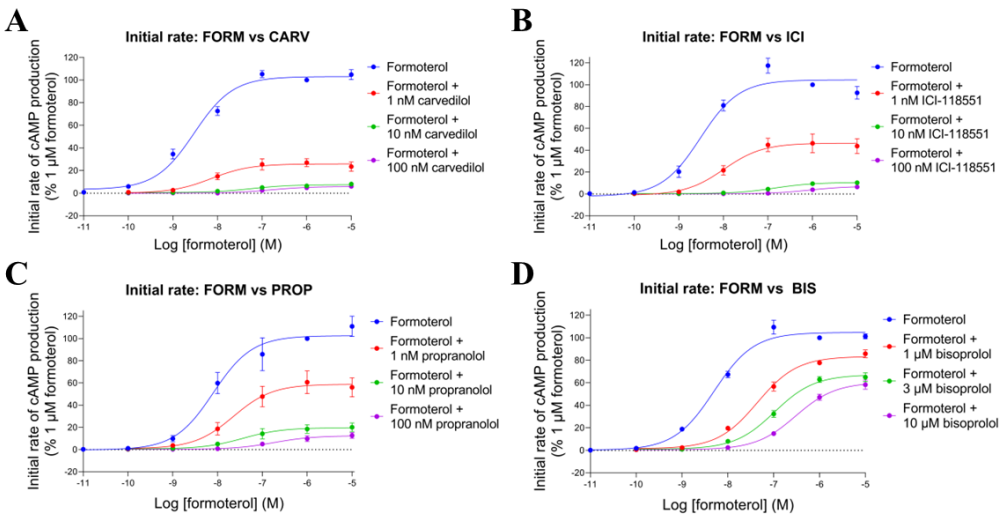

Figure 3.15: GloSensor^{TM} luminescence stimulated by formoterol in the presence and absence of 30 min preincubated antagonists/inverse agonists. (A-D) Mean initial rate concentration-response curves for formoterol (FORM) in the presence and absence of carvedilol (CARV; 1 nM – 100 nM; A), ICI-118551 (ICI; 1 nM – 100 nM; B), propranolol (PROP; 1 nM – 100 nM; C) and bisoprolol (BIS; 1 µM – 10 µM; D) in HEK293Gwt cells, expressed as a percentage of 1 µM formoterol. Data points represent mean ± SEM from five independent experiments (n = 5).

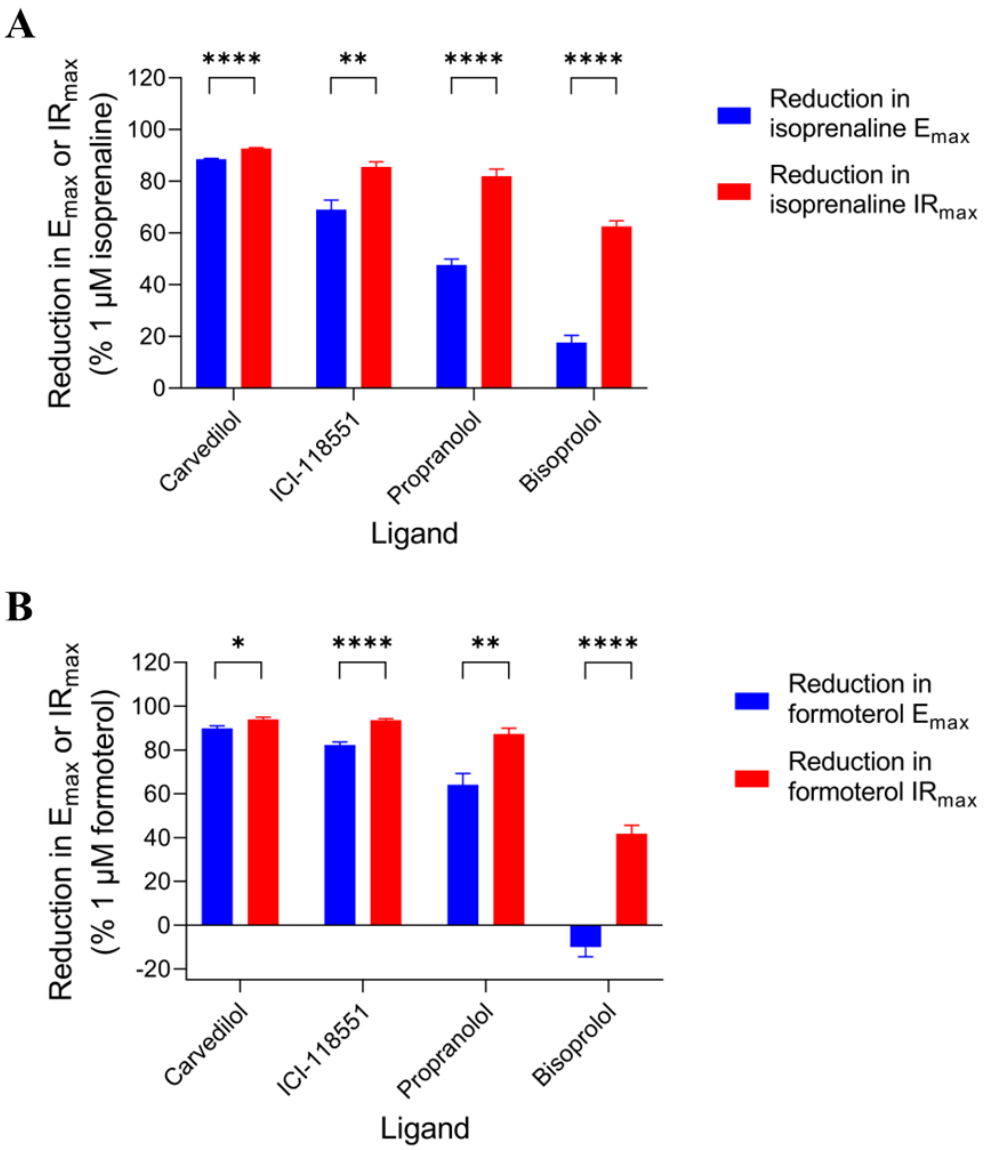

Figure 3.16: GloSensor^{TM} luminescence stimulated by agonists in the presence and absence of 30 min preincubated antagonists/inverse agonists. (A-B) Bar chart comparisons of reductions in mean E_{max} and IR_{max} values for isoprenaline (A) and formoterol (B) in the presence and absence of maximal concentrations of carvedilol, ICI-118551, propranolol (all 100 nM) and bisoprolol (10 µM) in HEK293Gwt cells. Data points represent mean ± SEM from five independent experiments (n = 5). Significant differences are indicated, determined by an unpaired t-test. $P < 0.05$ was used as the level for significance ($P < 0.05$ = *, $P < 0.01$ = **, $P < 0.0001$ = ****).

Antagonist	Log [antagonist] (M)	Isoprenaline E_{max} (% 1 µM isoprenaline) ± SEM	Isoprenaline IR_{max} (% 1 µM isoprenaline) ± SEM	Log isoprenaline EC_{50} (M) ± SEM	Log isoprenaline L_{50} (M) ± SEM
Carvedilol	0	100	100	-8.26 ± 0.04	-8.17 ± 0.03
	-9	36.50 ± 4.82 ****	36.86 ± 6.91 ****	-8.15 ± 0.11	-8.05 ± 0.11
	-8	14.40 ± 0.63 ****	10.13 ± 0.54 ****	-7.04 ± 0.11 ****	-7.17 ± 0.17 ****
	-7	11.46 ± 0.26 ****	7.31 ± 0.34 ****	-5.82 ± 0.08 ****	-5.90 ± 0.10 ****
ICI-118551	0	100	100	-8.16 ± 0.13	-8.22 ± 0.13
	-9	54.84 ± 3.45 ****	57.71 ± 5.91 ****	-7.92 ± 0.09	-7.99 ± 0.07
	-8	37.84 ± 3.45 ****	22.49 ± 1.93 ****	-7.41 ± 0.18 **	-7.79 ± 0.16
	-7	31.00 ± 3.70 ****	14.49 ± 2.01 ****	-7.05 ± 0.09 ****	-7.47 ± 0.12 **
Propranolol	0	100	100	-7.83 ± 0.07	-8.00 ± 0.18
	-9	84.74 ± 4.74 **	63.39 ± 7.28 ****	-7.72 ± 0.11	-7.92 ± 0.07

	-8	53.85 ± 3.36 ****	25.66 ± 2.15 ****	-7.45 ± 0.10 *	-7.68 ± 0.12
	-7	52.31 ± 2.28 ****	18.06 ± 2.78 ****	-6.55 ± 0.08 ****	-6.80 ± 0.06 ****
Bisoprolol	0	100	100	-7.97 ± 0.13	-8.14 ± 0.05
	-6	92.73 ± 3.85	64.51 ± 2.16 ****	-7.04 ± 0.07 ****	-7.10 ± 0.02 ****
	-5.5	89.37 ± 4.42	48.77 ± 2.55 ****	-6.57 ± 0.06 ****	-6.70 ± 0.06 ****
	-5	82.40 ± 2.85 **	37.42 ± 2.19 ****	-6.09 ± 0.05 ****	-6.06 ± 0.05 ****

Table 3.6: Isoprenaline mean E_{max}, IR_{max}, log EC_{50} and log L_{50} values ± SEM in the presence and absence of preincubated increasing concentrations of carvedilol, ICI-118551, propranolol and bisoprolol from concentration-response curves obtained by cAMP GloSensor™ in HEK293Gwt cells from five independent experiments (n = 5). Significant differences in responses to those seen in absence of antagonists/inverse agonists are indicated, determined by a one-way ANOVA with Tukey's multiple comparisons test. $P < 0.05$ was used as the level for significance ($P < 0.05$ = *, $P < 0.01$ = **, $P < 0.0001$ = ****).

Antagonist	Log [antagonist] (M)	Formoterol E_{max} (% 1 µM formoterol) ± SEM	Formoterol IR_{max} (% 1 µM formoterol) ± SEM	Log formoterol EC_{50} (M) ± SEM	Log formoterol L_{50} (M) ± SEM
Carvedilol	0	100	100	-8.90 ± 0.07	-8.52 ± 0.12
	-9	21.64 ± 2.18 ****	26.96 ± 3.61 ****	-8.13 ± 0.14 **	-8.12 ± 0.05
	-8	13.58 ± 1.52 ****	8.04 ± 1.49 ****	-7.20 ± 0.20 ****	-7.15 ± 0.17 ****
	-7	10.18 ± 1.26 ****	6.02 ± 1.02 ****	-6.18 ± 0.16 ****	-6.47 ± 0.32 ****
ICI-118551	0	100	100	-8.58 ± 0.11	-8.51 ± 0.11
	-9	38.15 ± 2.66 ****	46.38 ± 8.54 ****	-8.03 ± 0.20 *	-7.97 ± 0.04 **
	-8	20.49 ± 1.22 ****	10.27 ± 1.65 ****	-7.11 ± 0.13 ****	-6.80 ± 0.10 ****
	-7	17.78 ± 1.42 ****	6.45 ± 0.83 ****	-6.14 ± 0.07 ****	-6.05 ± 0.11 ****
Propranolol	0	100	100	-8.29 ± 0.15	-8.07 ± 0.17
	-9	65.15 ± 5.02 ****	60.63 ± 10.30 ***	-8.13 ± 0.21	-7.61 ± 0.13

	-8	47.59 ± 1.99 ****	20.06 ± 3.94 ****	-7.66 ± 0.25	-7.32 ± 0.19 *
	-7	35.86 ± 5.21 ****	12.69 ± 2.67 ****	-6.55 ± 0.25 ****	-6.46 ± 0.19 ****
Bisoprolol	0	100	100	-8.55 ± 0.08	-8.31 ± 0.05
	-6	115.53 ± 5.36	85.76 ± 3.50 *	-7.49 ± 0.11 ****	-7.33 ± 0.11 ****
	-5.5	106.45 ± 4.93	65.01 ± 3.99 ****	-7.12 ± 0.09 ****	-6.98 ± 0.09 ****
	-5	110.03 ± 4.42	58.27 ± 3.96 ****	-6.60 ± 0.09 ****	-6.51 ± 0.08 ****

Table 3.7: Formoterol mean E_{max}, IR_{max}, log EC_{50} and log L_{50} values ± SEM in the presence and absence of preincubated increasing concentrations of carvedilol, ICI-118551, propranolol and bisoprolol from concentration-response curves obtained by cAMP GloSensor^{TM} in HEK293Gwt cells from five independent experiments (n = 5). Significant differences in responses to those seen in absence of antagonists/inverse agonists are indicated, determined by a one-way ANOVA with Tukey's multiple comparisons test. $P < 0.05$ was used as the level for significance ($P < 0.05$ = *, $P < 0.01$ = **, $P < 0.001$ = ***, $P < 0.0001$ = ****).

3.3.4 – Use of functional data to determine antagonist binding affinities at the β_2-adrenoceptor

It is possible to use functional data in order to calculate the binding affinity of a competitive antagonist for its receptor, in terms of its equilibrium dissociation constant (K_D; originally denoted as pA_2) by performing Schild regression analysis of agonist vs antagonist responses. This requires calculation of the dose ratio parameter, which is the ratio of agonist concentrations required to produce a specific response in the presence and absence of the antagonist (calculated individually for each concentration of antagonist used). The Schild equation (Equation 5) can then be employed to produce a Schild plot, whereby an estimate for the antagonist log K_D is indicated by the x-intercept of the linear regression line (Equation 6) on the plot (Arunlakshana and Schild, 1959; Tallarida and Murray, 1987). Usually, these analyses are performed on data obtained under equilibrium binding conditions whereby a surmountable antagonism is observed (as was shown with bisoprolol peak responses), and the specific response used to calculate the dose ratio is the half-maximal (EC_{50}) agonist response (Arunlakshana and Schild, 1959; Tallarida and Murray, 1987). However, under the non-equilibrium conditions seen in this study whereby agonist maximal responses are depressed by increasing antagonist concentrations (as with propranolol, ICI-118551 and carvedilol), antagonist affinities can still be estimated. In these cases the EC_{50} values do not provide equivalent magnitudes of response, so instead equieffective agonist concentrations can be taken from an arbitrarily selected response level (where all conditions show a constant level of response occurring within the linear phase of the sigmoidal curve) to determine the dose ratios and thus still provide a sufficient estimate of antagonist K_D (Christopoulos et al., 1999). A graphical representation of how the dose ratios are calculated under equilibrium and non-equilibrium conditions was shown in Chapter 2 (Figures 2.8A and 2.8B).

Firstly, using the peak response data obtained throughout these experiments, Schild regression analysis was utilised to estimate antagonist log K_D values for the β_2AR, using both agonists isoprenaline and formoterol. As bisoprolol did not cause a depression in agonist maximal response (Figures 3.12D and 3.13D), the

EC_{50} response level could be used to determine dose ratios. Since propranolol and ICI-118551 did reduce agonist maximal responses (Figures 3.12B, 3.12C, 3.13B and 3.13C), equieffective agonist concentrations were taken from selected response levels (individually for each experimental repeat), approximately around 25-30% (propranolol) or 15-20% (ICI-118551) agonist response in absence of antagonist. However, because carvedilol almost entirely abolished agonist responses (Figures 3.12A and 3.13A), meaning no appropriate response level could be selected to calculate dose ratios, it was not possible to determine a log K_D value for carvedilol from the data obtained in this study. Schild plots were constructed for propranolol, ICI-118551 and bisoprolol (using both isoprenaline and formoterol peak response data) and are displayed in Figures 3.17A-3.17F. As expected, the determined log K_D values for each antagonist did not differ based on the agonist used ($P > 0.05$ in all cases), and the antagonist binding affinities were similar to those previously reported by Baker (2005), using radioligand competition binding assays (propranolol log K_D: -9.08 ± 0.06, ICI-118551 log K_D: −9.26 ± 0.03, and bisoprolol log K_D: −6.70 ± 0.05). The antagonist log K_D values estimated from the peak response data are stated in Table 3.8, alongside the determined Schild slopes which also represent a valuable parameter for determining antagonist behaviour. A Schild slope of approximately 1 implies a competitive antagonist behaviour, meanwhile slopes which deviate considerably from 1 may indicate non-competitive antagonism (Kenakin, 1982). Here, the Schild slopes calculated from both bisoprolol conditions are approximately 1 ($P > 0.05$ in both), whereas the propranolol and ICI-118551 slopes instead tended to deviate from 1, albeit only significantly so in one case (isoprenaline vs ICI-118551; $P < 0.05$).

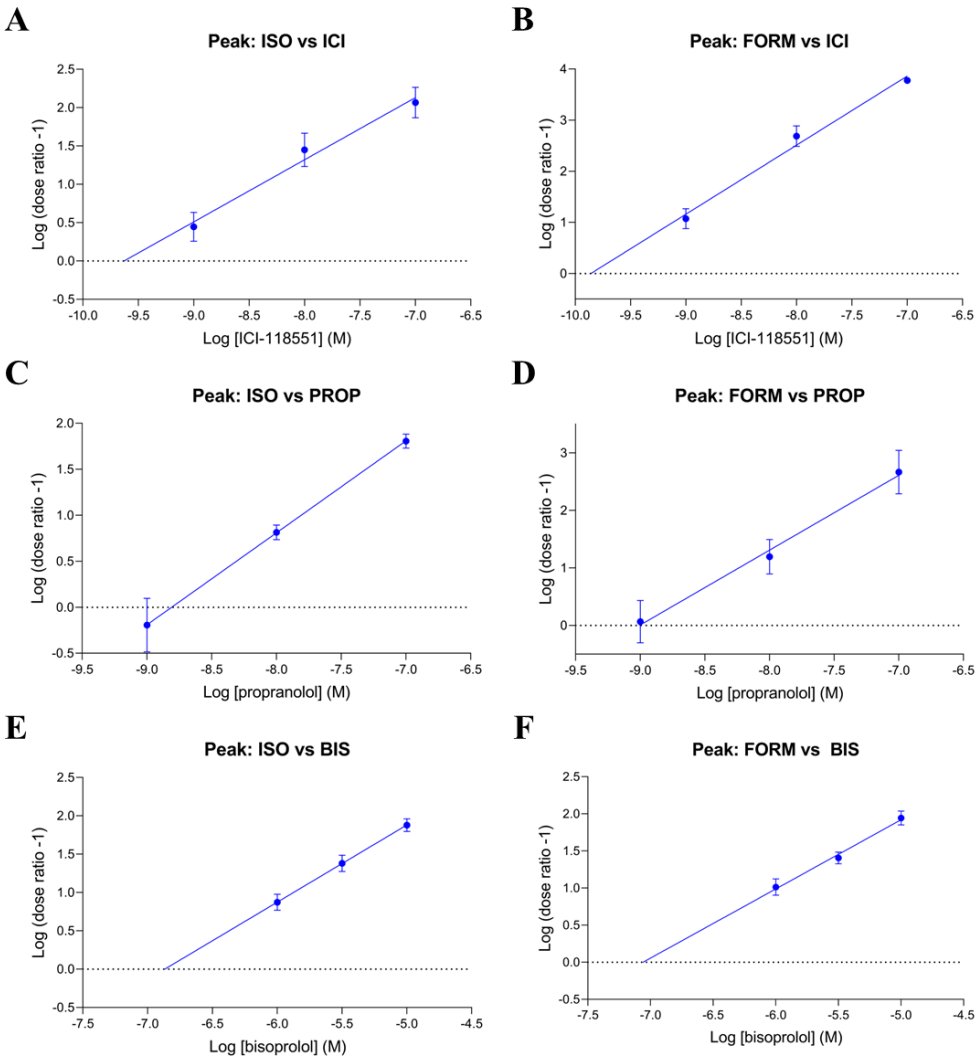

Figure 3.17: Schild regression analysis to determine antagonist binding affinities for the β_2AR from cAMP GloSensor^{TM} in HEK293Gwt cells. (A-F) Schild plots from peak response data for isoprenaline (ISO; A, C, E) or formoterol (FORM; B, D, F) versus ICI-118551 (ICI; A, B), propranolol (PROP; C, D) or bisoprolol (BIS; E, F). Data points represent mean log (dose ratio -1) ± SEM for each concentration of antagonist from five independent experiments (*n* = 5). The x-intercept provides an estimation of antagonist log K_D value.

Antagonist	Agonist	Estimated antagonist log K_D ± SEM	Schild slope ± SEM
ICI-118551	Isoprenaline	-9.70 ± 0.30	0.81 ± 0.09
	Formoterol	-9.93 ± 0.21	1.35 ± 0.11 *
Propranolol	Isoprenaline	-8.96 ± 0.29	1.00 ± 0.15
	Formoterol	-9.06 ± 0.29	1.30 ± 0.18
Bisoprolol	Isoprenaline	-6.89 ± 0.13	1.01 ± 0.05
	Formoterol	-7.15 ± 0.24	0.93 ± 0.11

Table 3.8: Estimated antagonist mean log K_D and Schild slope values ± SEM at the β_2AR for ICI-118551, propranolol and bisoprolol from peak response data obtained by cAMP GloSensor™ in HEK293Gwt cells from five independent experiments (n = 5). Significant deviation of Schild slopes from 1 are indicated, determined by an unpaired t-test. $P < 0.05$ was used as the level for significance ($P < 0.05$ = *).

The same Schild regression analyses were then performed using the data obtained from the initial rate of signal generation instead of the peak response. This time, bisoprolol was the only antagonist for which a log K_D value could be determined because the suppression of agonist maximal initial rates by propranolol, ICI-118551 and carvedilol were too drastic to select a valid response level for dose ratio calculation (Figures 3.14A-3.14C and 3.15A-3.15C). For bisoprolol, which caused a lesser but still significant reduction of the agonist maximal initial rates (Figures 3.14D and 3.15D), the response level used to determine dose ratio was individually selected for each experimental repeat, approximately 25-30% of agonist response in absence of antagonist. The Schild plots generated from these data are displayed in Figures 3.18A and 3.18B. Once again, the estimated bisoprolol log K_D value was similar under both agonist conditions ($P > 0.05$). Moreover, the log K_D values determined from this kinetics-based approach did not differ from those determined using the classic pharmacological approach using either isoprenaline (estimated bisoprolol log K_D from isoprenaline peak response vs initial rate data: -6.89 ± 0.13 vs -6.71 ± 0.04; $P > 0.05$) or formoterol (-7.15 ± 0.24 vs -6.84 ± 0.08; $P > 0.05$) as the agonist. Additionally, the Schild slopes for these data were both found to be significantly larger than 1 ($P < 0.05$ or less). Table 3.9 shows the determined log K_D values and Schild slopes for bisoprolol from the initial rate data.

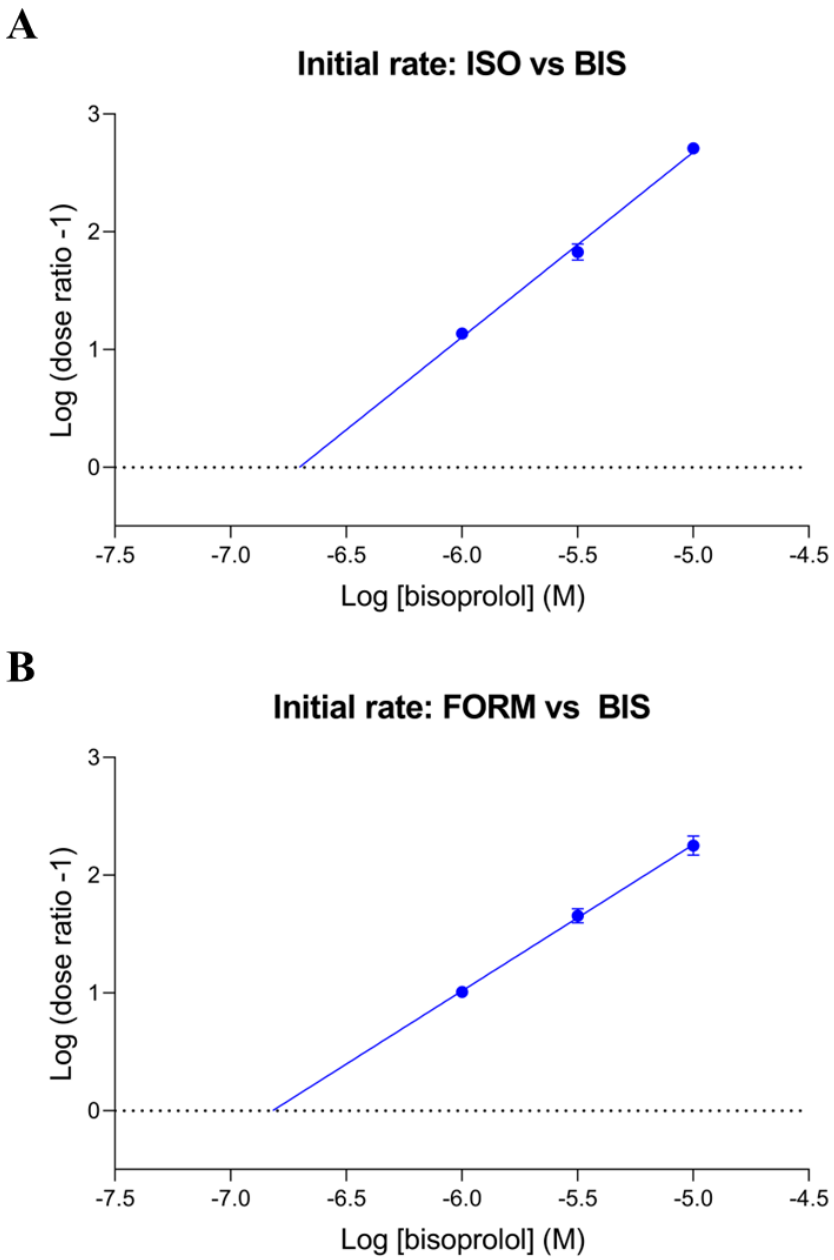

Figure 3.18: Schild regression analysis to determine antagonist binding affinities for the β_2AR from cAMP GloSensor^{TM} in HEK293Gwt cells. (A, B) Schild plots from initial rate data for isoprenaline (ISO; A) or formoterol (FORM; B) versus bisoprolol (BIS; A, B). Data points represent mean log (dose ratio -1) ± SEM for each concentration of antagonist from five independent experiments (n = 5). The x-intercept provides an estimation of antagonist log K_D value.

Antagonist	Agonist	Estimated antagonist log K_D ± SEM	Schild slope ± SEM
Bisoprolol	Isoprenaline	-6.71 ± 0.04	1.57 ± 0.04 ****
	Formoterol	-6.84 ± 0.08	1.24 ± 0.10 *

Table 3.9: Estimated antagonist mean log K_D and Schild slope values ± SEM at the β_2AR for bisoprolol from initial rate data obtained by cAMP GloSensor™ in HEK293Gwt cells from five independent experiments (n = 5). Significant deviation of Schild slopes from 1 are indicated, determined by an unpaired t-test. $P < 0.05$ was used as the level for significance ($P < 0.05$ = *, $P < 0.0001$ = ****).

3.3.5 – Investigating the effect of competing orthosteric agonists on cAMP production

Next, the effect of simultaneous addition of two competing orthosteric agonists of differing efficacies for the β_2AR was studied using the cAMP GloSensor^{TM} luminescence assay to assess the impact on cAMP production. It was demonstrated earlier in the study that salmeterol acts as a partial agonist for the β_2AR in HEK293Gwt cells, producing a substantially smaller maximal cAMP response than that of the full agonist isoprenaline (Figure 3.6). Firstly, increasing concentrations of isoprenaline were applied simultaneously alongside either a maximal concentration of salmeterol (1 μM) or HBSS (vehicle). This allowed construction of isoprenaline peak concentration-response curves in the presence and absence of salmeterol (Figure 3.19A). In the conditions where isoprenaline was added alongside vehicle, the expected sigmoidal increase in peak response from baseline up to a maximum was observed (1 μM isoprenaline normalised to 100%). Simultaneous addition of 1 μM salmeterol unsurprisingly increased peak cAMP production at low isoprenaline concentrations up to approximately the maximal response recorded for salmeterol previously (peak response at 10 pM isoprenaline increased from 2.68% ± 1.72% to 40.01% ± 3.09%; $P < 0.0001$). As isoprenaline concentration increases, peak cAMP production increases until it reaches the same maximal response as with isoprenaline alone (peak response at 10 μM isoprenaline: 99.04% ± 1.19% compared with 86.04% ± 6.28%; $P > 0.05$). In the presence of the competing salmeterol, the isoprenaline potency is reduced by approximately 100-fold (isoprenaline log EC_{50} reduced from -7.99 ± 0.06 to -6.00 ± 0.15; $P < 0.0001$).

It is also possible to determine the receptor binding affinity of partial agonists from functional data by competition with a full agonist. Using the data presented here, the affinity of salmeterol at the β_2AR was determined by employing a modified Gaddum equation (Equation 7) as described by Stephenson (1956) (see 2.12 – Data analysis and statistics). From the peak response data, the salmeterol log K_D was estimated as -7.93 ± 0.12, which is substantially lower than the -9.26 ± 0.06 previously reported by Baker (2010) using radioligand competition binding. However, it aligns more closely with similar findings both by Carter

and Hill (2005) (salmeterol log K_D: -8.3 ± 0.2) and McCrea and Hill (1993) (salmeterol K_D: 55.6 nM ± 28.2 nM, or approximately log K_D: -7.25), who employed much more similar techniques with those used in this study (measurements of functional β_2AR responses after simultaneous application of isoprenaline and salmeterol, followed by determination of salmeterol log K_D values using the same method by Stephenson (1956)).

Conversely, increasing concentrations of salmeterol were applied simultaneously alongside either a maximal concentration of isoprenaline (again 1 μM) or HBSS (vehicle) and peak salmeterol concentration-response curves in the presence and absence of isoprenaline were generated (Figure 3.19B). In the absence of isoprenaline, salmeterol produced the anticipated sigmoidal increase in peak response from baseline up to a reduced maximum (compared with isoprenaline maximal response). The simultaneous addition of 1 μM isoprenaline drastically increased peak response at low salmeterol concentrations (peak response at 10 pM salmeterol increased from 2.06% ± 0.82% to 100%; $P < 0.0001$). As salmeterol concentration is increased, peak cAMP production actually begins to decrease, until reaching its plateau around the same maximal response as salmeterol alone (peak response at 10 μM salmeterol: 41.21% ± 4.25% compared with 47.52% ± 4.00%; $P > 0.05$). A log IC_{50} value of -6.34 ± 0.13 was calculated for the observed inhibitory effect by salmeterol on the maximal isoprenaline (1 μM) response.

Kinetic analysis of these data revealed an almost identical trend in terms of initial rates of signal generation compared with the peak response data for both experiments, as shown in the initial rate concentration-response curves in Figures 3.19C and 3.19D. One notable difference was that the maximal initial rate of isoprenaline in the presence of 1 μM salmeterol did not ultimately reach the same level as with isoprenaline alone (Figure 3.19C; initial rate at 10 μM isoprenaline: 100% compared with 77.17% ± 5.80%; $P < 0.01$) despite having reached the same maximal response. Despite this, in the converse experiment, the addition of 1 μM isoprenaline did not have any effect on the salmeterol maximal initial rate (Figure 3.19D; initial rate at 10 μM salmeterol: 30.12% ± 2.31% compared with 32.18% ± 1.21%; $P > 0.05$). Finally, an estimate for the

binding affinity of salmeterol at the β_2AR was made again, this time based on the initial rate parameter. Salmeterol log K_D was this time determined as -7.68 ± 0.22, similar to that determined from the peak response data ($P > 0.05$). Moreover, the kinetic potency inhibitory effect, termed IL_{50} here, of salmeterol on 1 μM isoprenaline initial rate was also similar to that determined from the peak response data (log IL_{50}: -6.57 ± 0.14 compared with log IC_{50}: -6.34 ± 0.13; $P > 0.05$).

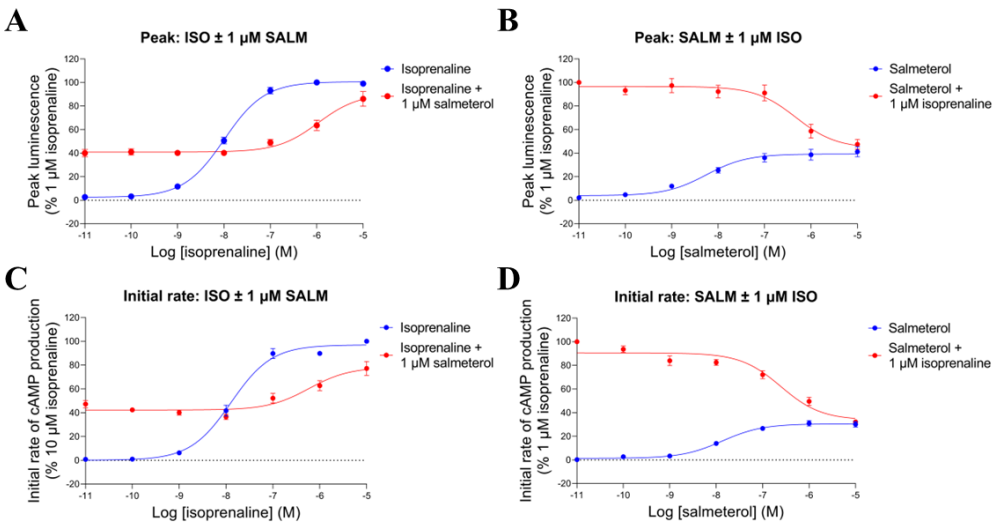

Figure 3.19: GloSensor^{TM} luminescence stimulated by simultaneous addition of agonists of differing efficacies. (A-D) Mean peak (A, B) and initial rate (C, D) concentration-response curves for isoprenaline (ISO) in the presence and absence of salmeterol (SALM; A, C) or salmeterol in the presence and absence of isoprenaline (B, D) in HEK293Gwt cells, expressed as a percentage of 1 µM isoprenaline. Data points represent mean ± SEM from five independent experiments (n = 5).

3.4 – Discussion

3.4.1 – Initial characterisation of the cAMP GloSensor™ luminescence assay

The initial aim of this study was to characterise the cAMP GloSensor™ luminescence assay by testing several ligands which act at distinct targets throughout the cAMP signalling pathway. The time-course data (Figure 3.1A) showed that addition of each of the tested ligands increased luminescence emission by the cAMP GloSensor™ biosensor, indicating (except for 8-CPT-cAMP) an increased cytosolic production of the second messenger cAMP (Fan et al., 2008; Binkowski et al., 2011). Isoprenaline and salmeterol activate the β_2AR, whist NECA acts at the A_{2A}AR and A_{2B}AR. Each of these receptors are endogenously expressed in HEK293 cells (Cooper et al., 1997; Friedman et al., 2002; Thomas and Smart, 2005; Goulding et al., 2018; Goulding et al., 2021a; Goulding et al., 2021b) and couple preferentially to G_s protein, which stimulates adenylate cyclase production of cAMP (Stiles et al., 1984; Fredholm et al., 1994). Forskolin instead stimulates cAMP production by binding directly to adenylate cyclase (Seamon and Daly, 1981; Zhang et al., 1997). 8-CPT-cAMP does not stimulate intracellular cAMP production, instead likely mimicking the action of the second messenger (Connolly et al., 1992; Parvathenani et al., 1998) to bind to the regulatory PKA subunit of the cAMP GloSensor™ biosensor directly and catalyse the oxidation of luciferin, resulting in the observed emission of luminescence. The differences in peak response amplitudes measured by the ligands (Figures 3.1A and 3.1B) are related to several factors, including the efficacy with which a ligand stabilises the active state of its target. For example, salmeterol produces a much reduced peak cAMP response when compared with isoprenaline because it has a lower intrinsic efficacy for activating the receptor. Another factor influencing the peak response is target expression levels. The endogenous expression of β_2AR, A_{2A}AR and A_{2B}AR in HEK293 cells are relatively low (Cooper et al., 1997; Friedman et al., 2002; Goulding et al., 2018; Goulding et al., 2021a; Goulding et al., 2021b), so responses are relatively small. Receptor overexpression should result in increased maximal responses achieved by the agonists, as well as other effects

on the pharmacology of the receptor response. This will be explored further in Chapter 4. The small response to HBSS observed (Figure 3.1A) is likely predominantly due to activation of other endogenous G_s-coupled receptors in HEK293 cells; this will also be discussed further in Chapter 4.

After the initial sharp rise in cAMP concentration after ligand application, the response reaches a peak and subsequently declines back toward the baseline. This is due to regulatory mechanisms such as receptor desensitisation and the breakdown of cAMP by PDEs (Francis et al., 2000; Moore et al., 2007a; Fan et al., 2008). The gradual diminishment of the luciferin substrate required for the luciferase reaction may also contribute toward the degradation of the response. In these experiments, the rate of decay of the NECA response was considerably slower than that of isoprenaline (Figure 3.1A). Since the rate of cAMP degradation by PDEs and the loss of luciferin substrate should be approximately the same, this observation suggests differences in the relative rates of desensitisation of β_2AR and A_{2A}AR/A_{2B}AR. Additionally, differences in receptor expression levels in HEK293 cells may also contribute. The slower rate of forskolin response decay was expected as no receptor desensitisation occurs in this case due to its direct action at adenylate cyclase, meaning the response is regulated entirely by PDE-mediated cAMP breakdown. The even slower decline in the response to 8-CPT-cAMP application might suggest a reduced ability by PDEs to breakdown the cAMP analogue, relative to endogenous cAMP molecules.

Catecholamines (such as the endogenous adrenaline and noradrenaline, as well as isoprenaline) are known to be relatively instable, particularly in physiological saline solutions, due to their susceptibility to oxidation (Sutor and Ten Bruggencate, 1990; Dhalla et al., 2010; Hughes and Smith, 2011). This can distort measured pharmacological parameters as the actual concentration of unoxidised ligand is lower than expected. The use of reductants like ascorbic acid has been common to prevent the rapid oxidation of catecholamines (Bendich et al., 1986; Hughes and Smith, 2011). Therefore, in order to determine whether the degradation of isoprenaline was substantial enough to affect its pharmacology during the time-frame of the cAMP GloSensor^{TM} assays

performed here, the effect of addition of ascorbic acid to the HBSS buffer was investigated. However, ascorbic acid application did not alter the isoprenaline maximal response or potency, neither did it have any discernible impact on the profile of the isoprenaline time-course signal (Figures 3.2A and 3.2B). It was therefore judged that isoprenaline oxidation was negligible during the time-frame of the cAMP GloSensor^{TM} assay measurement (1 h total) and thus the use of ascorbic acid was not required in this assay going forward.

Pre-treatment of HEK293Gwt cells with forskolin was shown to potentiate the peak isoprenaline response (Figure 3.3). However, this effect was modest in comparison with previous work, where Darfler et al. (1982) showed that forskolin was able to potentiate isoprenaline-mediated cAMP accumulation by as much as 8-10-fold. Additionally, no change in isoprenaline potency was observed, compared with a 2-3-fold potency shift previously (Darfler et al., 1982). Regardless, because the potentiation of the isoprenaline response by forskolin was larger than its effect on the vehicle (i.e., the peak isoprenaline + 10 nM forskolin cAMP response is more than additive than the individual isoprenaline and 10 nM forskolin responses), this still provides evidence for a synergistic activation between forskolin and $G_{\alpha s}$ protein, as has been reported previously (McHugh Sutkowski et al., 1994; Darfler et al., 1982; Insel and Ostrom, 2003).

One of the mechanisms by which cells regulate cAMP concentration inside cells is the breakdown of the second messenger molecule by PDEs (Francis et al., 2000; Ghosh et al., 2009). To assess the impact of this process on the character of cAMP GloSensor^{TM} luminescence responses, two inhibitors of PDE enzymes, the non-selective IBMX and PDE4-selective rolipram, were tested. As expected, the inhibitors both enhanced isoprenaline-mediated peak response and AUC (Figures 3.4A, 3.4C and 3.4D) due to the reduced ability of the enzymes to degrade cytosolic cAMP. The data gathered here provide evidence that PDE4 has a considerable role in regulating the concentration of cytosolic cAMP in HEK293 cells, since PDE4-selective rolipram potentiated both peak and AUC responses similarly to the non-selective IBMX. Previous studies have described the dominant role of the PDE4 subtype in regulating cAMP in HEK293 cells

(Lynch et al., 2005; Weninger et al., 2014). However, the combination of IBMX and rolipram further slowed the rate of decay of the isoprenaline response, indicating other PDEs also play some role. Contrastingly however, whilst IBMX also potentiated the small response to vehicle control, rolipram had no effect (Figures 3.4B, 3.4E and 3.4F), implying a lack of involvement of PDE4 in regulating cAMP at lower concentrations. PDEs are themselves regulated by intracellular cyclic nucleotide concentrations, so an increase in cAMP concentration leads to enhancement of PDE activity in order to subsequently accelerate the rate of cAMP degradation (Cheng and Grande, 2007; Ghosh et al., 2009). It is possible, therefore, that different PDE subtypes may become more active at distinct intracellular cAMP concentration thresholds. This could explain why rolipram has little effect on the small vehicle control response but considerably impacts the isoprenaline-mediated cAMP response, as PDE4 may only be sensitive to high cytosolic concentrations of cAMP. Whereas other PDE subtypes may be more sensitive to lower cAMP concentrations, thus IBMX shows a clear effect on both isoprenaline response and vehicle.

3.4.2 – Differences in the pharmacological and kinetic parameters of partial agonist-mediated cAMP production in a low receptor expression system

This study utilised the cAMP GloSensor^{TM} luminescence assay to investigate the kinetic parameters of β_2AR ligand activity and compare these with standard pharmacological parameters under very low, endogenous receptor expression conditions (Friedman et al., 2002; Goulding et al., 2021a; Goulding et al., 2021b). The ability of four β_2AR agonists of differing pharmacological efficacies (isoprenaline, formoterol, salbutamol, and salmeterol) to stimulate the production of cAMP in HEK293Gwt cells was examined. Analysis of the peak response data showed that salbutamol and salmeterol both elicited a markedly reduced maximal cAMP response compared with isoprenaline and formoterol (Figure 3.6), consistent with their partial agonism for the β_2AR (Baker et al., 2003a; Baker et al., 2003b; Hoffmann et al., 2004; Baker, 2010). The curve

fitting of the time-course data to a newly established kinetic equation, derived by Hoare et al. (2020b), allowed for the determination of the initial rate of signal generation. Whereas the 'peak response' parameter measures the maximal magnitude of cAMP concentration as the signal reaches its peak (followed by subsequent decline) due to the action of the regulatory mechanisms, the 'initial rate' parameter instead quantifies the initial linear phase of cAMP production immediately after agonist binding to the receptor before these regulatory mechanisms come into effect (Hoare et al., 2020b). The maximal initial rate, IR_{max}, therefore represents the ability of the agonist-occupied receptor to transduce a response prior to regulation and thus can provide a kinetic measure of agonist efficacy (Hoare et al., 2020b; Hoare et al., 2022). Concentration-response curves derived from the initial rate data for each agonist revealed that the partial agonists salbutamol and salmeterol also induced slower initial rates of production of cAMP (Figure 3.7B). The rank order of efficacy of the four tested ligands for the β_2AR remained the same in terms of their E_{max} and IR_{max} values (isoprenaline ≥ formoterol > salbutamol > salmeterol).

Direct comparison of agonist E_{max} values with their IR_{max} values from the same datasets revealed that the salbutamol and salmeterol IR_{max} values were significantly reduced compared to their E_{max} values, relative to those of the reference ligand isoprenaline (against which all data were normalised). Formoterol, however, showed no difference between E_{max} and IR_{max} values (Figure 3.8). This observation may be due to differential effects of regulatory mechanisms on distinct ligand-induced signals. For example, desensitisation of GPCRs occurs after binding by the receptor to intracellular β-arrestins, which sterically hinders further G protein coupling (Shenoy and Lefkowitz, 2003; Moore et al., 2007a). Therefore, the binding affinity of the agonist-occupied receptor for β-arrestins determines the rate of β-arrestin recruitment and hence the rate of receptor desensitisation. Several previous studies have established that different ligands can stabilise distinct GPCR conformations, which may confer varying G protein and β-arrestin binding affinities (Shukla et al., 2014b; Rankovic et al., 2016). A slower rate of receptor desensitisation would likely cause the rise phase of the time-course signal to plateau at a more gradual rate due to the reduced regulatory pressure on the cAMP response. This would allow

the response to peak at a higher magnitude than under faster desensitisation conditions, thus elevating the measured E_{max} value, but not that of the IR_{max} which is independent of regulatory mechanisms. This may account for the observed discrepancy between salbutamol and salmeterol E_{max} and IR_{max} values here. Indeed, many previous studies have uncovered decreased β_2AR desensitisation by both salbutamol (also referred to as albuterol) and salmeterol compared with higher efficacy agonists including isoprenaline and formoterol, particularly at the earlier time-points (less than 30 min) relevant here, due to reduced GRK binding, receptor phosphorylation and β-arrestin affinity by the salbutamol- or salmeterol-bound β_2AR (Clark et al., 1996; January et al., 1997; January et al., 1998; Tran et al., 2004; Moore et al., 2007b; Gimenez et al., 2015). Moreover, this would explain why forskolin also displayed substantially reduced IR_{max} values compared with E_{max} (Figures 3.6 and 3.7B), since it interacts directly with adenylate cyclase (Seamon and Daly, 1981; Zhang et al., 1997) and therefore receptor desensitisation is not a factor in the regulation of the cAMP response stimulated by forskolin.

Another factor that is worth considering is the relative binding affinities of the ligands for the receptor. One limitation of the initial rate of signal generation parameter is that is cannot account for ligand binding affinities and therefore, at submaximal ligand concentrations, ligand association rate may become the rate-limiting step rather than the agonist-occupied receptor's generation of the signal, thereby distorting initial rate values (Hoare et al., 2018; Hoare et al., 2022). However, the maximal initial rates are achieved at high ligand concentrations whereby sufficient ligand molecules should be present to bind rapidly to the receptor regardless of association rate, due to the effect of mass action (Hoare et al., 2020b). Therefore, although ligand association rates may affect measured kinetic potency (L_{50}) values, they are unlikely to account for the decreased IR_{max} values seen here. Salmeterol has a high binding affinity for the β_2AR relative to isoprenaline, formoterol and salbutamol due to both a fast association rate and a very slow dissociation rate with the receptor (Sykes and Charlton, 2012; Sykes et al., 2014). Despite its fast rate of association with β_2AR, salmeterol has been reported to have a slow onset of action (Johnson et al., 1993; Lötvall, 2001; Rosethorne et al., 2010). This may be due to the lipophilic nature of salmeterol

slowing its diffusion through aqueous solution and causing it to partition through the phospholipid cell membrane to access the receptor binding site (Rhodes et al., 1992; Johnson et al., 1993; Lötvall, 2001; Szczuka et al., 2009). Compared with less lipophilic ligands such as isoprenaline, formoterol and salbutamol which can access the receptor directly from the extracellular surface (Lötvall, 2001), this slows the onset of action of salmeterol. In addition, salmeterol has a much slower rate of dissociation with the β_2AR and a longer duration of action than the other tested ligands (Nials et al., 1993; Sykes and Charlton, 2012; Sykes et al., 2014), in part because it binds with high affinity to a β_2AR exosite consisting of residues from ECL2, ECL3 and the extracellular regions of TM6 and TM7 (Johnson et al., 1993; Green et al., 1996; Baker et al., 2015; Masureel et al., 2018). Salmeterol's slower dissociation rate means the time taken to reach binding equilibrium with the receptor is longer, which could potentially affect the initial rate of signal generation. Hoare et al. (2020b) have reported previously that slow ligand-receptor equilibration may have suppressed the initial rate of vasopressin-mediated cAMP production at the V_2 vasopressin receptor (V_2R), an effect that had earlier been predicted theoretically (Hoare et al., 2018). Ultimately though, these factors appear unlikely to play major roles in the differences between IR_{max} and E_{max} values observed here. This is because salbutamol is not particularly lipophilic (Rhodes et al., 1992; Johnson et al., 1993), exhibits a faster onset of action than salmeterol (Rosethorne et al., 2010) and comprises a dissociation rate at the β_2AR comparable to that of both isoprenaline and formoterol (Sykes and Charlton, 2012; Sykes et al., 2014), and yet salbutamol displays a similarly reduced IR_{max} as salmeterol (Figure 3.8). Therefore, reduced receptor desensitisation rate by partial agonists seems to be the key determinant in the reduction of IR_{max} relative to E_{max} values.

Whilst both the non-selective PDE inhibitor IBMX and the PDE4-selective rolipram substantially increased peak cAMP production mediated by isoprenaline through inhibition of cellular PDEs to prevent cAMP breakdown (Figures 3.9B), neither were able to alter the initial rate of production of cAMP (Figure 3.9C). This was unsurprising because, while the magnitude at which the response achieves its peak is dependent on the regulatory mechanisms counteracting the signal, the initial rate should be independent of these

mechanisms; instead measuring the rate of signal generation prior to their onset (Hoare et al., 2020b). On the other hand, it was hoped that the addition of PDE inhibitors may help to better define the specific mechanisms underlying the rate constants, k_1 and k_2. IBMX was shown to reduce k_2, whilst rolipram instead caused a reduction in k_1 (Table 3.5). Since no consistent effect could be determined on the rate constants by the PDE inhibitors, it was not possible to assign the rate constants to a specific regulatory mechanism (for example, k_2 to phosphodiesterase activity). Instead, they were considered operational rate constants and simply used to help fit the kinetic equation to the time-course data in order to define the initial response rates, which was the main focus in this study. Therefore, k_1 and k_2 have not been assessed further.

3.4.3 – Orthosteric antagonists acting at low receptor expression induce a hemi-equilibrium state which is amplified in kinetic parameters

In theory, a neutral antagonist is a ligand which binds to a receptor but does not shift the conformational state of the receptor toward either the inactive or active state and thus does not modulate receptor activity (Greasley and Clapham, 2006; Weis and Kobilka, 2018). An inverse agonist, on the other hand, stabilises the inactive state of the receptor and reduces constitutive activity (Greasley and Clapham, 2006; Berg and Clarke, 2018; Weis and Kobilka, 2018). Classifications of ligands as antagonists, inverse agonists or even weak partial agonists vary depending on differences in assay sensitivity, signal amplification, constitutive receptor activity and the cellular response being measured (Kenakin, 2004; Baker, 2010). In reality, few ligands appear to act as truly neutral antagonists, instead often exhibiting very weak partial agonism or inverse agonism (Kenakin, 2004; Greasley and Clapham, 2006; Baker, 2010). For example, propranolol, although often referred to as a β-adrenoceptor antagonist, has actually been found to display weak inverse activity at the β_2AR by reducing basal cAMP levels (Chidiac et al., 1994; Azzi et al., 2001; Baker et al., 2003a; Galandrin and Bouvier, 2006; Ferguson and Feldman, 2014). Furthermore, much

discussion has taken place over the classification of carvedilol, either as a weak inverse agonist (Yoshikawa et al., 1996; Wisler et al., 2007; Ferguson and Feldman, 2014), a weak partial agonist (Baker et al., 2003a; Benkel et al., 2022), or even as a β-arrestin biased agonist (Kim et al., 2008; Warne et al., 2012; Woo and Xiao, 2012) at the β_2AR. ICI-118551, however is generally considered a strong β_2AR-selective inverse agonist (Azzi et al., 2001; Baker et al., 2003a; Baker et al., 2003b; Hoffmann et al., 2004; Baker, 2005; Wisler et al., 2007). Bisoprolol is instead a β_1AR-selective inverse agonist (Iwata et al., 2001; Maack and Böhm, 2003; Hoffmann et al., 2004; Baker, 2005), but also shows some activity at the β_2AR (Baker et al., 2003a; Wisler et al., 2007).

In this study, application of each of the four antagonists/inverse agonists (propranolol, ICI-118551, carvedilol and bisoprolol) had no effect on basal cAMP levels in HEK293Gwt cells except very minor decreases at sub-micromolar concentrations (Figures 3.10A and 3.10B). This is because endogenous expression of the β_2AR in HEK293 cells is extremely low (Friedman et al., 2002; Goulding et al., 2021a; Goulding et al., 2021b), meaning no (or very little) constitutive receptor activity could be detected. Inverse agonists therefore appear simply as classical neutral antagonists in this system. This also provides some indication that the small response observed when vehicle control is applied to the cells is not stimulated predominantly by the β_2AR, as it is not inhibited by ICI-118551 or any of the other antagonists here. Instead, it is likely mediated by a combination of other endogenously expressed G_s-coupled receptors in HEK293 cells. This will be explored further in Chapter 4 but, for the purposes of this study, all data has been baseline-corrected against the vehicle (HBSS) response, hence why the HBSS condition in Figure 3.10B appears as zero (any inhibition of the response would therefore appear as a significantly negative response in the bar chart).

Preincubation of the slowly dissociating orthosteric antagonists carvedilol, ICI-118551 and propranolol (Sykes et al., 2014) concentration-dependently reduced the maximal peak response to both isoprenaline and formoterol (Figures 3.12A-3.12C and 3.13A-3.13C). This represents an insurmountable antagonism which is generally a characteristic of non-competitive allosteric antagonists (Gaddum

et al., 1955; Ariens et al., 1956; Vauquelin et al., 2002). In contrast, competitive orthosteric antagonists are classically considered to display a surmountable antagonism whereby increasing agonist concentration can overcome reductions in peak response and instead parallel rightward shifts in potency are observed (Gaddum et al., 1955; Ariens et al., 1956; Vauquelin et al., 2002). However, an apparent insurmountable antagonism effect can sometimes be produced by competitive antagonists in non-equilibrium conditions, as are likely to be present in the experiments performed here. This results from the failure of the preincubated antagonist-receptor complexes to dissociate sufficiently quickly to accommodate the required agonist binding (to the same binding site) to achieve a maximal response before regulatory mechanisms cause the response to peak and subsequently decay; the system is said to be in a state of hemi-equilibrium (Paton and Rang, 1965; Hopkinson et al., 2000; Vauquelin et al., 2002; Kenakin et al., 2006; Charlton and Vauquelin, 2010). The hemi-equilibrium phenomenon often occurs in low receptor expression systems where there is little receptor reserve to compensate for the 'loss' of a significant proportion of the receptors due to antagonist binding, reducing receptor reserve further (Kenakin et al., 2006; Charlton and Vauquelin, 2010; Goulding et al., 2021b). Extensive previous studies have also documented the resultant depression of the maximal agonist response (Kenakin and Cook, 1980; Liu et al., 1992; Christopoulos et al., 1999; Mould et al., 2014; Sykes et al., 2016), including on β_2AR-mediated responses by ICI-118551 (Hopkinson et al., 2000; Carter and Hill, 2005).

In contrast, preincubation with bisoprolol did not reduce maximal agonist responses (except for a slight reduction in isoprenaline, but not formoterol, E_{max} at the highest tested bisoprolol concentration), instead exhibiting a surmountable antagonism (Figures 3.12D and 3.13D). Bisoprolol has an extremely fast rate of dissociation with the β_2AR (Sykes et al., 2014), enabling sufficiently quick dissociation of antagonist-receptor complexes for the agonist to reach binding equilibrium in the required time for the maximal response to be achieved. The depression of the maximal response exhibited by each of the three slower dissociating antagonists reached a plateau whereby further increases in concentration of antagonist cause no further reduction in maximal response, instead rightward shifting agonist potency in a parallel manner. This observation

has also been reported previously (Liu et al., 1992; Christopoulos et al., 1999). Furthermore, the degree of reduction of agonist maximal responses correlated with the antagonist dissociation rates (carvedilol < ICI-118551 < propranolol < bisoprolol), according to Sykes et al. (2014).

Antagonist preincubation suppressed agonist maximal initial rates even more dramatically than maximal responses (Figures 3.16A and 3.16B). Even bisoprolol displayed a substantial reduction in IR_{max} at all tested concentrations despite its fast dissociation rate at the β_2AR. This was not surprising when accounting for the relative time of measurement of the initial rate and peak response parameters. In general, peak agonist-mediated cAMP responses were achieved approximately 2-5 min after agonist addition. Whereas the initial rate, although calculated by curve fitting of the entire time-course, represents the rate of generation of the cAMP signal within the first 0.2-0.5 min following addition of agonist, prior to the counteractive effects of regulatory mechanisms. Thus, fewer antagonist-receptor complexes will have dissociated during the relevant period of the response for measurement of the initial rate, compared with the later peak response, therefore further restricting the number of receptors available for agonist binding and resulting in lower agonist-mediated signal transduction during this period. By taking the reciprocal of the dissociation rate constants determined by Sykes et al. (2014), the residence times of each antagonist at the β_2AR can be estimated: 30.30 min (carvedilol), 4.76 min (ICI-118551), 2.17 min (propranolol) and 0.15 min (bisoprolol). These approximate residence times are compatible with the observations in this study whereby, for example, bisoprolol prevents the attainment of agonist binding equilibrium at the β_2AR in the required time-frame for initial rate measurement (0.2-0.5 min), but not for peak response (2-5 min). Meanwhile, the slowest dissociating antagonist carvedilol almost entirely abolished the initial rate response of both isoprenaline and formoterol, indicating that in the first couple of minutes after agonist application carvedilol is essentially showing irreversible binding and reducing the already limited number of receptors close to zero. While the effects of the hemi-equilibrium are exacerbated by further reductions in receptor reserve, increases in receptor expression should reverse the insurmountable antagonism seen here and restore agonist maximal responses (and initial rates), even in the

presence of slowly dissociating antagonists (Kenakin et al., 2006; Charlton and Vauquelin, 2010). In Chapter 4, similar agonist vs antagonist responses will be investigated in HEK293G cells stably overexpressing the β_2AR (HEK293G-β_2AR cells) to explore the role of receptor reserve in the nature of antagonist action and the hemi-equilibrium phenomenon.

3.4.4 – Kinetic data analysis can provide an accurate estimation of antagonist binding affinities and the nature of their antagonism

First described by Schild (1949) and Arunlakshana and Schild (1959), the method of Schild regression analysis has been an important tool for studying the complex interactions between agonists, antagonists and receptors, namely for determining competitive antagonist binding affinities for receptors using functional data and for pharmacological classification of ligands (Black et al., 1965; Black et al., 1972; Kenakin, 1982; Tallarida and Murray, 1987; Wyllie and Chen, 2007). It requires the calculation of dose ratios, which essentially represent the antagonist-induced rightward shift in agonist potency, at several distinct antagonist concentrations, followed by construction of a Schild plot in which the x-intercept of the linear regression line provides an estimate for antagonist binding dissociation constant (K_D). Moreover, the plotted Schild slope helps to elucidate the nature of the antagonism, be it competitive or otherwise (Kenakin, 1982). Usually, these analyses are performed where antagonist application simply elicits a parallel rightward shift in the agonist concentration-response without affecting the maximal response, however the same method can also be applied when depression of the agonist response maxima is observed (Arunlakshana and Schild, 1959; Kenakin, 1982; Tallarida and Murray, 1987; Christopoulos et al., 1999; Carter and Hill, 2005). As described earlier (see 3.3.4), rather than taking the EC_{50} agonist responses, equieffective agonist concentrations are instead taken to construct Schild plots, as performed in this study using both peak and initial rate data (Figures 3.17A-3.17F, 3.18A and 3.18B). Unfortunately, carvedilol binding affinity could not be determined

because it almost abolished agonist responses altogether. Moreover, use of the kinetic data only allowed calculation of the bisoprolol log K_D, for the same reason.

The antagonist log K_D values estimated here (Tables 3.8 and 3.9) were, as expected, unaffected by the agonist used and were largely in agreement with those determined previously by Baker (2005) through radioligand competition binding assays, which further validates this technique as a reliable method for characterising antagonist binding affinities. Interestingly, the estimation of bisoprolol binding affinity for the β_2AR did not differ based on the peak response or initial rate data, implying that Schild regression analysis of kinetic data may also provide an alternative, equally reliable estimation for antagonist binding affinities. From the peak response data, the Schild slopes (Table 3.8) for bisoprolol were very close to 1 (linear), evidencing the clear competitive action of bisoprolol. For propranolol and ICI-118551, this was less evident. Although a significant difference was only found in one of the four conditions, most of the Schild slopes deviated somewhat from 1 (with the exception of formoterol vs ICI-118551), which could be interpreted as a possible indication of non-competitive antagonist behaviour (Kenakin, 1982). However, both propranolol and ICI-118551 bind to the orthosteric site of the β_2AR and thus do act competitively with orthosteric agonists like isoprenaline and formoterol. Another reason for the deviation of Schild slopes from 1 is the existence of non-equilibrium conditions in the system (Kenakin, 1982). As has already been discussed, the slow receptor dissociation rates of propranolol and ICI-118551 (and carvedilol), but not bisoprolol, result in the state of hemi-equilibrium which caused the reduction in maximal agonist responses. This is the likely cause of the deviation of propranolol and ICI-118551 Schild slopes from 1, whilst bisoprolol (peak) Schild slopes did not. Supporting this, under the initial rate measurement bisoprolol also caused these hemi-equilibrium conditions, and as a result the Schild slopes derived from the kinetic bisoprolol data (Table 3.9) clearly deviate substantially from 1.

3.4.5 – The effective antagonism of the partial agonist salmeterol on isoprenaline-mediated cAMP responses

By simultaneously applying isoprenaline and salmeterol to HEK293Gwt cells and measuring resultant cAMP responses, insights into the competitive action of agonists of differing efficacies were revealed. Despite its agonist activity at the β_2AR, 1 μM salmeterol exhibited an antagonistic effect on isoprenaline-mediated cAMP production, causing a 100-fold rightward shift in isoprenaline potency (Figure 3.19A). This is due to salmeterol's competition with isoprenaline for the same receptor binding pocket, thereby essentially reducing the already limited number of available receptors (Friedman et al., 2002; Goulding et al., 2021a; Goulding et al., 2021b). Because of its lower intrinsic efficacy for signal transduction, the salmeterol-bound receptor cannot compensate for this loss of isoprenaline-mediated response beyond its maximal response (roughly 40% of maximal isoprenaline response in this experiment). Eventually, further increases in isoprenaline concentration allow the full agonist to outcompete salmeterol for receptor binding sites, thus restoring the maximal isoprenaline response (at 10 μM isoprenaline). Therefore, the antagonism displayed by salmeterol was surmountable. This is likely because, unlike the antagonists tested earlier, salmeterol was not preincubated and so had not reached binding equilibrium with the receptor prior to competition with isoprenaline. A previous study by McCrea and Hill (1993) showed a very similar effect of competing isoprenaline and salmeterol on cAMP responses in B50 neuronal cells. It was interesting that the estimated binding affinity of salmeterol for the β_2AR was much lower in this study than that determined through radioligand competition binding assays by Baker (2010). However, similar findings were made previously by Carter and Hill (2005) who determined salmeterol log K_D values via the same method (Stephenson, 1956) by investigating simultaneous addition of isoprenaline and salmeterol on β_2AR-β-arrestin-2 interactions using a β-galactosidase complementation assay and also by McCrea and Hill (1993), who studied the concurrent addition of these same agonists on cAMP responses in neuronal B50 cells and also used the same method by Stephenson (1956) for calculation of K_D values.

The converse experiment, in which increasing salmeterol concentrations were tested in the presence and absence of 1 μM isoprenaline, also highlighted the antagonistic effect by salmeterol on isoprenaline-mediated cAMP production. Salmeterol concentration-dependently inhibited the maximal isoprenaline response (Figure 3.19B), as the lower efficacy salmeterol began to outcompete isoprenaline for the limited receptor binding sites. This response inhibition reached a plateau at the maximal salmeterol response (approximately 40% of maximal isoprenaline response) and a log IC_{50} value could be derived for the inhibition of the isoprenaline response by salmeterol. When analysed kinetically these data very were similar (Figures 3.19C and 3.19D). Just as with the determination of bisoprolol log K_D values described earlier, calculation of salmeterol binding affinity for the β_2AR did not alter depending on the use of either peak response or initial rate data. Kinetic analysis of functional responses from complex ligand-receptor interactions can therefore provide an alternative, reliable route for determination of binding affinities of ligands at receptors.

3.5 – Conclusion

Kinetic analysis of the full profile of ligand-mediated β_2-adrenoceptor (β_2AR) responses obtained using the cAMP GloSensor^{TM} luminescence assay in HEK293Gwt cells, according to Hoare et al. (2020b), has enabled the determination of newly established kinetic parameters of ligand activity, including the initial rate of signal generation. Comparisons of these kinetic parameters with classic pharmacological ligand parameters showed a general correlation between maximal responses (E_{max}) and maximal initial rates (IR_{max}), but also revealed decreased IR_{max} values compared with E_{max} values of the partial agonists salbutamol and salmeterol, but not the full agonist formoterol, relative to the reference ligand isoprenaline. This may result from reduced desensitisation rates by partial agonist-occupied receptors, thus allowing the cAMP response to peak at a higher magnitude due to less regulatory pressure counteracting the signal. Additionally, with the exception of the fast-dissociating bisoprolol, preincubation of competitive antagonists substantially reduced agonist E_{max} values to varying degrees which correlated with their dissociation rates at the β_2AR. This was indicative of the existence of hemi-equilibrium conditions, resulting from extremely low receptor reserve in HEK293Gwt cells and the incomplete dissociation of antagonist in the time-frame required for maximal agonist response to be achieved. Determination of kinetic parameters revealed that this effect was more drastic in terms of the reduction of agonist IR_{max} values, with even bisoprolol causing a large reduction in agonist maximal initial rates. It has also been shown that these new kinetic parameters of ligand responses can be utilised to reliably determine ligand-receptor binding affinities.

Taken together, this study has demonstrated that analysing the kinetics of the entire time-course of agonist-stimulated receptor responses can uncover valuable new information about the pharmacological and kinetic properties of ligands and their complex interactions with receptors at low, endogenous expression levels in living cells. Therefore, quantifying these new kinetic parameters and considering them in combination with more standard pharmacological parameters can provide a fuller picture of ligand activity and potentially enable more accurate ligand characterisation.

Chapter 4

Investigating β_2-adrenoceptor mechanical stimulation and the effect of overexpression on receptor pharmacology

4.1 – Introduction

Many studies have previously examined the influence of receptor expression levels on ligand-receptor pharmacology (Kenakin, 1995; Kenakin, 1997; January et al., 1998; McDonald et al., 2003; Leach et al., 2007) and constitutive receptor activity (MacEwan and Milligan, 1996; Berg et al., 1999; Engelhardt et al., 2001; Leeb-Lundberg et al., 2001; Chanrion et al., 2008). Measurements of ligand parameters such as agonist efficacy and potency have been shown to be dependent on receptor expression levels (Hoyer and Boddeke, 1993; Kenakin, 1996; January et al., 1998; McDonnell et al., 1998; McDonald et al., 2003; Baker, 2010), as is the interpretation of antagonist behaviour (Hopkinson et al., 2000; Vauquelin et al., 2002; Carter and Hill, 2005; Kenakin et al., 2006; Charlton and Vauquelin, 2010). Moreover, constitutive activity, which is the ability of a receptor to initiate downstream signalling pathways ligand-independently by spontaneous conformational change to their active state (Cerione et al., 1984a; Costa and Herz, 1989; Cotecchia et al., 1990; Samama et al., 1993; Park et al., 2008), is rarely detectable in low or endogenous expression conditions but can often be readily measured upon exogenous overexpression of receptors (Lefkowitz et al., 1993; Berg et al., 1999; Leurs et al., 2000; Engelhardt et al., 2001; Leeb-Lundberg et al., 2001; Milligan, 2003; Berg and Clarke, 2018). This in turn provides an opportunity to study the activity of inverse agonists, which reduce constitutive signalling by stabilising the inactive receptor conformation (Costa and Herz, 1989; Greasley and Clapham, 2006; Berg and Clarke, 2018).

Mechanical stimulation is the ability of a receptor to recognise and respond to mechanical stimuli (rather than agonist binding) (Chachisvilis et al., 2006; Erdogmus et al., 2019; Hu et al., 2022; Wilde et al., 2022). This has been demonstrated in several GPCRs (Storch et al., 2012; Marullo et al., 2020; Wilde et al., 2022; Hu et al., 2022). GPCR mechanostimulation is thought to serve several physiological functions, in particular in the cardiovascular system where vessel blood flow may regulate processes including vasodilation and angiogenesis via mechanosensitive receptors expressed on vascular endothelial cells (Groves et al., 1995; Busch et al., 2015; Xu et al., 2018; Hong et al., 2020;

Tanaka et al., 2021; Hu et al., 2022). The mechanisms underpinning GPCR mechanostimulation are largely not well understood at present, although mechanically-induced active receptor conformations are thought to differ from those mediated by agonist binding (Zhang et al., 2009; Storch et al., 2012; Wang et al., 2018; Erdogmus et al., 2019; Poudel et al., 2023). In Chapter 1, a more detailed summary of our current understanding of GPCR mechanostimulation and its physiological relevance is provided (see 1.3.5 – Mechanostimulation of GPCRs).

Recent work by Virion et al. (2019) has revealed that the β_2-adrenoceptor (β_2AR) can act as a mechanosensor by transducing mechanical stimuli applied by meningococcus bacteria into β-arrestin-biased signalling pathways. In order to cross the blood-brain barrier and cause cerebrospinal meningitis and/or sepsis, meningococcus pili interact with human endothelial cells by binding to Neu5Ac sialic acid residues at the tip of N-glycan chains attached to the N-terminus of the β_2AR (Coureuil et al., 2010; Virion et al., 2019; Marullo et al., 2020; Marullo et al., 2022). The bacterial pili subsequently exert pulling traction forces on the N-glycans which are transduced by the receptor to promote GRK-mediated β-arrestin recruitment and activate ERK- and Src-mediated delocalisation of cytoskeletal proteins from endothelial junctions in order to cross the blood-brain barrier through resultant gaps in the endothelium (Coureuil et al., 2010; Lemichez et al., 2010; Virion et al., 2019; Marullo et al., 2020). The emergence of a mechanostimulatory function of the β_2AR, a receptor which is prevalently expressed in vascular smooth muscle and endothelial cells and implicated in cardiovascular processes such as vasodilation, opens up the question as to whether the β_2AR also plays a mechanosensory role in these physiological processes. The β_2AR mediates vasodilation primarily through cAMP-dependent phosphorylation of cellular proteins by PKA (Haynes et al., 1992; Velmurugan et al., 2019), however in the previous study by Virion et al. (2019), no production of cAMP was stimulated by β_2AR mechanostimulation.

Receptor glycosylation is a common type of post-translational modification of proteins which involves the attachment of one or more oligosaccharides (carbohydrates) to the protein by glycosidic bonds (Moremen et al., 2012; Reily

et al., 2019). In N-linked glycosylation, the large carbohydrate molecule is directed to a nitrogen in the side-chain of an asparagine residue within a specific consensus sequence NxS/T (where N refers to the asparagine, x can be any amino acid except proline and S/T is a serine or threonine residue) on the polypeptide by an oligosaccharyltransferase enzyme in the endoplasmic reticulum (Landolt-Marticorena and Reithmeier, 1994; Aebi, 2013; Bieberich, 2014). The other major type of glycosylation is O-linked glycosylation, whereby a carbohydrate is instead attached to an oxygen in the side-chain of one of several possible amino acids, but most often serine or threonine (Steen et al., 1998; An et al., 2009). N-glycan chains assist in the correct and efficient folding of proteins in the endoplasmic reticulum by increasing polypeptide solubility, altering the energy landscape of the unfolded and folded states and recruiting molecular chaperones which mediate the folding process (Ruddon and Bedows, 1997; Shental-Bechor and Levy, 2009; Aebi et al., 2010; Braakman and Hebert, 2013; Bieberich, 2014; Ahn et al., 2017; Esmail and Manolson, 2021). This in turn helps to increase protein stability and improve receptor trafficking (Vagin et al., 2009; Fiedler and Simons, 1995; Imperiali and O'Connor, 1999). Properly folded proteins are packaged into vesicles and trafficked via the Golgi apparatus to the cell membrane, while misfolded proteins are instead targeted for degradation by proteasomes (Römisch, 2005; Geva and Schuldiner, 2014; Tannous et al., 2015). The attachment of N-glycan chains to folding polypeptides not only increases the rate and success of correct folding, but can also block proteolytic cleavage sites and shield hydrophobic regions, thus increasing protein stability by preventing proteasomal degradation (Kundra and Kornfeld, 1999; Hanson et al., 2009; Braakman and Hebert, 2013; Esmail and Manolson, 2021).

Furthermore, receptor N-glycosylation has been shown to play roles in receptor function and signalling (George et al., 1986; Chen et al., 1998; Pang et al., 1999; Min et al., 2015; Li et al., 2017; Vuorio et al., 2021; Marullo et al., 2022). It has been implicated in many (patho-)physiological processes such as in the nervous system (neural development and transmission), the immune system (pathogen recognition and immune cell migration) and in cancer (tumour proliferation and metastasis) (Lau and Dennis, 2008; Zhao et al., 2008; Scott and Panin, 2014;

Taniguchi and Kizuka, 2015; Takahashi et al., 2016; Yale et al., 2018; de Haas et al., 2020). In addition to the recent finding that N-glycans mediate the transduction of meningococcus pili traction forces into intracellular signals at the β_2AR, several other studies have also implicated their potential importance in receptor mechanosensory functions (Knoepp et al., 2017; Knoepp et al., 2020; Marhuenda et al., 2021).

In this study, cAMP GloSensor^{TM} luminescence was measured using a newly developed stably overexpressing β_2AR HEK293G cell line (HEK293G-β_2AR) to assess the effect of high receptor expression on β_2AR responses to agonists and antagonists/inverse agonists. Ligand parameters were compared with those previously determined under low, endogenous β_2AR expression conditions. Additionally, a mechanosensory function of the β_2AR was revealed whereby a mechanical stimulus (caused by the linear motion of opening and closing the PHERAstar FSX door) was transduced into a transient cAMP signalling response. The role of receptor N-glycosylation in β_2AR mechanostimulation was explored by mutation of specific asparagine residues within the extracellular N-glycosylation recognition sequences of the receptor.

4.2 – Materials and methods

Molecular biology

All molecular biology was performed as described in Chapter 2 (see 2.3 – Molecular biology).

Cell culture

HEK293 cells stably expressing the cAMP GloSensor™ biosensor (HEK293Gwt) and HEK293 cells stably expressing both the TS-SNAP-β_2AR construct and the cAMP GloSensor™ biosensor (HEK293G-β_2AR) were used throughout this Chapter and were passaged and seeded into 96-well assay plates (including transient transfections where relevant) as described previously in Chapter 2 (See 2.4 – Cell culture).

Generation of new stable cell lines

The HEK293G-β_2AR cell line was developed as explained in Chapter 2 (see 2.5 – Generation of new stable cell lines).

cAMP GloSensor™ assay

Most of the data presented in this Chapter were obtained by performing the cAMP GloSensor™ assay. This technique was performed as described in Chapter 2 (see 2.7 – cAMP GloSensor™ assay).

HiBiT-LgBiT complementation assay

The HiBiT-LgBiT complementation assay was performed as stated in Chapter 2 (see 2.8 – HiBiT-LgBiT complementation assay).

Data analysis and statistics

Analysis of the data was carried out as stated in Chapter 2 (see 2.12 – Data analysis and statistics).

4.3 – Results

4.3.1 – Development and functional screening of a stable β_2-adrenoceptor-overexpressed HEK293G clonal cell line

In order to investigate the impact of increased receptor expression on ligand-receptor pharmacology and to compare functional responses with those seen under endogenous, low expression conditions, a new HEK293 clonal cell line was developed which stably overexpressed both the GloSensor™ biosensor and the human β_2-adrenoceptor (β_2AR). This was performed by transfection of a TS-SNAP-β_2AR construct into HEK293Gwt cells, simultaneous antibiotic selection for both the TS-SNAP-β_2AR and GloSensor™ plasmids, and subsequent dilution cloning to generate the new cell line from a single clone. This process was described in detail in Chapter 2 (see 2.5 – Generation of new stable cell lines) and the new, highly β_2AR-expressing cells were termed HEK293G-β_2AR cells. An important part of the dilution cloning stage of the process was to select a single clone to take forward from numerous candidates. A total of 48 clonal candidates were identified and functionally screened using the cAMP GloSensor™ luminescence assay.

Initially, each clone was tested for its luminescence output under four conditions: forskolin (100 μM), isoprenaline (100 nM), 30 min preincubation of ICI-118551 (100 nM) followed by isoprenaline (100 nM), and HBSS (vehicle control). Each condition was performed in singlet, and the clones were spread over three separate plates because all clones could not fit within one plate, each of which also contained HEK293Gwt controls for comparison. Many of the clonal candidates showed considerably increased peak response to isoprenaline compared to HEK293Gwt cells, potentially indicating successful overexpression of the β_2AR. These included the four clones 19, 25, 40 and 44, shown in Figure 4.1, which were selected from this initial screen and taken forward.

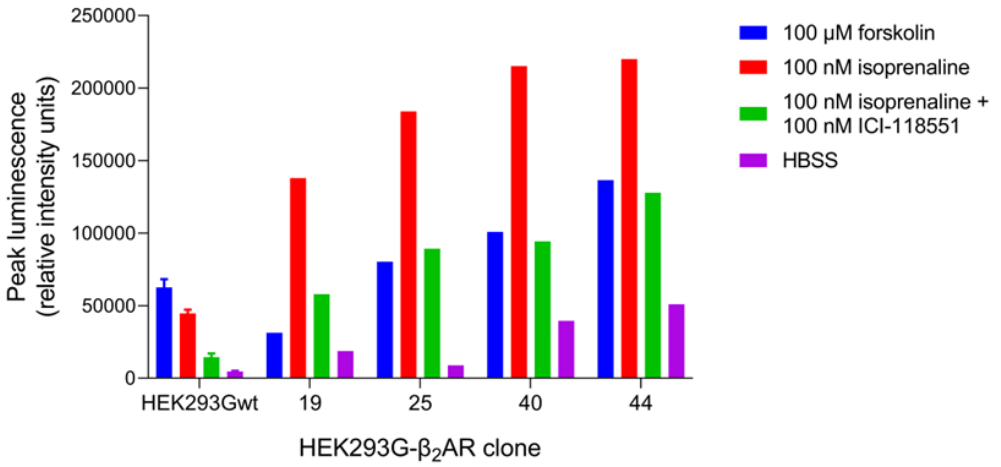

Figure 4.1: GloSensor™ luminescence stimulated by ligand-mediated cAMP production. Bar chart showing peak response for 100 µM forskolin, 100 nM isoprenaline, 100 nM isoprenaline + 30 min preincubated 100 nM ICI-118551 or HBSS (vehicle) applied to HEK293Gwt cells or four HEK293G-β_2AR clonal cell candidates. Data points represent mean ± SEM (HEK293Gwt) or absolute values (HEK293G-β_2AR), expressed as relative intensity units (RIU) of luminescence, from one (HEK293G-β_2AR) or three (HEK293Gwt) independent experiment(s) (n = 1 or 3).

Clones 19, 25, 40 and 44 were then further tested by performing agonist concentration-response curves using formoterol (Figures 4.2A-4.2D). Formoterol showed very similar functional activity with each clone, producing concentration-dependent responses in each case. Each clone showed markedly increased responses to formoterol than was seen in the HEK293Gwt controls and formoterol potency was also left-shifted in each case (compared with Figure 3.6). In addition, responses to both forskolin and to the vehicle control HBSS were also substantially increased compared to in HEK293Gwt cells. Similar results were obtained with each clone when using salmeterol instead of formoterol as the agonist (data not shown).

Since the functional responses by all four clones were very similar, each of the candidates would have been appropriate choices to select for use going forward. Clone 44 was ultimately selected to derive the clonal HEK293G-β_2AR cell line used throughout this Chapter. This was primarily because it showed a slightly larger HBSS response compared with the other clones, which would allow for interesting studies into the mechanism behind this response and into the effects of inverse agonists. In addition, clone 44 displayed consistently clean agonist responses and exhibited a similarly fast cell growth rate to that of HEK293Gwt cells.

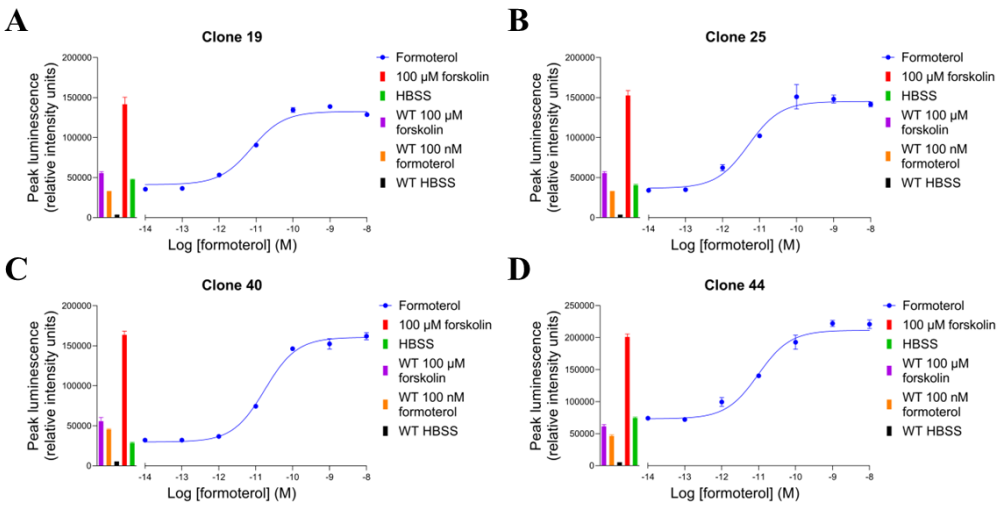

Figure 4.2: GloSensor^{TM} luminescence stimulated by formoterol-mediated cAMP production. Mean peak concentration-response curves for formoterol in HEK293G-β_2AR clonal cell candidates, plus 100 µM forskolin (HEK293G-β_2AR and HEK293Gwt), HBSS (HEK293G-β_2AR and HEK293Gwt) and 100 nM formoterol (HEK293Gwt) controls, expressed as expressed as relative intensity units (RIU) of luminescence. Data points represent mean ± SEM from triplicate measurements in one experiment (n = 1).

4.3.2 – Investigating mechanical stimulation of β_2-adrenoceptor-mediated cAMP responses

During the development of the HEK293G-β_2AR cell line, a large agonist-like response to application of the vehicle control HBSS was observed. A similar, but much smaller response had previously been observed in work involving HEK293Gwt cells (Figures 3.1A and 3.1B). Here, the responses to HBSS in HEK293Gwt cells and HEK293G-β_2AR cells were directly compared, with the combined time-course data for these responses displayed in Figure 4.3A. The HEK293G-β_2AR response was found to be substantially greater than HEK293Gwt, reaching a peak magnitude more than 10-fold larger (Figure 4.3B; 35638 RIU ± 2570 RIU, compared with 2880 RIU ± 1018 RIU; $P < 0.0001$) before ultimately decaying back toward the baseline. Moreover, considerable response remains of the HEK293G-β_2AR signal after 60 min, whereas the HEK293Gwt response has returned entirely to the baseline within the first 30 min. Interestingly, the initial basal luminescence read at $t = 0$ (0 min) is similar in both HEK293G-β_2AR and HEK293Gwt cells (Figure 4.3C; 480.13 RIU ± 61.45 RIU, compared with 266.87 RIU ± 116.56 RIU; $P > 0.05$).

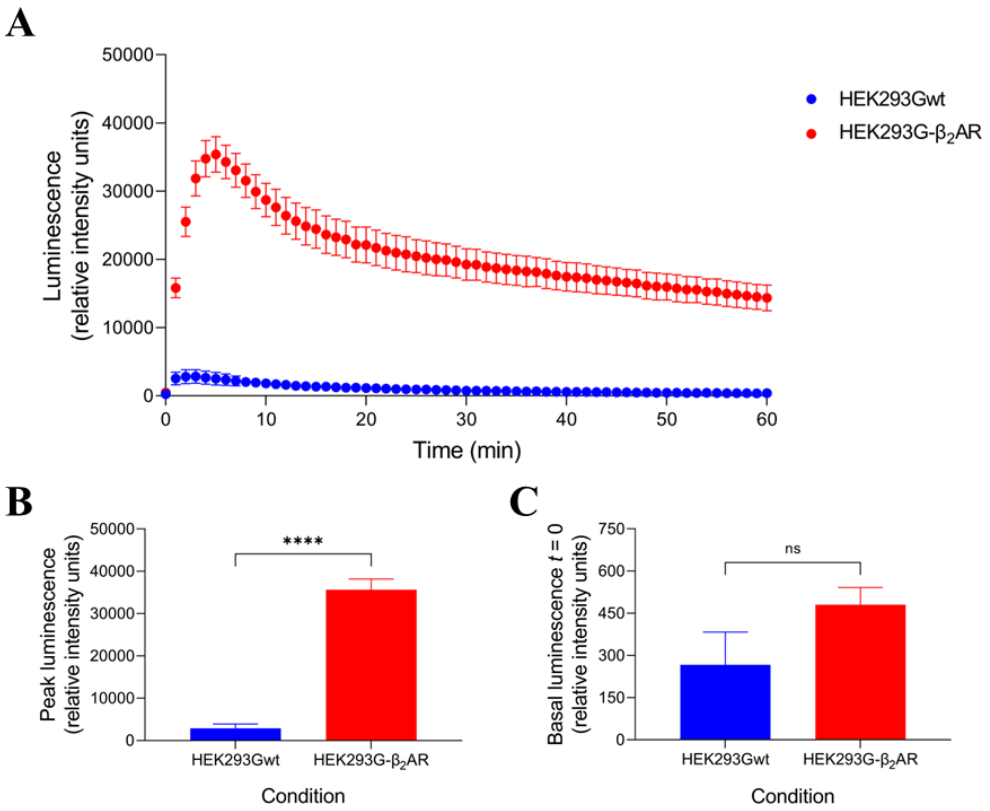

Figure 4.3: GloSensor™ luminescence stimulated by cAMP production after application of HBSS. (A) Combined GloSensor™ luminescence time-course data over 60 min following application of HBSS to HEK293Gwt or HEK293G-β_2AR cells. (B, C) Bar charts displaying mean peak (B) and $t = 0$ (C) response for HBSS in HEK293Gwt and HEK293G-β_2AR cells. Data points represent mean ± SEM expressed as relative intensity units (RIU) of luminescence, from five independent experiments ($n = 5$). Significant differences are indicated, determined by an unpaired *t*-test. $P < 0.05$ was used as the level for significance ($P \geq 0.05$ = ns, $P < 0.0001$ = ****).

To study ligand pharmacology in the β_2AR-overexpression system, four agonists were applied to HEK293G-β_2AR cells and luminescence was again measured using the cAMP GloSensor^{TM} assay. As in the studies in the low, endogenous expression system (Chapter 3), two full agonists (isoprenaline and formoterol) and two partial agonists (salbutamol and salmeterol) were used. Combined time-course data for increasing concentrations of each agonist are presented in Figures 4.4A-D. This time the GloSensor^{TM} time-course data has not been baseline-corrected, to allow the modulation of the vehicle response to be easily visualised. Each agonist stimulated a concentration-dependent increase in the cAMP response above that of the vehicle. Peak luminescence values were normalised against 1 nM isoprenaline (with the HBSS response adjusted to 0% to distinguish the agonist-mediated response) and taken to construct peak concentration-response curves, fitted to a standard sigmoidal curve using the Hill equation (Equation 1), shown in Figure 4.5. In contrast with the previous data from HEK293Gwt cells, all four agonists stimulated similar maximal responses ($P > 0.05$), including both of the partial agonists. The potencies of each ligand were leftward shifted in HEK293G-β_2AR cells compared with HEK293Gwt ($P < 0.0001$ for each; Tables 4.1 and 3.4), with formoterol, isoprenaline and salbutamol exhibiting 100-fold increases in potency, while salmeterol potency increased 10-fold. Table 4.1 displays the maximal responses (E_{max}) and potencies (log EC_{50}) of each agonist for the β_2AR in HEK293G-β_2AR cells.

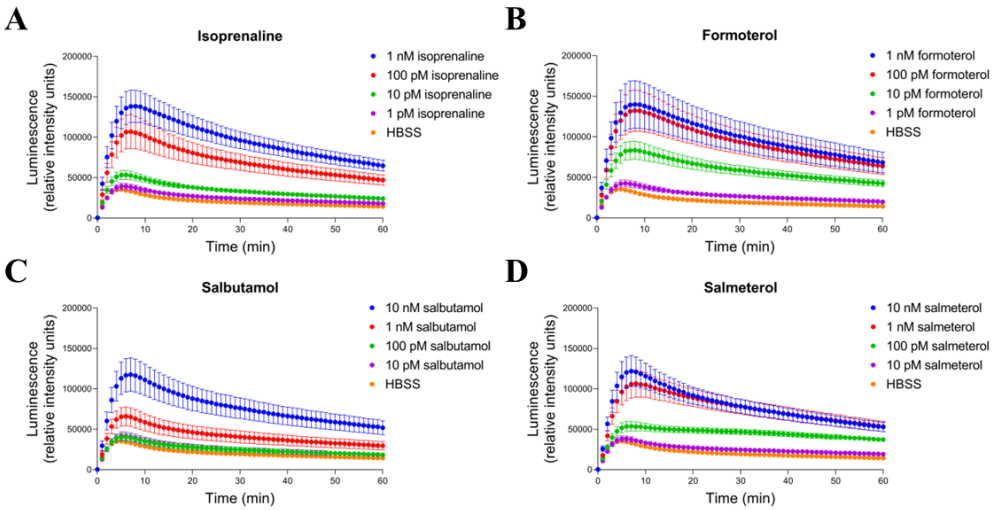

Figure 4.4: GloSensor^{TM} luminescence stimulated by ligand-mediated cAMP production. (A-D) Combined GloSensor^{TM} luminescence time-course data over 60 min following application of isoprenaline (1 pM – 1 nM; A), formoterol (1 pM – 1 nM; B), salbutamol (10 pM – 10 nM; C), salmeterol (10 pM – 10 nM; D) or HBSS (A-D) to HEK293G-β_2AR cells. Data points represent mean ± SEM expressed as relative intensity units (RIU) of luminescence, from five independent experiments (n = 5).

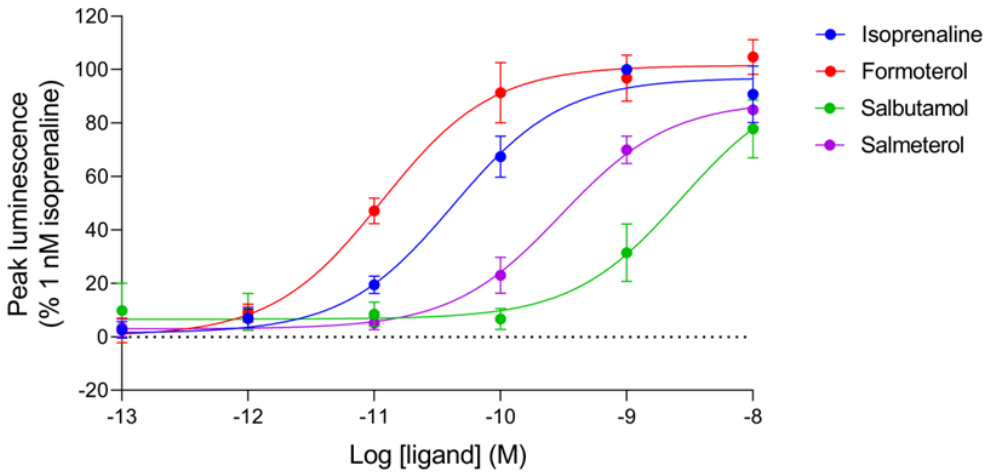

Figure 4.5: GloSensor^{TM} luminescence stimulated by ligand-mediated cAMP production. Mean peak concentration-response curves for isoprenaline formoterol, salbutamol and salmeterol in HEK293G-β_2AR cells expressed as a percentage of 1 nM isoprenaline with the HBSS response normalised to zero. Data points represent mean ± SEM from five independent experiments (n = 5). Significant differences were determined by a one-way ANOVA with Tukey's multiple comparisons test.

Agonist	E_{max} (% 1 nM isoprenaline) ± SEM	Log EC_{50} (M) ± SEM
Isoprenaline	100	-10.35 ± 0.15
Formoterol	104.73 ± 6.50	-10.95 ± 0.12
Salbutamol	77.81 ± 10.84	-8.46 ± 0.16
Salmeterol	84.94 ± 6.38	-9.53 ± 0.10

Table 4.1: Agonist mean E_{max} and log EC_{50} values ± SEM determined for isoprenaline, formoterol, salbutamol and salmeterol from concentration-response curves obtained by cAMP GloSensor^{TM} in HEK293G-β_2AR cells from five independent experiments (n = 5).

Next, five antagonists or inverse agonists were tested to investigate whether they modulated the large vehicle response in HEK293G-β_2AR cells. These included the four ligands tested in HEK293Gwt cells (propranolol, ICI-118551, carvedilol and bisoprolol) as well as carazolol. Combined time-course data are displayed in Figures 4.6A-4.6E for each of these antagonist/inverse agonists, which all caused a concentration-dependent reduction in the HBSS cAMP response. Carvedilol displayed a biphasic effect, whereby its inhibition of the cAMP response had reached a maximum level at 1 μM, but at 100 μM it appeared to entirely abolish cytosolic cAMP after roughly 10 min (Figure 4.6C). This was not seen from any of the other ligands, even at such high concentrations, and was assumed to be a non-specific effect. 100 μM carvedilol was therefore excluded from further analysis here. Peak luminescence values were again normalised, this time against the HBSS response, and peak concentration-response curves were generated (Figure 4.7) and fitted to a sigmoidal curve using the Hill equation (Equation 2). Each ligand reduced the peak cAMP response to a similar degree ($P > 0.05$), while the rank order of potency was as follows: carazolol = propranolol > ICI-118551 = carvedilol > bisoprolol. The maximal inhibitions of the peak response (I_{max}) and inhibitory potencies (log IC_{50}) for each of the ligands are stated in Table 4.2.

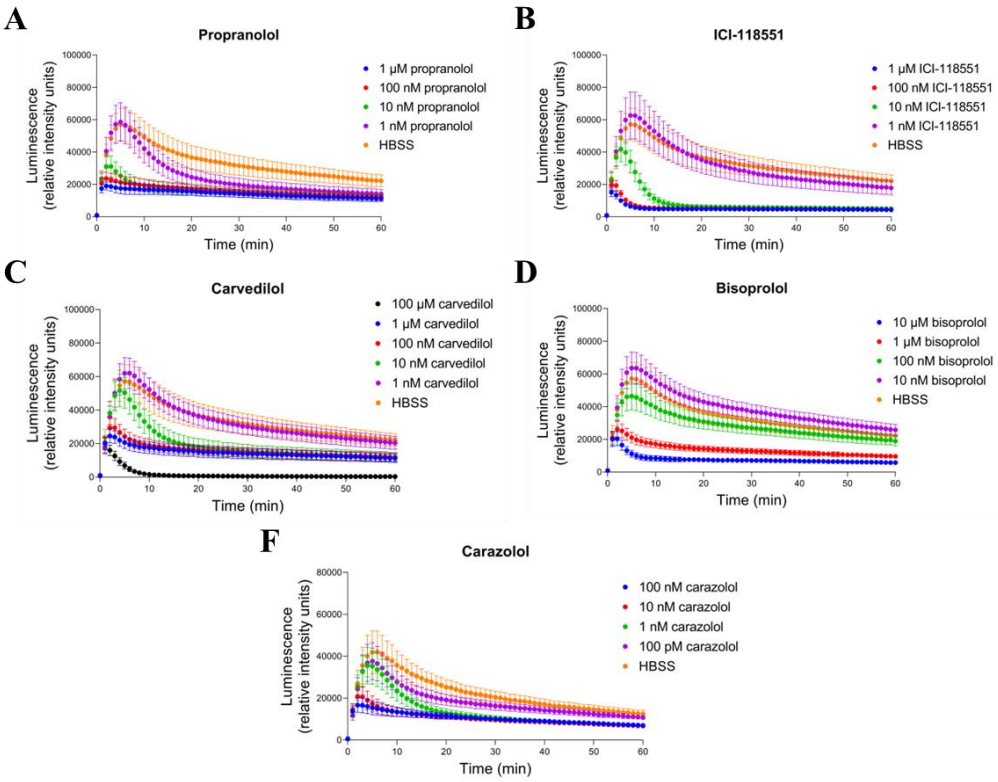

Figure 4.6: GloSensor^{TM} luminescence measured after application of antagonists/inverse agonists. (A-E) Combined GloSensor^{TM} luminescence time-course data over 60 min following application of propranolol (1 nM – 1 µM; A), ICI-118551 (1 nM – 1 µM; B), carvedilol (1 nM – 1 µM; C), bisoprolol (10 nM – 10 µM; D), carazolol (100 pM – 100 nM; E) or HBSS (A-E) to HEK293G-β_2AR cells. Data points represent mean ± SEM expressed as relative intensity units (RIU) of luminescence, from five independent experiments (n = 5).

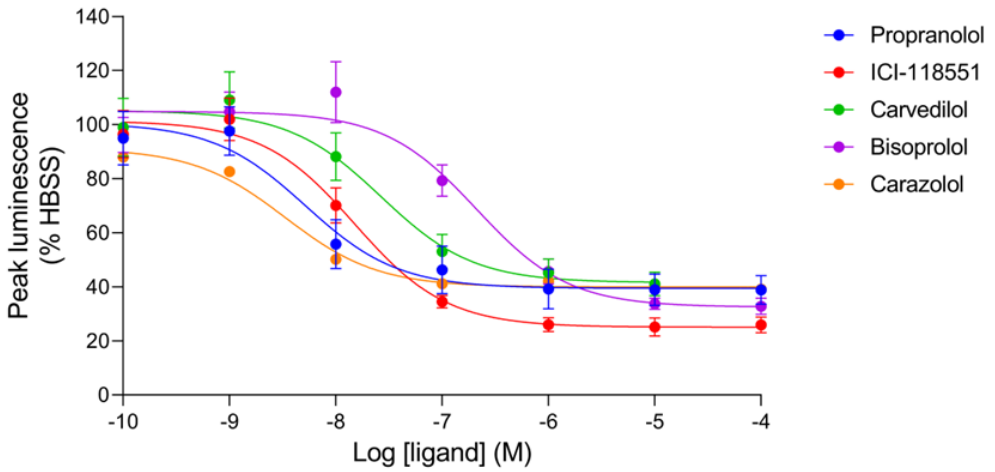

Figure 4.7: GloSensor^{TM} luminescence measured after application of antagonists/inverse agonists. Mean peak concentration-response curves for propranolol, ICI-118551, carvedilol, bisoprolol and carazolol in HEK293G-β_2AR cells expressed as a percentage of HBSS. Data points represent mean ± SEM from five independent experiments (n = 5). Significant differences were determined by a one-way ANOVA with Tukey's multiple comparisons test.

Antagonist/inverse agonist	I_{max} (% HBSS) ± SEM	Log IC_{50} (M) ± SEM
Propranolol	38.88 ± 5.31	-8.29 ± 0.08
ICI-118551	25.14 ± 3.36	-7.83 ± 0.05
Carvedilol	41.10 ± 4.32	-7.55 ± 0.08
Bisoprolol	32.82 ± 3.00	-6.68 ± 0.10
Carazolol	39.13 ± 3.38	-8.47 ± 0.05

Table 4.2: Antagonist/inverse agonist mean I_{max} and log IC_{50} values determined for propranolol, ICI-118551, carvedilol, bisoprolol and carazolol from peak concentration-response curves obtained by cAMP GloSensor™ in HEK293G-β_2AR cells from five independent experiments (n = 5).

To determine whether changes in flow induced by the addition of buffer to the cells immediately prior to the assay was responsible for the stimulation of cAMP production in response to vehicle, the GloSensor™ protocol was modified slightly to reduce the fluid flow in the wells. Normally, after 2 h incubation with the 50 µL GloSensor™ cAMP reagent (in HBSS) and subsequent basal luminescence read, 50 µL further HBSS or ligand (in HBSS) is added to each well, followed by luminescence measurements for 60 min. Hence this is referred to as a 50:50 buffer addition ratio here. This time, cells were incubated for 2 h in 90 µL GloSensor™ cAMP reagent, followed by addition of 10 µL HBSS or ligand before the 60 min luminescence measurement (ligand/reagent concentrations were adjusted accordingly). This is instead referred to here as a 90:10 buffer addition ratio. By adding a smaller volume of buffer into the wells, cells should be exposed to less flow of fluid. Figures 4.8A and 4.8B show that altering the buffer addition ratio as described had no effect on either the time-course or the peak magnitude of the response, respectively ($P > 0.05$). Next, the 50:50 buffer addition ratio was compared with a 'no addition' condition whereby no buffer was added to the HEK293G-β_2AR cells immediately prior to the 60 min luminescence read. A 10 µM ICI-118551 condition was also included. Again, there was no reduction in the cAMP response in the 'no addition' condition compared to HBSS ($P > 0.05$; Figures 4.9A and 4.9B), while ICI-118551 inhibited the response greatly ($P < 0.0001$). This same test was performed in HEK293Gwt cells to study the similar but much smaller response observed. Again, the 'no addition' condition had no effect on the production of cAMP in HEK293Gwt cells, and this time the addition of ICI-118551 also did not reduce the response ($P > 0.05$ for both; Figures 4.9C and 4.9D).

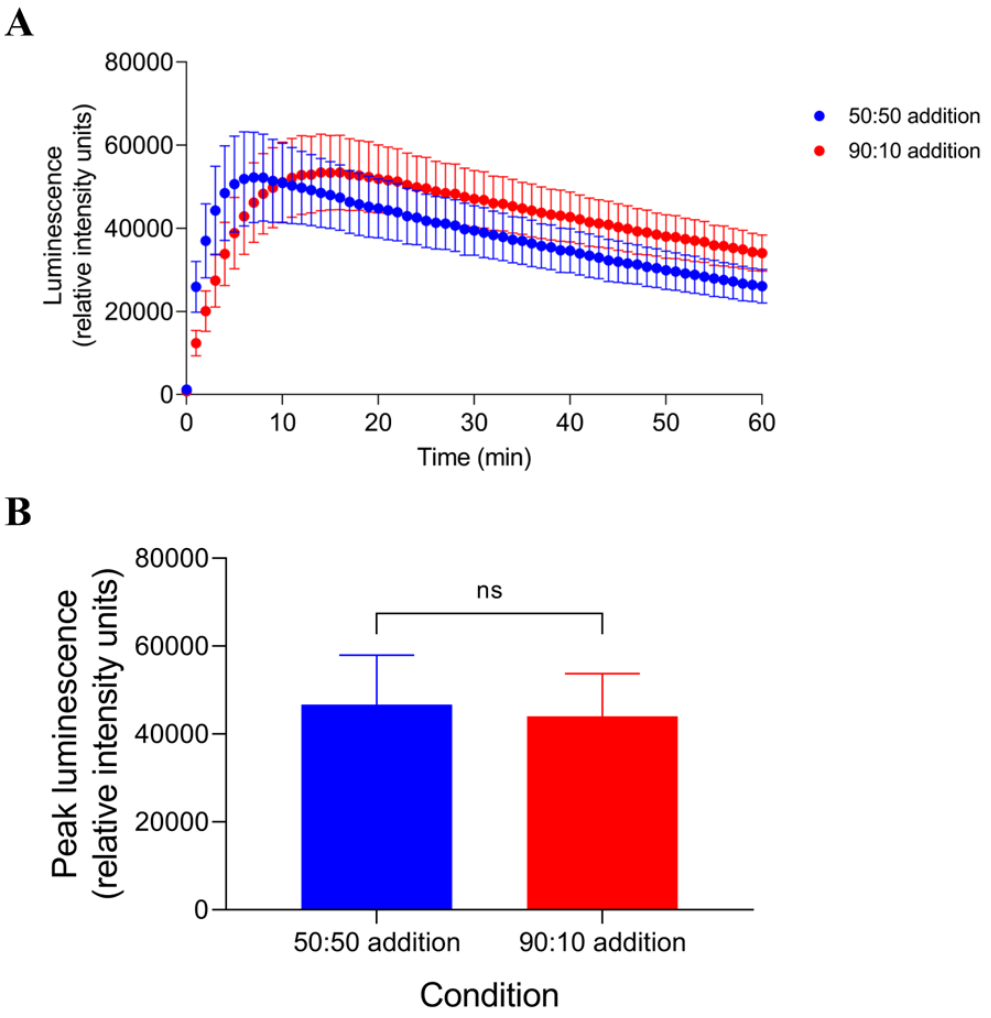

Figure 4.8: GloSensor™ luminescence stimulated by cAMP production. (A) Combined GloSensor™ luminescence time-course data over 60 min following application of 50:50 or 90:10 buffer addition ratios of HBSS to HEK293G-β_2AR cells. (B) Bar chart displaying mean peak response for 50:50 or 90:10 buffer addition ratios of HBSS in HEK293G-β_2AR cells. Data points represent mean ± SEM expressed as relative intensity units (RIU) of luminescence, from five independent experiments (n = 5). Significant differences are indicated, determined by an unpaired t-test. $P < 0.05$ was used as the level for significance ($P \geq 0.05$ = ns).

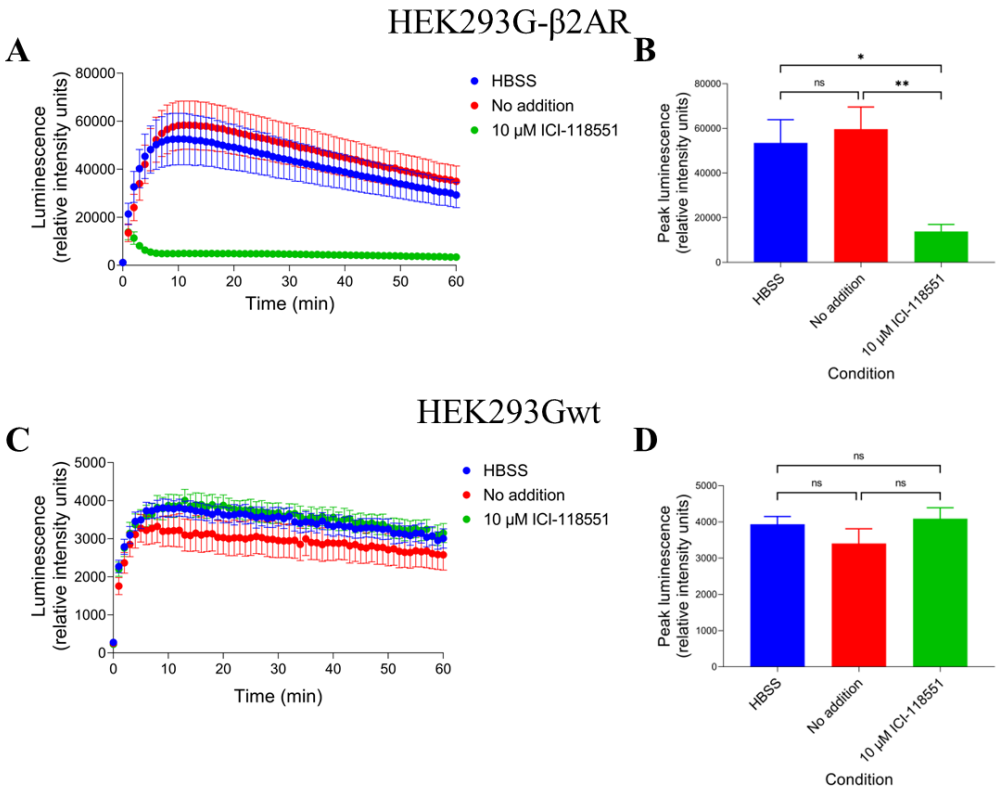

Figure 4.9: GloSensor™ luminescence stimulated by cAMP production. (A-D) Combined time-course GloSensor™ luminescence time-course data over 60 min (A, C) or bar charts displaying mean peak response (B, D) following application of HBSS, 'no addition' or 10 μM ICI-118551 to HEK293G-β_2AR cells (A, B) or HEK293Gwt cells (C, D). Data points represent mean ± SEM expressed as relative intensity units (RIU) of luminescence, from five independent experiments ($n = 5$). Significant differences are indicated, determined by a one-way ANOVA with Tukey's multiple comparisons test. $P < 0.05$ was used as the level for significance ($P \geq 0.05$ = ns, $P < 0.05$ = *, $P < 0.01$ = **).

When loading the microplate into the PHERAstar FSX microplate reader (BMG Labtech, Offenburg, Germany), the opening and/or closing of the door exposed the plate to a sustained linear motion as the tray was moved into position to measure luminescence. To determine whether this movement was able to initiate a mechanical response by the β_2AR, conditions of 1 μM isoprenaline, HBSS and 1 μM ICI-118551 were applied to HEK293G-β_2AR cells and luminescence was read for 60 min, but this time the PHERAstar door was reopened and then closed every 15 min (at 0 min, 15 min, 30 min and 45 min during the program) to provide the same linear movement to the cells each time. As can be observed by the combined time-course data shown in Figure 4.10A, each interval at which the PHERAstar door was opened and subsequently closed immediately caused a rapid increase in cAMP production, which quickly reached a peak and then began to decline. The application of isoprenaline produced a larger initial increase in cAMP levels than HBSS, followed by subsequent mechanical stimulations similar to those seen in the HBSS conditions. Application of ICI-118551 unsurprisingly largely antagonised the mechanical responses, although very small response increases can still be observed after each stimulation. The same experiment was then performed in completely dark conditions, whereby the plate was never exposed to light either at the start of the experiment or during each opening and closing of PHERAstar door, to rule out any effect of light sensitivity. The same sequential responses were indeed observed under these dark conditions (Figure 4.10B).

Next, the plate shaking function of the PHERAstar was employed instead of opening and closing of the PHERAstar door, allowing the rotation velocity, direction (linear or orbital) and duration to be modified to better characterise the mechanical response. 100 rpm velocity (for 5 s) was tested as this was the slowest setting and most closely mimicked that of the plate movement upon door closing. Unexpectedly, however, application of both linear and orbital 100 rpm shake functions caused no sequential cAMP responses after the initial response (which still resulted from the initial opening and closing of the door at the start of the assay), displayed in Figures 4.10C and 4.10D. Several other rotation velocities (200 rpm, 400 rpm) and durations (1 s) were also tested and produced similar results (Supplementary Figures 8.2A-8.2D). This method was then

altered slightly in Figure 4.11 by initially applying no ligand or buffer to any conditions (but the plate is still exposed to the linear motion from the PHERAstar door movement) before reading luminescence for 30 min. Subsequently, 1 μM isoprenaline, HBSS and 1 μM ICI-118551 were applied to the HEK293G-β_2AR cells which were also then subject to the same mechanical stimulation by the opening and closing of the PHERAstar door. Again, all conditions exhibited an initial rise in cAMP production, to which addition of ICI-118551 causes rapid diminishment back to the baseline whilst isoprenaline increases above that of the HBSS condition. Finally, the sequential mechanical stimulation experiments were also performed on HEK293Gwt cells to determine whether the response in these cells is also mediated through mechanical stimulation. Similar to the previous observations in HEK293G-β_2AR cells, Figure 4.12A shows that HEK293Gwt cells also responded to sequential mechanical stimulations by opening and closing the PHERAstar door, albeit on a much smaller scale. Again, no subsequent responses were observed when employing the linear 100 rpm shake function (Figure 4.12B) or at any other tested shaking condition (Supplementary Figures 8.3A-8.3D).

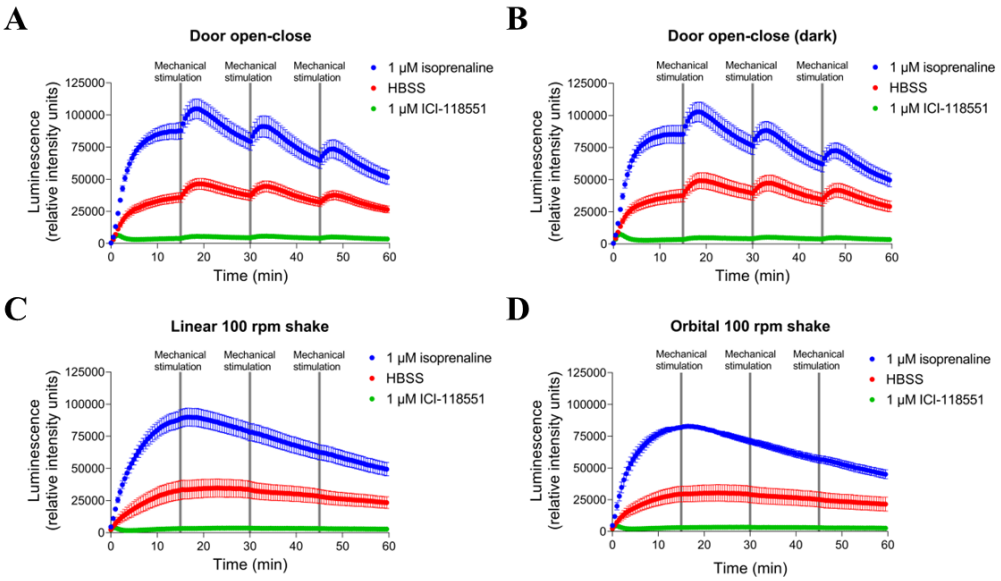

Figure 4.10: GloSensor™ luminescence stimulated by cAMP production. (A-D) Combined GloSensor™ luminescence time-course data over 60 min following application of isoprenaline (1 µM), HBSS or ICI-118551 (1 µM) and different sequential mechanical stimuli (at 0 min, 15 min, 30 min and 45 min): opening and closing of the PHERAstar FSX door (A), opening and closing of the PHERAstar FSX door in dark conditions (B), 5 s linear 100 rpm shake (C) and 5 s orbital 100 rpm shake (D) to HEK293G-β_2AR cells. Data points represent mean ± SEM expressed as relative intensity units (RIU) of luminescence, from five independent experiments (n = 5).

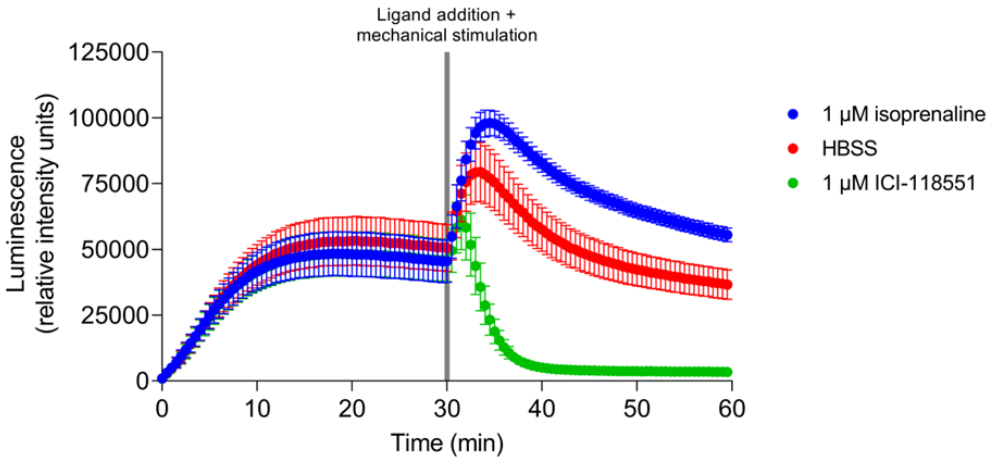

Figure 4.11: GloSensor^{TM} luminescence stimulated by cAMP production. Combined GloSensor^{TM} luminescence time-course data over 60 min following sequential mechanical stimuli (at 0 min and 30 min; opening and closing of the PHERAstar FSX door) and application (at 30 min) of isoprenaline (1 µM), HBSS or ICI-118551 (1 µM) to HEK293G-β_2AR cells. Data points represent mean ± SEM expressed as relative intensity units (RIU) of luminescence, from five independent experiments (n = 5).

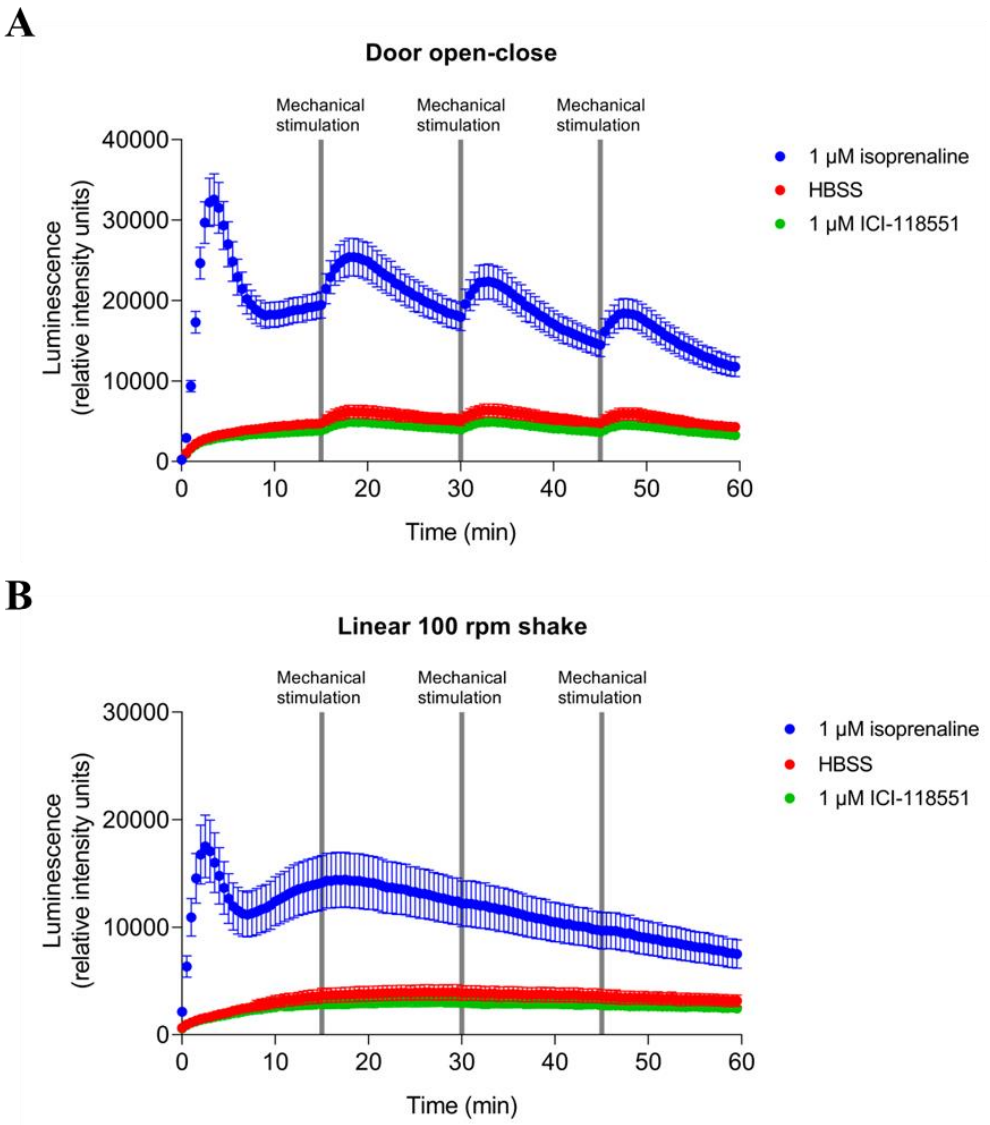

Figure 4.12: GloSensor™ luminescence stimulated by cAMP production. (A, B) Combined GloSensor™ luminescence time-course data over 60 min following application of isoprenaline (1 µM), HBSS or ICI-118551 (1 µM) and different sequential mechanical stimuli (at 0 min, 15 min, 30 min and 45 min): opening and closing of the PHERAstar FSX door (A) and 5 s linear 100 rpm shake (B) to HEK293Gwt cells. Data points represent mean ± SEM expressed as relative intensity units (RIU) of luminescence, from five independent experiments (n = 5).

4.3.3 – Determining the involvement of receptor N-glycosylation in mediating mechanical activation in the β_2-adrenoceptor

Using the methods described in Chapter 2 (see 2.3 – Molecular biology), several DNA constructs encoding the β_2AR were developed, including two mutant receptors which had either two or three asparagine residues residing at the N-terminus (Asn6 and Asn15) or ECL2 (Asn187) substituted for alanine residues. These residues are important in N-glycosylation of the β_2AR, a process that attaches oligosaccharide chains to specific asparagine residues of receptors, which is important for proper protein folding in the endoplasmic reticulum, protein stability and even signal transduction (Hanson et al., 2009; Aebi et al., 2010; Braakman and Hebert, 2013; Bieberich, 2014; Esmail and Manolson, 2021). Previous work has also shown that N-glycans attached to the N-terminus of the β_2AR are directly involved in conferring mechanosensitivity of the receptor to traction forces exerted by meningococcus pili (Virion et al., 2019; Marullo et al., 2020). To reveal whether a similar mechanism was responsible for mediating the stimulation of cAMP production in absence of agonists observed in this study, the two mutant receptor constructs (HiBiT-β_2AR_N6A_N15A and HiBiT-β_2AR_N6A_N15A_N187A) as well as a wildtype construct (HiBiT-β_2ARwt) were transiently transfected into HEK293Gwt cells and cAMP responses were compared using the cAMP GloSensor^{TM} assay. Substitution of the asparagine residues in the mutant receptors should prevent N-glycosylation as these residues act as the recognition sites for N-glycan oligosaccharide chains to bind to the receptor (Aebi, 2013; Bieberich, 2014).

Firstly, however, a HiBiT-LgBiT complementation assay was performed to measure relative NanoBiT luminescence emission indicating cell surface expression, in order to confirm a similar expression of each receptor construct on cell membranes. As depicted in Figure 4.13, a similar luminescence intensity was measured for each of the constructs, therefore indicating that receptor surface expression was unaffected by the asparagine mutations. It was also important to confirm that the expression and function of the GloSensor^{TM} biosensor was unaffected by the transient transfection. Combined cAMP GloSensor^{TM} time-course data from HEK293G cells transiently expressing each

receptor construct showed that the response to 100 μM forskolin was the same in each case (peak responses $P > 0.05$; Figure 4.14A). Additionally, the response to 1 μM isoprenaline was also unaffected in each of the receptor constructs (peak responses $P > 0.05$; Figure 4.14B).

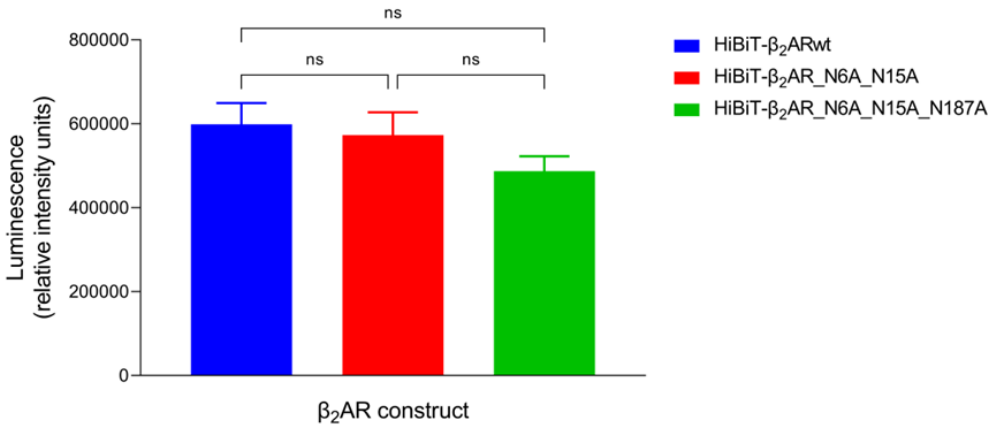

Figure 4.13: NanoBiT luminescence emission from HiBiT-LgBiT complementation. Bar chart displaying mean luminescence emission measured following simultaneous application of 0.2% LgBiT protein and 0.25% Nano-Glo® luciferase assay substrate to HEK293Gwt cells transiently transfected with HiBiT-β2ARwt, HiBiT-β2AR_N6A_N15A or HiBiT-β2AR_N6A_N15A_N187A receptor constructs. Data points represent mean ± SEM expressed as relative intensity units (RIU) of luminescence, from six independent experiments (n = 6). Significant differences are indicated, determined by a one-way ANOVA with Tukey's multiple comparisons test. $P < 0.05$ was used as the level for significance ($P \geq 0.05$ = ns).

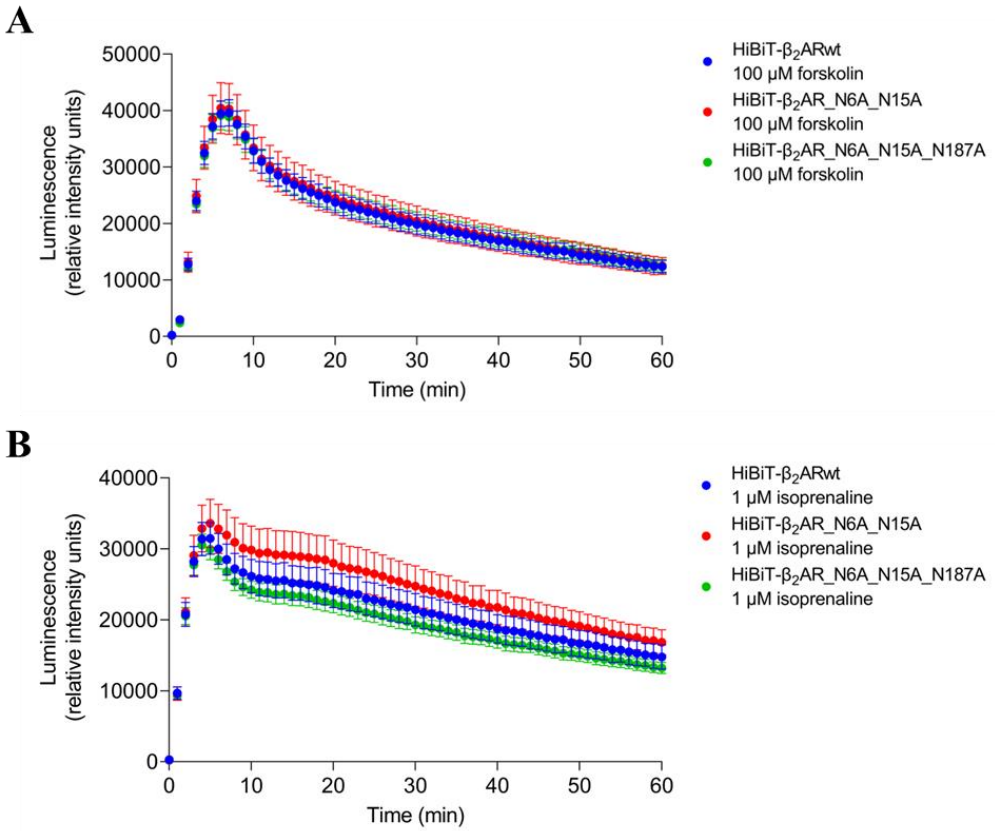

Figure 4.14: GloSensor™ luminescence stimulated by ligand-mediated cAMP production. (A, B) Combined GloSensor™ luminescence time-course data over 60 min following application of forskolin (100 µM; A) or isoprenaline (1 µM; B) to HEK293Gwt cells transiently transfected with HiBiT-β_2ARwt, HiBiT-β_2AR_N6A_N15A or HiBiT-β_2AR_N6A_N15A_N187A receptor constructs. Data points represent mean ± SEM expressed as relative intensity units (RIU) of luminescence, from six independent experiments (n = 6). Significant differences were determined by a one-way ANOVA with Tukey's multiple comparisons test.

Upon application of HBSS, however, decreased cAMP production was measured in cells transfected both with HiBiT-β_2AR_N6A_N15A (6776.78 RIU ± 751.50 RIU; $P < 0.05$) and particularly HiBiT-β_2AR_N6A_N15A_N187A (4766.00 RIU ± 566.03 RIU; $P < 0.001$), compared with HiBiT-β_2ARwt (9603.28 RIU ± 844.72 RIU; Figures 4.15A and 4.15B). However, with each of the constructs, including even HiBiT-β_2AR_N6A_N15A_N187A ($P < 0.05$), the response could still be inhibited by 1 μM ICI-118551 (Figures 4.15A and 4.15C).

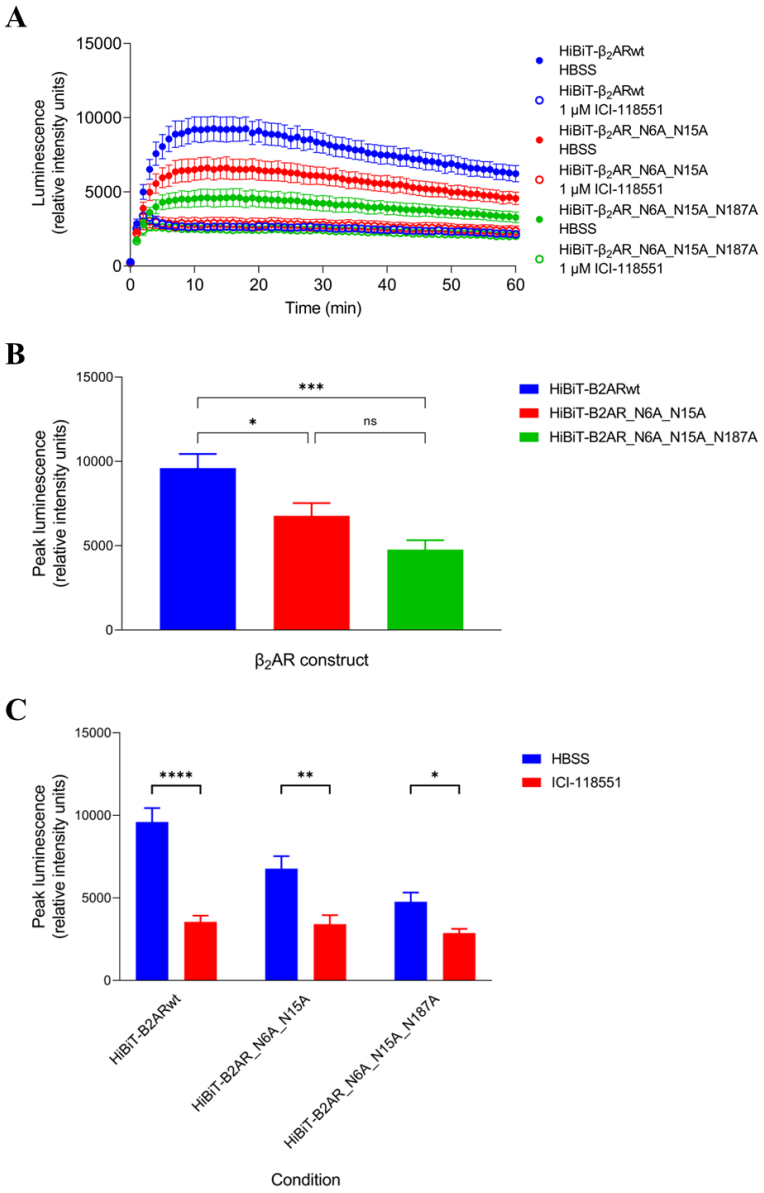

Figure 4.15: GloSensor™ luminescence stimulated by cAMP production. (A-C) Combined GloSensor™ luminescence time-course data over 60 min (A) or bar charts displaying mean peak response (B, C) following application of HBSS (A-C) or ICI-118551 (1 μM; A, C) to HEK293Gwt cells transiently transfected with HiBiT-β2ARwt, HiBiT-β2AR_N6A_N15A or HiBiT-β2AR_N6A_N15A_N187A receptor constructs. Data points represent mean ± SEM expressed as relative intensity units (RIU) of luminescence, from six independent experiments (n = 6). Significant differences are indicated, determined by a one-way ANOVA with Tukey's multiple comparisons test. $P <$ 0.05 was used as the level for significance ($P \geq 0.05$ = ns, $P < 0.05$ = *, $P < 0.01$ = **, $P < 0.001$ = ***, $P < 0.0001$ = ****).

A similar set of experiments were then performed but this time with an additional pcDNA3.1(+) plasmid-transfected control to directly compare the mechanical response in the presence and absence of transfected β_2AR constructs. This time, cAMP GloSensor^{TM} data are all normalised to the 100 μM forskolin response. Firstly, the pcDNA3.1(+) control was shown to produce almost no luminescence (except small background) compared with the β_2AR-transfected constructs in the HiBiT-LgBiT complementation assay ($P < 0.0001$; Figure 4.16A), confirming no transfection of a HiBiT-tagged receptor. The profile of forskolin responses were similar between conditions transfected with each receptor construct and the pcDNA3.1(+) control ($P > 0.05$; Figure 4.16B), whilst 1 μM isoprenaline produced approximately similar peak responses ($P > 0.05$) but the profile of the responses differed considerably with the pcDNA3.1(+) control showing a much faster rate of signal decay (Figure 4.16C).

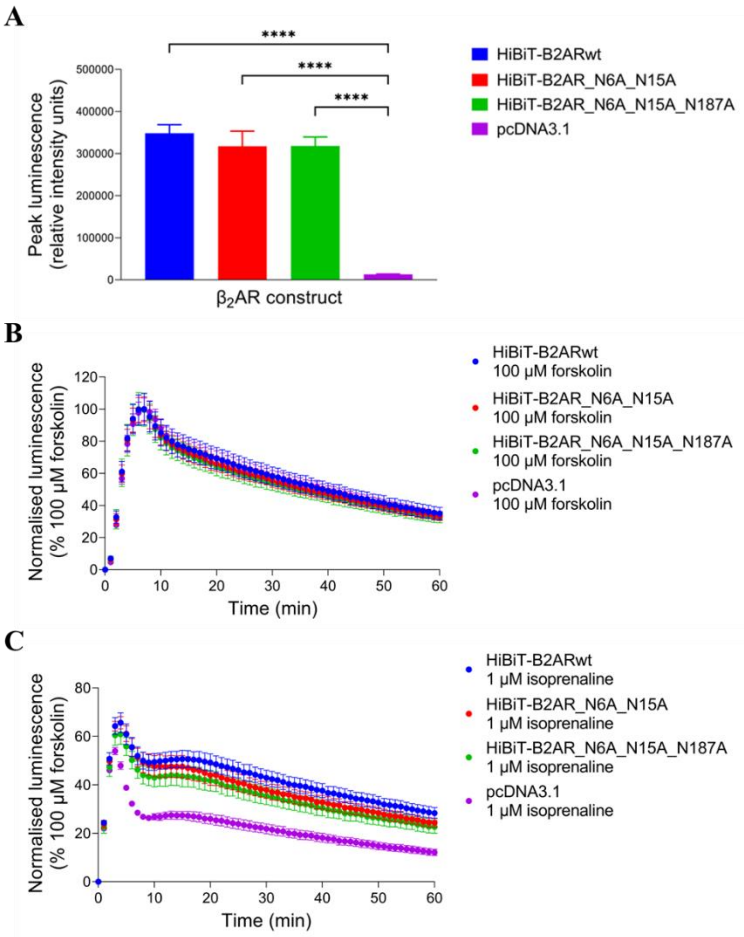

Figure 4.16: NanoBiT luminescence emission from HiBiT-LgBiT complementation and GloSensor™ luminescence stimulated by ligand-mediated cAMP production. (A) Bar chart displaying mean luminescence emission measured following simultaneous application of 0.2% LgBiT protein and 0.25% Nano-Glo® luciferase assay substrate to HEK293Gwt cells transiently transfected with HiBiT-β2ARwt, HiBiT-β2AR_N6A_N15A or HiBiT-β2AR_N6A_N15A_N187A receptor constructs or pcDNA3.1(+) control. (B, C) Combined GloSensor™ luminescence time-course data over 60 min following application of forskolin (100 µM; B) or isoprenaline (1 µM; C) to HEK293Gwt cells transiently transfected with HiBiT-β2ARwt, HiBiT-β2AR_N6A_N15A or HiBiT-β2AR_N6A_N15A_N187A receptor constructs or pcDNA3.1(+) control. Data points represent mean ± SEM expressed as relative intensity units (RIU) of luminescence (A) or as a percentage of 100 µM forskolin (B, C), from six independent experiments (n = 6). Significant differences are indicated, determined by a one-way ANOVA with Tukey's multiple comparisons test. $P <$ 0.05 was used as the level for significance ($P < 0.0001$ = ****).

The same trend was observed again between the three transfected β_2AR constructs after application of HBSS, whereby HiBiT-β_2ARwt showed the largest response which was slightly reduced in HiBiT-β_2AR_N6A_N15A and further reduced in HiBiT-β_2AR_N6A_N15A_N187A. Here, the pcDNA3.1(+) control appeared to show a slight further reduction again compared to HiBiT-β_2AR_N6A_N15A_N187A, although this was not found to be significant ($P > 0.05$; Figures 4.17A and 4.17B). Transfected cells were also exposed to repeated mechanical stimuli (opening and closing of the PHERAstar door every 15 min) to confirm the mechanostimulatory effect was altered by the mutations in the β_2AR. Once again, the order of magnitude of HBSS responses were the same (HiBiT-β_2ARwt > HiBiT-β_2AR_N6A_N15A > HiBiT-β_2AR_N6A_N15A_N187A > pcDNA3.1(+); Figure 4.18).

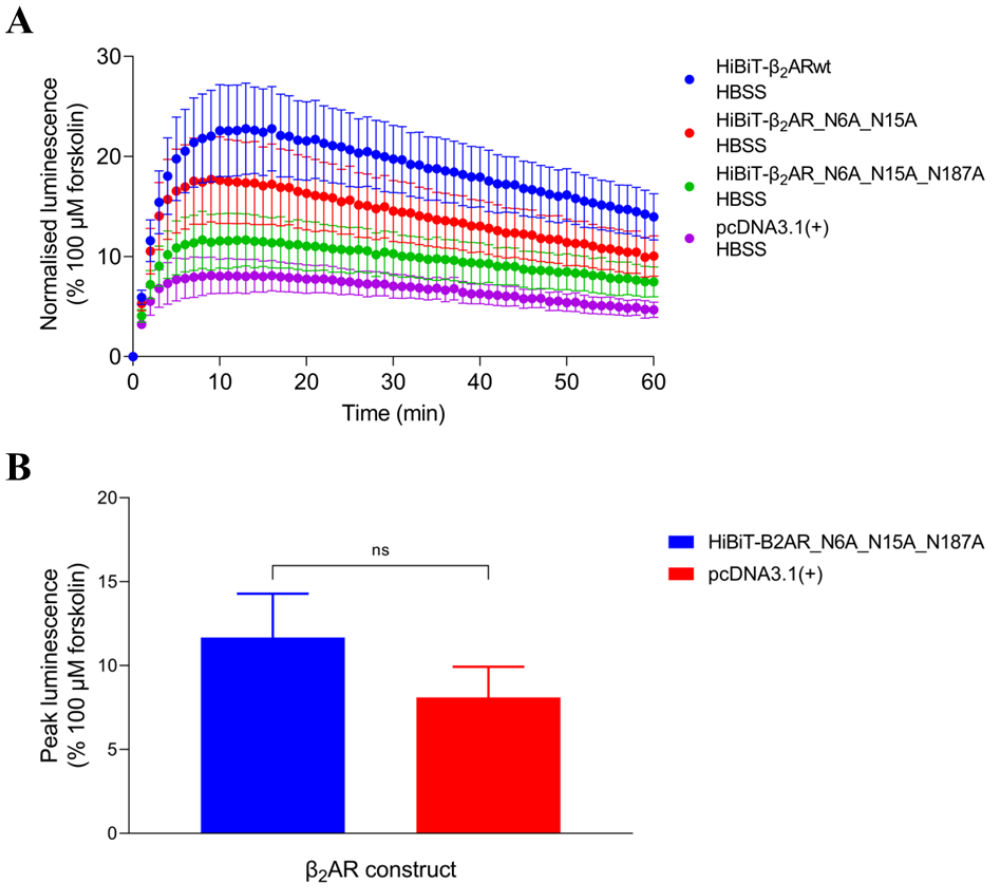

Figure 4.17: GloSensor™ luminescence stimulated by cAMP production. (A, B) Combined GloSensor™ luminescence time-course data over 60 min (A) or bar chart displaying mean peak response (B) following application of HBSS to HEK293Gwt cells transiently transfected with HiBiT-β2ARwt (A only), HiBiT-β2AR_N6A_N15A (A only) or HiBiT-β2AR_N6A_N15A_N187A (A, B) receptor constructs or pcDNA3.1(+) control (A, B). Data points represent mean ± SEM expressed as a percentage of 100 µM forskolin, from six independent experiments ($n = 6$). Significant differences are indicated, determined by a one-way ANOVA with Tukey's multiple comparisons test. $P < 0.05$ was used as the level for significance ($P \geq 0.05$ = ns).

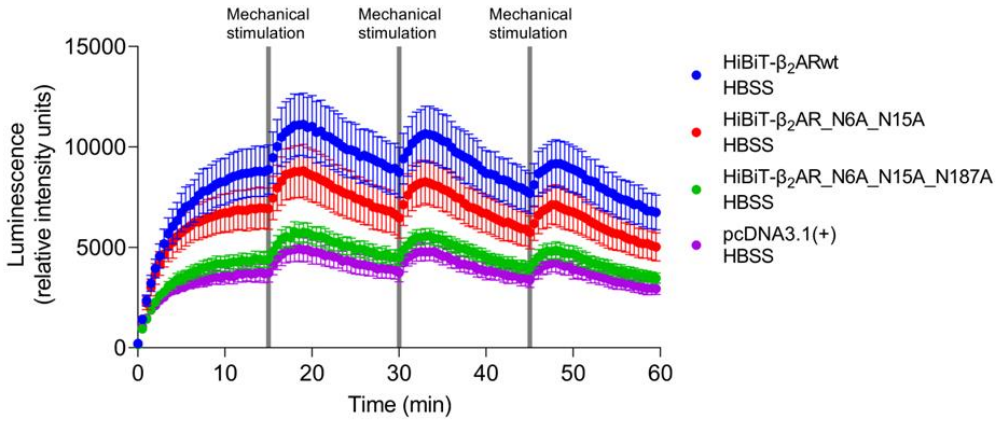

Figure 4.18: GloSensor^{TM} luminescence stimulated by cAMP production. Combined GloSensor^{TM} luminescence time-course data over 60 min following application of HBSS and sequential mechanical stimuli (at 0 min, 15 min, 30 min and 45 min): opening and closing of the PHERAstar FSX door to HEK293Gwt cells transiently transfected with HiBiT-β_2ARwt, HiBiT-β_2AR_N6A_N15A or HiBiT-β_2AR_N6A_N15A_N187A receptor constructs or pcDNA3.1(+) control. Data points represent mean ± SEM expressed as relative intensity units (RIU) of luminescence, from six independent experiments (n = 6).

4.3.4 – Studying the effect of receptor overexpression on the pharmacology and kinetics of agonist-mediated β_2-adrenoceptor cAMP GloSensor^{TM} responses

Agonist peak response parameters in HEK293G-β_2AR cells were discussed earlier in this Chapter (Figures 4.4A-4.4D, 4.5 and Table 4.1) and compared with HEK293Gwt data, whereby the partial agonists salbutamol and salmeterol produced greater maximal responses (E_{max} values were similar to those of isoprenaline and formoterol) and each of the four agonists showed a marked leftward shift in potency (log EC_{50}) at the receptor. Much like with the HEK293Gwt responses in Chapter 3, these data were also analysed kinetically by applying kinetic curve fitting to the time-course data, according to Hoare et al. (2020b). The relevant kinetic parameters, maximal initial rate (IR_{max}) and kinetic potency (L_{50}), were again determined from the ligand initial rates of signal generation. These values are shown in Table 4.3 alongside the equivalent E_{max} and EC_{50} values, and the initial rate concentration-response curves are displayed in Figure 4.19A, with data normalised against 1 nM isoprenaline (with the HBSS response adjusted to 0%) and fitted via the Hill equation (Equation 4) to a sigmoidal curve. As with the maximal responses, the maximal initial rates of all agonists were found to be similar ($P > 0.05$), whilst kinetic potencies were all leftward shifted compared with those calculated in HEK293Gwt cells ($P <$ 0.01 or less). Also, in contrast with the data obtained from HEK293Gwt cells, no differences were found between the E_{max} and IR_{max} values of any of the agonists in HEK293G-β_2AR cells ($P > 0.05$; Figure 4.19B). Moreover, there were no differences between agonist EC_{50} and L_{50} values either ($P > 0.05$).

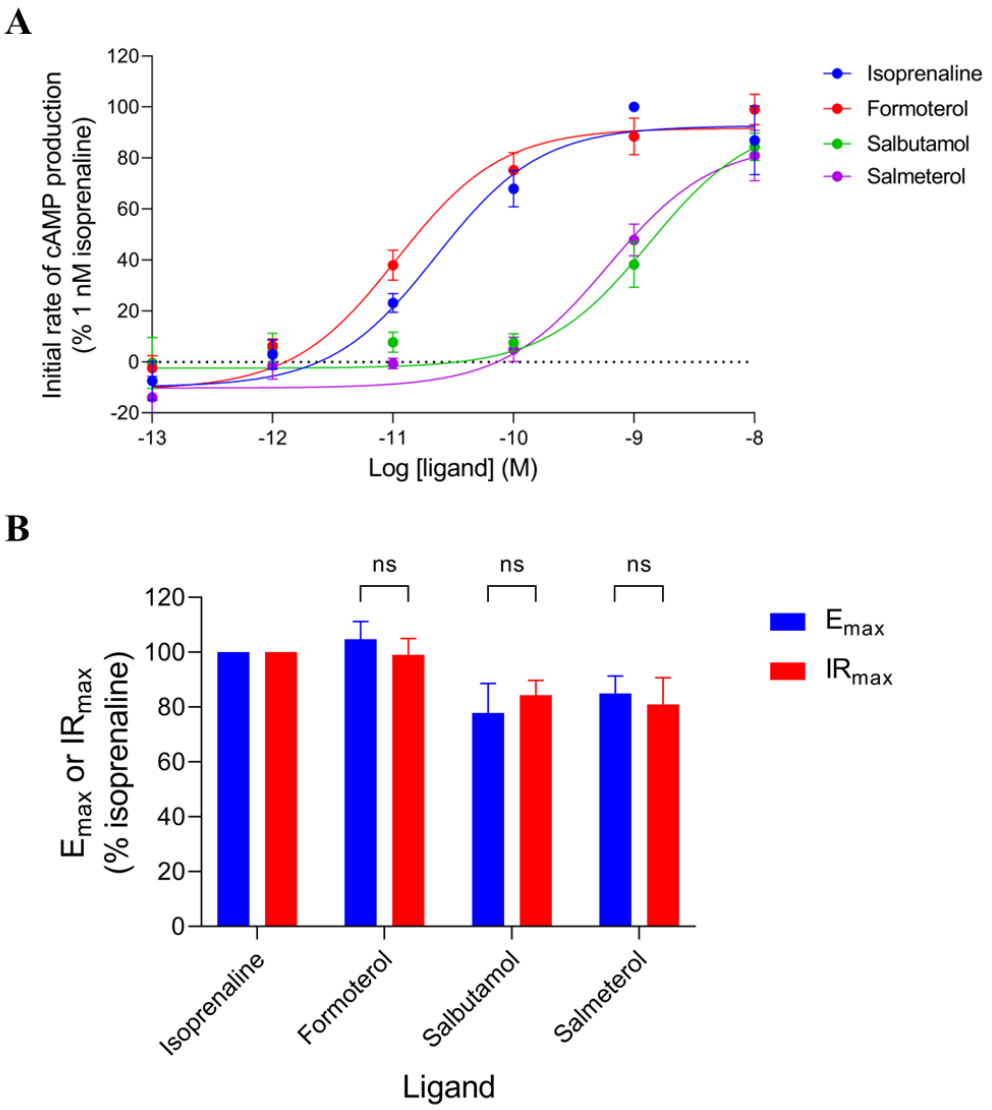

Figure 4.19: GloSensor^{TM} luminescence stimulated by ligand-mediated cAMP production. (A) Mean initial rate concentration-response curves for isoprenaline, formoterol, salbutamol and salmeterol in HEK293G-β_2AR cells expressed as a percentage of 1 nM isoprenaline with the HBSS response normalised to zero. (B) Bar chart comparisons of mean E_{max} and IR_{max} values for isoprenaline, formoterol, salbutamol and salmeterol, relative to isoprenaline in HEK293G-β_2AR cells. Data points represent mean ± SEM from five independent experiments (n = 5). Significant differences are indicated, determined by an unpaired t-test. $P < 0.05$ was used as the level for significance ($P \geq 0.05$ = ns).

Agonist	E_{max} (% 1 nM isoprenaline) ± SEM	IR_{max} (% 1 nM isoprenaline) ± SEM	Log EC_{50} (M) ± SEM	Log L_{50} (M) ± SEM
Isoprenaline	100	100	-10.35 ± 0.15	-10.58 ± 0.24
Formoterol	104.73 ± 6.50	99.01 ± 6.00	-10.95 ± 0.12	-10.97 ± 0.19
Salbutamol	77.81 ± 10.84	84.36 ± 5.36	-8.46 ± 0.16	-8.80 ± 0.15
Salmeterol	84.94 ± 6.38	80.94 ± 9.86	-9.53 ± 0.10	-9.45 ± 0.34

Table 4.3: Agonist mean E_{max}, IR_{max}, log EC_{50} and log L_{50} values ± SEM determined for isoprenaline, formoterol, salbutamol and salmeterol from concentration-response curves obtained by cAMP GloSensor™ in HEK293G-β_2AR cells from five independent experiments (n = 5).

Preincubation (30 min) of several antagonists or inverse agonists was then performed in HEK293G-β_2AR cells, prior to application of HBSS or increasing concentrations of isoprenaline and subsequent luminescence measurements. Just as application of each of the antagonists/inverse agonists reduced the HBSS response previously (Figure 4.7), preincubation of each of these ligands had the same effect here (each $P < 0.0001$; Figure 4.20A). In this case, preincubated ICI-118551 inhibited the HBSS response considerably further than the other ligands ($P < 0.05$ or less), but the rank order of inhibition remained the same as when the ligands were added immediately prior to assay (ICI-118551 > bisoprolol > propranolol = carvedilol). Comparing 30 min preincubation of each ligand as performed here with the earlier data where antagonists were applied at the start of the assay (termed 'simultaneous'; Figure 4.20B), inhibition of the HBSS response by ICI-118551 was significantly greater upon preincubation ($P < 0.001$), whereas each other ligand showed no further inhibition when preincubated for 30 min, compared to their application at the start of the assay ($P > 0.05$ for each).

Isoprenaline peak (Figures 4.21A-4.21D) and initial rate (Figures 4.22A-4.22D) concentration-response curves in the presence and absence of preincubated propranolol, ICI-118551, carvedilol and bisoprolol were constructed. Because of the inhibitory effect of the antagonists, the lowest concentrations of isoprenaline responses are seen to be negative in the graphs. Isoprenaline concentration-dependently increased the response up to a maximal level. Each of the antagonists, including the very slowly dissociating carvedilol, caused a parallel rightward shift in isoprenaline potency ($P < 0.001$ or less) and had no effect on isoprenaline maximal response even at the highest tested concentrations ($P > 0.05$ for each), representing a surmountable antagonism (Figures 4.21A-4.21D). Kinetic analysis revealed that the maximal initial rates of signal generation by isoprenaline were also unaffected by each of the antagonists ($P > 0.05$), whilst isoprenaline kinetic potencies were each shifted to a similar degree as calculated with the peak response data ($P > 0.05$; Figures 4.22A-4.22D, Table 4.4). All isoprenaline E_{max}, IR_{max}, log EC_{50} and log L_{50} values in the presence and absence of increasing concentrations of propranolol, ICI-118551, carvedilol and bisoprolol are shown in Table 4.4.

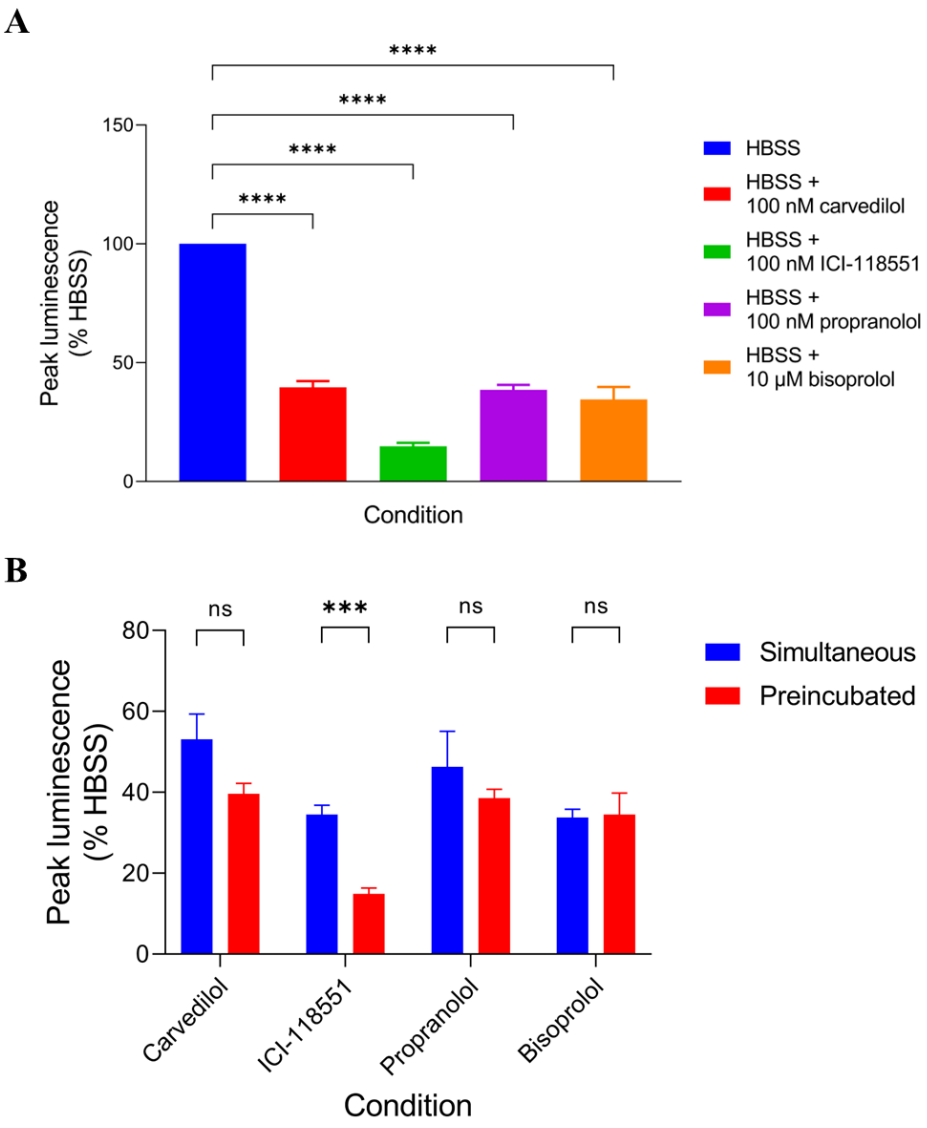

Figure 4.20: GloSensor™ luminescence stimulated by cAMP production. (A) Bar chart displaying mean peak response for HBSS after 30 min preincubation of carvedilol (100 nM), ICI-118551 (100 nM), propranolol (100 nM) and bisoprolol (10 µM) or vehicle in HEK293G-β_2AR cells expressed as a percentage of HBSS. (B) Bar chart comparisons of mean peak response values after application of carvedilol (100 nM), ICI-118551 (100 nM), propranolol (100 nM) and bisoprolol (10 µM) at the start of the assay ('simultaneous' condition) and with 30 min preincubation of the ligands ('preincubated') in HEK293G-β_2AR cells expressed as a percentage of HBSS. Data points represent mean ± SEM from five independent experiments (n = 5). Significant differences are indicated, determined by either a one-way ANOVA with Tukey's multiple comparisons test (A) or an unpaired t-test (B). $P < 0.05$ was used as the level for significance ($P \geq 0.05$ = ns, $P < 0.001$ = ***, $P < 0.0001$ = ****).

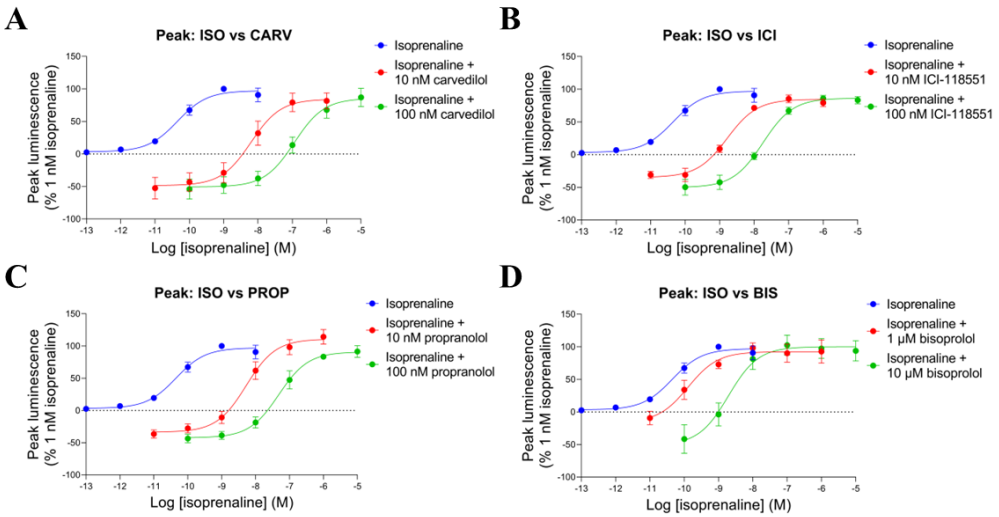

Figure 4.21: GloSensor™ luminescence stimulated by isoprenaline in the presence and absence of 30 min preincubated antagonists/inverse agonists. (A-D) Mean peak concentration-response curves for isoprenaline (ISO) in the presence and absence of carvedilol (CARV; 10 nM, 100 nM; A), ICI-118551 (ICI; 10 nM, 100 nM; B), propranolol (PROP; 10 nM, 100 nM; C) and bisoprolol (BIS; 1 µM, 10 µM; D) in HEK293G-β_2AR cells, expressed as a percentage of 1 nM isoprenaline with the HBSS response in absence of antagonist/inverse agonist normalised to zero. The isoprenaline data in absence of antagonist are taken from the previously constructed agonist peak concentration-response curves in Figure 4.5 and so are identical in each condition here. Data points represent mean ± SEM from five independent experiments (n = 5). Significant differences were determined by a one-way ANOVA with Tukey's multiple comparisons test.

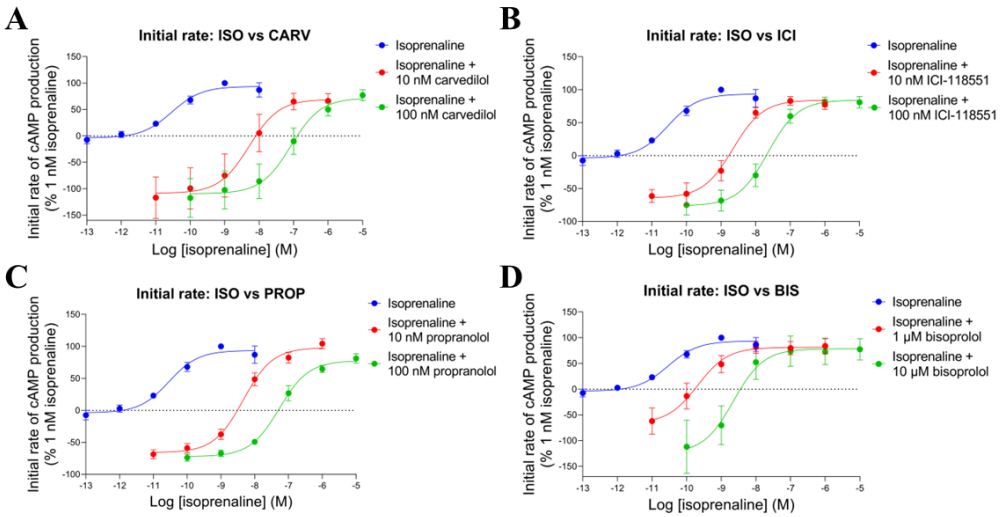

Figure 4.22: GloSensor^{TM} luminescence stimulated by isoprenaline in the presence and absence of 30 min preincubated antagonists/inverse agonists. (A-D) Mean initial rate concentration-response curves for isoprenaline (ISO) in the presence and absence of carvedilol (CARV; 10 nM, 100 nM; A), ICI-118551 (ICI; 10 nM, 100 nM; B), propranolol (PROP; 10 nM, 100 nM; C) and bisoprolol (BIS; 1 µM, 10 µM; D) in HEK293G-β_2AR cells, expressed as a percentage of 1 nM isoprenaline with the HBSS response in absence of antagonist/inverse agonist normalised to zero. The isoprenaline data in absence of antagonist are taken from the previously constructed agonist initial rate concentration-response curves in Figure 4.19 and so are identical in each condition here. Data points represent mean ± SEM from five independent experiments (n = 5). Significant differences were determined by a one-way ANOVA with Tukey's multiple comparisons test.

Antagonist	Log [antagonist] (M)	Isoprenaline E_{max} (% 1 nM isoprenaline) ± SEM	Isoprenaline IR_{max} (% 1 nM isoprenaline) ± SEM	Log isoprenaline EC_{50} (M) ± SEM	Log isoprenaline L_{50} (M) ± SEM
Carvedilol	0	100	100	-10.35 ± 0.15	-10.58 ± 0.24
	-8	81.61 ± 12.26	66.11 ± 13.89	-8.20 ± 0.10 ****	-8.38 ± 0.13 ****
	-7	87.04 ± 14.06	77.13 ± 10.15	-6.93 ± 0.11 ****	-7.11 ± 0.12 ****
ICI-118551	0	100	100	-10.35 ± 0.15	-10.58 ± 0.24
	-8	85.50 ± 6.02	82.94 ± 6.66	-8.78 ± 0.05 ****	-8.68 ± 0.08 ****
	-7	85.87 ± 4.63	81.19 ± 7.56	-7.73 ± 0.04 ****	-7.66 ± 0.08 ****
Propranolol	0	100	100	-10.35 ± 0.15	-10.58 ± 0.24
	-8	114.41 ± 11.34	104.32 ± 7.92	-8.31 ± 0.16 ****	-8.34 ± 0.14 ****
	-7	91.59 ± 8.96	81.17 ± 7.52	-7.32 ± 0.19 ****	-7.25 ± 0.17 ****
Bisoprolol	0	100	100	-10.35 ± 0.15	-10.58 ± 0.24

	-6	98.20 ± 7.71	83.85 ± 14.99	-9.86 ± 0.32	-9.59 ± 0.22 **
	-5	102.52 ± 15.44	77.49 ± 20.74	-8.69 ± 0.15 ***	-8.60 ± 0.10 ****

Table 4.4: Isoprenaline mean E_{max}, IR_{max}, log EC_{50} and log L_{50} values ± SEM in the presence and absence of preincubated increasing concentrations of carvedilol, ICI-118551, propranolol and bisoprolol from concentration-response curves obtained by cAMP GloSensor™ in HEK293G-β_2AR cells from five independent experiments (n = 5). Significant differences in responses to those seen in absence of antagonists/inverse agonists are indicated, determined by a one-way ANOVA with Tukey's multiple comparisons test. $P < 0.05$ was used as the level for significance ($P < 0.01$ = **, $P < 0.001$ = ***, $P < 0.0001$ = ****).

4.4 – Discussion

4.4.1 – Mechanical activation of the β_2-adrenoceptor can be modulated by agonists, inverse agonists and by sequential stimulation

The small response to the addition of vehicle control in HEK293Gwt cells noted in Chapter 3 (Figure 3.1A) was found to be considerably increased in the newly developed HEK293G-β_2AR cells (Figures 4.3A and 4.3B). Therefore, this could no longer be considered an addition artifact of the GloSensor^{TM} assay and so was studied further here. An important phenomenon in GPCR pharmacology is the concept of constitutive receptor activity, whereby GPCRs can exist in an active state in the absence of a bound agonist and thus still activate G proteins to mediate downstream pathways (Cerione et al., 1984a; Costa and Herz, 1989; Cotecchia et al., 1990; Samama et al., 1993; Park et al., 2008). Agonists act by stabilising the receptor active state to increase downstream signalling, whereas inverse agonists shift the conformational equilibrium the other way, stabilising the inactive state and reducing constitutive receptor activity (Costa and Herz, 1989; Greasley and Clapham, 2006; Berg and Clarke, 2018).

Under low, endogenous receptor expression conditions such as those used throughout Chapter 3 with HEK293Gwt cells (Friedman et al., 2002; Goulding et al., 2021a; Goulding et al., 2021b), constitutive receptor activity often cannot be detected as the signal is too low (Berg et al., 1999; Berg and Clarke, 2018). Indeed, no negative effect was seen by inverse agonists such as ICI-118551 on the vehicle response (Figures 3.10A and 3.10B), indicating a lack of detectable constitutive β_2AR activity in those conditions. Under high receptor expression conditions such as in HEK293G-β_2AR cells, constitutive activity is expected to be higher due to the larger number of receptors present (Lefkowitz et al., 1993; Berg et al., 1999; Leurs et al., 2000; Leeb-Lundberg et al., 2001; Milligan, 2003). Constitutive activity of the β_2AR has been specifically linked to its expression levels previously (Engelhardt et al., 2001). However, in this case, the time-course data in Figure 4.3A shows clearly that the response is transient and is initiated at approximately the start of the measurement, reaching a peak followed by a decay

of the signal in a manner similar to agonist-stimulated responses. If high intrinsic constitutive receptor activity was causing elevated cAMP levels, it would more likely appear as a constant high level of cAMP signal instead of the transient production of cAMP observed here, which appears to be responding to a stimulus. Furthermore, Figure 4.3C shows that at the initial luminescence read at $t = 0$ (which is the best indication of relative basal activity measured here), no difference in cAMP levels was observed between HEK293Gwt and HEK293G-β_2AR cells, suggesting that no increase in intrinsic constitutive activity is detected in the high receptor expression system.

The β_2AR partial agonists salbutamol and salmeterol produced maximal responses similar to those of isoprenaline and formoterol (Figure 4.5), thus appearing to act as full agonists here. Each agonist showed markedly increased potencies (in terms of log EC_{50} values) in this study, too, relative to the experiments performed on HEK293Gwt cells earlier (Tables 4.1 and 3.4). In amplified systems, such as those with high receptor expression, both the apparent efficacy and potency of partial agonists have been shown to increase (Hoyer and Boddeke, 1993; Kenakin, 1996; McDonnell et al., 1998; McDonald et al., 2003). Indeed, January et al. (1998) previously showed this exact effect using salbutamol and salmeterol, whereby responses to both partial agonists were similar to adrenaline in cells highly expressing the β_2AR, but were much reduced compared to the endogenous ligand in low expression cells. This effect is observed because, while partial agonists are less efficient at stabilising an active receptor conformation than full agonists, this is compensated for by the larger total number of receptors, and so the maximal response increases until it saturates at the detection limit of the GloSensor^{TM} biosensor, at which point the ligand potency then shifts leftward. Saturation of the response probably occurs because all of the luciferase enzymes in the cytosol are already bound to cAMP, so additional increases in cAMP concentration cannot elicit further enhancement of the luminescence output as there are no more free biosensor molecules available to bind. In this amplified, high receptor expression system, all four agonists are able to stimulate a cAMP response large enough to reach the detection limit of the biosensor.

However, these responses are more complex than simply agonist-mediated cAMP responses because even in the absence of agonist a large cAMP response is observed. As will be discussed further throughout this Chapter, this response is likely due to mechanical stimulation of the β_2AR, which shifts the conformational equilibrium of the receptor toward an active state (although activation by secretion of endogenous catecholamines cannot entirely be ruled out). This is a characteristic which has already been described in numerous GPCRs (Chachisvilis et al., 2006; Erdogmus et al., 2019; Hu et al., 2022; Wilde et al., 2022), including the β_2AR (Virion et al., 2019; Marullo et al., 2020). Response increases by the application of agonists are additive to this mechanical response (Figures 4.4A-4.4D). Similar additive action between agonists and mechanical stimuli have been reported in previous studies (Zhang et al., 2009; Scimia et al., 2012; Busch et al., 2015).

The four antagonists/inverse agonists propranolol, ICI-118551, carvedilol and bisoprolol had no clear inverse agonist effect when tested in HEK293Gwt cells (Figures 3.10A and 3.10B). The same four ligands were applied to HEK293G-β_2AR cells here, in addition to carazolol. Carazolol has previously been described as an extremely weak partial agonist (Baker, 2010; Sato et al., 2015) or a weak inverse agonist (Rosenbaum et al., 2007) for cAMP production at the β_2AR. The classification of the other four ligands as either antagonists, inverse agonists or even weak partial agonists was discussed in Chapter 3 (see 3.4.3). However, each of the five antagonists exhibited inhibition of the mechanical response to a similar degree (Figures 4.7). In each case, the cAMP response still rose briefly to a peak level (Figures 4.6A-4.6E) whilst the ligand was still equilibrating at the receptor, but the responses decayed very quickly, although not all the way back to the baseline. ICI-118551 in particular is very selective for the β_2AR, so inhibition by ICI-118511 (as well as the other antagonists) confirms that the response must be mediated through the β_2AR. Contrastingly, the small basal response in HEK293Gwt cells which was insensitive to these antagonists is likely mediated predominantly through other G_s-coupled receptors. In addition, this supports the concept that β_2AR mechanosensitivity is responsible for the observed cAMP response to vehicle, because both neutral antagonists and inverse agonists have been shown to reduce mechanically

stimulated receptor responses previously (Groves et al., 1995; Zou et al., 2004; Chachisvilis et al., 2006; Erdogmus et al., 2019). The data reported here also reemphasise the importance of measuring the full kinetic time-courses of receptor responses. If this experiment was performed as an endpoint assay with cAMP concentrations simply measured at a single time-point after ligand addition, then the existence of a transient mechanical stimulus would not have been discovered and instead these ligands would appear to act as classic inverse agonists reducing the constitutive activity of the highly-expressed β_2AR.

Sequential stimulation of the cAMP response was observed (Figure 4.10A) upon repeated opening and closing of the door of the PHERAstar FSX microplate reader (BMG Labtech, Offenburg, Germany), which exerted a sustained linear motion on the microplate tray (moving in and out of the position required for the luminescence reads). This suggested that these microplate movements were the cause of the β_2AR mechanostimulatory response, possibly due to induced movement in the extracellular matrix (ECM) environment around the cells. This ECM movement may result from changes in the flow of fluid (sometimes called shear stress) which commonly acts as a mechanical stimulus detected by mechanosensory GPCRs (Chachisvilis et al., 2006; Busch et al., 2015; Xu et al., 2018; Wilde et al., 2022). The addition of isoprenaline or ICI-118551 alongside the initial mechanical stimulation (at the start of assay; $t = 0$) again potentiated or antagonised the response, respectively, but restimulation at later time-points was still observed (to differing extents) after subsequent mechanical inputs. The same responses still occurred when performed in dark conditions (Figure 4.10B), which confirmed that the effect did not occur due to exposure to light upon the opening and closing of the PHERAstar door, meaning mechanical stimulation was the only plausible explanation remaining. Moreover, while the endogenous secretion of catecholamines by the HEK293 cells could not be explicitly ruled out as the cause of the β_2AR activation, this appears unlikely because the same sequential stimulation of the response was observed in HEK293Gwt cells (Figure 4.12A), which does not appear to be mediated predominantly by the β_2AR (no inhibition by ICI-118551 or other βAR antagonists). If the response was mediated by endogenous catecholamines, it would likely be inhibited by the

βAR antagonists even in HEK293Gwt cells. Instead, other G_s-coupled mechanosensory GPCRs probably mediate this response in HEK293Gwt cells.

It would be useful to be able to control and manipulate the mechanical stimulus that is applied to the cells to study the effect in more detail and optimise the mechanical response. In order to do this, the PHERAstar program was modified to include repeated plate shaking at selected conditions (velocity, direction and duration) every 15 min. However, none of the tested conditions were able to reproduce the sequential production of cAMP that was observed by the door open-close method in either HEK293G-β_2AR or HEK293Gwt cells (Figures 4.10C, 4.10D and 4.12B, as well as Supplementary Figures 8.2A-8.2D and 8.3A-8.3D). This suggests that only very specific mechanical stimuli (such as those induced upon opening/closing the PHERAstar door) are sensed by the β_2AR (and other G_s-coupled GPCRs) in order to shift the receptor conformational equilibrium toward an active state. Supporting this finding, previous work by Gaub and Müller (2017) also noted that the directionality of the mechanical force applied to cells (pulling vs pushing stimulus) affected the magnitude of mechanical stimulation by PIEZO1 cation channel receptors. Indeed, this feature may have considerable physiological relevance. In the vascular system, the direction (as well as magnitude and frequency) of fluid shear stress forces on vascular endothelial cells caused by the flow of blood is thought to have considerable impact on vascular physiology, influencing processes such as vascular remodelling and angiogenesis, vasodilation, inflammatory responses and atheroprotection (Davies, 1995; Chistiakov et al., 2017; Tanaka et al., 2021). Numerous GPCRs including but not limited to GPR68 (Xu et al., 2018), APJ (Busch et al., 2015), H_1R (Erdogmus et al., 2019) and B_2R (Groves et al., 1995; Chachisvilis et al., 2006) have been shown to act as mechanosensors in mediating some of these physiological responses.

4.4.2 – Receptor N-glycosylation confers mechanosensitivity in the β_2-adrenoceptor

N-linked receptor glycosylation is a vital process occurring within the endoplasmic reticulum, whereby the enzyme oligosaccharyltransferase attaches an oligosaccharide to a polypeptide at a specific asparagine residue within the consensus sequence NxS/T, whereby N indicates the asparagine residue, x can be any amino acid except proline and S/T refer to serine/threonine (Aebi, 2013; Bieberich, 2014). Three such sequences exist within the extracellular regions of the human β_2AR, resulting in potential glycosylation sites at Asn6, Asn15 and Asn187 (Dohlman et al., 1987; Li et al., 2017; Yang et al., 2021). There are an additional three NxS/T potential recognition sites throughout the β_2AR polypeptide sequence, Asn244 (ICL3), Asn405 and Asn409 (both C-terminal) (Supplementary Table 8.1), however these all occur within the cytoplasmic portions of the receptor, meaning they would not be relevant here. Regardless, it is unclear whether N-glycosylation occurs at intracellular sites of membrane proteins. In addition to protein folding and stability, which are well-known functions of receptor N-glycosylation (Hanson et al., 2009; Aebi et al., 2010; Braakman and Hebert, 2013; Bieberich, 2014; Esmail and Manolson, 2021), N-terminal N-glycan chains have previously been shown to directly mediate β_2AR mechanosensitivity to traction forces exerted by meningococcus pili (Virion et al., 2019; Marullo et al., 2020). Therefore, a mutant β_2AR construct which lacked both N-terminal glycosylation sites Asn6 and Asn15 (HiBiT-β_2AR_N6A_N15A) and another mutant receptor which also lacked these in addition to the ECL2 glycosylation site Asn187 (HiBiT-β_2AR_N6A_N15A_N187A) were developed to prevent N-glycosylation of the β_2AR, in order to study the impact of glycosylation on receptor surface expression, function and mechanosensitivity.

Firstly, it was important to confirm that mutation of the β_2AR glycosylation sites did not affect the surface expression of the receptor. Receptor N-glycosylation is important in correct protein folding and stability, which in turn influences receptor trafficking out of the endoplasmic reticulum and ultimately to the cell surface membrane (Helenius and Aebi, 2004; Vagin et al., 2009; Braakman and Hebert, 2013; Esmail et al., 2016; Esmail and Manolson, 2021). The HiBiT-

LgBiT complementation assay showed that both of the β_2AR mutants were expressed at the cell surface to a similar degree to that of the wildtype (unmutated) HiBiT β_2AR construct (HiBiT-β_2ARwt) (Figure 4.13), whilst a pcDNA3.1(+) control showed comparatively negligible (background) luminescence (Figure 4.16A). These results indicate that glycosylation of the β_2AR does not affect the trafficking of the receptor to the cell surface. This suggests it is also highly likely that the β_2AR does not require N-glycosylation for proper protein folding. Whereas many proteins do require N-linked glycan chains for proper folding and expression (Barbosa et al., 1987; Lanctôt et al., 1999; Vagin et al., 2009; Esmail et al., 2016; de Haas et al., 2020), others including the β_2AR have previously been shown to fold properly and be trafficked efficiently even in their absence (George et al., 1986; Helenius, 1994; Ruddon and Bedows, 1997; Li et al., 2017; Virion et al., 2019).

Some receptors lacking N-glycosylation may still be trafficked efficiently and thus expressed to a similar degree at the cell surface but are not fully functional (Hollmann et al., 1994; Gehle et al., 1997; Chen et al., 1998; Pang et al., 1999). However, previous studies have revealed that the β_2AR exhibits no decrease in function upon loss of N-glycan chains, either by removal of N-glycosylation sites by mutagenesis or by inhibition of the N-glycosylation process by inhibitors of important enzymes (George et al., 1986; Ostrowski et al., 1992; Virion et al., 2019). On the other hand, Li et al. (2017) found that mutation of glycosylation sites did alter β_2AR signalling (reduced isoprenaline potency, β-arrestin recruitment and internalisation). It should be noted that some of these studies mutated just the N-terminal glycosylation sites and did not consider the extra site on ECL2. In this study, no difference was found in the peak or profile of the response to a maximal concentration of isoprenaline between the wildtype β_2AR and either of the non-glycosylated mutant receptors (Figure 4.14B). When compared with the pcDNA3.1(+) control, the peak responses were surprisingly similar (Figure 4.16C), indicating that in these experiments the isoprenaline response even in the control-transfected cells was saturated. Therefore, it would be useful in future experiments to perform full isoprenaline concentration-response curves and determine relative isoprenaline potencies for each β_2AR construct and the control, to better confirm whether the mutations affected β_2AR

signalling in these experiments. Additionally, ligand binding experiments could be performed to check isoprenaline binding affinity was not reduced. However, in the pcDNA3.1(+) control, the profile of the decay phase of the response did differ visibly from the mutant β_2AR constructs, as well as the wildtype (Figure 4.16C), thus providing some evidence that receptor function was not altered by the mutation of the N-glycosylation sites.

Whereas no evidence was found for reduced receptor surface expression or function in the non-glycosylated mutant receptors, the mechanosensitivity of the β_2AR was clearly reduced by the mutations. Both HiBiT-β_2AR_N6A_N15A and to an even greater degree HiBiT-β_2AR_N6A_N15A_N187A constructs showed markedly reduced responses to HBSS application, although each were still susceptible to inhibition by ICI-118551 (Figures 4.15A-4.15C). This suggests that the N-glycan chains attached to residues Asn6, Asn15 and Asn187 play a substantial role in mediating mechanostimulatory responses in the β_2AR. Since these responses can still be inhibited by application of inverse agonist, N-glycosylation may not be the only mechanism conferring mechanical sensitivity to the receptor. Alternatively, since no difference was found in the HBSS response between the HiBiT-β_2AR_N6A_N15A_N187A construct and the pcDNA3.1(+) control (Figure 4.17A and 4.17B), the inhibitory effect of ICI-118551 may be due to endogenously expressed β_2ARs which still have their intact N-glycan chains, although the same inhibitory effect by ICI-118551 was not observed in HEK293Gwt cells (Figures 3.10A-3.10B). Therefore, whether other mechanisms which confer receptor mechanosensitivity exist remains unclear, but the presence of receptor N-glycan chains certainly have an amplifying effect on the β_2AR mechanical responses observed here. Sequential mechanical stimulation of each β_2AR construct (by repeated opening and closing of the PHERAstar FSX door every 15 min) further supported the observations reported here, whereby the rank order of magnitude of the responses to HBSS application was the same again: HiBiT-β_2ARwt > HiBiT-β_2AR_N6A_N15A > HiBiT-β_2AR_N6A_N15A_N187A > pcDNA3.1(+) (Figure 4.18).

Previous work by Virion et al. (2019) revealed the important role of N-terminal N-glycan chains in directly mediating the activation of endothelial cell β_2ARs

by meningococcus pili (Marullo et al., 2020). The bacterial pili bind to Neu5Ac sialic acid residues at the tip of the Asn6 and Asn15 N-glycan chains and exert pulling traction forces, which promotes GRK-dependent β-arrestin recruitment and initiates a signalling pathway ultimately facilitating the bacteria crossing the blood-brain barrier (Coureuil et al., 2010; Virion et al., 2019; Marullo et al., 2020). Here however, rather than a direct pulling force from bacterial pili, the source of mechanical stimulation is an indirect sustained linear motion on the microplate caused by the action of opening and closing the PHERAstar door. In that previous study, the involvement of the third N-glycosylation site at ECL2 was not investigated, whereas in this study the removal of this site reduced β_2AR mechanostimulation substantially further than just the two N-terminal sites.

It is straightforward to imagine how N-glycans, which are large, hydrophilic and branched structures extending away from the cell membrane and integrate with the ECM (Imperiali and O'Connor, 1999; Braakman and Hebert, 2013), may be particularly susceptible to gross movements of the cell. Their subsequent movements may in turn amplify conformational changes in the receptor to which they are linked, conferring mechanosensitivity and resulting in a transient signalling response. It is interesting that the β_2AR mechanical response to meningococcus pili traction forces has been shown to produce a β-arrestin-biased signalling cascade with no effect on the cAMP pathway (Coureuil et al., 2010; Virion et al., 2019; Marullo et al., 2020), whereas in this study mechanical activation of the β_2AR instead stimulated a substantial cAMP response. No β-arrestin recruitment or internalisation assays were performed here, but perhaps this could be examined in the future. Indeed, it would be useful to further validate the results obtained in this study by observing similar β_2AR mechanosensory functions using different assay types.

4.4.3 – Pharmacological and kinetic parameters of agonists and antagonists are dependent on receptor expression

Just as the maximal responses of partial agonists were increased to the same level as full agonists in HEK293G-β_2AR cells (discussed earlier), the maximal initial rates of the partial agonists salbutamol and salmeterol showed the same effect, reaching the same level as those of isoprenaline and formoterol (Figure 4.19A). In each case the ligand kinetic potencies also increased compared with those determined in HEK293Gwt cells (Tables 4.3 and 3.4). Similar to the maximal responses, this is because the GloSensor^{TM} biosensor reaches its detection limit (cAMP binding becomes saturated), which is dependent on the expression of the biosensor inside the cells. Since the initial rate of signal generation is related to intrinsic ligand efficacy (Hoare et al., 2020b; Hoare et al., 2022), it is unsurprising to see that these data follow the same trend as observed in the peak responses earlier. Furthermore, this meant that no difference was found between any agonist E_{max} and IR_{max} values here (Figure 4.21B), as all values were raised to the same maximal level as that of the reference ligand isoprenaline. Additionally, no differences in agonist EC_{50} and L_{50} values were observed either. Therefore, in this high expression system it was not possible to use the kinetic analysis to deduce potential differences in the pharmacological and kinetic properties of the agonists, as had been achieved in the low, endogenous expression system employed throughout Chapter 3. This highlights the usefulness of using endogenous receptor expression systems for some pharmacological analyses, as in some cases it can enable deduction of subtle differences between ligand parameters that may not be detectable in overexpression systems.

Preincubation of HEK293G-β_2AR cells with ICI-118551 for 30 min greatly increased inhibition of the mechanical response compared to addition of the inverse agonist immediately prior to the assay (Figures 4.20A and 4.20B). Inhibition by each of the other antagonists however was the same in both conditions. The reason for this disparity is not entirely clear, but ICI-118551 certainly acts with the greatest negative intrinsic efficacy of the ligands in this

study, in agreement with previous work (Azzi et al., 2001; Baker et al., 2003a; Baker et al., 2003b; Wisler et al., 2007).

In contrast to the equivalent experiments performed in HEK293Gwt cells (Figures 3.12A-3.12D), preincubation of HEK293G-β_2AR cells with each antagonist/inverse agonist produced a surmountable antagonism of the isoprenaline response, whereby the inhibitory effects of the antagonists were eventually overcome by increasing isoprenaline concentrations (Figures 4.21A-4.21D). Instead of a reduction in maximal response, a parallel rightward shift in agonist potency was observed, which is a classic characteristic of competitive, orthosteric antagonists acting within a system in equilibrium (Gaddum et al., 1955; Ariens et al., 1956; Vauquelin et al., 2002). Under low receptor expression conditions, antagonist preincubation reduced the already sparse number of available receptors for isoprenaline to bind in the required time-frame to achieve its peak response, leading to a state of hemi-equilibrium (Paton and Rang, 1965; Hopkinson et al., 2000; Vauquelin et al., 2002; Kenakin et al., 2006; Charlton and Vauquelin, 2010). Here however, the much greater number of receptors expressed on the surface of the cells (hence larger receptor reserve) easily compensates for the 'loss' of a proportion of these receptors to antagonist binding, so there are still enough free receptors for isoprenaline to bind in order to rapidly attain equilibrium and stimulate a maximal cAMP response (Vauquelin et al., 2002; Kenakin et al., 2006; Charlton and Vauquelin, 2010). Therefore, even the extremely slowly dissociating β_2AR antagonist carvedilol (Sykes et al., 2014) was unable to depress the maximal isoprenaline response in HEK293G-β_2AR cells. Isoprenaline maximal initial rates were also unaffected by preincubation of any of the antagonists (Figures 4.22A-4.22D), despite the even more drastic effect on the maximal initial rate parameters in HEK293Gwt cells (Figures 3.14A-3.14D), and the log shifts in isoprenaline L_{50} and EC_{50} values were similar in each case (Table 4.4). Together, the results discussed throughout this section have highlighted that receptor expression is an important factor in determining ligand pharmacological and kinetic parameters. These data have also confirmed that a lack of receptor reserve due to low, endogenous β_2AR expression was the cause of the hemi-equilibrium state and insurmountable antagonism effect observed in HEK293Gwt cells.

4.5 – Conclusion

Development of a stably overexpressing β_2-adrenoceptor (β_2AR) cell line (HEK293G-β_2AR cells) has enabled further investigations into β_2AR pharmacology using the cAMP GloSensor^{TM} luminescence assay. This has uncovered a mechanosensory function of the β_2AR whereby a transient cAMP signal was stimulated in response to a mechanical input. This response arose only from a very specific mechanical stimulus, namely the sustained linear motion exerted on the microplate during the opening and closing of the PHERAstar FSX door, but not from linear or orbital shaking protocols, and differential buffer volume additions (including 'no addition' conditions) also had no effect on the response. In addition, repeated application of the mechanical stimulus every 15 min was able to cause sequential receptor activation, and the response could be both potentiated by agonists and blocked by numerous β_2AR antagonists/inverse agonists. Virion et al. (2019) previously found that N-glycan chains at the N-terminus of the β_2AR were directly involved in transducing meningococcus pili traction forces into β-arrestin-biased responses. Removal of three extracellular N-glycosylation sites (namely Asn6 and Asn15 at the N-terminus, as well as Asn187 on ECL2), by mutation of the asparagine residues to alanine, substantially reduced the β_2AR mechanical response without altering receptor surface expression or functional response to isoprenaline, indicating that the N-glycan chains play an important role in conferring β_2AR mechanosensitivity. Some mechanical response remained even in absence of the N-glycosylation sites which could still be inhibited by ICI-118551, implying that other mechanosensory mechanisms may also exist. Finally, the observation of a small mechanical response in HEK293Gwt cells which could also be sequentially activated by repeated mechanical stimuli, but was insensitive to ICI-118551, indicates that mechanotransduction may be a common characteristic of other G_s-coupled GPCRs.

cAMP GloSensor^{TM} studies with the newly developed HEK293G-β_2AR cell line have also enabled comparisons of agonist-mediated β_2AR cAMP responses under high receptor expression conditions with those measured under low, endogenous expression conditions previously and provided new insights into

inverse agonist activity. In the high receptor expression system, both maximal responses and maximal initial rates of signal generation of the partial agonists salbutamol and salmeterol were elevated to the same level as those of the full agonists isoprenaline and formoterol. Therefore, no differences were found between agonist E_{max} and IR_{max} values under these conditions. Moreover, all agonist potencies were increased. Also, in contrast to the work performed in HEK293Gwt cells, preincubation with antagonists did not reduce either the isoprenaline maximal response or initial rate of signal generation. Instead, a parallel rightward shift in isoprenaline potency was observed in each case. This surmountable antagonism results from a larger receptor reserve which compensates for the 'loss' of receptors due to antagonist binding. Comparisons between agonist and antagonist pharmacological and kinetic analysis under high and low receptor expression conditions has outlined the substantial impact that receptor expression levels can have on the characterisation of ligand activity.

Chapter 5

Functional characterisation of β_2-adrenoceptor-derived pepducins

5.1 – Introduction

As discussed in Chapter 1 (see 1.3.3 – GPCR allostery and allosteric modulation), allosteric ligands are ligands which interact with receptors at sites topologically distinct from the orthosteric binding site (where the endogenous ligand interacts), called allosteric sites (Christopoulos and Kenakin, 2002; May et al., 2007; Christopoulos et al., 2014). Many allosteric ligands are able to modulate the receptor response to an orthosteric ligand, either potentiating (positive allosteric modulators; PAMs) or inhibiting (negative allosteric modulators; NAMs) orthosteric ligand responses by altering their receptor binding affinity and/or efficacy for signal transduction (Christopoulos and Kenakin, 2002; May et al., 2007; Keov et al., 2011). Some may instead simply bind to allosteric sites but not modify the orthosteric ligand response in any way (neutral allosteric ligands; NALs) (May et al., 2007; Christopoulos et al., 2014). Additionally, many allosteric ligands have been shown to modulate receptor activity in absence of orthosteric ligands, acting as either allosteric agonists or inverse agonists (Christopoulos and Kenakin, 2002; May et al., 2007; Keov et al., 2011; Lane et al., 2017). Allosteric modulators may provide therapeutic advantages over drugs acting at orthosteric sites, such as increased selectivity (due to lower evolutionary pressure at receptor allosteric sites compared to orthosteric sites) and reduced toxicity (because allosteric ligand saturability causes a 'ceiling level' effect of the response) (Christopoulos and Kenakin, 2002; May et al., 2007; Lane et al., 2017).

Other than pepducins, which are discussed below, several allosteric ligands have recently been discovered for the β_2AR. Firstly, two small molecule intracellular allosteric modulators, compound-15 (Ahn et al., 2017) and then compound-6 (Ahn et al., 2018), were discovered by screening DNA-encoded libraries. Compound-15 was shown to act as a NAM by inhibiting orthosteric agonist-mediated cAMP production and β-arrestin recruitment and enhancing inverse agonist activity (Ahn et al., 2017; Liu et al., 2017). Compound-6 instead showed PAM activity, increasing agonist binding affinity and signal transduction at the β_2AR (Ahn et al., 2018; Liu et al., 2019). It also showed a unique positive cooperativity with the β-blocker carvedilol (Pani et al., 2021). Since then,

another NAM has been reported, AS408, which binds in the transmembrane domain of the β_2AR (Liu et al., 2020), and several more allosteric ligands with varying degrees of PAM or NAM activity have since been screened based on computational identification of a novel allosteric site in the transmembrane region (Shah et al., 2022). Additionally, a novel intracellular β-arrestin-biased NAM of the β_2AR has very recently been reported, DFPQ, which could prove clinically useful due to its attenuation of airway smooth muscle desensitisation upon β-agonist application (Ippolito et al., 2023). There are also several endogenous allosteric ligands of the β_2AR as well as other GPCRs, including zinc (PAM) and sodium (NAM) cations (Swaminath et al., 2002; Swaminath et al., 2003; Katritch et al., 2014; Hori and Yokoyama, 2022; Wang et al., 2022) and also the lipid cholesterol, which can act as a PAM or NAM by stabilising either the active or inactive receptor states (Hanson et al., 2008; Manna et al., 2016; Jakubík and El-Fakahany, 2021).

Apart from small molecule ligands, another class of GPCR allosteric ligands is represented by the pepducins. These are short, N-terminally lipidated peptides whose sequences are derived from one of the three intracellular loops or C-terminal tail of their target GPCR (Covic et al., 2002a; Carlson et al., 2012; Zhang et al., 2015b). The hydrophobic lipid group enables translocation of pepducins across cell membranes by incorporating into the phospholipid bilayer and subsequently flipping to the intracellular side, remaining anchored at the cell membrane (Covic et al., 2002a; Covic et al., 2002b; Wielders et al., 2007; Carlson et al., 2012; Tsuji et al., 2013; Zhang et al., 2015b). The pepducins are then able to interact at the intracellular surface of their target receptor to regulate signalling responses (Covic et al., 2002a; Carlson et al., 2012; Zhang et al., 2015b). Pepducins have been developed for numerous GPCRs and can act as allosteric agonists, antagonists, inverse agonists, PAMs and NAMs (Tressel et al., 2011; Carlson et al., 2012; O'Callaghan et al., 2012a). They are also capable of displaying bias, likely through the stabilisation of distinct receptor conformations (Carlson et al., 2012; O'Callaghan et al., 2012a; Quoyer et al., 2013; Carr et al., 2014). Pepducins were reviewed more extensively in Chapter 1 (see 1.6 – Pepducins).

Pepducins have also been developed for the β_2AR. Carr et al. (2014) first designed approximately 50 peptide sequences derived from the three intracellular loops of the human β_2AR, attached to N-terminal palmitate tags. They found that several of the pepducins which derived from ICL3 of the receptor stimulated cAMP production without promoting β-arrestin recruitment (thus showing bias for G_s protein), whilst many pepducins derived from ICL1 instead had the opposite effect, promoting recruitment of β-arrestin to the β_2AR but not increasing cAMP concentrations (β-arrestin-biased) (Carr et al., 2014). ICL1-15 however acted neutrally, showing agonist activity for both pathways, meanwhile pepducins derived from ICL2 had no effect on either cAMP production or β-arrestin recruitment (Carr et al., 2014). Of the G_s-biased pepducins, some were found to act in a receptor-dependent manner (ICL3-7, ICL3-9), whilst others did not require expression of the receptor to activate G_s signalling pathways (ICL3-2, ICL3-8) (Carr et al., 2014). Later studies showed that the β-arrestin-biased pepducin ICL1-9 was able to facilitate cardiac contractility in cardiomyocytes via reduced G_i protein signalling and also promoted cardioprotective antiapoptotic pathways through β-arrestin coupling (Carr et al., 2016b; Grisanti et al., 2018). Conversely, ICL3-derived G_s-biased β_2AR pepducins were found to be ineffective at reversing airway smooth muscle contraction, compared with G_q-biased antagonist pepducins acting at other receptors (Carr et al., 2016a; Panettieri et al., 2018).

Here, five β_2AR pepducins (ICL3-2, ICL3-7, ICL3-8, ICL3-9 and ICL1-15; amino acid sequences are displayed in Table 2.1) were initially tested using the cAMP GloSensor^{TM} assay to confirm whether they acted as allosteric β_2AR agonists by stimulating cAMP production, as was shown previously by Carr et al. (2014). Additionally, the ability of each pepducin, as well as a range of orthosteric ligands, to promote CRE-mediated gene transcription was assessed by performing the CRE-SPAP assay. This assay measures signalling responses downstream of the second messenger cAMP which stimulates PKA-mediated phosphorylation of CREB, a transcription factor in the nucleus (Montminy et al., 1990; Lalli and Sassone-Corsi, 1994; Hill et al., 2001). The subsequent binding of phosphorylated CREB to one of the six CRE promoter sequences in the SPAP reporter gene initiates transcription of SPAP mRNA, which is then translated and

the protein is secreted from cells (Montminy et al., 1990; Lalli and Sassone-Corsi, 1994; Hill et al., 2001). SPAP cleaves the phosphate group of the pNPP dye added to the media, resulting in a measurable colour change which can be used to quantify SPAP gene transcription (Cullen and Malim, 1992; Hill et al., 2001). In this case, the measured gene transcription response was mediated by either orthosteric β_2AR ligands or pepducins. The ability of the pepducins to modify the response of an orthosteric agonist (positive or negative allosteric modulation) was also examined in both cAMP GloSensor^{TM} and CRE-SPAP assays.

5.2 – Materials and methods

Solubilisation of pepducins

The five pepducins ICL3-2, ICL3-7, ICL3-8, ICL3-9 and ICL1-15 were solubilised from lyophilised form as described already in Chapter 2 (see 2.2 – Solubilisation of pepducins).

Cell culture

HEK293 cells stably expressing the cAMP GloSensor™ biosensor (HEK293Gwt), CHO cells expressing the CRE-SPAP reporter (CHO-CRE-SPAPwt) and CHO cells stably expressing both the CRE-SPAP reporter and the human β_2AR (CHO-CRE-SPAP-β_2AR) were used throughout this Chapter and were passaged and seeded into 96-well assay plates as described previously in Chapter 2 (See 2.4 – Cell culture).

cAMP GloSensor™ assay

The cAMP GloSensor™ assay was performed throughout this Chapter as described in Chapter 2 (see 2.7 – cAMP GloSensor™ assay).

CRE-SPAP assay

The CRE-SPAP assay was performed throughout this Chapter as described in Chapter 2 (see 2.9 – CRE-SPAP assay).

Data analysis and statistics

Analysis of the data was carried out as stated in Chapter 2 (see 2.12 – Data analysis and statistics).

5.3 – Results

5.3.1 – Pepducin-mediated cAMP responses at the β_2-adrenoceptor under low receptor expression conditions

Bovine serum albumin (BSA) is a globular, largely inert protein which is commonly used in assays involving protein or peptide samples in order to prevent adsorption of the samples to glass or plasticware (for example, pipette tips or microplate surfaces) by coating the surfaces of these labware (Felgner and Wilson, 1976; Goebel-Stengel et al., 2011). In addition, BSA has been shown to increase solubility of lipophilic compounds in aqueous solutions (Huynh et al., 2014; Cai et al., 2019). For these reasons, addition of BSA to the HBSS buffer was considered important for assays involving pepducins, which are short peptide sequences attached to lipid palmitate tags (Covic et al., 2002a). Firstly, the concentration of BSA was optimised by testing the effect of increasing BSA concentrations (0.1%, 0.2% and 0.5%) in the HBSS buffer on the isoprenaline concentration-response in HEK293Gwt cells, shown in Figure 5.1. Although not statistically significant, 0.5% BSA appeared to somewhat reduce the maximal isoprenaline response (29.96% ± 8.55% reduction in isoprenaline E_{max}: $P > 0.05$). Lower concentrations of BSA had less effect on the response ($P > 0.05$ for both). It was thus determined that 0.1% BSA was an appropriate concentration to use in buffer preparations for pepducin tests going forward.

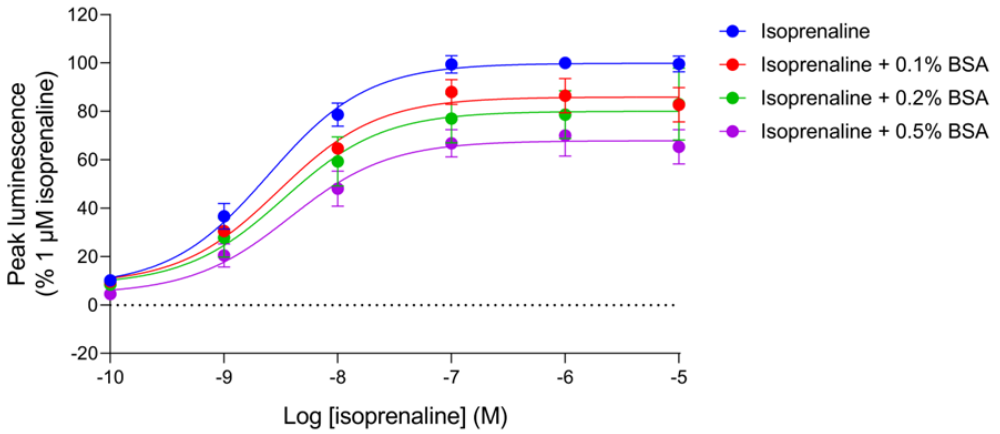

Figure 5.1: GloSensor^{TM} luminescence stimulated by isoprenaline in the presence and absence of BSA. Mean peak concentration-response curves for isoprenaline in the presence and absence of increasing concentrations of BSA (0.1%, 0.2%, 0.5%) in HEK293Gwt cells expressed as a percentage of 1 µM isoprenaline. Data points represent mean ± SEM from five independent experiments (n = 5). Significant differences were determined by a one-way ANOVA with Tukey's multiple comparisons test.

Five pepducins were tested for their abilities to stimulate cAMP production using the cAMP GloSensor^{TM} assay in HEK293Gwt cells. ICL3-2, ICL3-7, ICL3-8, ICL3-9 and ICL1-15 were each screened at three concentrations (100 nM, 1 μM and 10 μM). As described in Chapter 2 (see 2.2 – Solubilisation of pepducins), each pepducin was initially dissolved to 1 mM stock solutions in either 10% (ICL3-2, ICL3-7 and ICL3-8) or 50% (ICL3-9 and ICL1-15) DMSO. This meant at the highest tested pepducin concentration here (10 μM), cells were exposed to either 0.1% or 0.5% DMSO during the time-course of the assay, which was generally higher than during the earlier studies of orthosteric ligands. In order to negate any minor effects of DMSO on the luminescence signal, 0.1% or 0.5% DMSO was applied, respectively, to the HBSS vehicle controls for these experiments. As with earlier work in HEK293Gwt cells (Chapter 3), all GloSensor^{TM} data throughout this Chapter has been baseline-corrected by subtraction of the vehicle control response at equivalent time-points. Therefore, any increases in cAMP signal above baseline should be the result of pepducin activity, rather than any small basal (mechanical or DMSO) response.

The combined time-course data over 60 min after application of each of the five pepducins (Figures 5.2A-5.2E) as well as those for 1 μM isoprenaline and 100 μM forskolin (Figure 5.2F) are displayed. A variety of effects on the cAMP signal were observed. Several of the pepducins (ICL3-2, ICL3-7, ICL3-8 and 10 μM ICL3-9) appeared to transiently elevate cAMP concentration in an agonist-like manner, with a sharp initial rise in luminescence followed by a decline back to the baseline. In some cases, there was no clear 'peak' response and instead the cAMP signal appeared to more gradually increase and plateau at a level slightly above baseline (< 10 μM ICL3-9 and ICL1-15). However, all of these responses were very minor in comparison with those produced by isoprenaline or forskolin. Pepducin peak responses are shown in Figure 5.3, expressed as a percentage of the peak 1 μM isoprenaline response, in which each of the eight experimental repeats are displayed. In many of the pepducin conditions there was considerable inconsistency between each experimental repeat. Four of the pepducins, ICL3-7 (100 nM: 5.50% ± 1.63%; $P < 0.05$), ICL3-8 (10 μM: 6.07% ± 1.71%; $P < 0.05$), ICL3-9 (10 μM: 3.10% ± 0.96%; $P < 0.05$) and ICL1-15 (100 nM: 2.90% ± 0.70%; $P < 0.05$), produced statistically significant increases in peak cytosolic

cAMP concentrations, however ICL3-2 (10 μM: 6.07% ± 2.25%; $P > 0.05$) did not. Table 5.1 states the full set of peak responses measured in each pepducin condition.

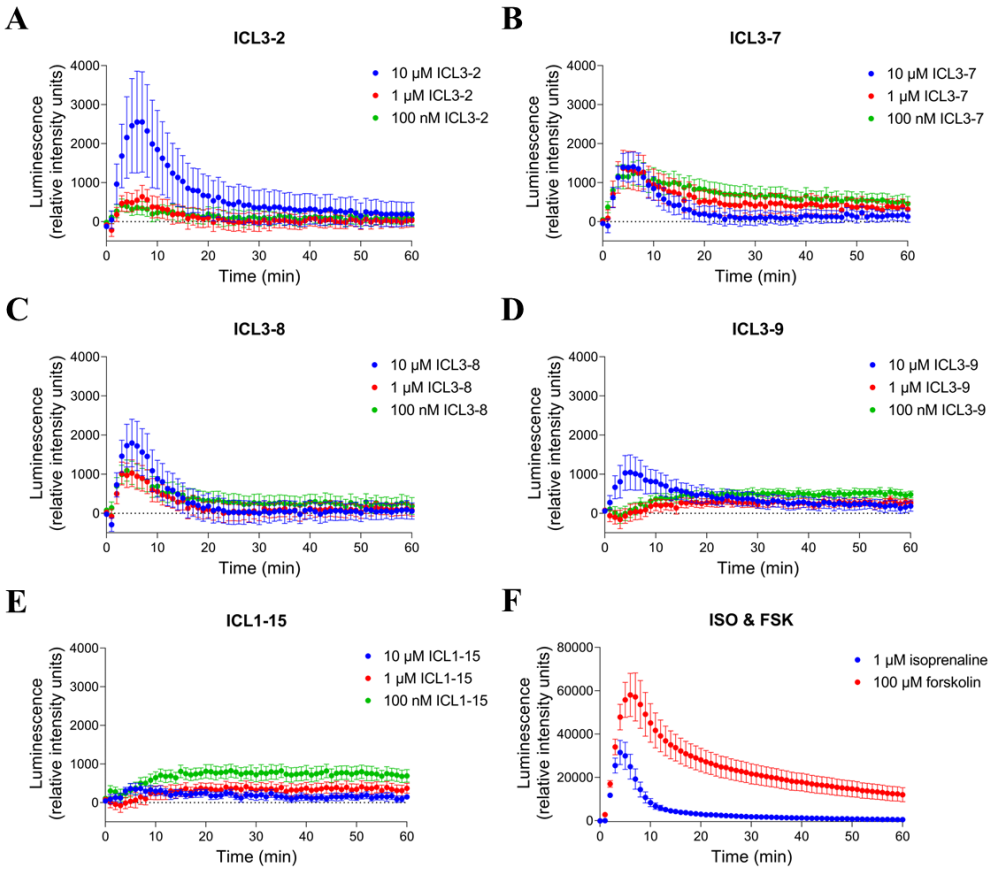

Figure 5.2: GloSensor^{TM} luminescence stimulated by ligand-mediated cAMP production. (A-F) Combined GloSensor^{TM} luminescence time-course data over 60 min following application of ICL3-2 (100 nM – 10 µM; A), ICL3-7 (100 nM – 10 µM; B), ICL3-8 (100 nM – 10 µM; C), ICL3-9 (100 nM – 10 µM; D), ICL1-15 (100 nM – 10 µM; E) or isoprenaline and forskolin (ISO & FSK; 1 µM and 100 µM, respectively; F) to HEK293Gwt cells. Data points represent mean ± SEM expressed as relative intensity units (RIU) of luminescence, from eight independent experiments (n = 8).

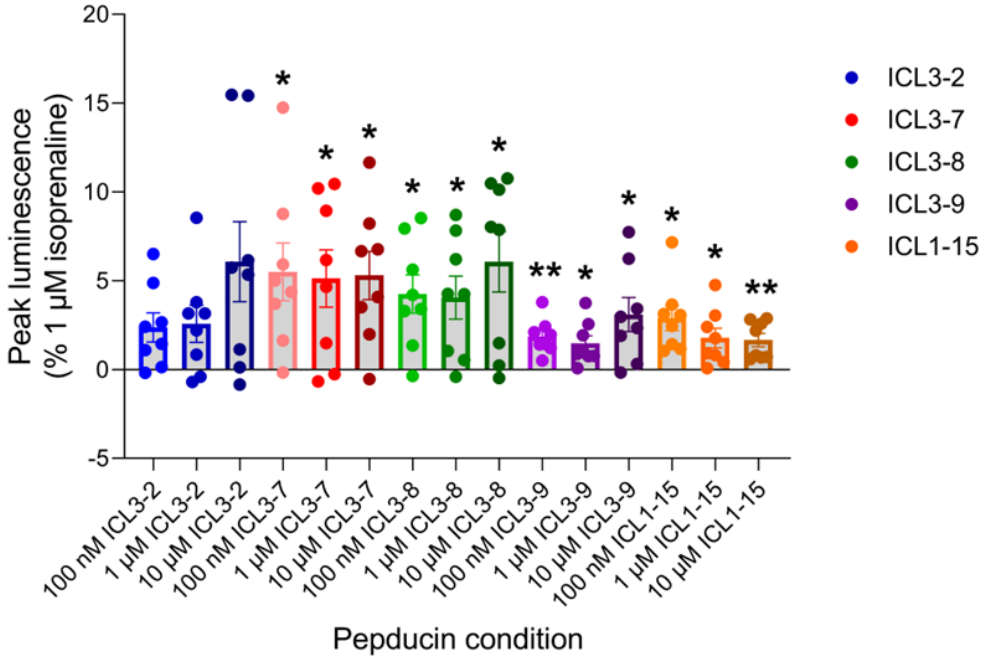

Figure 5.3: GloSensor^{TM} luminescence stimulated by pepducin-mediated cAMP production. Bar-dot plot displaying mean peak response for ICL3-2, ICL3-7, ICL3-8, ICL3-9 and ICL1-15 (all 100 nM – 10 µM) in HEK293Gwt cells, expressed as a percentage of 1 µM isoprenaline. Data points represent mean ± SEM (bars) from eight independent experiments (n = 8), with each individual experimental repeat displayed (dots). Significant increases in response over 0.1% (ICL3-2, ICL3-7 and ICL3-8) or 0.5% (ICL3-9 and ICL1-15) DMSO (vehicle) are indicated, determined by a two-way ANOVA with Tukey's multiple comparisons test. $P < 0.05$ was used as the level for significance ($P < 0.05$ = *, $P < 0.01$ = **).

Pepducin	Log [pepducin] (M)	Pepducin peak response (% 1 µM isoprenaline) ± SEM
ICL3-2	-7	2.37 ± 0.82
	-6	2.58 ± 1.04
	-5	6.07 ± 2.25
ICL3-7	-7	5.50 ± 1.63 *
	-6	5.13 ± 1.61 *
	-5	5.30 ± 1.35 *
ICL3-8	-7	4.25 ± 1.08 *
	-6	4.06 ± 1.21 *
	-5	6.07 ± 1.71 *
ICL3-9	-7	1.86 ± 0.35 **
	-6	1.48 ± 0.42 *
	-5	3.10 ± 0.96 *

ICL1-15	-7	2.90 ± 0.70 *
	-6	1.78 ± 0.56 *
	-5	1.66 ± 0.37 **

Table 5.1: Pepducin mean peak response ± SEM determined for ICL3-2, ICL3-7, ICL3-8, ICL3-9 and ICL1-15 obtained by cAMP GloSensor™ in HEK293Gwt cells from eight independent experiments (n = 8). Significant increases in response over 0.1% (ICL3-2, ICL3-7 and ICL3-8) or 0.5% (ICL3-9 and ICL1-15) DMSO (vehicle) are indicated, determined by a two-way ANOVA with Tukey's multiple comparisons test. $P < 0.05$ was used as the level for significance ($P < 0.05$ = *, $P < 0.01$ = **).

HEK293Gwt cells were then preincubated with each of the pepducins for 30 min, followed by application of 10 nM (EC_{50} concentration) isoprenaline to examine whether the pepducins were able to alter the response of an orthosteric agonist. The same three pepducin concentrations of 100 nM, 1 μM and 10 μM were used. Preincubation of ICI-118551 was also used for comparison. Figure 5.4 shows the effect of each pepducin condition on the isoprenaline peak response. Again, the same four pepducins, ICL3-7 (100 nM: 22.62% ± 5.15% increase in 10 nM isoprenaline peak response; $P < 0.01$), ICL3-8 (100 nM: 16.38% ± 5.33% increase; $P < 0.05$), ICL3-9 (100 nM: 14.70% ± 4.67% increase; $P < 0.05$) and ICL1-15 (100 nM: 18.12% ± 4.71% increase; $P < 0.05$), but not ICL3-2 (100 nM: 6.54% ± 5.26% increase; $P > 0.05$), produced statistically significant effects, each mildly increasing the isoprenaline response generally at their lowest tested concentrations but not at higher concentrations. ICI-118551 instead inhibited isoprenaline peak response at all tested concentrations (100 nM: 96.18% ± 2.05% reduction in 10 nM isoprenaline peak response; $P < 0.0001$).

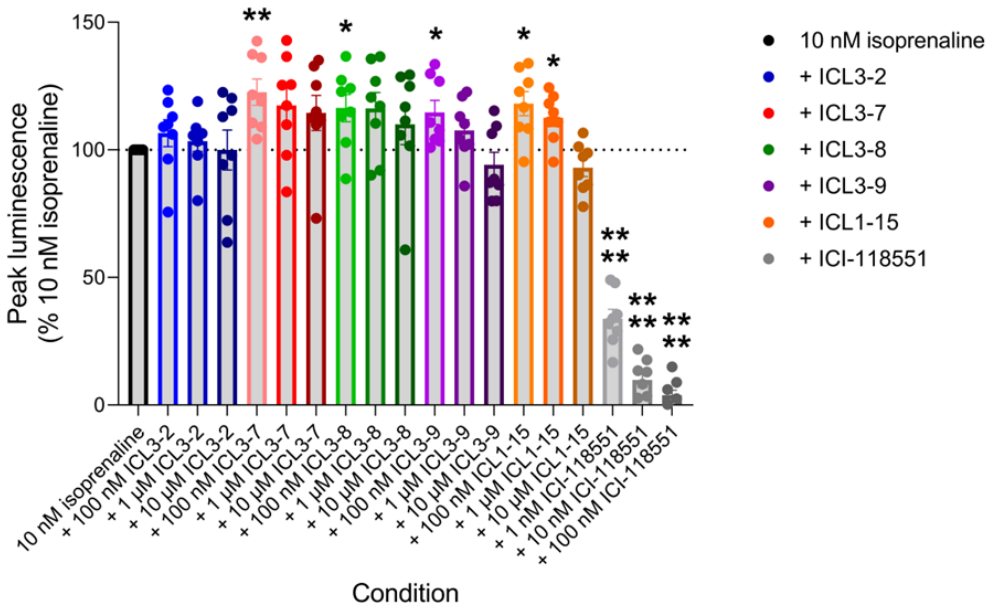

Figure 5.4: GloSensor^{TM} luminescence stimulated by isoprenaline in the presence and absence of 30 min preincubated ligands. Bar-dot plot displaying mean peak response for 10 nM isoprenaline in the presence and absence of ICL3-2, ICL3-7, ICL3-8, ICL3-9, ICL1-15 (all 100 nM – 10 µM) and ICI-118551 (1 nM – 100 nM) in HEK293Gwt cells, expressed as a percentage of 10 nM isoprenaline. Data points represent mean ± SEM (bars) from eight independent experiments (n = 8), with each individual experimental repeat displayed (dots). Significant differences in responses to those seen in absence of pepducins or inverse agonist are indicated, determined by a two-way ANOVA with Tukey's multiple comparisons test. $P < 0.05$ was used as the level for significance ($P < 0.05$ = *, $P < 0.01$ = **, $P < 0.0001$ = ****).

Ligand	Log [pepducin] (M)	Isoprenaline peak response (% 10 nM isoprenaline) ± SEM
ICL3-2	0	100
	-7	106.54 ± 5.26
	-6	103.38 ± 3.92
	-5	99.95 ± 7.84
ICL3-7	0	100
	-7	122.62 ± 5.15 **
	-6	117.41 ± 6.98
	-5	114.46 ± 6.84
ICL3-8	0	100
	-7	116.38 ± 5.33*
	-6	116.20 ± 6.31
	-5	109.95 ± 7.91
ICL3-9	0	100
	-7	114.70 ± 4.67 *

	-6	107.60 ± 4.23
	-5	94.15 ± 4.95
ICL1-15	0	100
	-7	118.12 ± 4.71 *
	-6	112.53 ± 3.30 *
	-5	92.97 ± 3.41
ICI-118551	0	100
	-9	33.76 ± 3.83 ****
	-8	9.79 ± 2.91 ****
	-7	3.82 ± 2.05 ****

Table 5.2: Isoprenaline mean peak response ± SEM in the presence and absence of preincubated increasing concentrations of ICL3-2, ICL3-7, ICL3-8, ICL3-9, ICL1-15 and ICI-118551 obtained by cAMP GloSensor^{TM} in HEK293Gwt cells from eight independent experiments (n = 8). Significant differences in responses to those seen in absence of pepducins or inverse agonist are indicated, determined by a two-way ANOVA with Tukey's multiple comparisons test. $P < 0.05$ was used as the level for significance ($P < 0.05$ = *, $P < 0.01$ = **, $P < 0.0001$ = ****).

5.3.2 – Characterisation of ligand-mediated gene transcription via the β_2-adrenoceptor using the CRE-SPAP assay

The minute and inconsistent nature of the pepducin-mediated cAMP GloSensor^{TM} responses made it very difficult to study pepducin activity further using that assay. It was therefore considered appropriate to select a different technique with which to examine the pepducins. The CRE-SPAP assay is a method which measures gene transcription responses taking place further downstream the cAMP signalling pathway (Hill et al., 2001). Measuring downstream signals often provides a degree of amplification of the signalling responses and thus can enhance the apparent activity of ligands, so that even weak partial agonists may produce substantial responses (Baker et al., 2003b; Buchwald, 2017). Furthermore, the assay was performed in CHO cells stably overexpressing not just the CRE-SPAP reporter but also the β_2AR. High receptor expression provides an additional level of signal amplification (McDonnell et al., 1998; Buchwald, 2017), as has already been demonstrated in this study (see Chapters 3 and 4). In addition, because CHO cells do not endogenously express the β_2AR (Baker et al., 2003a), performing the same pepducin experiments in the presence and absence of the stably transfected receptor would provide a simple method to determine the β_2AR-dependency of their activity. Therefore, this CRE-SPAP assay provided an ideal, amplified system to attempt further characterisation of the activity of pepducins. But prior to testing the pepducins, the assay was initially characterised using several orthosteric β_2AR ligands.

Firstly, four β_2AR agonists (isoprenaline, formoterol, salbutamol and salmeterol) and the adenylate cyclase activator forskolin were tested for their ability to stimulate CRE-mediated SPAP gene transcription in CHO cells stably expressing both the CRE-SPAP reporter gene and the human β_2AR. These cells are referred to as CHO-CRE-SPAP-β_2AR cells throughout. CRE-SPAP responses are expressed as absorbance (optical density; OD) at 405 nm throughout, which quantifies the media (SFM) colour change due to the production and secretion of SPAP after CRE-mediated gene transcription (Hill et al., 2001). Each agonist stimulated concentration-dependent SPAP production and these responses were normalised against 100 μM forskolin and fitted to a standard sigmoidal curve

using the Hill equation (Equation 1) to construct concentration-response curves for each β_2AR agonist and forskolin (Figure 5.5A). Each ligand produced comparable maximal responses ($P > 0.05$), similar to the cAMP GloSensor^{TM} data obtained in HEK293G-β_2AR cells (Figure 4.5) but not in HEK293Gwt cells (Figure 3.6), and β_2AR ligand potencies were also left-shifted (approximately 100-fold) compared with HEK293Gwt GloSensor^{TM} data ($P < 0.0001$ for each), with the exception of isoprenaline ($P > 0.05$; Tables 5.3 and 3.4). However, upon addition of 0.01% ascorbic acid to the SFM throughout the five hour ligand incubation step, the isoprenaline potency also increased to a similar degree (log EC_{50}: -7.62 ± 0.31 in absence of ascorbic acid, compared with -10.53 ± 0.10 in presence of ascorbic acid; $P < 0.0001$; Figure 5.5B), while the maximal response remained unchanged ($P > 0.05$).

Four other β_2AR ligands generally considered to act as antagonists or inverse agonists at the receptor (propranolol, ICI-118551, carvedilol and bisoprolol) were also tested using the CRE-SPAP assay. Indeed, each of these ligands were previously shown to act as β_2AR antagonists or inverse agonists in the cAMP GloSensor^{TM} work described in Chapters 3 and 4 (Figures 3.10A and 4.7). Data were again normalised against 100 μM forskolin and concentration-response curves were generated by fitting to a sigmoidal curve using the Hill equation (Equation 1). Interestingly, both propranolol and carvedilol produced concentration-dependent partial agonist SPAP responses (Figure 5.6). Carvedilol produced a more efficacious response than propranolol (carvedilol E_{max}: 26.31% ± 0.65% of 100 μM forskolin, compared with propranolol E_{max}: 19.05% ± 0.86%; $P < 0.0001$; Table 5.3), but propranolol acted with higher potency (propranolol log EC_{50}: -9.16 ± 0.15, compared with carvedilol log EC_{50}: -8.43 ± 0.02; $P < 0.01$). In contrast, both ICI-118551 (3.51% ± 0.41% decrease in basal response; $P < 0.01$) and bisoprolol (3.71% ± 1.02% decrease in basal response; $P < 0.01$) caused a slight decrease in basal SPAP production, perhaps suggesting a very minor inverse agonist activity from both ligands. However, no accurate log IC_{50} values could be determined for either ICI-118551 or bisoprolol as the responses were too small. The full set of determined E_{max} and log EC_{50} values for all ligands tested here are displayed in Table 5.3.

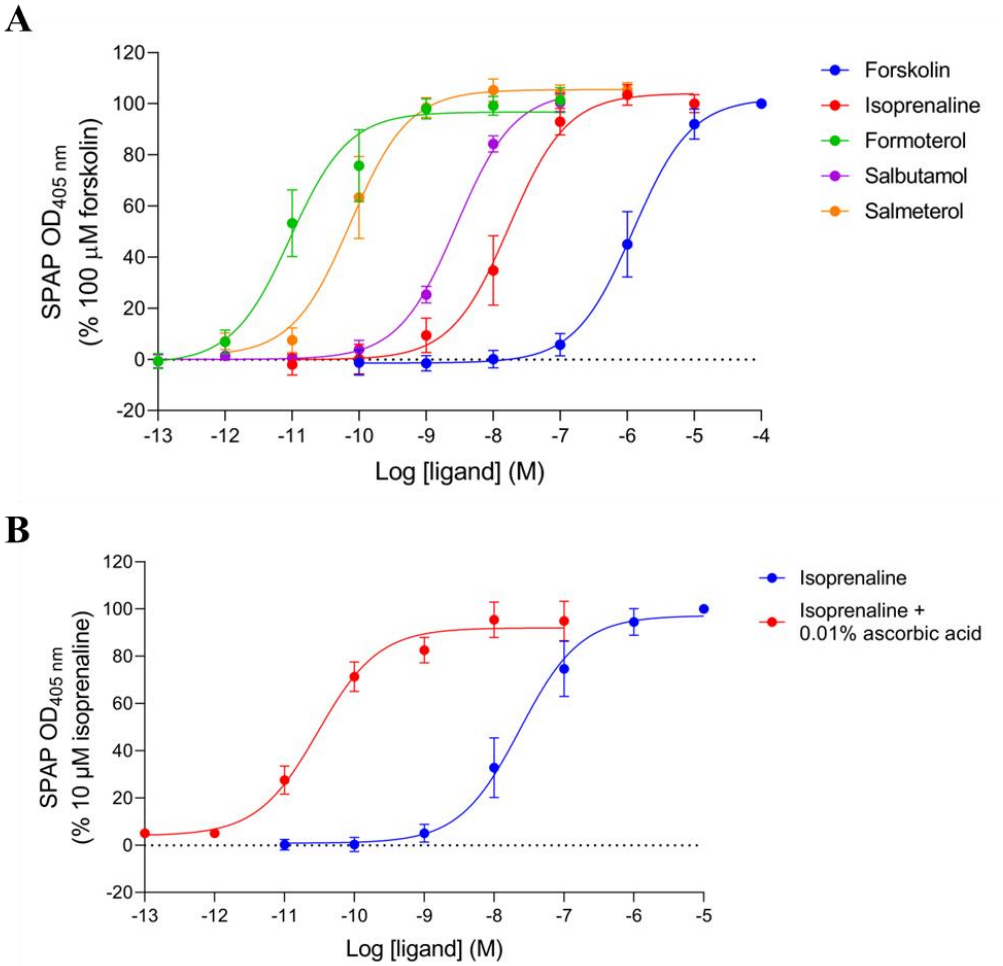

Figure 5.5: CRE-mediated SPAP production stimulated by agonists. (A) Mean concentration-response curves for forskolin, isoprenaline, formoterol, salbutamol and salmeterol in CHO-CRE-SPAP-β_2AR cells expressed as a percentage of 100 µM forskolin. (B) Mean concentration-response curves for isoprenaline in the presence and absence of 0.01% ascorbic acid in CHO-CRE-SPAP-β_2AR cells expressed as a percentage of 10 µM isoprenaline. Data points represent mean ± SEM from five independent experiments (n = 5). Significant differences were determined by a one-way ANOVA with Tukey's multiple comparisons test (A) or an unpaired t-test (B).

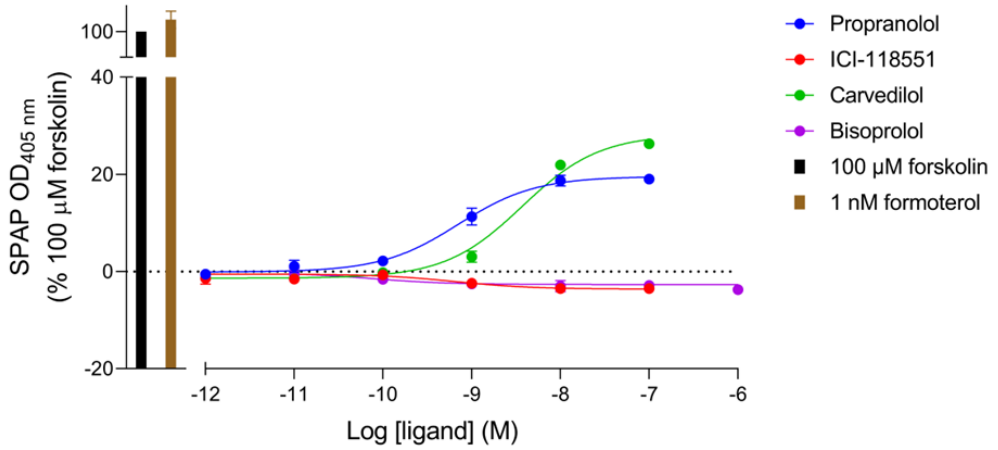

Figure 5.6: CRE-mediated SPAP production stimulated after antagonist application. Mean concentration-response curves for propranolol, ICI-118551, carvedilol and bisoprolol with 100 µM forskolin and 1 nM formoterol controls in CHO-CRE-SPAP-β_2AR cells expressed as a percentage of 100 µM forskolin. Data points represent mean ± SEM from five independent experiments (n = 5). Significant differences were determined by a one-way ANOVA with Tukey's multiple comparisons test.

Ligand	E_{max} (% 100 µM forskolin) ± SEM	Log EC_{50} (M) ± SEM
Forskolin	100	-5.93 ± 0.20
Isoprenaline	103.44 ± 3.98	-7.85 ± 0.25
Formoterol	101.37 ± 4.89	-11.23 ± 0.10
Salbutamol	100.50 ± 3.50	-8.55 ± 0.02
Salmeterol	105.38 ± 2.84	-10.13 ± 0.20
Carvedilol	26.31 ± 0.65	-8.43 ± 0.02
Propranolol	19.05 ± 0.86	-9.16 ± 0.15
ICI-118551	-3.51 ± 0.41	N/A
Bisoprolol	-3.71 ± 1.02	N/A

Table 5.3: Ligand E_{max} and log EC_{50} values ± SEM determined for forskolin, isoprenaline, formoterol, salbutamol, salmeterol, carvedilol, propranolol, ICI-118551 and bisoprolol from concentration-response curves obtained by CRE-SPAP in CHO-CRE-SPAP-β_2AR cells from five independent experiments (n = 5).

To confirm that these ligand responses were all mediated through the β_2AR, CHO cells stably expressing the CRE-SPAP reporter gene but not the β_2AR were used (termed CHO-CRE-SPAPwt cells throughout). Since these cells do not endogenously express the receptor (Baker et al., 2003a), this provides a useful measure of SPAP responses in the absence of the β_2AR. None of the eight β_2AR ligands were able to stimulate any increased production of SPAP over the basal response in CHO-CRE-SPAPwt cells ($P > 0.05$; Figures 5.7A and 5.7B). However, in a small number of conditions, minor negative responses were observed (10 pM ICI-118551: 3.23% ± 0.85% decrease in basal response, 10 pM carvedilol: 4.06% ± 0.88% decrease, 100 pM bisoprolol: 4.87% ± 0.96% decrease; each $P < 0.05$ or less), although this was not concentration-dependent. Forskolin on the other hand still produced a similarly large maximal response, albeit with slightly lower potency than in CHO-CRE-SPAP-β_2AR cells (log EC_{50}: -5.10 ± 0.13 in CHO-CRE-SPAPwt cells, compared with log EC_{50}: -5.93 ± 0.20 in CHO-CRE-SPAP-β_2AR cells; $P < 0.01$).

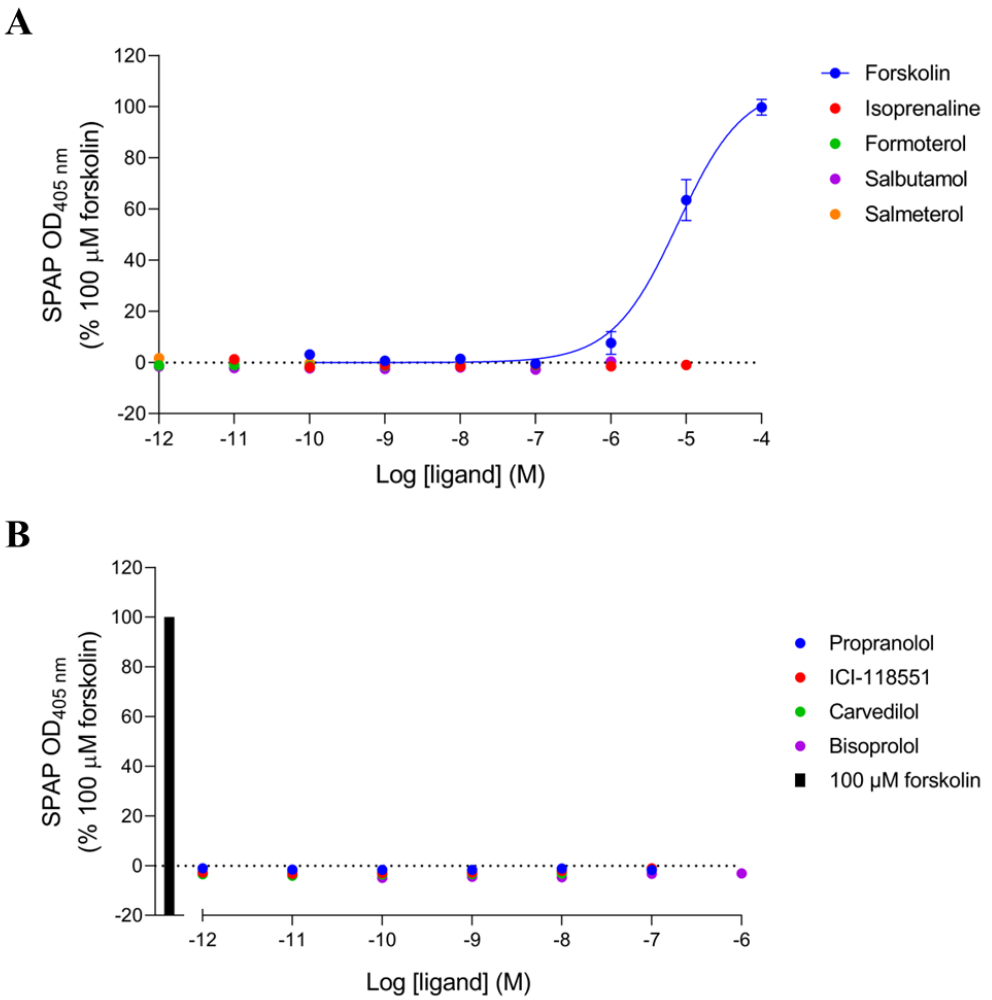

Figure 5.7: CRE-mediated SPAP production after application of ligands. (A, B) Mean concentration-response curves for forskolin, isoprenaline formoterol, salbutamol and salmeterol (A), or propranolol, ICI-118551, carvedilol, bisoprolol and 100 µM forskolin control (B) in CHO-CRE-SPAPwt cells expressed as a percentage of 100 µM forskolin. Significant differences were determined by a one-way ANOVA with Tukey's multiple comparisons test.

CHO-CRE-SPAP-β_2AR cells were then preincubated with each of the four antagonists for 30 min, prior to application of a range of formoterol concentrations. Formoterol concentration-response curves were constructed in the presence and absence of the antagonists, shown in Figures 5.8A-5.8D. In each case, antagonist application caused a parallel rightward shift in formoterol potency ($P < 0.0001$ in each case) in a concentration-dependent manner. Generally, no effect was observed on the maximal formoterol response ($P > 0.05$ in most cases), with the exception of two conditions where the formoterol maximal response was mildly reduced: 10 nM carvedilol (9.02% ± 2.00% reduction in formoterol E_{max}; $P < 0.05$) and 10 nM propranolol (14.44% ± 4.21% reduction in formoterol E_{max}; $P < 0.05$). These effects were not concentration dependent because in both cases application of higher antagonist concentration (100 nM) did not produce significant reduction of the formoterol E_{max} value. All formoterol E_{max} and log EC_{50} values under each antagonist condition are stated in Table 5.4. At lower formoterol concentrations, the small partial agonist effects of both carvedilol and propranolol can be observed again (Figures 5.8A and 5.8C). Similarly, a mild inverse agonist effect can be also seen by both ICI-118551 and bisoprolol at the lower agonist concentrations (Figures 5.8B and 5.8D).

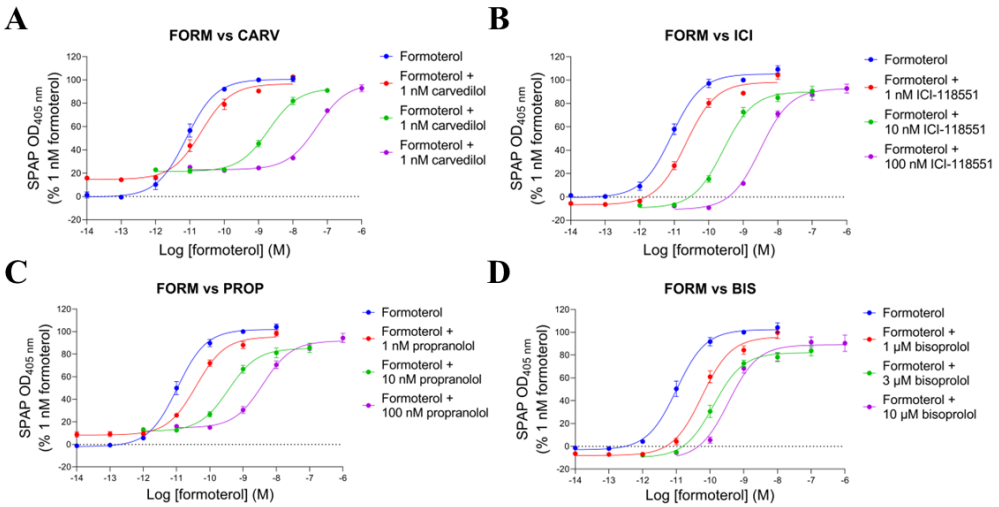

Figure 5.8: CRE-mediated SPAP production stimulated by formoterol in the presence and absence of 30 min preincubated antagonists/inverse agonists. (A-D) Mean concentration-response curves for formoterol (FORM) in the presence and absence of carvedilol (CARV; 1 nM – 100 nM; A), ICI-118551 (ICI; 1 nM – 100 nM; B), propranolol (PROP; 1 nM – 100 nM; C) and bisoprolol (BIS; 1 µM – 10 µM; D) in CHO-CRE-SPAP-β_2AR cells expressed as a percentage of 1 nM formoterol. Data points represent mean ± SEM from five independent experiments (n = 5).

Antagonist	Log [antagonist] (M)	Formoterol E_{max} (% 1 nM formoterol) ± SEM	Log formoterol EC_{50} (M) ± SEM
Carvedilol	0	100	-11.12 ± 0.11
	-9	102.54 ± 1.17	-10.66 ± 0.15 *
	-8	90.98 ± 2.00 *	-8.70 ± 0.04 ****
	-7	92.89 ± 16.88	-7.29 ± 0.05 ****
ICI-118551	0	100	-11.08 ± 0.09
	-9	104.34 ± 3.59	-10.66 ± 0.07 **
	-8	90.30 ± 4.35	-9.58 ± 0.04 ****
	-7	92.82 ± 3.82	-8.51 ± 0.04 ****
Propranolol	0	100	-10.98 ± 0.09
	-9	98.38 ± 2.32	-10.41 ± 0.09 **
	-8	85.56 ± 4.21 *	-9.46 ± 0.07 ****

	-7	94.31 ± 4.03	-8.41 ± 0.10 ****
Bisoprolol	0	100	-10.98 ± 0.10
	-9	99.74 ± 5.21	-10.24 ± 0.06 ****
	-8	83.80 ± 4.49	-9.90 ± 0.07 ****
	-7	91.38 ± 4.67	-9.45 ± 0.03 ****

Table 5.4: Formoterol mean E_{max} and log EC_{50} values ± SEM in the presence and absence of preincubated increasing concentrations of carvedilol, ICI-118551, propranolol and bisoprolol from concentration-response curves obtained by CRE-SPAP in CHO-CRE-SPAP-β_2AR cells from five independent experiments (n = 5). Significant differences in responses to those seen in absence of antagonists/inverse agonists are indicated, determined by a one-way ANOVA with Tukey's multiple comparisons test. $P < 0.05$ was used as the level for significance ($P < 0.05$ = *, $P < 0.01$ = **, $P < 0.0001$ = ****).

Just as with cAMP GloSensor™ data in HEK293Gwt cells, Schild regression analysis was performed using the formoterol vs antagonist concentration-response curves in Figures 5.8A-5.8D to estimate antagonist binding affinity at the β_2AR. This was done by employing the Schild equation (Equation 5), followed by generation of a Schild plot and the fitting of a linear regression line (Equation 6) to determine the antagonist log K_D value, which is represented by the x-intercept (Arunlakshana and Schild, 1959; Tallarida and Murray, 1987). Although there were no hemi-equilibrium-mediated depression of agonist maximal responses observed in the CRE-SPAP assay, due to the small partial agonist responses by carvedilol and propranolol it was not appropriate to use agonist EC_{50} concentrations to calculate dose ratios (in these cases the EC_{50} values would not provide equivalent response magnitudes). Therefore the 50% formoterol response in absence of antagonist was selected as the equieffective agonist concentration in each case to determine dose ratios here.

Schild plots were constructed for each antagonist, displayed in Figures 5.9A-5.9D, and estimated antagonist log K_D values for the β_2AR and Schild slopes are shown in Table 5.5. Estimated log K_D values for propranolol (CRE-SPAP vs GloSensor™ log K_D: -9.37 ± 0.15 vs -9.06 ± 0.29; $P > 0.05$) and bisoprolol (-6.86 ± 0.07 vs -7.15 ± 0.24; $P > 0.05$) were similar to those calculated using the cAMP GloSensor™ assay (Tables 3.8 and 5.5), whereas the log K_D values for ICI-118551 (-9.35 ± 0.05 vs -9.93 ± 0.21; $P < 0.05$) differed slightly between the two assays. No log K_D value could be determined for carvedilol using the cAMP GloSensor™ previously (due to drastic reduction of agonist maximal responses), so no comparison can be made here for carvedilol. Surprisingly, with the exception of bisoprolol ($P > 0.05$), the Schild slopes calculated for each antagonist deviated significantly from 1 ($P < 0.05$ or less for each), which usually indicates either a non-competitive antagonist behaviour or the presence of non-equilibrium conditions (Kenakin, 1982). Neither of these should be true in these cases since all the antagonists act competitively at the β_2AR orthosteric site, and the five hour ligand incubation period should be more than sufficient for the ligands to reach binding equilibrium with the receptor.

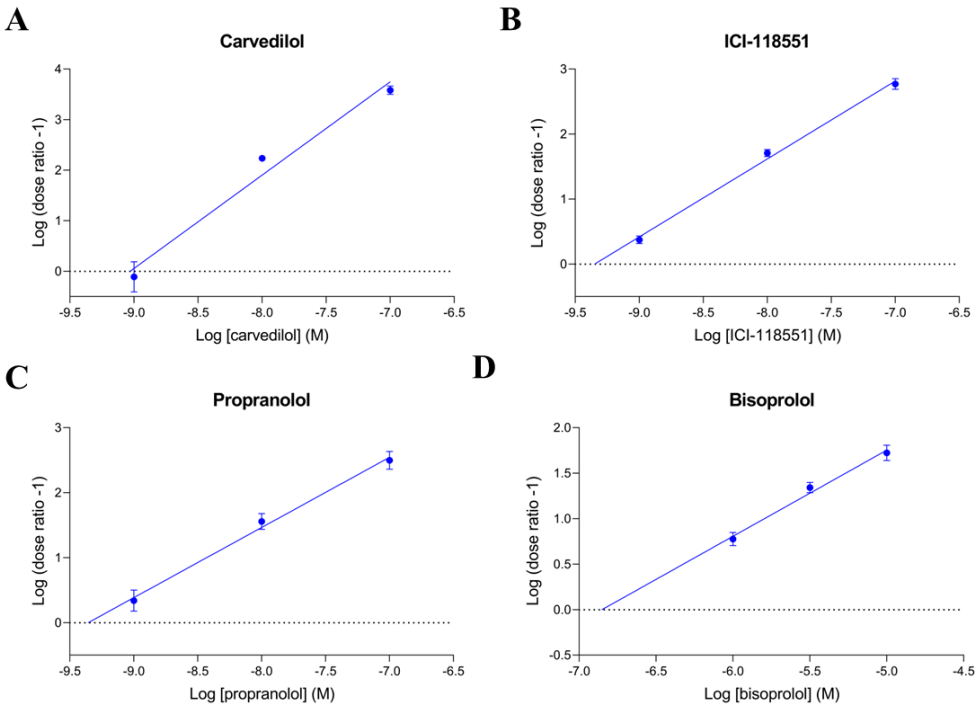

Figure 5.9: Schild regression analysis to determine antagonist binding affinities for the β_2AR from CRE-SPAP in CHO-CRE-SPAP-β_2AR cells. (A-D) Schild plots for formoterol versus carvedilol (A), ICI-118551 (B), propranolol (C) or bisoprolol (D). Data points represent mean log (dose ratio -1) ± SEM for each concentration of antagonist from five independent experiments (n = 5). The x-intercept provides an estimation of antagonist log K_D value.

Antagonist	Estimated antagonist log K_D ± SEM	Schild slope ± SEM
Carvedilol	-9.08 ± 0.15	1.85 ± 0.14 ***
ICI-118551	-9.35 ± 0.05	1.20 ± 0.03 ****
Propranolol	-9.37 ± 0.15	1.08 ± 0.03 *
Bisoprolol	-6.86 ± 0.07	0.95 ± 0.03

Table 5.5: Estimated antagonist mean log K_D and Schild slope values ± SEM at the β_2AR for carvedilol, ICI-118551, propranolol and bisoprolol from data obtained by CRE-SPAP in CHO-CRE-SPAP-β_2AR cells from five independent experiments (n = 5). Significant deviation of Schild slopes from 1 are indicated, determined by an unpaired t-test. $P < 0.05$ was used as the level for significance ($P < 0.05$ = *, $P < 0.001$ = ***, $P < 0.0001$ = ****).

5.3.3 – β_2-adrenoceptor gene transcription responses mediated by pepducins in an amplified, high receptor expression system

Having characterised the CRE-SPAP assay using several orthosteric ligands and shown that consistent ligand responses can be measured, pepducins were then applied to CHO-CRE-SPAP-β_2AR cells to examine whether they were able to stimulate gene transcription and subsequent production of SPAP. For these experiments, 0.1% BSA was applied to the SFM in order to limit peptide adhesion to the plasticware. Several orthosteric ligand responses were first tested in the presence of 0.1% BSA and both maximal responses and ligand potencies were all unaffected (data not shown). Each pepducin was tested at three concentrations (100 nM, 1 μM and 10 μM). Due to the differential DMSO concentrations used to solubilise the initial pepducin stocks (see 2.2 – Solubilisation of pepducins), 0.1% (ICL3-2, ICL3-7 and ICL3-8) or 0.5% (ICL3-9 and ICL1-15) DMSO were applied to the SFM vehicle control conditions, which were normalised to zero throughout these experiments. Any increase over this basal level therefore should indicate pepducin-mediated increases in SPAP-production.

Changes in CRE-mediated SPAP production after application of pepducins to CHO-CRE-SPAP-β_2AR cells are shown in Figure 5.10A, expressed as a percentage of 1 μM isoprenaline response (in absence of ascorbic acid). Each of the six experimental repeats are shown for each condition. As with the data observed in GloSensor^{TM}, there was considerable variation between experimental repeats, particularly at high pepducin concentrations. Because of this inconsistency, the only pepducin to produce a statistically significant gene transcription response over basal was ICL3-8 (1 μM: 10.43% ± 2.72% of 1 μM isoprenaline response; $P < 0.05$). Whereas the highest concentrations of ICL3-8 (10 μM: 32.20% ± 20.68%; $P > 0.05$), ICL3-2 (10 μM: 16.62% ± 8.83%; $P > 0.05$) and ICL3-7 (10 μM: 12.92% ± 10.65%; $P > 0.05$) all failed to reach the threshold for significance despite occasionally displaying substantially increased responses over basal and showing the largest mean responses of all conditions. Meanwhile, ICL3-9 (10 μM: -5.41% ± 1.81%; $P > 0.05$) and ICL1-15 (10 μM: -6.38% ± 2.45%; $P > 0.05$) both appeared to mildly reduce basal gene

transcription, but again these were not found to be statistically significant. Pepducin responses in each tested condition are displayed in Table 5.6.

The same test was then performed in CHO-CRE-SPAPwt cells lacking expression of the β_2AR, displayed in Figure 5.10B. This time responses are normalised to 100 μM forskolin as isoprenaline did not produce a response in these cells. Under these conditions, none of the pepducins had any effect on CRE-mediated SPAP production at any concentration ($P > 0.05$ in every condition). Moreover, all the variation between repeats was lost in absence of β_2AR expression.

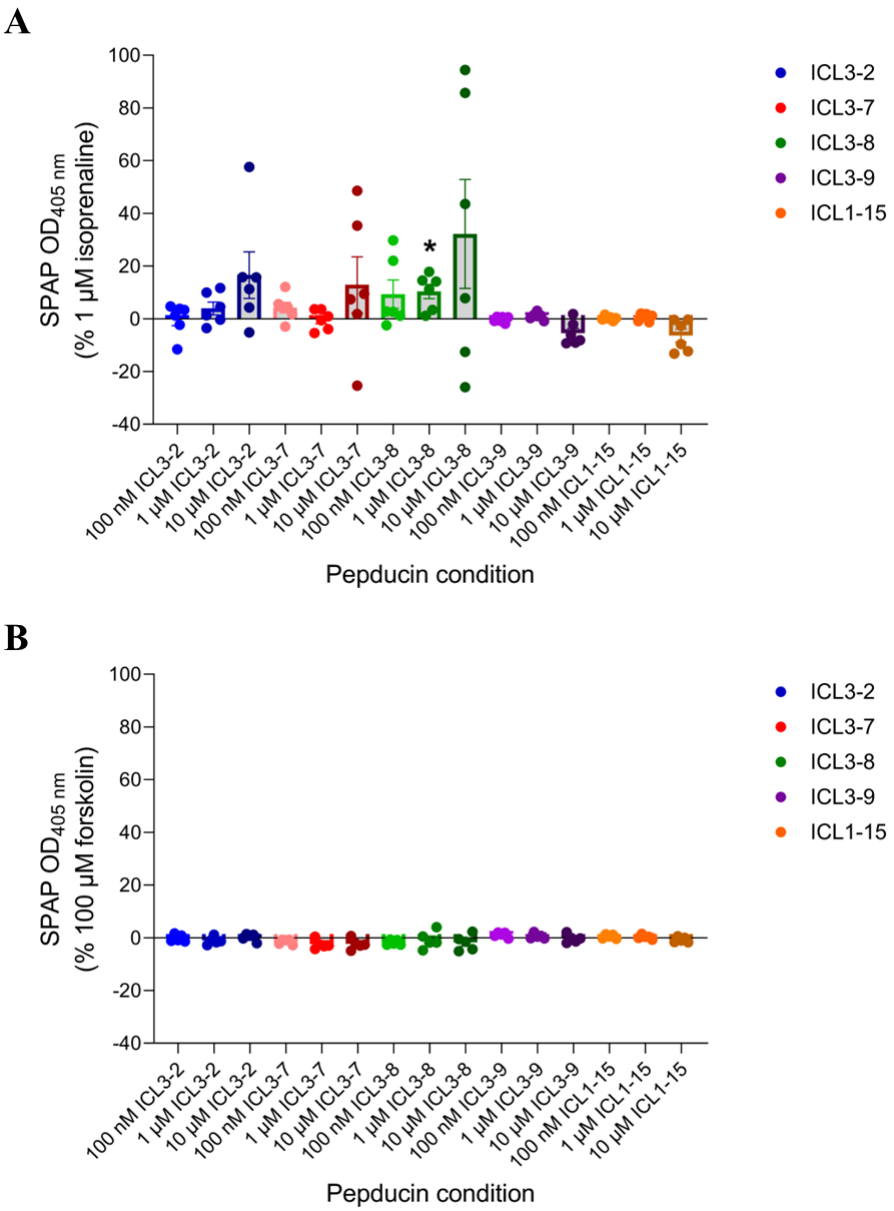

Figure 5.10: CRE-mediated SPAP production after application of pepducins. (A, B) Bar-dot plots displaying mean response for ICL3-2, ICL3-7, ICL3-8, ICL3-9 and ICL1-15 (all 100 nM – 10 µM) in CHO-CRE-SPAP-β_2AR cells (A) or CHO-CRE-SPAPwt cells (B), expressed as a percentage of 1 µM isoprenaline (A) or 100 µM forskolin (B). Data points represent mean ± SEM (bars) from six independent experiments (n = 6), with each individual experimental repeat displayed (dots). Significant increases in response over 0.1% (ICL3-2, ICL3-7 and ICL3-8) or 0.5% (ICL3-9 and ICL1-15) DMSO (vehicle) are indicated, determined by a two-way ANOVA with Tukey's multiple comparisons test. $P <$ 0.05 was used as the level for significance ($P < 0.05$ = *).

Pepducin	Log [pepducin] (M)	Pepducin response (% 1 μM isoprenaline) ± SEM
ICL3-2	-7	-0.09 ± 2.50
	-6	3.96 ± 2.43
	-5	16.62 ± 8.83
ICL3-7	-7	4.27 ± 2.02
	-6	-0.27 ± 1.55
	-5	12.92 ± 10.65
ICL3-8	-7	9.38 ± 5.39
	-6	10.43 ± 2.72 *
	-5	32.20 ± 20.68
ICL3-9	-7	-0.20 ± 0.43
	-6	1.08 ± 0.53
	-5	-5.41 ± 1.81

ICL1-15	-7	0.26 ± 0.34
	-6	0.63 ± 0.57
	-5	-6.38 ± 2.45

Table 5.6: Pepducin mean response ± SEM determined for ICL3-2, ICL3-7, ICL3-8, ICL3-9 and ICL1-15 obtained by CRE-SPAP in CHO-CRE-SPAP-β_2AR cells from six independent experiments (n = 6). Significant increases in response over 0.1% (ICL3-2, ICL3-7 and ICL3-8) or 0.5% (ICL3-9 and ICL1-15) DMSO (vehicle) are indicated, determined by a two-way ANOVA with Tukey's multiple comparisons test. $P < 0.05$ was used as the level for significance ($P < 0.05$ = *).

Finally, CHO-CRE-SPAP-β_2AR cells were preincubated for 30 min with each pepducin prior to application of 10 nM isoprenaline (EC_{50} concentration in absence of ascorbic acid). This was to determine whether any of the pepducins were able to allosterically modulate the production of SPAP stimulated by an orthosteric agonist. As shown in Figure 5.11, the most notable effect of the pepducins was once again to introduce a considerable degree of variation between repeated experiments, although there was a general inhibitory trend on the isoprenaline response, particularly by ICL3-7 (10 μM: 28.45% ± 7.27% reduction in 10 nM isoprenaline response; $P < 0.05$) and ICL3-8 (1 μM: 28.39% ± 3.65% reduction; $P < 0.01$), which significantly reduced the 10 nM isoprenaline response. Whereas ICL3-2 (100 nM: 13.00% ± 7.76% reduction; $P > 0.05$), ICL3-9 (1 μM: 21.42% ± 7.11% reduction; $P > 0.05$) and ICL1-15 (1 μM: 27.77% ± 8.51% reduction; $P > 0.05$) did not significantly alter the isoprenaline response and the effect did not appear to be concentration-dependent in any of the five pepducins. Isoprenaline SPAP responses in the presence and absence of the pepducins are stated in Table 5.7.

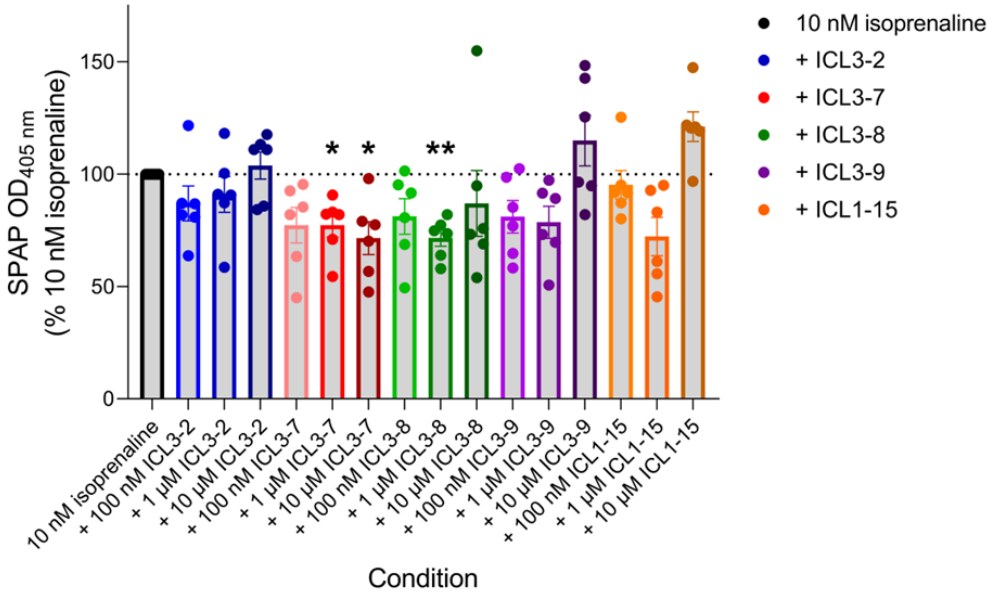

Figure 5.11: CRE-mediated SPAP production stimulated by isoprenaline in the presence and absence of 30 min preincubated pepducins. Bar-dot plot for 10 nM isoprenaline in the presence and absence of ICL3-2, ICL3-7, ICL3-8, ICL3-9 and ICL1-15 (all 100 nM – 10 µM) in CHO-CRE-SPAP-β_2AR cells, expressed as a percentage of 10 nM isoprenaline. Data points represent mean ± SEM (bars) from six independent experiments (n = 6), with each individual experimental repeat displayed (dots). Significant differences in responses to those seen in absence of pepducins or inverse agonist are indicated, determined by a two-way ANOVA with Tukey's multiple comparisons test. $P < 0.05$ was used as the level for significance ($P < 0.05$ = *, $P < 0.01$ = **).

Pepducins	Log [pepducin] (M)	Isoprenaline response (% 10 nM isoprenaline) ± SEM
ICL3-2	0	100
	-7	87.00 ± 7.76
	-6	91.01 ± 7.93
	-5	103.80 ± 6.02
ICL3-7	0	100
	-7	77.31 ± 7.93
	-6	77.27 ± 5.23 *
	-5	71.55 ± 7.27 *
ICL3-8	0	100
	-7	81.20 ± 7.91
	-6	71.61 ± 3.65 **
	-5	86.98 ± 14.62

ICL3-9	0	100
	-7	81.05 ± 7.27
	-6	78.58 ± 7.11
	-5	114.99 ± 11.28
ICL1-15	0	100
	-7	95.28 ± 6.38
	-6	72.23 ± 8.51
	-5	121.14 ± 6.55

Table 5.7: Isoprenaline mean response ± SEM in the presence and absence of preincubated increasing concentrations of ICL3-2, ICL3-7, ICL3-8, ICL3-9 and ICL1-15 obtained by CRE-SPAP in CHO-CRE-SPAP-β_2AR cells from six independent experiments ($n = 6$). Significant differences in responses to those seen in absence of pepducins or inverse agonist are indicated, determined by a two-way ANOVA with Tukey's multiple comparisons test. $P < 0.05$ was used as the level for significance ($P < 0.05$ = *, $P < 0.01$ = **).

5.4 – Discussion

5.4.1 – Pepducins were unable to produce substantial or consistent cAMP responses in HEK293Gwt cells

Previously, Carr et al. (2014) developed numerous β_2AR-dervied pepducins which they reported to act as allosteric agonists by stimulating cAMP production in HEK293 cells. They determined this by cell lysis following incubation with 10 μM pepducins and subsequent measurement of cAMP concentrations using a cAMP ELISA kit (Carr et al., 2014). Using this technique, several of the pepducins which derived from ICL3 of the β_2AR (ICL3-2, ICL3-7, ICL3-8 and ICL3-9) were shown to produce cAMP concentrations similar to the orthosteric partial agonist salbutamol, whilst others (including ICL1-15) produced smaller but still substantial responses (Carr et al., 2014). For this reason, the four pepducins which showed the highest efficacy for cAMP production, ICL3-2, ICL3-7, ICL3-8 and ICL3-9, as well as the ICL1-derived ICL1-15, were selected for this study. The abilities of these five pepducins to modulate cytosolic cAMP concentrations in real-time, and thus act as allosteric β_2AR agonists, was monitored using the cAMP GloSensor^{TM} assay in HEK293Gwt cells.

Although application of several of the pepducins (ICL3-2, ICL3-7, ICL3-8 and 10 μM ICL3-9, but not ICL1-15) produced small agonist-like increases in the cAMP signal which quickly peaked and subsequently declined back to the baseline (Figures 5.2A-5.2E), each of these responses were minute compared to those of isoprenaline and forskolin (Figure 5.2F). In contrast with the previous work by Carr et al. (2014), the largest responses (produced by ICL3-2, ICL3-7 and ICL3-8) achieved only approximately 5-6% of the maximal isoprenaline response (Table 5.1), much lower than that of salbutamol (previously shown to produce a cAMP response approximately 45% of isoprenaline in HEK293Gwt cells in this study; Table 3.4). One possible explanation for the differences between pepducin responses measured in the two studies is the use of the PDE inhibitor IBMX. In the study by Carr et al. (2014), 500 μM IBMX was applied to the cells to reduce PDE-mediated breakdown of cAMP and thus amplify relative intracellular cAMP concentrations (Cheng and Grande, 2007; Ghosh et

al., 2009). This would not necessarily explain why the pepducins achieved a similar response magnitude as salbutamol in that study but not here, as orthosteric agonist responses are also increased by the presence of IBMX (Figures 3.4A, 3.4C and 3.4D). However, the addition of IBMX in this study may have enabled detection of more robust pepducin-mediated cAMP responses and would be worth testing in the future. Considerable inconsistency between experimental repeats was also observed in many of the conditions (Figure 5.3). This is particularly exemplified by 10 μM ICL3-2 which showed a wide range of responses between 0% and 15% that of isoprenaline and did not produce a statistically significant response despite showing the largest mean response out of all the tested pepducins (Table 5.1). Some possible reasons for these observations are discussed in more detail later (see 5.4.3). Because of the small responses combined with large variations between experiments, it is difficult to determine the actual effect of the pepducins on cytosolic cAMP levels here and therefore it cannot be definitively concluded that they act as β_2AR allosteric agonists in this study. Leach et al. (2007) have previously noted that allosteric ligand efficacy may be difficult to detect under low receptor expression conditions, as were present here.

As there was limited evidence of agonist activity by the pepducins tested in this study, their ability to instead act as allosteric modulators of the β_2AR was examined. Allosteric modulators act by altering the activity of an orthosteric agonist at its receptor (Christopoulos and Kenakin, 2002; May et al., 2007; Christopoulos et al., 2014; Lane et al., 2017), hence a submaximal concentration of isoprenaline (10 nM; EC_{50} concentration) was applied to HEK293Gwt cells following preincubation of the pepducins to enable any potentiation (increased response) or inhibition (decreased response) of isoprenaline-mediated cAMP production to be easily detected. ICL3-7, ICL3-8, ICL3-9 and ICL1-15 each did slightly increase the peak isoprenaline response (up to roughly 15-20% increases; Figure 5.4), possibly implying some mild PAM activity by these pepducins. However, these effects were all observed at lower concentrations (generally 100 nM) of the pepducins. Upon application of higher concentrations (1 μM or higher), these effects were no longer observed and the pepducins did not alter the isoprenaline response. Again, each pepducin appeared to introduce

considerable response variation between experimental repeats. Therefore, evidence of allosteric modulation by any of the pepducins was not clear in the cAMP GloSensor^{TM} assay here.

5.4.2 – Pharmacological studies of β_2-adrenoceptor-mediated gene transcription responses

The CRE-SPAP assay was firstly used to study orthosteric ligand activity at the level of gene transcription. Both the partial agonists salbutamol and salmeterol produced maximal responses similar to those of the full agonists isoprenaline and formoterol (Figure 5.5A), and the log EC_{50} values of each ligand (except isoprenaline) were markedly leftward shifted in comparison to cAMP GloSensor^{TM} data performed in HEK293Gwt cells. This was similar to the observations when performing GloSensor^{TM} in HEK293G-β_2AR cells because CHO-CRE-SPAP-β_2AR cells also highly express the β_2AR, which has been shown to increase the apparent efficacies and potencies of agonists (Hoyer and Boddeke, 1993; Kenakin, 1996; January et al., 1998; McDonnell et al., 1998; McDonald et al., 2003). In addition, the CRE-SPAP assay measures responses much further downstream the signalling pathway than cAMP, at the level of gene transcription, which results in further amplification of signalling responses (McDonnell et al., 1998; Buchwald, 2017). Differences in β_2AR agonist pharmacological parameters between cAMP and gene transcription assays has been reported previously (McDonnell et al., 1998; Baker et al., 2003b; Baker et al., 2004).

Isoprenaline was the only agonist which initially showed a lower potency than expected in the CRE-SPAP assay. This was probably due to oxidation, to which catecholamines such as isoprenaline (as well as the endogenous β_2AR ligands adrenaline and noradrenaline) are particularly susceptible (Sutor and Ten Bruggencate, 1990; Dhalla et al., 2010; Hughes and Smith, 2011). Therefore, it is likely that the actual concentration of unoxidised isoprenaline was much lower than assumed, which would naturally affect the measurement of potency here. This is supported by the restoration of a more potent isoprenaline response upon

addition of ascorbic acid (Figure 5.5B), which acts as a strong reductant to prevent oxidation of catecholamines (Bendich et al., 1986; Hughes and Smith, 2011). Although ascorbic acid had no effect on the isoprenaline cAMP GloSensor^{TM} response (Figures 3.2A and 3.2B), the much longer ligand incubation period during CRE-SPAP (5 h) appears to be sufficient for substantial degradation of isoprenaline.

Both propranolol and carvedilol also stimulated an increase in CRE-mediated gene transcription (Figure 5.6), albeit to a lesser degree than the agonists discussed above. This was in contrast to GloSensor^{TM} assays, where the ligands either had no effect on (HEK293Gwt cells; Figure 3.10A) or reduced (HEK293G-β_2AR cells; Figure 4.7) cytosolic cAMP levels. These responses were found to be β_2AR-mediated because both were abolished in CHO-CRE-SPAPwt cells lacking β_2AR expression (Figure 5.7B). Similar findings have been reported previously by Baker et al. (2003a), where several β-blockers (including both propranolol and carvedilol) were found to display partial agonist activity at the β_2AR in terms of gene transcription. In that study, carvedilol additionally stimulated cAMP accumulation, which has also been shown in some other studies (Benkel et al., 2022) but was not the case here. However, propranolol is by all accounts an inverse agonist for cAMP production (Chidiac et al., 1994; Azzi et al., 2001; Baker et al., 2003a; Galandrin and Bouvier, 2006; Ferguson and Feldman, 2014). Baker et al. (2003a) discovered that the signalling pathway transduced by the β_2AR down to the level of gene transcription was not simply a linear cascade via cAMP- and PKA-mediated promotion of CRE. Instead, crosstalk with other signalling pathways was found (both cAMP-dependent and -independent) and propranolol was proposed to act via a non-G protein signalling partner to activate the p42/44 MAPK pathway, leading to stimulation of CRE-mediated gene transcription (Baker et al., 2003a). Although not currently established, if the signalling partner in question was β-arrestin then this could be an example of biased signalling. Numerous other studies have shown that both propranolol and carvedilol activate the MAPK ERK1/2 pathway, which is linked to β-arrestin (DeFea et al., 2000; Luttrell et al., 2001; Azzi et al., 2003; Galandrin and Bouvier, 2006; Wisler et al., 2007).

Contrastingly, it was difficult to determine the action of ICI-118551 and bisoprolol on gene transcription in this study. Both caused a concentration-dependent decrease in basal SPAP production (Figure 5.6), however the responses were so small (approximately 3-4% reduction of basal in both cases) that it is not clear that this is due to inverse agonist activity, especially since similarly small negative effects were observed in some ICI-118551 and bisoprolol conditions in CHO-CRE-SPAPwt cells lacking β_2AR expression (Figure 5.7B). Previously, Baker et al. (2003a) found that bisoprolol had no effect on basal SPAP production, whilst ICI-118551 did act as an inverse agonist but to a much weaker degree than in cAMP accumulation studies.

5.4.3 – The effect of pepducins on CRE-mediated SPAP production is inconclusive due to large response variation

Since cAMP responses produced by the pepducins were so small using the GloSensor^{TM} assay, it was thought that employing the high expression, amplified CRE-SPAP system, downstream of cAMP signalling, could enhance pepducin signalling responses in a similar manner to the amplification of salbutamol and salmeterol (which appeared as full agonists in this assay). Indeed, the mean magnitudes of the pepducin responses were larger in some conditions, particularly at 10 μM concentrations (Figure 5.10A), but this was also accompanied by much larger SEM values in these conditions. Because of this, only 1 μM ICL3-8 produced a significant increase in SPAP production. At 10 μM ICL3-8, responses in this condition ranged from around 90% of 1 μM isoprenaline response to a 30% reduction in basal activity between different experimental repeats. Therefore, it is difficult to surmise the true effect of the pepducins beyond a general trend of introducing considerable variation in gene transcription responses. Interestingly though, this inconsistent effect was shown to be β_2AR-dependent, as it was completely abolished in all pepducin conditions when performed in the absence of β_2AR expression (Figure 5.10B). Therefore, each pepducin does appear to be having some influence over β_2AR activity. This is perhaps surprising because ICL3-2 and ICL3-8 (the two pepducins which

tended to provide the largest functional responses in both assay types performed here) were previously shown to act independently of the β_2AR, instead likely directly activating G_s protein (Carr et al., 2014).

Moreover, ICL3-7 and ICL3-8 modestly inhibited the EC_{50} isoprenaline response, while the other pepducins also showed a general trend toward reduction of the response (up to 20-30% reduction; Figure 5.11). Once again though, this effect was not concentration-dependent in any of the pepducins and also varied largely between experimental repeats. Since Baker et al. (2003a) have shown that the CRE-mediated gene transcription response does not stem solely from a single linear signalling cascade downstream of cAMP, it is possible that the inconsistent pepducin responses may be mediated through another pathway via the β_2AR, either cAMP-dependent or -independent, as was shown for propranolol (Baker et al., 2003a). This could explain the discrepancy between the tendencies of the pepducins to produce small PAM (cAMP GloSensor^{TM}) or NAM (CRE-SPAP) effects in these two different assays. Although the similarly inconsistent responses observed in the cAMP GloSensor^{TM} assay may indicate that the CRE-SPAP responses here are at least in part cAMP-dependent.

There are a few potential explanations for the smaller than expected responses as well as the large degree of variation observed by the pepducins throughout this Chapter. Firstly, pepducins are generally thought to act at the intracellular surface of their target receptors which requires them to first translocate across the cell membrane (Covic et al., 2002a). The mechanism by which they likely do this requires the incorporation of their N-terminal palmitate tag into the lipid bilayer followed by a passive flip of the peptide sequence to the inside of the cell (Covic et al., 2002a; Covic et al., 2002b; Wielders et al., 2007; Carlson et al., 2012; Tsuji et al., 2013; Zhang et al., 2015b). This is clearly an essential step in the mechanism of action of pepducins. It is possible that the pepducins in this study lack efficacy for translocating the cell membrane and are therefore unable reach the intracellular receptor surface (or G_s protein) in order to exert their functional activity. Another possibility is that at the highest tested concentration of 10 μM, the pepducins may just be at the lower end of their response curves. This may explain not only the relatively small magnitude of responses but also

perhaps why they varied so much between replicates. Responses approaching the linear phase of the sigmoidal concentration-response curve will likely vary the most (and thus often display the largest SEM) because small differences in ligand concentrations or other factors between replicates will have a large impact on the measured response. Perhaps, therefore, if higher concentrations were applied (for example, 30 μM or 100 μM pepducin), larger and more consistent β_2AR responses could be measured. Although it must be noted that 10 μM pepducin concentrations were sufficient for cAMP stimulation in the study by Carr et al. (2014). Unfortunately, due to the relatively small amount of pepducin samples available, as well as issues around solubility in the assay buffers, it was not possible to test the pepducins at concentrations higher than 10 μM in these functional experiments. Additionally, it is possible that even the addition of 0.1% BSA to the buffers used in these assays could not prevent issues with peptide adhesion to the plasticware. This could introduce variation depending on different environmental factors in each experiment (how long the pepducins spend in microtubes or pipette tips during serial dilutions or assay preparation steps could affect the extent of their adhesion to the plastics). It may be worth attempting these experiments with higher BSA concentration in the future (for example, 0.2% or 0.5% BSA). Overall, the results from these experiments showed no convincing evidence of either allosteric agonist activity or allosteric modulation of orthosteric agonist activity by any of the pepducins.

5.5 – Conclusion

Functional studies into the activity of five pepducins derived from either ICL3 (ICL3-2, ICL3-7, ICL3-8 and ICL3-9) or ICL1 (ICL1-15) of the β_2AR were performed using cAMP GloSensor^{TM} (in HEK293Gwt cells) and CRE-SPAP assays. All five pepducins were previously shown to stimulate intracellular cAMP production by Carr et al. (2014). Here, although several of the pepducins (ICL3-7, ICL3-8, ICL3-9 and ICL1-15) raised cytosolic cAMP concentrations above the basal level, in each case the responses were very modest (up to approximately 6% of the maximal isoprenaline response). Only ICL3-8 produced a significant increase in CRE-mediated SPAP production, despite CRE-SPAP mean responses being somewhat larger than those obtained in GloSensor^{TM}. This had been expected due to the higher receptor expression conditions as well as the measurement of responses further downstream the signalling pathway providing a more amplified system. In both assays pepducin responses displayed considerable variation between experimental repeats, making it difficult to conclusively determine any agonist activity from any of the five pepducins. However, using cells which lacked β_2AR expression, the inconsistent CRE-SPAP responses were entirely abolished, suggesting the responses were β_2AR-mediated. Furthermore, the pepducins generally appeared to display a modest PAM effect in the cAMP GloSensor^{TM} assay by increasing the EC_{50} concentration isoprenaline peak response. Contrastingly however, in the CRE-SPAP assay the pepducins instead displayed some NAM activity by reducing the isoprenaline response. Therefore, the abilities of the pepducins to act as allosteric modulators and modify orthosteric ligand responses were also not clear.

Ultimately, although the each of the pepducins do appear to elicit some small effects on β_2AR signalling, the lack of substantial and consistent responses in both cAMP GloSensor^{TM} and CRE-SPAP assays reported here have made it very difficult to conclusively characterise the functional activity of any of the pepducins tested in this study.

Chapter 6

Binding and kinetic studies of orthosteric ligands and pepducins at the β_2-adrenoceptor

6.1 – Introduction

Earlier work in this study attempted to characterise the functional activity of five pepducins (ICL3-2, ICL3-7, ICL3-8, ICL3-9 and ICL1-15) at the β_2AR, in terms of both their stimulation of cAMP production and CRE-mediated SPAP transcription, as described in Chapter 5. In both assays, some evidence of activity was observed by each of the pepducins, to differing degrees, however the inconsistent nature of the measured responses made it difficult to conclude whether any of the peptides acted as allosteric agonists or modulators of orthosteric ligand activity. Therefore, in order to obtain a clearer idea of the action of the pepducins at the β_2AR, the next logical approach was to perform binding studies to directly assess the interactions of each pepducin with the receptor.

Structure-function studies of membrane-bound receptors in their native cellular environment has long proven difficult due to the complex and dynamic nature of the phospholipid bilayer in which they reside, as well as relatively low levels of endogenous expression and their lack of solubility in aqueous solutions (Seddon et al., 2004). Receptor solubilisation is a technique used to extract membrane-bound receptors from their cellular environment and isolate them from cellular regulation (le Maire et al., 2000; Seddon et al., 2004). It has been performed extensively for structural and biophysical studies of GPCRs (Rajesh et al., 2011; Tate, 2012; Lavington and Watts, 2020; Wiseman et al., 2020), including the β_2AR (Cherezov et al., 2007; Rasmussen et al., 2011b; Manglik et al., 2015; Gregorio et al., 2017; Harwood et al., 2021). The most commonly used class of solubilising agents are detergents, such as N-dodecyl-β-D-maltopyranoside (DDM) and lauryl maltose neopentyl glycol (LMNG), which are amphipathic molecules comprising both a polar hydrophilic head group and a hydrophobic tail, enabling them to aggregate to form soluble micelles (le Maire et al., 2000; Seddon et al., 2004; Milić and Veprintsev, 2015; Lyons et al., 2016; Munk et al., 2019; Errey and Fiez-Vandal, 2020). Detergents have been crucial for receptor solubilisation due to their ability to mimic the native cellular lipid bilayer and generally maintain the folding, function and thermostability of the protein (le Maire et al., 2000; Arachea et al., 2012; Milić and Veprintsev, 2015; Dawaliby

et al., 2016; Errey and Fiez-Vandal, 2020). Additionally, non-detergent solubilising agents such as styrene maleic acid lipid particles (SMALPs) and diisobutylene maleic acid lipid particles (DIBMALPs) have been developed in order to further improve solubilised protein stability and function (Knowles et al., 2009; Jamshad et al., 2015; Oluwole et al., 2017; Stroud et al., 2018; Lavington and Watts, 2020; Harwood et al., 2021).

As well as being a prerequisite for protein purification and crystallisation (le Maire et al., 2000; Palczewski, 2000; Cherezov et al., 2007; Rasmussen et al., 2011b; Tate, 2012), solubilised receptors have also been used in protein stability assays which are often employed to optimise the thermostability of receptors for structural studies (Alexandrov et al., 2008; Serrano-Vega et al., 2008; Robertson et al., 2011; Magnani et al., 2016). Receptor thermostability measurements can also be used as an indication of ligand binding because when ligands interact with the receptor binding site the receptor becomes locked into a stable conformational state and the number of hydrogen bonds throughout the structure increases, thus improving receptor thermostability (Fang, 2012; Zhang et al., 2015c; Bergsdorf et al., 2016; Hoare et al., 2023). Recently, a BRET-based thermostability assay (thermoBRET) has been developed by Hoare et al. (2023) which can be used to detect ligand binding to non-purified detergent-solubilised GPCRs. The thermoBRET assay utilises a thermostable mutant of nanoluciferase (tsNLuc) which, in the presence of its furimazine substrate, acts as a donor of luminescence (at ~450 nm wavelength) for the thiol-reactive sulfo-cyanine3 maleimide (SCM) dye (when in close proximity; ~10 nm) which acts as the acceptor and subsequently emits fluorescence (at ~550 nm) (Hoare et al., 2023). When the N-terminally tsNLuc-tagged receptor is incubated at increasing temperatures the protein begins to denature and unfold, exposing cysteine residues in the core of the receptor (transmembrane domain) to covalent attachment by the SCM dye (Hoare et al., 2023). The close proximity of the tsNLuc donor and SCM acceptor results in an increased nanoBRET signal, and the thermostability of the receptor can be calculated in terms of its melting temperature (T_m; the temperature at which half of the receptor population is unfolded) (Hoare et al., 2023). Ligand binding to the receptor has been shown to substantially rightward shift the receptor melting curve, thus increasing the T_m

value (Hoare et al., 2023). A FRET-based version of the assay (thermoFRET) has also been developed by Tippett et al. (2020), whereby a Terbium fluorescent donor replaces the tsNLuc used in thermoBRET.

Another technique which can be used to characterise ligand-receptor binding is time-resolved FRET (TR-FRET). The FRET technique relies on similar principles as BRET, however employing a fluorophore donor to replace the bioluminescent donor. Similar to BRET, if the excitation-emission spectra of the donor-acceptor pair overlap then, when in close proximity (~10 nm), direct energy transfer can occur from donor to acceptor, which is followed by acceptor emission (Saraheimo et al., 2013; Ergin et al., 2016). TR-FRET takes advantage of long-lived fluorescence emission by lanthanides to improve the FRET signal-to-noise ratio (Degorce et al., 2009; Ergin et al., 2016). Whereas fluorescence emitted by most fluorophores, including any background compounds present, decays rapidly within nanoseconds (ns), emission by lanthanides such as Terbium last for much longer, from microseconds (μs) to milliseconds (ms) (Degorce et al., 2009; Ergin et al., 2016). Therefore, following the initial excitation, fluorescence is measured after a short time delay (~50 μs) to reduce interference from background fluorescence (Degorce et al., 2009; Ergin et al., 2016). Here, Terbium is used as the donor (~620 nm wavelength emission) and the fluorescent ligand (S)-propranolol-green (F-propranolol; Hello Bio, Bristol, UK), which was originally developed by Baker et al. (2011), is used as the acceptor (~520 nm emission) (Degorce et al., 2009; Farmer et al., 2022) to measure fluorescent ligand binding to the Terbium-tagged β_2AR in homogenised membrane preparations. As well as providing a measure of the equilibrium dissociation constant (K_D) of the fluorescent 'tracer' ligand for the target receptor, this technique can allow determination of kinetic binding parameters of the tracer such as association rate constant (k_{on}) and dissociation rate constant (k_{off}), which in turn can provide a kinetic measure of the tracer's K_D (Bosma et al., 2017; Sykes and Charlton, 2018; Sykes et al., 2019). Moreover, the development of the Motulsky-Mahan "kinetics of competitive binding" model by Motulsky and Mahan (1984) has also enabled the quantification of the binding kinetics of unlabelled ligands competing with a characterised tracer ligand. Calculations of ligand binding kinetics have become increasingly

prevalent recently as the importance of understanding these parameters for the optimisation of therapeutics has become clearer (Sykes et al., 2019).

This study has employed the techniques described here to examine the interactions of ICL3-2, ICL3-7, ICL3-8, ICL3-9 and ICL1-15 with the β_2AR and their effect on the binding of orthosteric ligands at the receptor. Firstly, detergent-solubilisation of the β_2AR is optimised using thermoBRET and the influence of orthosteric ligand binding on measurements of receptor thermostability (in terms of its melting temperature; T_m) is characterised. The ability of pepducins to modify receptor thermostability themselves, or to alter the formoterol-induced stabilisation of the receptor, is then assessed. Additionally, TR-FRET is utilised to quantify both the equilibrium and kinetic binding parameters of a fluorescently-labelled tracer ligand (F-propranolol) and an unlabelled competing ligand (formoterol) at the β_2AR in homogenised membrane preparations, and the effect of pepducin application on these ligand binding kinetics is explored.

6.2 – Materials and methods

Molecular biology

All relevant molecular biology processes were carried out as previously described in Chapter 2 (see 2.3 – Molecular biology).

Cell culture

HEK293TR cells stably expressing either TS-tsNLuc-β_2AR (thermoBRET) or TS-SNAP-β_2AR (TR-FRET) receptor constructs were used throughout this Chapter and were passaged as stated previously in Chapter 2 (see 2.4 – Cell culture).

Membrane preparation

Membranes overexpressing either the TS-tsNLuc-β_2AR (thermoBRET) or TS-SNAP-β_2AR (TR-FRET) receptor constructs were prepared according to the procedures outlined in Chapter 2 (see 2.6 – Membrane preparation).

ThermoBRET assay

The thermoBRET assay was carried out as described in Chapter 2 (see 2.10 – ThermoBRET assay).

TR-FRET assay

The TR-FRET assay was performed as explained in Chapter 2 (see 2.11 – TR-FRET assay).

Data analysis and statistics

Analysis of the data was carried out as stated in Chapter 2 (see 2.12 – Data analysis and statistics).

6.3 – Results

6.3.1 – Investigating ligand-induced changes in β_2-adrenoceptor thermostability using the thermoBRET assay

Solubilisation of the β_2AR firstly needed to be optimised to provide a large nanoBRET signal-to-noise ratio in order to clearly observe a receptor melting curve after incubation of the receptor at increasing temperatures. This would provide a more accurate calculation of receptor T_m values. Therefore, in the initial thermoBRET experiments performed here, a temperature gradient between 22 °C – 52 °C was applied to the β_2AR (from HEK293TR cells overexpressing the TS-tsNLuc-β_2AR construct) solubilised in four different detergent conditions: 1% DDM, 1% DDM + 1% 3-[(3-cholamidopropyl)dimethylammonio]-2-hydroxy-1-propanesulfonate (CHAPSO) + 0.2% cholesteryl hemisuccinate tris salt (CHS), 0.5% LMNG and 0.5% LMNG + 1% CHAPSO + 0.2% CHS. DDM and LMNG are two of the most commonly used detergents to solubilise membrane proteins (Munk et al., 2019; Errey and Fiez-Vandal, 2020). They are considered 'mild' detergents because they generally have a less disruptive effect on the structural features of proteins and they comprise a low critical micelle concentration (CMC), which refers to the minimum detergent concentration required for individual detergent monomers to aggregate into micelles and is essential for protein solubilisation (le Maire et al., 2000; Seddon et al., 2004; Milić and Veprintsev, 2015; Errey and Fiez-Vandal, 2020). CHAPSO is a steroid-based detergent which is sometimes used separately or in addition to other detergents for protein solubilisation (Fargin et al., 1988; Milić and Veprintsev, 2015; Errey and Fiez-Vandal, 2020). CHS is an analogue of cholesterol with increased solubility and is commonly applied alongside detergents to increase receptor stability due to its binding to a conserved allosteric site in many GPCRs (Hanson et al., 2008; Lyons et al., 2016; Munk et al., 2019; Errey and Fiez-Vandal, 2020). The concentrations of each of these components were selected based on similar detergent concentrations used by Hoare et al. (2023) previously.

Considerable differences were observed between the four different detergent conditions in terms of both the maximal change in signal during receptor unfolding and the thermostability of the β_2AR. Firstly, solubilisation in DDM produced the largest increase in nanoBRET signal upon receptor denaturation (Figure 6.1A), although this was not shown to be significantly larger than LMNG over the three independent experiments ($P > 0.05$; determined by a one-way ANOVA with Tukey's multiple comparisons test). The addition of CHAPSO and CHS to both DDM and LMNG reduced the maximal nanoBRET signal achieved in both cases ($P < 0.05$ or less). Upon normalisation of each detergent condition to their own maxima, a clear rightward shift in the melting curves was also observed after addition of CHAPSO and CHS to both DDM and LMNG (Figure 6.1B; $P < 0.0001$ for both), indicating increased receptor thermostability. Moreover, solubilisation in LMNG provided a more thermostable β_2AR than in DDM (β_2AR T_m values 39.67 °C ± 0.15 °C and 35.82 °C ± 0.25 °C, respectively; $P < 0.0001$). The calculated T_m values for the β_2AR after solubilisation in each detergent condition are shown in Table 6.1, which were determined by fitting the Boltzmann sigmoidal equation (Equation 8) to the melting curves.

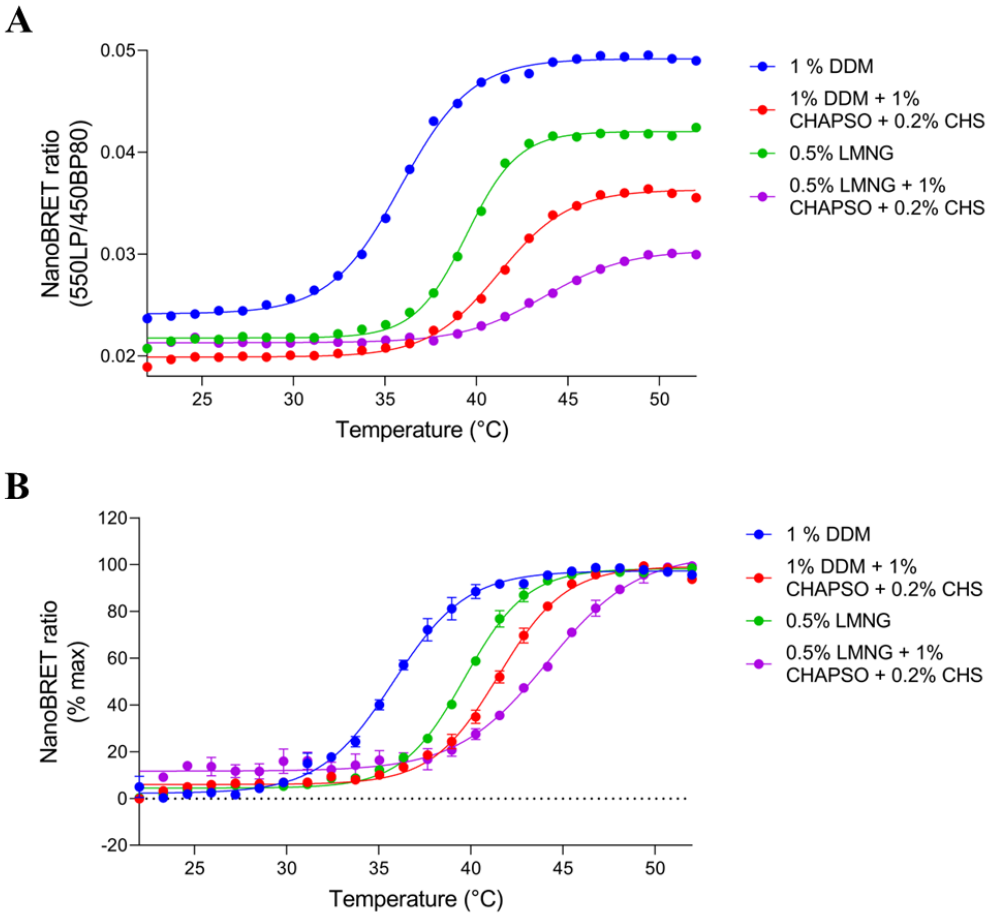

Figure 6.1: NanoBRET signal measured due to receptor unfolding at increasing temperatures. (A) Representative thermoBRET melting curves in one experiment over a 22 °C – 52 °C temperature gradient for the β_2AR solubilised in 1% DDM, 1% DDM + 1% CHAPSO + 0.2% CHS, 0.5% LMNG and 0.5% LMNG + 1% CHAPSO + 0.2% CHS. Data points represent mean ± SEM of sextuplicate measurements, expressed as 550LP/450BP80 nanoBRET ratio. Similar data were obtained in three independent experiments. (B) Combined thermoBRET melting curves over a 22 °C – 52 °C temperature gradient for the β_2AR solubilised in 1% DDM, 1% DDM + 1% CHAPSO + 0.2% CHS, 0.5% LMNG and 0.5% LMNG + 1% CHAPSO + 0.2% CHS. Data points represent mean ± SEM, expressed as a percentage of maximal nanoBRET ratio, from three independent experiments ($n = 3$). Significant differences in T_m values or maximal signal were determined by a one-way ANOVA with Tukey's multiple comparisons test.

Detergent	β_2AR T_m (°C) ± SEM
1% DDM	35.82 ± 0.25
1% DDM + 1% CHAPSO + 0.2% CHS	41.50 ± 0.21
0.5% LMNG	39.67 ± 0.15
0.5% LMNG + 1% CHAPSO + 0.2% CHS	44.22 ± 0.27

Table 6.1: β_2AR mean T_m values ± SEM determined after solubilisation in 1% DDM, 1% DDM + 1% CHAPSO + 0.2% CHS, 0.5% LMNG and 0.5% LMNG + 1% CHAPSO + 0.2% CHS obtained from thermoBRET melting curves from three independent experiments (n = 3). Significant differences in T_m values were determined by a one-way ANOVA with Tukey's multiple comparisons test.

Additionally, it was important for later studies that ligand application caused a substantial rightward shift in the receptor melting curve to clearly indicate ligand-receptor binding (due to increased receptor thermostability). Therefore, under each detergent condition, the addition of 1 μM propranolol was also tested. When solubilised in DDM, β_2AR thermostability increased greatly upon application of propranolol (β_2AR T_m: 35.82 °C ± 0.25 °C in absence of propranolol, compared with 44.37 °C ± 0.17 °C in presence of 1 μM propranolol; $P < 0.0001$), displayed in Figure 6.2B. Upon solubilisation in LMNG, however, the effect of propranolol addition instead substantially reduced the maximal nanoBRET signal achieved as temperature was increased (Figure 6.2A), at least within the temperature range tested here (up to 52 °C), and there was no significant change in the melting temperature of the receptor (β_2AR T_m: 39.67 °C ± 0.15 °C in absence of propranolol, compared with 43.10 °C ± 1.48 °C in presence of 1 μM propranolol; $P > 0.05$). Similar effects were observed upon application of 1 μM propranolol to the β_2AR solubilised in either DDM or LMNG in addition to CHAPSO and CHS (reduced maximal signal and lack of shift in T_m; data not shown). As a result, the detergent DDM was selected as the solubilising agent for the β_2AR for each experiment going forward.

Just as cholesterol binds allosterically to many GPCRs, sodium ions have also been shown to bind to a conserved allosteric GPCR site, including at the β_2AR (acting as NAMs of receptor activity) (Katritch et al., 2014; Wang et al., 2022). The standard composition of the CORE buffer (and solubilisation buffer) used throughout these experiments included a high concentration of sodium chloride (150 mM NaCl). To examine whether sodium ions contributed to the thermostability of the β_2AR through their allosteric interaction with the receptor, CORE buffer (20 mM HEPES, 150 mM NaCl, 10% glycerol, 0.5% BSA in ddH_2O, pH 7.45) and solubilisation buffer (CORE buffer plus detergent) containing no NaCl were prepared and tested here for comparison with the standard salt-containing buffer compositions. As shown in Figure 6.3, removal of NaCl had no effect on β_2AR thermostability (β_2AR T_m: 35.82 °C ± 0.25 °C in CORE buffer containing 150 mM NaCl, compared with 36.85 °C ± 1.55 °C in CORE buffer lacking NaCl; $P > 0.05$; determined by an unpaired t-test).

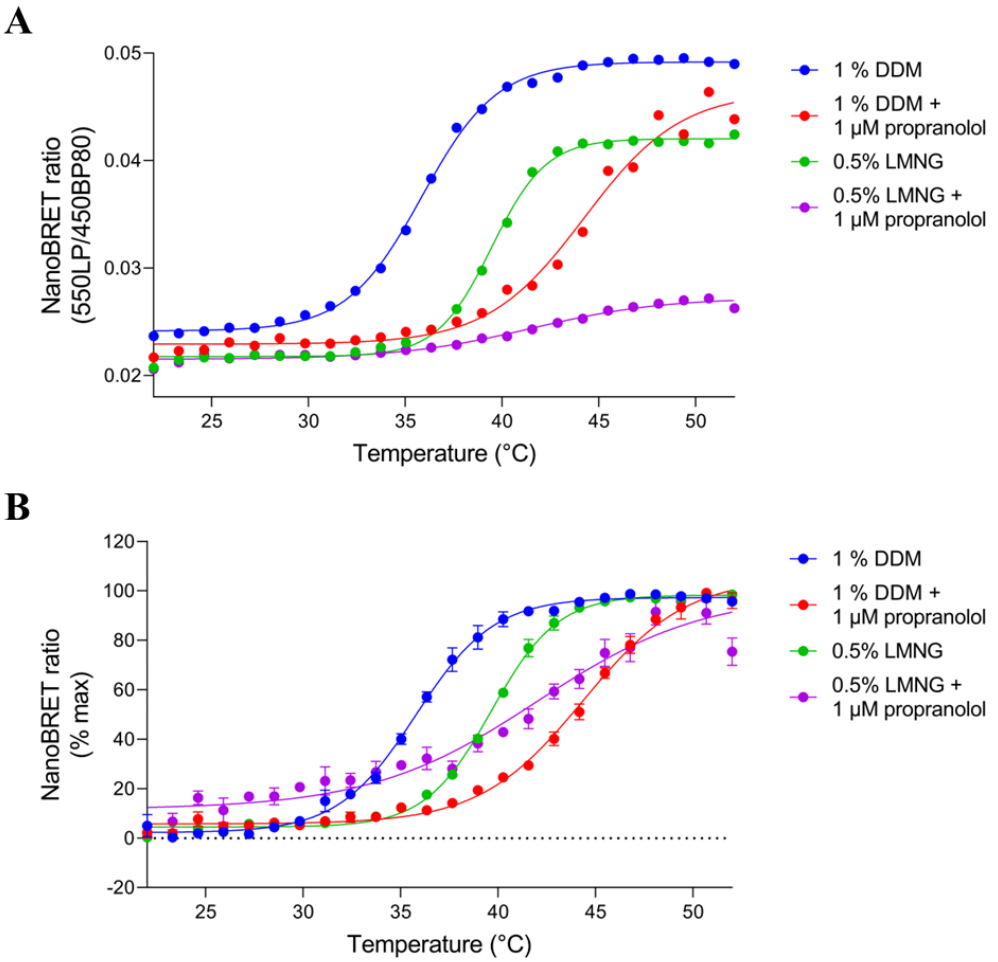

Figure 6.2: NanoBRET signal measured due to receptor unfolding at increasing temperatures. (A) Representative thermoBRET melting curves in one experiment over a 22 °C – 52 °C temperature gradient for the 1% DDM- and 0.5% LMNG-solubilised β_2AR in the presence and absence of 1 µM propranolol. Data points represent mean ± SEM of sextuplicate measurements, expressed as 550LP/450BP80 nanoBRET ratio. Similar data were obtained in three independent experiments. (B) Combined thermoBRET melting curves over a 22 °C – 52 °C temperature gradient for the 1% DDM- and 0.5% LMNG-solubilised β_2AR in the presence and absence of 1 µM propranolol. Data points represent mean ± SEM, expressed as a percentage of maximal nanoBRET ratio, from three independent experiments ($n = 3$). Significant differences in T_m values or maximal signal were determined by a one-way ANOVA with Tukey's multiple comparisons test.

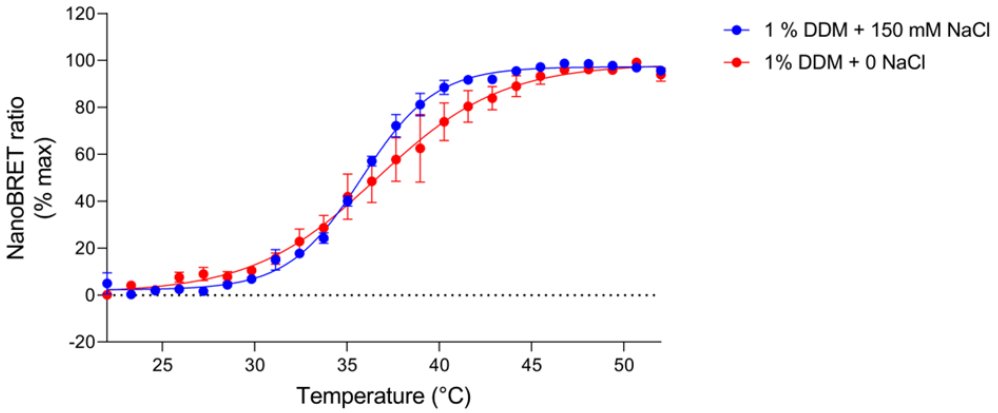

Figure 6.3: NanoBRET signal measured due to receptor unfolding at increasing temperatures. Combined thermoBRET melting curves over a 22 °C – 52 °C temperature gradient for the 1% DDM-solubilised β_2AR in high (150 mM NaCl) and zero (0 NaCl) salt conditions. Data points represent mean ± SEM, expressed as a percentage of maximal nanoBRET ratio, from three independent experiments (n = 3). Significant differences in T_m values were determined by an unpaired t-test.

Next, four β_2AR ligands (formoterol, salmeterol, propranolol and ICI-118551) were applied at high concentration (each 10 μM) to the DDM-solubilised receptor and a temperature gradient was applied (22 °C – 52 °C for CORE buffer control and 35 °C – 65 °C for ligand conditions because of the large T_m shift induced by ligands). In the presence of each of the ligands, the temperatures required to cause unfolding of the β_2AR were increased markedly (Figure 6.4A), and hence the calculated β_2AR T_m value was larger in each case (Figure 6.4B; $P < 0.0001$ for each). Formoterol had the most modest effect on β_2AR thermostability (T_m shift: 11.69 °C ± 0.53 °C; $P < 0.05$ or less, compared with the other ligands, determined by a one-way ANOVA with Tukey's multiple comparisons test). Salmeterol, propranolol and ICI-118551 all produced similarly large shifts in the β_2AR T_m value (14.30 °C ± 0.53 °C, 15.56 °C ± 0.49 °C and 14.02 °C ± 0.50 °C, respectively; $P > 0.05$ in each case). The calculated T_m value for the β_2AR after application of each ligand is stated in Table 6.2. At high temperatures of approximately 56 °C and above, the nanoBRET signal began to reduce in a temperature-dependent manner (Figure 6.4A). This effect was exactly the same regardless of which ligand was applied. Therefore, datapoints obtained at temperatures above 56 °C were excluded from the fitting of the Boltzmann sigmoidal equation (Equation 8) to the melting curves so that the T_m values were not distorted.

Two of the ligands, formoterol and ICI-118551, were then applied at increasing concentrations (1 nM – 10 μM) and a temperature gradient was applied between 25 °C – 55 °C to each ligand concentration. The increases in β_2AR thermostability by both ligands was found to be concentration-dependent and the rightward shift in thermostability had not reached a maximal shift even at 10 μM in each case (Figures 6.5A and 6.5B).

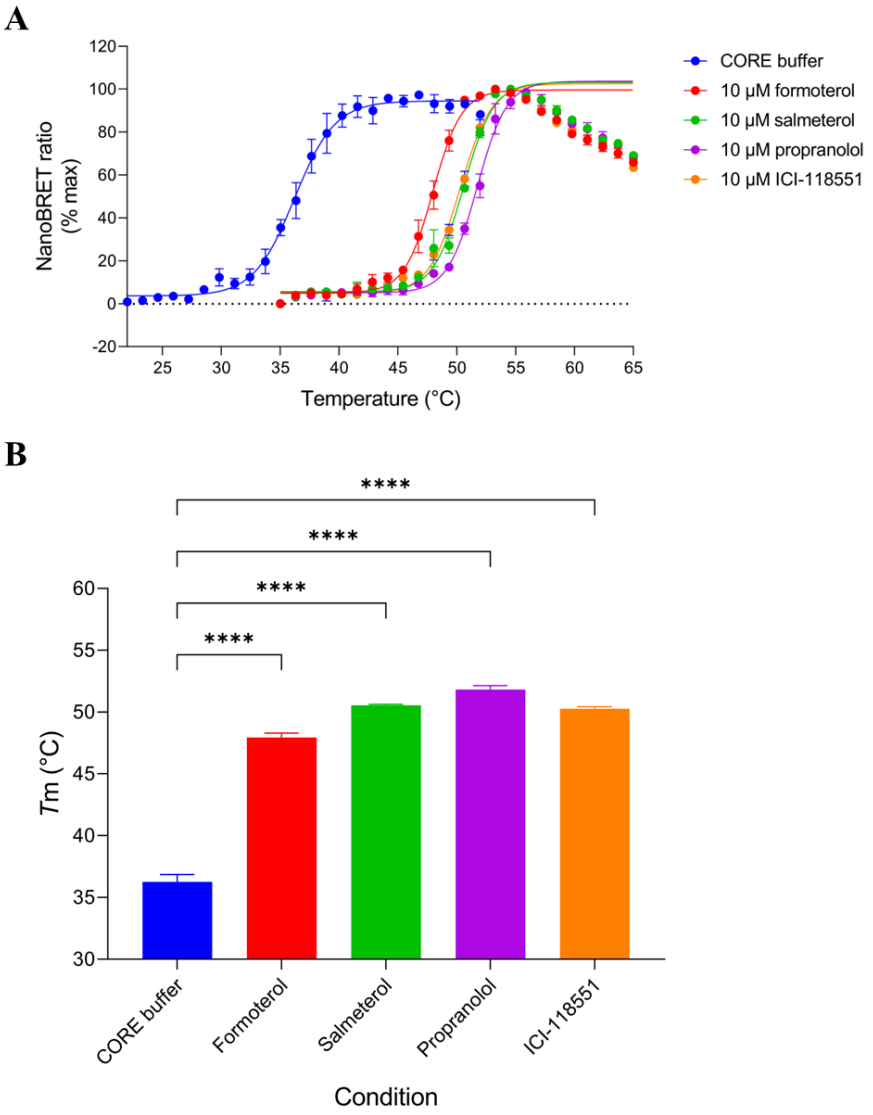

Figure 6.4: NanoBRET signal measured due to receptor unfolding at increasing temperatures. (A) Combined thermoBRET melting curves over a 22 °C – 52 °C (CORE buffer) or 35 °C – 65 °C (ligands) temperature gradient for the 1% DDM-solubilised β_2AR in the presence or absence of formoterol, salmeterol, propranolol and ICI-118851 (all 10 µM). Data points represent mean ± SEM, expressed as a percentage of maximal nanoBRET ratio, from three independent experiments (n = 3). (B) Bar chart displaying mean T_m values for the 1% DDM-solubilised β_2AR in the presence and absence of 10 µM formoterol, salmeterol, propranolol and ICI-118851. Data points represent mean ± SEM, expressed as °C from three independent experiments (n = 3). Significant differences in T_m values to those seen in absence of ligand are indicated, determined by a one-way ANOVA with Tukey's multiple comparisons test. $P < 0.05$ was used as the level for significance ($P < 0.0001$ = ****).

Condition	β_2AR T_m (°C) ± SEM
CORE buffer	36.26 ± 0.59
10 μM formoterol	47.95 ± 0.36 ****
10 μM salmeterol	50.56 ± 0.07 ****
10 μM propranolol	51.82 ± 0.33 ****
10 μM ICI-118551	50.28 ± 0.15 ****

Table 6.2: 1% DDM-solubilised β_2AR mean T_m values ± SEM determined in the presence and absence of formoterol, salmeterol, propranolol and ICI-118851 (all 10 μM) obtained from thermoBRET melting curves from three independent experiments (n = 3). Significant differences in T_m values to those seen in absence of ligand are indicated, determined by a one-way ANOVA with Tukey's multiple comparisons test. $P < 0.05$ was used as the level for significance ($P < 0.0001$ = ****).

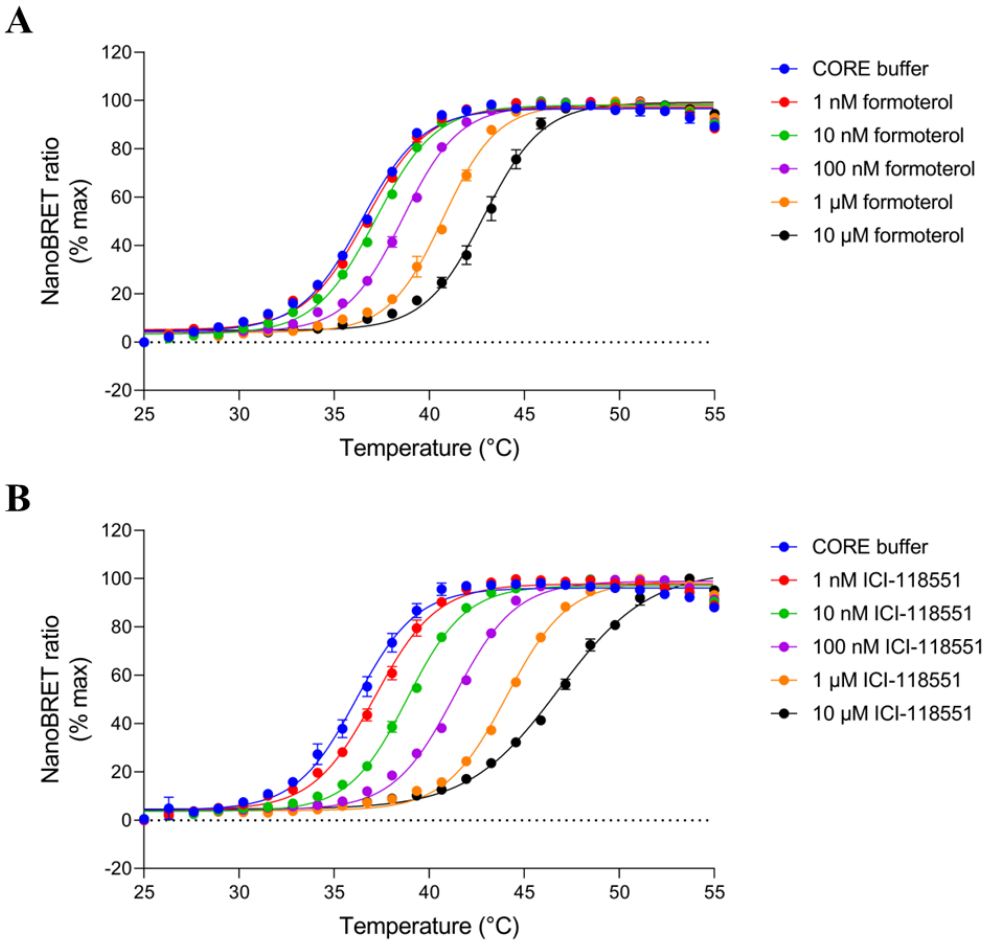

Figure 6.5: NanoBRET signal measured due to receptor unfolding at increasing temperatures. (A-B) Combined thermoBRET melting curves over a 25 °C – 55 °C temperature gradient for the 1% DDM-solubilised β_2AR in the presence or absence of increasing concentrations of formoterol (A) or ICI-118551 (B) (both 1 nM – 10 µM). Data points represent mean ± SEM, expressed as a percentage of maximal nanoBRET ratio, from three independent experiments (n = 3).

The thermoBRET assay can also be performed in an isothermal format in which the receptor is subjected to a constant melting temperature (approximately the T_m value) and the concentration of applied ligand is altered. In this assay format, changes in receptor thermostability are measured directly as increases or decreases in the nanoBRET signal. Upon the stabilisation of the receptor by a bound ligand, the same temperature which causes unfolding of a certain proportion of the unbound receptor population (for example, 50%; T_m) will unfold a lower proportion of ligand-bound receptors (due to increased thermostability), thereby restricting the exposure of transmembrane cysteine residues to the SCM dye and thus reducing the nanoBRET signal measured at that temperature (Hoare et al., 2023). Hence, as ligand concentrations are increased, a concentration-dependent reduction of the signal should be observed, from which ligand IC_{50} curves can be generated.

Here, a constant temperature of 36 °C, which was determined as the T_m value for the DDM-solubilised unbound β_2AR (Table 6.1), was applied to the β_2AR in the presence or absence of increasing concentrations of four orthosteric ligands, formoterol, salmeterol, propranolol and ICI-118551 (all 1 pM – 100 μM). The T_m value was selected because, being in the middle of the linear phase of the sigmoidal melting curve, the receptor should be the most sensitive to changes in thermostability at this temperature. Each of the four ligands caused a concentration-dependent reduction in the nanoBRET signal (Figure 6.6), which was normalised between the nanoBRET signal measured in absence of ligand (vehicle; 100%) and the highest tested concentration of ligand (100 μM in each case; 0%). The data were fitted to a sigmoidal curve using the Hill equation (Equation 2) and log IC_{50} values were determined for each ligand, stated in Table 6.3. The log IC_{50} values for each ligand were statistically similar ($P > 0.05$ between all ligands, determined by a one-way ANOVA with Tukey's multiple comparisons test), but a comparable rank order was observed between ligand T_m shifts and log IC_{50} values propranolol ≥ salmeterol ≥ ICI-118551 > formoterol (Tables 6.2 and 6.3).

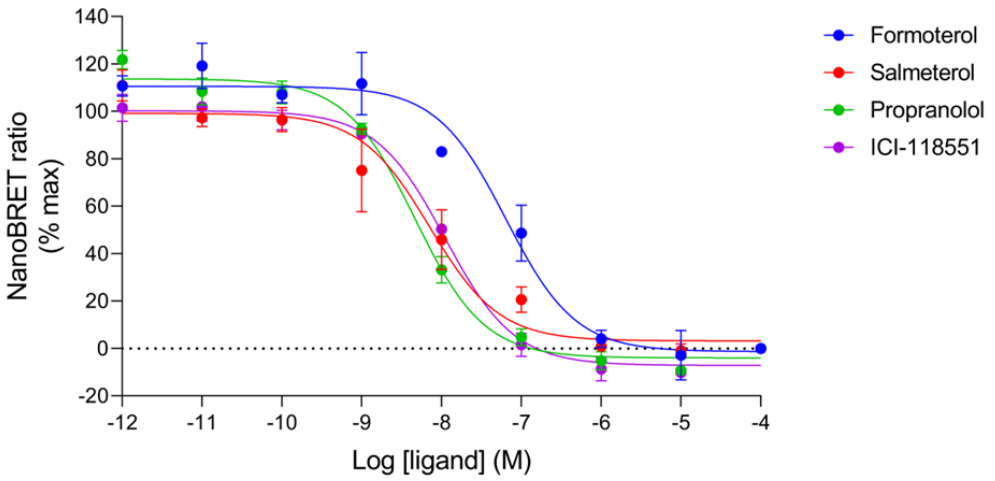

Figure 6.6: NanoBRET ratio measured due to receptor unfolding at a constant temperature with increasing ligand concentration. Isothermal thermoBRET IC_{50} curves at a constant 36 °C temperature for the 1% DDM-solubilised β_2AR in the presence of increasing concentrations of formoterol, salmeterol, propranolol and ICI-118551 (all 1 pM – 100 μM). Data points represent mean ± SEM, expressed as a percentage of the maximal nanoBRET ratio in the absence of ligand with zero determined as the signal from the highest concentration of tested ligand (100 μM in each case), from three independent experiments (n = 3). Significant differences in IC_{50} values were determined by a one-way ANOVA with Tukey's multiple comparisons test.

Ligand	Log IC_{50} (M) ± SEM
Formoterol	-7.16 ± 0.13
Salmeterol	-8.26 ± 0.49
Propranolol	-8.29 ± 0.09
ICI-118551	-7.95 ± 0.05

Table 6.3: Ligand mean log IC_{50} values ± SEM determined for formoterol, salmeterol, propranolol and ICI-118551 at the 1% DDM-solubilised β_2AR obtained from thermoBRET melting curves from three independent experiments (n = 3). Significant differences in IC_{50} values were determined by a one-way ANOVA with Tukey's multiple comparisons test.

6.3.2 – Effects of pepducins on the thermostability of the β_2-adrenoceptor

Since the binding of several orthosteric ligands had been shown to substantially increase β_2AR thermostability and cause clear rightward shifts in the receptor melting curves (Figure 6.4A), it was hoped that using the same technique and applying pepducins to the detergent-solubilised receptor could determine whether the pepducins are able to shift the thermostability of β_2AR in a similar manner, thus indicating pepducin binding at the β_2AR. This was initially tested by performing a temperature gradient (between 22 °C – 52 °C for all conditions) after application of high concentrations (each 10 μM) of ICL3-2, ICL3-7, ICL3-8, ICL3-9 and ICL1-15, or CORE buffer or DMSO vehicle controls. In each well the final DMSO concentration was made to 2.5%, except for the CORE buffer control (1.5% DMSO). Therefore, in the DMSO control condition, an additional 1% DMSO was applied to ensure a final concentration of 2.5% (same as highest pepducin conditions). Unlike each of the orthosteric ligands tested previously, none of the pepducins caused any shift in β_2AR thermostability or altered the T_m value compared to either the CORE buffer or DMSO vehicle controls (Figure 6.7; $P > 0.05$ in all cases). Receptor T_m values calculated from each condition are displayed in Table 6.4.

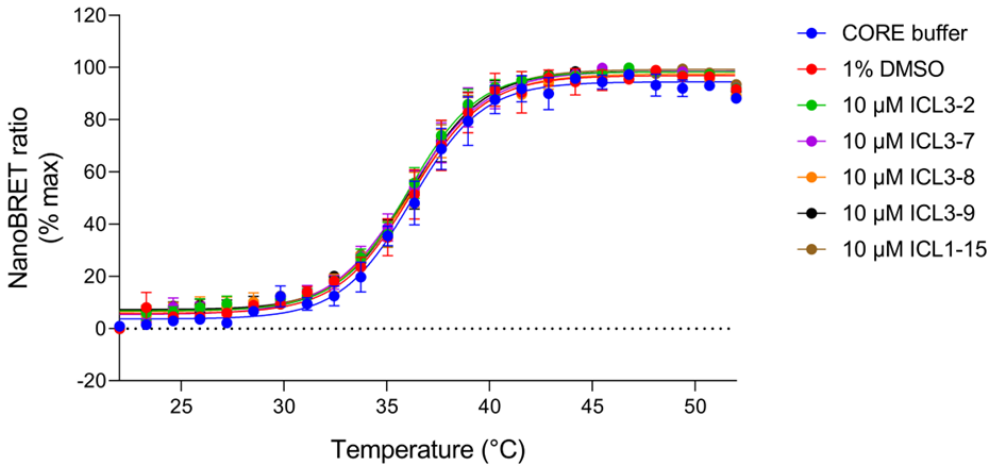

Figure 6.7: NanoBRET signal measured due to receptor unfolding at increasing temperatures. Combined thermoBRET melting curves over a 22 °C – 52 °C temperature gradient for the 1% DDM-solubilised β_2AR in the presence or absence of DMSO (1%), ICL3-2, ICL3-7, ICL3-8, ICL3-9 and ICL1-15 (each 10 µM). Data points represent mean ± SEM, expressed as a percentage of maximal nanoBRET ratio, from three independent experiments (n = 3). Significant differences in T_m values to those seen in absence of pepducin were determined by a one-way ANOVA with Tukey's multiple comparisons test.

Condition	β_2AR T_m (°C) ± SEM
CORE buffer	36.26 ± 0.59
1% DMSO	36.30 ± 0.78
10 μM ICL3-2	36.05 ± 0.48
10 μM ICL3-7	36.08 ± 0.59
10 μM ICL3-8	36.19 ± 0.49
10 μM ICL3-9	36.23 ± 0.56
10 μM ICL1-15	36.15 ± 0.38

Table 6.4: 1% DDM-solubilised β_2AR mean T_m values ± SEM determined in the presence and absence of DMSO (1%), ICL3-2, ICL3-7, ICL3-8, ICL3-9 and ICL1-15 (all 10 μM) obtained from thermoBRET melting curves from three independent experiments (n = 3). Significant differences in T_m values to those seen in absence of pepducin (or DMSO) were determined by a one-way ANOVA with Tukey's multiple comparisons test.

In order to verify that the pepducins had no effect on the thermostability of the receptor, the isothermal thermoBRET format was also performed. The β_2AR T_m value (36 °C) was again used as the constant temperature in this assay in the presence or absence of ICL3-2, ICL3-7, ICL3-8, ICL3-9 and ICL1-15 at a range of temperatures between 10 nM – 30 μM (half-log increases). Data were normalised between a 1% DMSO vehicle control (100%) and the 100 μM formoterol nanoBRET signal (0%), which represented a maximal reduction in the signal. None of the pepducins were found to alter the nanoBRET signal from that of the vehicle control within the concentration range tested (Figure 6.8; $P >$ 0.05 for each). As there was no reduction in the nanoBRET signal in any condition, no log IC_{50} values could be determined for any of the pepducins. Additionally, the same experiment was then repeated, but this time including a 30 min preincubation (at 4 °C to prevent inadvertent protein denaturation during this period) of the pepducins with the β_2AR prior to melting the receptor in the GeneTouch^{TM} Thermocycler (Bioer, Hangzhou, China), to allow more time for the pepducins to potentially achieve binding equilibrium with the receptor. However, even after the longer preincubation none of the pepducins had any effect on the measured nanoBRET signal (data not shown).

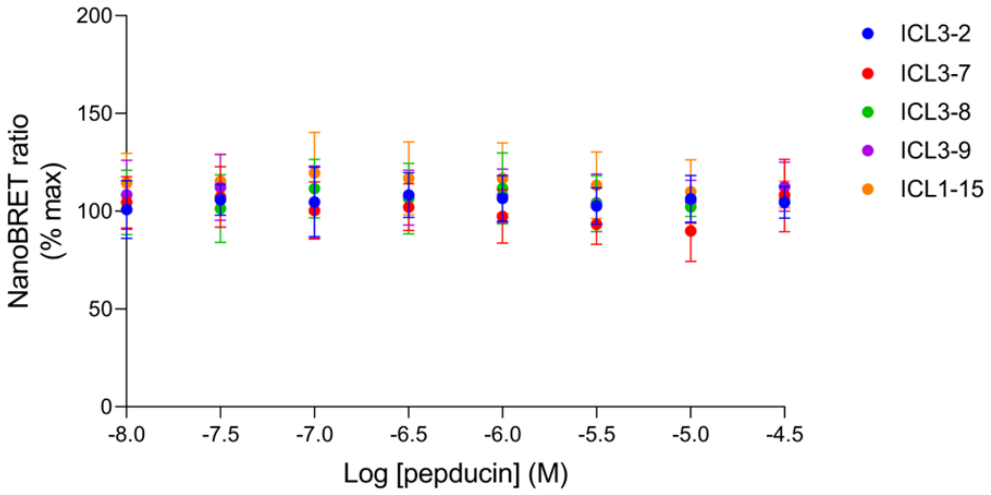

Figure 6.8: NanoBRET ratio measured due to receptor unfolding at a constant temperature with increasing pepducin concentration. Isothermal thermoBRET IC_{50} curves at a constant 36 °C temperature for the 1% DDM-solubilised β_2AR in the presence of increasing concentrations of ICL3-2, ICL3-7, ICL3-8, ICL3-9 and ICL1-15 (all 10 nM – 30 μM; half-log increases). Data points represent mean ± SEM, expressed as a percentage of the maximal nanoBRET ratio in the absence of ligand with zero determined as the 100 μM formoterol signal, from three independent experiments (n = 3). Significant differences were determined by a one-way ANOVA with Tukey's multiple comparisons test.

In an attempt to establish whether any of the pepducins could instead bind to a pre-bound agonist-receptor complex, 1 μM formoterol was preincubated with the β_2AR for 30 min at 4 °C prior to addition of increasing concentrations of ICL3-2, ICL3-7, ICL3-8, ICL3-9 or ICL1-15 (10 nM – 10 μM; half log increases) and subsequent protein melt, this time at a constant temperature of 41 °C. The choice of 1 μM concentration of formoterol was because this concentration of the ligand provided a submaximal thermostability shift in earlier tests (Figure 6.5A), so any further shift in thermostability (increased or decreased) resulting from pepducin addition could be readily detected by changes in the nanoBRET signal. The β_2AR T_m value in the presence of 1 μM formoterol was approximately 41 °C (Figure 6.5A), so this was the appropriate temperature to use for this assay. Here, data were normalised against the CORE buffer control (100%) and 10 μM formoterol (0%), which represented a maximal reduction in the nanoBRET signal. None of the pepducins either increased or decreased the 1 μM nanoBRET signal at any tested concentration ($P > 0.05$ in all cases), meaning that the thermostability of the preincubated ligand-receptor complex was unaffected (Figure 6.9A).

Finally, the converse experiment was then performed whereby the pepducins were instead preincubated with the β_2AR for 30 min at 4 °C, followed by 1 μM formoterol addition and subsequent 41 °C protein melt. This was done in order to determine any changes in the binding of formoterol to the receptor by the presence of preincubated pepducins. However, pepducin preincubation had no effect on the formoterol-mediated thermostability shift of the β_2AR, within the tested concentration range (Figure 6.9B; $P > 0.05$ throughout).

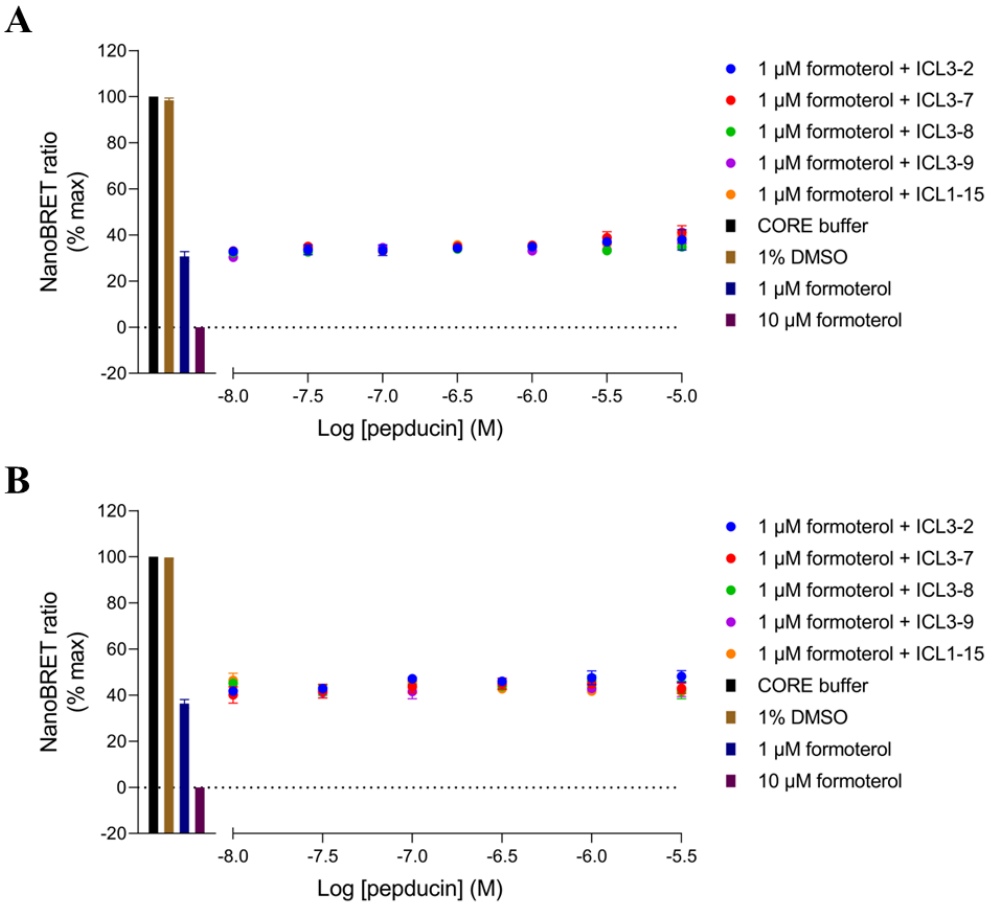

Figure 6.9: NanoBRET ratio measured due to receptor unfolding at a constant temperature with increasing pepducin concentration. (A-B) Isothermal thermoBRET IC_{50} curves at a constant 41 °C temperature for the 1% DDM-solubilised β_2AR in the presence of 1 µM formoterol and increasing concentrations of ICL3-2, ICL3-7, ICL3-8, ICL3-9 and ICL1-15 (10 nM – 10 µM in A, or 10 nM – 3 µM in B; half-log increases), with CORE buffer, 1% DMSO, 1 µM formoterol and 10 µM formoterol controls. 1 µM formoterol (A) or pepducins (B) were preincubated for 30 min at 4 °C before addition of the other and subsequent receptor melt. Data points represent mean ± SEM, expressed as a percentage of the maximal nanoBRET ratio in the absence of ligand with zero determined as the 10 µM formoterol signal, from three independent experiments (n = 3). Significant differences were determined by a one-way ANOVA with Tukey's multiple comparisons test.

6.3.3 – Using TR-FRET to examine orthosteric ligand binding kinetics at the β_2-adrenoceptor in the presence and absence of pepducins

Since no interactions with the detergent-solubilised β_2AR could be detected for any of the pepducins using the thermoBRET technique described above, subsequent attempts were made to study pepducin action at the receptor when residing in native, homogenised cell membranes by employing TR-FRET. As the pepducins are not themselves fluorescently tagged, this assay could not be used to directly assess pepducin binding to the receptor. Additionally, the fluorescent ligand used as the tracer here (F-propranolol) interacts with the orthosteric receptor binding site (Baker et al., 2011) whereas pepducins act allosterically (Covic et al., 2002a). Therefore, the pepducins do not compete for receptor binding with the tracer and hence pepducin binding kinetics at the β_2AR could not be determined using the TR-FRET technique described here, as displacement of the fluorescent ligand is required. Instead, the effect of pepducin addition on the receptor binding kinetics of both the fluorescent ligand and an unlabelled competing orthosteric ligand (formoterol) were examined.

Firstly, the binding of the fluorescent tracer ligand to the receptor was characterised. Increasing concentrations of F-propranolol (0.98 nM – 125 nM) were applied to homogenised HEK293TR cell membranes overexpressing the Terbium-labelled TS-SNAP-β_2AR construct, both in the presence and absence of a high concentration of alprenolol (3 μM). Alprenolol is an orthosteric β_2AR antagonist (Baker, 2005), so at high concentration it should fully displace F-propranolol binding at the β_2AR, thus providing a measure of non-specific binding (NSB; residual signal measured in absence of F-propranolol binding). The conditions in absence of alprenolol provide the total binding measurements and specific binding was calculated by subtraction of the NSB from the total binding. F-propranolol binding kinetics at the β_2AR were assessed by construction of an association plot using specific binding measurements over 20 min after application of each concentration of F-propranolol to the membranes (Figure 6.10A). Increasing F-propranolol concentrations are shown to elevate the maximal HTRF emission ratio, until a saturation of ligand-receptor binding

is achieved. Estimates of F-propranolol kinetic binding parameters (association and dissociation rate constants, k_{on} and k_{off}) were produced by fitting these data to an association kinetics equation (Equation 11). F-propranolol k_{on} and k_{off} values were estimated as 4.97 x10^7 M^{-1} min^{-1} ± 0.63 x10^7 M^{-1} min^{-1} and 0.17 min^{-1} ± 0.01 min^{-1}, respectively. Moreover, the kinetic K_D of the fluorescent ligand (calculated by k_{off} / k_{on}) was 3.62 nM ± 0.55 nM. These values are mostly consistent with previously determined F-propranolol kinetic binding parameters by Farmer et al. (2022) using the same technique, although the estimated association rate was slightly slower in that study, resulting in a somewhat reduced kinetic K_D value (F-propranolol k_{on}: 1.30 x10^7 M^{-1} min^{-1} ± 0.18 x10^7 M^{-1} min^{-1}, k_{off}: 0.18 min^{-1} ± 0.02 min^{-1}, kinetic K_D: 16.1 nM ± 3.1 nM (Farmer et al., 2022)).

An F-propranolol saturation plot was also generated, displayed in Figure 6.10B, from mean total, NSB and specific binding values from six repeated measurements at equilibrium (between 19-20 min after ligand application), normalised against the maximal specific binding (100%). Fitting of these data to one-site binding models (Equations 9 and 10), enabled estimation of the equilibrium K_D value of 3.52 nM ± 0.67 nM, which was similar to the kinetically derived K_D for F-propranolol in this study ($P > 0.05$; determined by an unpaired t-test). This value is also largely consistent with the binding affinities of several fluorescent propranolol derivatives reported previously (Baker et al., 2011), although Harwood et al. (2021) previously estimated the equilibrium K_D value of F-propranolol with the β_2AR in membranes to be roughly 10-fold lower (31.62 nM) than found here.

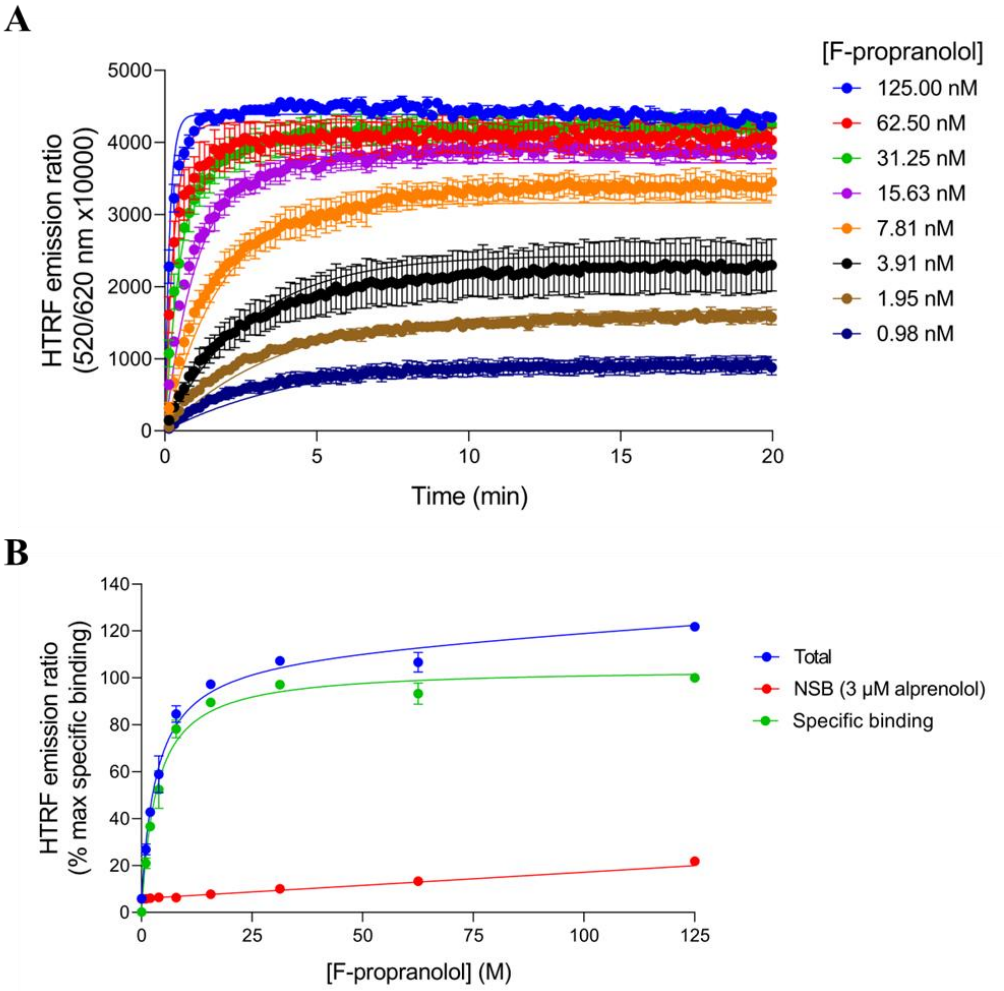

Figure 6.10: HTRF emission ratio measured due to total, NSB and specific binding of a fluorescent ligand to the Terbium-labelled receptor. (A) Combined TR-FRET association plot displaying specific binding over 20 min following application of increasing concentrations of F-propranolol (0.98 nM – 125 nM) to homogenised HEK293TR membranes overexpressing Terbium-labelled β_2AR. Data points represent mean ± SEM, expressed as 520/620 nm x10000 HTRF emission ratio, from three independent experiments ($n = 3$). (B) TR-FRET saturation plot displaying total, NSB and specific binding at equilibrium (between 19-20 min after ligand application) of increasing concentrations of F-propranolol (0.98 nM – 125 nM) in homogenised HEK293TR membranes overexpressing Terbium-labelled β_2AR. Data points represent mean ± SEM, expressed as a percentage of maximal specific binding, from three independent experiments ($n = 3$).

Subsequently, the same experiment was performed but this time including the application of 10 μM pepducin (ICL3-2, ICL3-7, ICL3-8, ICL3-9 and ICL1-15) or 1% DMSO (vehicle) simultaneously to F-propranolol addition. F-propranolol association (Figures 6.11A-6.11F) and saturation (Figures 6.12A-6.12F) plots for each condition were again constructed by performing the same analyses as already described. Kinetic and equilibrium binding parameters were then estimated for F-propranolol in the presence of each pepducin or DMSO and were compared to the equivalent parameters determined in the absence of the pepducins or DMSO (TR-FRET assay buffer only). None of the pepducins or DMSO had any effect on the equilibrium binding affinity of F-propranolol to the β_2AR ($P > 0.05$ for each). Similarly, no changes in F-propranolol kinetic binding affinity were found in any of the tested conditions ($P > 0.05$ in each case), however ICL3-7 did significantly increase the dissociation rate of the fluorescent ligand (F-propranolol k_{off}: 0.45 $min^{-1} \pm 0.08$ min^{-1} in presence of 10 μM ICL3-7, compared with 0.17 $min^{-1} \pm 0.01$ min^{-1} in absence of ICL3-7; $P < 0.05$). No other significant effects on association or dissociation rates were observed by any of the pepducins or DMSO ($P > 0.05$ throughout). Moreover, for each pepducin condition and the DMSO control, the estimated kinetic and equilibrium K_D values were similar ($P > 0.05$ for each; determined by unpaired t-tests). The full set of F-propranolol k_{on}, k_{off}, kinetic K_D and equilibrium K_D values in each condition are stated in Table 6.5.

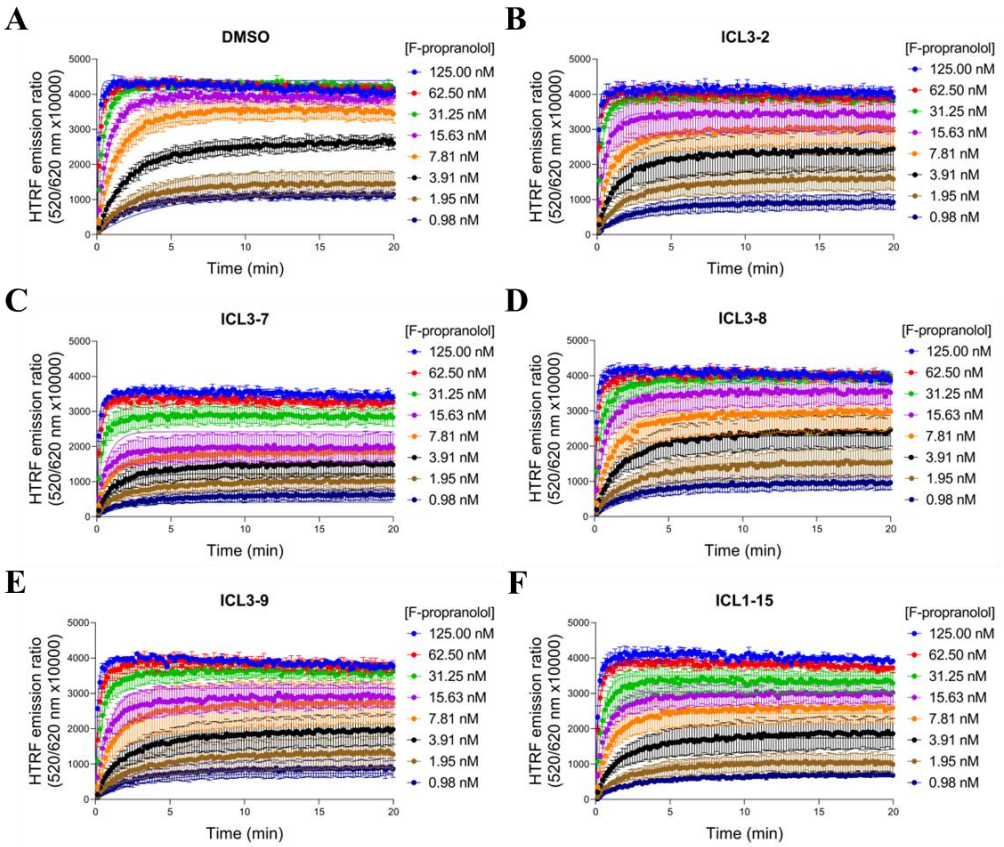

Figure 6.11: HTRF emission ratio measured due to specific binding of a fluorescent ligand to the Terbium-labelled receptor. (A-F) Combined TR-FRET association plots displaying specific binding over 20 min following application of increasing concentrations of F-propranolol (0.98 nM – 125 nM) in the presence of DMSO (1%; A), ICL3-2 (B), ICL3-7 (C), ICL3-8 (D), ICL3-9 (E) or ICL1-15 (F; all 10 μM) to homogenised HEK293TR membranes overexpressing Terbium-labelled β_2AR. Data points represent mean ± SEM, expressed as 520/620 nm x10000 HTRF emission ratio, from three independent experiments (n = 3).

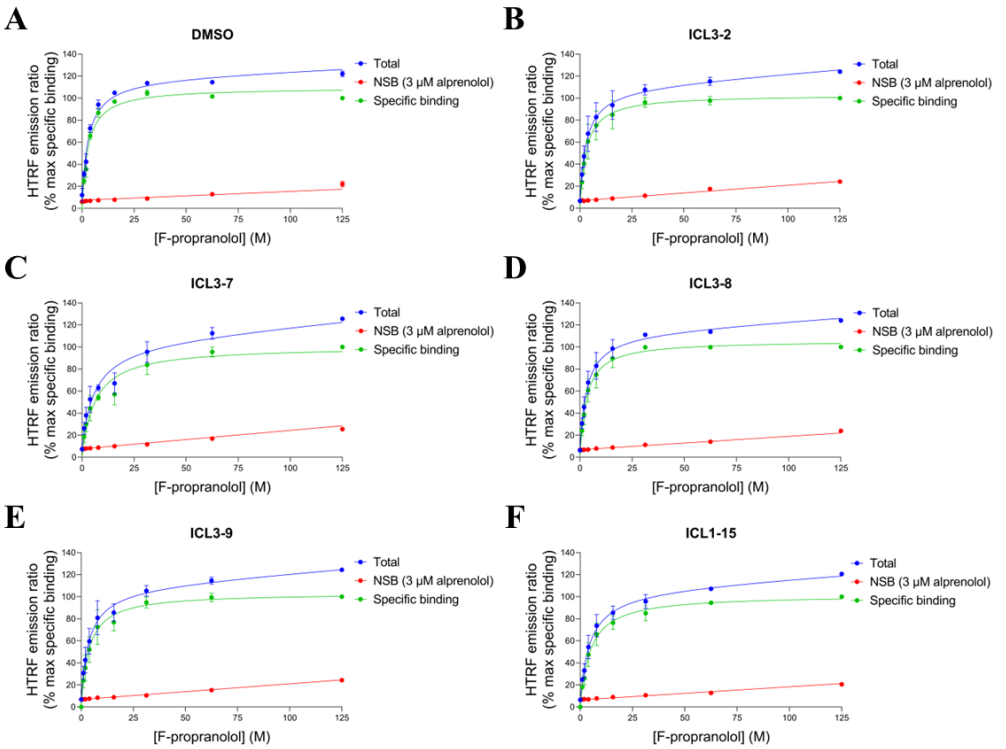

Figure 6.12: HTRF emission ratio measured due to total, NSB and specific binding of a fluorescent ligand to the Terbium-labelled receptor. (A-F) TR-FRET saturation plots displaying total, NSB and specific binding at equilibrium (between 19-20 min after ligand application) of increasing concentrations of F-propranolol (0.98 nM – 125 nM) in the presence of DMSO (1%; A), ICL3-2 (B), ICL3-7 (C), ICL3-8 (D), ICL3-9 (E) or ICL1-15 (F; all 10 µM) in homogenised HEK293TR membranes overexpressing Terbium-labelled β_2AR. Data points represent mean ± SEM, expressed as a percentage of maximal specific binding, from three independent experiments (n = 3).

Condition	F-propranolol k_{on} (M^{-1} min^{-1} $x10^7$) ± SEM	F-propranolol k_{off} (min^{-1}) ± SEM	F-propranolol kinetic K_D (nM) ± SEM	F-propranolol equilibrium K_D (nM) ± SEM
TR-FRET assay buffer	4.97 ± 0.63	0.17 ± 0.01	3.62 ± 0.55	3.52 ± 0.67
1% DMSO	6.73 ± 1.01	0.19 ± 0.01	3.00 ± 0.48	2.91 ± 0.41
10 μM ICL3-2	8.56 ± 1.52	0.33 ± 0.10	4.61 ± 2.24	4.28 ± 2.07
10 μM ICL3-7	6.93 ± 1.43	0.45 ± 0.08 *	7.07 ± 1.78	6.27 ± 1.65
10 μM ICL3-8	6.71 ± 1.58	0.23 ± 0.04	4.39 ± 2.16	4.01 ± 1.86
10 μM ICL3-9	6.05 ± 1.41	0.27 ± 0.07	5.95 ± 3.34	5.21 ± 2.84
10 μM ICL1-15	6.00 ± 0.92	0.34 ± 0.07	6.40 ± 2.35	5.79 ± 2.12

Table 6.5: F-propranolol mean k_{on}, k_{off}, kinetic K_D and equilibrium K_D values ± SEM determined in the presence and absence of DMSO (1%), ICL3-2, ICL3-7, ICL3-8, ICL3-9 and ICL1-15 (all 10 μM) obtained from TR-FRET association plots and saturation plots from three independent experiments ($n = 3$). Significant differences to those seen in absence of pepducin (or DMSO) are indicated, determined by a one-way ANOVA with Tukey's multiple comparisons test. $P < 0.05$ was used as the level for significance ($P < 0.05$ = *).

Formoterol competition binding experiments were then performed to investigate the binding parameters of unlabelled formoterol at the β_2AR in this system. An approximate K_D concentration of F-propranolol (4 nM) was applied to the membranes simultaneously with increasing concentrations of formoterol (0.21 nM – 450 nM), DMSO (vehicle) or 3 µM alprenolol (NSB). An association plot was again constructed from specific binding measurements over 20 min after application of the competing ligands to examine the binding kinetics of formoterol at the β_2AR, shown in Figure 6.13A. As formoterol concentration is increased, the maximal HTRF emission ratio achieved by F-propranolol binding to the receptor decreases. Formoterol k_{on} and k_{off} parameters were estimated as 6.15 x10^7 M^{-1} min^{-1} ± 1.79 x10^7 M^{-1} min^{-1} and 0.35 min^{-1} ± 0.07 min^{-1}, respectively, by applying the Motulsky-Mahan "kinetics of competitive binding" model (Equation 14) to these data (constrained to the HTRF emission ratio in the first 10 min after ligand addition only, in order to aid in the fitting of the data to the model), according to Motulsky and Mahan (1984). From these values, the kinetic K_I of the competing formoterol was determined as 5.97 nM ± 0.54 nM.

The effect of increasing formoterol concentrations on the 4 nM F-propranolol mean specific binding at equilibrium (from six repeated measurements between 19-20 min after ligand application) was then normalised between the maximal specific binding in the absence of formoterol (100%) and in the presence of the highest tested concentration of formoterol (0%) and plotted as an IC_{50} curve, fitted to a one-site binding model (Equation 12), displayed in Figure 6.13B. The determined formoterol IC_{50} value was then converted to an equilibrium K_I value of 6.33 nM ± 1.94 nM by using the method developed by Cheng and Prusoff (1973) (Equation 13), which was similar to the kinetic K_I value estimated for formoterol here ($P > 0.05$; determined by an unpaired t-test). Previous studies have provided somewhat varying estimations of formoterol binding parameters. Both Baker (2010) (formoterol K_D: 2.34 nM) and Farmer et al. (2022) (formoterol K_I: 5.01 nM) have reported formoterol binding affinities similar to those reported in this study. Contrastingly, Sykes et al. (2014) determined a kinetically-derived K_D value of 17.65 nM for formoterol, which was calculated from k_{on} and k_{off} rates which were both substantially faster than the k_{on} and k_{off}

rates found in this study (1.78×10^8 M^{-1} min^{-1} ± 0.21×10^8 M^{-1} min^{-1} and 3.00 min^{-1} ± 0.38 min^{-1}, respectively).

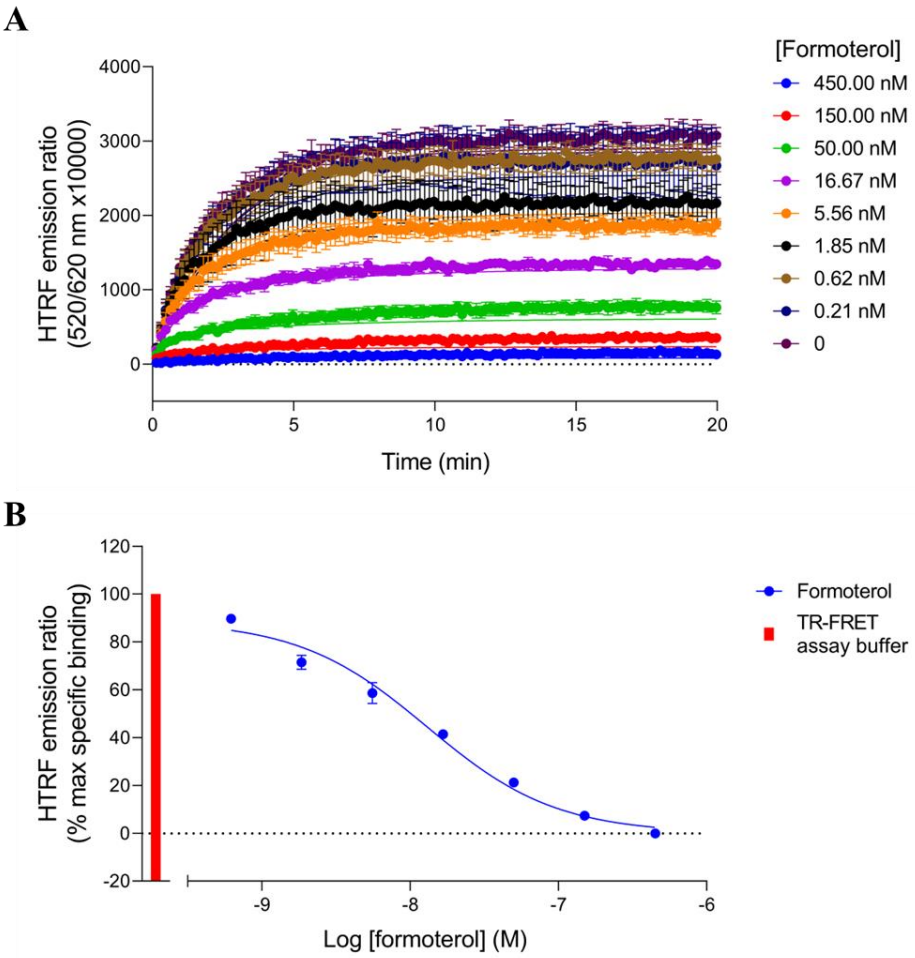

Figure 6.13: HTRF emission ratio measured due to specific binding of a fluorescent ligand to the Terbium-labelled receptor in competition with an unlabelled ligand. (A) Combined TR-FRET association plot displaying specific binding over 20 min following application of F-propranolol (4 nM) in the presence and absence of increasing concentrations of formoterol (0.21 nM – 450 nM) to homogenised HEK293TR membranes overexpressing Terbium-labelled β_2AR. Data points represent mean ± SEM, expressed as 520/620 nm x10000 HTRF emission ratio, from three independent experiments ($n = 3$). (B) TR-FRET IC_{50} curve displaying specific binding at equilibrium (between 19-20 min after ligand application) of F-propranolol (4 nM) in the presence of increasing concentrations of formoterol (0.62 nM – 450 nM) with TR-FRET assay buffer control in homogenised HEK293TR membranes overexpressing Terbium-labelled β_2AR. Data points represent mean ± SEM, expressed as a percentage of maximal specific binding in the absence of formoterol with zero determined as the signal from the highest concentration of formoterol (450 nM), from three independent experiments ($n = 3$).

The formoterol competition binding experiment was then repeated in the presence of 10 μM pepducin (ICL3-2, ICL3-7, ICL3-8, ICL3-9 and ICL1-15) simultaneously with both the 4 nM fluorescent tracer F-propranolol and the competing, unlabelled formoterol. These data were used to construct association plots (Figures 6.14A-6.14E) and IC_{50} curves (Figure 6.15) in the same processes as described above. Formoterol kinetic and equilibrium binding parameters were determined in the presence of each pepducin and comparisons were made with those values determined in the absence of pepducins (TR-FRET assay buffer only). The formoterol equilibrium inhibition constant, K_I, was not altered by addition of any of the tested pepducins ($P > 0.05$ throughout). Additionally, the kinetic binding affinity of formoterol remained unchanged in each case ($P > 0.05$ in all conditions). This was despite both ICL3-9 and ICL1-15 causing significant increases in the formoterol dissociation rate (formoterol k_{off}: 0.66 min^{-1} ± 0.05 min^{-1} in the presence of 10 μM ICL3-9 and 0.63 min^{-1} ± 0.02 min^{-1} in the presence of 10 μM ICL1-15, compared with 0.35 min^{-1} ± 0.07 min^{-1} in the absence of pepducins; $P < 0.05$ for both). None of the other pepducins modified the formoterol dissociation rate and none had any effect on the association rate of formoterol to the β_2AR ($P > 0.05$ for all other conditions). The kinetic and equilibrium K_I values were found to be similar in each case ($P > 0.05$ for each; determined by unpaired t-tests). Table 6.6 outlines the k_{on}, k_{off}, kinetic K_I and equilibrium K_I values determined for formoterol in each condition.

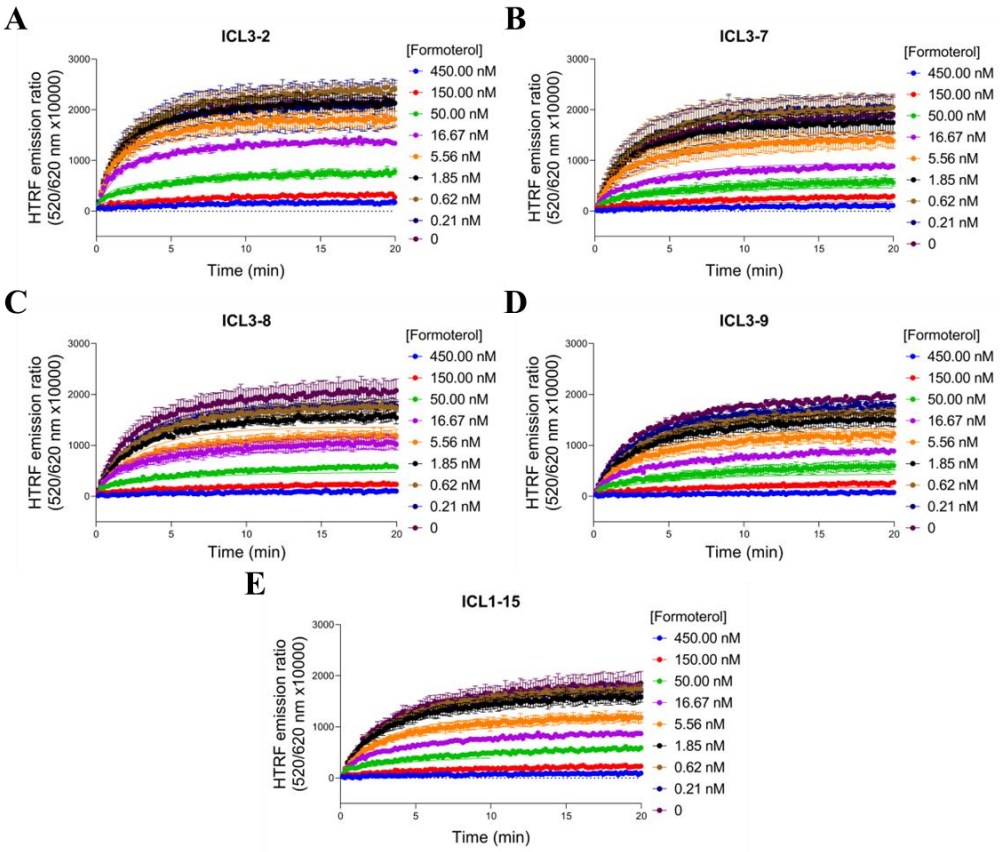

Figure 6.14: HTRF emission ratio measured due to specific binding of a fluorescent ligand to the Terbium-labelled receptor in competition with an unlabelled ligand. (A-E) Combined TR-FRET association plots displaying specific binding over 20 min following application of F-propranolol (4 nM) and ICL3-2 (A), ICL3-7 (B), ICL3-8 (C), ICL3-9 (D) or ICL1-15 (E; all 10 µM) in the presence and absence of increasing concentrations of formoterol (0.21 nM – 450 nM) to homogenised HEK293TR membranes overexpressing Terbium-labelled β_2AR. Data points represent mean ± SEM, expressed as 520/620 nm x10000 HTRF emission ratio, from three independent experiments (n = 3).

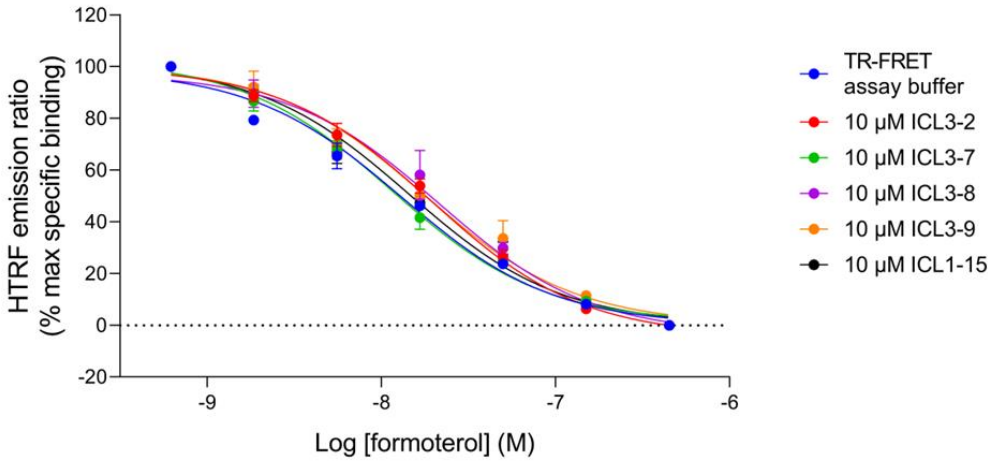

Figure 6.15: HTRF emission ratio measured due to specific binding of a fluorescent ligand to the Terbium-labelled receptor in competition with an unlabelled ligand. TR-FRET IC_{50} curves displaying specific binding at equilibrium (between 19-20 min after ligand application) of F-propranolol (4 nM) and ICL3-2, ICL3-7, ICL3-8, ICL3-9 or ICL1-15 (all 10 µM) in the presence of increasing concentrations of formoterol (0.62 nM – 450 nM) in homogenised HEK293TR membranes overexpressing Terbium-labelled β_2AR. Data points represent mean ± SEM, expressed as a percentage of maximal specific binding at the lowest concentration of formoterol (0.62 nM) with zero determined as the signal from the highest concentration of formoterol (450 nM), from three independent experiments (n = 3).

Condition	Formoterol k_{on} (M^{-1} min^{-1} x10^7) ± SEM	Formoterol k_{off} (min^{-1}) ± SEM	Formoterol kinetic K_I (nM) ± SEM	Formoterol equilibrium K_I (nM) ± SEM
TR-FRET assay buffer	6.15 ± 1.79	0.35 ± 0.07	5.97 ± 0.54	6.33 ± 1.94
10 μM ICL3-2	3.85 ± 0.26	0.34 ± 0.03	8.94 ± 0.94	9.26 ± 0.74
10 μM ICL3-7	7.32 ± 0.32	0.59 ± 0.13	8.03 ± 1.69	5.07 ± 0.63
10 μM ICL3-8	6.76 ± 0.57	0.56 ± 0.05	8.38 ± 0.70	7.40 ± 0.55
10 μM ICL3-9	8.16 ± 1.07	0.66 ± 0.05 *	8.49 ± 1.45	6.79 ± 1.08
10 μM ICL1-15	7.10 ± 0.47	0.63 ± 0.02 *	9.02 ± 0.81	7.10 ± 1.49

Table 6.6: Formoterol mean k_{on}, k_{off}, kinetic K_I and equilibrium K_I values ± SEM determined in the presence and absence of ICL3-2, ICL3-7, ICL3-8, ICL3-9 and ICL1-15 (all 10 μM) obtained from TR-FRET association plots and IC_{50} curves from three independent experiments ($n = 3$). Significant differences to those seen in absence of pepducin are indicated, determined by a one-way ANOVA with Tukey's multiple comparisons test. $P < 0.05$ was used as the level for significance ($P < 0.05$ = *).

6.4 – Discussion

6.4.1 – Ligand binding induces substantial increases in detergent-solubilised β_2-adrenoceptor thermostability

Initial thermoBRET experiments were designed to optimise the conditions in which the β_2AR was solubilised. Four detergent conditions were tested here: 1% DDM, 1% DDM + 1% CHAPSO + 0.2% CHS, 0.5% LMNG and 0.5% LMNG + 1% CHAPSO + 0.2% CHS. In this study, the LMNG-solubilised β_2AR showed a higher thermostability than when solubilised in DDM (Figure 6.1B). LMNG has also previously been reported to provide improved stability to solubilised GPCRs than DDM (Chae et al., 2010; Milić and Veprintsev, 2015). The effect of CHAPSO and CHS addition was to further stabilise the β_2AR under both DDM and LMNG conditions (Figure 6.1B). This was not an unexpected result because CHS, a cholesterol derivative, is regularly used to maintain solubilised receptor stability and function during purification and for structural studies such as crystallography (Weiß and Grisshammer, 2002; Hanson et al., 2008; Thompson et al., 2011; Errey and Fiez-Vandal, 2020). The order of detergent-solubilised β_2AR thermostability (in terms of T_m) observed here was the same as previously determined by Hoare et al. (2023) using the same thermoBRET technique: LMNG/CHAPSO/CHS > DDM/CHAPSO/CHS > LMNG > DDM.

However, when deciding which detergent to use for these experiments, the most important factor was not the receptor thermostability itself (as long as the receptor was stable enough for reliable studies). Instead, the ability to clearly detect ligand binding through shifts in the receptor's melting temperature (T_m) was key in order to examine pepducin binding at the receptor later. The addition of 1 μM propranolol caused a substantial rightward shift in DDM-solubilised β_2AR thermostability (approximately 9 °C increase in T_m; Figure 6.2B). In contrast, none of the other detergent conditions displayed any clear rightward shift in the melting curve upon propranolol application. Instead, the signal-to-noise ratio decreased in each case, making it difficult to detect receptor unfolding, at least in the temperature range tested here (LMNG shown in Figure 6.2A). It is possible that higher temperatures (> 52 °C) were required to cause

maximal unfolding of the receptor in these conditions as this was not tested. DDM also provided the best window of signal-to-noise in the absence of bound ligand (Figure 6.1A). This may indicate some detergent-based differences in the unfolding of the protein upon melting, whereby the exposure of cysteine residues in the core of the receptor to the SCM dye is reduced in LMNG (or in the presence of CHAPSO and CHS), compared with DDM alone. Taking all these factors into consideration, it was decided that DDM was the most appropriate detergent to proceed with.

Surprisingly, the removal of sodium chloride (NaCl) from the CORE buffer composition had little effect on the β_2AR melting curve (Figure 6.3), despite sodium ions having previously been demonstrated to interact with GPCRs including the β_2AR at physiologically relevant concentrations, such as the concentration in the standard CORE buffer composition here (150 mM NaCl) (Katritch et al., 2014; Zarzycka et al., 2019). Although the sodium binding pocket is conserved throughout most class A GPCRs, sodium binding affinity has been reported to vary widely between receptors (Zarzycka et al., 2019). In addition, sodium binding may be affected by solubilisation of the receptor into detergent micelles. It is possible that if sodium binding to the detergent-solubilised β_2AR is weak (low affinity), then it may only have minimal impact on receptor thermostability. Hence, the removal of sodium ions here does not cause a detectable leftward shift in the β_2AR T_m.

The application of β_2AR ligands prior to receptor melting markedly increased the thermostability of the β_2AR (~11-15 °C shift in T_m at 10 μM ligand concentration; Figures 6.4A and 6.4B). This effect was also shown to be concentration-dependent (Figures 6.5A and 6.5B). This assay therefore provides a useful indication of ligand-receptor binding. Ligand activity or efficacy did not appear to be an important factor in the stabilisation of the receptor since, out of the four ligands tested, two were agonists (of differing efficacies; formoterol and salmeterol) and two were inverse agonists (propranolol and ICI-118551) and this did not correlate with the degree of shift in the T_m value. Instead, the rightward shift in the receptor melting curves reflected the binding affinity of the ligands. The rank order of ligand-induced T_m shift was in agreement with the order of

pK_D values determined by Sykes et al. (2014): propranolol (pK_D value: 9.90 ± 0.03) > salmeterol (9.47 ± 0.01) = ICI-118551 (9.56 ± 0.03) > formoterol (7.28 ± 0.10). This observation was also reported previously (Hoare et al., 2023). Moreover, in the isothermal thermoBRET format, where a reduction in nanoBRET signal reflects increased receptor thermostability, determined IC_{50} values also correlated with these pK_D values (Table 6.3) (Sykes et al., 2014). The reduction in nanoBRET ratio at high temperatures (above 56 °C) was also observed at similar temperatures by Hoare et al. (2023). This was likely due to aggregation of the denatured proteins at these high temperatures which may reduce the exposure of the cysteine residues in the receptor core to the SCM dye, thus resulting in the loss of signal (Hoare et al., 2023). The effect was not due to denaturation of the tsNLuc at these temperatures as thermostabilising mutations provided the nanoluciferase a T_m of 87 °C, improved from 57 °C in the unmutated protein (Hoare et al., 2023).

6.4.2 – Pepducins are unable to alter β_2-adrenoceptor thermostability

The thermoBRET assay has been demonstrated as an ideal technique for examining ligand binding to receptors. Hence, this technique was used to assess whether pepducins can interact with the β_2AR. Although Hoare et al. (2023) did not report the effects of any allosteric ligands using the thermoBRET assay, allosteric ligand binding has previously been shown to increase receptor stability (Hanson et al., 2008; Liu et al., 2012; Kruse et al., 2013; Katritch et al., 2014; Zhang et al., 2015c), so any binding by the pepducins to allosteric receptor sites should cause a rightward shift in the β_2AR melting curve in a similar manner as the orthosteric ligands discussed already. However, in this study no evidence was found of pepducin binding to the β_2AR. None of the five pepducins tested were able to cause any shift in the melting temperature of the receptor (Figure 6.7) and, upon switching to the isothermal assay format, the pepducins had no effect on the measured nanoBRET ratio at 36 °C at any concentration (Figure 6.8). Even when a 30 min incubation period was added to the protocol after pepducin

addition (prior to receptor melting), in order to allow more time for the pepducins to equilibrate at the receptor, no change in signal was observed. This incubation had to be performed at 4 °C to prevent unwanted receptor denaturation during this period. At such low temperatures, ligands likely achieve binding equilibrium with receptors at a much slower rate than at higher temperatures, so perhaps even longer than 30 min would be required for the pepducin-receptor binding equilibrium to be reached. However, orthosteric ligands were able to substantially increase the thermostability of the receptor even without this incubation period.

Although it has generally proven difficult to directly determine receptor binding affinities for pepducins (Janz et al., 2011; Quoyer et al., 2013), some studies have demonstrated that pepducin agonists generally act with reduced potency when compared with orthosteric agonists (Tchernychev et al., 2010; Quoyer et al., 2013; Brouillette et al., 2020), which suggests that they may comprise lower receptor binding affinities. Indeed, Carr et al. (2014) found that ICL3-9 (EC_{50}: 4.7 μM ± 0.1 μM) acted with very low potency at the β_2AR despite showing a similar efficacy for cAMP production as salbutamol. For comparison, in the same study isoprenaline (EC_{50}: 8.23 nM ± 0.15 nM) acted with approximately 500-fold higher potency than ICL3-9 (Carr et al., 2014). In the thermoBRET assay, the degree of shift in receptor thermostability (in terms of T_m value), appears to be associated with ligand-receptor binding affinities. Therefore, it might be expected that pepducins would cause somewhat more modest shifts in the β_2AR melting curve than those observed by orthosteric ligands. Regardless, it seems unlikely that the effects of pepducin binding on receptor thermostability are so miniscule so as not to detect any changes in this sensitive assay system, especially at the micromolar concentrations used here (10 μM in the temperature gradient assay, and up to 30 μM in the isothermal format).

Since there was no evidence of pepducin binding to the unbound β_2AR, the next experiment aimed to determine whether they could instead interact with a pre-bound agonist-receptor complex. Each of the pepducins were shown to act as allosteric β_2AR agonists by Carr et al. (2014). Additionally, the data presented earlier in this study (Figures 5.3, 5.10A and 5.10B) also implied some β_2AR-

dependent agonist activity, although the data were too inconsistent to be conclusive (discussed throughout Chapter 5). Agonists display a higher binding affinity for the active receptor conformation (De Lean et al., 1980; Park et al., 2008; Weis and Kobilka, 2018) and so, by preincubating the receptor with formoterol and thereby stabilising the active state of the β_2AR population, the pepducin binding affinities should theoretically be increased. This could therefore provide a better opportunity to detect pepducin binding, which would be observed as a further increase in β_2AR thermostability (a reduction in the nanoBRET signal in the isothermal assay format used here). However, no such change in the nanoBRET signal was measured at any tested pepducin concentration (Figure 6.9A), indicating that the pepducins did not bind to the β_2AR even when stabilised in its active conformation by an orthosteric agonist. A useful additional test would have been to instead preincubate the β_2AR with an inverse agonist (for example, ICI-118551), to confirm that no detectable binding occurred between the pepducins and the receptor stabilised in its inactive state. Finally, the preincubation of pepducins with the receptor, followed by formoterol application (essentially the opposite of the previous experiment described) was performed. This time, differences in the nanoBRET signal measured here would imply a modification of the formoterol binding affinity for the β_2AR by the pepducins, which is a classic property of allosteric modulators (Christopoulos and Kenakin, 2002; May et al., 2007; Keov et al., 2011). Once again however, no pepducin effect was observed (increase or decrease) even at high concentrations (Figure 6.9B).

Previously, Carr et al. (2014) showed that ICL3-7, ICL3-9 and ICL1-15 were all β_2AR-dependent (although ICL3-2 and ICL3-8 acted β_2AR-independently). Earlier work in this study also showed that CRE-SPAP responses to each of the five pepducins were completely abolished in cells lacking expression of the β_2AR (Figure 5.10B). Considering this, it is surprising that no evidence of pepducin binding could be detected in the thermoBRET assay performed here. Pepducins are thought to traverse cell membranes by incorporation of the hydrophobic palmitate tag into the phospholipid bilayer and subsequently passively flipping across the membrane (Covic et al., 2002a; Carlson et al., 2012; Zhang et al., 2015b). The pepducin then remains attached to the membrane by

its palmitate tag and from here the peptide can interact with a target receptor at its intracellular surface (Covic et al., 2002a; Carlson et al., 2012; Zhang et al., 2015b). Perhaps then, the incorporation of the palmitate moiety into the bilayer is not just important for the translocation of the peptide inside the cell but is also a vital mechanism for the pepducin-receptor interaction to occur. This membrane-anchoring feature likely brings pepducins into closer proximity with their allosteric binding site and thus increases the effective local concentration of pepducin at the receptor surface. This mechanism could be disrupted by removal of the receptor from the native cell membrane by solubilisation into detergent (DDM in this case). It is likely that the palmitate tag interacts differently with the detergent micelles, which comprise distinct structural properties to the native phospholipid bilayer of cells, including the loss of endogenous membrane lipids (Seddon et al., 2004; Wiseman et al., 2020). Hence, the lack of membrane-anchoring may disrupt the interaction between pepducin and receptor, either due to reduced local concentration or a loss of binding affinity.

6.4.3 – Several pepducins alter orthosteric ligand binding kinetics at the β_2-adrenoceptor by increasing dissociation rates

As discussed above, it is possible that the anchoring of pepducins into the cell membrane is critical for their interaction with the target receptor. It was therefore important to study the action of the five pepducins at the β_2AR residing in the native cell membrane. To this end, TR-FRET kinetic binding assays were performed in homogenised HEK293TR cell membranes which transiently overexpressed the β_2AR, in order to study whether pepducins impacted the binding affinities or kinetics of orthosteric ligands at the receptor. This is a classic hallmark of allosteric ligands (Christopoulos and Kenakin, 2002; May et al., 2007). The action of an allosteric modulator generally manifests as a modification of either the affinity or efficacy (or both) of an orthosteric ligand for its target receptor (Christopoulos, 2002; May et al., 2007; Keov et al., 2011). Changes in affinity of the orthosteric ligand occur because the binding of an

allosteric ligand causes a shift in the receptor conformation which can alter the rate at which the orthosteric ligand associates or dissociates with the receptor (Christopoulos and Kenakin, 2002; May et al., 2007; Díaz et al., 2023). For example, a PAM may act by increasing the rate of association and/or decreasing the rate of dissociation of an orthosteric agonist for its receptor. Alternatively, a NAM might have the opposite effect. Several studies have reported the effects of allosteric modulators on orthosteric ligand binding kinetics, with changes in dissociation rate being more common (Stockton et al., 1983; Price et al., 2005; May et al., 2010; Guo et al., 2014; Doornbos et al., 2018). In addition, Farmer et al. (2022) showed that intracellular peptides were able to increase the binding affinities of several agonists (including formoterol) for the β_2AR, thus acting as PAMs at the receptor.

In this study, several of the pepducins displayed some indication of allosteric activity by modulating receptor binding kinetics to a modest degree. Ultimately, however, the action of the pepducins was still unclear. In the initial investigation into their effect on the binding properties of the fluorescent ligand F-propranolol, ICL3-7 modestly increased the dissociation rate of F-propranolol whilst not significantly altering the association rate of the ligand (Table 6.5). Although there is no direct evidence that this fluorescent derivative of propranolol comprises inverse efficacy, unlabelled propranolol is generally considered a weak inverse agonist of the β_2AR (Chidiac et al., 1994; Azzi et al., 2001). Evidence supporting this was also presented earlier in this study (Figure 4.7). Therefore, this finding may suggest some positive modulatory activity by ICL3-7, as increasing the inverse agonist dissociation rate is indicative of PAM behaviour (Christopoulos and Kenakin, 2002; May et al., 2007). However, this did not translate into a significant decrease in F-propranolol binding affinity, determined either kinetically or by equilibrium measurements. Moreover, any PAM activity by ICL3-7 should have been even more evident in the formoterol competition experiments. The binding properties of formoterol, which is classified as a highly efficacious agonist for the β_2AR (Baker, 2010) (also shown in this study; Figure 3.6), would likely be enhanced in the presence of a PAM (although not necessarily the case due to probe dependence). Upon addition of

ICL3-7, however, no changes in any of the binding properties of formoterol to the β_2AR were observed (Table 6.6).

Conversely, both ICL3-9 and ICL1-15 significantly increased the dissociation rate of formoterol at the β_2AR, thus implying some NAM activity by these two pepducins (Table 6.6). Once again, this did not result in any significant reduction in the formoterol binding affinity for the receptor in either case and no modification of F-propranolol binding kinetics were observed (Table 6.5). It may at first seem counterintuitive for these pepducins, which were previously shown to act as allosteric β_2AR agonists (Carr et al., 2014), to negatively modulate the β_2AR here. However, it has previously been shown that the effect of an allosteric ligand on orthosteric ligand affinity and efficacy may not necessarily be the same (Price et al., 2005; Keov et al., 2011). Price et al. (2005) found that numerous cannabinoid CB_1 receptor allosteric ligand analogues could potentiate orthosteric ligand binding affinity, whist simultaneously inhibiting signalling efficacy. Therefore, it is also plausible that these pepducins could act as allosteric agonists for the β_2AR but negatively modulate orthosteric agonist binding kinetics. Additional tests into the action of these pepducins on the binding properties of a competing strong inverse agonist (such as ICI-118551) would be useful to further support the findings here.

It is noteworthy that ICL3-2 and ICL3-8, which were found to act β_2AR-independently (instead directly activating G_s protein) by Carr et al. (2014), were the two pepducins which exerted no significant modification of the dissociation rate of either F-propranolol or formoterol here (Tables 6.5 and 6.6). Whereas each of the other pepducins (ICL3-7, ICL3-9 and ICL1-15), which were previously considered receptor-dependent (Carr et al., 2014), altered the dissociation rate of one of the two orthosteric ligands tested in this study, thus suggesting either PAM (ICL3-7) or NAM (ICL3-9 and ICL1-15) activity. However, since the effects on F-propranolol or formoterol dissociation rates were only minor and did not ultimately translate into alterations in ligand binding affinities, the allosteric effects of these pepducins is not entirely clear from the findings in this study and thus needs further investigation in the future.

6.5 – Conclusion

This study has demonstrated the use of the thermoBRET assay to determine ligand-receptor binding by measuring changes in receptor thermostability. High concentrations of orthosteric ligands (10 μM) increased the melting temperature (T_m) of the DDM-solubilised β_2AR by approximately 11 °C – 15 °C. The degree of thermostability shift correlated with ligand binding affinity for the receptor. However, when five distinct pepducins (ICL3-2, ICL3-7, ICL3-8, ICL3-9, and ICL1-15) were applied at the same high concentration, no changes in the receptor's T_m value were measured. Additionally, when the assay was performed in an isothermal format, no evidence of pepducins binding to the receptor (reduction in nanoBRET signal) could be detected. Upon preincubation of formoterol to stabilise the active receptor conformation and potentially increase pepducin binding affinity, the pepducins still had no impact on receptor thermostability, strongly suggesting that none of the pepducins could interact with the β_2AR in this assay. One possible explanation is the removal of the receptor from its native cell membrane during detergent solubilisation, thus preventing membrane anchoring by the N-terminal palmitate tag which could be vital for pepducin interaction with the receptor inside cells.

TR-FRET was then employed to investigate pepducin-mediated modulation of orthosteric ligand binding kinetics at the β_2AR in homogenised membranes. Several of the tested pepducins displayed an ability to modestly alter the dissociation rates of either the fluorescently labelled tracer ligand F-propranolol (ICL3-7) or the unlabelled competing agonist formoterol (ICL3-9 and ICL1-15), thereby suggesting potential PAM or NAM activity, respectively. However, in each case the binding affinities of the ligands were not significantly changed (either kinetically-derived or obtained at equilibrium). Interestingly, the two pepducins which did not modify the binding kinetics of either of the tested orthosteric ligands (ICL3-2 and ICL3-8) were previously shown to act receptor-independently by directly activating G_s protein by Carr et al. (2014). Further experiments are required to verify the allosteric effects of the pepducins on orthosteric ligand binding kinetics.

Chapter 7

General discussion

7.1 – General discussion

The β_2-adrenoceptor (β_2AR) is a prototypical class A GPCR which plays important roles in airway and vascular smooth muscle relaxation (bronchodilation and vasodilation, respectively) and has been successfully targeted by β-agonists in the treatment of asthma and other pulmonary diseases (Bai, 1992; Tanaka et al., 2005; Billington et al., 2013). It also contributes to cardiac contractility, which is regulated clinically by β-blockers (Madamanchi, 2007; Frishman and Saunders, 2011; Pérez-Schindler et al., 2013). Because the β_2AR has been one of the most extensively studied GPCRs, it provides an ideal model system for unravelling new insights into general GPCR functions and mechanisms of activity. To this end, this thesis has explored numerous distinct aspects of the pharmacology of the β_2AR. This includes investigations into the kinetics of agonist-stimulated cAMP responses in both low endogenous expression and stable overexpression systems in HEK293G cells (Chapters 3 and 4), β_2AR mechanostimulation mediated by receptor extracellular N-glycan chains (Chapter 4) and the functional and binding activities of peptidic intracellular allosteric ligands, pepducins, at the receptor (Chapters 5 and 6). The findings in this thesis have helped to improve our understanding of β_2AR pharmacology and may serve as useful building blocks for both future studies into the β_2AR (as well as other GPCRs) and ultimately the development of novel therapeutics to provide improved treatments for pulmonary or cardiovascular diseases.

7.1.1 – Kinetic analysis of agonist-mediated functional receptor responses can lead to more accurate ligand characterisation

The importance of considering the kinetic parameters of agonist-mediated receptor responses has become increasingly clear in recent years, with the development of new biosensors which have enabled real-time continuous measurements of receptor signalling (Lohse et al., 2008; Goulding et al., 2018; Greenwald et al., 2018; Dijon et al., 2021). Here, by fitting cAMP GloSensor^{TM} luminescence time-course data to the kinetic equation derived by Hoare et al.

(2020b), new kinetic parameters (IR_{max}, log L_{50}) of β_2AR agonist activity were determined and compared with standard pharmacological parameters (E_{max}, log EC_{50}). Although there was a general correlation between agonist maximal responses and maximal initial rates of signal generation, under low receptor expression conditions the partial agonists salbutamol and salmeterol exhibited reduced IR_{max} values compared with their E_{max} values, with respect to the reference ligand isoprenaline, whereas the full agonist formoterol did not. This effect is likely related to reduced rates of receptor desensitisation induced by lower efficacy ligands, which has been reported previously (Clark et al., 1996; January et al., 1997; January et al., 1998; Gimenez et al., 2015) and which would allow the time-course signal to plateau at a slower rate due to less counteractive pressure from regulatory mechanisms. No differences were observed between E_{max} and IR_{max} parameters in cells stably overexpressing the β_2AR because all agonist responses were amplified to a maximal level (including the lower efficacy partial agonists), masking the effects of distinct receptor desensitisation rates on the cAMP signal. A useful experiment to complement these results would be to kinetically measure agonist-induced β-arrestin recruitment to the β_2AR in live cells by use of BRET- or NanoBiT-based biosensors, as has been described previously (Storme et al., 2018; Dale et al., 2019; Dijon et al., 2021). This could be performed both in endogenous low receptor expression conditions and after stable overexpression of the β_2AR into cells to assess whether receptor expression directly influences the rates of receptor desensitisation mediated by agonists of differing efficacies. Additionally, the influence of β-arrestin expression on the dynamics of receptor recruitment and desensitisation could be directly tested in cells with endogenous expression of the β_2AR using CRISPR-based gene editing techniques to attach biosensors to the endogenous receptors, as has been shown previously (White et al., 2020). Kinetic analysis of data obtained from measurements of different signalling pathways may even provide new insights into the mechanisms underpinning biased signalling (Hoare et al., 2020a; Hoare et al., 2022).

Additionally, preincubation of β_2AR antagonists with differing dissociation rates under endogenous receptor expression conditions caused distinct effects on the E_{max} and IR_{max} values of agonist-induced cAMP signals. Due to the presence of

hemi-equilibrium conditions (because of very low receptor reserve) (Paton and Rang, 1965; Vauquelin et al., 2002; Hopkinson et al., 2000; Charlton and Vauquelin, 2010), slowly dissociating antagonists (carvedilol, ICI-118551 and propranolol) substantially reduced the maximal responses of both isoprenaline and formoterol, but the extremely fast dissociating antagonist bisoprolol did not. Whereas the agonist maximal initial rates were reduced even more drastically by each antagonist and even bisoprolol substantially decreased agonist IR_{max}. This was because the pre-formed antagonist-receptor complexes had even less time to dissociate (and thus allow agonist binding and subsequent stimulation of cAMP production) in the time-frame required for the determination of the initial rate parameter, compared with peak response. When performed in cells overexpressing the β_2AR, no effect on either the agonist maximal responses or maximal initial rates were observed because the greater receptor reserve meant that even at high antagonist concentrations there were plenty of spare receptors available for agonist binding and thus for stimulation of a maximal cAMP response to be rapidly achieved.

By analysing the entire time-courses of β_2AR-mediated cAMP responses using the approach outlined by Hoare et al. (2020b), it has been possible to reveal novel information about complex ligand-receptor interactions and their effects on receptor signalling profiles. Quantification of new kinetic parameters of agonist activity in addition to standard pharmacological parameters of efficacy and potency has provided a fuller picture of β_2AR ligand activity. This has highlighted the necessity to take into consideration all aspects of the signalling response (including the initiation of the response as well as the signal decay) when classifying ligand efficacy, potency and even perhaps biased signalling. These kinetic analyses could therefore be applied in future studies to enable more accurate characterisation of ligands, which could in turn advance our understanding of GPCR pharmacology and may lead to improved rational design and optimisation of new therapeutics based on these kinetic parameters.

7.1.2 – β_2-adrenoceptor sensitivity to mechanostimulation of cAMP production is conferred by receptor N-glycosylation

Many GPCRs have previously been reported to respond to mechanical stimuli, including several members of the class A subfamily (Chachisvilis et al., 2006; Erdogmus et al., 2019; Wilde et al., 2022; Hardman et al., 2023). Among other physiological processes, GPCR mechanostimulation in vascular endothelial cells has been implicated in a range of cardiovascular processes such as mediating vascular remodelling, controlling vascular tone, inflammatory responses and atheroprotection (Davies, 1995; Groves et al., 1995; Storch et al., 2012; Busch et al., 2015; Chistiakov et al., 2017; Hong et al., 2020; Tanaka et al., 2021; Hu et al., 2022). The β_2AR also displays mechanosensitivity, having recently been shown to transduce traction forces from meningococcus pili into GRK-mediated β-arrestin recruitment via N-terminal N-glycan chains in a process which enables the bacteria to cross the blood-brain barrier during infection (Virion et al., 2019; Marullo et al., 2020). In this study, overexpression of the β_2AR in HEK293G cells revealed that mechanostimulation of the β_2AR could also promote cAMP production by shifting the conformational equilibrium of the receptor toward an active state, resulting in a transient, agonist-like response. This response was both potentiated by agonists and blocked by inverse agonists, which is consistent with previous studies into mechanosensitive GPCRs (Zou et al., 2004; Chachisvilis et al., 2006; Zhang et al., 2009; Busch et al., 2015; Erdogmus et al., 2019). The β_2AR was also sensitive to restimulation by repeated mechanical inputs, although only very specific mechanical stimuli produced the cAMP response (the sustained linear motion exerted on the microplate by opening and closing the PHERAstar FSX door, but not linear or orbital shaking protocols). It is plausible that this is a physiologically relevant feature of β_2AR mechanical stimulation. Physiological processes in the vascular system have been shown to be affected by alterations in fluid shear stress force (such as direction, magnitude and frequency of the force) caused by changes in blood flow (Davies, 1995; Chistiakov et al., 2017; Tanaka et al., 2021).

After removal of the extracellular β_2AR N-glycosylation sites by mutation of three asparagine residues (Asn6, Asn15 and Asn187) into alanine, the β_2AR

cAMP response to mechanical stimulation was substantially reduced, whilst both receptor surface expression and response to the agonist isoprenaline were unaffected. This revealed that N-glycan chains attached to the extracellular domain of the receptor are responsible for conferring mechanosensitivity to the β_2AR. The involvement of N-glycan chains in β_2AR mechanotransduction was also discussed previously by Virion et al. (2019), although they instead reported GRK-dependent β-arrestin recruitment and did not observe any stimulation of cAMP production. It is likely that the large N-glycans structures which extend out from the cell membrane and integrate with the ECM are particularly susceptible to movement upon application of forces onto the cell. This may amplify the effect of the force on the receptor which results in conformational changes into an active state and the subsequent cAMP signalling response; thus N-glycan chains confer β_2AR mechanosensitivity. These results supplement the increasing body of evidence that receptor N-glycosylation has important physiological roles beyond protein folding and stability, such as in receptor function and signal transduction. Furthermore, a small mechanical response was also observed in HEK293Gwt cells (which endogenously express the β_2AR at very low levels), which was largely insensitive to ICI-118551, indicating that other endogenously expressed GPCRs in HEK293 cells may also stimulate cAMP production via similar mechanically-induced mechanisms.

In order to support the findings of this study, it would be imperative to confirm that the measured cAMP response is not in fact due to catecholamine release from cells (and subsequent agonist-mediated β_2AR activation) after exposure to the mechanical stimuli. This could be carried out by substitution of an aspartate residue, Asp113, residing in the orthosteric ligand binding pocket with an alanine residue (D113A mutation). Asp113 is essential for the binding of orthosteric ligands to the β_2AR and removal of this amino acid from the β_2AR sequence has shown to drastically hinder agonist-mediated signalling responses (Plazinska et al., 2015; Chan et al., 2016; Jones et al., 2020; Yang et al., 2020; Zhang et al., 2020; An et al., 2022). Therefore, by performing similar GloSensor^{TM} experiments as those in this study with a β_2AR D113A mutant, confirmation that the cAMP response was not due to catecholamine activity would be provided if no change was observed in the response to mechanical stimulation while agonist

responses were substantially decreased or abolished. With this possibility ruled out, the only remaining plausible explanation for the response is β_2AR mechanostimulation. It would also be extremely useful to confirm the findings in this study using distinct assays. The cAMP GloSensor^{TM} luminescence assay provides an extremely sensitive and amplified assay system which allows relatively small changes in cAMP signalling responses to be visualised in real-time (Fan et al., 2008; Binkowski et al., 2011). If similar results can be obtained in other assay types, for example BRET-based effector protein recruitment experiments which measure signal transduction upstream of cAMP signalling and have reduced signal amplification, then the evidence of β_2AR mechanostimulation will be even more compelling.

The revelation of a mechanosensory function of the β_2AR has given rise to the question of whether this process could play a role in the vascular system, since mechanostimulation of other GPCRs has already been shown to be important in vascular physiology (Davies, 1995; Chistiakov et al., 2017; Tanaka et al., 2021). An initial step to answer this question may be to perform the same cAMP GloSensor^{TM} experiments in a vascular endothelial cell line (stably expressing both the GloSensor^{TM} biosensor and the β_2AR) to uncover whether the β_2AR responds similarly to mechanical stimuli in a more physiologically relevant cell type. Furthermore, the involvement of β_2AR mechanostimulation in vasodilation could be investigated directly by isolating blood vessels (for example, mouse artery segments) and carrying out vascular myography experiments to measure changes in vascular tone, a technique which has been described previously (Hart, 2019; Wenceslau et al., 2021; Schubert et al., 2023). Changes in vessel diameter can be measured under different flow conditions (which provides the mechanical input) to determine mechanically stimulated dilation of blood vessels. To establish whether this process is mediated by the β_2AR, selective inverse agonists can be applied which should suppress β_2AR-mediated vasodilation but not affect that mediated by other receptors. Moreover, β_2AR gene-deficient vessels can also be tested as a negative control. This described method is similar to that carried out by Erdogmus et al. (2019) to uncover whether the H_1R mediates flow-induced vasodilation. Gaining a better understanding of the mechanisms underlying β_2AR mechanotransduction and its physiological

implications in the vascular system could unlock new avenues to combat cardiovascular diseases such as hypertension and atherosclerosis.

7.1.3 – The action of pepducins at the β_2-adrenoceptor remains largely unclear despite some evidence of allosteric activity

The actions of short N-terminally lipidated allosteric ligands called pepducins have previously been described for several GPCRs (Covic et al., 2002a; Carlson et al., 2012; Zhang et al., 2015b). Pepducins derived from the intracellular loops of the β_2AR were developed by Carr et al. (2014) and functional characterisation of their activity revealed that many of the pepducins acted as allosteric agonists of the β_2AR. Pepducins deriving from ICL3 generally showed a bias for stimulating cAMP production, whereas ICL1-derived pepducins instead preferentially recruited β-arrestin to the receptor (Carr et al., 2014). Of the ICL3-based pepducins, several were β_2AR-dependent whereas others acted independent of β_2AR expression, instead likely activating G_s protein directly (Carr et al., 2014). In an attempt to build on this previous work, five β_2AR-derived pepducins were selected for further characterisation in this study, ICL3-2, ICL3-7, ICL3-8, ICL3-9 and ICL1-15.

Changes in cytosolic cAMP concentrations were measured using the cAMP GloSensor^{TM} assay upon application of each pepducin to HEK293Gwt cells in an attempt to reproduce the findings of Carr et al. (2014), however despite several pepducins stimulating a statistically significant increase in cAMP above basal levels (ICL3-7, ICL3-8, ICL3-9 and ICL1-15, but not ICL3-2), the responses were all very small (mean responses up to approximately 6% of maximal isoprenaline response) and varied substantially between experimental repeats. The CRE-SPAP assay was then employed to measure amplified β_2AR-mediated gene transcription responses downstream of cAMP. Although some of the maximal pepducin responses were considerably larger (up to roughly 32% of maximal isoprenaline response) than in the GloSensor^{TM} assay, the CRE-SPAP responses were also even more inconsistent and only ICL3-8 produced a statistically significant increase in SPAP production over basal levels. These

responses were confirmed to be mediated through the β_2AR, because in CHO cells lacking β_2AR expression the responses were abolished entirely in each case. Due to the small and inconsistent nature of the pepducin responses, evidence that the pepducins could act as allosteric β_2AR agonists in this study was unconvincing. In both assays, the pepducins were also tested to determine whether they could alter the response of the orthosteric ligand isoprenaline. In GloSensor^{TM} each of the pepducins except ICL3-2 marginally increased the EC_{50} concentration isoprenaline peak response (indicative of some PAM activity at the β_2AR), whereas in CRE-SPAP there was a general trend toward inhibition of the isoprenaline response (statistically significant for ICL3-7 and ICL3-8, indicating NAM behaviour). Once again though, the most obvious effect of pepducin application was the introduction of considerable variation in the responses. Therefore, although there is some evidence that the pepducins are interacting with the β_2AR and interfering with agonist-mediated signal transduction, it has not been possible to classify any of the pepducins as either positive or negative allosteric modulators of the β_2AR from the data obtained in this study.

For future work attempting to elucidate the functional activity of β_2AR-derived pepducins, it may be sensible to initially replicate the ELISA-based cAMP experiments performed by Carr et al. (2014) under the same conditions (for example, in the presence of the PDE inhibitor IBMX). One plausible explanation for the findings in this study is that the pepducins may lack efficacy for traversing the cell membrane and thus cannot interact with the receptor's intracellular allosteric site. To investigate this, perhaps it would be useful to synthesize fluorescently labelled pepducin analogues, as has been done previously by Covic et al. (2002a), and perform FRET-based studies with a fluorescent donor tagged either to the intracellular side of the cell membrane or directly to the C-terminus of the β_2AR. This would enable determination of the presence of the pepducins at the intracellular side of the membrane or specifically at the allosteric site of the receptor, respectively. Alternatively, employing a fluorescent microscopy approach could allow visualisation of the fluorescently-tagged pepducins inside the cell.

Because functional assays did not provide conclusive evidence of pepducin allosteric activity at the β_2AR, binding studies were next performed to uncover pepducin interactions with the receptor. Using the thermoBRET assay, despite orthosteric ligands increasing DDM-solubilised β_2AR thermostability substantially (up to a 15 °C shift in β_2AR T_m value) which indicates ligand binding to the receptor (Hoare et al., 2023), none of the five pepducins had any effect on receptor thermostability. Even after the preincubation of formoterol with the receptor, application of pepducins still did not alter the measured nanoBRET signal, suggesting that the pepducins were unable to bind even to the stabilised active conformation of the receptor, which should increase the binding affinity of the pepducins since they were previously shown to act as allosteric agonists of the β_2AR (Carr et al., 2014). It is possible that the removal of the receptor from its native cell membrane and solubilisation into detergent micelles may disrupt the interaction with the pepducins. After translocating the cell membrane, pepducins are generally thought to remain anchored to the phospholipid bilayer via their N-terminal palmitate tag (Covic et al., 2002a; Carlson et al., 2012; Zhang et al., 2015b). This mechanism likely aids in localising pepducins in the vicinity of the receptor and may also improve pepducin-receptor binding affinity. Hence, distinct pepducin interactions with the differently structured detergent micelles may hinder their ability to interact with the β_2AR.

In membrane-based TR-FRET experiments, the impact of pepducins on the binding kinetics of firstly the fluorescently tagged tracer ligand, F-propranolol, and secondly an unlabelled competing ligand, formoterol, with the β_2AR were assessed. ICL3-7 increased the dissociation rate of F-propranolol at the β_2AR while ICL3-9 and ICL1-15 instead both increased the formoterol dissociation rate, suggesting possible PAM and NAM activity, respectively. In each case the ligand association rates were unaffected by the pepducins. Additionally, because of the relatively modest impact of the pepducins on ligand dissociation rates, neither the kinetic or equilibrium K_D values of F-propranolol or formoterol for the receptor were significantly modified. ICL3-2 and ICL3-8 did not alter any of the binding parameters of either ligand. In order to support the evidence of allosteric modulation found in this study, it would be useful to also evaluate the

effect of pepducin application on the binding kinetics of a whole range of agonists and inverse agonists to the β_2AR to determine whether induced changes in ligand dissociation rates consistently correlate with ligand activity (either agonist or inverse agonist) throughout.

It has not been possible in this study to directly confirm the binding of the pepducins to the β_2AR. One approach to directly determine pepducin-receptor binding that was used previously by Janz et al. (2011) involved the development of a $CXCR_4$ pepducin analogue by introduction of a photoactivatable leucine residue (photo-Leu) into the amino acid sequence which formed a covalent cross-link with the receptor upon UV-light application. Direct interaction between the receptor and the pepducin was subsequently confirmed by SDS-PAGE and in-gel fluorescence imaging because the pepducin also had a TAMRA fluorophore attached (Janz et al., 2011). Other effective (although time- and cost-intensive) methods to confirm binding between ligands and a receptor include structural studies such as x-ray crystallography or cryogenic electron microscopy (cryo-EM), which enable determination of three-dimensional receptor-ligand structures. To date, no cryo-EM or crystal structures of GPCRs bound to pepducins have been solved. Pepducins are a novel class of allosteric GPCR ligands which have shown promise as potential therapeutics in the future. Indeed, they may provide considerable advantages over orthosteric drugs due to the increased selectivity and lower toxicity associated with allosteric ligands (Christopoulos, 2002; May et al., 2007; Lane et al., 2017). β_2AR-dervied pepducins may become useful lead compounds in the development of improved asthma therapeutics, although in previous studies ICL3-derived G_s-biased β_2AR pepducins proved ineffective at reversing airway smooth muscle contraction (Panettieri et al., 2018). The inconclusive results from this study may also temper expectations of these peptide ligands becoming useful therapeutics, but regardless they remain useful tools to study GPCR (and more specifically, β_2AR) pharmacology.

7.2 – General conclusion

The β_2AR is a prototypical class A GPCR which represents an important therapeutic target, particularly due to its roles in pulmonary and cardiovascular physiology. This thesis has employed several techniques to address numerous aspects of β_2AR pharmacology, specifically agonist-mediated cAMP signalling kinetics, receptor mechanostimulation and the action of intracellular allosteric ligands called pepducins. Kinetic analysis of the full time-course of cAMP signalling responses under both low and high β_2AR expression conditions revealed important differences in pharmacological and kinetic agonist signalling parameters and can be used to provide a fuller picture of ligand activity. This work also highlighted the importance of considering receptor expression levels during ligand characterisation. Mechanical stimulation of the β_2AR initiated a transient cAMP response which could be potentiated by agonists or blocked by inverse agonists. Sensitivity to mechanostimulation was conferred by N-glycan chains attached to three sites on the extracellular receptor surface. β_2AR mechanotransduction may be important in mediating physiological processes in the vascular system such as vasodilation. The functional activity of pepducins at the β_2AR was difficult to characterise in this study due to the small and particularly variable nature of the signalling responses, but there was some evidence that several of the tested pepducins exhibited allosteric agonist activity. Additionally, although no evidence was found of pepducins interacting with the detergent-solubilised β_2AR, several pepducins did modify ligand dissociation rates from the β_2AR in homogenised native membranes, indicating possible allosteric modulation of orthosteric ligand binding to the receptor. It is hoped that the findings arising from this thesis have enhanced our understanding of different aspects of β_2-adrenoceptor pharmacology (and thus GPCR pharmacology more generally), which may eventually contribute towards the fundamental objective of developing novel therapeutics and improved treatments for diseases.

Chapter 8

Appendices and references

8.1 – Supplementary data

DNA insert	Amino acid sequence
HiBiT-β_2AR_N6A_N15A	MVSGWRLFKKISGSSGGSSGGSLGQPGAGSAFLLAPARSHAPDHDVTQQRDEVWVVGMGIVMSLIVLAIVFGNVLVITAIAKFERLQT VTNYFITSLACADLVMGLAVVPFGAAHILMKMWTFGNFWCEFWTSIDVLCVTASIETLCVIAVDRYFAITSPFKYQSLLTKNKARVIIL MVWIVSGLTSFLPIQMHWYRATHQEAINCYANETCCDFFTNQAYAIASSIVSFYVPLVIMVFVYSRVFQEAKRQLQKIDKSEGRFHVQN LSQVEQDGRTGHGLRRSSKFCLKEHKALKTLGIIMGTFTLCWLPFFIVNIVHVIQDNLIRKEVYILLNWIGYVNSGFNPLIYCRSPDFRIA FQELLCLRRSSLKAYGNGYSSNGNTGEQSGYHVEQEKENKLLCEDLPGTEDFVGHQGTVPSDNIDSQGRNCSTNDSLL
HiBiT-β_2AR_N6A_N15A_N187A	MVSGWRLFKKISGSSGGSSGGSLGQPGAGSAFLLAPARSHAPDHDVTQQRDEVWVVGMGIVMSLIVLAIVFGNVLVITAIAKFERLQT VTNYFITSLACADLVMGLAVVPFGAAHILMKMWTFGNFWCEFWTSIDVLCVTASIETLCVIAVDRYFAITSPFKYQSLLTKNKARVIIL MVWIVSGLTSFLPIQMHWYRATHQEAINCYAAETCCDFFTNQAYAIASSIVSFYVPLVIMVFVYSRVFQEAKRQLQKIDKSEGRFHVQN LSQVEQDGRTGHGLRRSSKFCLKEHKALKTLGIIMGTFTLCWLPFFIVNIVHVIQDNLIRKEVYILLNWIGYVNSGFNPLIYCRSPDFRIA FQELLCLRRSSLKAYGNGYSSNGNTGEQSGYHVEQEKENKLLCEDLPGTEDFVGHQGTVPSDNIDSQGRNCSTNDSLL

Supplementary Table 8.1: Translated amino acid sequences of the mutated HiBiT-β_2AR DNA insert fragments, with the HiBiT tag highlighted in blue, linker in black, the β_2AR in green and the mutated nucleotide bases in red.

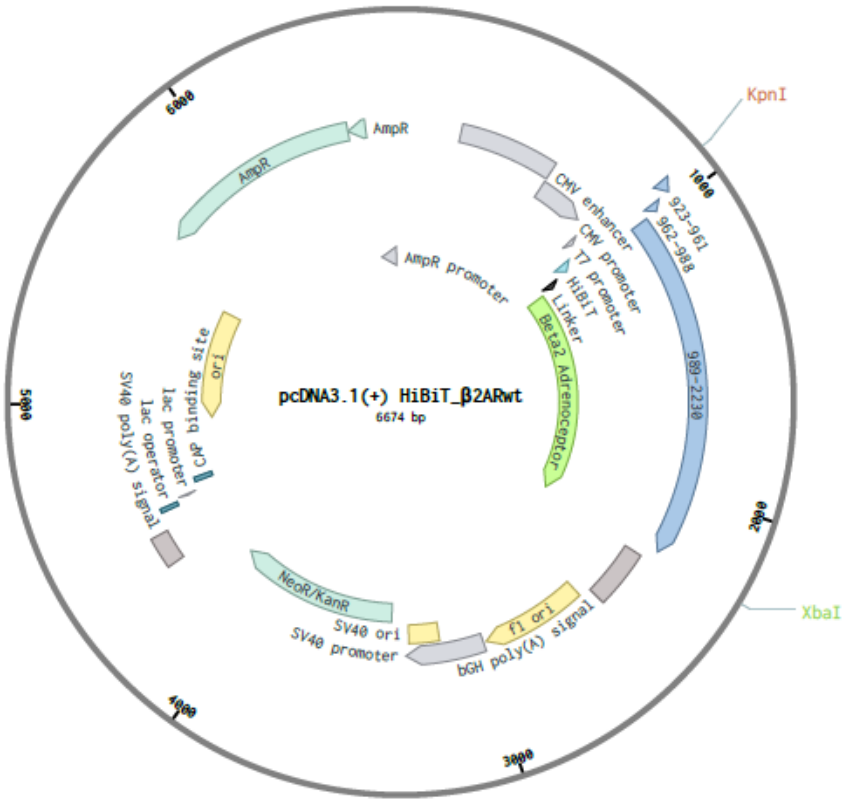

Supplementary Figure 8.1: Sequence map of the pcDNA3.1(+) HiBiT_β_2ARwt plasmid. The main features are displayed, including the HiBiT, linker and β_2AR regions, as well as the KpnI and XbaI endonuclease restriction sites and an ampicillin resistance gene. This image was obtained from Benchling.

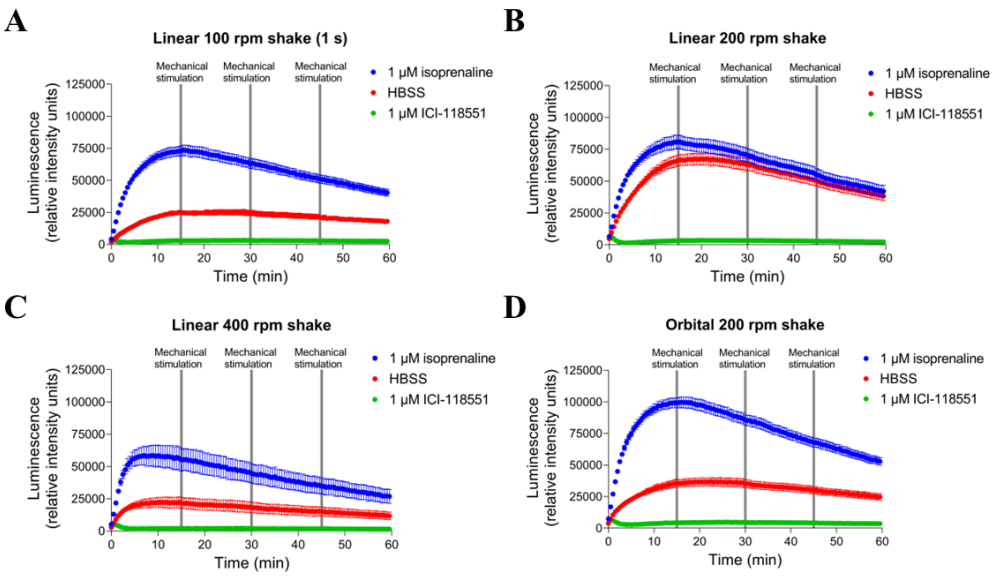

Supplementary Figure 8.2: GloSensor™ luminescence stimulated by cAMP production. (A-D) Combined GloSensor™ luminescence time-course data over 60 min following application of isoprenaline (1 µM), HBSS or ICI-118551 (1 µM) and different sequential mechanical stimuli (at 0 min, 15 min, 30 min and 45 min): 1 s linear 100 rpm shake (A), 5 s linear 200 rpm shake (B), 5 s linear 400 rpm shake (C) and 5 s orbital 200 rpm shake (D) to HEK293G-β_2AR cells. Data points represent mean ± SEM of triplicate measurements expressed as relative intensity units (RIU) of luminescence, from one experiment (n = 1).

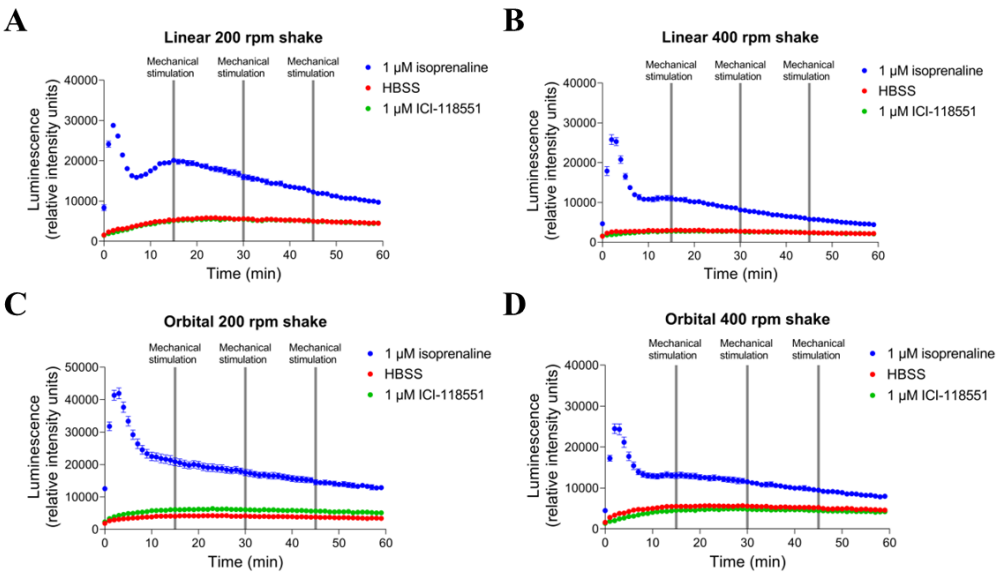

Supplementary Figure 8.3: GloSensor™ luminescence stimulated by cAMP production. (A-D) Combined GloSensor™ luminescence time-course data over 60 min following application of isoprenaline (1 µM), HBSS or ICI-118551 (1 µM) and different sequential mechanical stimuli (at 0 min, 15 min, 30 min and 45 min): 5 s linear 200 rpm shake (A), 5 s linear 400 rpm shake (B), 5 s orbital 200 rpm shake (C) and 5 s orbital 400 rpm shake (D) to HEK293Gwt cells. Data points represent mean ± SEM of triplicate measurements expressed as relative intensity units (RIU) of luminescence, from one experiment (n = 1).

8.2 – References

Aceto, J. F. & Baker, K. M. 1990. [Sar1]angiotensin II receptor-mediated stimulation of protein synthesis in chick heart cells. *American Journal of Physiology-Heart and Circulatory Physiology,* 258**,** H806-H813.

Aebi, M. 2013. N-linked protein glycosylation in the ER. *Biochimica et Biophysica Acta (BBA) - Molecular Cell Research,* 1833**,** 2430-2437.

Aebi, M., Bernasconi, R., Clerc, S. & Molinari, M. 2010. N-glycan structures: recognition and processing in the ER. *Trends in Biochemical Sciences,* 35**,** 74-82.

Agarwal, A., Covic, L., Sevigny, L. M., Kaneider, N. C., Lazarides, K., Azabdaftari, G., Sharifi, S. & Kuliopulos, A. 2008. Targeting a metalloprotease-PAR1 signaling system with cell-penetrating pepducins inhibits angiogenesis, ascites, and progression of ovarian cancer. *Molecular Cancer Therapeutics,* 7**,** 2746-2757.

Ahlquist, R. P. 1948. A study of the adrenotropic receptors. *American Journal of Physiology-Legacy Content,* 153**,** 586-600.

Ahn, S., Kahsai, A. W., Pani, B., Wang, Q. T., Zhao, S., Wall, A. L., Strachan, R. T., Staus, D. P., Wingler, L. M., Sun, L. D., Sinnaeve, J., Choi, M., Cho, T., Xu, T. T., Hansen, G. M., Burnett, M. B., Lamerdin, J. E., Bassoni, D. L., Gavino, B. J., Husemoen, G., Olsen, E. K., Franch, T., Costanzi, S., Chen, X. & Lefkowitz, R. J. 2017. Allosteric "beta-blocker" isolated from a DNA-encoded small molecule library. *Proceedings of the National Academy of Sciences of the United States of America,* 114**,** 1708-1713.

Ahn, S., Pani, B., Kahsai, A. W., Olsen, E. K., Husemoen, G., Vestergaard, M., Jin, L., Zhao, S., Wingler, L. M., Rambarat, P. K., Simhal, R. K., Xu, T. T., Sun, L. D., Shim, P. J., Staus, D. P., Huang, L. Y., Franch, T., Chen,

X. & Lefkowitz, R. J. 2018. Small-Molecule Positive Allosteric Modulators of the beta2-Adrenoceptor Isolated from DNA-Encoded Libraries. *Molecular Pharmacology,* 94**,** 850-861.

Aiello, E. A., Malcolm, A. T., Walsh, M. P. & Cole, W. C. 1998. β-Adrenoceptor activation and PKA regulate delayed rectifier K+ channels of vascular smooth muscle cells. *American Journal of Physiology-Heart and Circulatory Physiology,* 275**,** H448-H459.

Akinaga, J., García-Sáinz, J. A. & S. Pupo, A. 2019. Updates in the function and regulation of α1-adrenoceptors. *British Journal of Pharmacology,* 176**,** 2343-2357.

Alexander, S. P., Christopoulos, A., Davenport, A. P., Kelly, E., Marrion, N. V., Peters, J. A., Faccenda, E., Harding, S. D., Pawson, A. J., Sharman, J. L., Southan, C. & Davies, J. A. 2017. The concise guide to pharmacology 2017/18: G protein-coupled receptors. *British Journal of Pharmacology,* 174**,** S17-S129.

Alexandrov, A. I., Mileni, M., Chien, E. Y. T., Hanson, M. A. & Stevens, R. C. 2008. Microscale Fluorescent Thermal Stability Assay for Membrane Proteins. *Structure,* 16**,** 351-359.

Ammit, A. J., Hoffman, R. K., Amrani, Y., Lazaar, A. L., Hay, D. W. P., Torphy, T. J., Penn, R. B. & Panettieri, R. A. 2000. Tumor Necrosis Factor- α – Induced Secretion of RANTES and Interleukin-6 from Human Airway Smooth-Muscle Cells. *American Journal of Respiratory Cell and Molecular Biology,* 23**,** 794-802.

Amrani, Y. & Panettieri, R. A. 2003. Airway smooth muscle: contraction and beyond. *The International Journal of Biochemistry & Cell Biology,* 35**,** 272-276.

An, H. J., Froehlich, J. W. & Lebrilla, C. B. 2009. Determination of glycosylation sites and site-specific heterogeneity in glycoproteins. *Current Opinion in Chemical Biology,* 13**,** 421-426.

An, K., Zhu, X. & Bai, C. 2022. The Nature of Functional Features of Different Classes of G-Protein-Coupled Receptors. *Biology,* 11**,** 1839.

An, S. S., Bai, T. R., Bates, J. H. T., Black, J. L., Brown, R. H., Brusasco, V., Chitano, P., Deng, L., Dowell, M., Eidelman, D. H., Fabry, B., Fairbank, N. J., Ford, L. E., Fredberg, J. J., Gerthoffer, W. T., Gilbert, S. H., Gosens, R., Gunst, S. J., Halayko, A. J., Ingram, R. H., Irvin, C. G., James, A. L., Janssen, L. J., King, G. G., Knight, D. A., Lauzon, A. M., Lakser, O. J., Ludwig, M. S., Lutchen, K. R., Maksym, G. N., Martin, J. G., Mauad, T., Mcparland, B. E., Mijailovich, S. M., Mitchell, H. W., Mitchell, R. W., Mitzner, W., Murphy, T. M., Paré, P. D., Pellegrino, R., Sanderson, M. J., Schellenberg, R. R., Seow, C. Y., Silveira, P. S. P., Smith, P. G., Solway, J., Stephens, N. L., Sterk, P. J., Stewart, A. G., Tang, D. D., Tepper, R. S., Tran, T. & Wang, L. 2007. Airway smooth muscle dynamics: a common pathway of airway obstruction in asthma. *European Respiratory Journal,* 29**,** 834-860.

Anantharaman, V., Abhiman, S., De Souza, R. F. & Aravind, L. 2011. Comparative genomics uncovers novel structural and functional features of the heterotrimeric GTPase signaling system. *Gene,* 475**,** 63-78.

Andersson, K.-E., Lepor, H. & Wyllie, M. G. 1997. Prostatic α1-adrenoceptors and uroselectivity. *The Prostate,* 30**,** 202-215.

Arachea, B. T., Sun, Z., Potente, N., Malik, R., Isailovic, D. & Viola, R. E. 2012. Detergent selection for enhanced extraction of membrane proteins. *Protein Expression and Purification,* 86**,** 12-20.

Archer, M., Dogra, N., Dovey, Z., Ganta, T., Jang, H. S., Khusid, J. A., Lantz, A., Mihalopoulos, M., Stockert, J. A., Zahalka, A., Björnebo, L., Gaglani,

S., Noh, M. R., Kaplan, S. A., Mehrazin, R., Badani, K. K., Wiklund, P., Tsao, K., Lundon, D. J., Mohamed, N., Lucien, F., Padanilam, B., Gupta, M., Tewari, A. K. & Kyprianou, N. 2021. Role of α- and β-adrenergic signaling in phenotypic targeting: significance in benign and malignant urologic disease. *Cell Communication and Signaling,* 19**,** 78.

Ariens, E., Van Rossum, J. & Simonis, A. 1956. A theoretical basis of molecular pharmacology. I. Interactions of one or two compounds with one receptor system. *Arzneimittel-Forschung,* 6**,** 282-293.

Arunlakshana, O. & Schild, H. O. 1959. Some quantitative uses of drug antagonists. *British Journal of Pharmacology and Chemotherapy,* 14**,** 48-58.

Attramadal, H., Arriza, J. L., Aoki, C., Dawson, T. M., Codina, J., Kwatra, M. M., Snyder, S. H., Caron, M. G. & Lefkowitz, R. J. 1992. Beta-arrestin2, a novel member of the arrestin/beta-arrestin gene family. *Journal of Biological Chemistry,* 267**,** 17882-17890.

Azevedo Neto, J., Costanzini, A., De Giorgio, R., Lambert, D. G., Ruzza, C. & Calò, G. 2020. Biased versus Partial Agonism in the Search for Safer Opioid Analgesics. *Molecules,* 25**,** 3870.

Azzi, M., Charest, P. G., Angers, S., Rousseau, G., Kohout, T., Bouvier, M. & Piñeyro, G. 2003. β-arrestin-mediated activation of MAPK by inverse agonists reveals distinct active conformations for G protein-coupled receptors. *Proceedings of the National Academy of Sciences of the United States of America,* 100**,** 11406-11411.

Azzi, M., Piñeyro, G., Pontier, S., Parent, S., Ansanay, H. & Bouvier, M. 2001. Allosteric Effects of G Protein Overexpression on the Binding of β-Adrenergic Ligands with Distinct Inverse Efficacies. *Molecular Pharmacology,* 60**,** 999-1007.

Bai, T. R. 1992. Beta2 adrenergic receptors in asthma: A current perspective. *Lung,* 170**,** 125-141.

Baker, J. G. 2005. The selectivity of β-adrenoceptor antagonists at the human β1, β2 and β3 adrenoceptors. *British Journal of Pharmacology,* 144**,** 317-322.

Baker, J. G. 2010. The selectivity of β-adrenoceptor agonists at human β1-, β2- and β3-adrenoceptors. *British Journal of Pharmacology,* 160**,** 1048-1061.

Baker, J. G., Adams, L. A., Salchow, K., Mistry, S. N., Middleton, R. J., Hill, S. J. & Kellam, B. 2011. Synthesis and characterization of high-affinity 4,4-difluoro-4-bora-3a,4a-diaza-s-indacene-labeled fluorescent ligands for human β-adrenoceptors. *Journal of Medicinal Chemistry,* 54**,** 6874-6887.

Baker, J. G., Hall, I. P. & Hill, S. J. 2003a. Agonist and Inverse Agonist Actions of β-Blockers at the Human β2-Adrenoceptor Provide Evidence for Agonist-Directed Signaling. *Molecular Pharmacology,* 64**,** 1357-1369.

Baker, J. G., Hall, I. P. & Hill, S. J. 2003b. Influence of Agonist Efficacy and Receptor Phosphorylation on Antagonist Affinity Measurements: Differences between Second Messenger and Reporter Gene Responses. *Molecular Pharmacology,* 64**,** 679-688.

Baker, J. G., Hall, I. P. & Hill, S. J. 2004. Temporal Characteristics of cAMP Response Element-Mediated Gene Transcription: Requirement for Sustained cAMP Production. *Molecular Pharmacology,* 65**,** 986-998.

Baker, J. G., Proudman, R. G. W. & Hill, S. J. 2015. Salmeterol's Extreme β2 Selectivity Is Due to Residues in Both Extracellular Loops and Transmembrane Domains. *Molecular Pharmacology,* 87**,** 103-120.

Ballesteros, J. A. & Weinstein, H. 1995. [19] Integrated methods for the construction of three-dimensional models and computational probing of

structure-function relations in G protein-coupled receptors. *In:* Sealfon, S. C. (ed.) *Methods in Neurosciences.* Academic Press**,** 366-428.

Bang, I. & Choi, H. J. 2015. Structural features of β2 adrenergic receptor: crystal structures and beyond. *Molecules and cells,* 38**,** 105-111.

Barbato, E. 2009. Role of adrenergic receptors in human coronary vasomotion. *Heart,* 95**,** 603-608.

Barbosa, J. A., Santos-Aguado, J., Mentzer, S. J., Strominger, J. L., Burakoff, S. J. & Biro, P. A. 1987. Site-directed mutagenesis of class I HLA genes. Role of glycosylation in surface expression and functional recognition. *Journal of Experimental Medicine,* 166**,** 1329-1350.

Barnes, P. J. 1993. β-adrenoceptors on smooth muscle, nerves and inflammatory cells. *Life Sciences,* 52**,** 2101-2109.

Barnes, P. J. 1998. Pharmacology of Airway Smooth Muscle. *American Journal of Respiratory and Critical Care Medicine,* 158**,** S123-S132.

Bartlett, J. M. S. & Stirling, D. 2003. A Short History of the Polymerase Chain Reaction. *In:* Bartlett, J. M. S. & Stirling, D. (eds.) *PCR Protocols.* Totowa, NJ: Humana Press**,** 3-6.

Barwich, A.-S. & Bschir, K. 2017. The manipulability of what? The history of G-protein coupled receptors. *Biology & Philosophy,* 32**,** 1317-1339.

Bdioui, S., Verdi, J., Pierre, N., Trinquet, E., Roux, T. & Kenakin, T. 2018. Equilibrium Assays Are Required to Accurately Characterize the Activity Profiles of Drugs Modulating Gq-Protein-Coupled Receptors. *Molecular Pharmacology,* 94**,** 992-1006.

Beasley, R., Pearce, N., Crane, J. & Burgess, C. 1999. β agonists: What is the evidence that their use increases the risk of asthma morbidity and

mortality? *The Journal of Allergy and Clinical Immunology,* 104**,** S18-S30.

Beeh, K. M., Derom, E., Kanniess, F., Cameron, R., Higgins, M. & Van As, A. 2007. Indacaterol, a novel inhaled 2-agonist, provides sustained 24-h bronchodilation in asthma. *The European Respiratory Journal,* 29**,** 871-878.

Bendich, A., Machlin, L. J., Scandurra, O., Burton, G. W. & Wayner, D. D. M. 1986. The antioxidant role of vitamin C. *Advances in Free Radical Biology & Medicine,* 2**,** 419-444.

Benkel, T., Zimmermann, M., Zeiner, J., Bravo, S., Merten, N., Lim, V. J. Y., Matthees, E. S. F., Drube, J., Miess-Tanneberg, E., Malan, D., Szpakowska, M., Monteleone, S., Grimes, J., Koszegi, Z., Lanoiselée, Y., O'brien, S., Pavlaki, N., Dobberstein, N., Inoue, A., Nikolaev, V., Calebiro, D., Chevigné, A., Sasse, P., Schulz, S., Hoffmann, C., Kolb, P., Waldhoer, M., Simon, K., Gomeza, J. & Kostenis, E. 2022. How Carvedilol activates β2-adrenoceptors. *Nature Communications,* 13**,** 7109.

Benovic, J. L., Strasser, R. H., Caron, M. G. & Lefkowitz, R. J. 1986. Beta-adrenergic receptor kinase: identification of a novel protein kinase that phosphorylates the agonist-occupied form of the receptor. *Proceedings of the National Academy of Sciences of the United States of America,* 83**,** 2797-2801.

Berg, K. A. & Clarke, W. P. 2018. Making Sense of Pharmacology: Inverse Agonism and Functional Selectivity. *International Journal of Neuropsychopharmacology,* 21**,** 962-977.

Berg, K. A., Stout, B. D., Cropper, J. D., Maayani, S. & Clarke, W. P. 1999. Novel Actions of Inverse Agonists on 5-HT2C Receptor Systems. *Molecular Pharmacology,* 55**,** 863-872.

Bergsdorf, C., Fiez-Vandal, C., Sykes, D. A., Bernet, P., Aussenac, S., Charlton, S. J., Schopfer, U., Ottl, J. & Duckely, M. 2016. An Alternative Thiol-Reactive Dye to Analyze Ligand Interactions with the Chemokine Receptor CXCR2 Using a New Thermal Shift Assay Format. *SLAS Discovery,* 21**,** 243-251.

Berman, D. M., Wilkie, T. M. & Gilman, A. G. 1996. GAIP and RGS4 Are GTPase-Activating Proteins for the Gi Subfamily of G Protein α Subunits. *Cell,* 86**,** 445-452.

Berridge, C. W., Schmeichel, B. E. & España, R. A. 2012. Noradrenergic modulation of wakefulness/arousal. *Sleep Medicine Reviews,* 16**,** 187-197.

Berridge, C. W., Stellick, R. L. & Schmeichel, B. E. 2005. Wake-Promoting Actions of Medial Basal Forebrain β_2 Receptor Stimulation. *Behavioral Neuroscience,* 119**,** 743-751.

Berthelsen, S. & Pettinger, W. A. 1977. A functional basis for classification of α-adrenergic receptors. *Life Sciences,* 21**,** 595-606.

Bieberich, E. 2014. Synthesis, Processing, and Function of N-glycans in N-glycoproteins. *Advances in Neurobiology,* 9**,** 47-70.

Billington, C. K. & Hall, I. P. 2012. Novel cAMP signalling paradigms: therapeutic implications for airway disease. *British Journal of Pharmacology,* 166**,** 401-410.

Billington, C. K., Ojo, O. O., Penn, R. B. & Ito, S. 2013. cAMP regulation of airway smooth muscle function. *Pulmonary Pharmacology & Therapeutics,* 26**,** 112-120.

Billington, C. K. & Penn, R. B. 2003. Signaling and regulation of G protein-coupled receptors in airway smooth muscle. *Respiratory Research,* 4**,** 4.

Binkowski, B. F., Butler, B. L., Stecha, P. F., Eggers, C. T., Otto, P., Zimmerman, K., Vidugiris, G., Wood, M. G., Encell, L. P., Fan, F. & Wood, K. V. 2011. A Luminescent Biosensor with Increased Dynamic Range for Intracellular cAMP. *ACS Chemical Biology,* 6**,** 1193-1197.

Birnboim, H. C. & Doly, J. 1979. A rapid alkaline extraction procedure for screening recombinant plasmid DNA. *Nucleic Acids Research,* 7**,** 1513-1523.

Black, J. B., Premont, R. T. & Daaka, Y. 2016. Feedback regulation of G protein-coupled receptor signaling by GRKs and arrestins. *Seminars in Cell & Developmental Biology,* 50**,** 95-104.

Black, J. W., Duncan, W. A. & Shanks, R. G. 1965. Comparison of some properties of pronethalol and propranolol. *British Journal of Pharmacology and Chemotherapy,* 25**,** 577-591.

Black, J. W., Duncan, W. a. M., Durant, C. J., Ganellin, C. R. & Parsons, E. M. 1972. Definition and Antagonism of Histamine H2-receptors. *Nature,* 236**,** 385-390.

Black, J. W. & Leff, P. 1983. Operational models of pharmacological agonism. *Proceedings of the Royal Society of London. Series B. Biological Sciences,* 220**,** 141-162.

Boesenberg-Smith, K. A., Pessarakli, M. M. & Wolk, D. M. 2012. Assessment of DNA Yield and Purity: an Overlooked Detail of PCR Troubleshooting. *Clinical Microbiology Newsletter,* 34**,** 1-6.

Bootman, M. D. 2012. Calcium Signaling. *Cold Spring Harbor Perspectives in Biology,* 4**,** a011171-a011171.

Bosma, R., Mocking, T. a. M., Leurs, R. & Vischer, H. F. 2017. Ligand-Binding Kinetics on Histamine Receptors. *In:* Tiligada, E. & Ennis, M. (eds.)

Histamine Receptors as Drug Targets. New York, NY: Springer New York**,** 115-155.

Boussif, O., Lezoualc'h, F., Zanta, M. A., Mergny, M. D., Scherman, D., Demeneix, B. & Behr, J. P. 1995. A versatile vector for gene and oligonucleotide transfer into cells in culture and in vivo: polyethylenimine. *Proceedings of the National Academy of Sciences,* 92**,** 7297-7301.

Boyer, J. L., Waldo, G. L. & Harden, T. K. 1992. Beta gamma-subunit activation of G-protein-regulated phospholipase C. *Journal of Biological Chemistry,* 267**,** 25451-25456.

Braakman, I. & Hebert, D. N. 2013. Protein Folding in the Endoplasmic Reticulum. *Cold Spring Harbor Perspectives in Biology,* 5**,** a013201-a013201.

Brodde, O.-E. 1993. Beta-adrenoceptors in cardiac disease. *Pharmacology & Therapeutics,* 60**,** 405-430.

Brookman, L. J., Knowles, L. J., Barbier, M., Elharrar, B., Fuhr, R. & Pascoe, S. 2007. Efficacy and safety of single therapeutic and supratherapeutic doses of indacaterol versus salmeterol and salbutamol in patients with asthma. *Current Medical Research and Opinion,* 23**,** 3113-3122.

Brouillette, R. L., Besserer-Offroy, É., Mona, C. E., Chartier, M., Lavenus, S., Sousbie, M., Belleville, K., Longpré, J.-M., Marsault, É., Grandbois, M. & Sarret, P. 2020. Cell-penetrating pepducins targeting the neurotensin receptor type 1 relieve pain. *Pharmacological Research,* 155**,** 104750.

Buchwald, P. 2017. A three-parameter two-state model of receptor function that incorporates affinity, efficacy, and signal amplification. *Pharmacology Research & Perspectives,* 5**,** e00311.

Busch, R., Strohbach, A., Pennewitz, M., Lorenz, F., Bahls, M., Busch, M. C. & Felix, S. B. 2015. Regulation of the endothelial apelin/APJ system by hemodynamic fluid flow. *Cellular Signalling,* 27**,** 1286-1296.

Bylund, D. B. 2007. Alpha- and beta-adrenergic receptors: Ahlquist's landmark hypothesis of a single mediator with two receptors. *American Journal of Physiology-Endocrinology and Metabolism,* 293**,** E1479-E1481.

Cabrera-Vera, T. M., Vanhauwe, J., Thomas, T. O., Medkova, M., Preininger, A., Mazzoni, M. R. & Hamm, H. E. 2003. Insights into G Protein Structure, Function, and Regulation. *Endocrine Reviews,* 24**,** 765-781.

Cai, X., Madari, S., Walker, A., Paiva, A., Li, Y., Herbst, J., Shou, W. & Weller, H. 2019. Addition of Optimized Bovine Serum Albumin Level in a High-Throughput Caco-2 Assay Enabled Accurate Permeability Assessment for Lipophilic Compounds. *SLAS Discovery : Advancing the Science of Drug Discovery,* 24**,** 738-744.

Calebiro, D., Nikolaev, V. O., Gagliani, M. C., De Filippis, T., Dees, C., Tacchetti, C., Persani, L. & Lohse, M. J. 2009. Persistent cAMP-Signals Triggered by Internalized G-Protein–Coupled Receptors. *PLoS Biology,* 7**,** e1000172.

Cantor, R. S. 1997. Lateral Pressures in Cell Membranes: A Mechanism for Modulation of Protein Function. *The Journal of Physical Chemistry B,* 101**,** 1723-1725.

Carlson, K. E., Mcmurry, T. J. & Hunt, S. W. 2012. Pepducins: lipopeptide allosteric modulators of GPCR signaling. *Drug Discovery Today: Technologies,* 9**,** e33-e39.

Carr, R., 3rd, Du, Y., Quoyer, J., Panettieri, R. A., Jr., Janz, J. M., Bouvier, M., Kobilka, B. K. & Benovic, J. L. 2014. Development and characterization

of pepducins as Gs-biased allosteric agonists. *The Journal of Biological Chemistry,* 289**,** 35668-35684.

Carr, R., Koziol-White, C., Zhang, J., Lam, H., An, S. S., Tall, G. G., Panettieri, R. A. & Benovic, J. L. 2016a. Interdicting Gq Activation in Airway Disease by Receptor-Dependent and Receptor-Independent Mechanisms. *Molecular Pharmacology,* 89**,** 94-104.

Carr, R., Schilling, J., Song, J., Carter, R. L., Du, Y., Yoo, S. M., Traynham, C. J., Koch, W. J., Cheung, J. Y., Tilley, D. G. & Benovic, J. L. 2016b. β-arrestin–biased signaling through the β2-adrenergic receptor promotes cardiomyocyte contraction. *Proceedings of the National Academy of Sciences,* 113**,** E4107-E4116.

Carter, A. A. & Hill, S. J. 2005. Characterization of Isoprenaline- and Salmeterol-Stimulated Interactions between β2-Adrenoceptors and β-Arrestin 2 Using β-Galactosidase Complementation in C2C12 Cells. *Journal of Pharmacology and Experimental Therapeutics,* 315**,** 839-848.

Cassinotti, P. & Weitz, M. 1994. Increasing the sensitivity of a common CAT assay. *BioTechniques,* 17**,** 36, 38, 40.

Cerione, R. A., Codina, J., Benovic, J. L., Lefkowitz, R. J., Birnbaumer, L. & Caron, M. G. 1984a. Mammalian .beta.2-adrenergic receptor: reconstitution of functional interactions between pure receptor and pure stimulatory nucleotide binding protein of the adenylate cyclase system. *Biochemistry,* 23**,** 4519-4525.

Cerione, R. A., Sibley, D. R., Codina, J., Benovic, J. L., Winslow, J., Neer, E. J., Birnbaumer, L., Caron, M. G. & Lefkowitz, R. J. 1984b. Reconstitution of a hormone-sensitive adenylate cyclase system. The pure beta-adrenergic receptor and guanine nucleotide regulatory protein confer hormone responsiveness on the resolved catalytic unit. *Journal of Biological Chemistry,* 259**,** 9979-9982.

Chachisvilis, M., Zhang, Y.-L. & Frangos, J. A. 2006. G protein-coupled receptors sense fluid shear stress in endothelial cells. *Proceedings of the National Academy of Sciences,* 103**,** 15463-15468.

Chae, P. S., Rasmussen, S. G. F., Rana, R. R., Gotfryd, K., Chandra, R., Goren, M. A., Kruse, A. C., Nurva, S., Loland, C. J., Pierre, Y., Drew, D., Popot, J.-L., Picot, D., Fox, B. G., Guan, L., Gether, U., Byrne, B., Kobilka, B. & Gellman, S. H. 2010. Maltose–neopentyl glycol (MNG) amphiphiles for solubilization, stabilization and crystallization of membrane proteins. *Nature Methods,* 7**,** 1003-1008.

Chakroborty, D., Sarkar, C., Basu, B., Dasgupta, P. S. & Basu, S. 2009. Catecholamines Regulate Tumor Angiogenesis. *Cancer Research,* 69**,** 3727-3730.

Chalfie, M. 2009. Neurosensory mechanotransduction. *Nature Reviews Molecular Cell Biology,* 10**,** 44-52.

Chan, H. C. S., Filipek, S. & Yuan, S. 2016. The Principles of Ligand Specificity on beta-2-adrenergic receptor. *Scientific Reports,* 6**,** 34736.

Chang, A., Le, C. P., Walker, A. K., Creed, S. J., Pon, C. K., Albold, S., Carroll, D., Halls, M. L., Lane, J. R., Riedel, B., Ferrari, D. & Sloan, E. K. 2016. β2-Adrenoceptors on tumor cells play a critical role in stress-enhanced metastasis in a mouse model of breast cancer. *Brain, Behavior, and Immunity,* 57**,** 106-115.

Chanrion, B., Cour, C. M. L., Gavarini, S., Seimandi, M., Vincent, L., Pujol, J.-F., Bockaert, J., Marin, P. & Millan, M. J. 2008. Inverse Agonist and Neutral Antagonist Actions of Antidepressants at Recombinant and Native 5-Hydroxytryptamine2C Receptors: Differential Modulation of Cell Surface Expression and Signal Transduction. *Molecular Pharmacology,* 73**,** 748-757.

Charlton, S. J. & Vauquelin, G. 2010. Elusive equilibrium: the challenge of interpreting receptor pharmacology using calcium assays. *British Journal of Pharmacology,* 161**,** 1250-1265.

Chen, C. Y., Dion, S. B., Kim, C. M. & Benovic, J. L. 1993. Beta-adrenergic receptor kinase. Agonist-dependent receptor binding promotes kinase activation. *Journal of Biological Chemistry,* 268**,** 7825-7831.

Chen, D., Dang, H. & Patrick, J. W. 1998. Contributions of N-Linked Glycosylation to the Expression of a Functional α7-Nicotinic Receptor in Xenopus Oocytes. *Journal of Neurochemistry,* 70**,** 349-357.

Chen, K. M., Keri, D. & Barth, P. 2020. Computational design of G Protein-Coupled Receptor allosteric signal transductions. *Nature Chemical Biology,* 16**,** 77-86.

Cheng, J. & Grande, J. P. 2007. Cyclic nucleotide phosphodiesterase (PDE) inhibitors: novel therapeutic agents for progressive renal disease. *Experimental Biology and Medicine (Maywood),* 232**,** 38-51.

Cheng, Y.-C. & Prusoff, W. H. 1973. Relationship between the inhibition constant (KI) and the concentration of inhibitor which causes 50 per cent inhibition (I50) of an enzymatic reaction. *Biochemical Pharmacology,* 22**,** 3099-3108.

Cherezov, V., Rosenbaum, D. M., Hanson, M. A., Rasmussen, S. G. F., Thian, F. S., Kobilka, T. S., Choi, H. J., Kuhn, P., Weis, W. I., Kobilka, B. K. & Stevens, R. C. 2007. High-Resolution Crystal Structure of an Engineered Human 2-Adrenergic G Protein-Coupled Receptor. *Science,* 318**,** 1258-1265.

Chidiac, P., Hebert, T. E., Valiquette, M., Dennis, M. & Bouvier, M. 1994. Inverse agonist activity of beta-adrenergic antagonists. *Molecular Pharmacology,* 45**,** 490-499.

Chin, K.-V., Yang, W.-L., Ravatn, R., Kita, T., Reitman, E., Vettori, D., Cvijic, M. E., Shin, M. & Iacono, L. 2002. Reinventing the Wheel of Cyclic AMP. *Annals of the New York Academy of Sciences,* 968**,** 49-64.

Chistiakov, D. A., Orekhov, A. N. & Bobryshev, Y. V. 2017. Effects of shear stress on endothelial cells: go with the flow. *Acta Physiologica,* 219**,** 382-408.

Chotani, M. A., Mitra, S., Su, B. Y., Flavahan, S., Eid, A. H., Clark, K. R., Montague, C. R., Paris, H., Handy, D. E. & Flavahan, N. A. 2004. Regulation of α2-adrenoceptors in human vascular smooth muscle cells. *American Journal of Physiology-Heart and Circulatory Physiology,* 286**,** H59-H67.

Christopoulos, A. 2002. Allosteric binding sites on cell-surface receptors: novel targets for drug discovery. *Nature Reviews Drug Discovery,* 1**,** 198-210.

Christopoulos, A., Changeux, J. P., Catterall, W. A., Fabbro, D., Burris, T. P., Cidlowski, J. A., Olsen, R. W., Peters, J. A., Neubig, R. R., Pin, J. P., Sexton, P. M., Kenakin, T. P., Ehlert, F. J., Spedding, M. & Langmead, C. J. 2014. International Union of Basic and Clinical Pharmacology. XC. Multisite Pharmacology: Recommendations for the Nomenclature of Receptor Allosterism and Allosteric Ligands. *Pharmacological Reviews,* 66**,** 918-947.

Christopoulos, A. & Kenakin, T. 2002. G Protein-Coupled Receptor Allosterism and Complexing. *Pharmacological Reviews,* 54**,** 323-374.

Christopoulos, A., Parsons, A. M., Lew, M. J. & El-Fakahany, E. E. 1999. The assessment of antagonist potency under conditions of transient response kinetics. *European Journal of Pharmacology,* 382**,** 217-227.

Cipolletta, E., Del Giudice, C., Santulli, G., Trimarco, B. & Iaccarino, G. 2017. Opposite effects of β2-adrenoceptor gene deletion on insulin signaling in

liver and skeletal muscle. *Nutrition, Metabolism and Cardiovascular Diseases,* 27**,** 615-623.

Cisowski, J., O'callaghan, K., Kuliopulos, A., Yang, J., Nguyen, N., Deng, Q., Yang, E., Fogel, M., Tressel, S., Foley, C., Agarwal, A., Hunt, S. W., Iii, Mcmurry, T., Brinckerhoff, L. & Covic, L. 2011. Targeting Protease-Activated Receptor-1 with Cell-Penetrating Pepducins in Lung Cancer. *The American Journal of Pathology,* 179**,** 513-523.

Clapham, D. E. & Neer, E. J. 1997. G protein βγ subunits. *Annual Review of Pharmacology and Toxicology,* 37**,** 167-203.

Clark, R. B., Allal, C., Friedman, J., Johnson, M. & Barber, R. 1996. Stable activation and desensitization of beta 2-adrenergic receptor stimulation of adenylyl cyclase by salmeterol: evidence for quasi-irreversible binding to an exosite. *Molecular Pharmacology,* 49**,** 182-189.

Clarkson, M. W., Gilmore, S. A., Edgell, M. H. & Lee, A. L. 2006. Dynamic Coupling and Allosteric Behavior in a Nonallosteric Protein. *Biochemistry,* 45**,** 7693-7699.

Congreve, M., De Graaf, C., Swain, N. A. & Tate, C. G. 2020. Impact of GPCR Structures on Drug Discovery. *Cell,* 181**,** 81-91.

Conn, P. J., Christopoulos, A. & Lindsley, C. W. 2009. Allosteric modulators of GPCRs: a novel approach for the treatment of CNS disorders. *Nature Reviews Drug Discovery,* 8**,** 41-54.

Connolly, B. J., Willits, P. B., Warrington, B. H. & Murray, K. J. 1992. 8-(4-Chlorophenyl)thio-cyclic AMP is a potent inhibitor of the cyclic GMP-specific phosphodiesterase (PDE VA). *Biochemical Pharmacology,* 44**,** 2303-2306.

Cooper, J., Hill, S. J. & Alexander, S. P. H. 1997. An endogenous A2B adenosine receptor coupled to cyclic AMP generation in human embryonic kidney (HEK 293) cells. *British Journal of Pharmacology,* 122**,** 546-550.

Costa, T. & Herz, A. 1989. Antagonists with negative intrinsic activity at delta opioid receptors coupled to GTP-binding proteins. *Proceedings of the National Academy of Sciences,* 86**,** 7321-7325.

Cotecchia, S., Exum, S., Caron, M. G. & Lefkowitz, R. J. 1990. Regions of the alpha 1-adrenergic receptor involved in coupling to phosphatidylinositol hydrolysis and enhanced sensitivity of biological function. *Proceedings of the National Academy of Sciences,* 87**,** 2896-2900.

Coureuil, M., Lécuyer, H., Scott, M. G. H., Boularan, C., Enslen, H., Soyer, M., Mikaty, G., Bourdoulous, S., Nassif, X. & Marullo, S. 2010. Meningococcus Hijacks a β2-Adrenoceptor/β-Arrestin Pathway to Cross Brain Microvasculature Endothelium. *Cell,* 143**,** 1149-1160.

Covic, L., Gresser, A. L., Talavera, J., Swift, S. & Kuliopulos, A. 2002a. Activation and inhibition of G protein-coupled receptors by cell-penetrating membrane-tethered peptides. *Proceedings of the National Academy of Sciences,* 99**,** 643-648.

Covic, L., Misra, M., Badar, J., Singh, C. & Kuliopulos, A. 2002b. Pepducin-based intervention of thrombin-receptor signaling and systemic platelet activation. *Nature Medicine,* 8**,** 1161-1165.

Creed, S. J., Le, C. P., Hassan, M., Pon, C. K., Albold, S., Chan, K. T., Berginski, M. E., Huang, Z., Bear, J. E., Lane, J. R., Halls, M. L., Ferrari, D., Nowell, C. J. & Sloan, E. K. 2015. β2-adrenoceptor signaling regulates invadopodia formation to enhance tumor cell invasion. *Breast Cancer Research,* 17**,** 145.

Cukic, V., Lovre, V., Dragisic, D. & Ustamujic, A. 2012. Asthma and Chronic Obstructive Pulmonary Disease (COPD) - Differences and Similarities. *Mater Sociomed,* 24**,** 100-105.

Cullen, B. R. & Malim, M. H. 1992. [31] Secreted placental alkaline phosphatase as a eukaryotic reporter gene. *Methods in Enzymology.* Academic Press**,** 362-368.

Cullum, S. A., Veprintsev, D. B. & Hill, S. J. 2023. Kinetic analysis of endogenous β2-adrenoceptor-mediated cAMP GloSensor™ responses in HEK293 cells. *British Journal of Pharmacology,* 180**,** 1304-1315.

D'alonzo, G. E., Nathan, R. A., Henochowicz, S., Morris, R. J., Ratner, P. & Rennard, S. I. 1994. Salmeterol Xinafoate as Maintenance Therapy Compared With Albuterol in Patients With Asthma. *JAMA,* 271**,** 1412-1416.

Daaka, Y., Luttrell, L. M. & Lefkowitz, R. J. 1997. Switching of the coupling of the β2-adrenergic receptor to different g proteins by protein kinase A. *Nature,* 390**,** 88-91.

Dale, N. C., Johnstone, E. K. M., White, C. W. & Pfleger, K. D. G. 2019. NanoBRET: The Bright Future of Proximity-Based Assays. *Frontiers in Bioengineering and Biotechnology,* 7**,** 56.

Daly, C. J. & Mcgrath, J. C. 2011. Previously unsuspected widespread cellular and tissue distribution of β-adrenoceptors and its relevance to drug action. *Trends in Pharmacological Sciences,* 32**,** 219-226.

Darfler, F. J., Mahan, L., Koachman, A. & Insel, P. 1982. Stimulation of forskolin of intact S49 lymphoma cells involves the nucleotide regulatory protein of adenylate cyclase. *Journal of Biological Chemistry,* 257**,** 11901-11907.

Davies, P. F. 1995. Flow-mediated endothelial mechanotransduction. *Physiological Reviews,* 75**,** 519-560.

Dawaliby, R., Trubbia, C., Delporte, C., Masureel, M., Van Antwerpen, P., Kobilka, B. K. & Govaerts, C. 2016. Allosteric regulation of G protein–coupled receptor activity by phospholipids. *Nature Chemical Biology,* 12**,** 35-39.

De Belly, H., Paluch, E. K. & Chalut, K. J. 2022. Interplay between mechanics and signalling in regulating cell fate. *Nature Reviews Molecular Cell Biology,* 23**,** 465-480.

De Haas, P., Hendriks, W. J. a. J., Lefeber, D. J. & Cambi, A. 2020. Biological and Technical Challenges in Unraveling the Role of N-Glycans in Immune Receptor Regulation. *Frontiers in chemistry,* 8**,** 55.

De Lean, A., Stadel, J. M. & Lefkowitz, R. J. 1980. A ternary complex model explains the agonist-specific binding properties of the adenylate cyclase-coupled beta-adrenergic receptor. *Journal of Biological Chemistry,* 255**,** 7108-7117.

De Vries, L., Zheng, B., Fischer, T., Elenko, E. & Farquhar, M. G. 2000. The Regulator of G Protein Signaling Family. *Annual Review of Pharmacology and Toxicology,* 40**,** 235-271.

Defea, K. A., Zalevsky, J., Thoma, M. S., Déry, O., Mullins, R. D. & Bunnett, N. W. 2000. β-Arrestin–Dependent Endocytosis of Proteinase-Activated Receptor 2 Is Required for Intracellular Targeting of Activated Erk1/2. *Journal of Cell Biology,* 148**,** 1267-1282.

Degorce, F., Card, A., Soh, S., Trinquet, E., Knapik, G. P. & Xie, B. 2009. HTRF: A technology tailored for drug discovery - a review of theoretical aspects and recent applications. *Current Chemical Genomics,* 3**,** 22-32.

Deshpande, D. A., Theriot, B. S., Penn, R. B. & Walker, J. K. L. 2008. β-Arrestins specifically constrain β2-adrenergic receptor signaling and function in airway smooth muscle. *The FASEB Journal,* 22**,** 2134-2141.

Dessauer, C. W., Scully, T. T. & Gilman, A. G. 1997. Interactions of Forskolin and ATP with the Cytosolic Domains of Mammalian Adenylyl Cyclase. *Journal of Biological Chemistry,* 272**,** 22272-22277.

Dessy, C. & Balligand, J.-L. 2010. Beta3-Adrenergic Receptors in Cardiac and Vascular Tissues: Emerging Concepts and Therapeutic Perspectives. *In:* Vanhoutte, P. M. (ed.) *Advances in Pharmacology.* Academic Press**,** 135-163.

Dewire, S. M., Ahn, S., Lefkowitz, R. J. & Shenoy, S. K. 2007. β-Arrestins and Cell Signaling. *Annual Review of Physiology,* 69**,** 483-510.

Dézsi, C. A. & Szentes, V. 2017. The Real Role of β-Blockers in Daily Cardiovascular Therapy. *American Journal of Cardiovascular Drugs,* 17**,** 361-373.

Dhalla, N. S., Adameova, A. & Kaur, M. 2010. Role of catecholamine oxidation in sudden cardiac death. *Fundamental & Clinical Pharmacology,* 24**,** 539-546.

Díaz, Ó., Martín, V., Renault, P., Romero, D., Guillamon, A. & Giraldo, J. 2023. Allosteric binding cooperativity in a kinetic context. *Drug Discovery Today,* 28**,** 103441.

Dijon, N. C., Nesheva, D. N. & Holliday, N. D. 2021. Luciferase Complementation Approaches to Measure GPCR Signaling Kinetics and Bias. *G Protein-Coupled Receptor Screening Assays: Methods and Protocols.* Springer US**,** 249-274.

Dixon, A. S., Schwinn, M. K., Hall, M. P., Zimmerman, K., Otto, P., Lubben, T. H., Butler, B. L., Binkowski, B. F., Machleidt, T. & Kirkland, T. A. 2016.

NanoLuc complementation reporter optimized for accurate measurement of protein interactions in cells. *ACS Chemical Biology,* 11**,** 400-408.

Dixon, R. a. F., Kobilka, B. K., Strader, D. J., Benovic, J. L., Dohlman, H. G., Frielle, T., Bolanowski, M. A., Bennett, C. D., Rands, E., Diehl, R. E., Mumford, R. A., Slater, E. E., Sigal, I. S., Caron, M. G., Lefkowitz, R. J. & Strader, C. D. 1986. Cloning of the gene and cDNA for mammalian β-adrenergic receptor and homology with rhodopsin. *Nature,* 321**,** 75-79.

Docherty, J. R. 1998. Subtypes of functional α1- and α2-adrenoceptors. *European Journal of Pharmacology,* 361**,** 1-15.

Dohlman, H. G., Bouvier, M., Benovic, J. L., Caron, M. G. & Lefkowitz, R. J. 1987. The multiple membrane spanning topography of the beta 2-adrenergic receptor. Localization of the sites of binding, glycosylation, and regulatory phosphorylation by limited proteolysis. *Journal of Biological Chemistry,* 262**,** 14282-14288.

Dohlman, H. G., Thorner, J., Caron, M. G. & Lefkowitz, R. J. 1991. Model systems for the study of seven-transmembrane-segment receptors. *Annual Review of Biochemistry,* 60**,** 653-688.

Donohue, J. F. 2004. Therapeutic Responses in Asthma and COPD: Bronchodilators. *Chest,* 126**,** 125S-137S.

Doornbos, M. L. J., Vermond, S. C., Lavreysen, H., Tresadern, G., Ijzerman, A. P. & Heitman, L. H. 2018. Impact of allosteric modulation: Exploring the binding kinetics of glutamate and other orthosteric ligands of the metabotropic glutamate receptor 2. *Biochemical Pharmacology,* 155**,** 356-365.

Dorr, P., Westby, M., Dobbs, S., Griffin, P., Irvine, B., Macartney, M., Mori, J., Rickett, G., Smith-Burchnell, C., Napier, C., Webster, R., Armour, D., Price, D., Stammen, B., Wood, A. & Perros, M. 2005. Maraviroc (UK-

427,857), a Potent, Orally Bioavailable, and Selective Small-Molecule Inhibitor of Chemokine Receptor CCR5 with Broad-Spectrum Anti-Human Immunodeficiency Virus Type 1 Activity. *Antimicrobial Agents and Chemotherapy,* 49**,** 4721-4732.

Downes, G. B. & Gautam, N. 1999. The G Protein Subunit Gene Families. *Genomics,* 62**,** 544-552.

Drake, M. T., Shenoy, S. K. & Lefkowitz, R. J. 2006. Trafficking of G Protein-Coupled Receptors. *Circulation Research,* 99**,** 570-582.

Dubois, J.-M., Ouanounou, G. & Rouzaire-Dubois, B. 2009. The Boltzmann equation in molecular biology. *Progress in Biophysics and Molecular Biology,* 99**,** 87-93.

Eckert, K. A. & Kunkel, T. A. 1991. DNA polymerase fidelity and the polymerase chain reaction. *Genome Research,* 1**,** 17-24.

Ejiofor, S. & Turner, A. M. 2013. Pharmacotherapies for COPD. *Clinical Medicine Insights: Circulatory, Respiratory and Pulmonary Medicine,* 7**,** CCRPM.S7211.

Engelhardt, S., Grimmer, Y., Fan, G.-H. & Lohse, M. J. 2001. Constitutive Activity of the Human β1-Adrenergic Receptor in β1-Receptor Transgenic Mice. *Molecular Pharmacology,* 60**,** 712-717.

England, C. G., Ehlerding, E. B. & Cai, W. 2016. NanoLuc: A Small Luciferase Is Brightening Up the Field of Bioluminescence. *Bioconjugate Chem,* 27**,** 1175-1187.

Erdogmus, S., Storch, U., Danner, L., Becker, J., Winter, M., Ziegler, N., Wirth, A., Offermanns, S., Hoffmann, C., Gudermann, T. & Mederos Y Schnitzler, M. 2019. Helix 8 is the essential structural motif of mechanosensitive GPCRs. *Nature Communications,* 10**,** 5784.

Ergin, E., Dogan, A., Parmaksiz, M., Elçin, E. A. & Elçin, M. Y. 2016. Time-Resolved Fluorescence Resonance Energy Transfer [TR-FRET] Assays for Biochemical Processes. *Current Pharmaceutical Biotechnology,* 17**,** 1222-1230.

Errey, J. C. & Fiez-Vandal, C. 2020. Production of membrane proteins in industry: The example of GPCRs. *Protein Expression and Purification,* 169**,** 105569.

Esmail, S. & Manolson, M. F. 2021. Advances in understanding N-glycosylation structure, function, and regulation in health and disease. *European Journal of Cell Biology,* 100**,** 151186.

Esmail, S., Yao, Y., Kartner, N., Li, J., Reithmeier, R. a. F. & Manolson, M. F. 2016. N-Linked Glycosylation Is Required for Vacuolar H+-ATPase (V-ATPase) a4 Subunit Stability, Assembly, and Cell Surface Expression. *Journal of Cellular Biochemistry,* 117**,** 2757-2768.

Evans, B. A., Merlin, J., Bengtsson, T. & Hutchinson, D. S. 2019. Adrenoceptors in white, brown, and brite adipocytes. *British Journal of Pharmacology,* 176**,** 2416-2432.

Exton, J. H. 1996. Regulation of Phosphoinositide Phospholipases by Hormones, Neurotransmitters, and Other Agonists Linked to G Proteins. *Annual Review of Pharmacology and Toxicology,* 36**,** 481-509.

Fagerholm, V., Haaparanta, M. & Scheinin, M. 2011. α2-Adrenoceptor Regulation of Blood Glucose Homeostasis. *Basic & Clinical Pharmacology & Toxicology,* 108**,** 365-370.

Fan, F., Binkowski, B. F., Butler, B. L., Stecha, P. F., Lewis, M. K. & Wood, K. V. 2008. Novel Genetically Encoded Biosensors Using Firefly Luciferase. *ACS Chemical Biology,* 3**,** 346-351.

Fang, Y. 2012. Ligand–receptor interaction platforms and their applications for drug discovery. *Expert Opinion on Drug Discovery,* 7**,** 969-988.

Fargin, A., Faye, J. C., Le Maire, M., Bayard, F., Potier, M. & Beauregard, G. 1988. Solubilization of a tamoxifen-binding protein. Assessment of its molecular mass. *Biochemical Journal,* 256**,** 229-236.

Farmer, J. P., Mistry, S. N., Laughton, C. A. & Holliday, N. D. 2022. Development of fluorescent peptide G protein-coupled receptor activation biosensors for NanoBRET characterization of intracellular allosteric modulators. *The FASEB Journal,* 36**,** e22576.

Feldman, R. & Gros, R. 1998. Impaired Vasodilator Function in Hypertension The Role of Alterations in Receptor–G Protein Coupling. *Trends in Cardiovascular Medicine,* 8**,** 297-305.

Feldman, R. D. & Gros, R. 2006. Defective vasodilatory mechanisms in hypertension: a G-protein-coupled receptor perspective. *Current Opinion in Nephrology and Hypertension,* 15**,** 135-140.

Felgner, P. L. & Wilson, J. E. 1976. Hexokinase binding to polypropylene test tubes: Artifactural activity losses from protein binding to disposable plastics. *Analytical Biochemistry,* 74**,** 631-635.

Ferguson, S. S., Barak, L. S., Zhang, J. & Caron, M. G. 1996. G-protein-coupled receptor regulation: role of G-protein-coupled receptor kinases and arrestins. *Canadian Journal of Physiology and Pharmacololgy,* 74**,** 1095-1110.

Ferguson, S. S. G. & Feldman, R. D. 2014. β-Adrenoceptors as Molecular Targets in the Treatment of Hypertension. *Canadian Journal of Cardiology,* 30**,** S3-S8.

Ferrandon, S., Feinstein, T. N., Castro, M., Wang, B., Bouley, R., Potts, J. T., Gardella, T. J. & Vilardaga, J.-P. 2009. Sustained cyclic AMP production

by parathyroid hormone receptor endocytosis. *Nature Chemical Biology,* 5**,** 734-742.

Ferro, A., Queen, L. R., Priest, R. M., Xu, B., Ritter, J. M., Poston, L. & Ward, J. P. 1999. Activation of nitric oxide synthase by beta 2-adrenoceptors in human umbilical vein endothelium in vitro. *British Journal of Pharmacology,* 126**,** 1872-1880.

Fiedler, K. & Simons, K. 1995. The role of N-glycans in the secretory pathway. *Cell,* 81**,** 309-312.

Filipek, S. 2019. Molecular switches in GPCRs. *Current Opinion in Structural Biology,* 55**,** 114-120.

Finlay, D. B., Duffull, S. B. & Glass, M. 2020. 100 years of modelling ligand–receptor binding and response: A focus on GPCRs. *British Journal of Pharmacology,* 177**,** 1472-1484.

Flock, T., Ravarani, C. N. J., Sun, D., Venkatakrishnan, A. J., Kayikci, M., Tate, C. G., Veprintsev, D. B. & Babu, M. M. 2015. Universal allosteric mechanism for Gα activation by GPCRs. *Nature,* 524**,** 173-179.

Foord, S. M., Bonner, T. I., Neubig, R. R., Rosser, E. M., Pin, J.-P., Davenport, A. P., Spedding, M. & Harmar, A. J. 2005. International Union of Pharmacology. XLVI. G Protein-Coupled Receptor List. *Pharmacological Reviews,* 57**,** 279-288.

Francis, S. H., Turko, I. V. & Corbin, J. D. 2000. Cyclic nucleotide phosphodiesterases: Relating structure and function. *Progress in Nucleic Acid Research and Molecular Biology.* Academic Press**,** 1-52.

Fredericks, Z. L., Pitcher, J. A. & Lefkowitz, R. J. 1996. Identification of the G protein-coupled receptor kinase phosphorylation sites in the human β2-adrenergic receptor. *Journal of Biological Chemistry,* 271**,** 13796-13803.

Fredholm, B. B., Abbracchio, M. P., Burnstock, G., Daly, J. W., Harden, T. K., Jacobson, K. A., Leff, P. & Williams, M. 1994. Nomenclature and classification of purinoceptors. *Pharmacological Reviews,* 46**,** 143-156.

Fredriksson, R., Lagerström, M. C., Lundin, L.-G. & Schiöth, H. B. 2003. The G-Protein-Coupled Receptors in the Human Genome Form Five Main Families. Phylogenetic Analysis, Paralogon Groups, and Fingerprints. *Molecular Pharmacology,* 63**,** 1256-1272.

Freedman, N. J. & Lefkowitz, R. J. 2004. Anti-beta(1)-adrenergic receptor antibodies and heart failure: causation, not just correlation. *Journal of Clinical Investigation,* 113**,** 1379-1382.

Friedland, J. C., Lee, M. H. & Boettiger, D. 2009. Mechanically Activated Integrin Switch Controls α5β1 Function. *Science,* 323**,** 642-644.

Friedman, J., Babu, B. & Clark, R. B. 2002. β2-Adrenergic Receptor Lacking the Cyclic AMP-Dependent Protein Kinase Consensus Sites Fully Activates Extracellular Signal-Regulated Kinase 1/2 in Human Embryonic Kidney 293 Cells: Lack of Evidence for Gs/Gi Switching. *Molecular Pharmacology,* 62**,** 1094-1102.

Frishman, W. H. & Saunders, E. 2011. β-Adrenergic blockers. *Journal of Clinical Hypertension (Greenwich),* 13**,** 649-653.

Furness, S. G. B., Liang, Y.-L., Nowell, C. J., Halls, M. L., Wookey, P. J., Dal Maso, E., Inoue, A., Christopoulos, A., Wootten, D. & Sexton, P. M. 2016. Ligand-Dependent Modulation of G Protein Conformation Alters Drug Efficacy. *Cell,* 167**,** 739-749.e711.

Gacasan, S. B., Baker, D. L. & Parrill, A. L. 2017. G protein-coupled receptors: the evolution of structural insight. *AIMS Biophysics,* 4**,** 491-527.

Gaddum, J. H., Hameed, K. A., Hathway, D. E. & Stephens, F. F. 1955. Quantitative studies of antagonists for 5-hydroxytryptamine. *Quarterly*

Journal of Experimental Physiology and Cognate Medical Sciences, 40**,** 49-74.

Galandrin, S. & Bouvier, M. 2006. Distinct Signaling Profiles of β1 and β2 Adrenergic Receptor Ligands toward Adenylyl Cyclase and Mitogen-Activated Protein Kinase Reveals the Pluridimensionality of Efficacy. *Molecular Pharmacology,* 70**,** 1575-1584.

Gao, Q. B. & Wang, Z. Z. 2006. Classification of G-protein coupled receptors at four levels. *Protein Engineering Design and Selection,* 19**,** 511-516.

Gaspardone, A., Crea, F., Kaski, J. C. & Maseri, A. 1991. Effects of beta2-adrenoceptor stimulation on exercise-induced myocardial ischemia. *The American Journal of Cardiology,* 68**,** 111-114.

Gaub, B. M. & Müller, D. J. 2017. Mechanical Stimulation of Piezo1 Receptors Depends on Extracellular Matrix Proteins and Directionality of Force. *Nano Letters,* 17**,** 2064-2072.

Gehle, V. M., Walcott, E. C., Nishizaki, T. & Sumikawa, K. 1997. N-Glycosylation at the conserved sites ensures the expression of properly folded functional ACh receptors. *Molecular Brain Research,* 45**,** 219-229.

George, S. T., Ruoho, A. E. & Malbon, C. C. 1986. N-glycosylation in expression and function of beta-adrenergic receptors. *Journal of Biological Chemistry,* 261**,** 16559-16564.

Geva, Y. & Schuldiner, M. 2014. The Back and Forth of Cargo Exit from the Endoplasmic Reticulum. *Current Biology,* 24**,** R130-R136.

Ghosh, R., Sawant, O., Ganpathy, P., Pitre, S. & Kadam, V. 2009. Phosphodiesterase inhibitors: their role and implications. *International Journal of PharmTech Research,* 1**,** 1148-1160.

Gillis, A., Gondin, A. B., Kliewer, A., Sanchez, J., Lim, H. D., Alamein, C., Manandhar, P., Santiago, M., Fritzwanker, S., Schmiedel, F., Katte, T. A., Reekie, T., Grimsey, N. L., Kassiou, M., Kellam, B., Krasel, C., Halls, M. L., Connor, M., Lane, J. R., Schulz, S., Christie, M. J. & Canals, M. 2020. Low intrinsic efficacy for G protein activation can explain the improved side effect profiles of new opioid agonists. *Science Signaling,* 13**,** eaaz3140.

Gillis, R. D., Botteri, E., Chang, A., Ziegler, A. I., Chung, N.-C., Pon, C. K., Shackleford, D. M., Andreassen, B. K., Halls, M. L., Baker, J. G. & Sloan, E. K. 2021. Carvedilol blocks neural regulation of breast cancer progression in vivo and is associated with reduced breast cancer mortality in patients. *European Journal of Cancer,* 147**,** 106-116.

Gimenez, L. E., Baameur, F., Vayttaden, S. J. & Clark, R. B. 2015. Salmeterol Efficacy and Bias in the Activation and Kinase-Mediated Desensitization of β2-Adrenergic Receptors. *Molecular Pharmacology,* 87**,** 954-964.

Goebel-Stengel, M., Stengel, A., Taché, Y. & Reeve, J. R., Jr. 2011. The importance of using the optimal plasticware and glassware in studies involving peptides. *Analytical Biochemistry,* 414**,** 38-46.

Goldstein, D. S. 2001. Adrenaline and Noradrenaline. *Encyclopedia of Life Sciences.* John Wiley & Sons, Ltd (Ed.).

Goodman, O. B., Krupnick, J. G., Santini, F., Gurevich, V. V., Penn, R. B., Gagnon, A. W., Keen, J. H. & Benovic, J. L. 1996. β-Arrestin acts as a clathrin adaptor in endocytosis of the β2-adrenergic receptor. *Nature,* 383**,** 447-450.

Goulding, J., Kondrashov, A., Mistry, S. J., Melarangi, T., Vo, N. T. N., Hoang, D. M., White, C. W., Denning, C., Briddon, S. J. & Hill, S. J. 2021a. The use of fluorescence correlation spectroscopy to monitor cell surface β2-

adrenoceptors at low expression levels in human embryonic stem cell-derived cardiomyocytes and fibroblasts. *The FASEB Journal,* 35**,** e21398.

Goulding, J., May, L. T. & Hill, S. J. 2018. Characterisation of endogenous A 2A and A 2B receptor-mediated cyclic AMP responses in HEK 293 cells using the GloSensor™ biosensor: Evidence for an allosteric mechanism of action for the A 2B -selective antagonist PSB 603. *Biochemical Pharmacology,* 147**,** 55-66.

Goulding, J., Mistry, S. J., Soave, M., Woolard, J., Briddon, S. J., White, C. W., Kellam, B. & Hill, S. J. 2021b. Subtype selective fluorescent ligands based on ICI 118,551 to study the human β2-adrenoceptor in CRISPR/Cas9 genome-edited HEK293T cells at low expression levels. *Pharmacology Research & Perspectives,* 9**,** e00779.

Grandoch, M., Roscioni, S. S. & Schmidt, M. 2010. The role of Epac proteins, novel cAMP mediators, in the regulation of immune, lung and neuronal function. *British Journal of Pharmacology,* 159**,** 265-284.

Gray, D. W. & Marshall, I. 1992. Novel signal transduction pathway mediating endothelium-dependent beta-adrenoceptor vasorelaxation in rat thoracic aorta. *British Journal of Pharmacology,* 107**,** 684-690.

Greasley, P. J. & Clapham, J. C. 2006. Inverse agonism or neutral antagonism at G-protein coupled receptors: A medicinal chemistry challenge worth pursuing? *European Journal of Pharmacology,* 553**,** 1-9.

Green, S. A., Spasoff, A. P., Coleman, R. A., Johnson, M. & Liggett, S. B. 1996. Sustained Activation of a G Protein-coupled Receptor via "Anchored" Agonist Binding. *Journal of Biological Chemistry,* 271**,** 24029-24035.

Greenwald, E. C., Mehta, S. & Zhang, J. 2018. Genetically Encoded Fluorescent Biosensors Illuminate the Spatiotemporal Regulation of Signaling Networks. *Chemical Reviews,* 118**,** 11707-11794.

Gregorio, G. G., Masureel, M., Hilger, D., Terry, D. S., Juette, M., Zhao, H., Zhou, Z., Perez-Aguilar, J. M., Hauge, M., Mathiasen, S., Javitch, J. A., Weinstein, H., Kobilka, B. K. & Blanchard, S. C. 2017. Single-molecule analysis of ligand efficacy in β(2)AR-G-protein activation. *Nature,* 547**,** 68-73.

Grisanti, L. A., Thomas, T. P., Carter, R. L., De Lucia, C., Gao, E., Koch, W. J., Benovic, J. L. & Tilley, D. G. 2018. Pepducin-mediated cardioprotection via β-arrestin-biased β2-adrenergic receptor-specific signaling. *Theranostics,* 8**,** 4664-4678.

Groves, P., Kurz, S., Just, H. & Drexler, H. 1995. Role of Endogenous Bradykinin in Human Coronary Vasomotor Control. *Circulation,* 92**,** 3424-3430.

Guimarães, S. & Moura, D. 2001. Vascular Adrenoceptors: An Update. *Pharmacological Reviews,* 53**,** 319-356.

Gundry, J., Glenn, R., Alagesan, P. & Rajagopal, S. 2017. A Practical Guide to Approaching Biased Agonism at G Protein Coupled Receptors. *Frontiers in Neuroscience,* 11**,** 17.

Guo, D., Venhorst, S. N., Massink, A., Van Veldhoven, J. P. D., Vauquelin, G., Ijzerman, A. P. & Heitman, L. H. 2014. Molecular mechanism of allosteric modulation at GPCRs: insight from a binding kinetics study at the human A1 adenosine receptor. *British Journal of Pharmacology,* 171**,** 5295-5312.

Gurevich, E. V. & Gurevich, V. V. 2006. Arrestins: ubiquitous regulators of cellular signaling pathways. *Genome Biology,* 7**,** 236.

Gurevich, V. V. & Gurevich, E. V. 2013. Chapter Three - Structural Determinants of Arrestin Functions. *In:* Luttrell, L. M. (ed.) *Progress in Molecular Biology and Translational Science.* Academic Press**,** 57-92.

Gurevich, V. V. & Gurevich, E. V. 2019. GPCR Signaling Regulation: The Role of GRKs and Arrestins. *Frontiers in Pharmacology,* 10**,** 125.

Gusach, A., Maslov, I., Luginina, A., Borshchevskiy, V., Mishin, A. & Cherezov, V. 2020. Beyond structure: emerging approaches to study GPCR dynamics. *Current Opinion in Structural Biology,* 63**,** 18-25.

Gutkind, J. S. & Kostenis, E. 2018. Arrestins as rheostats of GPCR signalling. *Nature Reviews Molecular Cell Biology,* 19**,** 615-616.

Hall, I. 2000. Second messengers, ion channels and pharmacology of airway smooth muscle. *European Respiratory Journal,* 15**,** 1120-1127.

Hallsworth, M. P., Twort, C. H. C., Lee, T. H. & Hirst, S. J. 2001. β2-Adrenoceptor agonists inhibit release of eosinophil-activating cytokines from human airway smooth muscle cells. *British Journal of Pharmacology,* 132**,** 729-741.

Hanania, N. A., Sharafkhaneh, A., Barber, R. & Dickey, B. F. 2002. β -Agonist Intrinsic Efficacy. *American Journal of Respiratory and Critical Care Medicine,* 165**,** 1353-1358.

Hanson, M. A., Cherezov, V., Griffith, M. T., Roth, C. B., Jaakola, V.-P., Chien, E. Y. T., Velasquez, J., Kuhn, P. & Stevens, R. C. 2008. A Specific Cholesterol Binding Site Is Established by the 2.8 Å Structure of the Human β2-Adrenergic Receptor. *Structure,* 16**,** 897-905.

Hanson, M. A. & Stevens, R. C. 2009. Discovery of New GPCR Biology: One Receptor Structure at a Time. *Structure,* 17**,** 8-14.

Hanson, S. R., Culyba, E. K., Hsu, T.-L., Wong, C.-H., Kelly, J. W. & Powers, E. T. 2009. The core trisaccharide of an N-linked glycoprotein intrinsically accelerates folding and enhances stability. *Proceedings of the National Academy of Sciences,* 106**,** 3131-3136.

Hardman, K., Goldman, A. & Pliotas, C. 2023. Membrane force reception: mechanosensation in GPCRs and tools to address it. *Current Opinion in Physiology,* 35**,** 100689.

Hart, J. 2019. Vascular Myography to Examine Functional Responses of Isolated Blood Vessels. *In:* Bełtowski, J. (ed.) *Vascular Effects of Hydrogen Sulfide: Methods and Protocols.* New York, NY: Springer New York**,** 205-217.

Harwood, C. R., Sykes, D. A., Hoare, B. L., Heydenreich, F. M., Uddin, R., Poyner, D. R., Briddon, S. J. & Veprintsev, D. B. 2021. Functional solubilization of the β2-adrenoceptor using diisobutylene maleic acid. *iScience,* 24**,** 103362.

Hauser, A. S., Attwood, M. M., Rask-Andersen, M., Schiöth, H. B. & Gloriam, D. E. 2017. Trends in GPCR drug discovery: new agents, targets and indications. *Nature Reviews Drug Discovery,* 16**,** 829-842.

Haynes, J., Robinson, J., Saunders, L., Taylor, A. E. & Strada, S. J. 1992. Role of cAMP-dependent protein kinase in cAMP-mediated vasodilation. *American Journal of Physiology-Heart and Circulatory Physiology,* 262**,** H511-H516.

Hein, L. 2006. Adrenoceptors and signal transduction in neurons. *Cell and Tissue Research,* 326**,** 541-551.

Helenius, A. 1994. How N-linked oligosaccharides affect glycoprotein folding in the endoplasmic reticulum. *Molecular Biology of the Cell,* 5**,** 253-265.

Helenius, A. & Aebi, M. 2004. Roles of N-Linked Glycans in the Endoplasmic Reticulum. *Annual Review of Biochemistry,* 73**,** 1019-1049.

Herlitze, S., Garcia, D. E., Mackie, K., Hille, B., Scheuer, T. & Catterall, W. A. 1996. Modulation of Ca2+ channels βγ G-protein py subunits. *Nature,* 380**,** 258-262.

Hill, A. 1910. Proceedings of the Physiological Society: January 22, 1910. *The Journal of Physiology,* 40**,** i-vii.

Hill, S. J., Baker, J. G. & Rees, S. 2001. Reporter-gene systems for the study of G-protein-coupled receptors. *Current Opinion in Pharmacology,* 1**,** 526-532.

Hillenbrand, M., Schori, C., Schöppe, J. & Plückthun, A. 2015. Comprehensive analysis of heterotrimeric G-protein complex diversity and their interactions with GPCRs in solution. *Proceedings of the National Academy of Sciences of the United States of America,* 112**,** E1181-E1190.

Hoare, B. L., Tippett, D. N., Kaur, A., Cullum, S. A., Miljuš, T., Koers, E. J., Harwood, C. R., Dijon, N., Holliday, N. D., Sykes, D. A. & Veprintsev, D. B. 2023. ThermoBRET: a ligand-engagement nanoscale thermostability assay applied to GPCRs. *bioRxiv***,** 2020.2008.2005.237982.

Hoare, S. R., Tewson, P. H., Sachdev, S., Connor, M., Hughes, T. & Quinn, A. M. 2022. Quantifying the kinetics of signaling and arrestin recruitment by nervous system G-protein coupled receptors. *Frontiers in Cellular Neuroscience,* 15**,** 814547.

Hoare, S. R. J., Pierre, N., Moya, A. G. & Larson, B. 2018. Kinetic operational models of agonism for G-protein-coupled receptors. *Journal of Theoretical Biology,* 446**,** 168-204.

Hoare, S. R. J., Tewson, P. H., Quinn, A. M. & Hughes, T. E. 2020a. A kinetic method for measuring agonist efficacy and ligand bias using high resolution biosensors and a kinetic data analysis framework. *Scientific Reports,* 10**,** 1766.

Hoare, S. R. J., Tewson, P. H., Quinn, A. M., Hughes, T. E. & Bridge, L. J. 2020b. Analyzing kinetic signaling data for G-protein-coupled receptors. *Scientific Reports,* 10**,** 12263.

Hoffmann, C., Leitz, M. R., Oberdorf-Maass, S., Lohse, M. J. & Klotz, K. N. 2004. Comparative pharmacology of human **?**-adrenergic receptor subtypes?characterization of stably transfected receptors in CHO cells. *Naunyn-Schmiedeberg's Archives of Pharmacology,* 369**,** 151-159.

Hollenberg, M. D., Mihara, K., Polley, D., Suen, J. Y., Han, A., Fairlie, D. P. & Ramachandran, R. 2014. Biased signalling and proteinase-activated receptors (PARs): targeting inflammatory disease. *British Journal of Pharmacology,* 171**,** 1180-1194.

Hollenberg, M. D., Saifeddine, M., Sandhu, S., Houle, S. & Vergnolle, N. 2004. Proteinase-activated receptor-4: Evaluation of tethered ligand-derived peptides as probes for receptor function and as inflammatory agonists in vivo. *British Journal of Pharmacology,* 143**,** 443-454.

Hollmann, M., Maron, C. & Heinemann, S. 1994. N-glycosylation site tagging suggests a three transmembrane domain topology for the glutamate receptor GluR1. *Neuron,* 13**,** 1331-1343.

Hong, K. S., Kim, K. & Hill, M. A. 2020. Regulation of blood flow in small arteries: mechanosensory events underlying myogenic vasoconstriction. *Journal of Exercise Rehabilitation,* 16**,** 207-215.

Hopkinson, H. E., Latif, M. L. & Hill, S. J. 2000. Non-competitive antagonism ofβ2-agonist-mediated cyclic AMP accumulation by ICI 118551 in BC3H1 cells endogenously expressing constitutively activeβ2-adrenoceptors. *British Journal of Pharmacology,* 131**,** 124-130.

Hori, T. & Yokoyama, S. 2022. Chapter 4 - Ions as GPCR allosteric modulators. *In:* Laprairie, R. B. (ed.) *Allosteric Modulation of G Protein-Coupled Receptors.* Academic Press**,** 47-69.

Horinouchi, T., Tanaka, Y. & Koike, K. 2003. Beta-adrenoceptor subtypes involved in relaxations of guinea-pig gastrointestinal smooth muscles: distribution and signaling pathway of beta 3-adrenoceptors. *Nihon Yakurigaku Zasshi,* 122 Suppl**,** 54p-56p.

Howarth, P. H., Knox, A. J., Amrani, Y., Tliba, O., Panettieri, R. A. & Johnson, M. 2004. Synthetic responses in airway smooth muscle. *Journal of Allergy and Clinical Immunology,* 114**,** S32-S50.

Hoyer, D. & Boddeke, H. W. G. M. 1993. Partial agonists, full agonists, antagonists: dilemmas of definition. *Trends in Pharmacological Sciences,* 14**,** 270-275.

Hrometz, S. L., Edelmann, S. E., Mccune, D. F., Olges, J. R., Hadley, R. W., Perez, D. M. & Piascik, M. T. 1999. Expression of Multiple α1-Adrenoceptors on Vascular Smooth Muscle: Correlation with the Regulation of Contraction. *Journal of Pharmacology and Experimental Therapeutics,* 290**,** 452-463.

Hu, G.-M., Mai, T.-L. & Chen, C.-M. 2017. Visualizing the GPCR Network: Classification and Evolution. *Scientific Reports,* 7**,** 15495.

Hu, Y., Chen, M., Wang, M. & Li, X. 2022. Flow-mediated vasodilation through mechanosensitive G protein-coupled receptors in endothelial cells. *Trends in Cardiovascular Medicine,* 32**,** 61-70.

Hughes, I. E. & Smith, J. A. 2011. The stability of noradrenaline in physiological saline solutions. *Journal of Pharmacy and Pharmacology,* 30**,** 124-126.

Huynh, F. K., Green, M. F., Koves, T. R. & Hirschey, M. D. 2014. Chapter Twenty - Measurement of Fatty Acid Oxidation Rates in Animal Tissues

and Cell Lines. *In:* Galluzzi, L. & Kroemer, G. (eds.) *Methods in Enzymology.* Academic Press**,** 391-405.

Ibarrondo, J., Marino, A., Font, J., Trueba, M. & Macarulla, J. M. 1989. GTP and its non-hydrolysable analogues stimulate polyphosphoinositide hydrolysis in plasma membranes of rat hepatocytes. *Biochemical Society Transactions,* 17**,** 1006-1008.

Imperiali, B. & O'connor, S. E. 1999. Effect of N-linked glycosylation on glycopeptide and glycoprotein structure. *Current Opinion in Chemical Biology,* 3**,** 643-649.

Inglese, J., Koch, W. J., Touhara, K. & Lefkowitz, R. J. 1995. Gβγ interactions with PH domains and Ras-MAPK signaling pathways. *Trends in Biochemical Sciences,* 20**,** 151-156.

Insel, P. A. & Ostrom, R. S. 2003. Forskolin as a tool for examining adenylyl cyclase expression, regulation, and G protein signaling. *Cellular and Molecular Neurobiology,* 23**,** 305-314.

Ippolito, M., De Pascali, F., Hopfinger, N., Komolov, K. E., Laurinavichyute, D., Reddy, P. a. N., Sakkal, L. A., Rajkowski, K. Z., Nayak, A. P., Lee, J., Lee, J., Cao, G., Donover, P. S., Reichman, M., An, S. S., Salvino, J. M., Penn, R. B., Armen, R. S., Scott, C. P. & Benovic, J. L. 2023. Identification of a β-arrestin-biased negative allosteric modulator for the β2-adrenergic receptor. *Proceedings of the National Academy of Sciences,* 120**,** e2302668120.

Irannejad, R., Tomshine, J. C., Tomshine, J. R., Chevalier, M., Mahoney, J. P., Steyaert, J., Rasmussen, S. G. F., Sunahara, R. K., El-Samad, H., Huang, B. & Von Zastrow, M. 2013. Conformational biosensors reveal GPCR signalling from endosomes. *Nature,* 495**,** 534-538.

Iwata, M., Yoshikawa, T., Baba, A., Anzai, T., Nakamura, I., Wainai, Y., Takahashi, T. & Ogawa, S. 2001. Autoimmunity Against the Second Extracellular Loop of β1-Adrenergic Receptors Induces β-Adrenergic Receptor Desensitization and Myocardial Hypertrophy In Vivo. *Circulation Research,* 88**,** 578-586.

Jakubík, J. & El-Fakahany, E. E. 2021. Allosteric Modulation of GPCRs of Class A by Cholesterol. *International Journal of Molecular Sciences,* 22**,** 1953.

Jamshad, M., Charlton, J., Lin, Y.-P., Routledge, Sarah j., Bawa, Z., Knowles, Timothy j., Overduin, M., Dekker, N., Dafforn, Tim r., Bill, Roslyn m., Poyner, David r. & Wheatley, M. 2015. G-protein coupled receptor solubilization and purification for biophysical analysis and functional studies, in the total absence of detergent. *Bioscience Reports,* 35**,** e00188.

January, B., Seibold, A., Allal, C., Whaley, B. S., Knoll, B. J., Moore, R. H., Dickey, B. F., Barber, R. & Clark, R. B. 1998. Salmeterol-induced desensitization, internalization and phosphorylation of the human β 2 -adrenoceptor. *British Journal of Pharmacology,* 123**,** 701-711.

January, B., Seibold, A., Whaley, B., Hipkin, R. W., Lin, D., Schonbrunn, A., Barber, R. & Clark, R. B. 1997. β2-Adrenergic Receptor Desensitization, Internalization, and Phosphorylation in Response to Full and Partial Agonists. *Journal of Biological Chemistry,* 272**,** 23871-23879.

Janz, J. M., Ren, Y., Looby, R., Kazmi, M. A., Sachdev, P., Grunbeck, A., Haggis, L., Chinnapen, D., Lin, A. Y., Seibert, C., Mcmurry, T., Carlson, K. E., Muir, T. W., Hunt, S., 3rd & Sakmar, T. P. 2011. Direct interaction between an allosteric agonist pepducin and the chemokine receptor CXCR4. *Journal of the American Chemical Society,* 133**,** 15878-15881.

Ji, T. H., Grossmann, M. & Ji, I. 1998. G Protein-coupled Receptors: I. Diversity of receptor-ligand interactions. *The Journal of Biological Chemistry,* 273**,** 17299-17302.

Johannessen, L., Remsberg, J., Gaponenko, V., Adams, K. M., Barchi, J. J., Tarasov, S. G., Jiang, S. & Tarasova, N. I. 2011. Peptide Structure Stabilization by Membrane Anchoring and its General Applicability to the Development of Potent Cell-Permeable Inhibitors. *ChemBioChem,* 12**,** 914-921.

Johnson, M. 1998. The β -Adrenoceptor. *American Journal of Respiratory and Critical Care Medicine,* 158**,** S146-S153.

Johnson, M., Butchers, P. R., Coleman, R. A., Nials, A. T., Strong, P., Summer, M. J., Vardey, C. J. & Whelan, C. J. 1993. The pharmacology of salmeterol. *Life Sciences,* 52**,** 2131-2143.

Johnson, P. R. A., Roth, M., Tamm, M., Hughes, M., Ge, Q., King, G., Burgess, J. K. & Black, J. L. 2001. Airway Smooth Muscle Cell Proliferation Is Increased in Asthma. *American Journal of Respiratory and Critical Care Medicine,* 164**,** 474-477.

Jones, E. M., Lubock, N. B., Venkatakrishnan, A. J., Wang, J., Tseng, A. M., Paggi, J. M., Latorraca, N. R., Cancilla, D., Satyadi, M., Davis, J. E., Babu, M. M., Dror, R. O. & Kosuri, S. 2020. Structural and functional characterization of G protein–coupled receptors with deep mutational scanning. *eLife,* 9**,** e54895.

Kamenetsky, M., Middelhaufe, S., Bank, E. M., Levin, L. R., Buck, J. & Steegborn, C. 2006. Molecular details of cAMP generation in mammalian cells: a tale of two systems. *Journal of Molecular Biology,* 362**,** 623-639.

Kaneider, N. C., Agarwal, A., Leger, A. J. & Kuliopulos, A. 2005. Reversing systemic inflammatory response syndrome with chemokine receptor pepducins. *Nature Medicine,* 11**,** 661-665.

Kassel, K. M., Wyatt, T. A., Panettieri, R. A. & Toews, M. L. 2008. Inhibition of human airway smooth muscle cell proliferation by β2-adrenergic receptors and cAMP is PKA independent: evidence for EPAC involvement. *American Journal of Physiology-Lung Cellular and Molecular Physiology,* 294**,** L131-L138.

Katritch, V., Cherezov, V. & Stevens, R. C. 2013. Structure-Function of the G Protein–Coupled Receptor Superfamily. *Annual Review of Pharmacology and Toxicology,* 53**,** 531-556.

Katritch, V., Fenalti, G., Abola, E. E., Roth, B. L., Cherezov, V. & Stevens, R. C. 2014. Allosteric sodium in class A GPCR signaling. *Trends in Biochemical Sciences,* 39**,** 233-244.

Katsumi, A., Orr, A. W., Tzima, E. & Schwartz, M. A. 2004. Integrins in Mechanotransduction *. *Journal of Biological Chemistry,* 279**,** 12001-12004.

Kenakin, T. 1995. Agonist-receptor efficacy I: mechanisms of efficacy and receptor promiscuity. *Trends in Pharmacological Sciences,* 16**,** 188-192.

Kenakin, T. 1996. The classification of seven transmembrane receptors in recombinant expression systems. *Pharmacological Reviews,* 48**,** 413-463.

Kenakin, T. 1997. Differences between natural and recombinant G protein-coupled receptor systems with varying receptor/G protein stoichiometry. *Trends in Pharmacological Sciences,* 18**,** 456-464.

Kenakin, T. 2004. Efficacy as a Vector: the Relative Prevalence and Paucity of Inverse Agonism. *Molecular Pharmacology,* 65**,** 2-11.

Kenakin, T. 2009. Quantifying Biological Activity in Chemical Terms: A Pharmacology Primer To Describe Drug Effect. *ACS Chemical Biology,* 4**,** 249-260.

Kenakin, T. 2013. New concepts in pharmacological efficacy at 7TM receptors: IUPHAR review 2. *British Journal of Pharmacology,* 168**,** 554-575.

Kenakin, T. 2017. Theoretical Aspects of GPCR-Ligand Complex Pharmacology. *Chemical Reviews,* 117**,** 4-20.

Kenakin, T. 2019. Analytical Pharmacology: How Numbers Can Guide Drug Discovery. *ACS Pharmacology and Translational Science,* 2**,** 9-17.

Kenakin, T. & Christopoulos, A. 2013. Signalling bias in new drug discovery: detection, quantification and therapeutic impact. *Nature Reviews Drug Discovery,* 12**,** 205-216.

Kenakin, T., Jenkinson, S. & Watson, C. 2006. Determining the Potency and Molecular Mechanism of Action of Insurmountable Antagonists. *Journal of Pharmacology and Experimental Therapeutics,* 319**,** 710-723.

Kenakin, T. P. 1982. The Schild regression in the process of receptor classification. *Canadian Journal of Physiology and Pharmacology,* 60**,** 249-265.

Kenakin, T. P. & Cook, D. A. 1980. N, N-Diethy1-2-(1-pyridyl)ethylamine, a partial agonist for the histamine receptor in guinea pig ileum. *Canadian Journal of Physiology and Pharmacology,* 58**,** 1307-1310.

Keov, P., Sexton, P. M. & Christopoulos, A. 2011. Allosteric modulation of G protein-coupled receptors: A pharmacological perspective. *Neuropharmacology,* 60**,** 24-35.

Kim-Fuchs, C., Le, C. P., Pimentel, M. A., Shackleford, D., Ferrari, D., Angst, E., Hollande, F. & Sloan, E. K. 2014. Chronic stress accelerates pancreatic cancer growth and invasion: A critical role for beta-adrenergic signaling in the pancreatic microenvironment. *Brain, Behavior, and Immunity,* 40**,** 40-47.

Kim, I. M., Tilley, D. G., Chen, J., Salazar, N. C., Whalen, E. J., Violin, J. D. & Rockman, H. A. 2008. β-Blockers alprenolol and carvedilol stimulate β-arrestin-mediated EGFR transactivation. *Proceedings of the National Academy of Sciences of the United States of America,* 105**,** 14555-14560.

Klein Herenbrink, C., Sykes, D. A., Donthamsetti, P., Canals, M., Coudrat, T., Shonberg, J., Scammells, P. J., Capuano, B., Sexton, P. M., Charlton, S. J., Javitch, J. A., Christopoulos, A. & Lane, J. R. 2016. The role of kinetic context in apparent biased agonism at GPCRs. *Nature Communications,* 7**,** 10842.

Knoepp, F., Ashley, Z., Barth, D., Baldin, J.-P., Jennings, M., Kazantseva, M., Saw, E. L., Katare, R., Alvarez De La Rosa, D., Weissmann, N. & Fronius, M. 2020. Shear force sensing of epithelial Na+ channel (ENaC) relies on N-glycosylated asparagines in the palm and knuckle domains of αENaC. *Proceedings of the National Academy of Sciences,* 117**,** 717-726.

Knoepp, F., Ashley, Z., Barth, D., Kazantseva, M., Szczesniak, P. P., Clauss, W. G., Althaus, M., Rosa, D. a. D. L. & Fronius, M. 2017. Mechanical activation of epithelial Na+ channel relies on an interdependent activity of the extracellular matrix and extracellular N-glycans of αENaC. *bioRxiv***,** 102756.

Knowles, T. J., Finka, R., Smith, C., Lin, Y.-P., Dafforn, T. & Overduin, M. 2009. Membrane Proteins Solubilized Intact in Lipid Containing Nanoparticles Bounded by Styrene Maleic Acid Copolymer. *Journal of the American Chemical Society,* 131**,** 7484-7485.

Kobilka, B. 2013. The Structural Basis of G-Protein-Coupled Receptor Signaling (Nobel Lecture). *Angewandte Chemie International Edition,* 52**,** 6380-6388.

Kobilka, B., Kobilka, T., Daniel, K., Regan, J., Caron, M. & Lefkowitz, R. 1988. Chimeric alpha 2-,beta 2-adrenergic receptors: delineation of domains

involved in effector coupling and ligand binding specificity. *Science,* 240**,** 1310-1316.

Kobilka, B. K. 2007. G protein coupled receptor structure and activation. *Biochimica et Biophysica Acta (BBA) - Biomembranes,* 1768**,** 794-807.

Kobilka, B. K. 2011. Structural insights into adrenergic receptor function and pharmacology. *Trends in Pharmacological Sciences,* 32**,** 213-218.

Kobilka, B. K. & Deupi, X. 2007. Conformational complexity of G-protein-coupled receptors. *Trends in Pharmacological Sciences,* 28**,** 397-406.

Koch, W. J., Inglese, J., Stone, W. & Lefkowitz, R. 1993. The binding site for the beta gamma subunits of heterotrimeric G proteins on the beta-adrenergic receptor kinase. *Journal of Biological Chemistry,* 268**,** 8256-8260.

Kohout, T. A., Nicholas, S. L., Perry, S. J., Reinhart, G., Junger, S. & Struthers, R. S. 2004. Differential Desensitization, Receptor Phosphorylation, -Arrestin Recruitment, and ERK1/2 Activation by the Two Endogenous Ligands for the CC Chemokine Receptor 7. *Journal of Biological Chemistry,* 279**,** 23214-23222.

Komolov, K. E. & Benovic, J. L. 2018. G protein-coupled receptor kinases: Past, present and future. *Cellular Signalling,* 41**,** 17-24.

Kopperud, R., Krakstad, C., Selheim, F. & Døskeland, S. O. 2003. cAMP effector mechanisms. Novel twists for an 'old' signaling system. *FEBS Letters,* 546**,** 121-126.

Kozanoglu, I., Yandim, M. K., Cincin, Z. B., Ozdogu, H., Cakmakoglu, B. & Baran, Y. 2013. New indication for therapeutic potential of an old well-known drug (propranolol) for multiple myeloma. *Journal of Cancer Research and Clinical Oncology,* 139**,** 327-335.

Kozasa, T. 1998. p115 RhoGEF, a GTPase Activating Protein for G12 and G13. *Science,* 280**,** 2109-2111.

Krueger, K. M., Daaka, Y., Pitcher, J. A. & Lefkowitz, R. J. 1997. The Role of Sequestration in G Protein-coupled Receptor Resensitization. *Journal of Biological Chemistry,* 272**,** 5-8.

Krupnick, J. G. & Benovic, J. L. 1998. The role of receptor kinases and arrestins in G protein-coupled receptor regulation. *Annual Review of Pharmacology and Toxicology,* 38**,** 289-319.

Kruse, A. C., Ring, A. M., Manglik, A., Hu, J., Hu, K., Eitel, K., Hübner, H., Pardon, E., Valant, C., Sexton, P. M., Christopoulos, A., Felder, C. C., Gmeiner, P., Steyaert, J., Weis, W. I., Garcia, K. C., Wess, J. & Kobilka, B. K. 2013. Activation and allosteric modulation of a muscarinic acetylcholine receptor. *Nature,* 504**,** 101-106.

Kühn, H. 1978. Light-regulated binding of rhodopsin kinase and other proteins to cattle photoreceptor membranes. *Biochemistry,* 17**,** 4389-4395.

Kumar, A. & Kaur, J. 2014. Primer Based Approach for PCR Amplification of High GC Content Gene: Mycobacterium Gene as a Model. *Molecular Biology International,* 2014**,** 1-7.

Kume, H., Hall, I. P., Washabau, R. J., Takagi, K. & Kotlikoff, M. I. 1994. Beta-adrenergic agonists regulate KCa channels in airway smooth muscle by cAMP-dependent and -independent mechanisms. *Journal of Clinical Investigation,* 93**,** 371-379.

Kundra, R. & Kornfeld, S. 1999. Asparagine-linked Oligosaccharides Protect Lamp-1 and Lamp-2 from Intracellular Proteolysis. *Journal of Biological Chemistry,* 274**,** 31039-31046.

Kurose, H. 2003. Gα12 and Gα13 as key regulatory mediator in signal transduction. *Life Sciences,* 74**,** 155-161.

Kurozumi, S., Kaira, K., Matsumoto, H., Hirakata, T., Yokobori, T., Inoue, K., Horiguchi, J., Katayama, A., Koshi, H., Shimizu, A., Oyama, T., Sloan, E. K., Kurosumi, M., Fujii, T. & Shirabe, K. 2019. β2-Adrenergic receptor expression is associated with biomarkers of tumor immunity and predicts poor prognosis in estrogen receptor-negative breast cancer. *Breast Cancer Research and Treatment,* 177**,** 603-610.

Lagerström, M. C. & Schiöth, H. B. 2008. Structural diversity of G protein-coupled receptors and significance for drug discovery. *Nature Reviews Drug Discovery,* 7**,** 339-357.

Lalli, E. & Sassone-Corsi, P. 1994. Signal transduction and gene regulation: the nuclear response to cAMP. *Journal of Biological Chemistry,* 269**,** 17359-17362.

Lanctôt, P. M., Leclerc, P. C., Escher, E., Leduc, R. & Guillemette, G. 1999. Role of N-Glycosylation in the Expression and Functional Properties of Human AT1 Receptor. *Biochemistry,* 38**,** 8621-8627.

Lander, E. S., Linton, L. M., Birren, B., Nusbaum, C., Zody, M. C., Baldwin, J., Devon, K., Dewar, K., Doyle, M., Fitzhugh, W., Funke, R., Gage, D., Harris, K., Heaford, A., Howland, J., Kann, L., Lehoczky, J., Levine, R., Mcewan, P., Mckernan, K., Meldrim, J., Mesirov, J. P., Miranda, C., Morris, W., Naylor, J., Raymond, C., Rosetti, M., Santos, R., Sheridan, A., Sougnez, C., Stange-Thomann, N., Stojanovic, N., Subramanian, A., Wyman, D., Rogers, J., Sulston, J., Ainscough, R., Beck, S., Bentley, D., Burton, J., Clee, C., Carter, N., Coulson, A., Deadman, R., Deloukas, P., Dunham, A., Dunham, I., Durbin, R., French, L., Grafham, D., Gregory, S., Hubbard, T., Humphray, S., Hunt, A., Jones, M., Lloyd, C., Mcmurray, A., Matthews, L., Mercer, S., Milne, S., Mullikin, J. C., Mungall, A., Plumb, R., Ross, M., Shownkeen, R., Sims, S., Waterston, R. H., Wilson, R. K., Hillier, L. W., Mcpherson, J. D., Marra, M. A., Mardis, E. R., Fulton, L. A., Chinwalla, A. T., Pepin, K. H., Gish, W. R., Chissoe, S. L., Wendl, M. C., Delehaunty, K. D., Miner, T. L.,

Delehaunty, A., Kramer, J. B., Cook, L. L., Fulton, R. S., Johnson, D. L., Minx, P. J., Clifton, S. W., Hawkins, T., Branscomb, E., Predki, P., Richardson, P., Wenning, S., Slezak, T., Doggett, N., Cheng, J.-F., Olsen, A., Lucas, S., Elkin, C., Uberbacher, E., Frazier, M., et al. 2001. Initial sequencing and analysis of the human genome. *Nature,* 409**,** 860-921.

Landolt-Marticorena, C. & Reithmeier, R. a. F. 1994. Asparagine-linked oligosaccharides are localized to single extracytosolic segments in multi-span membrane glycoproteins. *Biochemical Journal,* 302**,** 253-260.

Lands, A. M., Arnold, A., Mcauliff, J. P., Luduena, F. P. & Brown, T. G. 1967a. Differentiation of Receptor Systems activated by Sympathomimetic Amines. *Nature,* 214**,** 597-598.

Lands, A. M., Luduena, F. P. & Buzzo, H. J. 1967b. Differentiation of receptors responsive to isoproterenol. *Life Sciences,* 6**,** 2241-2249.

Lane, J. R., May, L. T., Parton, R. G., Sexton, P. M. & Christopoulos, A. 2017. A kinetic view of GPCR allostery and biased agonism. *Nature Chemical Biology,* 13**,** 929-937.

Langer, S. Z. 1974. Presynaptic regulation of catecholamine release. *Biochemical Pharmacology,* 23**,** 1793-1800.

Langin, D., Tavernier, G. & Lafontan, M. 1995. Regulation of beta3-adrenoceptor expression in white fat cells*. *Fundamental & Clinical Pharmacology,* 9**,** 97-106.

Laporte, S. A., Oakley, R. H., Zhang, J., Holt, J. A., Ferguson, S. S., Caron, M. G. & Barak, L. S. 1999. The beta2-adrenergic receptor/betaarrestin complex recruits the clathrin adaptor AP-2 during endocytosis. *Proceedings of the National Academy of Sciences of the United States of America,* 96**,** 3712-3717.

Lau, K. S. & Dennis, J. W. 2008. N-Glycans in cancer progression. *Glycobiology,* 18**,** 750-760.

Laverty, R. 1978. Catecholamines: Role in Health and Disease. *Drugs,* 16**,** 418-440.

Lavington, S. & Watts, A. 2020. Lipid nanoparticle technologies for the study of G protein-coupled receptors in lipid environments. *Biophysical Reviews,* 12**,** 1287-1302.

Le Maire, M., Champeil, P. & Møller, J. V. 2000. Interaction of membrane proteins and lipids with solubilizing detergents. *Biochimica et Biophysica Acta (BBA) - Biomembranes,* 1508**,** 86-111.

Leach, K., Sexton, P. M. & Christopoulos, A. 2007. Allosteric GPCR modulators: taking advantage of permissive receptor pharmacology. *Trends in Pharmacological Sciences,* 28**,** 382-389.

Leblais, V., Delannoy, E., Fresquet, F., Bégueret, H., Bellance, N., Banquet, S., Allières, C., Leroux, L., Desgranges, C., Gadeau, A. & Muller, B. 2007. β-adrenergic relaxation in pulmonary arteries: preservation of the endothelial nitric oxide-dependent β2 component in pulmonary hypertension. *Cardiovascular Research,* 77**,** 202-210.

Lee, H. Y., Kim, S. D., Shim, J. W., Kim, H. J., Kwon, J. Y., Kim, J.-M., Baek, S.-H., Park, J. S. & Bae, Y.-S. 2010. Activation of human monocytes by a formyl peptide receptor 2-derived pepducin. *FEBS Letters,* 584**,** 4102-4108.

Leeb-Lundberg, L. M. F., Kang, D. S., Lamb, M. E. & Fathy, D. B. 2001. The Human B1 Bradykinin Receptor Exhibits High Ligand-independent, Constitutive Activity. *Journal of Biological Chemistry,* 276**,** 8785-8792.

Lefkowitz, R. J. 2004. Historical review: A brief history and personal retrospective of seven-transmembrane receptors. *Trends in Pharmacological Sciences,* 25**,** 413-422.

Lefkowitz, R. J., Cotecchia, S., Samama, P. & Costa, T. 1993. Constitutive activity of receptors coupled to guanine nucleotide regulatory proteins. *Trends in Pharmacological Sciences,* 14**,** 303-307.

Lehman, I. R. 1974. DNA Ligase: Structure, Mechanism, and Function. *Science,* 186**,** 790-797.

Lemichez, E., Lecuit, M., Nassif, X. & Bourdoulous, S. 2010. Breaking the wall: targeting of the endothelium by pathogenic bacteria. *Nature Reviews Microbiology,* 8**,** 93-104.

Lessard, S. J., Rivas, D. A., Chen, Z.-P., Van Denderen, B. J., Watt, M. J., Koch, L. G., Britton, S. L., Kemp, B. E. & Hawley, J. A. 2009. Impaired Skeletal Muscle β-Adrenergic Activation and Lipolysis Are Associated with Whole-Body Insulin Resistance in Rats Bred for Low Intrinsic Exercise Capacity. *Endocrinology,* 150**,** 4883-4891.

Leurs, R., Pena, M. S. R., Bakker, R. A., Alewijnse, A. E. & Timmerman, H. 2000. Constitutive activity of G protein coupled receptors and drug action. *Pharmaceutica Acta Helvetiae,* 74**,** 327-331.

Li, F., Godoy, M. D. & Rattan, S. 2004. Role of Adenylate and Guanylate Cyclases in β1-, β2-, and β3-Adrenoceptor-Mediated Relaxation of Internal Anal Sphincter Smooth Muscle. *Journal of Pharmacology and Experimental Therapeutics,* 308**,** 1111-1120.

Li, K., Zhang, H., Qiu, J., Lin, Y., Liang, J., Xiao, X., Fu, L., Wang, F., Cai, J., Tan, Y., Zhu, W., Yin, W., Lu, B., Xing, F., Tang, L., Yan, M., Mai, J., Li, Y., Chen, W., Qiu, P., Su, X., Gao, G., Tai, P. W. L., Hu, J. & Yan, G. 2016. Activation of Cyclic Adenosine Monophosphate Pathway

Increases the Sensitivity of Cancer Cells to the Oncolytic Virus M1. *Molecular Therapy,* 24**,** 156-165.

Li, X., Zhou, M., Huang, W. & Yang, H. 2017. N-glycosylation of the β2 adrenergic receptor regulates receptor function by modulating dimerization. *The FEBS Journal,* 284**,** 2004-2018.

Licht, T., Tsirulnikov, L., Reuveni, H., Yarnitzky, T. & Ben-Sasson, S. A. 2003. Induction of pro-angiogenic signaling by a synthetic peptide derived from the second intracellular loop of S1P3 (EDG3). *Blood,* 102**,** 2099-2107.

Liggett, S. B. 2011. Phosphorylation Barcoding as a Mechanism of Directing GPCR Signaling. *Science Signaling,* 4**,** pe36-pe36.

Lin, H.-H., Ng, K.-F., Chen, T.-C. & Tseng, W.-Y. 2022. Ligands and Beyond: Mechanosensitive Adhesion GPCRs. *Pharmaceuticals,* 15**,** 219.

Liu, C. & Montell, C. 2015. Forcing open TRP channels: Mechanical gating as a unifying activation mechanism. *Biochemical and Biophysical Research Communications,* 460**,** 22-25.

Liu, W., Chun, E., Thompson, A. A., Chubukov, P., Xu, F., Katritch, V., Han, G. W., Roth, C. B., Heitman, L. H., Ijzerman, A. P., Cherezov, V. & Stevens, R. C. 2012. Structural Basis for Allosteric Regulation of GPCRs by Sodium Ions. *Science,* 337**,** 232-236.

Liu, X., Ahn, S., Kahsai, A. W., Meng, K. C., Latorraca, N. R., Pani, B., Venkatakrishnan, A. J., Masoudi, A., Weis, W. I., Dror, R. O., Chen, X., Lefkowitz, R. J. & Kobilka, B. K. 2017. Mechanism of intracellular allosteric beta2AR antagonist revealed by X-ray crystal structure. *Nature,* 548**,** 480-484.

Liu, X., Kaindl, J., Korczynska, M., Stößel, A., Dengler, D., Stanek, M., Hübner, H., Clark, M. J., Mahoney, J., Matt, R. A., Xu, X., Hirata, K., Shoichet,

B. K., Sunahara, R. K., Kobilka, B. K. & Gmeiner, P. 2020. An allosteric modulator binds to a conformational hub in the β2 adrenergic receptor. *Nature Chemical Biology,* 16**,** 749-755.

Liu, X., Masoudi, A., Kahsai, A. W., Huang, L.-Y., Pani, B., Staus, D. P., Shim, P. J., Hirata, K., Simhal, R. K., Schwalb, A. M., Rambarat, P. K., Ahn, S., Lefkowitz, R. J. & Kobilka, B. 2019. Mechanism of β2AR regulation by an intracellular positive allosteric modulator. *Science,* 364**,** 1283-1287.

Liu, Y. J., Shankley, N. P., Welsh, N. J. & Black, J. W. 1992. Evidence that the apparent complexity of receptor antagonism by angiotensin II analogues is due to a reversible and syntopic action. *British Journal of Pharmacology,* 106**,** 233-241.

Lodowski, D. T. 2003. Keeping G Proteins at Bay: A Complex Between G Protein-Coupled Receptor Kinase 2 and Gbetagamma. *Science,* 300**,** 1256-1262.

Logothetis, D. E., Kurachi, Y., Galper, J., Neer, E. J. & Clapham, D. E. 1987. The βγ subunits of GTP-binding proteins activate the muscarinic K+ channel in heart. *Nature,* 325**,** 321-326.

Lohse, M. J., Benovic, J. L., Codina, J., Caron, M. G. & Lefkowitz, R. J. 1990. β-Arrestin: a Protein that Regulates β-adrenergic Receptor Function. *Science,* 248**,** 1547-1550.

Lohse, M. J., Nikolaev, V. O., Hein, P., Hoffmann, C., Vilardaga, J.-P. & Bünemann, M. 2008. Optical techniques to analyze real-time activation and signaling of G-protein-coupled receptors. *Trends in Pharmacological Sciences,* 29**,** 159-165.

Lohse, M. J., Nuber, S. & Hoffmann, C. 2012. Fluorescence/Bioluminescence Resonance Energy Transfer Techniques to Study G-Protein-Coupled

Receptor Activation and Signaling. *Pharmacological Reviews,* 64**,** 299-336.

Lopez, A. D., Shibuya, K., Rao, C., Mathers, C. D., Hansell, A. L., Held, L. S., Schmid, V. & Buist, S. 2006. Chronic obstructive pulmonary disease: current burden and future projections. *European Respiratory Journal,* 27**,** 397-412.

Lötvall, J. 2001. Pharmacological similarities and differences between β2-agonists. *Respiratory Medicine,* 95**,** S7-S11.

Lu, M. & Wu, B. 2016. Structural studies of G protein-coupled receptors. *IUBMB Life,* 68**,** 894-903.

Luttrell, L. M. 2005. Composition and Function of G Protein-Coupled Receptor Signalsomes Controlling Mitogen-Activated Protein Kinase Activity. *Journal of Molecular Neuroscience,* 26**,** 253-264.

Luttrell, L. M. 2008. Reviews in Molecular Biology and Biotechnology: Transmembrane Signaling by G Protein-Coupled Receptors. *Molecular Biotechnology,* 39**,** 239-264.

Luttrell, L. M., Ferguson, S. S. G., Daaka, Y., Miller, W. E., Maudsley, S., Della Rocca, G. J., Lin, F. T., Kawakatsu, H., Owada, K., Luttrell, D. K., Caron, M. G. & Lefkowitz, R. J. 1999. β-Arrestin-Dependent Formation of β2 Adrenergic Receptor-Src Protein Kinase Complexes. *Science,* 283**,** 655-661.

Luttrell, L. M., Roudabush, F. L., Choy, E. W., Miller, W. E., Field, M. E., Pierce, K. L. & Lefkowitz, R. J. 2001. Activation and targeting of extracellular signal-regulated kinases by β-arrestin scaffolds. *Proceedings of the National Academy of Sciences,* 98**,** 2449-2454.

Lynch, M. J., Baillie, G. S., Mohamed, A., Li, X., Maisonneuve, C., Klussmann, E., Van Heeke, G. & Houslay, M. D. 2005. RNA Silencing Identifies

PDE4D5 as the Functionally Relevant cAMP Phosphodiesterase Interacting with Arrestin to Control the Protein Kinase A/AKAP79-mediated Switching of the 2-Adrenergic Receptor to Activation of ERK in HEK293B2 Cells. *The Journal of Biological Chemistry,* 280**,** 33178-33189.

Lyons, J. A., Shahsavar, A., Paulsen, P. A., Pedersen, B. P. & Nissen, P. 2016. Expression strategies for structural studies of eukaryotic membrane proteins. *Current Opinion in Structural Biology,* 38**,** 137-144.

Maack, C. & Böhm, M. 2003. Different inverse agonist activities of β-adrenergic receptor antagonists—pharmacological characterization and therapeutical implications in the treatment of chronic heart failure. *International Congress Series,* 1249**,** 39-53.

Macewan, D. J. & Milligan, G. 1996. Inverse agonist-induced up-regulation of the human beta2-adrenoceptor in transfected neuroblastoma X glioma hybrid cells. *Molecular Pharmacology,* 50**,** 1479-1486.

Madamanchi, A. 2007. Beta-adrenergic receptor signaling in cardiac function and heart failure. *McGill journal of medicine : MJM : an international forum for the advancement of medical sciences by students,* 10**,** 99-104.

Madden, K. S., Szpunar, M. J. & Brown, E. B. 2011. β-Adrenergic receptors (β-AR) regulate VEGF and IL-6 production by divergent pathways in high β-AR-expressing breast cancer cell lines. *Breast Cancer Research and Treatment,* 130**,** 747-758.

Magistrelli, L. & Comi, C. 2020. Beta2-Adrenoceptor Agonists in Parkinson's Disease and Other Synucleinopathies. *Journal of Neuroimmune Pharmacology,* 15**,** 74-81.

Magnani, F., Serrano-Vega, M. J., Shibata, Y., Abdul-Hussein, S., Lebon, G., Miller-Gallacher, J., Singhal, A., Strege, A., Thomas, J. A. & Tate, C. G.

2016. A mutagenesis and screening strategy to generate optimally thermostabilized membrane proteins for structural studies. *Nature Protocols,* 11**,** 1554-1571.

Mahn, K., Ojo, O. O., Chadwick, G., Aaronson, P. I., Ward, J. P. T. & Lee, T. H. 2010. Ca2+ homeostasis and structural and functional remodelling of airway smooth muscle in asthma. *Thorax,* 65**,** 547-552.

Manglik, A., Kim, T. H., Masureel, M., Altenbach, C., Yang, Z., Hilger, D., Lerch, M. T., Kobilka, T. S., Thian, F. S., Hubbell, W. L., Prosser, R. S. & Kobilka, B. K. 2015. Structural Insights into the Dynamic Process of β2-Adrenergic Receptor Signaling. *Cell,* 161**,** 1101-1111.

Manna, M., Niemelä, M., Tynkkynen, J., Javanainen, M., Kulig, W., Müller, D. J., Rog, T. & Vattulainen, I. 2016. Mechanism of allosteric regulation of β2-adrenergic receptor by cholesterol. *eLife,* 5**,** e18432.

Marhuenda, E., Fabre, C., Zhang, C., Martin-Fernandez, M., Iskratsch, T., Saleh, A., Bauchet, L., Cambedouzou, J., Hugnot, J.-P., Duffau, H., Dennis, J. W., Cornu, D. & Bakalara, N. 2021. Glioma stem cells invasive phenotype at optimal stiffness is driven by MGAT5 dependent mechanosensing. *Journal of Experimental & Clinical Cancer Research,* 40**,** 139.

Marullo, S., Doly, S., Saha, K., Enslen, H., Scott, M. G. H. & Coureuil, M. 2020. Mechanical GPCR Activation by Traction Forces Exerted on Receptor N-Glycans. *ACS Pharmacology & Translational Science,* 3**,** 171-178.

Marullo, S., Scott, M. G. H., Enslen, H. & Coureuil, M. 2022. Mechanical Activation of the β2-Adrenergic Receptor by Meningococcus: A Historical and Future Perspective Analysis of How a Bacterial Probe Can Reveal Signalling Pathways in Endothelial Cells, and a Unique Mode of Receptor Activation Involving Its N-Terminal Glycan Chains. *Frontiers in Endocrinology,* 13**,** 883568.

Masoli, M., Fabian, D., Holt, S., Beasley, R. & Program, G. I. F. A. 2004. The global burden of asthma: executive summary of the GINA Dissemination Committee Report. *Allergy,* 59**,** 469-478.

Masureel, M., Zou, Y., Picard, L. P., Van Der Westhuizen, E., Mahoney, J. P., Rodrigues, J., Mildorf, T. J., Dror, R. O., Shaw, D. E., Bouvier, M., Pardon, E., Steyaert, J., Sunahara, R. K., Weis, W. I., Zhang, C. & Kobilka, B. K. 2018. Structural insights into binding specificity, efficacy and bias of a beta2AR partial agonist. *Nature Chemical Biology,* 14**,** 1059-1066.

Maurel, D., Comps-Agrar, L., Brock, C., Rives, M.-L., Bourrier, E., Ayoub, M. A., Bazin, H., Tinel, N., Durroux, T., Prézeau, L., Trinquet, E. & Pin, J.-P. 2008. Cell-surface protein-protein interaction analysis with time-resolved FRET and snap-tag technologies: application to GPCR oligomerization. *Nature Methods,* 5**,** 561-567.

May, L. T., Leach, K., Sexton, P. M. & Christopoulos, A. 2007. Allosteric Modulation of G Protein–Coupled Receptors. *Annual Review of Pharmacology and Toxicology,* 47**,** 1-51.

May, L. T., Self, T. J., Briddon, S. J. & Hill, S. J. 2010. The effect of allosteric modulators on the kinetics of agonist-G protein-coupled receptor interactions in single living cells. *Molecular Pharmacology,* 78**,** 511-523.

Mccrea, K. E. & Hill, S. J. 1993. Salmeterol, a long-acting β2-adrenoceptor agonist mediating cyclic AMP accumulation in a neuronal cell line. *British Journal of Pharmacology,* 110**,** 619-626.

Mcdonald, J., Barnes, T. A., Okawa, H., Williams, J., Calo, G., Rowbotham, D. J. & Lambert, D. G. 2003. Partial agonist behaviour depends upon the level of nociceptin/orphanin FQ receptor expression: studies using the ecdysone-inducible mammalian expression system. *British Journal of Pharmacology,* 140**,** 61-70.

Mcdonnell, J., Latif, M. L., Rees, E. S., Bevan, N. J. & Hill, S. J. 1998. Influence of receptor number on the stimulation by salmeterol of gene transcription in CHO-K1 cells transfected with the human β2-adrenoceptor. *British Journal of Pharmacology,* 125**,** 717-726.

Mchugh Sutkowski, E., Tang, W.-J., Broome, C. W., Robbins, J. D. & Seamon, K. B. 1994. Regulation of forskolin interactions with type I, II, V, and VI adenylyl cyclases by Gs. alpha. *Biochemistry,* 33**,** 12852-12859.

Merlin, J., Sato, M., Nowell, C., Pakzad, M., Fahey, R., Gao, J., Dehvari, N., Summers, R. J., Bengtsson, T., Evans, B. A. & Hutchinson, D. S. 2018. The PPARγ agonist rosiglitazone promotes the induction of brite adipocytes, increasing β-adrenoceptor-mediated mitochondrial function and glucose uptake. *Cellular Signalling,* 42**,** 54-66.

Milić, D. & Veprintsev, D. B. 2015. Large-scale production and protein engineering of G protein-coupled receptors for structural studies. *Frontiers in Pharmacology,* 6**,** 66.

Milligan, G. 2003. Constitutive Activity and Inverse Agonists of G Protein-Coupled Receptors: a Current Perspective. *Molecular Pharmacology,* 64**,** 1271-1276.

Min, C., Zheng, M., Zhang, X., Guo, S., Kwon, K.-J., Shin, C. Y., Kim, H.-S., Cheon, S. H. & Kim, K.-M. 2015. N-linked Glycosylation on the N-terminus of the dopamine D2 and D3 receptors determines receptor association with specific microdomains in the plasma membrane. *Biochimica et Biophysica Acta (BBA) - Molecular Cell Research,* 1853**,** 41-51.

Minneman, K. P., Hedberg, A. & Molinoff, P. B. 1979. Comparison of beta adrenergic receptor subtypes in mammalian tissues. *Journal of Pharmacology and Experimental Therapeutics,* 211**,** 502-508.

Minneman, K. P., Pittman, R. N. & Molinoff, P. B. 1981. beta-Adrenergic Receptor Subtypes: Properties, Distribution, and Regulation. *Annual Review of Neuroscience,* 4**,** 419-461.

Mittal, S., Bjørnevik, K., Im, D. S., Flierl, A., Dong, X., Locascio, J. J., Abo, K. M., Long, E., Jin, M., Xu, B., Xiang, Y. K., Rochet, J.-C., Engeland, A., Rizzu, P., Heutink, P., Bartels, T., Selkoe, D. J., Caldarone, B. J., Glicksman, M. A., Khurana, V., Schüle, B., Park, D. S., Riise, T. & Scherzer, C. R. 2017. β2-Adrenoreceptor is a regulator of the α-synuclein gene driving risk of Parkinson's disease. *Science,* 357**,** 891-898.

Moldoveanu, B., Otmishi, P., Jani, P., Walker, J., Sarmiento, X., Guardiola, J., Saad, M. & Yu, J. 2009. Inflammatory mechanisms in the lung. *Journal of Inflammation Research,* 2**,** 1-11.

Montminy, M. R., Gonzalez, G. A. & Yamamoto, K. K. 1990. Regulation of camp-inducible genes by creb. *Trends in Neurosciences,* 13**,** 184-188.

Montoya, A., Varela-Ramirez, A., Dickerson, E., Pasquier, E., Torabi, A., Aguilera, R., Nahleh, Z. & Bryan, B. 2019. The beta adrenergic receptor antagonist propranolol alters mitogenic and apoptotic signaling in late stage breast cancer. *Biomedical Journal,* 42**,** 155-165.

Moore, C. a. C., Milano, S. K. & Benovic, J. L. 2007a. Regulation of Receptor Trafficking by GRKs and Arrestins. *Annual Review of Physiology,* 69**,** 451-482.

Moore, R. H., Khan, A. & Dickey, B. F. 1998. Long-acting Inhaled β2-Agonists in Asthma Therapy. *Chest,* 113**,** 1095-1108.

Moore, R. H., Millman, E. E., Godines, V., Hanania, N. A., Tran, T. M., Peng, H., Dickey, B. F., Knoll, B. J. & Clark, R. B. 2007b. Salmeterol Stimulation Dissociates β2-Adrenergic Receptor Phosphorylation and

Internalization. *American Journal of Respiratory Cell and Molecular Biology,* 36**,** 254-261.

Moremen, K. W., Tiemeyer, M. & Nairn, A. V. 2012. Vertebrate protein glycosylation: diversity, synthesis and function. *Nature Reviews Molecular Cell Biology,* 13**,** 448-462.

Morgan, A. J., Murray, K. J. & Challiss, R. a. J. 1993. Comparison of the effect of isobutylmethylxanthine and phosphodiesterase-selective inhibitors on cAMP levels in SH-SY5Y neuroblastoma cells. *Biochemical Pharmacology,* 45**,** 2373-2380.

Morrison, D. K. & Davis, R. J. 2003. Regulation of MAP Kinase Signaling Modules by Scaffold Proteins in Mammals. *Annual Review of Cell and Developmental Biology,* 19**,** 91-118.

Motulsky, H. J. & Mahan, L. C. 1984. The kinetics of competitive radioligand binding predicted by the law of mass action. *Molecular Pharmacology,* 25**,** 1-9.

Mould, R., Brown, J., Marshall, F. H. & Langmead, C. J. 2014. Binding kinetics differentiates functional antagonism of orexin-2 receptor ligands. *British Journal of Pharmacology,* 171**,** 351-363.

Munk, C., Mutt, E., Isberg, V., Nikolajsen, L. F., Bibbe, J. M., Flock, T., Hanson, M. A., Stevens, R. C., Deupi, X. & Gloriam, D. E. 2019. An online resource for GPCR structure determination and analysis. *Nature Methods,* 16**,** 151-162.

Murakami, A., Yajima, T., Sakuma, H., Mclaren, M. J. & Inana, G. 1993. X-Arrestin: a new retinal arrestin mapping to the X chromosome. *FEBS Letters,* 334**,** 203-209.

Muramatsu, I., Ohmura, T., Kigoshi, S., Hashimoto, S. & Oshita, M. 1990. Pharmacological subclassification of α1-adrenoceptors in vascular smooth muscle. *British Journal of Pharmacology,* 99**,** 197-201.

Murchison, C. F., Zhang, X.-Y., Zhang, W.-P., Ouyang, M., Lee, A. & Thomas, S. A. 2004. A Distinct Role for Norepinephrine in Memory Retrieval. *Cell,* 117**,** 131-143.

Naline, E., Trifilieff, A., Fairhurst, R. A., Advenier, C. & Molimard, M. 2007. Effect of indacaterol, a novel long-acting 2-agonist, on isolated human bronchi. *European Respiratory Journal,* 29**,** 575-581.

Nemeth, E. F. 2013. Allosteric modulators of the extracellular calcium receptor. *Drug Discovery Today: Technologies,* 10**,** e277-e284.

Neubig, R. R., Spedding, M., Kenakin, T. & Christopoulos, A. 2003. International Union of Pharmacology Committee on Receptor Nomenclature and Drug Classification. XXXVIII. Update on Terms and Symbols in Quantitative Pharmacology. *Pharmacological Reviews,* 55**,** 597-606.

Neves, S. R., Ram, P. T. & Iyengar, R. 2002. G Protein Pathways. *Science,* 296**,** 1636-1639.

Nials, A. T., Sumner, M. J., Johnson, M. & Coleman, R. A. 1993. Investigations into factors determining the duration of action of the β2-adrenoceptor agonist, salmeterol. *British Journal of Pharmacology,* 108**,** 507-515.

Nicholas, A. P., Hökfely, T. & Pieribone, V. A. 1996. The distribution and significance of CNS adrenoceptors examined with in situ hybridization. *Trends in Pharmacological Sciences,* 17**,** 245-255.

Nobles, K. N., Xiao, K., Ahn, S., Shukla, A. K., Lam, C. M., Rajagopal, S., Strachan, R. T., Huang, T.-Y., Bressler, E. A., Hara, M. R., Shenoy, S. K., Gygi, S. P. & Lefkowitz, R. J. 2011. Distinct Phosphorylation Sites on

the β2-Adrenergic Receptor Establish a Barcode That Encodes Differential Functions of β-Arrestin. *Science Signaling,* 4**,** ra51-ra51.

O'callaghan, K., Kuliopulos, A. & Covic, L. 2012a. Turning Receptors On and Off with Intracellular Pepducins: New Insights into G-protein-coupled Receptor Drug Development. *The Journal of Biological Chemistry,* 287**,** 12787-12796.

O'callaghan, K., Lee, L., Nguyen, N., Hsieh, M.-Y., Kaneider, N. C., Klein, A. K., Sprague, K., Van Etten, R. A., Kuliopulos, A. & Covic, L. 2012b. Targeting CXCR4 with cell-penetrating pepducins in lymphoma and lymphocytic leukemia. *Blood,* 119**,** 1717-1725.

Oakley, R. H., Laporte, S. A., Holt, J. A., Barak, L. S. & Caron, M. G. 2001. Molecular Determinants Underlying the Formation of Stable Intracellular G Protein-coupled Receptor-β-Arrestin Complexes after Receptor Endocytosis*. *Journal of Biological Chemistry,* 276**,** 19452-19460.

Oluwole, A. O., Danielczak, B., Meister, A., Babalola, J. O., Vargas, C. & Keller, S. 2017. Solubilization of Membrane Proteins into Functional Lipid-Bilayer Nanodiscs Using a Diisobutylene/Maleic Acid Copolymer. *Angewandte Chemie International Edition,* 56**,** 1919-1924.

Ostrowski, J., Kjelsberg, M. A., Caron, M. G. & Lefkowitz, R. J. 1992. Mutagenesis of the beta2-adrenergic receptor: how structure elucidates function. *Annual Review of Pharmacology and Toxicology,* 32**,** 167-183.

Otsuka, A., Shinbo, H., Matsumoto, R., Kurita, Y. & Ozono, S. 2008. Expression and functional role of β-adrenoceptors in the human urinary bladder urothelium. *Naunyn-Schmiedeberg's Archives of Pharmacology,* 377**,** 473-481.

Paek, J., Kalocsay, M., Staus, D. P., Wingler, L., Pascolutti, R., Paulo, J. A., Gygi, S. P. & Kruse, A. C. 2017. Multidimensional Tracking of GPCR Signaling via Peroxidase-Catalyzed Proximity Labeling. *Cell,* 169**,** 338-349.e311.

Palczewski, K. 2000. Crystal Structure of Rhodopsin: A G Protein-Coupled Receptor. *Science,* 289**,** 739-745.

Palczewski, K., Buczyłko, J., Kaplan, M. W., Polans, A. S. & Crabb, J. W. 1991. Mechanism of rhodopsin kinase activation. *Journal of Biological Chemistry,* 266**,** 12949-12955.

Palczewski, K., Kumasaka, T., Hori, T., Behnke, C. A., Motoshima, H., Fox, B. A., Trong, I. L., Teller, D. C., Okada, T., Stenkamp, R. E., Yamamoto, M. & Miyano, M. 2000. Crystal Structure of Rhodopsin: A G Protein-Coupled Receptor. *Science,* 289**,** 739-745.

Palmqvist, M., Ibsen, T., Mellén, A. & Lötvall, J. 1999. Comparison of the Relative Efficacy of Formoterol and Salmeterol in Asthmatic Patients. *American Journal of Respiratory and Critical Care Medicine,* 160**,** 244-249.

Pándy-Szekeres, G., Munk, C., Tsonkov, T. M., Mordalski, S., Harpsøe, K., Hauser, A. S., Bojarski, A. J. & Gloriam, D. E. 2018. GPCRdb in 2018: adding GPCR structure models and ligands. *Nucleic Acids Research,* 46**,** D440-d446.

Panettieri, R. A., Kotlikoff, M. I., Gerthoffer, W. T., Hershenson, M. B., Woodruff, P. G., Hall, I. P. & Banks-Schlegel, S. 2008. Airway Smooth Muscle in Bronchial Tone, Inflammation, and Remodeling. *American Journal of Respiratory and Critical Care Medicine,* 177**,** 248-252.

Panettieri, R. A., Pera, T., Liggett, S. B., Benovic, J. L. & Penn, R. B. 2018. Pepducins as a potential treatment strategy for asthma and COPD. *Current Opinion in Pharmacology,* 40**,** 120-125.

Pang, R. T.-K., Ng, S. S.-M., Cheng, C. H.-K., Holtmann, M. H., Miller, L. J. & Chow, B. K.-C. 1999. Role of N-Linked Glycosylation on the Function and Expression of the Human Secretin Receptor. *Endocrinology,* 140**,** 5102-5111.

Pani, B., Ahn, S., Rambarat, P. K., Vege, S., Kahsai, A. W., Liu, A., Valan, B. N., Staus, D. P., Costa, T. & Lefkowitz, R. J. 2021. Unique Positive Cooperativity Between the β-Arrestin–Biased β-Blocker Carvedilol and a Small Molecule Positive Allosteric Modulator of the β2-Adrenergic Receptor. *Molecular Pharmacology,* 100**,** 513-525.

Park, P. S. H., Lodowski, D. T. & Palczewski, K. 2008. Activation of G Protein–Coupled Receptors: Beyond Two-State Models and Tertiary Conformational Changes. *Annual Review of Pharmacology and Toxicology,* 48**,** 107-141.

Parvathenani, L. K., Buescher, E. S., Chacon-Cruz, E. & Beebe, S. J. 1998. Type I cAMP-dependent Protein Kinase Delays Apoptosis in Human Neutrophils at a Site Upstream of Caspase-3. *Journal of Biological Chemistry,* 273**,** 6736-6743.

Paton, W. D. M. & Rang, H. P. 1965. The uptake of atropine and related drugs by intestinal smooth muscle of the guinea-pig in relation to acetylcholine receptors. *Proceedings of the Royal Society of London. Series B. Biological Sciences,* 163**,** 1-44.

Pavoine, C. & Defer, N. 2005. The cardiac β2-adrenergic signalling a new role for the cPLA2. *Cellular Signalling,* 17**,** 141-152.

Penn, R. B. & Benovic, J. L. 2011. Regulation of G Protein–Coupled Receptors. *Comprehensive Physiology.* 125-164.

Pérez-Schindler, J., Philp, A. & Hernandez-Cascales, J. 2013. Pathophysiological relevance of the cardiac β2-adrenergic receptor and its potential as a therapeutic target to improve cardiac function. *European Journal of Pharmacology,* 698**,** 39-47.

Peterson, L., Ismond, K. P., Chapman, E. & Flood, P. 2014. Potential Benefits of Therapeutic Use of β2-Adrenergic Receptor Agonists in Neuroprotection and Parkinson's Disease. *Journal of Immunology Research,* 2014**,** 103780.

Pfister, C., Chabre, M., Plouet, J., Tuyen, V., De Kozak, Y., Faure, J. & Kuhn, H. 1985. Retinal S antigen identified as the 48K protein regulating light-dependent phosphodiesterase in rods. *Science,* 228**,** 891-893.

Pierce, K. L., Premont, R. T. & Lefkowitz, R. J. 2002. Seven-transmembrane receptors. *Nature Reviews Molecular Cell Biology,* 3**,** 639-650.

Pingoud, A. & Jeltsch, A. 2001. Structure and function of type II restriction endonucleases. *Nucleic Acids Research,* 29**,** 3705-3727.

Pitcher, J., Inglese, J., Higgins, J., Arriza, J., Casey, P., Kim, C., Benovic, J., Kwatra, M., Caron, M. & Lefkowitz, R. 1992. Role of beta gamma subunits of G proteins in targeting the beta-adrenergic receptor kinase to membrane-bound receptors. *Science,* 257**,** 1264-1267.

Plazinska, A., Plazinski, W. & Jozwiak, K. 2015. Agonist binding by the β2-adrenergic receptor: an effect of receptor conformation on ligand association-dissociation characteristics. *European Biophysics Journal,* 44**,** 149-163.

Pon, C. K., Lane, J. R., Sloan, E. K. & Halls, M. L. 2016. The β2-adrenoceptor activates a positive cAMP-calcium feedforward loop to drive breast cancer cell invasion. *The FASEB Journal,* 30**,** 1144-1154.

Poudel, B., Rajeshwar T, R. & Vanegas, J. M. 2023. Membrane mediated mechanical stimuli produces distinct active-like states in the AT1 receptor. *Nature Communications,* 14**,** 4690.

Premont, R. T. & Gainetdinov, R. R. 2007. Physiological Roles of G Protein–Coupled Receptor Kinases and Arrestins. *Annual Review of Physiology,* 69**,** 511-534.

Price, M. R., Baillie, G. L., Thomas, A., Stevenson, L. A., Easson, M., Goodwin, R., Mclean, A., Mcintosh, L., Goodwin, G., Walker, G., Westwood, P., Marrs, J., Thomson, F., Cowley, P., Christopoulos, A., Pertwee, R. G. & Ross, R. A. 2005. Allosteric Modulation of the Cannabinoid CB1 Receptor. *Molecular Pharmacology,* 68**,** 1484-1495.

Pupo, A. S., Duarte, D. A., Lima, V., Teixeira, L. B., Parreiras-E-Silva, L. T. & Costa-Neto, C. M. 2016. Recent updates on GPCR biased agonism. *Pharmacological Research,* 112**,** 49-57.

Quoyer, J., Janz, J. M., Luo, J., Ren, Y., Armando, S., Lukashova, V., Benovic, J. L., Carlson, K. E., Hunt, S. W., 3rd & Bouvier, M. 2013. Pepducin targeting the C-X-C chemokine receptor type 4 acts as a biased agonist favoring activation of the inhibitory G protein. *Proceedings of the National Academy of Sciences of the United States of America,* 110**,** E5088-5097.

Rajesh, S., Knowles, T. & Overduin, M. 2011. Production of membrane proteins without cells or detergents. *New Biotechnology,* 28**,** 250-254.

Rakesh, K., Yoo, B., Kim, I.-M., Salazar, N., Kim, K.-S. & Rockman, H. A. 2010. β-Arrestin-Biased Agonism of the Angiotensin Receptor Induced by Mechanical Stress. *Science Signaling,* 3**,** ra46-ra46.

Ranade, Sanjeev s., Syeda, R. & Patapoutian, A. 2015. Mechanically Activated Ion Channels. *Neuron,* 87**,** 1162-1179.

Rankovic, Z., Brust, T. F. & Bohn, L. M. 2016. Biased agonism: An emerging paradigm in GPCR drug discovery. *Bioorganic & Medicinal Chemistry Letters,* 26**,** 241-250.

Rask-Andersen, M., Almén, M. S. & Schiöth, H. B. 2011. Trends in the exploitation of novel drug targets. *Nature Reviews Drug Discovery,* 10**,** 579-590.

Rasmussen, S. G., Choi, H. J., Fung, J. J., Pardon, E., Casarosa, P., Chae, P. S., Devree, B. T., Rosenbaum, D. M., Thian, F. S., Kobilka, T. S., Schnapp, A., Konetzki, I., Sunahara, R. K., Gellman, S. H., Pautsch, A., Steyaert, J., Weis, W. I. & Kobilka, B. K. 2011a. Structure of a nanobody-stabilized active state of the beta(2) adrenoceptor. *Nature,* 469**,** 175-180.

Rasmussen, S. G., Choi, H. J., Rosenbaum, D. M., Kobilka, T. S., Thian, F. S., Edwards, P. C., Burghammer, M., Ratnala, V. R., Sanishvili, R., Fischetti, R. F., Schertler, G. F., Weis, W. I. & Kobilka, B. K. 2007. Crystal structure of the human beta2 adrenergic G-protein-coupled receptor. *Nature,* 450**,** 383-387.

Rasmussen, S. G., Devree, B. T., Zou, Y., Kruse, A. C., Chung, K. Y., Kobilka, T. S., Thian, F. S., Chae, P. S., Pardon, E., Calinski, D., Mathiesen, J. M., Shah, S. T., Lyons, J. A., Caffrey, M., Gellman, S. H., Steyaert, J., Skiniotis, G., Weis, W. I., Sunahara, R. K. & Kobilka, B. K. 2011b. Crystal structure of the beta2 adrenergic receptor-Gs protein complex. *Nature,* 477**,** 549-555.

Rath, G., Balligand, J.-L. & Chantal, D. 2012. Vasodilatory Mechanisms of Beta Receptor Blockade. *Current Hypertension Reports,* 14**,** 310-317.

Regard, J. B., Sato, I. T. & Coughlin, S. R. 2008. Anatomical Profiling of G Protein-Coupled Receptor Expression. *Cell,* 135**,** 561-571.

Reid, J. L. 1986. Alpha-adrenergic receptors and blood pressure control. *American Journal of Cardiology,* 57**,** E6-E12.

Reily, C., Stewart, T. J., Renfrow, M. B. & Novak, J. 2019. Glycosylation in health and disease. *Nature Reviews Nephrology,* 15**,** 346-366.

Reiter, E., Ahn, S., Shukla, A. K. & Lefkowitz, R. J. 2012. Molecular Mechanism of β-Arrestin-Biased Agonism at Seven-Transmembrane Receptors. *Annual Review of Pharmacology and Toxicology,* 52**,** 179-197.

Rennard, S., Bantje, T., Centanni, S., Chanez, P., Chuchalin, A., D'urzo, A., Kornmann, O., Perry, S., Jack, D., Owen, R. & Higgins, M. 2008. A dose-ranging study of indacaterol in obstructive airways disease, with a tiotropium comparison. *Respiratory Medicine,* 102**,** 1033-1044.

Reynolds, K., Richard, M. & Ranganathan, R. 2011. Hot Spots for Allosteric Regulation on Protein Surfaces. *Cell,* 147**,** 1564-1575.

Rhee, S. G. & Bae, Y. S. 1997. Regulation of Phosphoinositide-specific Phospholipase C Isozymes. *Journal of Biological Chemistry,* 272**,** 15045-15048.

Rhodes, D. G., Newton, R., Butler, R. & Herbette, L. 1992. Equilibrium and kinetic studies of the interactions of salmeterol with membrane bilayers. *Molecular Pharmacology,* 42**,** 596-602.

Ring, A. M., Manglik, A., Kruse, A. C., Enos, M. D., Weis, W. I., Garcia, K. C. & Kobilka, B. K. 2013. Adrenaline-activated structure of β2-

adrenoceptor stabilized by an engineered nanobody. *Nature,* 502**,** 575-579.

Robertson, N., Jazayeri, A., Errey, J., Baig, A., Hurrell, E., Zhukov, A., Langmead, C. J., Weir, M. & Marshall, F. H. 2011. The properties of thermostabilised G protein-coupled receptors (StaRs) and their use in drug discovery. *Neuropharmacology,* 60**,** 36-44.

Römisch, K. 2005. Endoplasmic reticulum-associated degradation. *Annual Review of Cell and Developmental Biology,* 21**,** 435-456.

Roscioni, S. S., Kistemaker, L. E. M., Menzen, M. H., Elzinga, C. R. S., Gosens, R., Halayko, A. J., Meurs, H. & Schmidt, M. 2009. PKA and Epac cooperate to augment bradykinin-induced interleukin-8 release from human airway smooth muscle cells. *Respiratory Research,* 10**,** 88.

Roscioni, S. S., Maarsingh, H., Elzinga, C. R. S., Schuur, J., Menzen, M., Halayko, A. J., Meurs, H. & Schmidt, M. 2011. Epac as a novel effector of airway smooth muscle relaxation. *Journal of Cellular and Molecular Medicine,* 15**,** 1551-1563.

Rosenbaum, D. M., Cherezov, V., Hanson, M. A., Rasmussen, S. G. F., Thian, F. S., Kobilka, T. S., Choi, H.-J., Yao, X.-J., Weis, W. I., Stevens, R. C. & Kobilka, B. K. 2007. GPCR Engineering Yields High-Resolution Structural Insights into β2-Adrenergic Receptor Function. *Science,* 318**,** 1266-1273.

Rosenbaum, D. M., Rasmussen, S. G. F. & Kobilka, B. K. 2009. The structure and function of G-protein-coupled receptors. *Nature,* 459**,** 356-363.

Rosenbaum, D. M., Zhang, C., Lyons, J. A., Holl, R., Aragao, D., Arlow, D. H., Rasmussen, S. G., Choi, H. J., Devree, B. T., Sunahara, R. K., Chae, P. S., Gellman, S. H., Dror, R. O., Shaw, D. E., Weis, W. I., Caffrey, M.,

Gmeiner, P. & Kobilka, B. K. 2011. Structure and function of an irreversible agonist-β(2) adrenoceptor complex. *Nature,* 469**,** 236-240.

Rosendorff, C. 1993. Beta-blocking agents with vasodilator activity. *Journal of Hypertension,* 11**,** S37-S40.

Rosethorne, E. M., Turner, R. J., Fairhurst, R. A. & Charlton, S. J. 2010. Efficacy is a contributing factor to the clinical onset of bronchodilation of inhaled β2-adrenoceptor agonists. *Naunyn-Schmiedeberg's Archives of Pharmacology,* 382**,** 255-263.

Ross, E. M. & Wilkie, T. M. 2000. GTPase-Activating Proteins for Heterotrimeric G Proteins: Regulators of G Protein Signaling (RGS) and RGS-Like Proteins. *Annual Review of Biochemistry,* 69**,** 795-827.

Ross, T. D., Coon, B. G., Yun, S., Baeyens, N., Tanaka, K., Ouyang, M. & Schwartz, M. A. 2013. Integrins in mechanotransduction. *Current Opinion in Cell Biology,* 25**,** 613-618.

Rovati, G. E., Capra, V. & Neubig, R. R. 2007. The Highly Conserved DRY Motif of Class A G Protein-Coupled Receptors: Beyond the Ground State. *Molecular Pharmacology,* 71**,** 959-964.

Ruddon, R. W. & Bedows, E. 1997. Assisted Protein Folding. *Journal of Biological Chemistry,* 272**,** 3125-3128.

Ruffolo, R. R. 1985. Distribution and function of peripheral α-adrenoceptors in the cardiovascular system. *Pharmacology Biochemistry and Behavior,* 22**,** 827-833.

Ruffolo, R. R. & Hieble, J. P. 1994. α-Adrenoceptors. *Pharmacology & Therapeutics,* 61**,** 1-64.

Samama, P., Cotecchia, S., Costa, T. & Lefkowitz, R. J. 1993. A mutation-induced activated state of the beta 2-adrenergic receptor. Extending the

ternary complex model. *Journal of Biological Chemistry,* 268**,** 4625-4636.

Santos, N. M. D., Gardner, L. A., White, S. W. & Bahouth, S. W. 2006. Characterization of the Residues in Helix 8 of the Human β1-Adrenergic Receptor That Are Involved in Coupling the Receptor to G Proteins *. *Journal of Biological Chemistry,* 281**,** 12896-12907.

Santos, R., Ursu, O., Gaulton, A., Bento, A. P., Donadi, R. S., Bologa, C. G., Karlsson, A., Al-Lazikani, B., Hersey, A., Oprea, T. I. & Overington, J. P. 2017. A comprehensive map of molecular drug targets. *Nature Reviews Drug Discovery,* 16**,** 19-34.

Saraheimo, S., Hepojoki, J., Nurmi, V., Lahtinen, A., Hemmilä, I., Vaheri, A., Vapalahti, O. & Hedman, K. 2013. Time-Resolved FRET -Based Approach for Antibody Detection – A New Serodiagnostic Concept. *PLoS One,* 8**,** e62739.

Sardi, I., Giunti, L., Bresci, C., Buccoliero, A. M., Degl'innocenti, D., Cardellicchio, S., Baroni, G., Castiglione, F., Da Ros, M., Fiorini, P., Giglio, S., Genitori, L., Aricò, M. & Filippi, L. 2013. Expression of β-adrenergic receptors in pediatric malignant brain tumors. *Oncology Letters,* 5**,** 221-225.

Sato, T., Baker, J., Warne, T., Brown, G. A., Leslie, A. G. W., Congreve, M. & Tate, C. G. 2015. Pharmacological Analysis and Structure Determination of 7-Methylcyanopindolol–Bound β1-Adrenergic Receptor. *Molecular Pharmacology,* 88**,** 1024-1034.

Schertler, G. F. X., Villa, C. & Henderson, R. 1993. Projection structure of rhodopsin. *Nature,* 362**,** 770-772.

Schild, H. O. 1949. pAx and competitive drug antagonism. *British Journal of Pharmacology and Chemotherapy,* 4**,** 277-280.

Schiöth, H. B. & Fredriksson, R. 2005. The GRAFS classification system of G-protein coupled receptors in comparative perspective. *General and Comparative Endocrinology,* 142**,** 94-101.

Scholz, N., Dahse, A.-K., Kemkemer, M., Bormann, A., Auger, G. M., Vieira Contreras, F., Ernst, L. F., Staake, H., Körner, M. B., Buhlan, M., Meyer-Mölck, A., Chung, Y. K., Blanco-Redondo, B., Klose, F., Jarboui, M. A., Ljaschenko, D., Bigl, M. & Langenhan, T. 2023. Molecular sensing of mechano- and ligand-dependent adhesion GPCR dissociation. *Nature,* 615**,** 945-953.

Scholz, N., Gehring, J., Guan, C., Ljaschenko, D., Fischer, R., Lakshmanan, V., Kittel, R. J. & Langenhan, T. 2015. The Adhesion GPCR Latrophilin/CIRL Shapes Mechanosensation. *Cell Reports,* 11**,** 866-874.

Schubert, R., Gaynullina, D., Shvetsova, A. & Tarasova, O. S. 2023. Myography of isolated blood vessels: Considerations for experimental design and combination with supplementary techniques. *Frontiers in Physiology,* 14**,** 1176748.

Schwartz, M. A. 2010. Integrins and Extracellular Matrix in Mechanotransduction. *Cold Spring Harbor Perspectives in Biology,* 2**,** a005066-a005066.

Schwinn, M. K., Machleidt, T., Zimmerman, K., Eggers, C. T., Dixon, A. S., Hurst, R., Hall, M. P., Encell, L. P., Binkowski, B. F. & Wood, K. V. 2018. CRISPR-Mediated Tagging of Endogenous Proteins with a Luminescent Peptide. *ACS Chemical Biology,* 13**,** 467-474.

Scimia, M. C., Hurtado, C., Ray, S., Metzler, S., Wei, K., Wang, J., Woods, C. E., Purcell, N. H., Catalucci, D., Akasaka, T., Bueno, O. F., Vlasuk, G. P., Kaliman, P., Bodmer, R., Smith, L. H., Ashley, E., Mercola, M., Brown, J. H. & Ruiz-Lozano, P. 2012. APJ acts as a dual receptor in cardiac hypertrophy. *Nature,* 488**,** 394-398.

Scott, H. & Panin, V. M. 2014. The role of protein N-glycosylation in neural transmission. *Glycobiology,* 24**,** 407-417.

Seamon, K. & Daly, J. W. 1981. Activation of adenylate cyclase by the diterpene forskolin does not require the guanine nucleotide regulatory protein. *Journal of Biological Chemistry,* 256**,** 9799-9801.

Sears, M. R. & Lötvall, J. 2005. Past, present and future—β2-adrenoceptor agonists in asthma management. *Respiratory Medicine,* 99**,** 152-170.

Sears, M. R., Taylor, D. R., Print, C. G., Lake, D. C., Li, Q., Flannery, E. M., Yates, D. M., Lucas, M. K. & Herbison, G. P. 1990. Regular inhaled beta-agonist treatment in bronchial asthma. *The Lancet,* 336**,** 1391-1396.

Seddon, A. M., Curnow, P. & Booth, P. J. 2004. Membrane proteins, lipids and detergents: not just a soap opera. *Biochimica et Biophysica Acta (BBA) - Biomembranes,* 1666**,** 105-117.

Serezani, C. H., Ballinger, M. N., Aronoff, D. M. & Peters-Golden, M. 2008. Cyclic AMP: master regulator of innate immune cell function. *American Journal of Respiratory Cell and Molecular Biology,* 39**,** 127-132.

Serrano-Vega, M. J., Magnani, F., Shibata, Y. & Tate, C. G. 2008. Conformational thermostabilization of the β1-adrenergic receptor in a detergent-resistant form. *Proceedings of the National Academy of Sciences,* 105**,** 877-882.

Sevigny, L. M., Zhang, P., Bohm, A., Lazarides, K., Perides, G., Covic, L. & Kuliopulos, A. 2011. Interdicting protease-activated receptor-2-driven inflammation with cell-penetrating pepducins. *Proceedings of the National Academy of Sciences,* 108**,** 8491-8496.

Shah, S. D., Lind, C., De Pascali, F., Penn, R. B., Mackerell, A. D. & Deshpande, D. A. 2022. In silico identification of a β2-adrenoceptor allosteric site

that selectively augments canonical β2AR-Gs signaling and function. *Proceedings of the National Academy of Sciences,* 119**,** e2214024119.

Shan, T., Ma, Q., Zhang, D., Guo, K., Liu, H., Wang, F. & Wu, E. 2011. β2-adrenoceptor blocker synergizes with gemcitabine to inhibit the proliferation of pancreatic cancer cells via apoptosis induction. *European Journal of Pharmacology,* 665**,** 1-7.

Shear, M., Insel, P. A., Melmon, K. L. & Coffino, P. 1976. Agonist-specific refractoriness induced by isoproterenol. Studies with mutant cells. *Journal of Biological Chemistry,* 251**,** 7572-7576.

Shenoy, S. K. & Lefkowitz, R. J. 2003. Multifaceted roles of β-arrestins in the regulation of seven-membrane-spanning receptor trafficking and signalling. *Biochemical Journal,* 375**,** 503-515.

Shenoy, S. K. & Lefkowitz, R. J. 2005. Receptor-specific Ubiquitination of β-Arrestin Directs Assembly and Targeting of Seven-transmembrane Receptor Signalosomes *. *Journal of Biological Chemistry,* 280**,** 15315-15324.

Shental-Bechor, D. & Levy, Y. 2009. Folding of glycoproteins: toward understanding the biophysics of the glycosylation code. *Current Opinion in Structural Biology,* 19**,** 524-533.

Shi, L., Liapakis, G., Xu, R., Guarnieri, F., Ballesteros, J. A. & Javitch, J. A. 2002. 2 Adrenergic Receptor Activation: Modulation of the proline kink in tramsmembrane 6 by a rotamer toggle switch. *The Journal of Biological Chemistry,* 277**,** 40989-40996.

Shimada, I., Ueda, T., Kofuku, Y., Eddy, M. T. & Wüthrich, K. 2019. GPCR drug discovery: integrating solution NMR data with crystal and cryo-EM structures. *Nature Reviews Drug Discovery,* 18**,** 59-82.

Shukla, A. K., Singh, G. & Ghosh, E. 2014a. Emerging structural insights into biased GPCR signaling. *Trends in Biochemical Sciences,* 39**,** 594-602.

Shukla, A. K., Violin, J. D., Whalen, E. J., Gesty-Palmer, D., Shenoy, S. K. & Lefkowitz, R. J. 2008. Distinct conformational changes in β-arrestin report biased agonism at seven-transmembrane receptors. *Proceedings of the National Academy of Sciences,* 105**,** 9988-9993.

Shukla, A. K., Westfield, G. H., Xiao, K., Reis, R. I., Huang, L.-Y., Tripathi-Shukla, P., Qian, J., Li, S., Blanc, A., Oleskie, A. N., Dosey, A. M., Su, M., Liang, C.-R., Gu, L.-L., Shan, J.-M., Chen, X., Hanna, R., Choi, M., Yao, X. J., Klink, B. U., Kahsai, A. W., Sidhu, S. S., Koide, S., Penczek, P. A., Kossiakoff, A. A., Woods Jr, V. L., Kobilka, B. K., Skiniotis, G. & Lefkowitz, R. J. 2014b. Visualization of arrestin recruitment by a G-protein-coupled receptor. *Nature,* 512**,** 218-222.

Slosky, L. M., Caron, M. G. & Barak, L. S. 2021. Biased Allosteric Modulators: New Frontiers in GPCR Drug Discovery. *Trends in Pharmacological Sciences,* 42**,** 283-299.

Small, K. M., Mcgraw, D. W. & Liggett, S. B. 2003. Pharmacology and physiology of human adrenergic receptor polymorphisms. *Annual Review of Pharmacology and Toxicology,* 43**,** 381-411.

Smith, J. S., Lefkowitz, R. J. & Rajagopal, S. 2018. Biased signalling: from simple switches to allosteric microprocessors. *Nature Reviews Drug Discovery,* 17**,** 243-260.

Soave, M., Kellam, B., Woolard, J., Briddon, S. J. & Hill, S. J. 2020. NanoBiT complementation to monitor agonist-induced adenosine A1 receptor internalization. *SLAS Discovery : Advancing the Science of Drug Discovery,* 25**,** 186-194.

Sonawane, N. D., Szoka, F. C., Jr. & Verkman, A. S. 2003. Chloride Accumulation and Swelling in Endosomes Enhances DNA Transfer by Polyamine-DNA Polyplexes *. *Journal of Biological Chemistry,* 278**,** 44826-44831.

Stanojkovic, T. P., Zizak, Z., Mihailovic-Stanojevic, N., Petrovic, T. & Juranic, Z. 2005. Inhibition of proliferation on some neoplastic cell lines-act of carvedilol and captopril. *Journal of experimental & clinical cancer research : CR,* 24**,** 387-395.

Steen, P. V. D., Rudd, P. M., Dwek, R. A. & Opdenakker, G. 1998. Concepts and Principles of O-Linked Glycosylation. *Critical Reviews in Biochemistry and Molecular Biology,* 33**,** 151-208.

Stephenson, R. P. 1956. A modification of receptor theory. *British Journal of Pharmacology,* 11**,** 379-393.

Stevens, R. C., Cherezov, V., Katritch, V., Abagyan, R., Kuhn, P., Rosen, H. & Wüthrich, K. 2013. The GPCR Network: a large-scale collaboration to determine human GPCR structure and function. *Nature Reviews Drug Discovery,* 12**,** 25-34.

Stich, V., Glisezinski, I. D., Crampes, F., Suljkovicova, H., Galitzky, J., Riviere, D., Hejnova, J., Lafontan, M. & Berlan, M. 1999. Activation of antilipolytic α2-adrenergic receptors by epinephrine during exercise in human adipose tissue. *American Journal of Physiology-Regulatory, Integrative and Comparative Physiology,* 277**,** R1076-R1083.

Stiles, G. L., Caron, M. G. & Lefkowitz, R. J. 1984. Beta-adrenergic receptors: biochemical mechanisms of physiological regulation. *Physiological Reviews,* 64**,** 661-743.

Stockton, J. M., Birdsall, N. J., Burgen, A. S. & Hulme, E. C. 1983. Modification of the binding properties of muscarinic receptors by gallamine. *Molecular Pharmacology,* 23**,** 551-557.

Stoffel, R. H., Pitcher, J. A. & Lefkowitz, R. J. 1997. Targeting G protein-coupled receptor kinases to their receptor substrates. *The Journal of Membrane Biology,* 157**,** 1-8.

Storch, U., Schnitzler, M. M. Y. & Gudermann, T. 2012. G protein-mediated stretch reception. *American Journal of Physiology-Heart and Circulatory Physiology,* 302**,** H1241-H1249.

Storme, J., Cannaert, A., Van Craenenbroeck, K. & Stove, C. P. 2018. Molecular dissection of the human A3 adenosine receptor coupling with β-arrestin2. *Biochemical Pharmacology,* 148**,** 298-307.

Strader, C. D., Fong, T. M., Tota, M. R., Underwood, D. & Dixon, R. a. F. 1994. Structure and function of G protein-coupled receptors. *Annual Review of Biochemistry,* 63**,** 101-132.

Strotmann, R., Schröck, K., Böselt, I., Stäubert, C., Russ, A. & Schöneberg, T. 2011. Evolution of GPCR: Change and continuity. *Molecular and Cellular Endocrinology,* 331**,** 170-178.

Stroud, Z., Hall, S. C. L. & Dafforn, T. R. 2018. Purification of membrane proteins free from conventional detergents: SMA, new polymers, new opportunities and new insights. *Methods,* 147**,** 106-117.

Sturton, R. G., Trifilieff, A., Nicholson, A. G. & Barnes, P. J. 2007. Pharmacological Characterization of Indacaterol, a Novel Once Daily Inhaled 2 Adrenoceptor Agonist, on Small Airways in Human and Rat Precision-Cut Lung Slices. *The Journal of Pharmacology and Experimental Therapeutics,* 324**,** 270-275.

Süel, G. M., Lockless, S. W., Wall, M. A. & Ranganathan, R. 2003. Evolutionarily conserved networks of residues mediate allosteric communication in proteins. *Nature Structural Biology,* 10**,** 59-69.

Sukharev, S. I., Blount, P., Martinac, B., Blattner, F. R. & Kung, C. 1994. A large-conductance mechanosensitive channel in E. coli encoded by mscL alone. *Nature,* 368**,** 265-268.

Sun, Z., Guo, S. S. & Fässler, R. 2016. Integrin-mediated mechanotransduction. *Journal of Cell Biology,* 215**,** 445-456.

Sunahara, R. K., Dessauer, C. W. & Gilman, A. G. 1996. Complexity and Diversity of Mammalian Adenylyl Cyclases. *Annual Review of Pharmacology and Toxicology,* 36**,** 461-480.

Sutor, B. & Ten Bruggencate, G. 1990. Ascorbic acid: A useful reductant to avoid oxidation of catecholamines in electrophysiological experiments in vitro? *Neuroscience Letters,* 116**,** 287-292.

Swaminath, G., Lee, T. W. & Kobilka, B. 2003. Identification of an Allosteric Binding Site for Zn2+on the β2 Adrenergic Receptor *. *Journal of Biological Chemistry,* 278**,** 352-356.

Swaminath, G., Steenhuis, J., Kobilka, B. & Lee, T. W. 2002. Allosteric Modulation of β2-Adrenergic Receptor by Zn2+. *Molecular Pharmacology,* 61**,** 65-72.

Sykes, D. A., Bradley, M. E., Riddy, D. M., Willard, E., Reilly, J., Miah, A., Bauer, C., Watson, S. J., Sandham, D. A., Dubois, G. & Charlton, S. J. 2016. Fevipiprant (QAW039), a Slowly Dissociating CRTh2 Antagonist with the Potential for Improved Clinical Efficacy. *Molecular Pharmacology,* 89**,** 593-605.

Sykes, D. A. & Charlton, S. J. 2012. Slow receptor dissociation is not a key factor in the duration of action of inhaled long-acting β2-adrenoceptor agonists. *British Journal of Pharmacology,* 165**,** 2672-2683.

Sykes, D. A. & Charlton, S. J. 2018. Single Step Determination of Unlabeled Compound Kinetics Using a Competition Association Binding Method Employing Time-Resolved FRET. *In:* Mavromoustakos, T. & Kellici, T. F. (eds.) *Rational Drug Design: Methods and Protocols.* New York, NY: Springer New York**,** 177-194.

Sykes, D. A., Parry, C., Reilly, J., Wright, P., Fairhurst, R. A. & Charlton, S. J. 2014. Observed Drug-Receptor Association Rates Are Governed by Membrane Affinity: The Importance of Establishing "Micro-Pharmacokinetic/Pharmacodynamic Relationships" at the β2-Adrenoceptor. *Molecular Pharmacology,* 85**,** 608-617.

Sykes, D. A., Stoddart, L. A., Kilpatrick, L. E. & Hill, S. J. 2019. Binding kinetics of ligands acting at GPCRs. *Molecular and Cellular Endocrinology,* 485**,** 9-19.

Syrovatkina, V., Alegre, K. O., Dey, R. & Huang, X.-Y. 2016. Regulation, Signaling, and Physiological Functions of G-Proteins. *Journal of Molecular Biology,* 428**,** 3850-3868.

Szczuka, A., Wennerberg, M., Packeu, A. & Vauquelin, G. 2009. Molecular mechanisms for the persistent bronchodilatory effect of the β2-adrenoceptor agonist salmeterol. *British Journal of Pharmacology,* 158**,** 183-194.

Takahashi, M., Kizuka, Y., Ohtsubo, K., Gu, J. & Taniguchi, N. 2016. Disease-associated glycans on cell surface proteins. *Molecular Aspects of Medicine,* 51**,** 56-70.

Takemoto, J., Masumiya, H., Nunoki, K., Sato, T., Nakagawa, H., Ikeda, Y., Arai, Y. & Yanagisawa, T. 2008. Potentiation of Potassium Currents by Beta-Adrenoceptor Agonists in Human Urinary Bladder Smooth Muscle Cells: A Possible Electrical Mechanism of Relaxation. *Pharmacology,* 81**,** 251-258.

Tallarida, R. J. & Murray, R. B. 1987. pA2 Analysis I: Schild Plot. *Manual of Pharmacologic Calculations: With Computer Programs.* New York, NY: Springer New York**,** 53-56.

Tanaka, K., Joshi, D., Timalsina, S. & Schwartz, M. A. 2021. Early events in endothelial flow sensing. *Cytoskeleton,* 78**,** 217-231.

Tanaka, Y., Horinouchi, T. & Koike, K. 2005. New insights into β-adrenoceptors in smooth muscle: distribution of receptor subtypes and molecular mechanisms triggering muscle relaxation. *Clinical and Experimental Pharmacology and Physiology,* 32**,** 503-514.

Tang, W.-J. & Gilman, A. G. 1991. Type-Specific Regulation of Adenylyl Cyclase by G Protein βγ Subunits. *Science,* 254**,** 1500-1503.

Taniguchi, N. & Kizuka, Y. 2015. Chapter Two - Glycans and Cancer: Role of N-Glycans in Cancer Biomarker, Progression and Metastasis, and Therapeutics. *In:* Drake, R. R. & Ball, L. E. (eds.) *Advances in Cancer Research.* Academic Press**,** 11-51.

Tannous, A., Pisoni, G. B., Hebert, D. N. & Molinari, M. 2015. N-linked sugar-regulated protein folding and quality control in the ER. *Seminars in Cell & Developmental Biology,* 41**,** 79-89.

Tashkin, D. P. & Fabbri, L. M. 2010. Long-acting beta-agonists in the management of chronic obstructive pulmonary disease: current and future agents. *Respiratory Research,* 11**,** 149.

Tate, C. G. 2012. A crystal clear solution for determining G-protein-coupled receptor structures. *Trends in Biochemical Sciences,* 37**,** 343-352.

Tchernychev, B., Ren, Y., Sachdev, P., Janz, J. M., Haggis, L., O'shea, A., Mcbride, E., Looby, R., Deng, Q., Mcmurry, T., Kazmi, M. A., Sakmar, T. P., Hunt, S. & Carlson, K. E. 2010. Discovery of a CXCR4 agonist pepducin that mobilizes bone marrow hematopoietic cells. *Proceedings of the National Academy of Sciences,* 107**,** 22255-22259.

Thomas, P. & Smart, T. G. 2005. HEK293 cell line: A vehicle for the expression of recombinant proteins. *Journal of Pharmacological and Toxicological Methods,* 51**,** 187-200.

Thompson, A. A., Liu, J. J., Chun, E., Wacker, D., Wu, H., Cherezov, V. & Stevens, R. C. 2011. GPCR stabilization using the bicelle-like architecture of mixed sterol-detergent micelles. *Methods,* 55**,** 310-317.

Thompson, G. L., Lane, J. R., Coudrat, T., Sexton, P. M., Christopoulos, A. & Canals, M. 2016. Systematic analysis of factors influencing observations of biased agonism at the mu-opioid receptor. *Biochemical Pharmacology,* 113**,** 70-87.

Tippett, D. N., Hoare, B., Miljus, T., Sykes, D. A. & Veprintsev, D. B. 2020. ThermoFRET: A novel nanoscale G protein coupled receptor thermostability assay functional in crude solubilised membrane preparations. *bioRxiv***,** 2020.2007.2007.191957.

Touhara, K., Inglese, J., Pitcher, J. A., Shaw, G. & Lefkowitz, R. J. 1994. Binding of G protein beta gamma-subunits to pleckstrin homology domains. *Journal of Biological Chemistry,* 269**,** 10217-10220.

Tran, T. M., Friedman, J., Qunaibi, E., Baameur, F., Moore, R. H. & Clark, R. B. 2004. Characterization of Agonist Stimulation of cAMP-Dependent Protein Kinase and G Protein-Coupled Receptor Kinase Phosphorylation

of the β2-Adrenergic Receptor Using Phosphoserine-Specific Antibodies. *Molecular Pharmacology,* 65**,** 196-206.

Tressel, S. L., Koukos, G., Tchernychev, B., Jacques, S. L., Covic, L. & Kuliopulos, A. 2011. Pharmacology, Biodistribution, and Efficacy of GPCR-Based Pepducins in Disease Models. *In:* Biology, M. I. M. (ed.). Humana Press**,** 259-275.

Tsuji, M., Ueda, S., Hirayama, T., Okuda, K., Sakaguchi, Y., Isono, A. & Nagasawa, H. 2013. FRET-based imaging of transbilayer movement of pepducin in living cells by novel intracellular bioreductively activatable fluorescent probes. *Organic & Biomolecular Chemistry,* 11**,** 3030-3037.

Ullman, A. & Svedmyr, N. 1988. Salmeterol, a new long acting inhaled beta 2 adrenoceptor agonist: comparison with salbutamol in adult asthmatic patients. *Thorax,* 43**,** 674-678.

Vagin, O., Kraut, J. A. & Sachs, G. 2009. Role of N-glycosylation in trafficking of apical membrane proteins in epithelia. *American Journal of Physiology-Renal Physiology,* 296**,** F459-F469.

Valant, C., Felder, C. C., Sexton, P. M. & Christopoulos, A. 2012. Probe Dependence in the Allosteric Modulation of a G Protein-Coupled Receptor: Implications for Detection and Validation of Allosteric Ligand Effects. *Molecular Pharmacology,* 81**,** 41-52.

Van Neuren, A. S., Müller, G., Klebe, G. & Moroder, L. 1999. Molecular Modelling Studies on g Protein-Coupled Receptors: From Sequence to Structure? *Journal of Receptors and Signal Transduction,* 19**,** 341-353.

Vanhoutte, P. M. 2001. Endothelial Adrenoceptors. *Journal of Cardiovascular Pharmacology,* 38**,** 796-808.

Vatner, D. E., Knight, D. R., Homcy, C. J., Vatner, S. F. & Young, M. A. 1986. Subtypes of beta-adrenergic receptors in bovine coronary arteries. *Circulation Research,* 59**,** 463-473.

Vauquelin, G., Van Liefde, I., Birzbier, B. B. & Vanderheyden, P. M. 2002. New insights in insurmountable antagonism. *Fundamental and Clinical Pharmacology,* 16**,** 263-272.

Velmurugan, B. K., Baskaran, R. & Huang, C.-Y. 2019. Detailed insight on β-adrenoceptors as therapeutic targets. *Biomedicine & Pharmacotherapy,* 117**,** 109039.

Venkatakrishnan, A. J., Deupi, X., Lebon, G., Heydenreich, F. M., Flock, T., Miljus, T., Balaji, S., Bouvier, M., Veprintsev, D. B., Tate, C. G., Schertler, G. F. X. & Babu, M. M. 2016. Diverse activation pathways in class A GPCRs converge near the G-protein-coupling region. *Nature,* 536**,** 484-487.

Venkatakrishnan, A. J., Deupi, X., Lebon, G., Tate, C. G., Schertler, G. F. & Babu, M. M. 2013. Molecular signatures of G-protein-coupled receptors. *Nature,* 494**,** 185-194.

Venter, J. C., Adams, M. D., Myers, E. W., Li, P. W., Mural, R. J., Sutton, G. G., Smith, H. O., Yandell, M., Evans, C. A., Holt, R. A., Gocayne, J. D., Amanatides, P., Ballew, R. M., Huson, D. H., Wortman, J. R., Zhang, Q., Kodira, C. D., Zheng, X. H., Chen, L., Skupski, M., Subramanian, G., Thomas, P. D., Zhang, J., Miklos, G. L. G., Nelson, C., Broder, S., Clark, A. G., Nadeau, J., Mckusick, V. A., Zinder, N., Levine, A. J., Roberts, R. J., Simon, M., Slayman, C., Hunkapiller, M., Bolanos, R., Delcher, A., Dew, I., Fasulo, D., Flanigan, M., Florea, L., Halpern, A., Hannenhalli, S., Kravitz, S., Levy, S., Mobarry, C., Reinert, K., Remington, K., Abu-Threideh, J., Beasley, E., Biddick, K., Bonazzi, V., Brandon, R., Cargill, M., Chandramouliswaran, I., Charlab, R., Chaturvedi, K., Deng, Z., Francesco, V. D., Dunn, P., Eilbeck, K., Evangelista, C., Gabrielian, A.

E., Gan, W., Ge, W., Gong, F., Gu, Z., Guan, P., Heiman, T. J., Higgins, M. E., Ji, R.-R., Ke, Z., Ketchum, K. A., Lai, Z., Lei, Y., Li, Z., Li, J., Liang, Y., Lin, X., Lu, F., Merkulov, G. V., Milshina, N., Moore, H. M., Naik, A. K., Narayan, V. A., Neelam, B., Nusskern, D., Rusch, D. B., Salzberg, S., Shao, W., Shue, B., Sun, J., Wang, Z. Y., Wang, A., Wang, X., Wang, J., Wei, M.-H., Wides, R., Xiao, C., Yan, C., et al. 2001. The Sequence of the Human Genome. *Science,* 291**,** 1304-1351.

Virion, Z., Doly, S., Saha, K., Lambert, M., Guillonneau, F., Bied, C., Duke, R. M., Rudd, P. M., Robbe-Masselot, C., Nassif, X., Coureuil, M. & Marullo, S. 2019. Sialic acid mediated mechanical activation of β2 adrenergic receptors by bacterial pili. *Nature Communications,* 10**,** 4752.

Vogel, R., Mahalingam, M., Lüdeke, S., Huber, T., Siebert, F. & Sakmar, T. P. 2008. Functional Role of the "Ionic Lock"—An Interhelical Hydrogen-Bond Network in Family A Heptahelical Receptors. *Journal of Molecular Biology,* 380**,** 648-655.

Vuorio, J., Škerlová, J., Fábry, M., Veverka, V., Vattulainen, I., Řezáčová, P. & Martinez-Seara, H. 2021. N-Glycosylation can selectively block or foster different receptor–ligand binding modes. *Scientific Reports,* 11**,** 5239.

Wachter, S. B. & Gilbert, E. M. 2012. Beta-Adrenergic Receptors, from Their Discovery and Characterization through Their Manipulation to Beneficial Clinical Application. *Cardiology,* 122**,** 104-112.

Wacker, D., Fenalti, G., Brown, M. A., Katritch, V., Abagyan, R., Cherezov, V. & Stevens, R. C. 2010. Conserved binding mode of human beta2 adrenergic receptor inverse agonists and antagonist revealed by X-ray crystallography. *Journal of the American Chemical Society,* 132**,** 11443-11445.

Walker, J., Penn, R., Hanania, N., Dickey, B. & Bond, R. 2011. New perspectives regarding β2-adrenoceptor ligands in the treatment of asthma. *British Journal of Pharmacology,* 163**,** 18-28.

Walker, J. M. 2009. The Bicinchoninic Acid (BCA) Assay for Protein Quantitation. *In:* Walker, J. M. (ed.) *The Protein Protocols Handbook.* Totowa, NJ: Humana Press**,** 11-15.

Wang, J., Hanada, K., Gareri, C. & Rockman, H. A. 2018. Mechanoactivation of the angiotensin II type 1 receptor induces β-arrestin-biased signaling through Gαi coupling. *Journal of Cellular Biochemistry,* 119**,** 3586-3597.

Wang, X., Yuan, S. & Chan, H. C. S. 2022. Translocation Mechanism of Allosteric Sodium Ions in β2-Adrenoceptor. *Journal of Chemical Information and Modeling,* 62**,** 3090-3095.

Warne, T., Edwards, Patricia c., Leslie, Andrew g. W. & Tate, Christopher g. 2012. Crystal Structures of a Stabilized β1-Adrenoceptor Bound to the Biased Agonists Bucindolol and Carvedilol. *Structure,* 20**,** 841-849.

Wei, W.-C., Bianchi, F., Wang, Y.-K., Tang, M.-J., Ye, H. & Glitsch, M. D. 2018. Coincidence Detection of Membrane Stretch and Extracellular pH by the Proton-Sensing Receptor OGR1 (GPR68). *Current Biology,* 28**,** 3815-3823.e3814.

Weis, W. I. & Kobilka, B. K. 2018. The Molecular Basis of G Protein–Coupled Receptor Activation. *Annual Review of Biochemistry,* 87**,** 897-919.

Weiß, H. M. & Grisshammer, R. 2002. Purification and characterization of the human adenosine A2a receptor functionally expressed in Escherichia coli. *European Journal of Biochemistry,* 269**,** 82-92.

Weiss, J. M., Morgan, P. H., Lutz, M. W. & Kenakin, T. P. 1996. The Cubic Ternary Complex Receptor–Occupancy Model I. Model Description. *Journal of Theoretical Biology,* 178**,** 151-167.

Welte, T. & Groneberg, D. A. 2006. Asthma and COPD. *Experimental and Toxicologic Pathology,* 57**,** 35-40.

Wenceslau, C. F., Mccarthy, C. G., Earley, S., England, S. K., Filosa, J. A., Goulopoulou, S., Gutterman, D. D., Isakson, B. E., Kanagy, N. L., Martinez-Lemus, L. A., Sonkusare, S. K., Thakore, P., Trask, A. J., Watts, S. W. & Webb, R. C. 2021. Guidelines for the measurement of vascular function and structure in isolated arteries and veins. *American Journal of Physiology-Heart and Circulatory Physiology,* 321**,** H77-H111.

Weninger, S., Van Craenenbroeck, K., Cameron, R. T., Vandeput, F., Movsesian, M. A., Baillie, G. S. & Lefebvre, R. A. 2014. Phosphodiesterase 4 interacts with the 5-HT4(b) receptor to regulate cAMP signaling. *Cellular Signalling,* 26**,** 2573-2582.

Westfield, G. H., Rasmussen, S. G. F., Su, M., Dutta, S., Devree, B. T., Chung, K. Y., Calinski, D., Velez-Ruiz, G., Oleskie, A. N., Pardon, E., Chae, P. S., Liu, T., Li, S., Woods, V. L., Steyaert, J., Kobilka, B. K., Sunahara, R. K. & Skiniotis, G. 2011. Structural flexibility of the Gαs α-helical domain in the β2-adrenoceptor Gs complex. *Proceedings of the National Academy of Sciences,* 108**,** 16086-16091.

Wettschureck, N. & Offermanns, S. 2005. Mammalian G Proteins and Their Cell Type Specific Functions. *Physiological Reviews,* 85**,** 1159-1204.

Whalen, E. J., Rajagopal, S. & Lefkowitz, R. J. 2011. Therapeutic potential of β-arrestin- and G protein-biased agonists. *Trends in Molecular Medicine,* 17**,** 126-139.

Whaley, B. S., Yuan, N., Birnbaumer, L., Clark, R. B. & Barber, R. 1994. Differential expression of the beta-adrenergic receptor modifies agonist stimulation of adenylyl cyclase: a quantitative evaluation. *Molecular Pharmacology,* 45**,** 481-489.

Wheatley, M., Wootten, D., Conner, M., Simms, J., Kendrick, R., Logan, R., Poyner, D. & Barwell, J. 2012. Lifting the lid on GPCRs: the role of extracellular loops. *British Journal of Pharmacology,* 165**,** 1688-1703.

White, C. W., Caspar, B., Vanyai, H. K., Pfleger, K. D. G. & Hill, S. J. 2020. CRISPR-Mediated Protein Tagging with Nanoluciferase to Investigate Native Chemokine Receptor Function and Conformational Changes. *Cell Chemical Biology,* 27**,** 499-510.e497.

Wielders, S. J. H., Bennaghmouch, A., Reutelingsperger, C. P. M., Bevers, E. M. & Lindhout, T. 2007. Anticoagulant and antithrombotic properties of intracellular protease-activated receptor antagonists. *Journal of Thrombosis and Haemostasis,* 5**,** 571-576.

Wild, C., Cunningham, K. A. & Zhou, J. 2014. Allosteric Modulation of G Protein-Coupled Receptors: An Emerging Approach of Drug Discovery. *Austin Journal of Pharmacology and Therapeutics,* 2**,** 1101.

Wilde, C., Mitgau, J., Suchý, T., Schöneberg, T. & Liebscher, I. 2022. Translating the force—mechano-sensing GPCRs. *American Journal of Physiology-Cell Physiology,* 322**,** C1047-C1060.

Wilson, C., Wilson, S., Piercy, V., Sennitt, M. V. & Arch, J. R. S. 1984. The rat lipolytic β-adrenoceptor: Studies using novel β-adrenoceptor agonists. *European Journal of Pharmacology,* 100**,** 309-319.

Wilson, J. M., Lorimer, E., Tyburski, M. D. & Williams, C. L. 2015. β-Adrenergic receptors suppress Rap1B prenylation and promote the metastatic phenotype in breast cancer cells. *Cancer Biology & Therapy,* 16**,** 1364-1374.

Wiseman, D. N., Otchere, A., Patel, J. H., Uddin, R., Pollock, N. L., Routledge, S. J., Rothnie, A. J., Slack, C., Poyner, D. R., Bill, R. M. & Goddard, A.

D. 2020. Expression and purification of recombinant G protein-coupled receptors: A review. *Protein Expression and Purification,* 167**,** 105524.

Wisler, J. W., Dewire, S. M., Whalen, E. J., Violin, J. D., Drake, M. T., Ahn, S., Shenoy, S. K. & Lefkowitz, R. J. 2007. A unique mechanism of beta-blocker action: Carvedilol stimulates beta-arrestin signaling. *Proceedings of the National Academy of Sciences,* 104**,** 16657-16662.

Wold, E. A., Chen, J., Cunningham, K. A. & Zhou, J. 2019. Allosteric Modulation of Class A GPCRs: Targets, Agents, and Emerging Concepts. *Journal of Medicinal Chemistry,* 62**,** 88-127.

Won, C.-K. & Oh, Y. S. 2000. cAMP-induced stellation in primary astrocyte cultures with regional heterogeneity. *Brain Research,* 887**,** 250-258.

Woo, A. Y. H. & Xiao, R.-P. 2012. β-Adrenergic receptor subtype signaling in heart: From bench to bedside. *Acta Pharmacologica Sinica,* 33**,** 335-341.

Wootten, D., Christopoulos, A., Marti-Solano, M., Babu, M. M. & Sexton, P. M. 2018. Mechanisms of signalling and biased agonism in G protein-coupled receptors. *Nature Reviews Molecular Cell Biology,* 19**,** 638-653.

Wright, S. C. & Bouvier, M. 2021. Illuminating the complexity of GPCR pathway selectivity – advances in biosensor development. *Current Opinion in Structural Biology,* 69**,** 142-149.

Wyllie, D. J. A. & Chen, P. E. 2007. Taking The Time To Study Competitive Antagonism. *British Journal of Pharmacology,* 150**,** 541-551.

Xiao, K. & Liu, H. 2016. "Barcode" and Differential Effects of GPCR Phosphorylation by Different GRKs. *In:* Gurevich, V. V., Gurevich, E. V. & Tesmer, J. J. G. (eds.) *G Protein-Coupled Receptor Kinases.* New York, NY: Springer New York**,** 75-120.

Xu, J., Mathur, J., Vessières, E., Hammack, S., Nonomura, K., Favre, J., Grimaud, L., Petrus, M., Francisco, A., Li, J., Lee, V., Xiang, F.-L., Mainquist, J. K., Cahalan, S. M., Orth, A. P., Walker, J. R., Ma, S., Lukacs, V., Bordone, L., Bandell, M., Laffitte, B., Xu, Y., Chien, S., Henrion, D. & Patapoutian, A. 2018. GPR68 Senses Flow and Is Essential for Vascular Physiology. *Cell,* 173**,** 762-775.e716.

Yale, A. R., Nourse, J. L., Lee, K. R., Ahmed, S. N., Arulmoli, J., Jiang, A. Y. L., Mcdonnell, L. P., Botten, G. A., Lee, A. P., Monuki, E. S., Demetriou, M. & Flanagan, L. A. 2018. Cell Surface N-Glycans Influence Electrophysiological Properties and Fate Potential of Neural Stem Cells. *Stem Cell Reports,* 11**,** 869-882.

Yan, H., Deshpande, D. A., Misior, A. M., Miles, M. C., Saxena, H., Riemer, E. C., Pascual, R. M., Panettieri, R. A. & Penn, R. B. 2011. Anti-mitogenic effects of β-agonists and PGE2 on airway smooth muscle are PKA dependent. *The FASEB Journal,* 25**,** 389-397.

Yang, A., Yu, G., Wu, Y. & Wang, H. 2021. Role of β2-adrenergic receptors in chronic obstructive pulmonary disease. *Life Sciences,* 265**,** 118864.

Yang, F., Ling, S., Zhou, Y., Zhang, Y., Lv, P., Liu, S., Fang, W., Sun, W., Hu, L. A., Zhang, L., Shi, P. & Tian, C. 2020. Different conformational responses of the β2-adrenergic receptor-Gs complex upon binding of the partial agonist salbutamol or the full agonist isoprenaline. *National Science Review,* 8**,** nwaa284.

Yao, F., Svensjö, T., Winkler, T., Lu, M., Eriksson, C. & Eriksson, E. 1998. Tetracycline Repressor, tetR, rather than the tetR–Mammalian Cell Transcription Factor Fusion Derivatives, Regulates Inducible Gene Expression in Mammalian Cells. *Human Gene Therapy,* 9**,** 1939-1950.

Yasuda, N., Miura, S.-I., Akazawa, H., Tanaka, T., Qin, Y., Kiya, Y., Imaizumi, S., Fujino, M., Ito, K., Zou, Y., Fukuhara, S., Kunimoto, S., Fukuzaki,

K., Sato, T., Ge, J., Mochizuki, N., Nakaya, H., Saku, K. & Komuro, I. 2008. Conformational switch of angiotensin II type 1 receptor underlying mechanical stress-induced activation. *EMBO reports,* 9**,** 179-186.

Yatabe, J., Sanada, H., Yatabe, M. S., Hashimoto, S., Yoneda, M., Felder, R. A., Jose, P. A. & Watanabe, T. 2009. Angiotensin II type 1 receptor blocker attenuates the activation of ERK and NADPH oxidase by mechanical strain in mesangial cells in the absence of angiotensin II. *American Journal of Physiology-Renal Physiology,* 296**,** F1052-F1060.

Yoshikawa, T., Port, J. D., Asano, K., Chidiak, P., Bouvier, M., Dutcher, D., Roden, R. L., Minobe, W., Tremmel, K. D. & Bristow, M. R. 1996. Cardiac adrenergic receptor effects of carvedilol. *European Heart Journal,* 17**,** 8-16.

Zamah, A. M., Delahunty, M., Luttrell, L. M. & Lefkowitz, R. J. 2002. Protein Kinase A-mediated Phosphorylation of the β2-Adrenergic Receptor Regulates Its Coupling to Gs and Gi: Demonstration in a Reconstituted System *. *Journal of Biological Chemistry,* 277**,** 31249-31256.

Zarzycka, B., Zaidi, S. A., Roth, B. L. & Katritch, V. 2019. Harnessing Ion-Binding Sites for GPCR Pharmacology. *Pharmacological Reviews,* 71**,** 571-595.

Zhang, D., Zhao, Q. & Wu, B. 2015a. Structural Studies of G Protein-Coupled Receptors. *Molecules and cells,* 38**,** 836-842.

Zhang, G., Liu, Y., Ruoho, A. E. & Hurley, J. H. 1997. Structure of the adenylyl cyclase catalytic core. *Nature,* 386**,** 247-253.

Zhang, P., Covic, L. & Kuliopulos, A. 2015b. Pepducins and Other Lipidated Peptides as Mechanistic Probes and Therapeutics. *Methods in Molecular Biology***,** 191-203.

Zhang, P., Gruber, A., Kasuda, S., Kimmelstiel, C., O'callaghan, K., Cox, D. H., Bohm, A., Baleja, J. D., Covic, L. & Kuliopulos, A. 2012. Suppression of Arterial Thrombosis Without Affecting Hemostatic Parameters With a Cell-Penetrating PAR1 Pepducin. *Circulation,* 126**,** 83-91.

Zhang, X., Stevens, R. C. & Xu, F. 2015c. The importance of ligands for G protein-coupled receptor stability. *Trends in Biochemical Sciences,* 40**,** 79-87.

Zhang, Y.-L., Frangos, J. A. & Chachisvilis, M. 2009. Mechanical stimulus alters conformation of type 1 parathyroid hormone receptor in bone cells. *American Journal of Physiology-Cell Physiology,* 296**,** C1391-C1399.

Zhang, Y., Yang, F., Ling, S., Lv, P., Zhou, Y., Fang, W., Sun, W., Zhang, L., Shi, P. & Tian, C. 2020. Single-particle cryo-EM structural studies of the β2AR–Gs complex bound with a full agonist formoterol. *Cell Discovery,* 6**,** 45.

Zhao, P. & Furness, S. G. B. 2019. The nature of efficacy at G protein-coupled receptors. *Biochemical Pharmacology,* 170**,** 113647.

Zhao, Y.-Y., Takahashi, M., Gu, J.-G., Miyoshi, E., Matsumoto, A., Kitazume, S. & Taniguchi, N. 2008. Functional roles of N-glycans in cell signaling and cell adhesion in cancer. *Cancer Science,* 99**,** 1304-1310.

Zhou, C., Chen, X., Zeng, W., Peng, C., Huang, G., Li, X., Ouyang, Z., Luo, Y., Xu, X., Xu, B., Wang, W., He, R., Zhang, X., Zhang, L., Liu, J., Knepper, T. C., He, Y. & Mcleod, H. L. 2016. Propranolol induced G0/G1/S phase arrest and apoptosis in melanoma cells via AKT/MAPK pathway. *Oncotarget,* 7**,** 68314-68327.

Zhu, X., Finlay, D. B., Glass, M. & Duffull, S. B. 2019. Model-free and kinetic modelling approaches for characterising non-equilibrium

pharmacological pathway activity: Internalisation of cannabinoid CB 1 receptors. *British Journal of Pharmacology,* 176**,** 2593-2607.

Zidar, D. A., Violin, J. D., Whalen, E. J. & Lefkowitz, R. J. 2009. Selective engagement of G protein coupled receptor kinases (GRKs) encodes distinct functions of biased ligands. *Proceedings of the National Academy of Sciences of the United States of America,* 106**,** 9649-9654.

Zou, Y., Akazawa, H., Qin, Y., Sano, M., Takano, H., Minamino, T., Makita, N., Iwanaga, K., Zhu, W., Kudoh, S., Toko, H., Tamura, K., Kihara, M., Nagai, T., Fukamizu, A., Umemura, S., Iiri, T., Fujita, T. & Komuro, I. 2004. Mechanical stress activates angiotensin II type 1 receptor without the involvement of angiotensin II. *Nature Cell Biology,* 6**,** 499-506.